CRANFIELD UNIVERSITY

B. M. Salihu

STRESS ANALYSIS OF DRILLSTRING THREADED CONNECTIONS

SCHOOL OF ENGINEERING

DOCTOR OF PHILOSOPHY
Academic Year: 2010/2011

Supervisor: Prof. F. P. Brennan
November 2011

CRANFIELD UNIVERSITY

SCHOOL OF ENGINEERING

DOCTOR OF PHILOSOPHY

Academic Year 2010 - 2011

B. M. Salihu

STRESS ANALYSIS OF DRILLSTRING THREADED CONNECTIONS

Supervisor: Prof. F. P. Brennan

November 2011

This thesis is submitted in partial fulfilment of the requirements for the degree of Doctor of Philosophy

ABSTRACT

The demand for energy from developed and developing economies of the world is driving the search for energy resources to more challenging environments. The exploration and exploitation of hydrocarbons now requires the drillbit to hit pay zones from drillships or platforms that are located on water surfaces below which is, possibly, in excess of ten thousand feet of water above the sea bed. From Brazil, to the Gulf of Mexico and the Gulf of Guinea on the western coast of Africa, hitherto unfamiliar, but now common, concepts in the drilling parlance such as ultra-deep drilling (UDD), ultra-extended-reach drilling (uERD) and slimhole drilling, are employed to reach and produce reservoirs which a few decades ago would seem technologically impossible to produce.

This is expected to exert tremendous demands on the physical and mechanical properties of the drillstring components. Limiting factors for reaching and producing oil and gas resources hidden very deep in the subsurface are both the capacity of the drilling rig to support the weight of the drillstring, which in some instances can be several kilometres long, and the bending, tensile and impact stresses the string has to withstand in well trajectories that are getting both longer and more tortuous.

Associated with this increased well depths and complex well trajectories is the prohibitive cost penalty of a failed drillstring. The in-service failure of drillstrings has always been an issue in the industry long before the wells become this deep and complex. The global oil and gas industry estimates the cost of string failure to be in excess of quarter of a billion dollars annually.

Researchers are continuously looking for ways to design against string failure and improve the level of confidence in drillstrings. Defect-tolerant design, tooljoint geometry modification and surface coldworking are just a few of the ideas that have gained mileage in this effort. Others that are now in consideration are the use of non-conventional materials such as aluminium and titanium alloys for drillstring components. More novel, still, is the use of a combination of two materials - one ‘softer’ than the other to form a hybrid string of two materials of unequal moduli of elasticity. This is done to make the string lighter, reduce stress concentration factor at the connections and place fatigue resistant materials in areas of high well bore curvature.

In this work a computational technique in the form of two-dimensional finite element analysis is used to develop a robust model of a drillstring connection and to analyse the stresses on the model of a threaded connection of standard drillstring tooljoint made from alloy steel. Further comparative analyses were undertaken on models of drillstrings made from a newly developed drillstring material for ultra-deep drilling, the UD-165, aluminium and titanium alloys and, finally, on hybrid drillstrings made from two different materials of unequal moduli of elasticity.

The aim is not only to develop and validate a better method of computational drillstring analysis but also to use the model to investigate and suggest areas of optimisation that will benefit industry especially in the areas hybrid strings.

Keywords:

Hybrid Strings, Computational Mechanics, Fatigue, Ultra-Deep Drilling, Extended-Reach Drilling, Unconventional Drillstrings, Aluminium Drillstrings, Titanium Drillstrings

ACKNOWLEDGEMENTS

I wish to start by thanking God Almighty for his love and guidance throughout my life and in particular the role He played in this project.

I wish to thank my supervisor Professor Feargal P. Brennan for his excellent supervision of this work. I would like to express my deep and sincere gratitude to Feargal for being an excellent mentor and for availing me with his deep experience and knowledge of the subject matter of my research in particular and the technologies and intricacies of the offshore engineering / oil and gas industry in general.

My special gratitude to my wife, Safiyyah and my children, Khadijah, Aishah, Ahmad and Bello Jr, for being part of this journey. I thank them all for their love, patience and support. I wish to also acknowledge the kind support and encouragement of my father-in-law, the late Professor Abubakar Aliyu Gwandu.

My sincere thanks go to Dr. Martin Lugg and Dr. Raymond Kare of TSC Limited for taking a keen interest in my research work and their valuable input on the use of Automated Thread Inspection (ATI) technology in drillstring inspection. I wish to also thank DAMT Ltd and in particular Mr. Tony Ing and Mr. Bob Johnson for help and guidance in developing the two-dimensional finite element model of the NC46 connector used in this work.

Special thanks go to all my research colleagues at both the NDE Centre of the University College London and at the Offshore Engineering and Naval Architecture Research Group of Cranfield University. To Bijan, Andy, Song, Abdul, Amir, Tanya, Wilson, Payam and Xiaojian, I will always cherish the companionship we shared both on and off work.

Finally, I wish to thank Mrs. Sam Skears our ever-helpful Departmental Administrator for her assistance.

DEDICATION

This work is dedicated to my father Alhaji Saleh Maradun, who was gone before it started, my mother Hajiya Hadiza Ismaila and my father-in-law Professor Abubakar Aliyu Gwandu who were gone before it ended, my wife, Safiyyah, my children Khadijah, Aishah and Ahmad who have been here all through and to my son, Bello Jr., who arrived as it was coming to an end.

TABLE OF CONTENTS

LIST OF FIGURES

LIST OF TABLES

NOTATION

A	=	Cross-Sectional Area
A_b, A_n,	=	Cross-Sectional Area of Bolt and/or Nut
a	=	Thread Pitch
C	=	Maximum Permissible Dogleg Severity
D, d_m	=	Mean Thread Diameter
E	=	Young's Modulus (Modulus of Elasticity)
$E_{(x,y...)}$	=	Error of the Approximate Solution
H	=	Thread Load Concentration Factor
I	=	Second Moment of Area
K_{ij}	=	Stiffness Matrix
K_t	=	Theoretical Stress Concentration Factor
L	=	Length of Thread in Engagement
l	=	Length of Thread in Engagement
M	=	Bending Moment of a Beam
P, P_0	=	Tensile Force on a Bolt
q	=	Force Transmitted from Bolt to Nut per unit length of nut
R	=	Thread Fillet Radius
R	=	Relative Phase Retardation (Photoelasticity)
R_1..... R_n	=	Resistance Values in Strain Gauge Resistors
R_G	=	Nominal Strain Gauge Resistance
$R_{(x;a)}$	=	Residual of the Approximate Trial Solution
ΔR	=	Change in Resistance
S_b	=	Heywood Fillet Stress
S_a, S_b	=	Axial and Bending Stress (H-K-Pedersen Formula)
a, b, e	=	Flank Load Proximity Terms (H-K-Pedersen Formula)
T	=	Torque
t	=	Thickness of Tooth projection
$U_{(x,y...)}$, $_{(x,y...)}$	=	Exact and Approx. Soln. for a Finite Sum of Functns
$\tilde{U}_G(x)$	=	Approximate Galerkin Solution
u, u_b, u_n	=	Axial Displacements
V_o, V_{Ex}	=	Output voltage, Excitation voltage (Strain Gauge)
W	=	Applied Load on Tooth Flank
w	=	Distributed Load on a Beam

x	=	Distance from the Seat of a nut
y	=	Distance along a Load Bearing Beam
Z	=	Section modulus
σ	=	Tensile Stress Along a Load Bearing Beam
$\sigma_x, \sigma_y, \tau_{xy}$	=	Directional Stress Components
$\delta, \delta_0, \delta_n$	=	Displacement Values in Bolt/Nut Arrangement
α	=	Spring Constant of the Thread
2α	=	Thread Angle
γ	=	Lead Angle
$\varepsilon, \varepsilon_a$	=	Strain, Axial Strain
$\varepsilon_x, \varepsilon_y, \gamma_{xy}$	=	Directional Strain Components
μ	=	Coefficient of Friction
β	=	Load Angle (Heywood-Kelly-Pedersen Formula)
$\phi_0 .... \phi_N$	=	Known Polynomial Functions

Abbreviations:

AISI	=	American Iron and Steel Institute
API	=	American Petroleum Institute
ATI	=	Automated Thread Inspection
BS	=	British Standard
BSR	=	Bending Stress Ratio
BSRA	=	British Shipbuilding Research Association
CFD	=	Controlled Failure Design
DC	=	Drill Collars
DOFs	=	Degress of Freedom
DP	=	Drill Pipe
ERD	=	Extended Reach Drilling
FE	=	Finite Element
FEA	=	Finite Element Analysis
FEM	=	Finite Element Modelling
GF	=	Gauge Factor (Strain Gauge)
HB	=	Brinnel Hardness
HCF	=	High Cycle Fatigue
HWDP	=	Heavy-Weight Drill Pipe

ID	=	Inside (internal) Diameter
LCF	=	Low Cycle Fatigue
LEFM	=	Linear Elastic Fracture Mechanics
LET	=	Last Engaged Thread
NC	=	Numbered Connection
NDE	=	Non-Destructive Evaluation
NDT	=	Non-Destructive Testing
OD	=	Outside (external) Diameter
POD	=	Probability of Detection
RSC	=	Rotary Shouldered Connection
S – N	=	Stress-Life
SST	=	Super Strength Threads
SCC	=	Stress Corrosion Cracking
SCF	=	Stress Concentration Factor
SIF	=	Stress Intensity Factor
TSC	=	Technical Software Consultants
UDD	=	Ultra-Deep Drilling
UERD	=	Ultra-Extended Reach Drilling

1 Introduction: In-Service Failure of Oilwell Drillstrings

1.1 Introduction

Because of the seemingly insatiable demand for energy from advanced and developing economies, the search and exploitation of new hydrocarbon resources is taking place in an economic climate characterised by rising oil prices and challenging environmental concerns. Production from new fields and (re)development of mature reservoirs that require creative well trajectories and deeper offshore developments, sometimes under water depths of over ten thousand feet, also require longer, and thus heavier, strings.

In the fifteen years from 1995 to 2010 the number of wells drilled in the U.S. that are deeper than 4500 m (15000 ft) have more than doubled. This is a reflection of a developing trend globally where ultra-deep drilling (UDD) and ultra extended-reach drilling (uERD) are becoming the norm rather than the exception. Projects under execution or in the planning stage in areas such as Gulf of Mexico, Brazil, Gulf of Guinea, Trinidad, Malaysia and the ultra-deep gas recovery project beneath the Caspian Sea all point to a drive by the industry to push the limit of existing drilling technologies [1.1].

Since the advent of deepwater drilling, a major challenge in the drilling industry is the capacity and mechanical properties of the engineering materials in use to withstand high operational demands in terms of their stress and fatigue resistance. This is more apparent in oilwell drillstrings that are not only expected to retain their designed mechanical properties, withstand additional hook loads (i.e., the hanging weight of the string in the well) due to the additional string weight occasioned by deep and ultra-deep drilling, but to also withstand bending stresses and fatigue occasioned by uERD and tortuous well trajectories. Clearly, there is a need for robust engineering investigations and analyses for the development of drillstring materials that can serve as an

alternative to carbon steel from which almost all conventional drillstrings are made.

Environmental considerations may require wells to be designed to hit reservoirs that are located stratigraphically under a surface location that has a fragile eco-system with the drilling rig located on a remote and less environmentally sensitive location. Lakes, National Parks and onshore remote areas and other environmentally sensitive locations can thus be protected using ERD and horizontal drilling technologies. When considering cost of field development, the operational footprints of oilwell drilling can also be minimized using such technology as there will be less requirement for drill sites, artificial islands and offshore platforms as the lateral extent of the reservoir can be accessed from fewer surface spud points than in conventional straight hole drilling. This has a huge impact on the economics of field development.

Titanium as a drillstring material comes with the advantage of higher strength and light weight. Because of its durability and toughness it is mainly used in ERD projects that expose the string to high bending and cyclic stresses. But because of its relatively high cost, most titanium drillstrings are of a smaller diameter and have found wide application in slimhole drilling.

In-service failure of a drillstring is normally due to high stress concentrations at the root of the threaded tooljoint connections when subjected to fatigue due to cyclic loading. This is normally exacerbated by the presence of dog-legs, which are measures of the deviation of the well trajectory from the 0^{o} vertical direction. This deviation from vertical produces a tension/compression cycle at points of stress concentration that will accelerate the initiation of fatigue cracks or the acceleration of the cracks towards a critical point that will ultimately lead to sudden fatigue failure in the string. Macdonald et al [1.2] believes that an understanding of the interaction between the local stresses at the tooljoint and global tensile stresses in the string will also contribute to the design of a fail-safe string.

Oil wells are drilled with a drill stem that consists, normally, of a series of 10m long hollow steel tubulars that are joined at threaded connections called tooljoints. The stem transmits rotary and vertical motion to the drill bit. The cyclic stresses due to fatigue that the drillstem undergoes gives rise to the initiation, and eventual propagation, of fatigue cracks that will ultimately lead to the failure of the string in service, which will, in turn, lead to days of costly retrieval operations (termed “fishing” in industry parlance) and other remedial operations before normal drilling activities can resume. Considering that the current daily hire rate for deep water drilling rig is over $400,000.00 it is not difficult to see why drillstring failure in service costs the global oil and gas over a quarter of a billion dollars annually [1.2].

Various methods and procedures are used to prevent this failure. Principal of these include material choice and treatment to delay the onset of crack initiation and proper and systematic tubular management through non-destructive inspection and the maintenance of an up-to-date service record.

This work aims to develop a fully validated and robust finite element model that will look at the response of the various non-conventional drillstring materials to preload and applied axial load in relation to the materials’ wide applicability as a stand-alone equimodulus strings or in a hybrid string configuration where one material is used as the pin (male) material and the other as a box (female) material in a drillstring connection.

Various methods of applying preload to a mating thread finite element model were considered and compared before one, considered to be a more robust method, was chosen for the study of loading and stresses in an oil well drillstring connection. The method so chosen uses the FEA code’s contact algorithm to mimic frictional contact and the cantilever effect of the lead angle of the thread flank. The axial load on the model was introduced using a simple pull action at the top of the string while the string is restrained from upward axial movement through the use of boundary conditionals applied to the bottom of the string. Because the elements used in the simulation are the CAX4 axisymmetric

quadrilateral elements that mimic a fully revolved model, there was no need to restrain the radial ends of the model.

The work succeeds in presenting a finite element model for the analysis of drillstring-threaded connections. The model was used to study the application of alternative and hybrid drillstring materials to the current industry need of deeper and longer reach well trajectories.

1.2 Trends in Ultra-Deep and (Ultra) Extended Reach Drilling

ERD evolved from simple directional and horizontal wells. The current rise in the study and application of Extended-Reach Drilling (ERD) and Ultra-Extended Reach Drilling (uERD) is not unconnected with the need by operators to access hitherto unreachable or commercially uneconomical reservoirs by extending the lateral departure of the well trajectory. A major area of concern in ERD is drillstring reliability. As stated earlier, ERD is undertaken using expensive rigs where an unplanned trip, or pulling the string out of hole, due to string failure can have a huge impact on the project because of costs associated with the daily hire rate of the rig, other ancillary services and the depth of the wells.

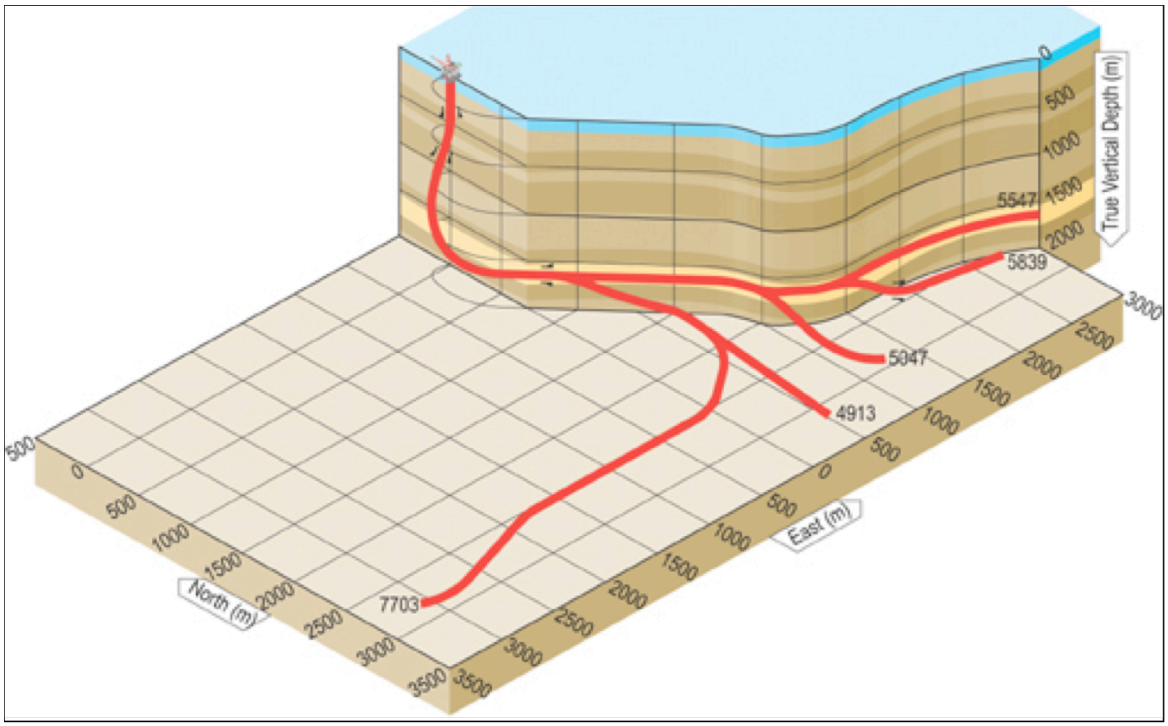

[7.1] Figure 1-1: Horizontal and Multilateral Wells [1.3]

Lateral, or multi-lateral, extended reach drilling has the advantage of drilling laterally (horizontally) into a reservoir thereby increasing production from a single well by enlarging its drainage area. An enlarged drainage area can swing a reservoir or field from being economically not viable to viable. Achieving such technical or commercial viability is connected to concerns that range from

environmental to the physical limitations of the drilling rig or drillstring components.

However, high energy prices occasioned by an increased energy demand has brought about a push by oil and gas companies to seek ways of drilling deeper high-displacement wells to access these reservoirs.

In this work, ERD wells are defined as wells with a horizontal throw versus true vertical depth ratio greater than 2:1 [1.4]. UDD wells on the hand are defined as wells that are deeper than 7620 m (25,000 ft) and a horizontal reach versus true vertical depth ratio of less than 1:4 [1.5]. Clearly, from this definition it can be seen that while the major area of concern in ERD wells will be high torque values, in UDD wells high tensile loads are likely to dominate as the major concern. Because of torque and drag management tools and techniques that have proven to be cheaper and more successful in preventing string failure in ERD wells, most of the current interest lies in the search and application of new materials that have higher strength (as in the case of the high strength steels) or high strength to weight ratios (as in the case of composites, aluminium and titanium alloys [1.4]. From a drillstring design point of view, the major difference between UDD and ERD wells is the manner in which the string is loaded.

1.2.1 Demand Versus Capability for Deep Offshore Drilling

Global trends in deep offshore drilling show a steep increase in activities. Since 1995, wells drilled in the U. S. with vertical depth of over 15,000 ft have more than doubled and the number of rigs capable of drilling deeper than that has nearly tripled. In September 2009, BP reported drilling the deepest well ever drilled. The well, which extends about 12 KMs from the rig floor, was drilled in the Tiber Prospect in the Gulf of Mexico [1.6].

Figure 1-2 below gives us an indication of where the industry is headed in terms of rig and tubular requirements. It can be seen that in 2009/2010 alone more

than 150 major discoveries were made globally in more than 4500 feet (1370m) of water. A drillship with a capacity to drill that deep will have a hook load capacity of over 1250 tonnes. Nearly twenty (20) newbuild rigs of such capacity were ordered in the first for months of this year at a cost of over 13 billion Dollars [1.7].

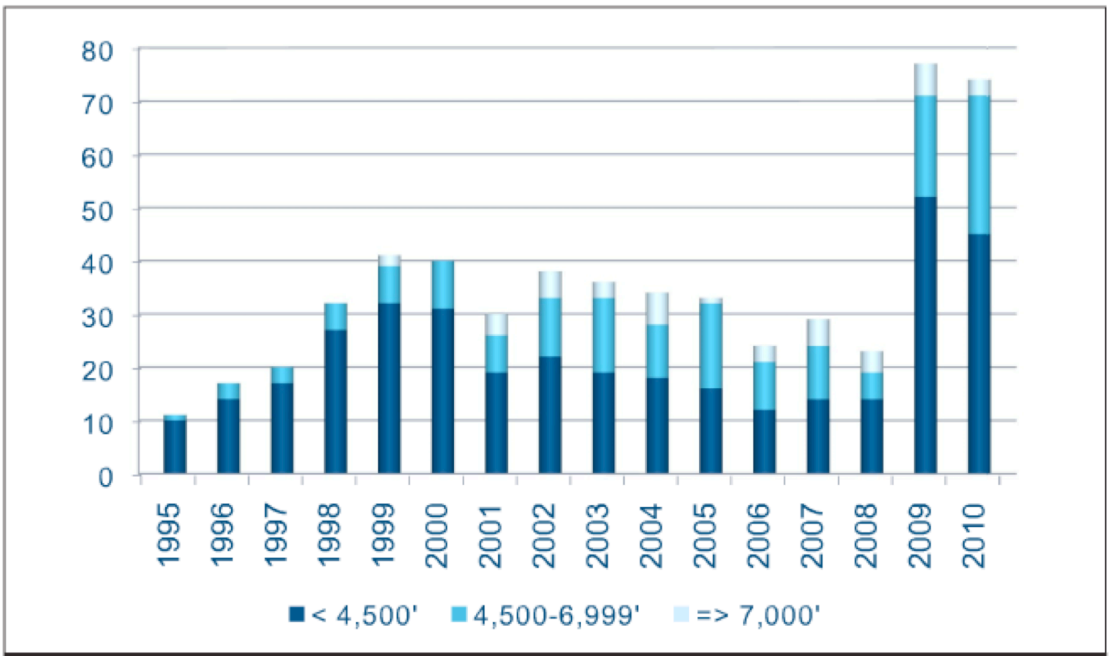

Figure 1-2: Major Oil and Gas Discoveries from 1995 – 2010 [1.8]

A study of the industry database, as shown in Figure 1-3 below, indicate that the capacity to drill long horizontal departures is stronger than the ability to drill deeper wells such as the Tiber Prospect well. However, global demand for energy and the industry's new-found interest in deposits locked very deep in the earth indicate that it is just a matter of time until the UDD envelope gets extended again.

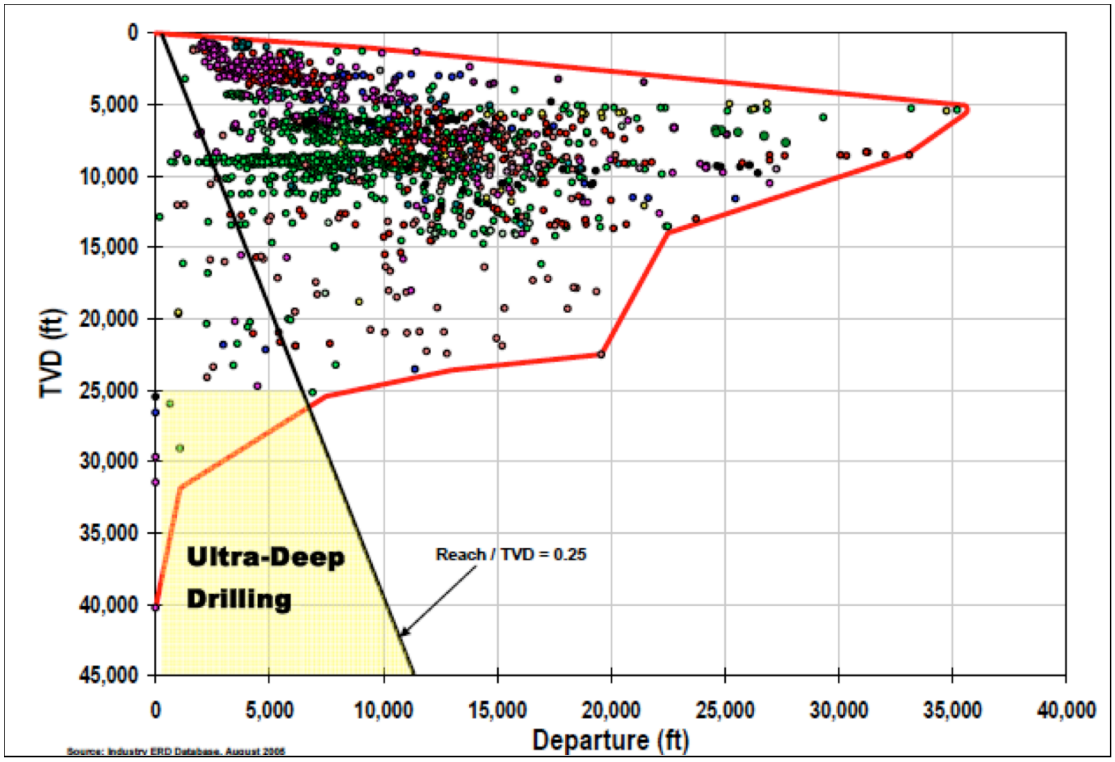

Figure 1-3:Extend Well Departures (ERD) Vs Ultra-Deep Drilling Envelop

[1.9]

In light of the above, the industry is already in search of technologies that will extend the capacity of the rigs and strings to explore much deeper than we are currently doing. While it is possible to build higher capacity rigs, a more appropriate technology will be the extension of the capacity of the existing rigs through technologies such as slimhole drilling and the use of hybrid and lighter drillstring materials.

1.3 Failure Mitigation In Drillstrings

Drillstring operations to enable exploitation of hydrocarbon reserves are an essential part of the worlds largest industry. As the more extensive reservoirs became fewer, more drilling operations than ever are required to tap wells previously considered economically marginal. In addition, demanding operations such as slim hole and directional drilling techniques are employed to an increasing extent thereby affecting the designed capabilities of the drillstring. These 'unconventional' operations have the net effect of increasing the stresses experienced by the string and accelerate the time to failure of the string [1.10].

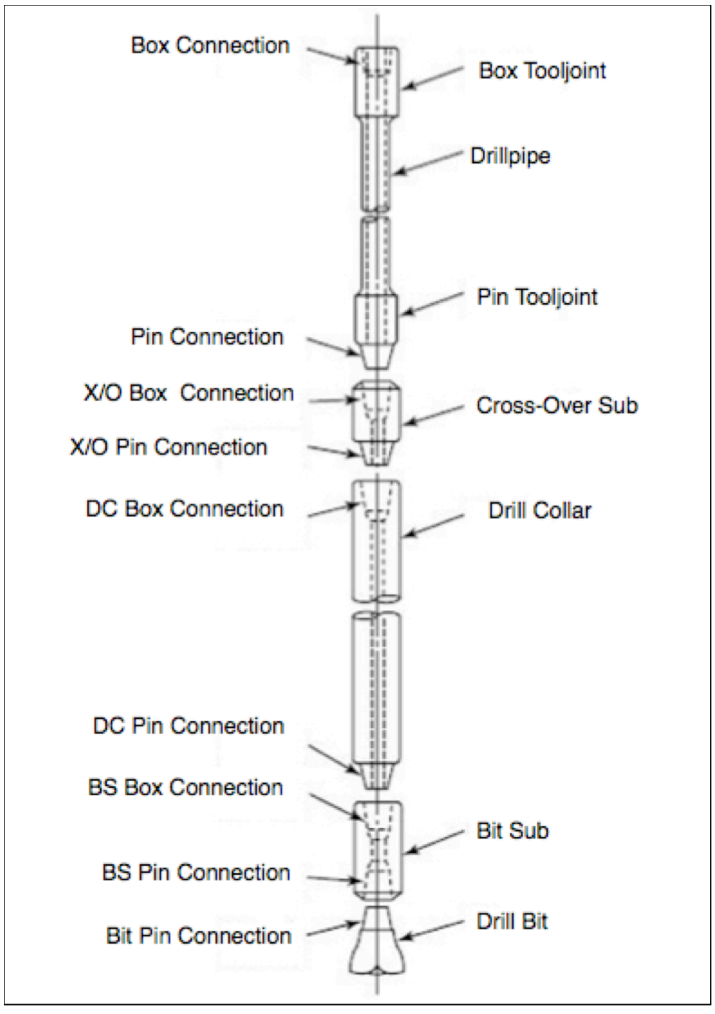

Figure 1-4: Drillstring Components in Straight Hole Configuration

At the lower end of the drillstring are various components plus the drill bit that

are collectively termed the bottom hole assembly (BHA). These include thick-walled drill collars that are used to add weight to the bit and the heavyweight drill pipe (HWDP) that is used in the transition zone between the drillstring and BHA to reduce the severity of the effects of stiffness change [1.11]. The transition zone is where tension in the string in the shallow end changes to compression of the string at the deeper end. Figure 1-4 above shows a schematic of the components that make up the drill stem. The term “drillstring” is used universally in the industry to mean the drillpipes and the BHA [1.12].

In the Fatigue Analysis of Drillstrings - (FADS) – investigation [1.13], a joint industry project carried out at the NDE Centre of the University College London in 1990, an analysis of failure history showed that most failures occurred about 300 feet from the bit, i.e., in the BHA area. It also showed that the last engaged thread (LET) of the pin or box carries the highest stress peaks and thus a higher SCF and susceptibility to crack initiation. Other analyses conducted, [1.14], [1.2], [1.15] suggested that the location of the maximum stress in a threaded connection is in the thread root of the first fully engaged loaded tooth of the pin and the first fully engaged loaded tooth of the box depending on the presence of preload. These location are shown as (a) and (b) in Figure 1-5 below

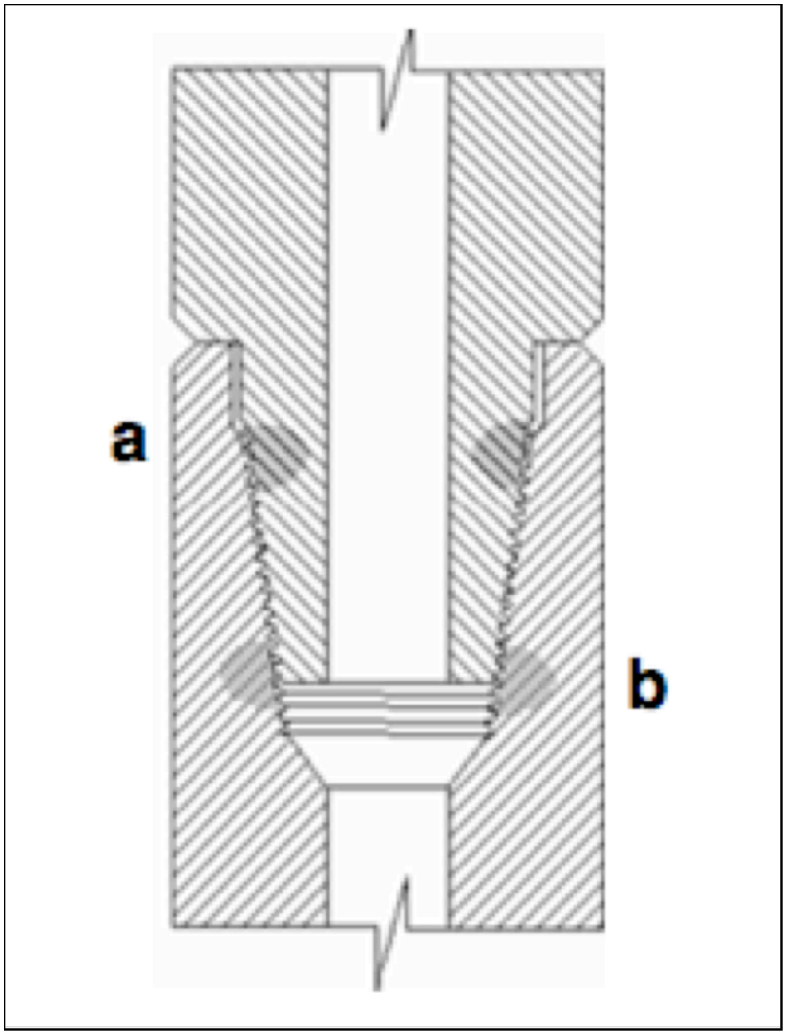

Figure 1-5: Last Engaged Thread (LET) on (a) Pin and (b) Box

1.4 Controlled Failure Design Applied to Drillstring Connections

In controlled failure design, limited failure is deemed acceptable as a warning of, or precursor to, a catastrophic failure. As early as 1967 Irwin, et al. [1.16] proposed the leak-before-break (LBB) criterion as a means of estimating the necessary toughness of pressure vessel steels so that surface crack could grow through the wall of the vessel before catastrophic fracture. This design technique has grown to include various methods that can be used to encourage a component to fail in a 'friendly', non-critical manner. In the analyses of drillstring fatigue failure, two failure types were identified, a twist-off and a washout where the former is the parting of the string catastrophically which will lead to massive costs to the operator and the latter is the gradual loss of the integrity of the string which can be detected on surface through loss of pressure and will call for an action to be taken to prevent total failure of the string [1.17]. One of the methods used in controlled failure design is the introduction of surface compressive residual stresses to harden the surface of the component.

Specialist inspection and monitoring regimes are then built into the maintenance programme to monitor the initiation and growth to near-criticality of defects. The applicability of controlled-failure design methodology to drillstrings has the potential of saving the global oil and gas industry massive sums of money by arresting the failure of drillstring components to locations and times that are not operation critical. This is shown in Figure 1-8 below. Oil well drillstrings are joined at threaded tool joints that are made up or broken up as the drilled depth increases or the downhole tools are pulled from bottom. Conventional wisdom calls for the modification of a threaded connection's stress distribution profile to reduce or eliminate peak stresses that are usually found in the last engaged thread of the pin or box connection. Controlled failure design on the other hand, understands the inevitability of some failures and so encourages the concentration of peak stresses in a particular, predetermined part of the thread

(in this case, the pin) that can be designed to give a leak-before-break (LBB) warning.

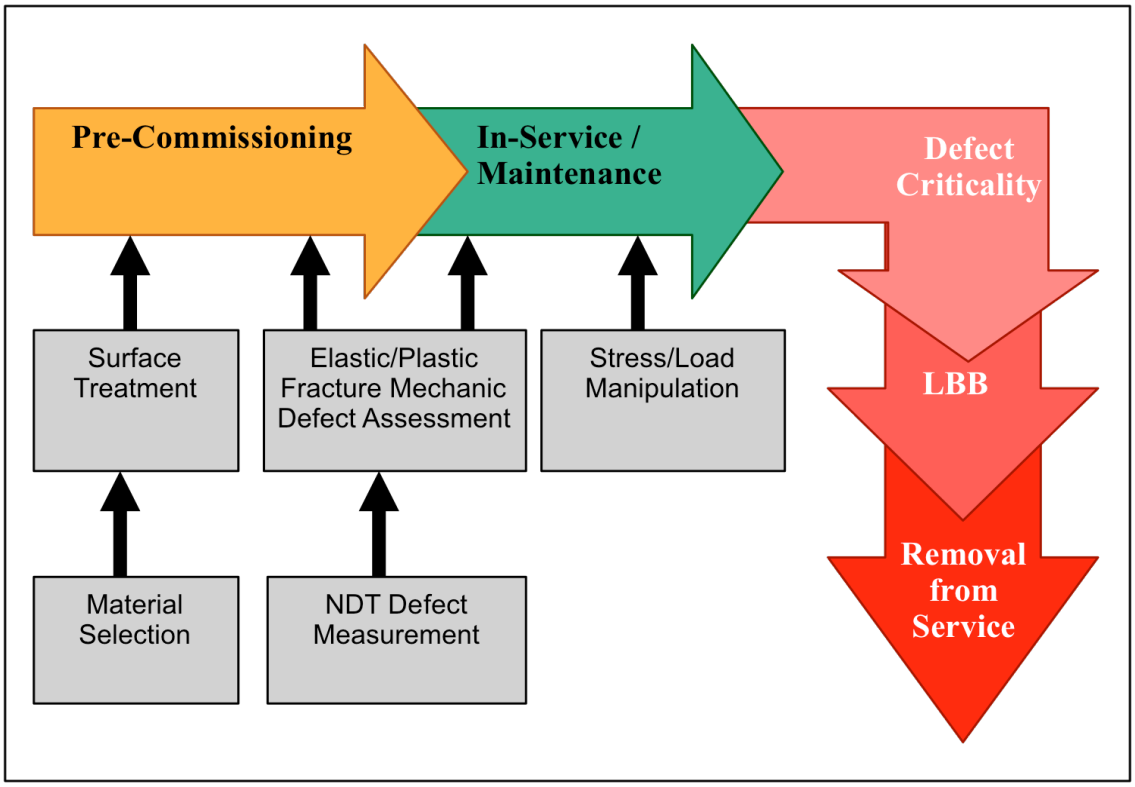

Figure 1-6: Applying Controlled Failure Design to Drillstring Components

Some technologies and processes applied in controlled failure design work on the material at microscopic levels.

According to Toor [1.18], this design method attempts to use ingenious ways to prevent sudden catastrophic failure in components. These ways include:

(1) Use of material that are as flaw-tolerant as possible

(2) Innovative design concepts such as multiple load paths

(3) Stress level selection and control which lead to slow progression of fatigue cracks during service life

(4) Inspection procedures that lead to defect detection prior to impairment of the structure's load capacity

(5) Process control - during manufacturing and processing so that the initial flaw

is small and the basic fracture properties are not impaired by the manufacturing processing.

Controlled failure design looks at innovative ways to use 1 to 5 above in determining not only how a component can function with sub-critical flaws but also how growing and advancing defects can be made to behave in ways that are beneficial to the engineering process the material is or will be engaged in and also to lend itself to evaluation and monitoring regimes that will help in knowing when to withdraw the component from service before it fails catastrophically.

1.4.1 Inducing Compressive Residual Stress Through Cold Working

The fatigue life property of a material is influenced by an induced residual stress. Residual stresses are internal local structural stresses in self-equilibrium through the cross-section. While residual stresses will not lead to plastic failure of structure, they contribute significantly to the stress state near the crack tip. Residual stresses can be classified into microstresses and macrostresses [1.19].

Microstresses are only present in two-phase materials where they maintain balance between the phases. Although they are evenly distributed over the entire cross-section of the material, their value will be different in the phases present. They do not influence fatigue crack initiation or the propagation rate. Macrostresses, on the other hand, are the same in all the phases present in the material. They are introduced to a macrostress-free structure after solidification or by the introduction of plastic strain gradient locally through overload or surface preparation at a temperature below the metal's crystallization temperature. In controlled failure design residual stress refers to a material macrostress [1.20].

The benefit of residual stresses is due, primarily, to the observed effect it has on a material's fatigue life properties. Tensile residual stresses are known to

decrease fatigue life while compressive residual stresses are known to increase fatigue life. Shot peening is one of the methods of inducing compressive stresses in materials and the magnitude of beneficial compressive residual stress produced using this method can be as high as 50-60% of the material's Ultimate Tensile Stress (UTS) [1.21].

The beneficial form of residual stress, also known as strain hardening, can be quantified by calculating the degree of plastic deformation, or percentage cold work (%CW) in the worked material [1.22].

$$\%CW = \left(\frac{A_0 + A_d}{A_0} \right) \times 100 \text{.....} 1.1$$

Values obtained from the solving for %CW in Eq. (1.1) are then read on a curve pertaining to the material on a special chart to obtain the increase in tensile stress.

Germany's Wohler Institute first investigated the benefits of thread root cold rolling in the 1930s when about 20-65% improvement in fatigue strength was observed. By mid-30s the American railroad industry was practicing surface stressing of components to reduce fatigue failures [1.23]. The first reported investigation into thread rolling in the UK was by the British Shipbuilding Research Association (BSRA) in the 1950's [1.19].

Kristoffersen [1.19] reported from several investigations on the increase of fatigue threshold in materials from the application of residual stress while Ngiam and Brennan [1.24] reported the application of stitch rolling to control the rate and shape of crack propagation.

1.4.2 Drillstring Defect Inspection

The two widely used drillstring inspection methods are the American Petroleum

Institute Recommended Practice 7G: Recommended practice for Drill Stem Design and Operating Limits and the DS-1 Volume 3: Drill Stem Inspection standard. The former is known simply as API RP7G while the latter is known as the DS-1 standard. As expected with other engineering and technical standards, these standards are used to ensure reproducible results during inspection/testing, no matter when, where or who conducts the inspection. The reliability and acceptability of a drillstring inspection depends on these and other less known standards [1.25].

Generally, Non-destructive testing (NDT) techniques are limited by the time it takes undetected cracks to grow to critical size and, consequently, cause failure. In the absence of a better method to address this limitation, a maintenance regime that incorporates defect assessment and a reliable inspection technique is invaluable to the continued fitness-for-purpose of any structure especially if the defect-tolerant design approach is considered

Non-Destructive Testing (NDT) methods in common use in the inspection of oilwell drillstrings include visual, magnetic, ultrasonic and electromagnetic.

1.5 Research Methodology

Investigations into failures of drillstring components will naturally and logically gravitate towards fatigue and stress concentrations. An overwhelming amount of academic and technical literature all point to fatigue as the primary cause of drillstring failure. While stress concentrations in standard bolt and nut connections have elicited a lot of interest, very little work has been done in the analysis of stresses made from non-conventional materials or when the string is a hybrid of tubulars made from different materials.

The methodology used in this work breaks down the research investigation into three main parts that are chronologically executed:

I. A critical study of earlier research work done in the area of thread load and stress distribution.

II. The development of an alternative and more robust method of using finite element analysis to simulate loading and stress response in threaded connectors. In particular, emphasis is made on developing and validating a unique preload modelling technique and using the technique/model to investigate stress response from non-conventional materials.

III. The possibility of the application of various non-conventional types of drillstring materials as oilwell drillstring tubulars. This is undertaken to verify the advantageous properties of the materials under investigation.

1.5.1 Stages of the Simulation

The stages required for the simulation process and the software code required to achieve each is shown in Figure 1-12 below. The design of the simulation process takes into consideration the need to make the input/output parameters of the simulations completely independent and easily variable, thereby making the process entirely parametric such that sketching, meshing and input file modifications can be used to obtain unlimited number of geometries, material types and elastic properties as inputs in the simulation.

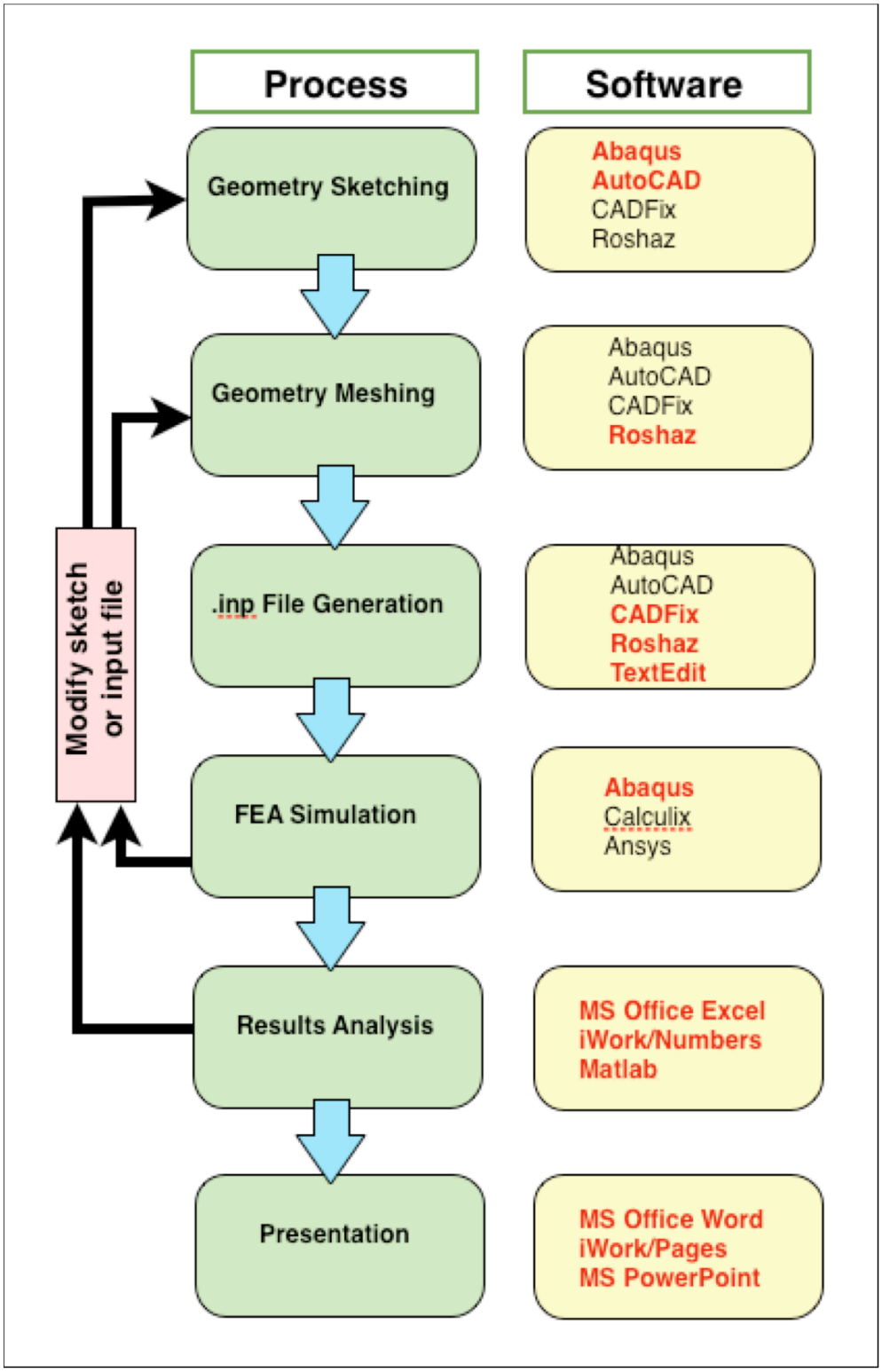

Figure 1-7: Stages of the Simulation

Once a benchmark model, which in this case is a standard NC46 connection made from AISI 4145H carbon steel, is sketched, meshed, fully solved and

validated - the model can be modified at any of the three (3) input stages to reflect varied tool joint geometries and material elastic properties. That way the entire simulation process can be made fully parametric.

A schematic of the simulation workflow can be seen in Appendix A: Simulation Workflow

1.6 Scope of Thesis

This chapter introduces the current trends in oil and gas exploration that have forced the industry and researchers to re-think conventional and routine methods of exploiting hydrocarbon resources, particularly in the area of the drillstring operating envelope. Drilling tubulars and their properties which, as it currently stands, are some of the limiting factors of how deep and far from the spud point a well can be drilled, are discussed. The research work then aims at developing and validating ways of simulating loading and stress response of these strings and applying this new method to both conventional and non-conventional drillstring materials.

In Chapter Two a detailed literature review looks into the work undertaken by various researchers in load and stress distribution in threaded connections generally and oilwell drillstring connections particularly. Work done using various stress analysis techniques by various analysts is then discussed. The effect of the environment in which the string operates is then discussed noting in particular the importance of fatigue, well tortuosity, preload, corrosion and thread/string geometry. The chapter ends with a look at the work done using finite element analysis in the study of drillstring stresses.

As the analysis tool used in this work, Finite Element Analysis (FEA), is discussed in Chapter Three. The understanding of the theories and principles of the FEA method and its history and the governing equations of stress modelling are explored. The governing equations in stress modeling in FEA are discussed and the possible sources of errors in any given solutions are discussed.

Chapter Four then goes on to show how the axisymmetric two-dimensional FEA model used in the work was developed. Results obtained from the earlier model are compared to those obtained from a benchmark study using the model developed in this work. The loads and stresses in the connector and the working limits that form the operational boundaries of the connection are also discussed.

In Chapter Five, the results of the simulations undertaken using the 2-D model are presented. These include the results from the benchmark parameters used to validate the model and also those of the comparative studies undertaken using the elastic properties of high strength steels and various other 'non-conventional' drillstring materials. The model is further used to investigate the effect of using hybrid, non-equimodulus strings where the connection is a combination of two different materials – one hard and the other soft. Using this latter study, it is shown that it is possible to obtain beneficial reduction in stress concentration in the connection when the box material in the connection is softer than the pin material. This is an FEA validation of an earlier work by Dragoni [1.26].

A discussion of the results including their operational relevance in today's oilfields is presented in Chapter Six. Fatigue and its effect on the life of drillstrings is discussed and the fatigue life of the connections studied is compared. The results from the simulations are then looked at in relation to the fatigue and stress performance of the various hybrid configurations studied.

In Chapter Seven the findings are then looked at in relation to their operational impact on drilling operations. A conclusion is then drawn from these finding and suggestions proffered for future work.

1.7 Reference

[1.1] **Smith, J. E., Chandler, R. B. and Boster, P. L.**. *"Titanium Drillpipe for Ultra-deep and Deep Directional Drilling"* SPE Paper No. 67722 presented at the SPE/IADC Drilling Conference, Amsterdam, February 2001

[1.2] **Macdonald, K.A. and Deans, W.F.**, *"Stress Analysis of Drillstring Threaded Connections Using the Finite Element Method"*; Engineering Failure Analysis, Vol 2, No. 1 pp. 1-30, 1995

[1.3] **Image courtesy of Baker Hughes Inteq,** published in E P Magazine of August 2007 and accessed at www.epmag.com/archives/features/583.htm on 19th of November 2009.

[1.4] **Jenkins, M., Rodriguex, A.C., Linke, C. and Mader, G.**, *"Can Aluminium Drill Pipe Extend the Operating Envelope for ERD Projects"*; IADC/SPE Paper no. 128910 presented at the IADC/SPE Drilling Conference and Exhibition; New Orleans; February 2010

[1.5] **Jellison, M.J., Chandler, B.R., Payne, M.L. and Shepard, J.S.**, *"Ultradeep Drilling Pushes Drillstring Technology Innovation"*; SPE Paper No. 104827 presented at the 15th SPE Middle East Oil & Gas Show and Conference in March 2007

[1.6] **The Star Online**: Published September 3rd, 2009. Accessed at http://biz.thestar.com.my/news/story.asp?file=/2009/9/3/business/20090903073841&sec=business on 25th February 2011.

[1.7] **Petroleum Review Magazine**, *"Ultra-deep Armada Sails In"*, June 2011; Energy Institute, UK

[1.8] **Image courtesy of ENSCO/PCF**; published in Petroleum Review Magazine of June 2011.

[1.9] **Chandler, R.B., Jellison, M.J., Payne, M.L. and Shepard, J.S**, *"Advanced and Emerging Drillstring Technologies Overcome Operational Challenges"*; World Oil, Vol. 227 No. 10; October, 2006

[1.10] **Azar, J. J. and Samuel, R.**, *"Drilling Engineering"*; PennWell Corporation, 2007, Pp 319

[1.11] **Devereaux, S.**, *"Drilling Technology in Non-Technical Language"* PennWell Corporation; 1999, Pp 53

[1.12] Azar**, J. J. and Samuel, R.**, *"Drilling Engineering"*; PennWell Corporation, 2007, Pp 319

[1.13] **NDE Centre, University College London**, *"Fatigue Analysis of Drillstrings – FADS"*, Joint Industry, Project Final Report, 1990.

[1.14] **NDE Centre, University College London**, *"Reliable Operations of Drillstrings - RODS"*, Joint Industry Project, Final Report, 2002

[1.15] Tafreshi **A. and Dover, W. D.**; *"Stress analysis of drillstring threaded connections using the finite element method"*; Int J Fatigue 15 No 5 (1993) pp 429-438

[1.16] **Irwin, G. R., Krafft, J. M., Paris, P. C., Wells, A. A.**, *"Basic Aspects of Crack Growth and Fracture"*, NLR Report 6598, Washington DC, November 1967

[1.17] **Knight, M.J., Brennan, F.P. and Dover, W.D.**; *"Controlled Failure Design of Drillstring threaded connections"*; Fatigue and Fracture of Engineering Materials and Structures; Vol. 26, pp 1081-1091; 2003

[1.18] **Toor, P. M.**, *"On Damage Tolerance Design of Fuselage Structure – Circumferential Cracks"*, Engineering Fracture Mechanics, Vol. 26, No. 5, pp771-778, 1987

[1.19] **Kristoffersen, S.**, *"Improved Fatigue Performance of Threaded Drillstring Connections by Cold Rolling"*, Dr. Ing Thesis, Norwegian University of Science and Technology, 2002

[1.20] **Burrell, N. K.**, *"Controlled Shot Peening to Produce Residual Compressive Stress and Improved Fatigue Life",* Proceedings of conference held in April 1980, Chicago, Illinois. Pp 139-149

[1.21] **Calister, W. D.**, *"Fundamentals of Material Science and Engineering"*; John Wiley and Sons Inc. Pp 254; 2005

[1.22] **Moore, H. F.**, Murra, W. M., Almen, J. O., Horger, O. J., Kosting, P. R., *"Surface Stressing of Metals"*, ASM Congress and Exposition, Cleveland, February 1946.

[1.23] **Taylor, B., Wilson, ,G. J.**, *"An investigation of the Effects of Thread Root Cold Rolling on the Fatigue Strength of Bolts"*, The British Shipbuilding Resaerch Association, Report # 186, 1955.

[1.24] **Ngiam, S.S. and Brennan, F. P.**, *"Experimental Investigation of Crack Shape Evolution in Cold Rolled Components"*, International Conference on Fatigue Crack Paths, Parma, 2003.

[1.25] **American Petroleum Institute**, "*API RP 7G:Recommended practice for Drill Stem Design and Operating Limits"*; American Petroleum Institute 16th Ed. Aug. 1998

[1.26] **Dragoni, E.**, *"Effect of Nut Compliance on Screw Thread Load Distribution"*, Journal of Strain Analysis. Vol. 25 No. 3, 1990

2 Literature Review: Load and Stress Distribution in Threads

Threaded fasteners are important in engineering design because they provide an economical and non-destructive means of assembling engineering components. Investigations have shown that the first few threads near the loaded face of the connection may carry as much as 60% of the total load carried by the entire connection thereby giving rise to high stress concentrations at the root of the first engaged thread [2.1].

Threaded fasteners influence the strength, durability and reliability of some assemblies and, in light of this, analyses of loads and stresses in bolts and nuts remain a very important part of fastener technology and has been an area of intense study for nearly a century. This chapter aims to present the various research work undertaken in the area of stress distribution in threaded fasteners.

Industries such as aircraft and aerospace are concerned with both weight and reliability. In these and similar industries the cost of R&D for a new fastener technology is insignificant compared to the cost of failure. The aircraft industry led the way in the development of standardised fasteners in the decades before the Second World War and since then the aerospace industry has been the leader in the development of high-strength fastening systems and engineered joints [2.2].

A few physical and geometrical improvements that have been attempted with a measure of success include the use of preload to modify load distribution in the connection [2.3], cold rolling of the thread roots to induce compressive residual stress [2.4], asymmetric thread forms to modify point of thread shank contact to keep the cantilevered bending moment down [2.2], the introduction of stress relief features [2.5], modification of the taper angle in conical threads [2.6], and improvement of fatigue life through control of bore eccentricity [2.7], etc.
Future trends in fastener technology will see the use of different materials for the

nut or bolt as simulated mathematically by Dragoni [2.8], through the variation of the nut's Young's Modulus and the use of shape memory alloys in minimizing the tendency to loosening in mating fastener parts [2.9].

2.1 Early Studies on Thread Load Distribution

Numerous investigations of threaded fastener load distribution that were carried out between 1918 and 1960 still govern the theory and understanding of how stresses, load distributions and deformations interact in a threaded fastener [2.10], [2.1], [2.11], [2.12], [2.13], [2.14]. Almost all of the studies carried out concentrated on the optimization of the loads and stresses in a bid to obtain a more uniform distribution and thus reduce peak stresses on specific areas of the fastener, which will in turn reduce the susceptibility of failure due to fatigue. Various models were suggested on how to correct for the non-uniform distribution which sees threads farther away from the free end of the connection bearing the highest loads and thus more likely to be locations of peak stress and failure initiation.

The first recorded attempt to understand the stress distribution in threads was undertaken by Stromeyer in 1918 [2.10]. He used the Bernoulli-Euler beam theory for the calculated deflections and the stresses.

There are many reasons why the Bernoulli-Euler bending theory cannot be applied to the classic thread root stress problems. One is the nature of the geometry of the thread as a load bearing projection. As can be easily demonstrated, the Bernoulli-Euler theory is more applicable to straight, long beams. In situations where the beam is curved and short, as in the case of threads or contacting gears, an alternative theory must be developed to address this peculiarity. However, the most important reason why the Bernoulli-Euler theory cannot be applied to thread root stress problems is that while linearity is one of the main attributes of the Bernoulli-Euler theory - thread loading is not a linear problem as it comes with issues of contact and plasticity.

In the same vein, because stress concentrations arise when uniformity of geometry is disrupted, a study of thread stresses and loading will involve considerations of geometry that are beyond those accounted for by the classical beam theory.

Stromeyer worked out a parabolic distribution of the stress in the threads by

relating it to riveted joints, in which case, for rivets on a plate in shear, the highest load is borne by the rivet that is farthest from the free end of the plate in shear. As stated above, the deflections in the member were calculated using the Bernoulli-Euler bending theory while stresses were calculated in the same manner but with some refinements and arbitrary assumptions in the theory. To calculate the stresses, Stromeyer neglected the effects of friction, also compression of the nut and recessions due to radial displacements were neglected.

Stromeyer's work showed the difficulty in modelling thread load distribution because threaded fasteners, unlike simple geometrical models, have very complex geometries. In a bid to simplify the model and arrive at an acceptable mathematical solution, the three-dimensional problem of load distribution in thread geometries was reduced to a two-dimensional planer problem of riveted joints with considerations based purely on elastic extensions. Since the aim of the model was to optimize the distribution of the load by making it more uniform across all the threads in the connection, it was acknowledged that exponential distribution of the curve would only exist if successive rivets were placed infinitely close together. He suggested differential pitching between the nut and bolt to correct for this non-uniform distribution. Stromeyer also observed that the bending of the threads affected the overall load distribution.

Stromeyer's work was important in anticipating, in general terms, some of the conclusions reached by later researchers such as in the understanding of the effect of variable pitch and variation of the load carried by a tooth to the distance of the free face of the nut.

In 1929 while discussing the elastic theory of bolt construction as part of his work of the analysis on stresses on plate rotors in turbo generators, Den Hartog presented a similar parabolic solution for this stress distribution as Stromeyer. According to him, when a nut and bolt of equal pitch are tightened the bolt elongates and the nut is compressed. As such, the mating pitches are no longer equal and thus the distribution of stress will also not be equal [2.1].

Studying an ACME threaded bolts of turbine plate rotors, Den Hartog thought of the contacting faces of the bolt and nut as two faces of a contacting cantilever. He considered only bending deflections and not axial recessions due to radial compression in threads and to radial displacement in bolts and nuts.

Figure 2-2 below shows, according to his analysis, the percentage of load carried by threads a distance (x) along the length of the nut and it showed that about 60% of the load was carried by threads that are a distance of less than 25% of the length of the nut from the loaded face of the nut.

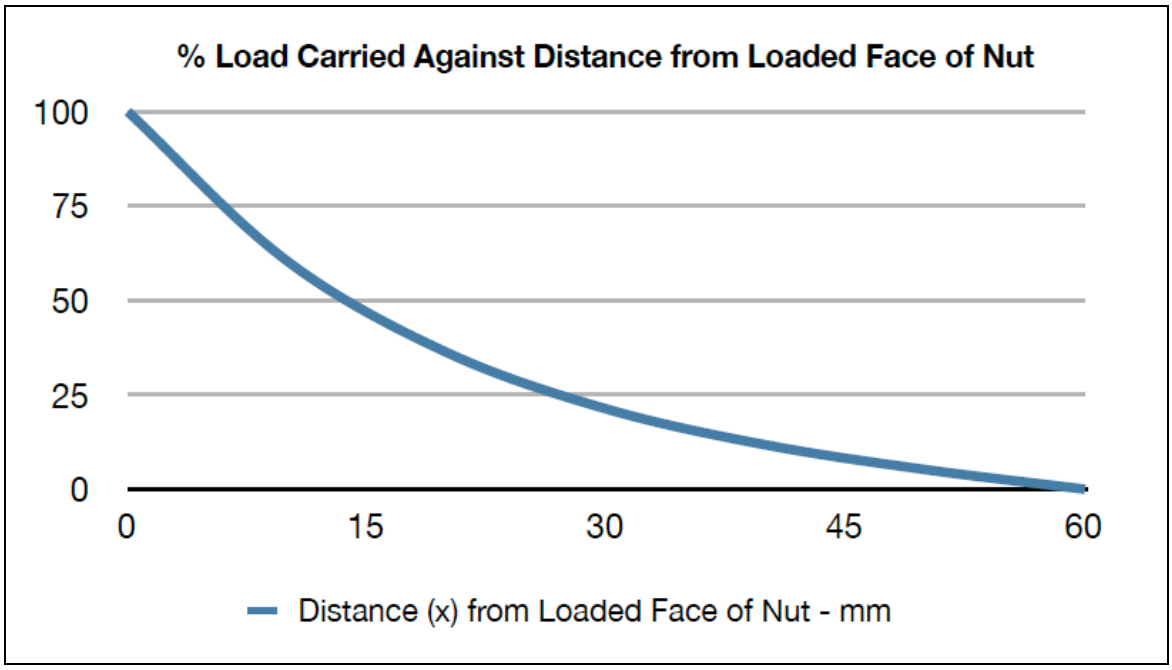

Figure 2-1: Percentage of Load Carried by Threads [2.1]

The results were obtained based on the assumption that the material of the nut and bolt is non-yielding such that the peak stress of the seat of the nut is nine times as the average stress - the average stress here is the stress calculated under the assumption of an equally distributed load along the bolt.

Den Hartog went on to show the effect of a uniform difference in pitch as being parabolic with the highest load concentrations at the bearing and free faces of the nut and the lowest load on the threads at the mid-distance of the connection. According to him, it is possible to obtain a difference in pitch by tapering the nut.

He showed that, theoretically, a uniform load distribution can be approached by making the nut slightly paraboloidal in shape.

Using a purpose built mirror extensometer to measure radial displacements, v, and a Martens extensometer to measure the axial displacements, u, Goodier [2.11] proved Den Hartog's observation in 1940 using actual bolts and nuts under loading.

Goodier measured the axial and radial displacements of a loaded circular nut from which he calculated the loads at various sections of the nut. He discovered that load distribution in a circular nut approached uniformity at higher loads even though at low loads it is concentrated at the loaded end of the nut. He showed the presence and magnitude of various strains contributing to the relief of load concentration. The experiment was carried out with a standard 1-1-1/4" bolt and nut subjected to a load of 11.3 kN (25,000 lb) and 22.6 kN (50,000 lbs) where it was estimated through stress analysis that yield would occur at the latter of the two loads and not the former.

For Goodier, the contention was that the threads can be regarded as a cantilever "gallery" built into the walls of the mating parts of the connection. The threads will bend under load and the displacements and stresses can be obtained roughly using beam equations and these values so obtained will have an order of magnitude as those due to simple stretching of the bolt and compression of the nut.

The bending in the cantilever can then be assumed to have taken up the gaps due to this elastic action of stretching and contraction. Goodier broke the total deformations in the connector into three mechanisms, namely;

1. Axial contraction of the nut wall and extension of the bolt core,
2. Bending of the two threads as cantilevers, and,
3. Circumferential stretch of the nut wall.
4. Circumferential contraction of bolt.

Because thread contact requires the same deformation of nut and bolt along the bearing surface of the cantilevers, the axial contraction of the nut wall and the extension of the bolt core (mechanism '1') has to be explained in terms of other type of deformations. Thus it was deduced to be primarily responsible for the load concentration and can be shown to cause complete concentration on an infinitesimal length of thread at base.

Although Den Hartog's calculation may show that thread bending (mechanism '2') can turn this into a smooth distribution with concentration at the base (by incorporating variable pitch), circumferential stretch of the wall (mechanism '3') also has an effect similar to that of thread bending by creating an axial tensile strain at the threads which offsets the compressive strain in the nut wall. Which means that, although both mechanisms '2' and '3' may help in some way towards reducing the effect of load concentration due to mechanism '1', mechanism '1' still remains the primary culprit.

Goodier then suggested means of reducing the load on the connection. If u_b and u_n denote the axial displacements of a point on a helical middle line of the thread surfaces in contact at a distance x from the baseline, then the condition of the two points remaining on contact is given by;

$$\frac{du_b}{dx} = \frac{du_n}{dx} \qquad \text{.....(2.15)}$$

Any of the three mechanisms that contribute to either of the two derivatives above will be important in determining the distribution of load in the connection. Mechanism '1' will contribute to

$$\frac{du_n}{dx}$$

by a value equal to the axial strain of that particular thread in contact. Axial strain is the strain in direction of the applied load, or,

$$\varepsilon_A = \frac{\sigma_A}{E} \text{.....(2.16)}$$

As it has been determined that the main source of load concentration is axial strain of the thread and the positive modifying influence of the other mechanisms, then any situation that increases thread bending, thread recessions and wall bending will have a favourable effect on load distribution. A reduction in wall thickness may bring about an increase in all three but it may also have the negative effect of increasing the axial strain.

Reduction of friction in the thread areas in contact and the abutment (shoulder) will bring about more radial expansion that should improve load distribution.

Other methods expounded by Goodier include the modification of the axial bending of the wall through the reduction of the area of contact at the base of the nut which will bring about an approach to zero bending moment, making axial cuts into the external surface of the wall to improve bending flexibility and increasing the fineness of the threads which may reduce the thread bending but since finer threads will have more helical length it will have less deflections under the same load.

Using photoelasticity, Hetenyi [2.12], in 1943, undertook a study of six (6) threaded nut designs to determine the effect of different bolt designs on the value of the Stress Concentration Factor (SCF).

In the photoelastic stress analysis method, components to be tested are cast in photoelastic material, normally Araldite or Bakelite. The model is then statically loaded then heated and cooled in a controlled manner. This has the effect of freezing in-place photoelastic stress patterns in the specimen. When examined under polarized light the frozen stress patterns are revealed. Hetenyi undertook his studies to determine what role fastener dimensions and designs will have on the value and location of SCFs in the models.

Hetenyi's results, as shown in Figure 2-3 below, confirm the location of the peak SCF in all his models to be at the root of the first engaged thread with SCF

values ranging from 3.85 for the conventional nut type and the lowest observed in the nuts with the tapered thread (3.10) and that with the tapered lip (3.00). The three other nut types used in the experiment, namely; nuts with outer supports, with spherical washer or double thread give similar SCF results as the conventional nut. The results of Hetenyi's study were later used by Sopwith who showed good correlation between experimental and theoretical thread loads, except on the loaded face of the nut.

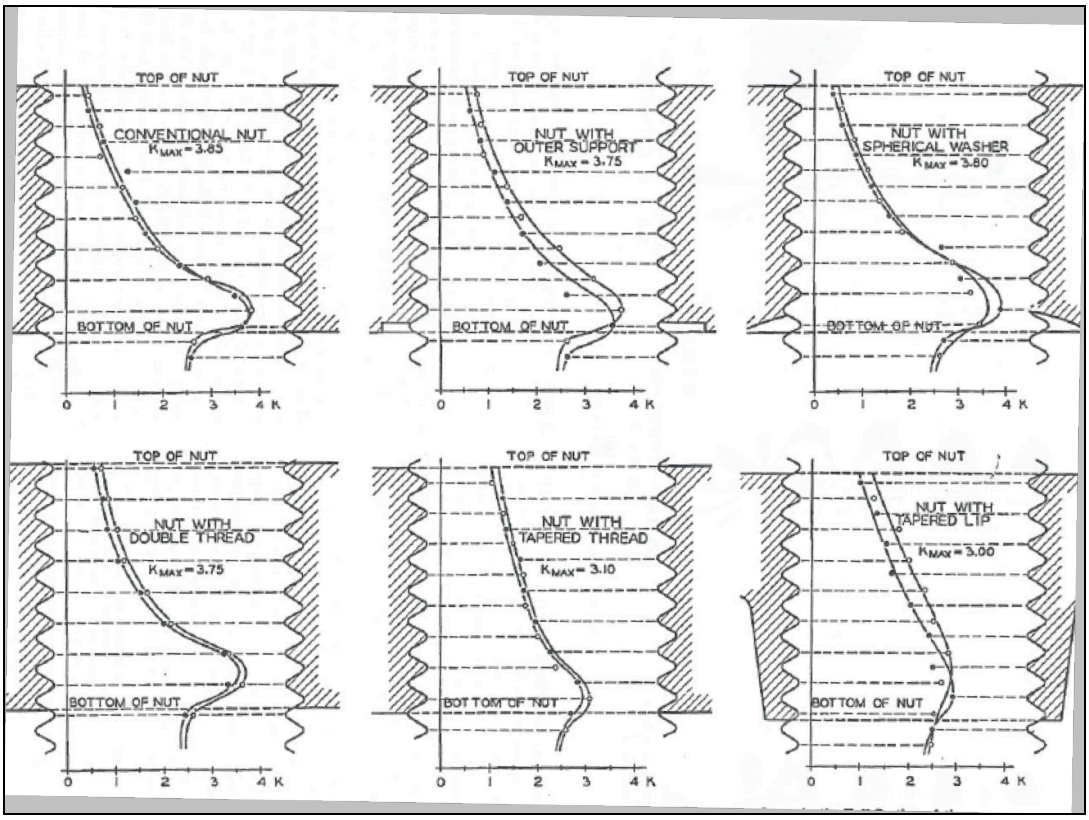

Figure 2-2: Hetenyi's Results Showing K_{max} for Different Nut Geometry [2.12]

Sopwith [2.13] agreed that the uniform load distribution obtained by Goodier at the higher loads was because yielding has occurred. He also confirmed Hetenyi's observation of the location of peak stress on the bolt as being the first fully engaged thread of the nut.

He carried out investigations that expanded on Den Hartog's solution. In his experimental work he studied the actions of axial strains within a threaded connection by assuming the treads to be contacting cantilevers - an assumption

carried over from the work of Den Hartog and Goodier. He proposed that the relative displacements were due to tooth bending and axial strains in bolt and nut body; an axial recession due to the radial compression of threads in the nut and bolt, and an axial recession due to radial contraction of the bolt and expansion of the nut caused by radial pressure between the nut and bolt. Recession, here, is used to refer to the axial separation of two threads originally in contact.

Sopwith further went ahead and proposed methods that can be employed to improve on the load distribution in the connector. He showed the effects of varying the ratio of length of the thread in engagement to the mean diameter of the thread $\left(L/D\right)$, the ratio of the pitch of the thread, a to the mean diameter of the thread $\left(a/D\right)$, the thread angle, 2α, the coefficient of friction, μ, etc to the thread load concentration factor, H. The thread load concentration factor, H is defined as the ratio of the load carried by a particular thread to the average load per thread. The lower the H value the closer the load distribution is to being uniform.

Understanding the limitations of Sopwith's model due to the many assumptions employed to arrive at a theoretical solution - which many thought renders it unusable for the determination of the precise load distribution in a practical sense, Heywood used photoelastic method to investigate bending stresses at the root (or fillet) of the tooth and he proposed an empirical relationship based on his observations that is robust enough to be applied to almost all cases of loaded projections including cantilevers, gear teeth and threads.

Heywood [2.15] considered an earlier solution for the fillet stress of gear teeth provided in 1893 by W. Lewis. Lewis' solution as published in the Proceedings of the Engineers' Club, Philadelphia in 1893 [2.14] which arrives at the fillet stress from the consideration of bending moment applied to the tooth. Heywood, was able to show from his photo elastic study the presence of a tensile fillet stress at the root of the projection, which goes on to show that the stress concentration factor does not remain constant but varies according to the position of the application of the load on the flank.

Heywood's analysis was able to show that the nominal stress obtained from his

photoelatic results is considerably higher than the nominal stress as obtained using a simple bending moment formula. To correct for this, a term which depends on the proximity of the load to the fillet, was added to the nominal bending moment term M such that the calculated fillet stress, $S_b = K(M + L)$ was shown by Heywood [2.15] as;

$$S_b = \left[1 + 0.26\left(\frac{e}{R}\right)^{0.7}\right]\left[\left[\frac{1.5a}{e^2}\right] + \sqrt{\frac{0.36}{be}}\left(1 + \frac{1}{4}\sin\gamma\right)\right]\frac{F}{t} \quad \text{.....(2.17)}$$

Where F is the load applied to the flank, t is the thickness of the projection and the dimensions a, b, e, R and the angle γ are as shown in Figure 2-4 below.

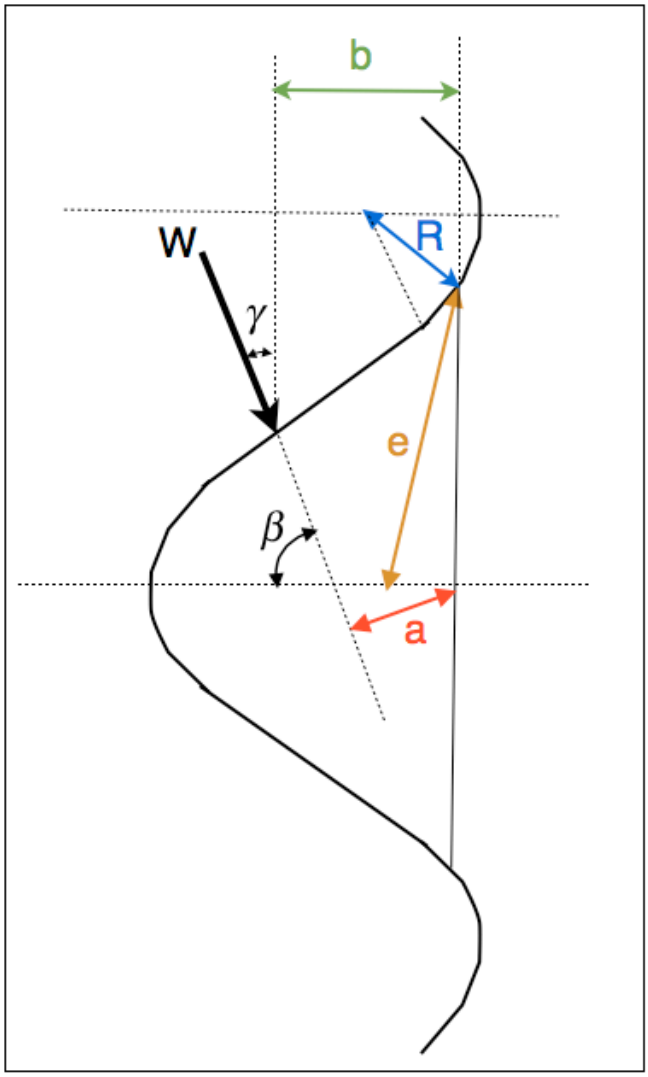

Figure 2-3: Parameters Used by Heywood for Calculating Fillet Stress

In eq. (2.17) above, $\left[1+0.26\left(\frac{e}{R}\right)^{0.7}\right]$ is the geometric stress riser (or stress concentration factor), K; $\left[\frac{1.5a}{e^2}\right]$ is the bending moment term, M; $\left[\sqrt{\frac{0.36}{be}}\left(1+\frac{1}{4}\sin\gamma\right)\right]$ is the fillet proximity term, L; while $\frac{W}{t}$ is the load term.

It can be seen that this formula allows for extremes in geometry and loading. For example, in the case of a long cantilever subjected to uniform bending moment in which the term, L can be eliminated or for a projection with large fillet radius, R, in which the stress concentration factor approaches unity.

Kelly and Pedersen [2.14] presented a revised form of the Heywood formula in which the fillet stress, S_b, is no longer shown to be equal to $K(M+L)$ but to $K(A+B+C)$ where A is the bending moment, and terms B and C are associated with the proximity of the point of loading on the flank.

$$S_b=\left[1+0.26\left(\frac{e}{R}\right)^{0.7}\right]\left[\frac{W}{t}\right]\left[\left(\frac{1.5a}{e^2}\right)+\frac{Cos\beta}{2e}+\frac{0.45}{\sqrt{(be)}}\right]\text{.....(2.18)}$$

Definitions of the terms used in the above formula are shown below in Figure 2-5 below.

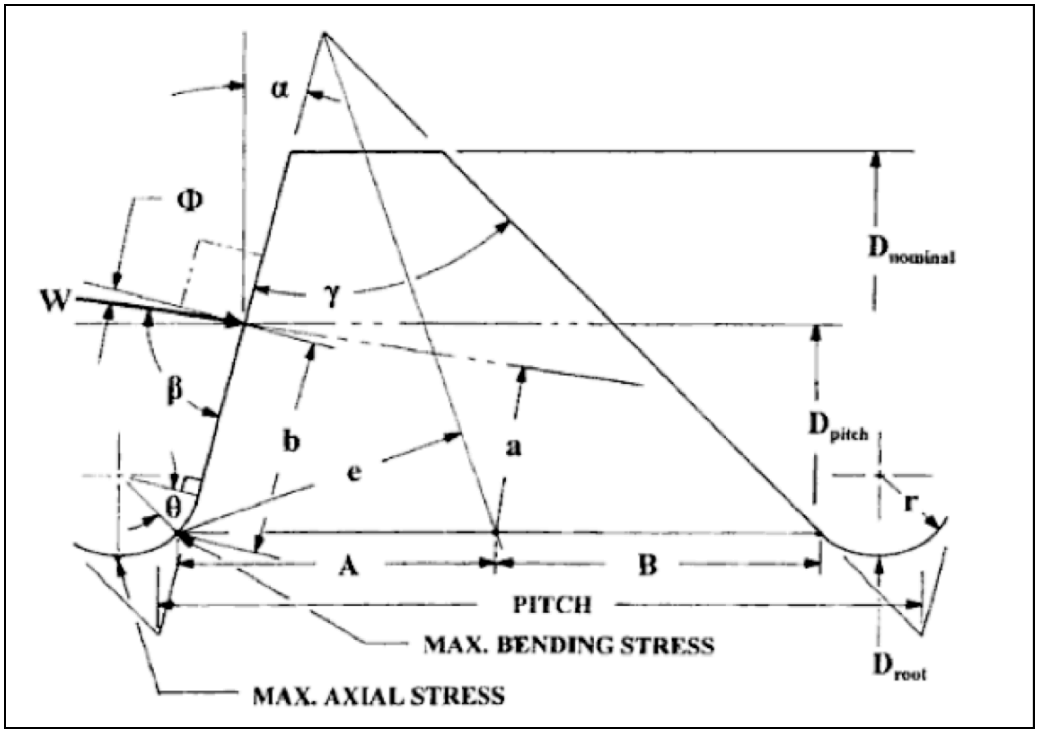

Figure 2-4: Parameters used in the Kelly-Pedersen-Heywood Formula

The combined stress at the root of the thread is a combination of the bending stress S_b as shown in the Kelley-Pedersen-Heywood formula in eq. (2.18) above and the thread axial stress, S_a, as depicted in Figure 2-5 (MAX. AXIAL STRESS) above, these two stress values do not occur at the same location on the root. The axial stress, S_a, at the roots is the local load at the thread in question plus the load from the threads upstream from it, i.e., passing through it to reach those threads all divided by the root area. From the foregoing discussion, at the first thread, the load is understood to be the total applied axial load on the connection. It depreciates linearly to zero as it reaches the thread farthest from the point of application of the load. S_a can then be said to be a product of the nominal axial load and the axial stress concentration factor.

Through photoelastic study Heywood was able to show this combined stress to be [2.15]

$$S_{Combined} = \frac{S_b + S_a}{\left[1 + c\left(\frac{S_b}{S_a}\right)\right]} \quad \text{.....(2.19)}$$

Where c is $\left[(60-\alpha)44\right]^2$

From eq. (2.19) it can be seen that fatigue failure is more likely to occur at the first engaged thread because not only does it have the highest combined stress value but also because the thread loading is highest at that point and the axial load is equal to the total load carried by the connection.

Published work by Stoeckly and Macke [2.16] shows the effect of introducing a taper to the threads of the bolt or the nut. Their results, obtained through theoretical analyses, experimental work using a similar setup as Sopwith and backed by ten years' experience on high pressure/high temperature turbine bolting, show that introducing a taper will have the effect of reducing the total load carried by, and the stresses on, the bottom thread and those on top thread are increased. They also show that by introducing a taper, load distribution across all threads is now influenced by the magnitude of the load. Other variables such as bolt diameter, thread pitch, coefficient of friction, nut length and nut diameter are generally unaffected by the introduction of a taper.

In a series of experimental and theoretical analyses, Junker and Wallace [2.17] observed that tightening a bolt to a stress equal to the material's yield will bring about better reliability and fatigue resistance through the increase of minimum preload in the bolt. This can be achieved through a method they described as "yield control" in which the connection is tightened to the yield of the fastener material using automatic or manual wrenches calibrated to detect the material yield.

Following in the footsteps of Den Hartog, Goodier and Sopwith, Dragoni undertook a theoretical study of the effect of nut compliance on the load distribution profile of a thread [2.8]. Noticing that most of the theoretical works undertaken in the area of thread load distribution assume material homogeneity between the nut and bolt, he sought to obtain further beneficial load distribution profile by varying the compliance (or stiffness) of the nut. He achieved this by varying the Modulus of Elasticity, E, of the nut. He extended Sopwith's thread load equations to incorporate a case of elements in the connection having axially

variable moduli of elasticity. The advantage of a stiff bolt in a soft nut has been addressed earlier so he was able to show the theoretical possibility of achieving a uniform load distribution by making the nut progressively softer as the load bearing face is approached.

What has been shown by the foregoing early works on thread load distribution is that:

1. The greatest single cause of elevated load and stress concentrations is the elongation of the bolt core due to tensile stresses and axial contraction of the nut due to compressive stresses.

2. The highest load is carried by thread farthest from the free end of the connector. This is normally the first engaged thread of the nut which exhibits high SCFs and becomes the most likely point for the initiation of failure. This load is normally in the region of three times the average load. Within elastic limit, changes in the magnitude of loading have little or no effect in this distribution.

3. In case of ductile materials yielding at the locations of peak stress leads to a more uniform and favourable distribution of stresses in a connection subjected to static loading and unfavourable when the connection is in dynamic loading such as in cases of impact or oscillating loads.

4. As could be expected, geometry plays a critical role in the location of the exact areas of these high stress concentrations.

5. For the purpose of theoretical estimations, loads and stresses on threads of the connector can be approximated to mating cantilevers and as such variations of the Bernoulli-Euler beam theory can be used to calculate forces and stresses in the connector.

6. Factors are identified that can be used to achieve (theoretical) a more uniform load distribution in the connection if that is what is desired.

7. It is possible to achieve a more uniform load distribution by varying the

geometric, loading and material parameters of the components in the threaded connection.

To summarise the above, Den Hartog developed a relationship between the load distribution and applied load, the geometry and chemo-mechanical properties of the connection. He also went ahead and looked at the effect of pitch on load distribution and how varying one will affect the other. His observations were validated through physical observations of the axial and radial displacements of a loaded connection using extensometers by Goodier. Sopwith then undertook a detailed theoretical analysis of the loads and stresses governing thread load distribution. Stoeckley and Macke (introduction of a taper), Dragoni (variable nut/bolt materials) and Wallace and Junker (working limits) would later test and modify these theories. However, Heywood contended that a critical factor influencing the failure of a threaded connection, or any loaded projection such as cantilevers and gear teeth, is the maximum fillet stress. Working from an existing flllet stress formula known as the Lewis formula, he used photoelasticity to develop a robust and more acceptable formula known as the Heywood (later the Kelly-Pedersen-Heywood) formula that can be used for the determination of fillet stress on a tooth and thus the load bearing capacity of the same projection.

From the earlier theoretical and experimental works discussed here it can be seen that a groundwork has been laid in the deterministic study of not only load and stress distribution but also load bearing capacity of a threaded connection. The theoretical models discussed here can be used as the background to further studies in root stress criticality in the presence of external factors such as fatigue, operating environments, and operational modifications such as preload and friction. The results so obtained can be used to optimize the geometry or chemo-mechanical properties of the connection or as input parameters into fracture mechanics calculations and stress analyses.

2.1.1 Photoelastic Models

As mentioned in the preceding section, major investigations were undertaken by researchers such as Hetenyi, Sopwith and Heywood to validate earlier works in thread root stress analysis undertaken by earlier researchers using other methods.

Photoelastic method allows for a three dimensional study of load and stress distribution in photoelastic models of components. If carefully and correctly applied it can give results on stress concentrations with errors not exceeding +/- 3% [2.14]. It takes advantage of the principle of birefringence, exhibited by certain transparent solids in which light passing through a birefringent material experiences two refractive indices as shown in Figure 2-6 below. Many optical crystals exhibit the property of birefringence, or double refraction. For most of the experimental photoelastic work carried out in the area of thread stress analysis, the material used was Araldite or Bakelite.

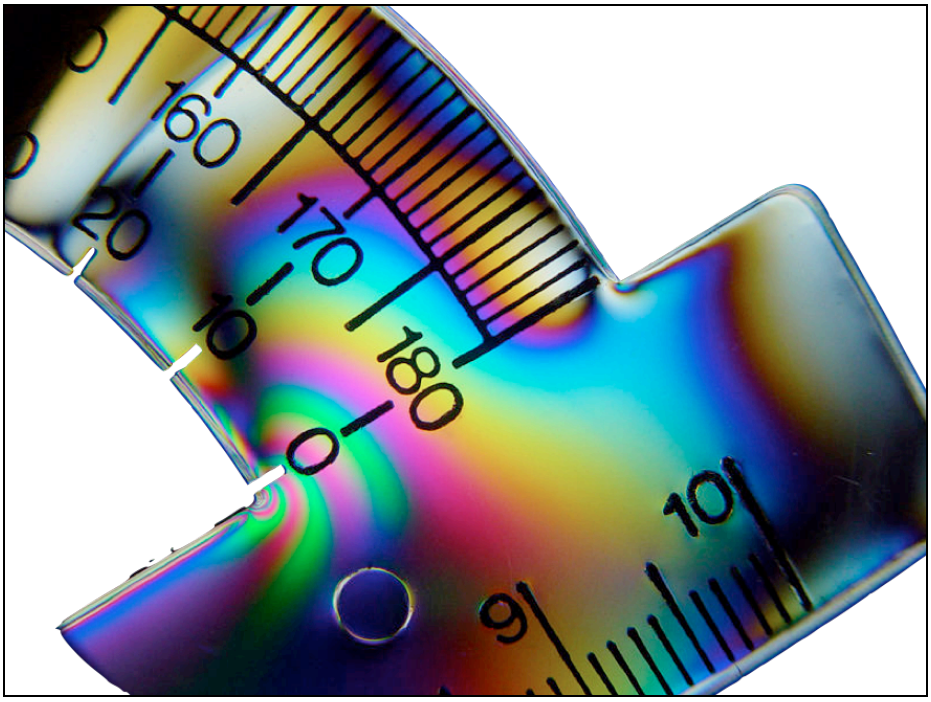

Figure 2-5: Example of Birefringence [2.18]

When a ray of light is passed through a specimen, it gets resolved along two

principal stress directions and each of the two components experiences a different refractive index. When the two waves are brought together in a polariscope a fringe pattern is observed that is a function of the relative retardation. By studying the fringe pattern, stress states in various parts of the specimen can be determined [2.19].

By their geometry and application, threads, especially in the theoretically expected areas of peak stress to be analysed, are inaccessible to be subjected to the conventional experimental stress measurement techniques such as strain gauging and also because mathematical solutions in such an analysis easily become cumbersome due to the number of variables that must be factored in, photoelasticity remains one of the most important tools that can be employed in 3D thread stress analysis.

In 1972 Weiner and True [2.20] conducted one of the first photoelastic studies of drillstring threaded connections.

They modelled an API 4-1/2" IF DC connection under bending loads, and they were able to observe the varied stress distribution within the connection. They concluded that there would be little benefit in modifying the thread design. However, they did argue that the joints must be made-up sufficiently tight to keep the connection together at the shoulders under the expected bending loads.

In an attempt to compare Sopwith's theoretical load distribution to an experimental load distribution obtained directly - as against being deduced from stress concentrations on nut deformations, Patterson and Kenny [2.21] developed a technique using three dimensional photoelastic method to study loads in small components. They reported that the results obtained for tests undertaken on an Araldite bolt model compare favourably with those obtained from Sopwith's theoretical distribution. Using two full scale models of 30mm nuts and a bolt made from Araldite, and applying the same frozen - stress method as Hetenyi, they were able to show that it is possible to directly determine load distribution in a threaded component using photoelasticity. They also suggested

that stress concentration distribution should not be used to predict load distributions.

In a later study they [2.22] replicated Hetenyi's work using an Araldite model of a bolt. Using photoelasticity as the main method of investigation in combination with the finite element method to determine the deflection factor of the thread, they observed that the nut thread run-out region influences the root stresses at the loaded end of the bolt. The incomplete thread exhibits a lower stiffness and load bearing capacity than a fully formed thread, hence the only discrepancy between their experimental observation and with Sopwith's theoretical solution.

Broadbent and Fessler [2.23] studied load distribution in photoelastic models by taking accurate measurements of shear stress distribution across the roots of the threads. The obtained values were then integrated between adjacent fillets to obtain the load carried by the thread. Models were loaded with preload, axial tension and a combination of the two loads and studied to see the effect of distribution of thread loads due the different load setups. Using an automatic micropolariscope to study the shear force concentration in specimens with a frozen stress state, it was observed that a maximum value of shear stress concentration was observed in specimens that were subjected to preload only as against tensile loads only or a combination of tensile loads and preload.

In 1990 as part of the FADS study at the Non-Destructive Evaluation Centre of the University College London, Fessler and Buchan [2.24] produced three photoelastic models of an NC-50 DC connection and subjected them to pre-load, pre-load and bending and pre-load and torsional loading. They found out that for each loading scenario, the maximum stress occurred near the thread root of the pin and was within one pitch of the start of the connection. This conforms to the known and established theory of uneven load distribution in threaded connections, and confirms that the first loaded tooth of the connection to be most critical.

2.1.2 Strain Gauged Models

Before the use of electrical strain gauges became widespread, stress analysis experiments were done using extensometers. Electrical strain gauges use the principle of the Whetstone Bridge to measure the strain (elongation or contraction) in a material. Since a change in electrical resistance of a conducting wire is directly proportional to its extension, a wire bonded to the surface under investigation will give accurate readings of strain on the surface of the material through changes in the electrical resistance of the wire.

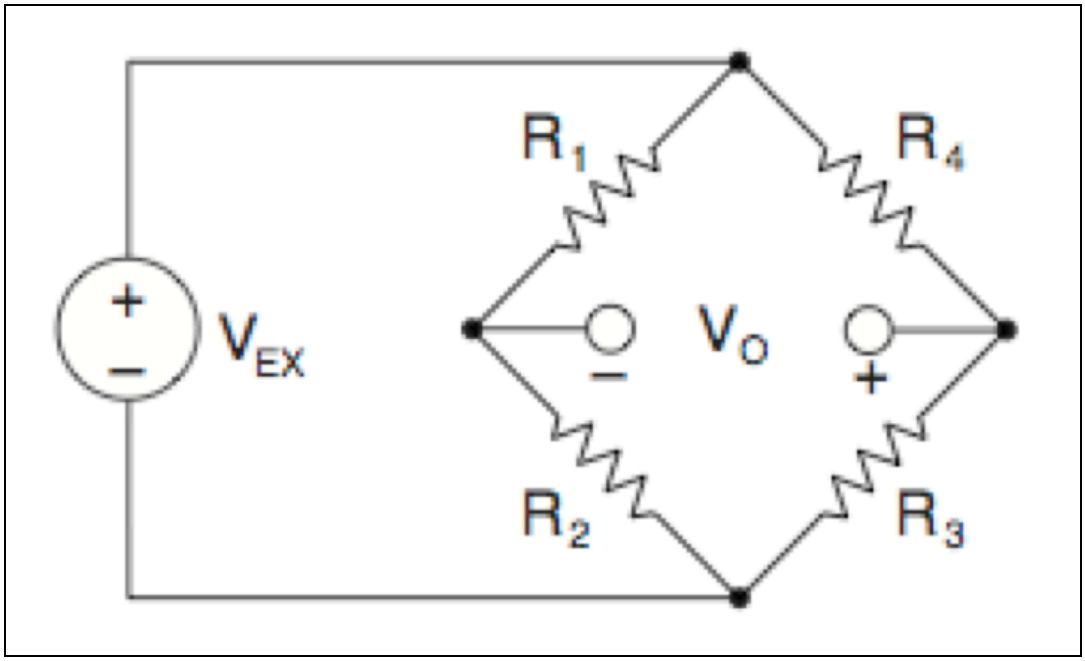

Figure 2-6: A Simple Whetstone Bridge

The sensitivity of a strain gauge to strain is known as its Gauge Factor (GF) and is normally 2 for most metallic gauges. Gauge factor is defined as the ratio of fractional change in electrical resistance to the fractional change in length (strain), which is mathematically expressed as [2.25];

$$GF = \frac{\Delta R/R}{\Delta l/l} = \frac{\Delta R/R}{\varepsilon} \quad \text{.....2.20}$$

However, from the configuration of the bridge shown above in Figure 2-7, it can be said that the output voltage, V_0 of the bridge will be equal to

$$V_0 = \left[\frac{R_3}{R_3 + R_4} - \frac{R_2}{R_1 + R_2} \right] \times V_{Ex} \text{.....2.21}$$

From eq. (2.21) above, when the voltage output equals zero the bridge can be said to be *balanced*. Any change in resistance in any arm of the bridge will result in a nonzero output voltage.

Therefore, if we replace R4 in Figure 2-7 above with an active strain gauge, R_G, any changes in the strain gauge resistance will unbalance the bridge and produce a nonzero output voltage. If the nominal resistance of the strain gauge is designated as R_G, then the strain-induced change in resistance, ΔR, can be expressed as

$$\Delta R = R_G \times GF \times \varepsilon \text{.....(2.23)}$$

Assuming that $R_1 = R_2$ and $R_3 = R_G$, the bridge equation above can be rewritten to express V_0 / V_{Ex} as a function of strain.

Although due to the nature of threads it is difficult and impractical to attach strain gauges on them many experiments were reported to have been carried out to determine the distribution of stresses on threads. Smith and Carlin [2.41] employed the use of strain gauges in the performance study of a new thread design, the Super Strength Threads (SST), on an NC-46 drill collars. The gauges were attached on both a standard NC connection and on an SST connection. After making up the connection, it was found that test results indicate that the SST connection could be made-up to higher torque levels than the standard NC connection. However, no detail was given on how the strain gauges were bonded to the connection neither was any strain gauge data presented in the report.

Brennan and Kare [2.42] successfully used gauges to study the overcoming of

make-up torque on a rotary-shouldered connection (RSC). They successfully bonded gauges to the external surface of a made-up 6-5/8” REG drill collar. The specimen was axially loaded to study the overcoming of make-up torque, which can be detected by the opening of the rotary-shouldered connection (RSC). The results showed no opening thereby indicating that the RSC retained its integrity at that applied axial load. Bending loads were not considered in this experiment as it was carried out using purely tensile loads.

2.2 Operational and Environmental Effects on Drillstring Integrity

In the course of drilling operations, the drillstring connection is expected to withstand tensile, compressive and bending loads occasioned by the requirements of the drilling operations. This is further complicated by the wellbore, which may not be rectilinear, may contain corrosive drilling fluids in the drillpipe and annulus and abrasive formation solids in the annulus and on the wellbore wall. The combined effect of this is the introduction of further over-torquing of the string due to friction between the string and the wellbore and additional load on the connection due to drag will be experienced as the string is pulled. Reductions of fatigue life and stress corrosion cracking (SCC) in the presence of high temperature corrosive drilling mud are also a factor [2.28].

2.2.1 Reasons for Failure of Drill Stem Components

Pitts [2.29] estimated that 73% of drillpipe defects found were due to fatigue. In a similar study, Hill [2.30] gave a general estimate of the impact of fatigue failure to the industry and concluded that fatigue causes 65% of failures and has significant impact on 12% more and that combined excessive tension and torque led to failure in 13% of the cases.

2.2.2 Influence of Dog-Leg Severity (DLS) on Drill Stem Fatigue

A dogleg is a location in a well where the trajectory of the wellbore in three-dimensional spaces changes very rapidly. This is a location where the wellbore is no longer considered to be rectilinear and will, thus, impose cyclic bending stresses on the section of drillpipe currently situated and rotating there. Dogleg Severity (DLS) is a measure of intensity of the dogleg. It is normally reported in two-dimensional angular degrees per 30 metres (or 100 ft) length of the drillstem.

To determine a component's fatigue strength at any given point, the maximum and minimum stress values at that point are calculated then used to obtain the

average stress and the stress amplitude. Where average stress, σ_{Ave} is $\frac{\sigma_{Max}+\sigma_{Min}}{2}$ and the stress amplitude, σ_{Amp} is $\frac{\sigma_{Max}-\sigma_{Min}}{2}$. By plotting a point of σ_{Ave} and σ_{Amp} for a particular location on the component on the Goodman diagram it can be ascertained whether that component will have infinite life at that location or if it will fail at that location [2.31].

Lubinski [2.32] used a modified form of the Goodman Diagram, shown in Figure 2-8 below, to propose a method of determining a permissible dogleg severity (DLS) below which fatigue damage will not occur depending on the tensile load and pipe's characteristics. In his submission, the maximum allowable DLS is reported as being dependent on axial tensile load, weight on bit, weight on hook, bending moment, length between tool-joints and the reaction force on the string at wall contact points. Lubinski's work is the basis of the American Petroleum Institute Recommended Practice 7G (API RP7G) [2.33], which puts forward practical analytical and graphical methods to ensure good and safe working conditions of drillstrings.

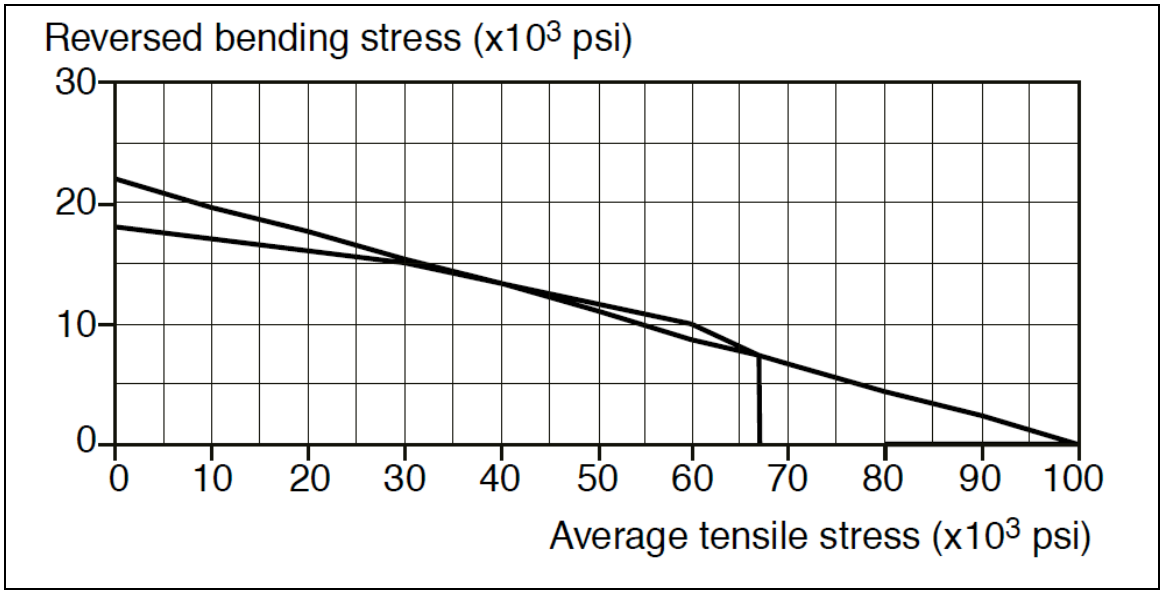

Figure 2-7: Lubinski's Modified Goodman Diagram [2.33]

While the Lubinski method can be used in all locations on the drillstring, another

method recommended presented in the API RP7G for the optimization of stress response of the Bottom Hole Assembly (BHA) section is the Bending Strength Ratio (BSR), which is the ratio of the section modulus of the box to that of the pin. Higher BSR means the connection is pin weak and lower BSR means the connection is box weak. The best-shouldered connections to be used in the BHA are selected or optmised using the BSR which basically compares the box and pin stiffness.

If the outside diameter of the connection is D, the box thread root diameter is b, the pin thread root diameter is R and d is the inside diameter of the pin, then the section modulus, Z of the box and pin will be

$$Z_{box} = 0.098\frac{\left(D^4 - b^4\right)}{D} \text{ and } Z_{pin} = 0.098\frac{\left(R^4 - d^4\right)}{R}$$

respectively. Which makes the bending stress ratio, $BSR = \frac{Z_{box}}{Z_{pin}}$

While API RP 7G recommends a BSR range of 2.25 to 2.75 with the optimum at 2.5 [2.33], Baryshnikov [2.34] and Hill [2.35] proposed BSR ratios of 1.9 to 3.2. Figure 2-9 shows a typical BSR diagram for a connection illustrating values of pin and box weakness.

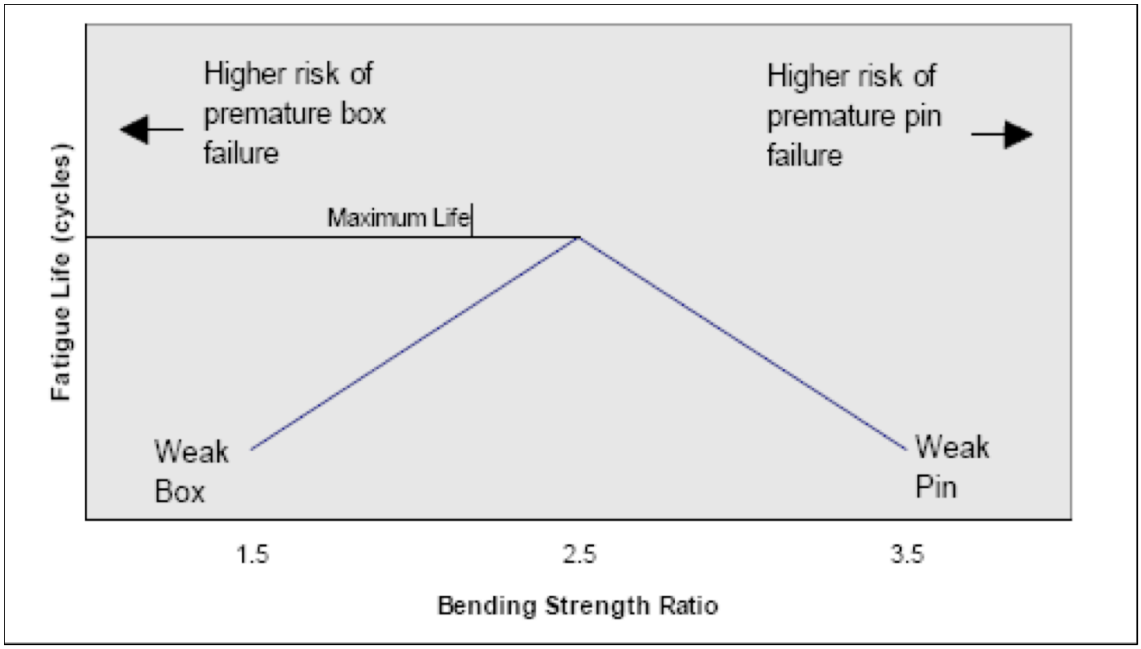

Figure 2-8: Bending Strength Ratio Criterion

2.2.3 Influence of Preload on Drillstem Stress Distribution

Preload is achieved by the application of torque, which involves converting angular (rotational) motion to a linear axial motion. This motion is converted into a pressure force as the contacting thread flanks (cantilevers) and abutment (shoulders) as the bolt and nut press against each other. According to Baha'i [2.36] the application of preload increases the amount of load carried by the LET of the bolt and has little effect on the tooth at the opposite end (the FET).

A discussion on the theory of torque and preload is presented in Appendix B3 – Theory of Torque and Preload.

Preloading, or tightening after make-up of the connections, directly affects the static stress distribution within the connection. Using a bolted joint diagram as shown in Figure 2-11 below, the force-deflection state of a preloaded joint can be illustrated [2.37].

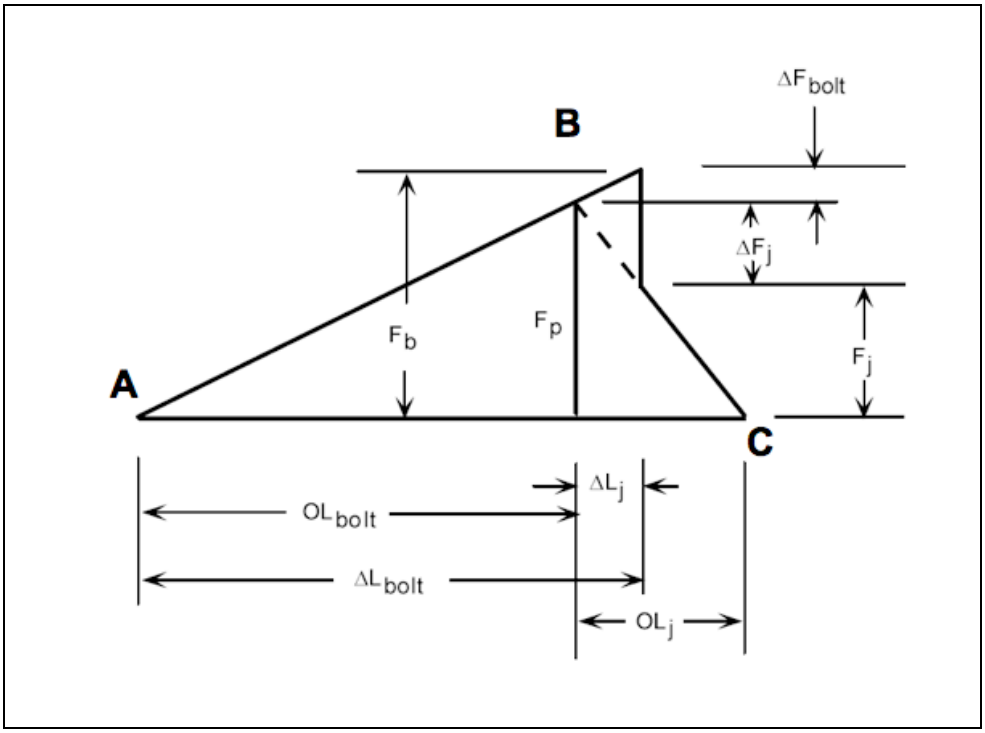

Figure 2-9: Bolted Joint Diagram

When the connection is made up, the pin extends by OL_{Bolt} and joint reduces by OL_{Joint}. The tension in the pin is opposed by an equal and opposite force in the joint, and the connection is said to be preloaded, F_P. Upon the application of an external tensile load, the pin further elongates to ΔL_J and the joint is compressed to OL_J, but since the pin and joint have different stiffness values, equal changes in deformation result in unequal changes of force. The net result is that the load in the pin only increases by a proportion ΔF_{Bolt} of the external load P. The remainder is a reduction in the compression force, ΔF_J of the joint.

Tafreshi and Dover [2.5] reported that for the standard NC46 connection with preloading, the maximum SCF at the unengaged teeth of the pin and box is only 8% lower (from 3.97 to 3.65) and 4% lower (from 5.80 to 5.57) than the maximum SCF for the engaged teeth of the pin and box, respectively. But for the standard NC46 without preloading, the maximum SCFs at the unengaged teeth of the pin and box are 13.5% lower (from 15.10 to 13.06) and 18% lower (from 7.53 to 6.18) than the maximum SCF of the engaged teeth of the pin and

box, respectively.

Using FEA Macdonald and Deans [2.3] investigated the relationship between the nominal applied load and the resulting peak and local elastic stresses at the critical thread roots and observed that at the peak stresses at the pin and box converge at higher stresses; concluding that the benefit of reduced SCF afforded the pin is lost once the preload is overcome at higher stress ranges.

An assembly that is not properly made-up will lead to instability in the connection which may bring about the separation of the seal at the shoulder which may, in turn, allow drilling fluids to seep into the threads and across the torque shoulder. It could also cause downhole make-up or wobbling in the connection – the former may lead to galling, or cold welding, and the latter may lead to the separation of the connection [2.38]. To avoid this, a design torque value is always kept lower than make-up torque value. A safety margin of 1% is recommended by the API in API-RP7 [2.33].

It is worth noting here that factors which influence preload such as high downhole pressures, severe bending and vibrations are not adequately compensated for with this low safety margin.

2.2.4 Influence of Drilling Environment on Drillstring Material

Two undesirable effects of corrosion reported by Hill [2.30] are the acceleration of the crack initiation phase by creating high stress areas and the acceleration of the crack propagation phase by attacking the newly exposed metal at the crack tip. High SCFs are known to occur in the areas of no apparent stress concentration when tiny pits due pitting corrosion occasioned by reaction between the pipe material and drilling fluids act as stress raisers or Sulfide Stress Cracking (SSC), which occurs when H_2S from the drilled formation reacts with the iron in the DP to form atomic hydrogen which may diffuse in the pipe and collect at high stress locations. This is further aggravated by the high acidity and temperature in some drilling fluids [2.28].

Lopez, et al. [2.39] reported enhanced metallurgical properties in API X-80 steel exposed to a H_2S saturated aqueous solution after heat treatment. Various heat treatment scenarios were tested with water-sprayed, quenched and tempered specimens exhibiting better SSC resistance than others. They discovered that under similar corrosive environments and stress intensity factors, crack propagation in the ferritic matrix (heat treated through water spraying and quenching) was severely limited when compared to a cementite structure (heat treated through quenching and tempering). In a closer look at the effect of microstructure to a metal's resistance to SSC, Zhao, et al. [2.40] subjected metals of three different microstructures to bent-beam test in aqueous H_2S solution and confirmed the superiority of an acicular ferrite-dominated (needle-shaped) microstructure over ultra-fine ferrite and ferritic-pearlitic microstructure.

Generally, corrosion has been known to reduce the endurance limit in any *S-N* curve. Corrosion fatigue cracks seem to invariably start at the corroded interface between the MnS inclusions and the matrix and then grow under cyclic loads [2.41]. However, the susceptibility of the string to corrosion can be reduced through surface treatment of the exposed pipe body such as nitrocarburizing and coating the pipe body to prevent abrasion from the sands. Coatings such as aluminum or zinc can act as sacrificial cathodes that diminish the potential difference and increase fatigue life. Corrosion resistance and fatigue strength has been seen to improve after oxidation treatment and nitrocarburization [2.39].

The benefits of thread root cold rolling were first investigated by Germany's Wohler Institute in the 1930s. Ifergane *et al.* [2.42] studied the effect on fatigue lifetime of the manufacturing sequence of aeronautical bolts made from AISI 4340 alloy steel. Their results showed that maximum fatigue life is obtained in bolts that are cold-rolled following heat treatment and not vice-versa.

Kristoffersen [2.43] reported from several investigations on the increase of fatigue threshold in materials from the application of compressive residual stress. In his investigations, full scale tests were carried out on pipes cut from

drillstrings and incorporated with a thread. The threads were cold rolled and fatigue tested in a full scale four-point rotating-bending fatigue test rig. It was shown that cold rolling has brought significant fatigue life improvements.

The application of the newly-developed technique of stitch rolling to control the rate and shape of crack propagation was reported by Ngiam and Brennan [2.44]. The experiment was carried out on three Grade 275A mild steel plates subjected to different cold rolling procedures and subjected to medium cycle fatigue tests under bending. While cold rolling was seen to have a positive effect on the crack initiation and propagation of all the specimens, the fatigue life of stitch rolled specimens was seen to have significantly improved.

2.2.5 Influence of Thread and Connection Geometry

In 2004 Majzoobi, et al. [2.45] studied the effect of thread pitch on the fatigue life of ISO (10 – 24 mm dia.) and (unified bolts 7/6" -1" dia.) threads. They concluded that in both cases (ISO and Unified), the coarse threads have a better fatigue life performance than the fine ones. Observing that in the case of the unified bolts, this only holds on the basis of equal stress and not equal load.

Knight and Brennan [2.7] used the FEA method to investigate the effect of bore eccentricity in a drill collar connection under various stress levels and concluded that a significant reduction of fatigue life is attributable to it. With a 3.5% bore eccentricity, 7.36% and 7.32% increase of maximum SCF at the pin and box were reported for the un-preloaded and preloaded connection respectively.

2.2.6 Stress Relief Features and Failure Mitigation

Stress Relief Groove Pin (SRGP) and a Bore Back Box (BBB) are features sometimes introduced to reduce these peak stresses. Both features involve the removal of metal at predetermined locations on the pin and the box to eliminate the stress concentration effects on unengaged thread roots. Both have been

shown to result in longer fatigue life for the connection.

Macdonald [2.46] undertook an investigation into the effect of stress relief features on stresses at the critical thread roots and pin bore of an API NC-6I NMDC connection. For a 50 MPa tension loading, peak stresses in the pin were significantly reduced by the presence of SRGP (-26%) and increased (+75%) in the box; although in absolute terms, the peak stresses in the pin are still higher.

Tafreshi and Dover [2.5] reported that for a preloaded connection, SCF reduction of 23% and 7% was observed in the case of a bore back feature on the box a stress relief groove in the pin respectively when compared to a preloaded connection with no stress relief features in the box and pin. Without preloading, the pin SCF was reduced by about 14.5% but the box SCF was increased by about 13% when these stress relief features are incorporated as against a standard connection with no stress relief features.

2.3 Finite Element Investigations Undertaken on Drillstrings

Burnett [2.47] defines the finite element method (FEM) as “a computer-aided mathematical technique for obtaining approximate numerical solutions to the abstract equations of calculus that predict the response of physical systems subjected to external influences”.

Finite Element Analysis is a way of getting a numerical solution to a specific problem involving field quantities. This is done by breaking up the continuum into substructures called *elements* which are joined at points called *nodes*. The elements and nodes are based on a global/local coordinates on which a response to an applied load can be deduced.

Pick and Burns [2.48] performed a finite element analysis of the stress distribution of a thick walled pressure vessel threaded connection in 1971. For ease of analysis they assumed the model to be two-dimensional and to be axisymmetric along its longitudinal axis. They also ignored the thread helix angle. Brennan [2.49] observed that their result compares well with previous load investigations, thus presenting the potential use of the method in stress analysis of drillstring connections.

In 1981 Tanaka et al. [2.50] used the FEA method to investigate the applicability of the method in the study of bolt load distribution. Applying the method to nut and bolt assembly with fastened plate, they developed a numerical method of analysing these and similar joints with multiple contact surfaces and with more complicated contact problems such as Hertzian stresses. They also showed a way to analyse the ratio of tooth load to axial tension by introducing pitch and flank angle modifications.

Observing that most of the earlier FEA studies in thread load distribution were mainly limited to linear elastic deformation of the contacting members, Zhao [2.51] investigated the elasto-plastic stress distributions within straight and tapered bolt-nut connectors using the virtual contact loading method. Using a

simplified axisymmetric model, he used virtual contact loads to simulate the elasto-plastic contact phenomena between the mating screw flanks and arrived at detailed stress and load distributions along the threads. Like in other earlier studies he was able to show that critical stress occurs at the thread roots and the first pair of thread roots are the first to undergo the plastic deformation. Earlier theoretical researchers such as Den Hartog and Sopwith agreed that the near uniform stress distribution at elevated loads may be due plastic deformation at the location of peak loading, Zhao's attempt was to use the FEA method to illustrate that.

Izumi et al. [2.52] investigated the mechanisms of the tightening and the loosening process due to shear loading using a three-dimensional finite element (FE) method. In their study they did not look at detailed stress distribution but rather based the investigation of the process purely on contact analysis. Their study showed weak nonlinearity between tightening torque and obtained preload which was attributed to the non-uniform distribution of the contact pressure. Comparing their FE analysis to experimental results they were able to show agreement in how the loosening progresses in the presence of shear loading. Their work shows the applicability of 3D FE modelling in the analysis of bolt design and operability.

2.3.1 Industry-Sponsored Investigations Undertaken at NDE-UCL

In a series of industry-sponsored studies undertaken at the Non-destructive Evaluation (NDE) Centre of the University College London, namely FADS [2.24], PDF [2.53] and RODS [2.54], an attempt was made to understand the distribution of load in drillstring threaded connections using the FEA method and, in some cases, a hybrid method that included FEA and other investigation techniques. The investigations aimed to study means of optimizing the service life of the threaded connections under study which may help in the reduction of incidences of downhole failure. A summary of the three research projects undertaken at the NDE Centre of the UCL are presented in Appendix C: Summary of Drillstring Investigations Undertaken at the UCL-NDE Centre.

2.3.2 Other FEA Investigations on Drillstrings

As stated in the discussion above on preload, Tafreshi and Dover [2.5] undertook an FE analysis for the standard API NC46 connection under axial, bending and torsional loads and reported that in both the preloaded and unpreloaded cases the maximum SCF is in the threads of the box.

Also studied in their investigation was the effect of geometry changes on the stress and load distribution in the connector. This was achieved by the introduction of bore back, stress relief features and changes in the thread root taper. Beneficial results were observed in the introduction of the bore back and stress relief features where the peak SCF in the pin and box was reduced by 23% and 7% respectively. Using these features was shown to help in overcoming the high SCF values observed at the unengaged tooth. Modification of the thread root profile was also shown to improve the fatigue resistance of the connector.

MacDonald and Deans' [2.3] work as reported above used the FEA method to investigate the relationship between the nominal applied load and the resulting peak and local elastic stresses at the critical thread roots and observed that the pin and box converge at higher stresses; concluding that the benefit of reduced SCF afforded the pin is lost once the preload is overcome at higher stress ranges. Their work was undertaken on an API NC61 connector with a V-Profile thread form.

Although they reported the pin as having a higher peak stress value than the box, like Tafreshi and Dover, they reported the box as being the critical component even though the stress criticality is occasioned by considering the effects of fatigue loading and by relating the individual preload and tensile load cases to local and peak stress ranges and mean levels.

Two important observations were recorded in this analysis. Firstly, the direction of maximum principal stress was shown to be tangential to the root, which is the location of peak stress, but progressively aligns to the axial direction away from the root. This is an invaluable tool for post mechanical failure investigation

because it gives a curved crack propagation profile at the location of peak stress. Secondly, notch stress at the root, known theoretically as the sum of the linearised axial and bending stress components, displays a non-proportional behaviour in the case of the pin where the local peak stress at the last engaged tooth (LET) is shown to be a nonlinear function of the nominal pipe stress. The box LET, on the hand was generally unaffected by the preload and thus exhibit a linear response to the applied stress. The change in gradient of the local stress response at a given nominal stress makes it possible to define exactly where the tooth preload is overcome in compression and the shoulder preload is released in tension.

Baragetti and Baryshnikov [2.55] investigated the working limits of the API NC50 connection by means of a numerical FE analysis. The aim of the study was to investigate the influence of friction and fatigue resistance of the connections at stresses that are at, or near, maximum levels. Their work was backed up by tests carried out with full scale specimens with full reference to API standards.

They were able to define working limits for the connections made up with low make-up torque concluding that at higher values of torque considerations must have to be given to the galling behaviour of the connection and, of course, to the change in fatigue resistance profile.

In a follow-up study Baragetti, [2.58] using the same technique of numerical SCF validation with full scale tests, proposed means to quantify the effect of varying the taper on the connection in terms of stress state, loads carried by the threads and the pressure on the thread flanks. For this study, considering the nonlinearity inherent in the problem due to effects of contact and the behaviour of the material, an axisymmetric model was used as against a 3-D model. The application of the make-up torque was simulated by introducing an axial load in the box shoulder by means of an elemental thermal load. Analyses were carried out to study the effect of varying the taper on the trends of the load carried by each thread, the contact pressure on the flanks of the most stressed threads and on the trends of the von Mises stresses in correspondence with the thread

root of the pin.

The study showed that reducing the value of the taper of the pin element from the standard 0.16667 m/m to 0.15667 m/m gives a better performance in terms of thread load distribution and contact pressure on the thread flanks. A more uniform thread load distribution was observed with the load carried by the last engaged thread (LET) dropping from 33% to 11%. This is expected to bring about a reduction in the peak and mean values of pressure on the thread flanks and also lower plastic deformation at the root of the LET.

Baha'i [2.36] used a hybrid technique that uses an FE analysis to study the variation of SCF in threaded connectors due to the application of external axial and bending loads and then used the data obtained from the FE analysis to obtain parametric equations describing SCF in terms of these parameters. He then proposed the use of such equations in carrying out thread design optimisations based on minimum axial and bending SCFs.

2.4 Aims and Objectives

Load and stress distribution in a threaded connection is a complex phenomenon. There are many factors at play and an analyses that looks at these various factors in isolation is bound to miss critical elements that have, as a result of these different factors, an influence on one another and in turn changing the global and microscopic response of the connection in load distribution and stress criticality.

While, due to the limitations of the tools at their disposal, earlier researchers could be forgiven for approaching this subject in such a way that singular parameters were varied, observed and reported, there exist now an array of simulation tools that can be used to model - in one run - variations in more than one parameter. Dragoni's attempt to mathematically model the effect of varying the material properties of the nut in order to obtain a more uniform distribution is one case in point [2.8], as it can be the starting point in simulating various other parameters in direct consequence of that variation in a material property.

What has been attempted here is the use of the finite element method to study different materials in equimodulus and hybrid configurations to ascertain their stress response in the presence of preload and axial loading. This is then viewed in relation to the known fatigue properties of the various materials in order to suggest the optimum application of the materials as drillstring materials in extended-reach and ultra-deep drilling scenarios.

Using the Finite Element Method (FEM) it is possible to:

1. Model and analyse the effect of varying the coefficient of friction (μ) in the contact simulation to see how that will affect the stresses on the mating teeth and preload shoulder of the connection. It is also possible to build a response pattern of the connector to varying magnitudes of preload for a fixed value of coefficient of friction and vice-versa. This was undertaken on an AISI 4145H NC46 model for the purpose of model validation and convergence study.

2. Track the effect of varying multiple parameters such as μ, E, υ, etc to the integrity of the equimodulus and hybrid strings then use that to suggest optimum values of a variable parameter such as string hookload load under study for safe operation of the string. This is particularly true in the hybrid string scenario where a trade-off may be necessary between cost and mechanical benefits of the various materials.
3. Finally, because as discussed earlier in this chapter, most failures are due to fatigue, the stress response of the various materials studied is linked to their fatigue properties.

From the aforesaid, the aim and objectives for these investigations, and ultimately, the research work is to:

A. Validate the developed finite element model of the string against earlier literature and experimental work so as to give an indication of the model's robustness and accuracy.
B. Investigate and develop alternative loading or string configuration arrangements that can be suitably applied to optimize life of the string, especially in UDD and uERD applications.
C. Develop and undertake FEA stress analysis on hybrid string arrangements in which tubulars or tooljoints made from two different materials are used in a given string to take advantage of each of the materials' beneficial properties such as reduction of the string's hanging weight (as in the case of aluminium and titanium alloys) or enhance its stress response (as in the case of the newly developed high strength steel alloys).
D. Determine which components should be placed in high dogleg locations or placed deeper in the well due to the material's fatigue strength or yield strength respectively.

2.5 Conclusion

Drillstrings are engineered to work in tension, deliver compressive load and torque to the bit at depth and resist internal burst and external collapse pressures due to the mud hydrostatic [2.57]. The undesirability of mechanical failures in the string is due mainly to the losses of operational time and high cost of fishing operations that are required to remove the failed string from the well, the cost of abandoned string in hole and/or the cost of performing remedial actions on the well so that drilling operation can recommence. In most of the investigations undertaken and reported in this work features of thread load distribution discussed above such as the location of peak stress in a nut-bolt connection, the effect of geometry and the ability to optimize the load distribution by making it more uniform and thus reduce peak stress concentrations, all remain true.

In the current operational realities of ultra-deep drilling and extended reach/ultra extended reach drilling (ER/uERD) the drillstring is expected to withstand axial tension due to a suspended string that may, in some cases, be longer than ten kilometers and experience high bending stresses due to torsional loading occasioned by tortuous well trajectories. Investigations into the importance of operational factors such as dogleg severity (DLS) and corrosive drilling mud and geometric factors such as the introduction of taper and stress relief features have been undertaken by various researchers where it has been shown that stress corrosion cracking and cyclic stress amplitude due to wellbore tortuousity are all factors present in normal drilling operations that have a direct bearing on the service life of the drillstem.

The finite element method was used by the NDE Centre of the University College London and subsequently by many other researchers such as Tafreshi & Dover, Macdonald & Deans, Baryshnikov & Baragetti and Baha'i to undertake various analysis on stress and load distribution and to propose methods to optimize the distribution and reduced the intensity of peak stress concentrations at critical areas. Due to computational cost most of the studies were undertaken

using elastostatic axisymmetric two-dimensional FEA models as they have been proven to provide acceptable results in the study of axially and preload connections. A three-dimensional model was used by Tafreshi & Dover to analyse torsion and bending.

2.6 References

[2.1] **Den Hartog, J.P.**, *"The Mechanics of Plate Rotors for Turbo-Generators"* 1929, Trans A.S.M.E., vol. 51, part 1, Applied Mechanics Section, p. 1, Paper No. APM 51-1

[2.2] **Smith, C.**, *"Carroll Smiths Nuts, Bolts, Fasteners and Plumbing Handbook"* MBI Publishing Co, 1990, Pp 209.

[2.3] **Macdonald, K.A. and Deans, W.F.**, *"Stress Analysis of Drillstring Threaded Connections Using the Finite Element Method"*; Engineering Failure Analysis, Vol 2, No. 1 pp. 1-30, 1995

[2.4] **Kristoffersen, S.**, *"Improved Fatigue Performance of Threaded Drillstring Connections by Cold Rolling"*, Dr. Ing Thesis, Norwegian University of Science and Technology, 2002

[2.5] **Tafreshi, A. and Dover, W.D.**, *"Stress Analysis of Drillstring Threaded Connections using the Finite Element Method"* Int J Fatigue 15 No 5 (1993) pp 429-438

[2.6] **Barragetti, S.**, *"Effects of Taper Variation on Conical Threaded Connections Load Distribution"*, Transactions of the ASM, Vol. 124, June 2002. Pp 320-329.

[2.7] **Knight, M.J., Brennan, F.P.**, "*Fatigue life improvement of drill collars through control of bore eccentricity"*; Engineering Fracture Analysis 6 (1998), pp 301-319.

[2.8] **Dragoni, E,** *"Effect of nut compliance on screw thread load distribution"*, Journal of Strain Analysis, Vol 25 No 3, 1990

[2.9] **Zhang, X. Nie, J. Hou, G.**; *"Development of anti-Loosening Nuts Using Shape Memory Alloys"*, Materials Science Forum 327, pp 35-38, 2000

[2.10] **Stromeyer, C.E.**, *"Stress Distribution in Bolts and Nut"*, Trans. Inst. Nav. Architects, vol 60, pp 112-121, 1918

[2.11] **Goodier, J.N.**, *"The Distribution of Load on the Threads of Screws"* 1940 Trans. A.S.M.E. vol. 62 p A-10

[2.12] **Hetenyi, M.**, *"A photoelastic Study of Bolt and Nut Fastenings"* 1943 Trans. A.S.M.E., vol. 65, p.A-93

[2.13] **Sopwith, D. G.**, "*The Distribution of Loads in Screw Threads"*; Proc. I.Mech.E, 1949, vol 160, p.124

[2.14] **Kelley, B. W. and Pedersen, R.**, *"The Beam Strength of Modern Gear-Tooth Design"*; Transactions of the Society of Automotive Engineers, 1958. Pp 137-157.

[2.15] **Heywwod, R. B.**, *"Design Against Fatigue"* Chapman and Hall Ltd., London 1962. Pp 261-265.

[2.16] **Stoeckly, E.E., and Macke, H.J.**, *"The effect of taper on screw thread load distribution"*, Transactions of the American Society of Mechanical Engineers, 1952, 74, pp 103-112.

[2.17] **Junker, G.H., Wallace P.W.**, *"The Bolted Joint: Economy of Design through Improved Analysis and Assemble Methods"*; Proc Inst Mech Engrs Vol 198B No 14, 1984, pp 255-266

[2.18] Image courtesy of http://commons.wikimedia.org/wiki/File:Plastic_Protractor_Polarized_05375.jpg accessed on June 12th 2010.

[2.19] **Kuske, A. and Robertson, G.**, *"Photoelastic Stress Analysis"* John Wiley and Sons, 1974. Pp. 72

[2.20] **Weiner, P.D., and True, M.E.**, *"A Means of Increasing Drill Collar Connection Life"* ASME paper 72-PET-65 presented at ASME Petroleum Mechanical Engineering Conference with Pressure Vessels and Piping Conference, New Orleans, September 1972.

[2.21] **Patterson, E.A. and Kenny, B.**, *""Load and Stress Distribution in Screw Threads"*, Experimental Mechanics, September 1985, pp 208-213

[2.22] **Patterson, E.A. and Kenny, B.**, *"A modification to the theory for the load distribution in conventional bolts and nuts"*, Journal of Strain Analysis, 1986, 21, pp 17-23

[2.23] **Broadbent, T.P., and Fessler, H.**, *"Distribution of thread loads in screwed tubular connections"*, Proceedings of Fatigue of Offshore Structure Conference, London, 1988

[2.24] **NDE Centre, University College London**, *"Fatigue Analysis of Drillstrings – FADS"*, Joint Industry Project, Final Report, 1990.

[2.25] **Perry, C.C. and Lissner, H. R.**, *"The Strain Gauge Primer"* McGraw-Hill Book Company; Second Edition, 1962. Pp.18

[2.26] **Smith, J.E., and Carlin, F.J.**, *"Options to Increase Drillstring Reliability and Decrease Tool Joint Break-in Costs"*, IADC/SPE Paper 19961, March 1990

[2.27] **Brennan, F.P., Kare, R.F.**, *"An Experimental Analysis of Preload in Threaded Connections"*, Proceedings of the International Conference on Offshore Mechanics and Arctic Engineering – OMAE, Vol. III, pp 235-241, 1994

[2.28] **Gonzalez-Rodriguez, J. G. and Procter, R. P. M.**, *"Environmental Cracking of AISI4145 Steel in Drilling Muds"*; Corrosion Science. Vol. 35, Nos. 1-4; Pp 515-520, 1993.

[2.29] **Pitts, J. P.**, *"Trip Inspection, Testing Gain Favor as Insurance",* Drill Bit, 303, 885.

[2.30] **Hill, T. H.**, *"A Unified Approach to Drillstem Failure Prevention"*; SPE Drilling Engineer, December 1992

[2.31] **Shigley, J.E.**, *"Mechanical Engineering Design: First Metric Edition*", McGraw-Hill Book Company; 1986. Pp. 262-268,

[2.32] **Lubinski, A.**, *"Maximum Permissible Doglegs in Rotary Boreholes"*; Journal of Petroleum Technology, February, 1991

[2.33] **American Petroleum Inst.**, *"API RP7G: Recommended Practice for Drill Stem Design and Operating Limits''*, Sixteenth Edition, 1998

[2.34] **Baryshnikov, A.**, *"Optimization of Rotary-Shouldered Connection Reliability and Failure Analysis"* Drilling Conference IADC/SPE 27535, Dallas, 1994

[2.35] **Hill, T.H.**, *"Standard DS-1, Drillstem Design and Inspection"* T.H. Hill Assoc. Inc., DEA Proj. 74, 2nd ed. March 1998

[2.36] **Baha'i, H.**, *"A Parametric Model for Axial and Bending Stress Concentration Factors in API Drillstring Threaded Connectors"*; Int. Journal of Pressure Vessels and Piping 78; 2001; pp 495-505

[2.37] **Ouqi Zhang**, *"Discussions on Behaviour of Bolted Joints in Tension"*, Transactions of ASME, vol127, May 2005, p506-510

[2.38] **Lyons, W.C. and Plisga, G. J.**, *"Standard Handbook of Petroleum and Natural Gas Engineering"* Gulf Professional Publishing, 2005. Pp. 4-186;

[2.39] **Lopez, H. F.**, Bharadwaj, R., Albarran, J. L.,and Martinez, L, *"The role of heat treating on the sour gas resistance of an X-80 steel for oil and gas transport"*, Metallurgical and Materials Transactions; Volume 30, Number 9 ; September, 1999; pp 2419-2428

[2.40] **Zhao, M.C. Tang, B., Shan, Y., and Yang, K.**; *"Role of microstructure on sulfide stress cracking of oil and gas pipeline steels"*; Metallurgical and Materials Transactions; Volume 34, No. 5, May 2003; pp 1089-1096

[2.41] **Karim Khani, M.**; *"Corrosion Fatigue in Nitrocarburized Quenched and Tempered Steels"*, Metallurgical and Materials Transactions, 27A; May 1996.

[2.42] **Ifergane, S., Stern, N., Kogan, E., Shemesh, G., Sheinkopf, H., and Eliezer, D.**, *"The Effect of manufacturing on processes on the fatigue lifetime of aeronautical bolts"*, Engineering Fracture Analysis 8 (2001), pp 227-235.

[2.43] **Kristoffersen, S.**, *"Improved Fatigue Performance of Threaded Drillstring Connections by Cold Rolling"*, Dr. Ing Thesis, Norwegian University of Science and Technology, 2002, Pp 88-100

[2.44] **Ngiam, S.S. and Brennan, F. P.**, *"Experimental Investigation of Crack Shape Evolution in Cold Rolled Components"*, International Conference on Fatigue Crack Paths, Parma, 2003.

[2.45] **Majzoobi, G.H., Farrahi, G.H. and. Habibi, N.**, *"Experimental evaluation of the effect of thread pitch on fatigue life of bolts"*,International Journal of Fatigue 27 (2005) 189–196

[2.46] **Macdonald, K.A.**, *"The Effectiveness of Stress Relief Features in Austenitic Drillcollar Connections"*, Engineering Failure Analysis. Vol. 3. No. 4, pp. 267-279~ 1996

[2.47] **Burnett, D. S.**, *"Finite Element Analysis: From Concepts to Application"* Addison-Wesley Publishing Company; 1988

[2.48] **Pick, R.J. and Burns, D.J.**, *"Finite Element Analysis of Threaded End Closures of Thick-Walled Vessels"*, Proceedings of the Institute of Mechanical Engineers, Pp. 15-25, January 1971

[2.49] **Brennan, F.P.**, *"Fatigue and Fracture Mechanics Analysis of Threaded Connections"*, Ph.D Thesis, University College London, 1992

[2.50] **Tanaka, M., Miyazawa, H., Asaba, E. and Hong, K.**, *"Application of the Finite Element Method to Bolt-Nut Joints"*, Bulletin of the JSME, vol. 24, No. 192, pp 1064-1071, June 1981

[2.51] **Zhao, H.**; *"Stress Concentration Factors Within Bolt-Nut Connectors Under Elasto-Plastic Deformation"*; Int. Journal of Fatigue; vol. 20, N0. 9; pp 651-659. 1998

[2.52] **Izumi, S., Yokoyama, T., Iwasaki, A., Sakai, S.**, *"Three-dimensional finite element analysis of tightening and loosening mechanism of threaded fastener"*; Engineering Failure Analysis 12; pp 604–615; 2005

[2.53] **NDE Centre, University College London**, "Prevention of Downhole Failure – PDF", Final Report, Joint Industry Project, NDE Centre, Univ. College London

[2.54] **NDE Centre, University College London**, *"Reliable Operations of Drillstrings - RODS"*, Joint Industry Project, Final Report, 2002

[2.55] **Baragetti, S., and Baryshnikov, A.**; *"Rotary Shouldered Thread Connections: Working Limits Under Combined Static Loading"*; Journal of Mechanical Design, Transactions of the ASME; vol 123, September 2001; pp 456-463

[2.56] **Baragetti, S.**, *"Effects of Taper Variation on Conical Threaded Connections Load Distribution"*, Journal of Mechanical Design, Transactions of the ASME; Vol 124, June 2002; Pp 320-329

[2.57] **Azar, J. J. and Samuel, R.**, *"Drilling Engineering"*; PennWell Corporation, 2007, Pp 319-340

3 Theory and Principles of the Finite Element Method

3.1 Theory of Finite Element Analysis

Finite Element Analysis, FEA, is a branch of computational solid mechanics that deals with the application of loads and stresses to a structure that is analyzed for specific physical results. Burnett [3.1] defines FEA as ".....a computer-aided mathematical technique for obtaining approximate numerical solutions to the abstract equations of calculus that predict the response of physical systems subjected to external influences".

3.1.1 History of the Finite Element Method

When R Courant published his paper introducing the concept of FEA [3.2] little of it was noticed or found useful by engineers. Courant's paper utilized the Ritz method of numerical analysis and minimization of variational calculus to obtain approximate solutions to vibration systems. In 1956 M. J. Turner, et al. [3.3] used similar applications of numerical systems to study and analyze the odd-shaped delta wings, which are too short for beam theory to be reliable. The wing was modelled as an assemblage of smaller panels of simple triangular shape. This was the first recorded practical application of the FE method. To solve for torsion in elasticity, Courant defined piecewise polynomials over a triangularized region and in a later paper by Schonberg in 1946, the theory of splines was introduced recommending the use of piecewise polynomials for approximation and interpolation [3.4].

As early as 1941, Hrenikoff proposed the idea that elastic behaviour of physically continuous plate could be approximated, under certain loading conditions, to a framework of physically-separate, one-dimensional rods and beams, connected together at discrete points [3.5]. But engineers' earlier disinterest in the concept of numerically analysing discretised structures was due to the unavailability of computing power to undertake such analyses. With

the introduction of stored-program digital computers in the 1950s, several scientists took the well-established framework-analysis procedures and reformulated them into a matrix format ideally suited for efficient automatic computation [3.4].

The term “Finite Element” first appeared in 1960 and by the mid-60s the mathematical validity of the method was recognized and it was expanded from its structural beginnings to include heat transfer, groundwater flow, magnetic fields and other areas [3.6]. But up to early-1970s FEA was limited to expensive mainframe computers generally owned by the aeronautics, automotive, defence and nuclear industries. Because of the massive decline in computing cost, robust general-purpose FE software became available. By the late 1980s similar software programs were available for microcomputers complete with colour graphics and pre- and post-processing modules. The element concept, the matrix method and digital computers have been combined to provide a powerful structural analysis tool for engineers.

3.1.2 Basic Theory of the Finite Element Method

FEA is dependent upon the discretisation of a structure into substructures called *elements* attached to each other at points called *nodes*, and the physical interrelationships between these nodes are then converted to equations and solved mathematically.

This is achieved through the construction of a “trial” solution for a finite sum of functions, applying an optimizing criterion to the functions and an estimation of how accurately the trial solution approximates to the exact solution obtained from a governing equation that mathematically defines the physical system.

To do that, a governing equation and boundary conditions that define the physical problem are identified. The solution to the governing equations will give an exact solution, $U_{(x)}$ for a 1-D problem or $U_{(x,y)}$ and $U_{(x,y,z)}$ for 2-D and 3-D

problems respectively, while the trial solution that approximates to the exact solution, $\tilde{U}_{(x)}$, or $\tilde{U}_{(x,y)}$ and $\tilde{U}_{(x,y,z)}$ as the case may be is solved numerically using the power of computing. The closeness of the approximate solution to the exact solution is termed the Error, $E_{(x)}$, and is the difference between the exact and approximate solution, or,

$$U_{(x)} - \tilde{U}_{(x)} = E_{(x)} \quad \text{.....(3.1)}$$

The governing equations for stress modeling are presented in Appendix B4: Governing Equations for Stress Modelling.

3.1.3 The Steps to an FEA Solution:

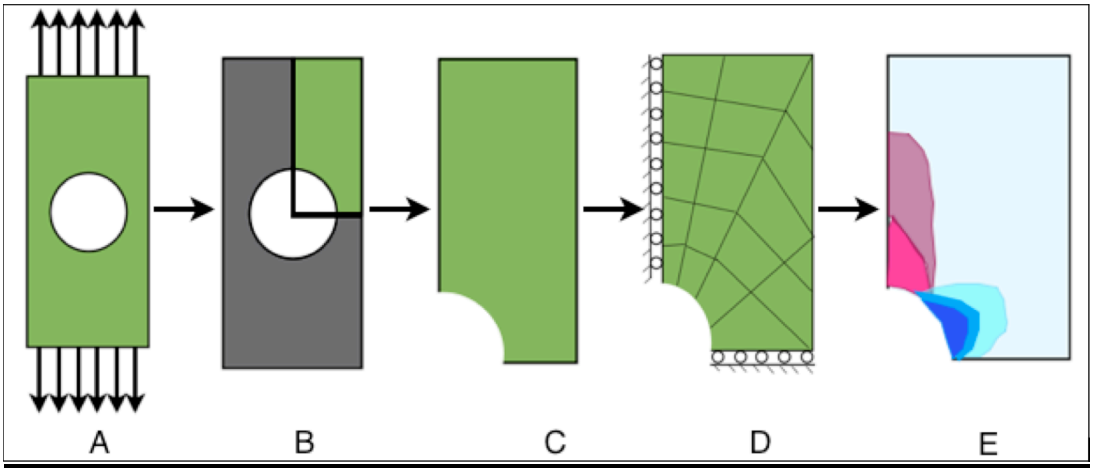

Figure 3-1: Steps to a Finite Element Solution

As shown in Figure 3-1 above, there are generally five steps to an FEA solution, namely, definition of the problem (A), reduction of the problem based on symmetry (B & C), discretisation of the problem and application of boundary conditions (D), solution of the problem and visualisation of the results (E).

However, in the computational FEA solution the above five steps are resolved in eight different steps:-

1) Derive the governing equations of the physical problem

2) Divide the physical problem into units called “elements” - a collection of elements is termed a ‘mesh’

3) In each element, the governing equations (normally differential equations) are transformed into algebraic equations. These algebraic equations are called element equations and they are an approximation of the governing equations. The algebraic equations are also called weak formulations.

   (Note: Algebraic equations are easier to handle by computers than calculus equations)

4) The terms in the element equations are numerically solved by a computer for each element in the mesh and assembled based on element connectivity

5) The result of the solution is compiled into a larger set of algebraic equations called the system equations (characterizing the response of the entire system to the external load)

6) The system equations are then modified to include the boundary conditions of the system

7) The system equations are then solved again by the computer

8) A result is then generated and viewed on a post-processor

The Finite Element Method is a numerical method that provides solutions to problems that would otherwise be difficult to obtain. The method is currently applicable to stress analysis, fracture, fluid flow, heat transfer and magnetic fields. The mathematical principles that underlie the processes undertaken by the FEA code are discussed below.

3.2 Mathematical Principles of the Finite Element Method

The FE method can be applied to almost all problems of continua where a physical quantity over an area (element) is to be deduced from a value of the quantity at specific points (nodes). These include physical and thermal stresses, strains, loads and moments. A simple three-member truss is sometimes used to give an introduction to the mathematical principles of the finite element method [3.7].

While the explanation in the reference above looks at a specific element, a number of similar equations are generated by the FE software to solve for the same unknowns in multiple elements that make up the mesh of a structural body. FEA has the power to solve for both static and dynamic analyses in consideration of whether inertial forces are a factor in the analysis or not [3.8].

3.2.1 The Trial-Solution Method

FEA uses the Trial-Solution method to derive the element equations and arrive at this approximate solution. The Trial-Solution procedure is characterized by three principal operations as listed below and shown graphically on Figure 3-2 below;

1. The construction of the trial solution;
2. The optimization of the solution; and
3. The estimation of the accuracy of the approximate solution to the exact solution.

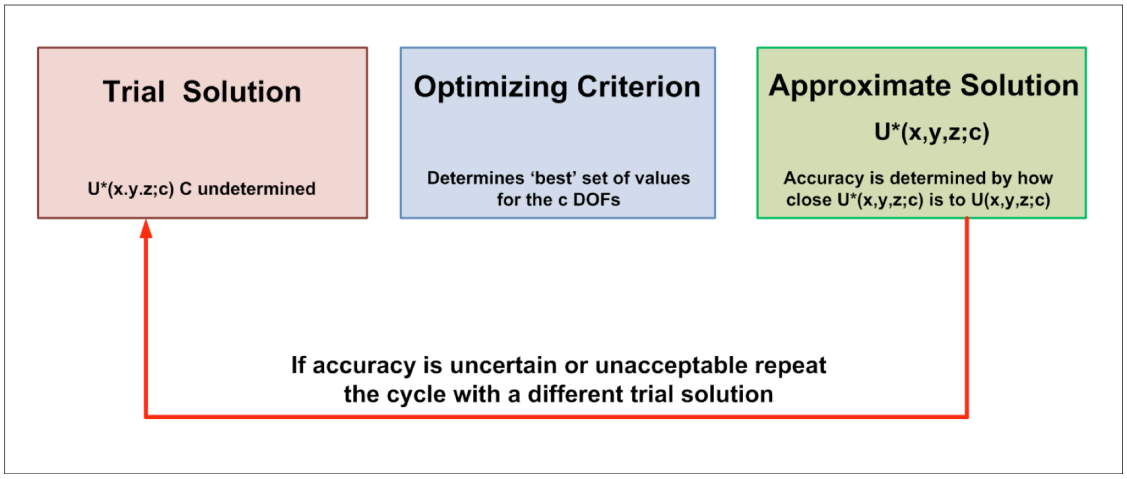

Figure 3-2: The FEA Trial-Solution Method [3.1]

3.2.1.1 Construction of a trial Solution

For a one-dimensional physical problem, $U_{(x)}$, is the trial solution, $\tilde{U}_{(x)}$ is constructed with a finite sum of functions;

$$\tilde{U}_{(x;a)} = \phi_0(x) + a_1\phi_1(x) + a_2\phi_2(x) + \ldots\ldots\ldots + a_N\phi_N(x) \ldots\ldots\ldots\ldots\ldots\ldots (3.12)$$

Where $\phi_0(x)$ to $\phi_N(x)$ are known functions (called trial, or coordinate, functions), x represents all the independent variables in the problem and the coefficients a_1 to a_N are undetermined parameters sometimes called generalized coordinates. The trial solution works by constructing expressions for each of the trial functions in terms of specific, known functions.

For the governing and boundary condition equations of stress modelling, if we choose the first few terms of a polynomial as our functions, then our trial solution will be;

$$\tilde{U}_{(x;a)} = a_1 + a_2x + a_2x^2 + \ldots\ldots\ldots + a_Nx^{N-1} \ldots\ldots\ldots\ldots\ldots\ldots (3.13)$$

3.2.1.2 Applying the Optimizing Criterion

As shown in Fig 3.2, the next stage is to apply an optimizing criterion on the Trial-Solution. This is done through the use one of the two main criteria; The Methods of Weighted Residuals (MWR) and the Ritz Variational Method (RVM). The WMR has four methods of approximate solution; the collocation method, the subdomain method, the least squares method and the Galerkin method.

The RVM is normally applied when the governing equations are variational (integral) and for optimization it seeks to minimize some physical quantity such as energy. The MWR method on the hand is mainly applicable when the governing equations are differential and for optimization it seeks to minimise an expression of error in the differential equation and not in the unknown value of displacement, U. The Galerkin method, in which the weighted average of the residual error over the entire domain is required to be zero, is the most popular of the MWR methods [3.9].

3.2.1.3 Estimating the Accuracy of the Solution

The last stage in the FE method is to estimate the accuracy of the solutions obtained to see which one is most accurate to the approximate solution. This aims to compare the various results obtained, which are then plotted on a chart to see how close they are to each other and, more importantly, how close they are to the exact solution.

3.2.2 Modelling Errors

As shown in eq. 3.1 and demonstrated in the preceding section, solution errors are part of the algorithm of an FEA code and any solution obtained remains an approximation of the exact solution. The approximate solution is optimized in order to obtain a solution with an accuracy that approaches the exact solution.

However, other type of errors exist that are occasioned by various factors inherent in the FEA method used or in the definition of the physical problem or the model. Therefore modelling errors can be classified into two main types; those due to incorrect problem definition and those due to incorrect model definition [3.10]. Examples of these are:

3.2.2.1 Errors due to incorrect problem definition

Some of the errors analyst must be aware of are due to how the problem itself is defined. Listed below are some of the more common ones.

a. Physics is not applicable or statics is not suitable
b. Problem cannot be isolated
c. Boundary conditions complicated
d. Linear materials are not suitable
e. Loading model not consistent or the load causes stiffening
f. Temperature effects are required
g. Solution varies with time
h. Friction dominates the solution

3.2.2.2 Errors due to incorrect model definition

Other type of errors are due to how the model to be used in the analyses is defined. These include;

a. Units are not consistent or the origin location is incorrect
b. Geometry does not replicate problem or the mesh does not conform to the model geometry
c. Mesh is too coarse in areas of interest or mesh is overly distorted in areas of loading or response
d. Type of element used is not suitable for the problem
e. Missing constraints (geometry duplicated)
f. Loaded faces missing
g. Symmetry/asymmetry not defined correctly

h. Incorrect material properties

The aim remains to eliminate known errors as part of the optimization process of the model. One method generally employed to reduce errors that are inherent in the system is the application of convergence studies to check the validity of the obtained results or the closeness of those results to the calculated mathematical response of the model [3.11.]. Convergence checks on the element (type, density, etc) and applied variables (load, friction coefficient, preload) are usually undertaken to study the suitability of an element type, the validity of the results as the mesh gets finer or the limits of the effect of an applied external load.

3.3 Modelling Variables of the Finite Element Method

3.3.1 Nodes and Elements

Each element possesses a set of distinguishing points called nodal points or nodes for short. Nodes serve a dual purpose; definition of element geometry (or geometric nodes), and home for degrees of freedom (or connection nodes). Geometric and connection nodes may be one and the same. In lower-order elements, nodes are usually located at the corners or end points of elements, but in the so-called refined or higher-order elements nodes are also placed on sides or faces, as well as possibly the interior of the element [3.8].

Elements are said to be of a given order (linear, quadratic or cubic) in reference to the interpolation of the element's nodal results to the interior of the element. This determines how calculated results can vary across an element, and is important if you have high gradients of strain. A beam or plate in bending is a good example of this phenomenon, where it is possible for the strain to change from positive to negative over a small distance. Linear elements do not have mid-side nodes [3.8].

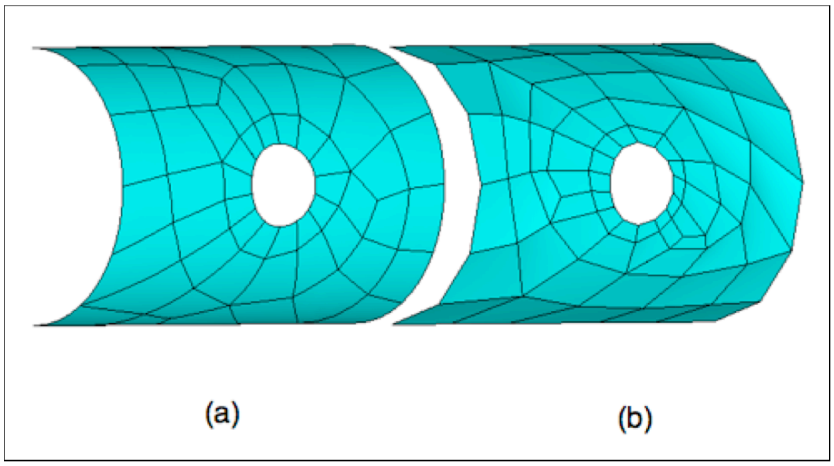

Figure 3-3: Second- (a) and First-Order (b) Elements

Quadratic elements, on the other hand, have mid-side nodes. The shape function for strains varies in some nonlinear fashion between the corner nodes.

Whereas linear elements are flat on both the sides and in-plane, a quadratic element can follow a curvature in both directions and is more accurate for a given number of nodes in the model. For example, in a tube with a hole, as shown on Figure 3-3 above, the curvature is maintained around the edges of the hole as well as on the curved edge of the panel.

In picking an element order for this work the following considerations were made:

1) Computational efficiency and error sensitivity - because a linear element is probably better in a mapped mesh than a free mesh.
2) Linear bricks give good results due to the “extra shapes” (full integration) if the elements are regularly shaped.
3) For out-of-plane, plate type bending, there isn’t much difference between linear and quadratic elements.
4) In nonlinear analysis, as in the case of possible plasticity at the tooth root on the connector, a finer mesh of linear elements is computationally more efficient, robust, stable and more accurate than a coarser quadratic mesh with a comparable number of nodes.

3.3.1.1 Element Characterisation

a. Family (Element Types)

	LINEAR	QUADRATIC	CUBIC
	Increasing order		
1D			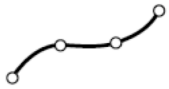
2D	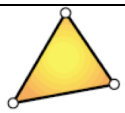	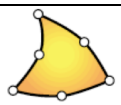	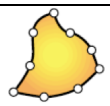
2D	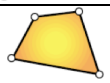	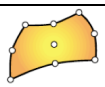	
3D	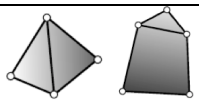	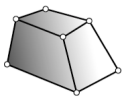	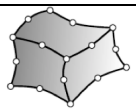

Table 3-1 Element Types

Table 3-1 above shows the element families that are most commonly used in computational stress analysis. One of the major distinctions between different element families is the geometry type that each family assumes. The categorization above shows the element types in increasing degree of dimensionality and order [3.8], [3.12].

Some Abaqus/Standard element families have a standard formulation as well as some alternative formulations such as the hybrid elements C3D8H and B31H that are identified by the letter H at the end of their names.

3.3.1.1.1 Degrees of Freedom (DOFs)

Degrees of freedom (DOF) of an element specify the state of the element. They also function as “handles” through which adjacent elements are connected. DOFs are defined as the values (and possibly derivatives) of a primary field variable at connector node points. As illustrated below, each node has number

of DOFs that is directly related to its dimension in space.

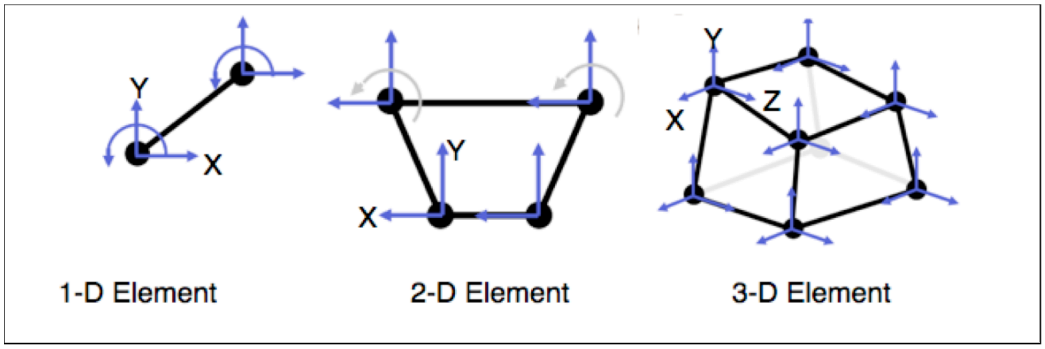

Figure 3-4: Nodal Degrees of Freedom (DOFs)

DEGREES OF FREEDOM					
DOF 1	**DOF 2**	**DOF 3**	**DOF 4**	**DOF 5**	**DOF 6**
Translation in the X Direction	Translation in the Y Direction	Translation in the Z Direction	Rotation in the X Direction	Rotation in the Y Direction	Rotation in the Z Direction

Table 3-2 Degrees of Freedom (DOFs)

3.3.1.1.2 Number of Nodes

As stated above, displacements or other degrees of freedom are calculated at the nodes of the element. At any other point in the element, the displacements are obtained by interpolating from the nodal displacements. Usually the number of nodes used in the element determines the interpolation order. Elements that have nodes only at their corners, such as the 8-node brick use linear interpolation in each direction and are often called linear elements or first-order elements. Elements with mid-side nodes, such as the 20-node brick use quadratic interpolation and are often called quadratic elements or second-order elements. Modified triangular or tetrahedral elements with mid-side nodes, such as the 10-node tetrahedron use a modified second-order interpolation and are often called modified or modified second-order elements.

3.3.1.1.3 Formulation

An element's formulation refers to the mathematical theory used to define the element's behavior. In the Lagrangian (or material) description of behavior the

element deforms with the material. In the alternative Eulerian (or spatial) description elements are fixed in space as the material flows through them. Eulerian methods are used commonly in fluid mechanics simulations [3.18]. Stress/displacement elements in Abaqus are based on the Lagrangian formulation.

3.3.1.1.4 Integration

FEA codes use numerical techniques to integrate various quantities over the volume of each element, thus allowing complete generality in material behaviour. Using Gaussian quadrature for most elements, the Abaqus code used in this work evaluates the material response at each integration point in each element. Some continuum elements in the Abaqus code can use full or reduced integration, a choice that can have a significant effect on the accuracy of the element for a given problem[3.15]. In the Abaqus code the letter R is used at the end of the element name to label reduced-integration elements. For example, CAX4R is the 4-node, reduced-integration, axisymmetric, solid element.

3.3.1.2 Element Choice

The work reported here was undertaken on an NC46 drilling tubular connection. The revolved shape and the complicated geometry of the teeth area on the NC46 tubular presents a geometric discontinuity that calls for a conservative choice of elements. An earlier method of solving the problem encountered in simulating these geometric discontinuities is the creation of adequately meshed sub-models at areas of concern [3.16], [3.17], [3.18].

This, as can be expected, always turns out to be more computationally expensive than using a single model.

While higher order elements and the use of hybrid of element types, for example a combination of quadrilateral and triangular elements, can give

adequate coverage of all parts of the model including the tight tooth roots and thread run-out areas, the design approach adopted in this work is to use first order linear quadrilateral elements all through the model but to make the mesh finer in areas of interests which are primarily the tooth root areas and the shoulder area.

The author kept an eye on the potential problem areas in the model and ensured that an accurate load path is created in the model especially in areas of transition from the fine to the coarse mesh and higher to lower stress gradients.

The work was undertaken using linear axisymmetric elements (CAX4) for the two-dimensional analysis and brick elements (C3D8) for the three-dimensional. The element choice is influenced by the requirements of the simulation and the possibility of varying the mesh density in the area of interest in the drillstring tooth geometry. In the two-dimensional analysis, the axisymmetric elements used are seen to be ideal for the revolved nature of the physical model.

3.3.1.3 Solution Accuracy Checks

Solution accuracy checks are undertaken on an FEA model to map out likely sources of errors in the model apart from solution errors which may be present in the code itself. Convergence studies and mesh adaptivity (or mesh convergence) checks, undertaken as part of the solution accuracy checks are very important methods in the determination of the accuracy of a solution.

Convergence studies are done to understand the effect of varying the some input parameters of the model to the analysis output. This could be due to the applied input values being too high or too low for accurate analysis or the design of the model in terms of finite element properties such as size, dimension or aspect ratio of elements. Mesh convergence studies, on the other hand, are undertaken to determine the physical size of the elements required in a model to ensure that the results of an analysis are not affected by changing

the size of the mesh. The two extremes of mesh density, i.e., very coarse to very fine, can produce unequal and disproportionate results. For a very coarse mesh there will be a likelihood of an incorrect solution and for a too fine a mesh the analysis can end up being both computationally and financial expensive.

3.3.1.3.1 Mesh Convergence Checks

There are two types of mesh convergence checks that can be carried out in relation to a given element. These are classified as “H” type convergence and “P” type convergence. “H” type convergence of the approximate solution is achieved by refining the element mesh density as parametrized by the mesh size *h*. In contrast, the *P* method achieves convergence by refining the degree of the polynomial approximation within each element while the element mesh spacing *h* is held fixed [3.19], [3.20]. In other words, by changing the number of nodes (degrees of freedom) in a given element. Figure 3-4 below shows the difference between the “H” and “P” convergence schemes.

However, only “H” type convergence studies were undertaken in this work as the choice of element type and polynomial element order has been decided for reasons mentioned in Section 3.4.1.2 above.

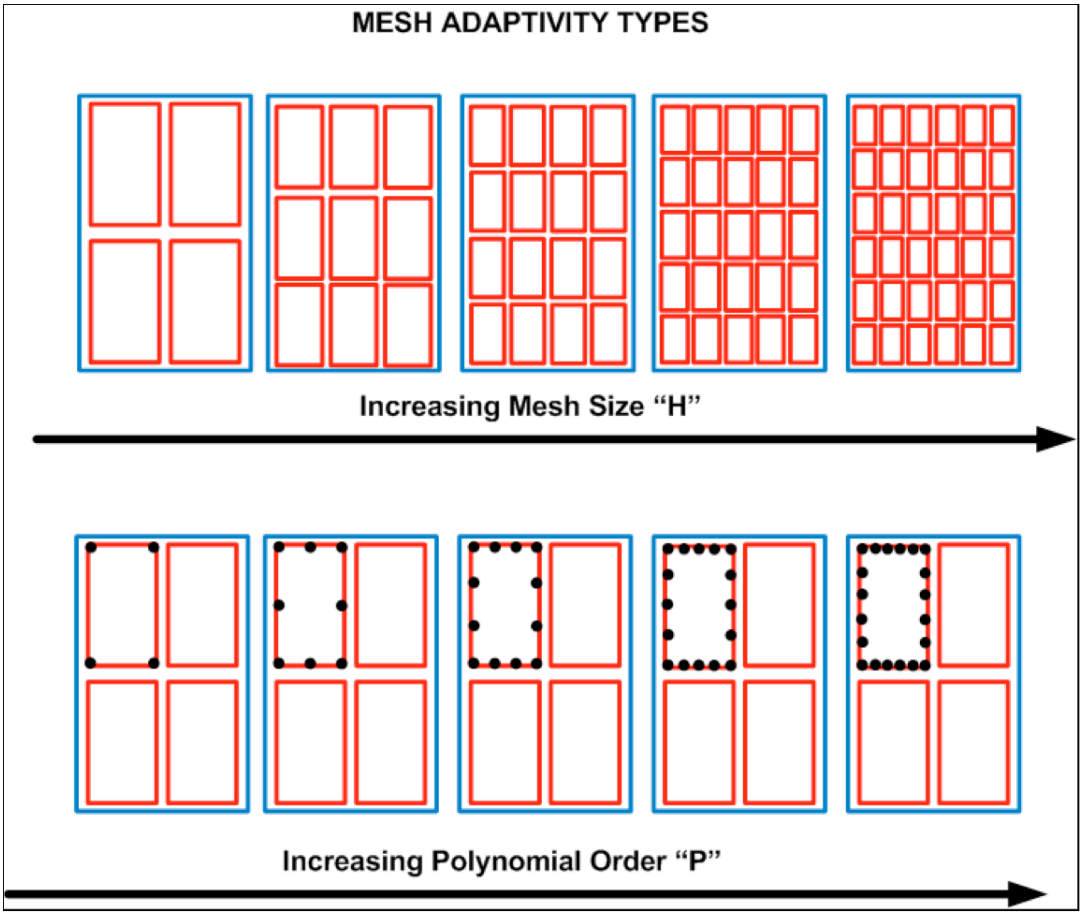

Figure 3-4: Mesh Adaptivity Types

Since, as stated above, the extremes of mesh density can produce an incorrect solution if too coarse and high analysis costs if too fine, a fine mesh is needed in regions of high stress (and strain) gradient which occur at geometric discontinuities, where a coarser mesh will suffice in areas of constant stress, low stress gradient or of little interest to the investigation.

3.3.1.3.2 Convergence Study Results

In an earlier study, Macdonald and Deans studied the effect of varying the mesh densities on a drillstring threaded connection FE model and found out that a significant mesh refinement is needed to accurately represent the stress distribution around the thread root radius [3.18]. They discovered that maximum peak stress is only obtained with more refined meshes but an optimum mesh

density had to be chosen such that optimized and acceptable results, with low associated computational costs are obtained.

In this work, while undertaking validation analyses, various convergence studies were undertaken to understand the effect a variation of some input variables of the model have on the accuracy of the model's output.
Figure 3-5 below shows the general trend obtained by the author when various FEA output parameters were studied against an increasing element density in a "H"-type convergence check undertaken on the 2D-axisymmetric model of the NC46 connector. The mesh at the thread root represents a geometric discontinuity and also acts as our principal area of interest in the study of peak stresses and SCF in the connector.

The mesh at the thread root was progressively refined and made finer covering a range of mesh density seedings (from 4 to 36) in a series of two-dimensional axisymmetric models. The boundary conditions and loads were kept the same for each of the models and each of the simulations.

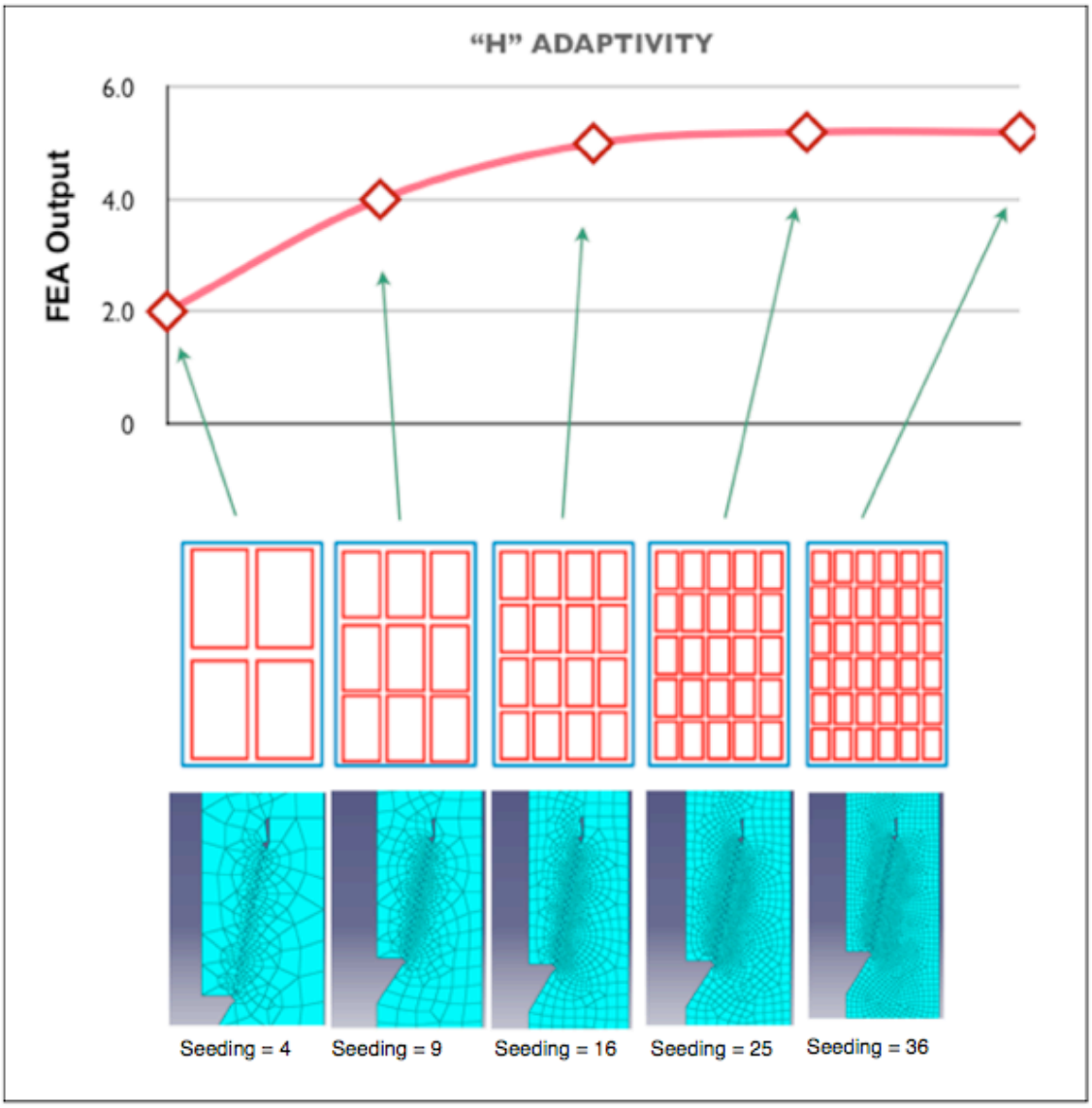

Figure 3-5: Mesh Convergence Results

Because stress concentration is a localized phenomenon that progressively dissipates with distance, a graduated mesh that gets finer as it approaches the areas of interest can be used. Also, since the local stresses at locations away from the thread root discontinuity are not of primary interest, a coarse mesh was used at those areas. Although accurate stress values will not be obtained at these areas of coarse mesh, care was taken to ascertain that correct and accurate load paths were obtained from the point of loading to the thread root discontinuity.

A convergence study was undertaken to determine the convergence values for an assigned mesh in terms of the Stress Concentration Factor (SCF). As can be seen from Figure 3-6 below, a convergence point, defined as the point where a change in the mesh density will have no effect on the output values in the pin and box threads was determined.

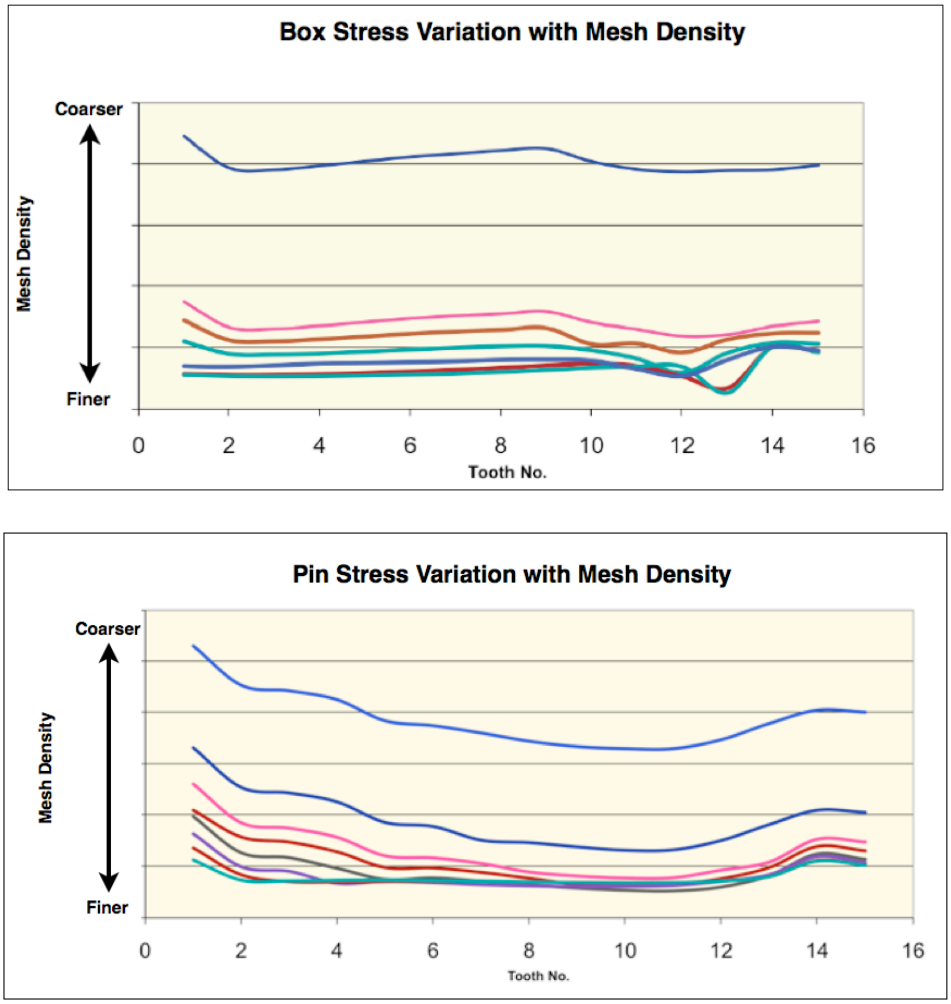

Figure 3-6: Root Stress Vs Mesh Density for a 2-D Axisymmetric Model

It can be seen from the chart above that convergence was achieved with a given mesh fineness in both the pin and box threads. At the convergence value increase in external axial loading and/or preload will have no effect on the Stress Concentration Factor (SCF).

3.4 Conclusion

The finite element method (FEM) is a widely used analysis tool that has its roots in mathematical and engineering theories. The steps employed in obtaining a finite element solution to a given problem involve the derivation of the governing mathematical equations that define the physical problem, the transformation of those (normally differential) equations into approximate algebraic equations that render themselves to easy computation using a computer code that renders the results to numerical or graphical output.

Solutions obtained from a finite element solution are affected by both solution variables and modelling variables. While solution variables look at those factors inherent in the mathematical solution based on which the finite element method solves the problem based on the input variables such as loading, coefficient of friction, stiffness, etc., modelling variables, on the hand, includes the mesh size and density and element order (linear, quadratic, cubic).

Because of the complex nature of stress and load distribution in drillstring threads convergence analysis and validation with earlier published theoretical and experimental work was undertaken on the model developed for this work.

3.5 References

[3.1] **Burnett, D. S.**; *"Finite Element Analysis: From Concepts to Application"*; Addison-Wesley Publishing Company; 1988

[3.2] **Courant, R.**,*"Variational methods for the solution of problems of equilibrium and vibrations,"* Bull. Amer. Math. Soc., 49 (1943), pp. 1–23.

[3.3] **Turner, M. J., Clough, R. W., Martin, H. C, and Topp, L. J.**, *"Stiffness and Deflection Analysis of Complex Structures",* Journal of the Aeronautical Sciences, Vol. 23, No. 9, p. 805-823, 1956

[3.4] **Schonberg, I. J.**, *"Contributions to the Problem of Approximation of Equidistant Data by Analytic Functions. Part A. On The Problem of Smoothing or Graduation. A First Class of Analytic Approximation Formulae"*, Quart Appl Math, 4: 45-99, 1946

[3.5] **Hrenikoff, A.**, *"Solutions of Problems in Elasticity by The Framework Method",* Journal of Applied Mechanics, 8. Pp169-175, 1941

[3.6] **Cook, R. D.**, *"Finite Element Modeling for Stress Analysis",* John Wiley & Sons, Inc. 1994, pp. 3.

[3.7] http://www.sv.vt.edu/classes/MSE2094_NoteBook/97ClassProj/num/midkiff/theory.html accessed on 5th January 2012.

[3.8] **Dassault Systemes**, "*Getting Started with Abaqus version 6.7-1"*, Dassault Systems, 2007

[3.9] **Seshu, P.**, *"Textbook of Finite element Analysis"* Prentice-Hall of India Pvt Limited; 2006. Pp. 16-20

[3.10] **Reddy, J. N.**, *"An Introduction to the Finite Element Method"* McGraw Hill International Editions; 1986; Pp. 9

[3.11] http://nafems.org/resources/cfdconvergence/Page0/ accessed on the 16/12/2011.

[3.12] **Felippa, C.**, *"Introduction to Finite Element Methods"*, Department of Aerospace Engineering Sciences University of Colorado at Boulder, 2008

[3.13] **Dassault Systemes**, "*Getting Started with Abaqus version 6.7-1"*, Dassault Systems, 2007

[3.14] **Zhang, L., Gerstenberger, A., Wang, X. and Liu, W. K.**, *"Immersed Finite Element Method"*; Computer Methods in Applied Mechanics and Engineering, Vol. 193; Pp. 2051-2067.

[3.15] , "Abaqus 6.7 Analysis Users Manual, Volume 1: Introduction Spatial Modeling, Execution and Output"; Dassault Systemes; 2007; Section 2.5.1.

[3.16] **NDE Centre, University College London**, *"Fatigue Analysis of Drillstrings – FADS"*, Joint Industry Project, Final Report, 1990.

[3.17] **NDE Centre, University College London**, *"Prevention of Downhole Failure – PDF"*, Final Report, Joint Industry Project,

[3.18] **Macdonald, K.A. and Deans, W.F.**; *"Stress Analysis of Drillstring Threaded Connections Using the Finite Element Method"*, Engineering Failure Analysis, Vol 2, No. 1 pp. 1-30, 1995

[3.19] **Shih, R.**, "An introduction to Finite Element Analysis Using Creo Simulation 1.0", Published by SDC Publications, 2011; Pp. 9-18

[3.20] http://nafems.org/resources/knowledgebase/001/ accessed on 16/12/2011

4 Development of the 2-D Axisymmetric FE Model

4.1 Early Finite Element Models of a Drillstring Connection

As discussed in earlier chapters, a mesh generation program was developed using the FORTRAN77 programming language to generate a two-dimensional axisymmetric model of some selected drillstring connection types and dimensions. The program is capable of generating an Abaqus input code for the solution of two different loading scenarios, viz, Preload + Axial Loading and Axial Loading only. The full FORTRAN77 code and an example of a generated input file as well as input files for the developed model are presented as Appendix F.

4.1.1 The FORTRAN77 Mesh Generator

From the various studies on drillstring stress and fatigue undertaken by UCL NDE Centre a detailed FORTRAN program was developed by the Centre to generate input files for the dedicated finite element analysis software, ABAQUS [4.1], [4.2], [4.3].

The developed program was adopted by the writer to generate a baseline mesh and FEA result prior to the development of the writer's own FEA model. The program provides the option to model the connector with pre-load (make-up) and axial load. By design, the connection is a taper jack screw that forces the pin/box shoulder together forming a structural member by means of a metal to metal seal. In doing so, an alternative load path is created through the shoulder interface when the connection is made-up. This has the effect of transferring the critical thread root from the pin to the box connector. In terms of FE modelling this is achieved by connecting the nodes of the pin and box at the shoulder interface, thus effectively welding the shoulder together.

The program allows the user to input a number of variables such as type of connector, joint dimensions, and the application (or not) of pre-load. To avoid a situation where, upon the application of loading, the pin section goes through the box section, contact must be simulated between the pin and box threads. ABAQUS “Gap elements”, which consists of two-nodes and a separation distance, are used to model this contact [4.4]. If the nodes are overlapped (or the separation distance is reached) ABAQUS will disable any further displacement at the specified nodal points. Gap elements use direction cosines to define their direction of action using their pressure angle of the thread faces.

The program accepts the user input in the form of the variables listed below, generates an input file in ABAQUS format and automatically exits. The input file is then loaded and run on an FEA program.

4.1.1.1 Programmed Geometries

The program generates two-dimensional axisymmetric finite element meshes for a range of different sized drill collar connections. It is able to produce input files that model the NC26, NC38, NC-46, NC-50, API 6-5/8REG and API 7-5/8REG connections.

4.1.1.2 Variables

Although earlier versions use a Visual FORTRAN with windows-style dialogue boxes and menus the current FE mesh generation programme opens on a text-based menu screen, shown in Figure 4-1 below, that is compatible with FORTRAN77.

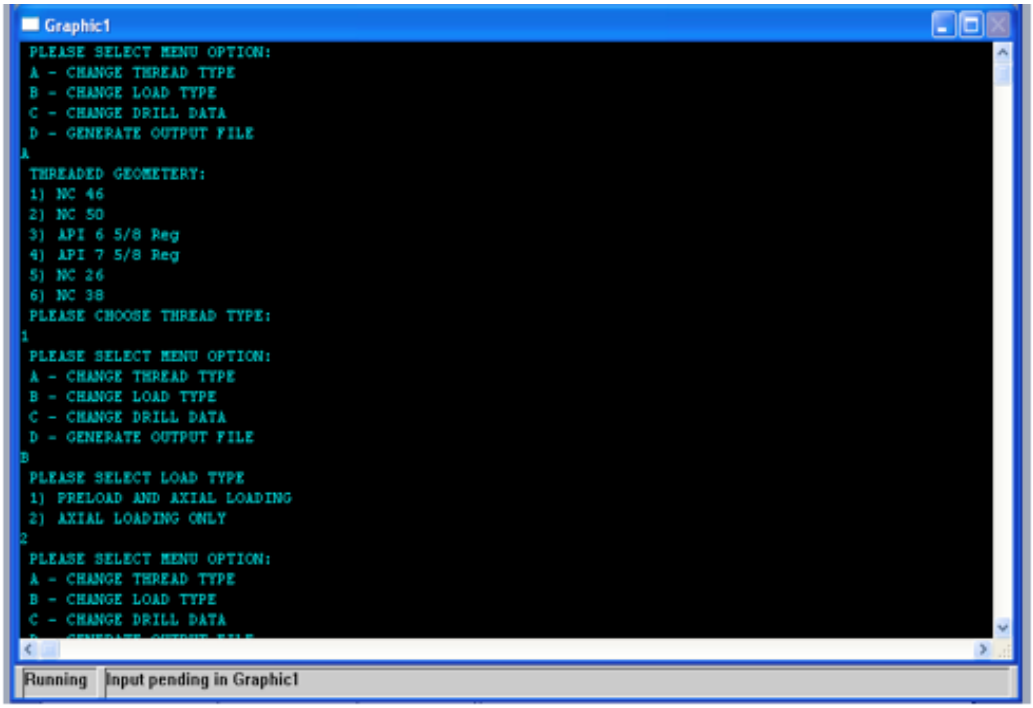

Figure 4-1: The FORTRAN77 Mesh Generator User Interface

The input variables taken by the program are

Thread Type (IDST): These include the NC26, NC38, NC-46, NC-50, API 6-5/8REG and API 7-5/8REG.

Load Type: Two types of loading conditions available in the program; axial loading only and axial + preloading.

Drillstring Data (OD, DI): The outer/inner diameters of either the pin or box are selected in the text-based user interface and input through the keyboard.

Output File Name (FNAME, TITLE): The user is requested to enter the name of the ABAQUS input file to be created.

Some input variable from earlier versions have been removed from the current version. These are; Bevel diameter of pin and box shoulder (DR), Total length of assembly (SLEN), Total Axial loading in Newtons (PFORCE).

4.1.1.3 Limitations of the Generated Model

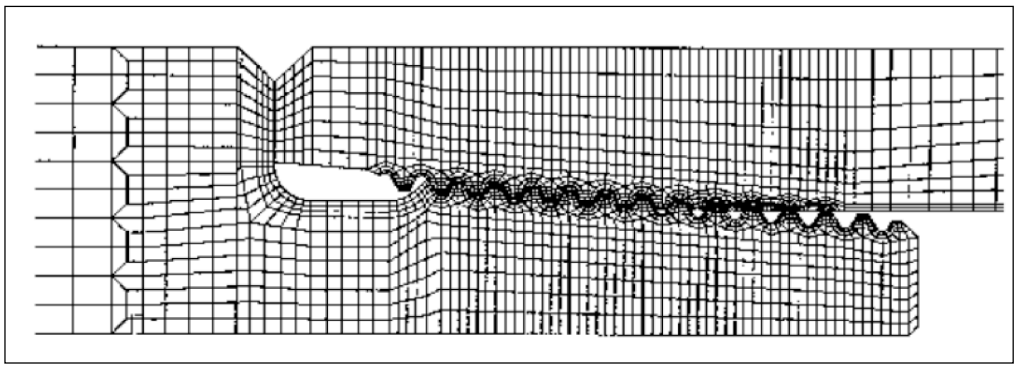

Figure 4-2: Generated FE Mesh of an NC50 Connection

From a line-by-line study of the mesh-generation program, it was discovered that when the IPRE=1 is activated for an axial + preload simulation (IPRE is the command that switches the analyses from axial loading to axial + preload loading) the program simulates preloading by locking the box and pin at the interface nodes. This has the negative effect of negating the principal mechanism through which preloading works, which is the generation of load transfer at contacting interfaces of the shoulder and teeth.

Also, the loading exerted on the string does not change in either the axial only or the axial + preload scenarios. The stress distribution modelling does not also change in either of the two scenarios.

The model generated is axisymmetric with eight-node quadrilateral elements for the general mesh and two-node gap elements for contact between the thread teeth. The program has the option to model the connector with preload. A generated model of NC50 connection is shown in Figure 4-2 above.

Other practical limitations of the model make it imperative to develop new

means of generating more functional models and meshes that are more robust and that could lend themselves to modifications on the fly at the whim of the stress analyst. Some of these limitations are:

1. While it is practically feasible, and it happens in most thread loading scenarios, to apply an internal load (preload) to the connection and to achieve and maintain connection integrity without the application of an external tensile (or compressive) load, it is practically not feasible to achieve such integrity in the presence of just an axial load, as suggested by the mesh generation program when the axial-only loading scenario is activated.

2. To achieve seamless interfacing between the pre-processing and processing module in the FEA code, and to make the parameters easier to modify, it is better for a model to be sketched, meshed and all simulation input parameters (loads, BCs and contact parameters) incorporated within the same FEA code.

3. Because, the mesh is imported into the Abaqus code as an ‘orphan’ mesh, the stress analysts will have no means of altering the mesh for optimization purposes. The mesh densities, element sizes and aspect ratios are part of the program output and cannot be modified through the available user interface or when the generated input file is loaded into the FEA code.

4. There currently exists ample computing power to handle not only the development of sophisticated models from the native sketching modules of various FEA codes but also to build even more stand-alone parts from non-native CAD and 3D modelling software and import same into the FEA pre-processor for meshing and processing [4.5].

4.2 Two-Dimensional Axisymmetric Modelling

4.2.1 Modification of the FORTRAN77 Mesh Generation software

One of the major shortcomings of the mesh-generation software is in the analysis of contact between the teeth and shoulder of the mating box and pin of the tooljoint. On the teeth, gap elements (ABAQUS Keyword: GAPUNI) were used to model the contact interaction and load transfer. On the shoulder of the tooljoint, to model pressure load transfer due to preload, the software generates a mesh in which the box and pin are joined as a single unit on the shoulder with nodes permanently attached. Abaqus-generated visualisation of both scenarios can be seen in Figure 4-3 (a) and Figure 4-3 (b) below.

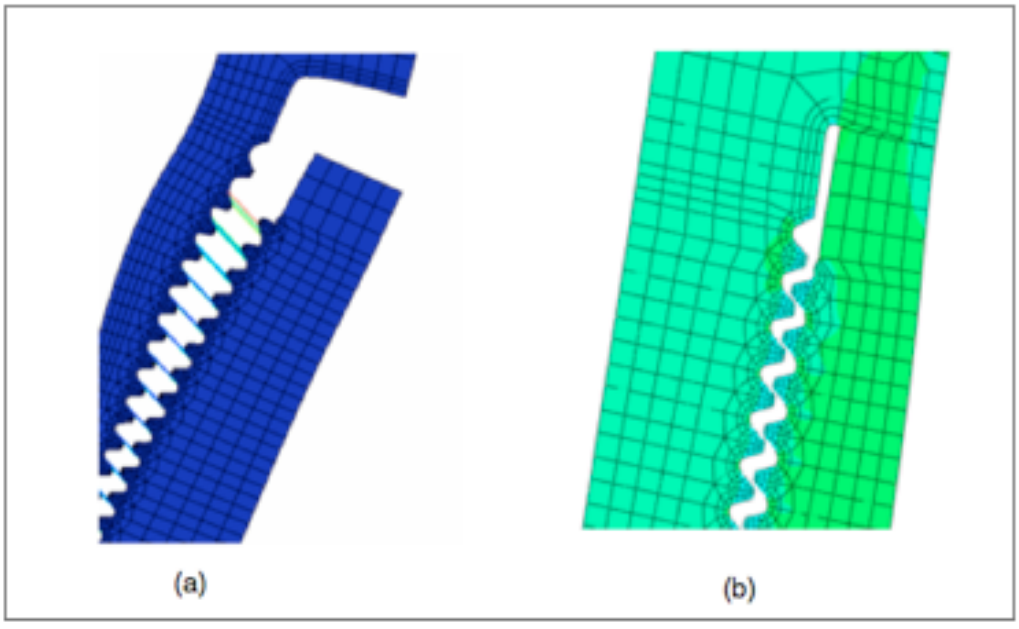

Figure 4-3: FEA Meshes: Gap Elements (a) and Load on Shoulder (b)

Both situations are disadvantageous and may not assist us in developing a robust FEA model for the various analyses we intend to undertake in tooljoint stresses. Another disadvantage is the inability of the gap elements model to

take into consideration the presence of thread compound (dope) and other environmental “film” adhesions on the tooth that can modify the coefficient of friction and affect the load transfer and frictional slip situation. It is proposed to solve the gap element problem by using alternative element definitions that can be simulated using the current versions of the ABAQUS code. This can be achieved by switching from element-based contact simulation to surface-based contact simulation such as friction modelling and defining points and reaction of contact locations in two components identified as “slave” and “master” [4.6].

4.2.1.1 Elimination of Gap Elements

Gap elements are used in the 2-D axisymmetric mesh generated by the FORTRAN77 program to model contact behaviour between nodes [4.6]. Unlike the fixed constraints identified in the derivation in Chapter 2 above, where nodal displacement, U, is equated to a fixed value, gap elements are multi-freedom (multi-point) constraints in which the value of the constraint is a function of the value of given nodal displacement components.

In earlier analysis carried out by Tafreshi and Dover [4.7] contact gap elements were used to model compressive forces between contacting teeth for the analysis of load transfer and also in the shoulder area in the unpreloaded joints in bending. Modelling with gap elements on axisymmetric solid elements did not pose any problem but using the same gap elements with parabolic 3-D solid brick and wedge elements was problematic because the finite element method resolves pressure on an element into equivalent nodal forces. For parabolic elements compressive surface pressure on an element can generate tensile nodal forces at the corner nodes.

Current versions of most FEA packages now perform contact analysis using frictional contact simulation across a “master” and a “slave” surface but it is still advisable to model a representation of the contacting surfaces to save

computational time. Yi-Cheng et al. analysed the contact interaction between helical gears by undertaking an FEA analysis of only one pair of such gears [4.8].

So the first objective was to modify the FORTRAN77 program to generate meshes that eliminate the gap elements and in place of them provide a generated mesh that lends itself to the delineation of surfaces as 'master' and 'slave' on which a contact simulation can be performed. Lines in the source code of the mesh generation program referring to contact surfaces were modified to obtain surface elements with nil contact simulation.

4.2.1.2 Introduction of Contact Surfaces

The generated mesh was modified within the ABAQUS software to introduce the surfaces on the teeth and the shoulder in which to apply a contact interaction. Figure 4-4 and Figure 4-5 below show a step-by-step procedure used to achieve this on NC46 thread profile.

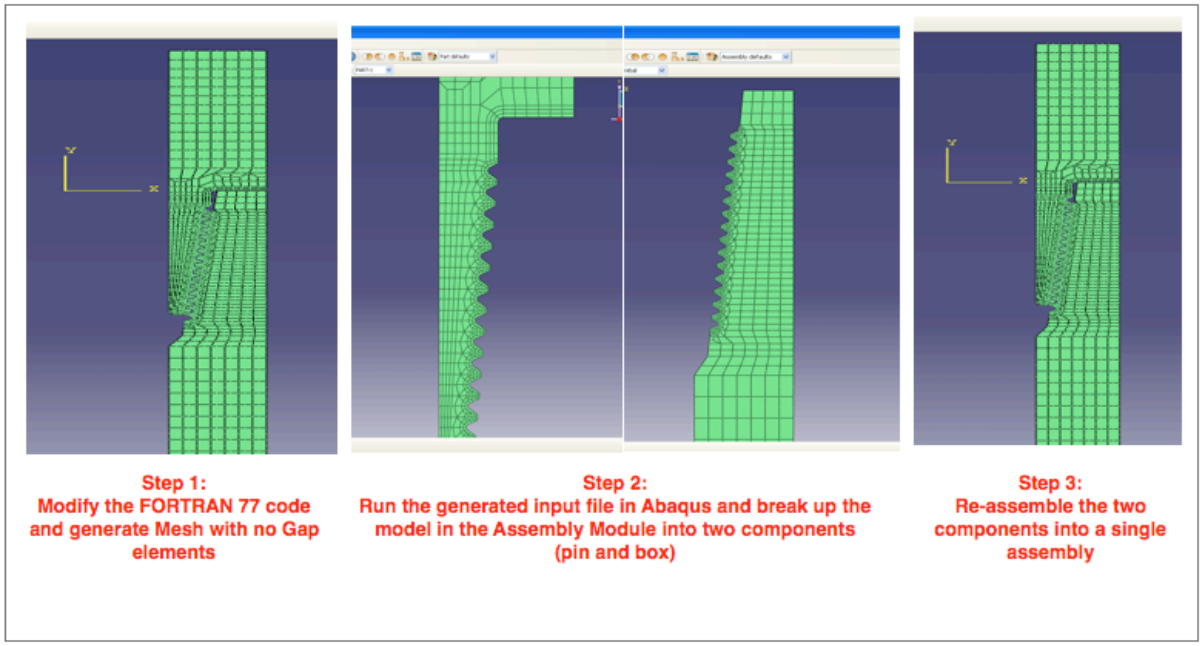

Figure 4-4: Introducing Contact Interaction; Breaking up the Model

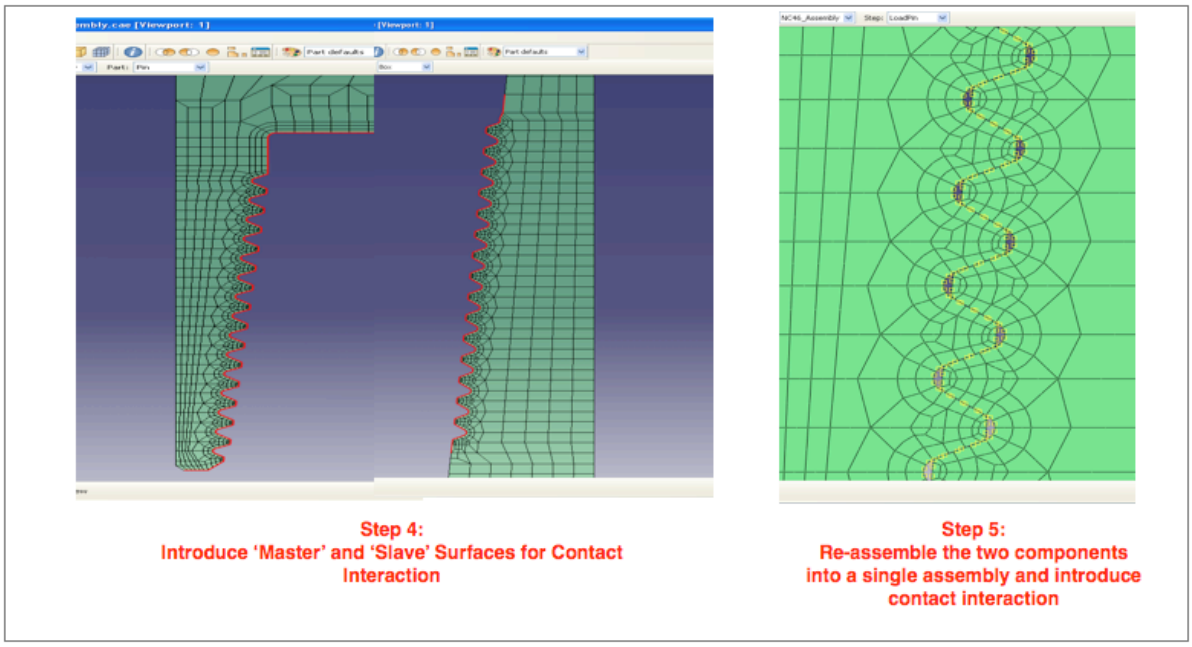

Figure 4-5: Introducing Contact Interaction; Re-assembling the Model

Step 1: After the modification of the source code of the FORTRAN77 mesh-generation software to remove gap elements and welded nodes, a mesh is generated through an input file and the generated mesh is loaded into the ABAQUS 'Part' module.

Step 2: The generated mesh is then broken up into two component parts, namely, the pin and box.

Step 3: The two parts are then loaded back into the ABAQUS Assembly Module and assembled as separate but mating parts.

Step 4: The parts are then assigned the necessary material, loading and boundary condition properties. The contacting areas of interest, namely, the pin/box teeth and the pin/box shoulder are given a 'surface' definition on which contact properties can subsequently be applied to a slave and master surface.

Step 5: The two contacting surfaces can now be rendered to contact simulation in which contact interaction properties can be modified parametrically and a full study of the model vis-à-vis loading, stresses, reactions and contact simulation can be undertaken.

4.2.1.3 Replacing the Mesh-Generated Model

The challenge at this stage is to develop a two-dimensional axisymmetric model that can better replace the mesh-generated model in terms of applicability and robustness. Such a model can be developed native in the FEA code to be used in the investigations or developed from external pre-processing program(s). For better control of the pre-processing stage, an external file developed outside the FEA code and imported into the FEA code should be of a stage that is before the meshing stage, for example, an external sketch file to be meshed by the FEA code. The model so created must be computationally efficient in solution and validated with earlier FEA work and robust enough to be adaptable to other connection types and loading scenarios.

4.2.2 Development of the Two-Dimensional Axisymmetric Model

4.2.2.1 Development of the Model

Figure 4-6 below shows a model sketched natively in the FEA code (a) and a model obtained from the FORTRAN77 mesh generator (b). The sketched model of the NC46 connector was dimensioned to a tolerance of 0.05mm with dimensional data sourced from the Drilling Data Handbook [4.9] and other published literature [4.7]. The model can be seen to be meshed uniformly and freely by the FEA code. At this stage it is meshed using quadrilateral plane stress (CPS4) elements. As their name implies, the CPS4 elements do not assume or recognize the existence of a third dimension and considers the model as a thin plate of unit thickness (z value) [4.6]. The reason why CPS4 elements are used at this stage is to simplify the study of the behaviour of the model in terms of loading, contact and boundary conditions. Ultimately, the model will be meshed with CAX4 axisymmetric elements with a capacity to be swept around all theta values of the connector.

As discussed in an earlier chapter, Pick and Burns used a 2-D axisymmetric model in performing the first FE analysis of a threaded connection in 1971

[4.10]. A similar model was used by Tafreshi and Dover [4.7] in the analysis of axial loading in connections and the analysis of SCFs. The assumption of 3D behaviour in a 2D FE model is considered valid since in large connections with relatively small pitches, helix angles are small. Also, Chen et al. [4.11] while studying the helical effect on threaded connections using 3D finite element analysis, concluded that axisymmetric 2-D analysis can give good estimation of stress distribution in medium to coarse mesh threads. Since thread designs do not use thread run out as load bearing section, the 2-D model can be assumed to be accurate in modelling peak stresses due to tensile load, effect of preload on tensile stress and the effect of friction on tooth load transfer. However a 3D model would still be required to undertake analyses of torsional and bending stresses in the joint.

At this stage it can be seen that the meshing will require a high level of optimization in order to obtain optimum load transfer across the elements, variable mesh density on opposing contacting slave and master surfaces and fine meshing in areas of interest, especially at locations where peak stresses are expected such as thread roots and the connection shoulder.

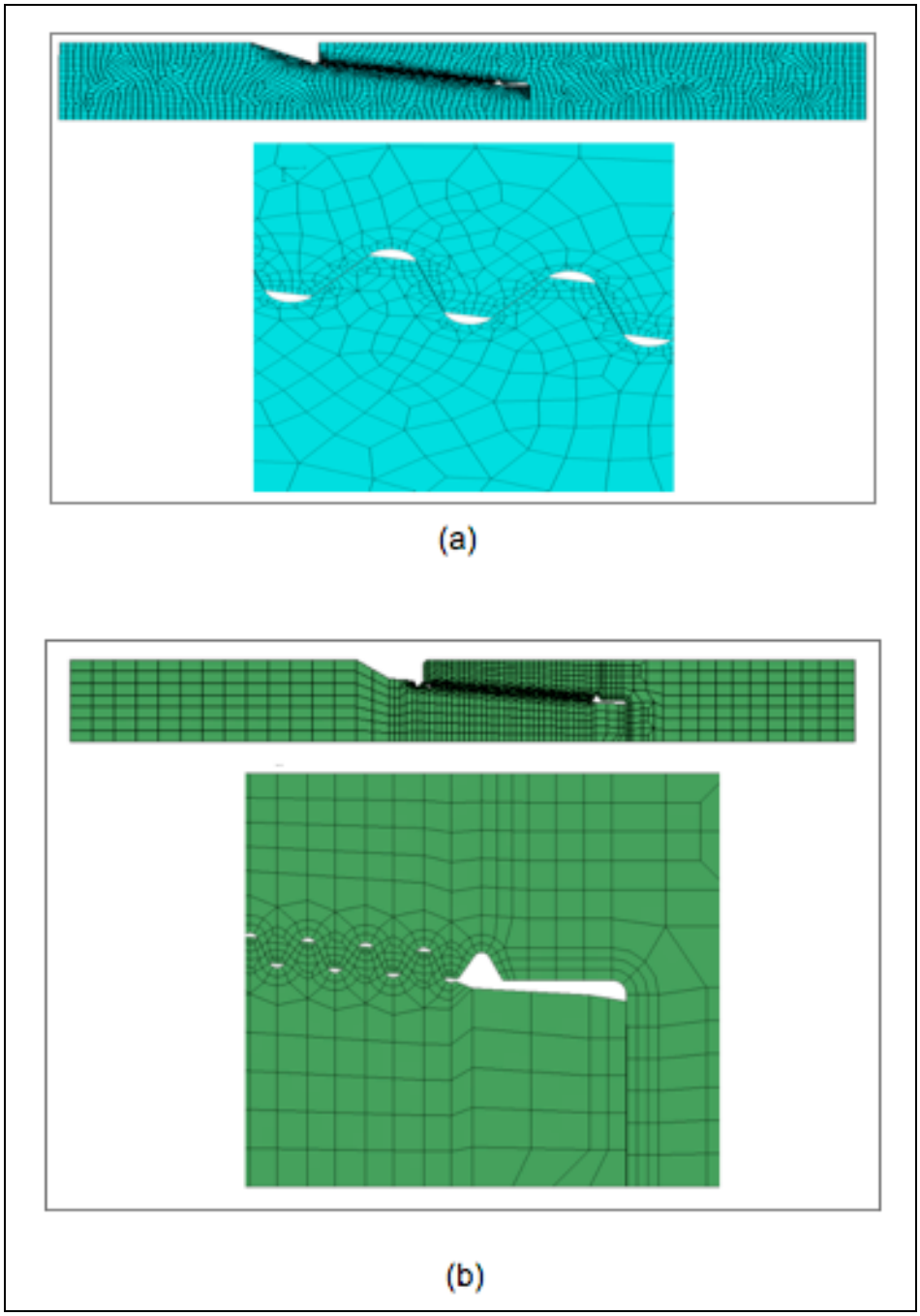

Figure 4-6: Model Sketched from FE Code (a) and from Mesh Generator (b)

While a near-optimized mesh that shows good element choice and a clear load path is obtained on the model generated from the FORTRAN77 mesh generator (b), the issues aforementioned such as the inability of the analyst to modify the mesh are still there. Therefore obtaining an optimized, variable mesh from such a model will not be possible. Also, as can be observed in Figure 4-6 (b), the

model was meshed with the use of a different contact algorithm in mind, viz., gap elements, and not specifically designed for surface/friction contact algorithm. To simulate contact behaviour in light of input variables such friction coefficient, (μ), and by extension, the drill floor action of applying a thread dope and the presence of other lubricating media such as drilling fluids, there is need to design the model to simulate contact using two contacting surfaces under the action of friction.

In view of the above, the sketched model is subjected to iterative meshing to obtain simulation parameters acceptable to the investigation. These include an optimized load path, contact surfaces and load bearing faces. Figure 4-7 below show an attempt to optimize the sketched model by creating better load path and finer meshes on the teeth area, the shoulder and the thread roots. As can be seen the tooth meshes still show a master/slave configuration as required by the chosen contact algorithm. At every stage of this process, the results obtained from the simulation are closely observed, recorded and validated with existing literature.

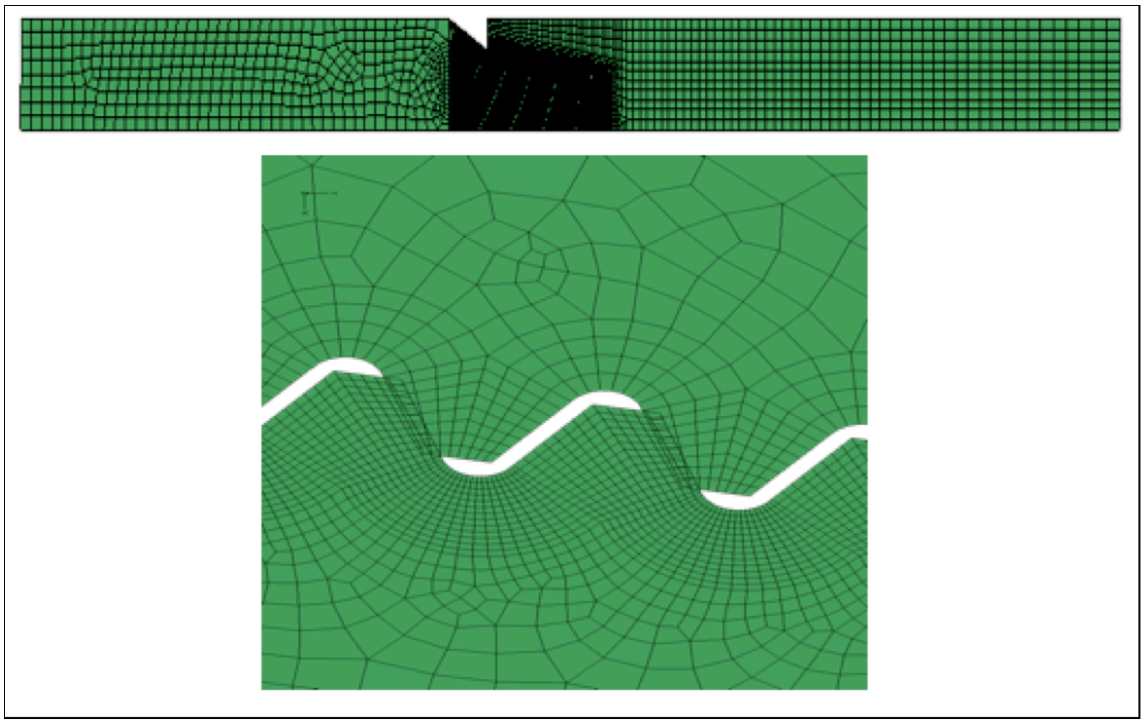

Figure 4-7: Mesh Optimisation

The next step in the model optimization process is the switching the model from using CSP4 elements to the axisymmetric CAX4 elements since this element type is the one ultimately to be used for the simulations. It is also at this stage that the mesh and the geometry of the model are optimized and sets introduced to properly delineate the model. The optimization of the mesh will entail further fine-tuning the CAX4 elements especially around contact surfaces and areas of expected peak stress. It will also involve the introduction of special geometric lines to be used in the calculation of forces induced in the connector due to 'tightening', or application of make-up torque, on the connector and the introduction of external axial tensile force. This is discussed in a later section of this chapter.

Finally, the type and magnitude of axial loading selected for the introduction of tensile stress on the connector is decided and applied. The magnitude of the axial loading is determined in relation with the materials yield strength and internal stresses due to the application of preload.

The part of the connector geometry that requires some modification is the length of the body of the model itself. The lengthening is aimed at reducing the localized effect of the application of the axial load on the top of the connector. Figure 4-8 below shows the lengthened body, tooth area with element aspect ratio transition and the thread roots with the fine mesh around the roots area.

The introduction of sets, as shown below in Figure 4-9, is not only to enable the model to have variable meshing whereby the meshes get finer around the areas of interest but also to provide a means of moving the teeth area of one component relative to those of the other. The interference fit method of simulating preload which will be used in the investigation requires moving and overlapping one contact surface over the other and resolving the interference (overlap) using the Abaqus keyword command, '*SHRINK'.

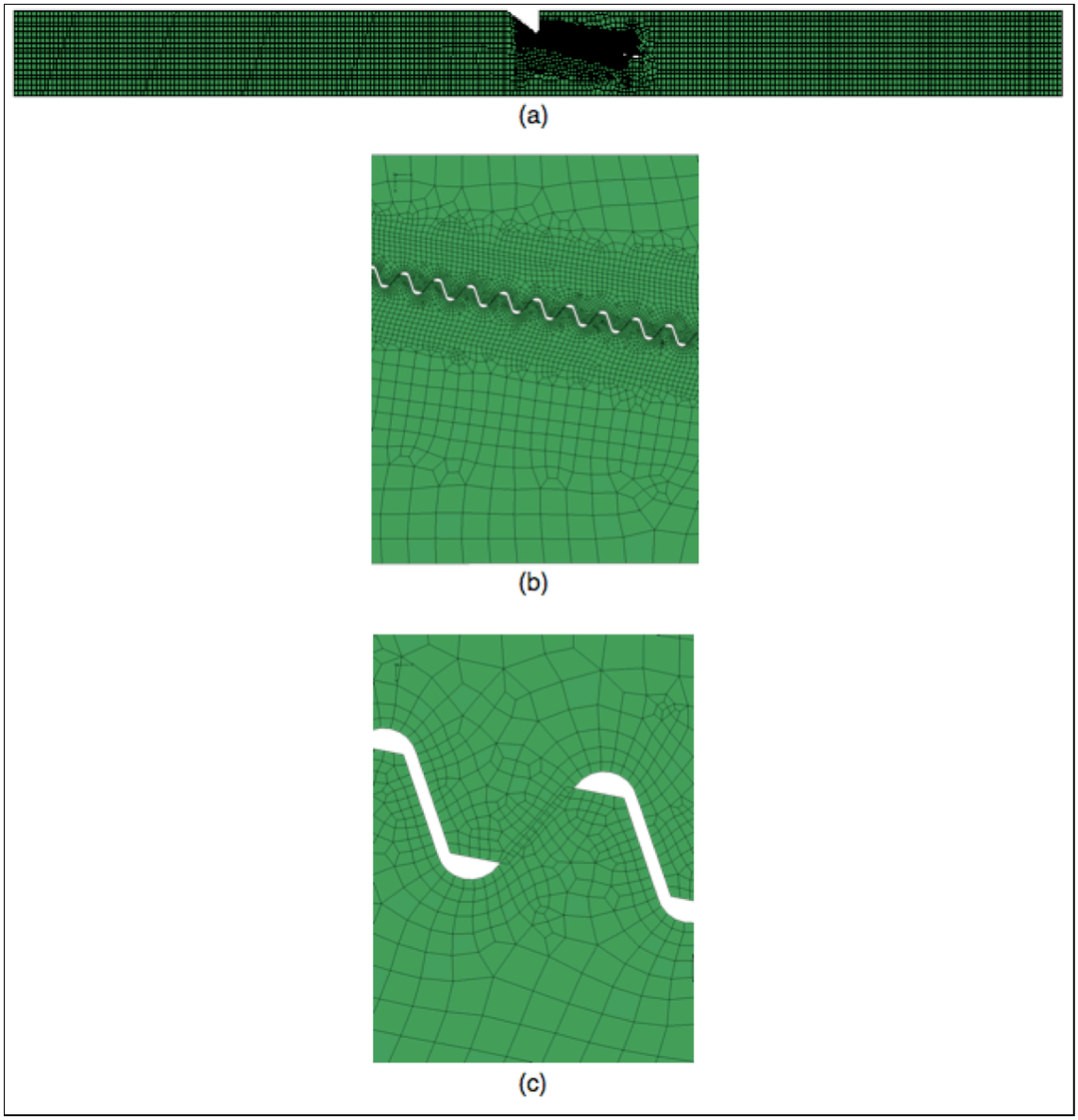

Figure 4-8: Final NC46 Mesh

Finally, unlike the mesh generated model which uses concentrated loading (Keyword: *CLOAD) on nodes at the top of the model to apply the axial pull, the final model will use a distributed pressure load (Keyword: *DLOAD) in order to avoid infinite stresses at the nodal point of load application that are expected with a concentrated force.

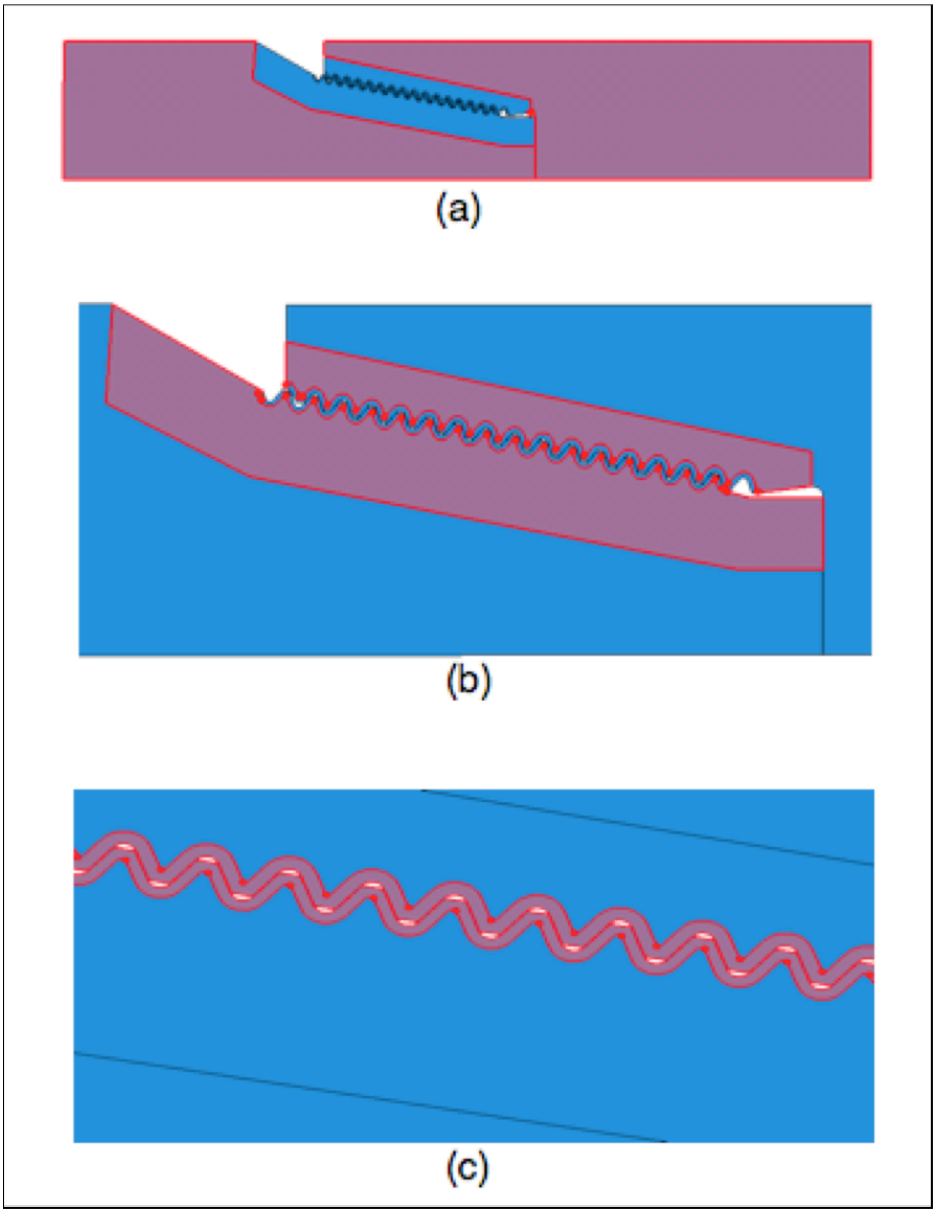

Figure 4-9: Sets: Body (a), Near Teeth (b) and Teeth (c)

4.2.2.2 Modeling with Axisymmetric Elements

The model using quadrilateral axisymmetric elements (CAX4) the freedom to move in the axial (Z) direction only. This is because the axisymmetric elements sweep out a full circle and the hoop stiffness of the connector will resists any tendency to move in the radial (r) direction and/or rotate about the (θ) direction. This is shown in Figure 4-10 below.

The FEA codes understand that each quadrilateral axisymmetric element face (CAX4) represent a complete ring that extends 360^{o} about a given axis. The ring is only free to move in the axial (z) direction. Attempt to move an element in the radial direction will only expand the ring and cause stress in the ring from that movement. The axial direction is therefore a direction of rigid body motion, which means the model is free to move in the axial direction but it is constrained in some way not to move.

The CAX4 element simulates a three-dimensional model swept about an axis for all values of theta, ideal for the modelling a threaded connector.

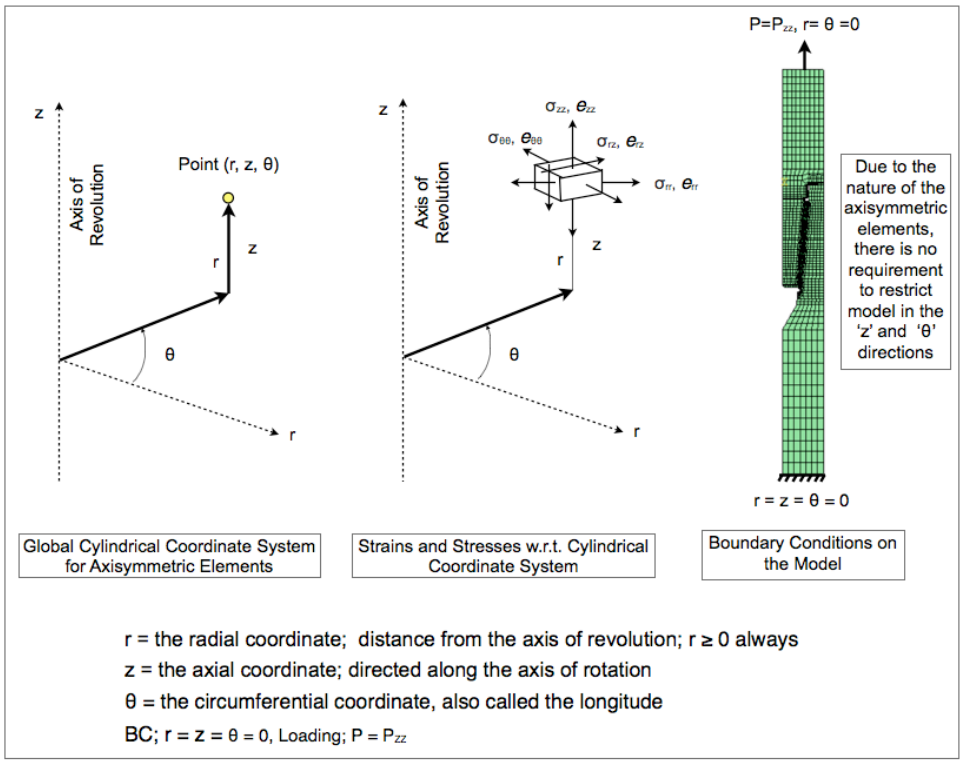

Figure 4-10: Boundary Conditions of Axisymmetric Elements [4.12]

4.3 Comparison and Validation of Results

The model developed was validated using earlier work undertaken by Tafreshi and Dover in 1993 [4.7]. In this validation exercise, the model was subjected to the same loading conditions as Tafreshi and Dover's model even though, as discussed, there will be no application of axial tension in unpreloaded connections in the actual investigation. Stress concentration factor, SCF, values at the root of threads are observed and reported for the pin and box components of the connection.

As shown in from Figure 4-11 below, the high SCF values at the first thread root, which is the last engaged thread, LET, of the pin, observed by Tafreshi and Dover and predicted from the literature and numerical investigations, was replicated within minor margins of error by the FEA model developed for this work. The model shows that in the unpreloaded case a peak SCF of about 12.9 is observed against the 15.10 observed by Tafreshi and Dover. While none of the input parameters in the simulation such as the applied external loading were modified, the lower SCF at the LET in the unpreloaded FEA model can be attributed to the change in contact algorithm and the variable mesh seeding that ensures, as recommended by NAFEMS, the professional body for finite element practitioners, that a finer mesh is used at the thread roots or areas of peak stress [4.13].

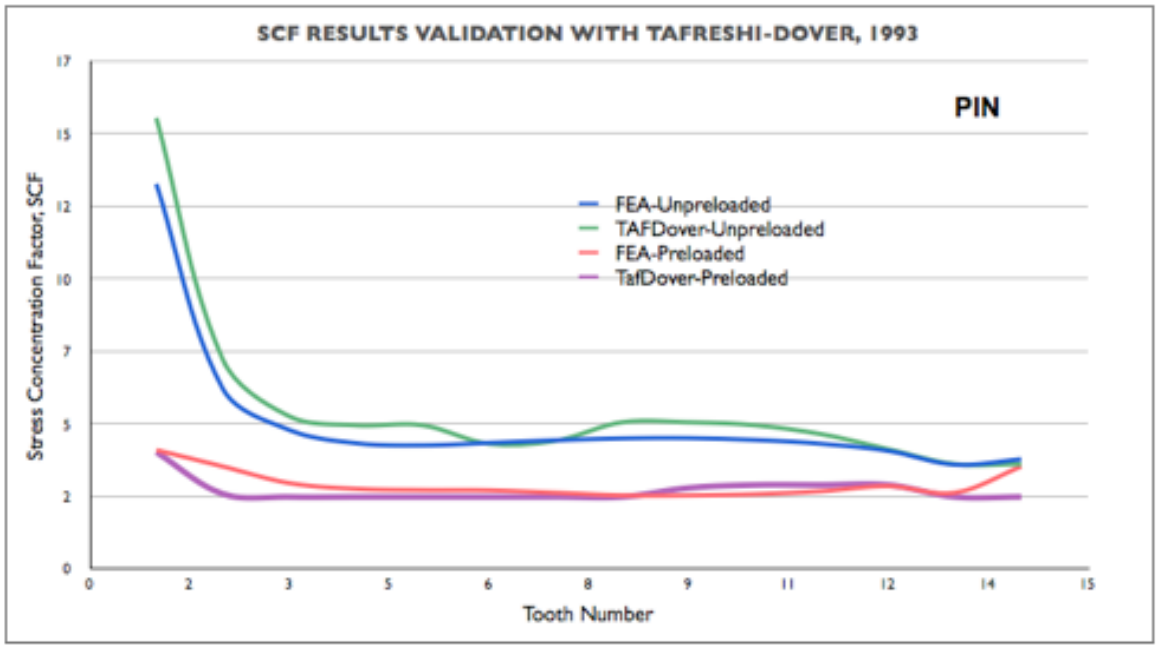

Figure 4-11: Validating Pin SCF Value: FEA and Tafreshi-Dover

Similar to the expected physical behaviour described, stress concentration factor values in a preloaded member will be lower than those in an unpreloaded member. Both the pin and box exhibit high SCF values across all teeth in the presence of axial loading and absence of preload. It is an expected physical attribute of the connection that because of the introduction of compressive stresses in a preloaded member, there will be a drop in peak tensile stresses due to the application preload. Just like the Tafreshi and Dover model, the 2-D axisymmetric FEA model exhibits this attribute in both the pin and box threads.

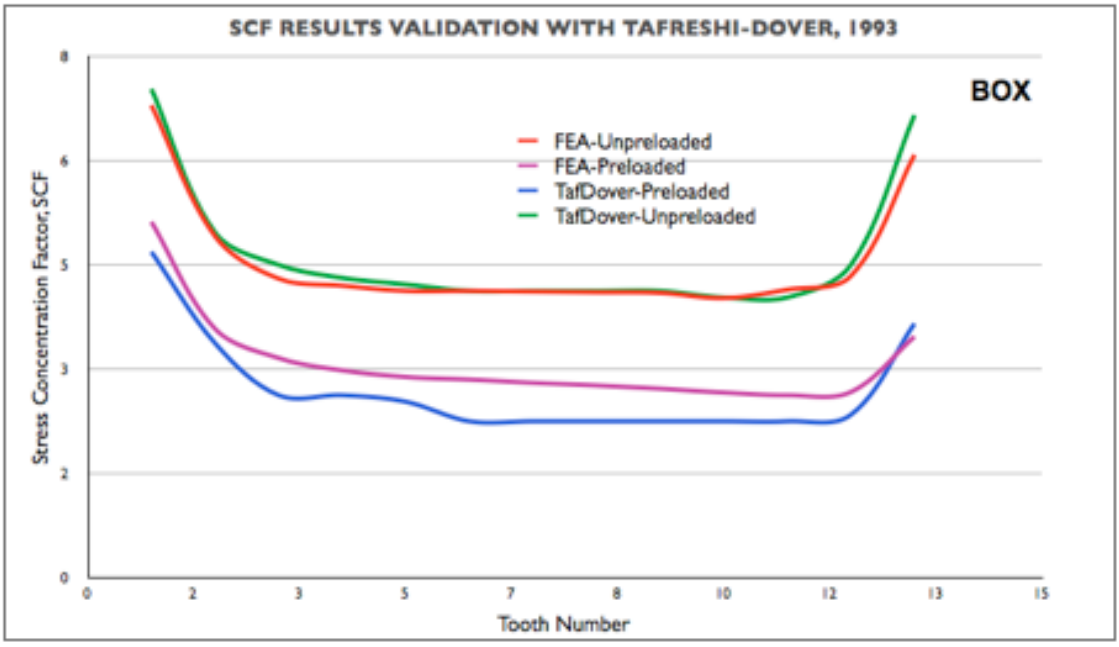

Figure 4-12: Validating Box SCF Value: FEA and Tafreshi-Dover

Figure 4-11 and Figure 4-12 above show the results from comparing the 2-D FEA model to the results obtained by Tafreshi-Dover. Conclusively, it can be seen that the use of surface contact modelling in the analysis software can be used to replace gap elements in the analysis of stresses and loads in 2-D axisymmetric FEA model. The enhanced meshing in the model also provides the analyst with more flexibility as to where to use fine or coarse mesh in optimizing the model.

It is important to note that both investigations are but an approximation of the complex stress regimes that occur in actual threaded connections. They both do not take into account the existence in an actual model of a helix and a thread run-out region.

4.4 Connection Nomenclature Used in this Work

The nomenclature used in this work is shown graphically below. The female component of the connector is termed the BOX while the male component is termed the PIN. The abutment, where the top pin of the pin meets with the top of the box, is the termed the SHOULDER. The locations of peak stress in each component in the analysis of threaded connections is the last engaged tooth of the component. The last engaged tooth is termed the LET. The conventions used in numbering the pin and box threads is to count downwards on a made-up connection. Connections made up on the drill floor have the box facing up while the pin 'stabbed' into the box. As such, from the aforesaid convention, the LET of the pin is at the first engaged tooth of the pin while the LET of the box is at the last engaged tooth of the box. This is shown graphically in Figure 4-13 below.

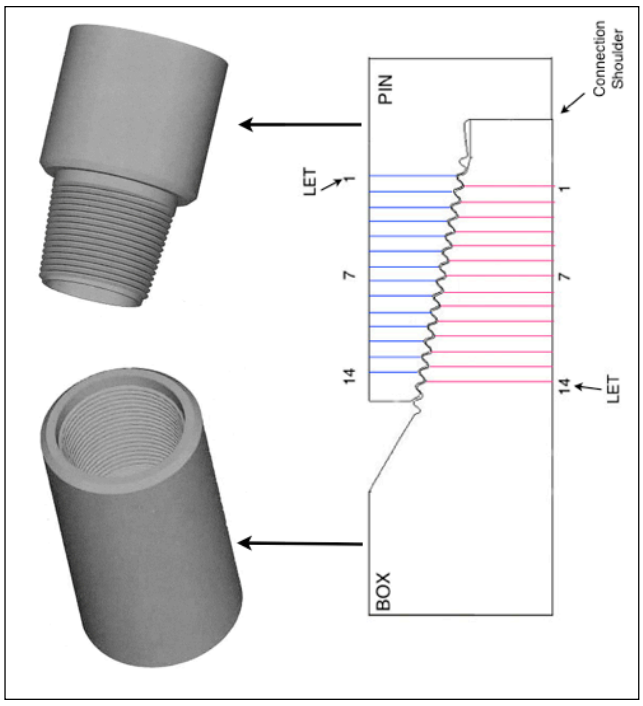

Figure 4-13: NC46 Threaded Connection Nomenclature

4.5 Loads and Stresses on a Threaded Connector

4.5.1 Numerical Determination of Thread Root Stress

Using the principles of mechanics and the Bernoulli-Euler beam theory, a formula can be derived to calculate the total stress on the root of the pin and box components. The formula will take into consideration the three stress components acting on the root, namely; the bearing (or direct) stress, bending stress and shear stress. However, it should be noted here that the use of the Bernoulli-Euler equation is but an oversimplification of the of the stress state of a threaded connection. This simplification lends itself to 'field' use where a quick answer is sought to determine the effect of loading on a member. This method is not suitable for detailed engineering design and research work.

From the dimension of the thread geometry, we can arrive at the correct inputs for these formulae. The thickness of the cantilever (as an input in the Bernoulli-Euler equation) is related to number of teeth in the connection.

Dimensions of the NC46 Connector	
Outside Diameter, OD	0.15875 m
Internal Diameter, ID	0.08255 m
Mean Thread Diameter, d_m	0.10373 m
Diameter at Thread Root, d_r	$\approx$ 0.10373 m
Thread Pitch, P	0.00633 m
Thread Depth, h	0.0055 m
Width of Screw at Root, b	3/4 of P = 0.0047475 m
Threads Engaged, n	13

Table 4-1 Geometric Dimensions of the NC46 Connector

The total stress on a threaded connection can be found by calculating and summing up the three main stress components; namely, the bearing stress, the bending stress and the shear stress;

$$\sigma_{bearing} = \frac{F}{A} = \frac{F}{\pi . d_m . h . n} \quad \text{.....(4.1)}$$

$$\sigma_{bending} = \frac{My}{I} \quad \text{.....(4.2)}$$

where the moment is,

$$M = \frac{F.\,h}{2} \quad \text{.....(4.3)}$$

the distance of the centroid is,

$$y = \frac{b}{2} \quad \text{.....(4.4)}$$

the second moment of area is,

$$I = \frac{\pi.\,d_m.\,n.\,b^3}{12} \quad \text{.....(4.5)}$$

Therefore, eq. (4.2) becomes

$$\sigma_{bending} = \frac{F.\,h}{2}.\left(\frac{12}{\pi.\,d_m.\,n.\,b^3}\right)\frac{b}{2} = \frac{3.\,F.\,h}{\pi.\,d_m.\,n.\,b^2} \quad \text{.....(4.6)}$$

Finally, the shear stress due to the applied load and the geometry of the connection is

$$\tau = \frac{3.\,F}{2.\,A} = \frac{3.\,F}{2.\,\pi.\,d_r.\,n.\,b} \quad \text{.....(4.7)}$$

where; F = force applied on the connection, A = area on which the force is applied, d_m = mean diameter of the connection, d_r = diameter of the connection

at the tooth root, h = thread depth, M = moment of a force acting on the flank of a tooth, y = distance of the centroid to the extreme fibre of the tooth, I = Second moment of area, n = number of threads engaged. The total stress at the thread root is calculated as

$$\sigma_{bearing} = \sigma_{bearing} + \sigma_{bending} + \tau \text{.....(4.8)}$$

If we apply an external axial tensile load of 2KN on the connector then ignoring the effect of the taper and assuming that the mean thread diameter d_m is same as the diameter at thread root, d_r then by substituting in eqs. (4.1), (4.6) and (4.7), the calculated values of the three stress components above is;

$$\sigma_{bearing} = \frac{F}{A} = \frac{F}{\pi . d_m . h . n} = \frac{2E03}{\pi \times 0.00010373 \times 0.005 \times 13} = 0.00472 MPa$$

$$\sigma_{bending} = \frac{3 . F . h}{\pi . d_m . n . b^2} = \frac{2E03 \times 0.0055}{\pi \times 0.00010373 \times 13 \times 0.004745^2} = 345.78 MPa$$

$$\tau = \frac{3 . F}{2 . \pi . d_r . n . b} = \frac{3 \times 2E03}{2 \times \pi \times 0.10373 \times 13 \times 0.0047475} = 0.06031 MPa$$

Substituting the above values in eq. (4.8), the total stress at the root of the connector when an axial tensile load of 2000N is applied is;

$$\sigma_{Total} = \sigma_{bearing} + \sigma_{bending} + \tau = 345.785 MPa$$

However, as can be recalled from the discussion in Chapter 2, an alternative

formula, the Kelley-Pederson-Heywood equation [4.14] could also be used for the determination of the maximum stress at the root of the thread. This formula calculates the root stress induced by a load acting on a very short cantilever beam such as gear tooth, saw tooth or screw thread.

Through photoelastic study, Heywood was able to show that the total or combined stress, $\sigma_{combined}$, at the root of the thread is obtained through the formula in eq. (4.9) below, which is the maximum stress value obtained as the combination, (not algebraic summation), of the maximum bending stress and the maximum axial stress at the base of the fillet [4.15].

$$\sigma_{Combined} = \frac{\sigma_b + \sigma_a}{\left[1 + c\left(\frac{\sigma_b}{\sigma_a}\right)\right]} \quad \text{.....4.9}$$

Where σ_a is the axial stress, which is a product of the axial load and the stress concentration factor, SCF, at the root. The SCF at the root can be equated to 3 because the axial stress is expected to act at approximately the centre of the root of the tooth. c is equal to $c = \left[(60 - \alpha)44\right]^2$ (where α is the thread angle) and σ_b is the bending stress as obtained using the Kelley-Pederson-Heywood formula as shown in eq. (4.10) below.

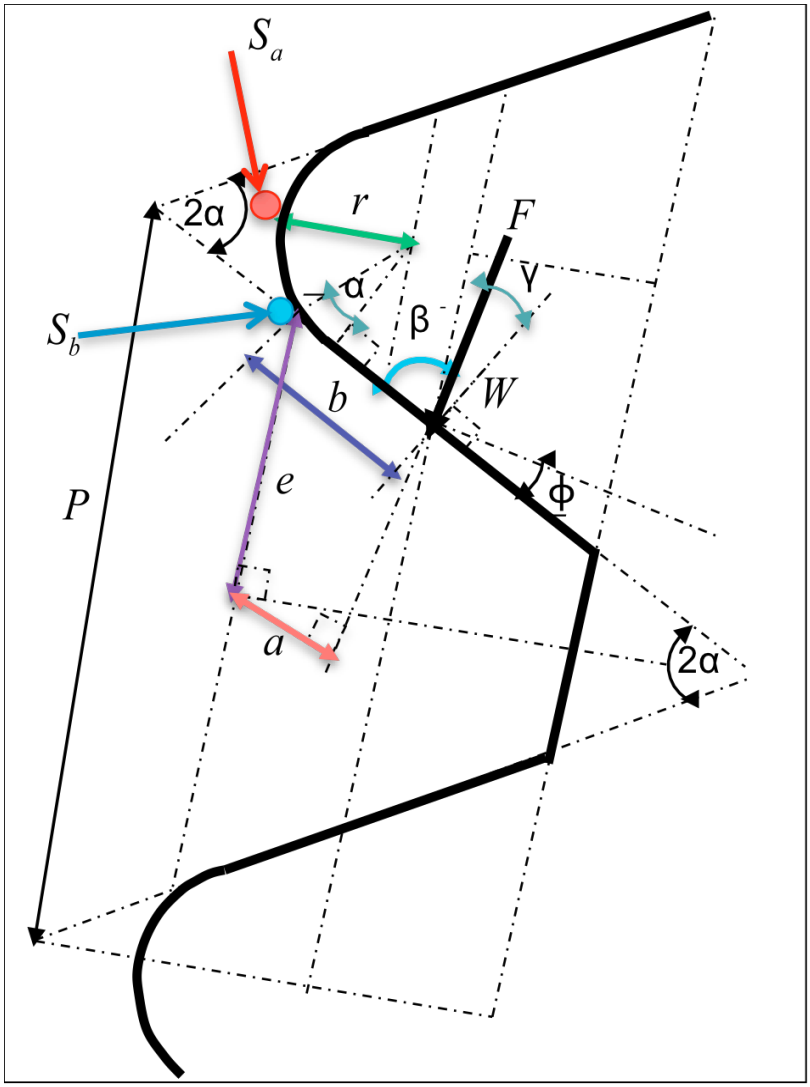

Figure 4-14: Application of the K-P-H Formula for the NC46 Connector

$$\sigma_{Bending} = \left[1 + 0.26\left(\frac{e}{r}\right)^{0.7}\right]\left[\frac{F}{t}\right]\left[\frac{1.5a}{e^2} + \frac{Cos\beta}{2e} + \frac{0.45}{(be)^{\frac{1}{2}}}\right] \quad \text{.....4.10}$$

Using the original model sketch of the NC46 connector the input values for the Kelley-Pedersen-Heywood formula shown above were obtained for the aforementioned quantities: F = force applied on the connection = 200N, t = thickness of the cantilever - unrolled length of the thread = circumference of thread (mean thread radius = 184mm) = 1156.1mm , γ = the friction angle

which is the arctangent of the coefficient of friction value = arctan (0.08) = 4.5°, β = force angle = 90-γ = 90° - arctan (0.08) = 90° – 4.5° = 85.5° , e = length of line perpendicular to the beam axis from the root to the thread axis = 2.28mm, a = length of line from mid-section of the base to the load line = 0.28mm, b = length of line from root of thread to the point of action of force = 1.46mm, r = thread fillet radius = 0.97mm. These values were obtained by using a sketching and dimensioning tool in the FEA software, Abaqus.

Subtituting the values obtained from the thread geometry into the Kelley-Pedersen-Haywood equation, we have;

$$\sigma_{Bending} = \left[1+0.26\left(\frac{e}{r}\right)^{0.7}\right]\left[\frac{F}{t}\right]\left[\frac{1.5a}{e^2}+\frac{Cos\beta}{2e}+\frac{0.45}{(be)^{\frac{1}{2}}}\right]$$

$$= \left[1+0.26\left(\frac{2.28}{0.97}\right)^{0.7}\right]\left[\frac{2.0\times 3}{1156.1}\right]\left[\frac{(1.5\times 0.28)}{2.28^2}+\frac{Cos86}{2\times 2.28}+\frac{0.45}{(1.46\times 2.28)^{\frac{1}{2}}}\right]$$

$$= 0.2622 MPa$$

Since, the constant, $c = \left[(60-\alpha)44\right]^2 = \left[(60-30)\times 44\right]^2 = 1742400$

Then the combined stress is equal to

$$\sigma_{Combined} = \frac{\sigma_b + \sigma_a}{\left[1+c\left(\frac{\sigma_b}{\sigma_a}\right)\right]} = \frac{0.2622+600}{\left[1+1.7424\left(\frac{0.2622}{600}\right)\right]} = 600.3 MPa$$

The above calculation takes into consideration the geometry of a single thread. The Kelley-Pederson-Heywood formula is used to calculate the stress at the root of a single tooth. Because we are looking at a single thread, the two formulae do not take into consideration the gradual reduction of the intensity of the load as we move farther away from the loaded face of the connection or the shoulder.

The amount of load “seen” by the tooth closest to the loaded face of the pin, the last engaged tooth (LET) in this case is 30% of the total applied load. In other words, the load seen by successive teeth decrease proportionally with their distance from the loaded face of the connection. To obtain the stress at the root of each tooth, the load “seen” by each tooth flank must be determined and used as the input load value for the stress calculation of each individual tooth. This can only be iterated if the load at each thread root can be precisely determined. However we can predict with mathematical certainty that unless a thread root farther away from the loaded face is mechanically damaged and thus a location of higher stress concentration factor is introduced in the tooljoint at that location, the failure will be initiated at the point of highest stress concentration factor, which we have determined to be at the LET of the tooljoint.

However, since in the Kelley-Pedersen-Heywood formula we are considering stress due an axial load acting at a point in a single thread root, and since the load is assumed to concentrate at a unit area (mm^2) then the stress at that point can be assumed to be the load (200N) acting on a millimeter square of the thread root, that is 200 MPa. Furthermore, since the load is acting axially, the stress can be said to concentrated at the root of the thread which forms a circle whose radius is the fillet radius, r, of the thread. Because of this geometry, the stress concentration factor (SCF) at that location can be assumed to be that of a circular hole in a loaded plate [4.16]. The applied axial load of 200N acting

on a unit area (1 mm^2) on the thread flank when multiplied by the SCF of 3 will give a stress 600 MPa at that location.

The only difference between the derived formula and the Kelley-Pederson-Heywood formula is that in the derived formula the load is assumed to be applied across the length of the unrolled teeth of the entire thread where it acts as a cantilever. While in the Kelley-Pederson-Heywood formula the load is applied at a point in a single root of a tooth in the thread.

The importance of the finite element tool in this regard is the ability to discretise the entire connection and calculate the peak stress values at each root node and as such determine the value of stress at each root and thus identify the location of peak root stress. This discretisation process will automatically take into account the complicated geometry of the connection and, using an optimized mesh, load paths and stress values at each thread root can then be obtained.

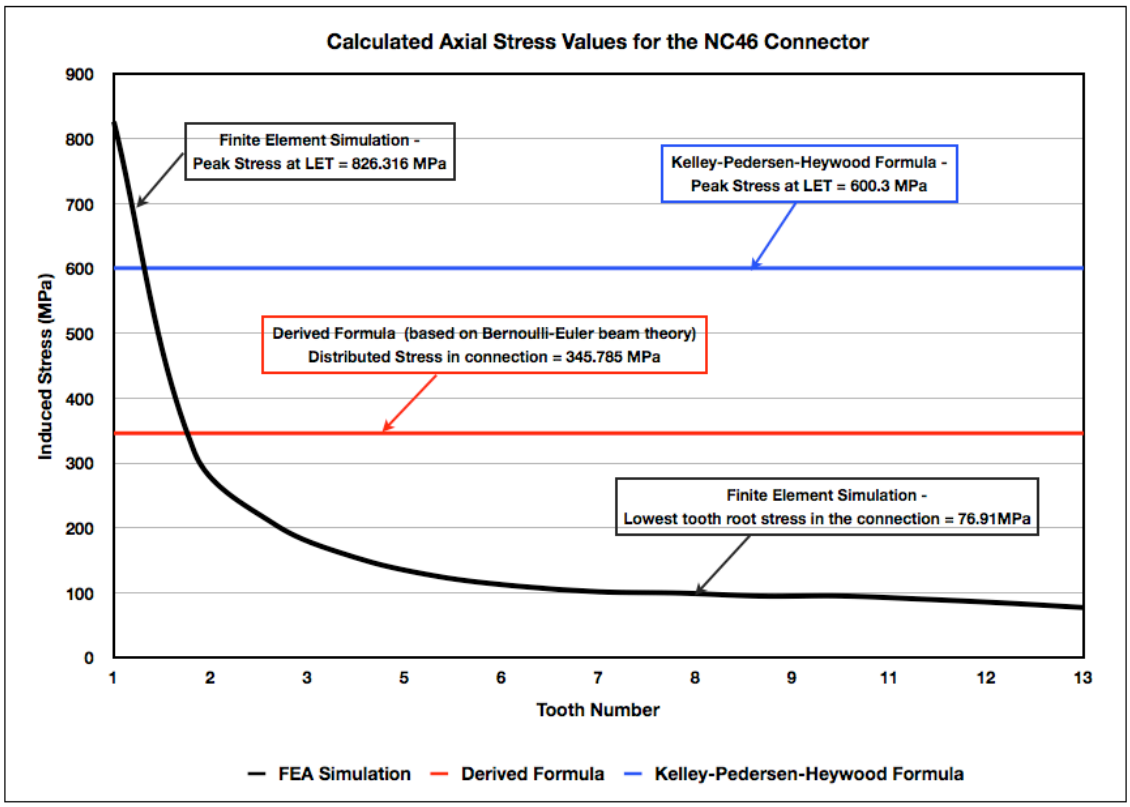

Figure 4-15: Numerical and FEA S_{yy} Values for the NC46 Connector

Figure 4-15 above shows the results obtained using the two formulae compared with the finite element results for the S_{yy} axial stress values at the thread root for an NC46 connector.

The FEA model shows a range of root stresses between **826.316 MPa** in the root of the last engaged tooth (LET) and **76.91 MPa** in the root of the 13th tooth. The value of the individual tooth stresses is shown as the black line.

Using the classical beam theory (Bernoulli-Euler), the values obtained for a representative average tooth root stress is lower at **345.785 MPa.** This is higher than the average FEA stress in the connection (**182.77 MPa)** but lower than the FEA S_{yy} stress value at the LET. But since it can be safely assumed that most of the 2000N load is seen by the LET then it can be said that the stress value obtained using the classical beam theory can be assumed to be acting at the LET and as such the peak stress in the connection according to this formula.

That makes it about 40% of the value obtained from an FEA simulation of the same loading scenario at the LET.

The value obtained using the Kelley-Pedersen-Heywood formula for the same representative tooth stress is **600.3 MPa**. Following the same assumptions as above, that equates to slightly more than 73% of the S_{yy} value at the LET that was obtained from the FEA simulation.

The low value obtained from the classical beam theory is the lowest of three at **345.785 MPa**. This can be attributed to the few assumptions made in the calculations above. Principal of these assumptions is that the load is not concentrated on the flank of one tooth, that according to Kelley-Pedersen-Heywood formula can be said to bear the applied load singularly and directly, but instead it is distributed across the entire length of the thread which is assumed to be acting as cantilever or a bank of cantilevers [4.17], [4.18]. The effect of the loaded shoulder (abutment) was also not taken into consideration. The other reason is that the effect of taper and helix was not taken into consideration.

At **600.3 MPa,** the root stress value obtained using the Kelley-Pedersen-Haywood formula is also lower than the peak stress at the same location as obtained using the FEA simulation. This is expected because a later work that included the use of fatigue tests by Weigle, Laselle and Puertell proved, through experimentation, that the Kelley-Pedersen-Heywood formula under-predicts the actual stress values obtained [4.19].

The numerical analyses done with the two formulae above both ignore the existence of helical and taper angles of the physical NC46 connection. The taper, but not the helix, is incorporated in the FEA model. But in both the numerical analysis and the FEA analysis the same geometric dimensions were used and a load of 2000N was used to apply axial tensile pull on the connector in the classical beam theory while a lower factor load of 200N was used in the

FEA analysis and the Kelley-Pedersen-Heywood formula to take account of the reduced dimensions in the model used.

Another factor not considered in the above comparison is that, while it is possible to simulate an unpreloaded string numerically or using a computational analysis method such as FEA, it is not physically feasible to axially load up and retain the integrity of a connector without an internal load (preload) that ensures compressive and tensile contact loading of the individual teeth, and thus the integrity of the connection. Unlike oilwell drillstrings, most threaded connections in service perform service using nothing but preload without the need of an externally applied force. Application of an external axial load in a threaded connector without an internal load (preload) is bound to cause the parting of the connector at the abutment (shoulder) and thus render the integrity of the connection to nil.

The aim of the analysis above is to provide a comparison between the results obtained from a simple benchmark FEA study and results from two formulae that can be used to calculate stresses in the thread root. This is a 'first step' validation of the finite element model developed.

4.5.2 Preload on the Connector

Good make-up should create optimum preload conditions in the connection. This make-up will guarantee maximum connection reliability under applied static or dynamic loads. The relationship between contact friction, make-up torque and applied preload was well established in Farr's [4.20] and Brennan & Kare's [4.21] work where the coefficient of friction, μ, is shown to be a factor in the amount of torque required to produce a given preload value. As for the recommended μ values in actual drilling operations, the make-up torque values recommended for drillstring connections in API-RP7G were determined using a coefficient of friction of 0.08. Bailey et al. [4.22] undertook 20 comparative tests between lead-based, copper-based and zinc-based thread compounds

and arrived at coefficient of friction (μ) values ranging from 0.08 to 0.12 [4.23].

The coefficient of friction was also numerically shown, in the Kelley-Pedersen-Heywood formula in eq. (4.10) above, to affect the stress induced on the flank of tooth (or short cantilever) where the friction angle, γ, is said to be the arctangent of the coefficient of friction (μ) value.

Stress analysis on drill strings is undertaken so the results can be used in experimental and numerical operations such as in fatigue life calculations and as fracture mechanics input parameters. But stress analysis on drill strings is difficult because of the varying contribution of tooth geometry, tooth stiffness, connection stiffness and the role played by preload all add to the stress distribution profile and these contributions are not easily quantifiable. Any method used in the simulation of load and preload application in the connector must take into consideration these challenges. As will be discussed below, while the application of load and subsequently obtaining stress, strain or displacement results may seem straightforward, simulating preload is a bit more complicated as it has to take into account that not only the materials in contact, but also the geometry of the connector and the presence (or absence) of a film of lubricant between the contacting surfaces, such as thread dope.

4.5.2.1 Earlier Contact Methods

Gap elements were used in the 2-D axisymmetric mesh generated by the FORTRAN77 program to model contact behaviour between nodes. Gap elements are multi-freedom (multi-point) constraints in which the value of the constraint is a function of the value of given nodal displacement components [4.24]. These elements were programmed to model load transfer between contacting nodes. Abaqus defines the clearance between gap elements, h, as;

$$h = d + n \times (u_2 - u_1) \text{.....} 4.11$$

where d is the initial separation distance, n is the contact direction, u_2 and u_1 are the total displacements at the first and second nodes of the gap element. When h becomes negative the gap elements are closed and the constraint $h = 0$ is imposed.

While earlier FEA work used of gap elements in contact simulation, the writer believes that better contact algorithms in the current versions of almost all FEA codes have now superseded the use of gap elements in contact simulation. Using this new contact simulation method, load transfer between nodes and elements can be modelled using an algorithm that recognises one surface as the slave and the other as master [4.25]. The Abaqus FEA code enforces contact by forming equations involving groups of nearby nodes.

The contact algorithm in Abaqus/Standard, the FEA code used in this work, is built around the Newton-Raphson technique. The technique examines the state of all contact interactions at the start of each increment to establish whether slave nodes are open or closed. If a node is closed, the code determines whether it is sliding or sticking. It then applies a constraint for each closed node and removes constraints from any node where the contact state changes from closed to open after which it carries out an iteration and updates the configuration of the model using the calculated corrections [4.6].

In this work, the application of preload in the simulation was obtained using the interference fit method because it best mimics the actual load transfer scenario in the physical connector. The slight overlap (or interference) introduced that is resolved using the *SHRINK Abaqus command uses displacement control to mimic the force that is introduced using torque to load up the connector.

4.5.2.2 Methods of Applying Preload

Preload added to a connector will introduce tensile/compressive mean stress which, in turn, will reduce the alternating stresses and hence increase the

fatigue life of the connector. In real-life applications, without preloading the connector, there will be relative movement of the two parts (pin and box) that make up the connector which will give rise to galling, fretting and excessive wear in the tooth and shoulder area [4.27].

There are four (4) main methods of applying preload in the finite element analysis of a bolted assembly. These methods are:

4.5.2.2.1 Direct Force on bolt and nut

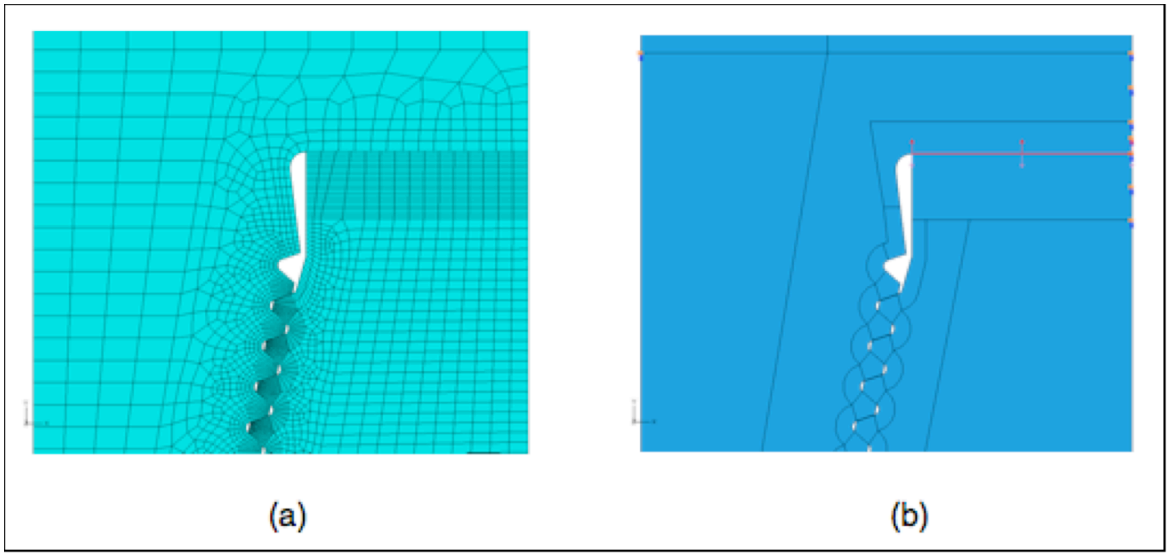

Figure 4-16: Direct Load on the Shoulder of the NC46 Model

In the case where forces are applied directly to one of the two contact areas (the shoulder, in this case) as shown in Figure 4-16 above. The forces, which are equal and acting in opposite directions, are expected to induce a compressive force that simulates preload on the two contacting surfaces.

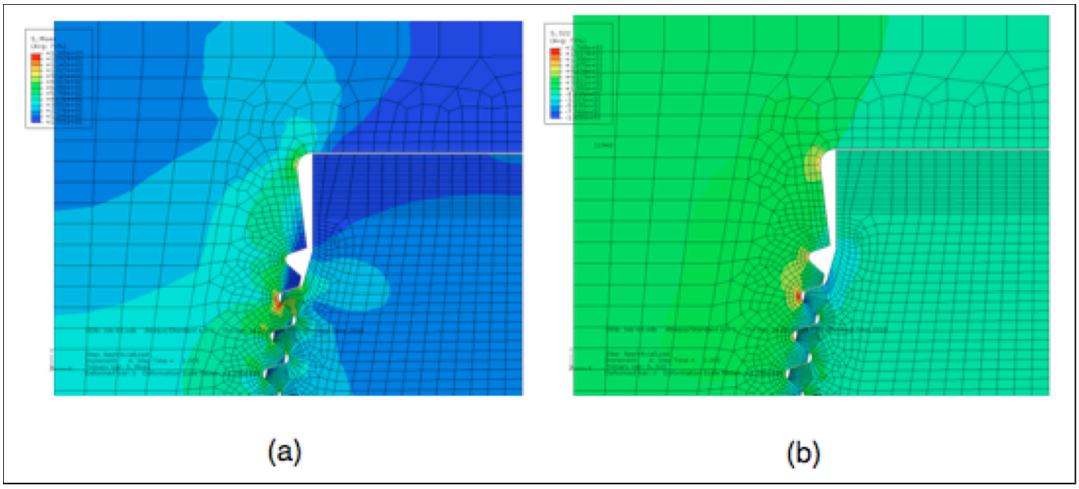

Figure 4-17: Stress Contours for Direct Load on Shoulder

It can be seen from Figure 4-17 above showing the S_{yy} and the von Mises stress contours that while appreciable stress is shown around the shoulder and the pin LET (from Figure 4-18b - von Mises), the overriding effect is the high compressive stresses (in blue) at the shoulder as can be seen from Figure 4-18a.

A closer examination of the effect of this type of preload application to the stress distribution at the roots can be seen from Figure 4-18 below which shows the SCF distribution in the root of the teeth of the model in the presence of a direct preload applied on the shoulder. It can be seen that the effect of the preload force when applied in this manner is restricted to the LET and the few (two or three) teeth downstream from the LET.

This behaviour is not in concordance with the behaviour observed using either theoretical or other analytical methods of applying preload. Neither is it supported by any earlier work done.

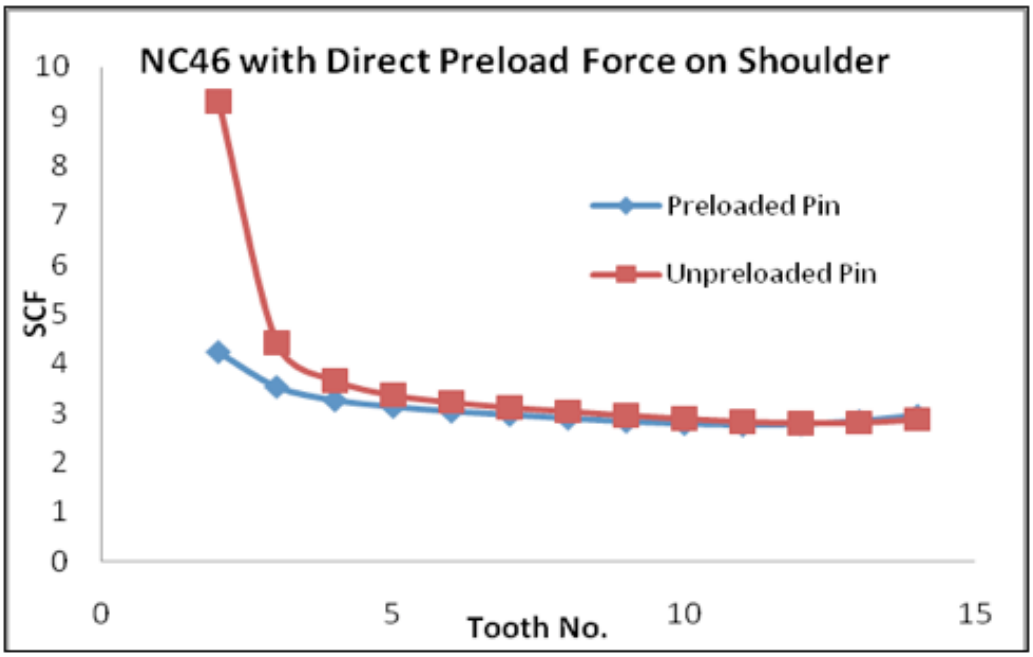

Figure 4-18: Preload SCF in NC46 Connector with Direct Load on Shoulder

4.5.2.2.2 Thermal Stress Method

Thermal loading can also be used to load up the structure at a location near the abutment (shoulder) to create a thermal stress on the location which will, in turn, exert a displacement. Depending on where and how the loading is applied combined with knowledge of the elastic and thermal expansivity properties of the material, a force of a given value can be applied at the shoulder to simulate preload.

Using the developed 2-D axisymmetric model of the NC46 connector, a location just below the shoulder was picked on the box as shown in Figure 4-19 (a) and (b) below.

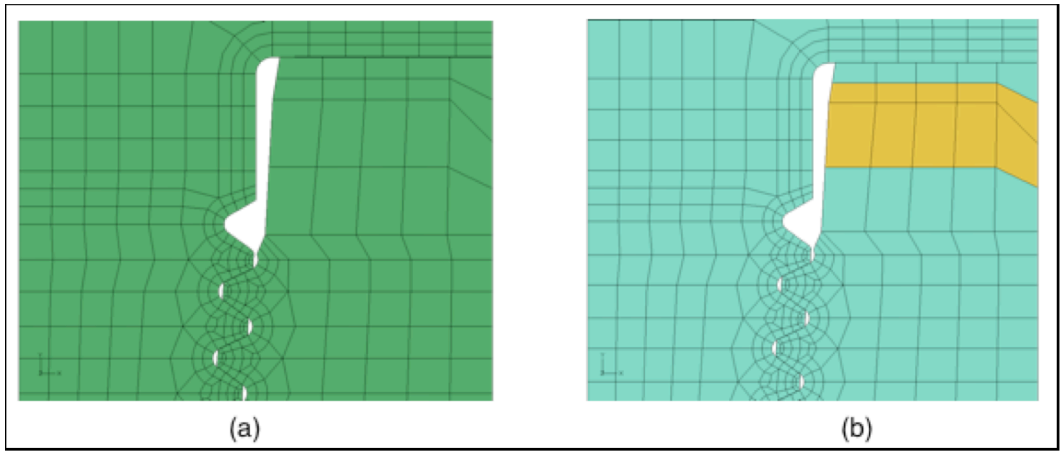

Figure 4-19: Thermal Load on the NC46 Model Showing Thermal Strip (b)

An external tensile load of 20 MPa was applied to the top of the pin to simulate an externally applied load while the Coefficient of Friction (μ) was set at 0.07. In all other material parameters, such as Coefficient of Thermal Expansion (α = 1.2 x 10^{-5}/^{o}C), Modulus of Elasticity (E = 203 x 10^{3} MPa) and Poisson Ration (υ = 0.3) values for steel were used. Results for S_{yy} values were analysed at the pin LET to observe the effect of the application of preload using this method. As can be seen from the stress contours in Figure 4-20 below, while there is appreciable global effect to the S_{yy} values, the most noticeable effect was observed at the point of the application of the load.

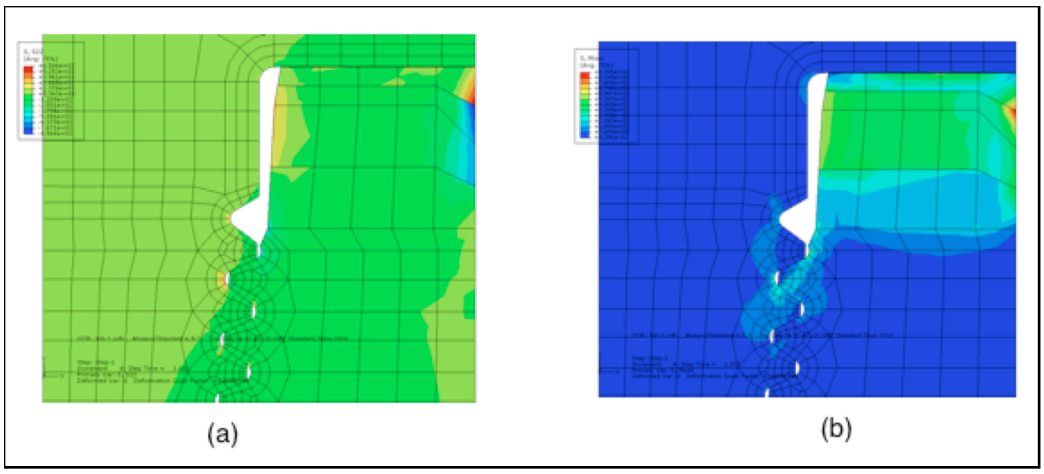

Figure 4-20: Thermally Loaded Connector: S_{yy} (a) and von Mises Stress (b)

Baragetti, while discussing the effect of taper variation on the load distribution of a NC50 connector, simulated preload through the application of thermal stress on a strip of elements located in a position as to have the effect of loading up the connector on the shoulder thereby obtaining a preload force in the abutment [4.28].

In order to obtain the optimum make-up torque value, various FE analyses on the model were undertaken in which the input thermal stress (temperature) was progressively increased to obtain the required preload value. With the knowledge of the relationship between the induced axial load and preload and also that of axial load and make-up torque, it was found to be possible to simulate the application of make-up torque by varying the temperature.

Figure 4-21 below shows the values obtained from the experiment described above. For validation, the values obtained for the NC46 connector are then compared to those obtained by Baragetti.

Application of thermal load on connector shoulders remains a theory that can be determined through numerical calculations or finite element simulation but practical applications of it, within the limiting envelop of the materials' physical and elastic properties, remains impractical because temperatures far in excess of the materials' melting point have to be used in order to obtain any usable result.

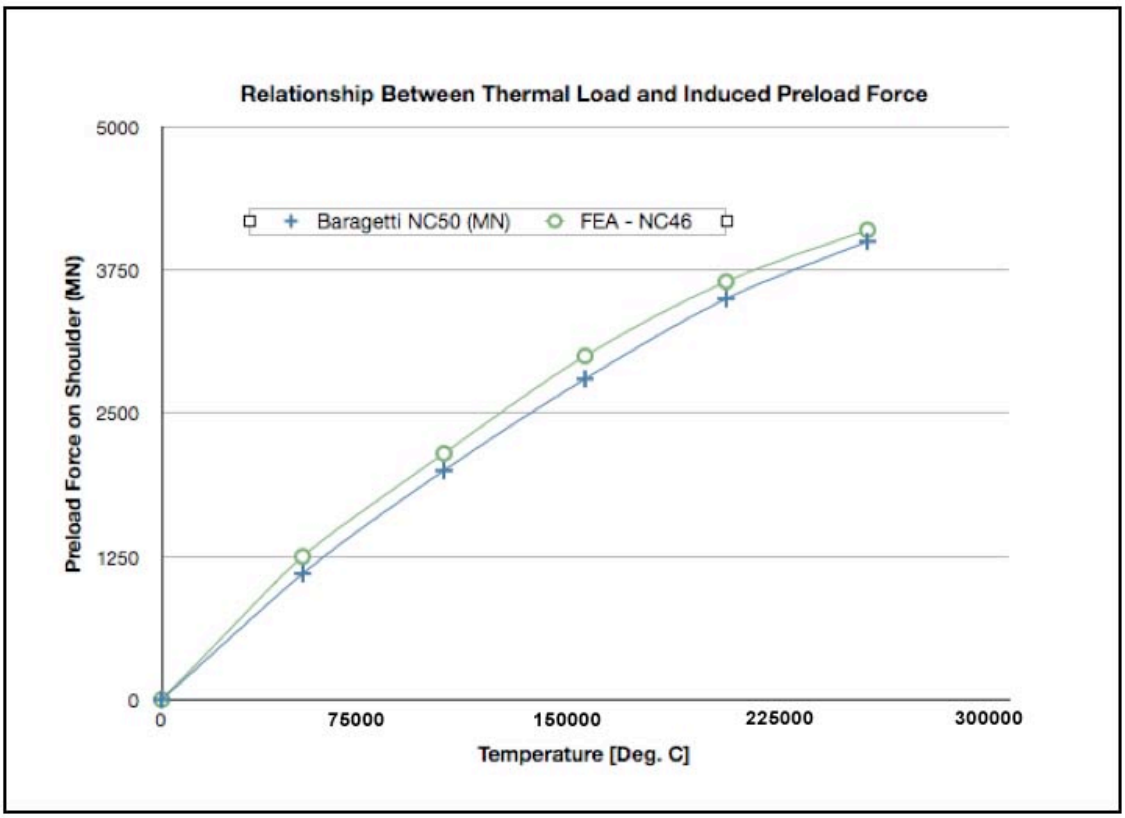

Figure 4-21: Thermal Stress Plotted Against Preload Force on Shoulder

4.5.2.2.3 Pretension Surface Method

This preload method replicates actual preloading that occurs in practice when the pin is screwed up tight into the box. Since the pin in the computer model cannot be rotated in the box to apply make-up torque and tighten the connection, the threads can be moved in relation to the abutment (shoulder) faces. If the pretension force is too high the fasteners may yield or fail catastrophically and if it is too low it may compromise the integrity of the connection. An amount of load that will give the exact required preload must be estimated either through iteration with different load values or through the use of values used in an earlier similar work.

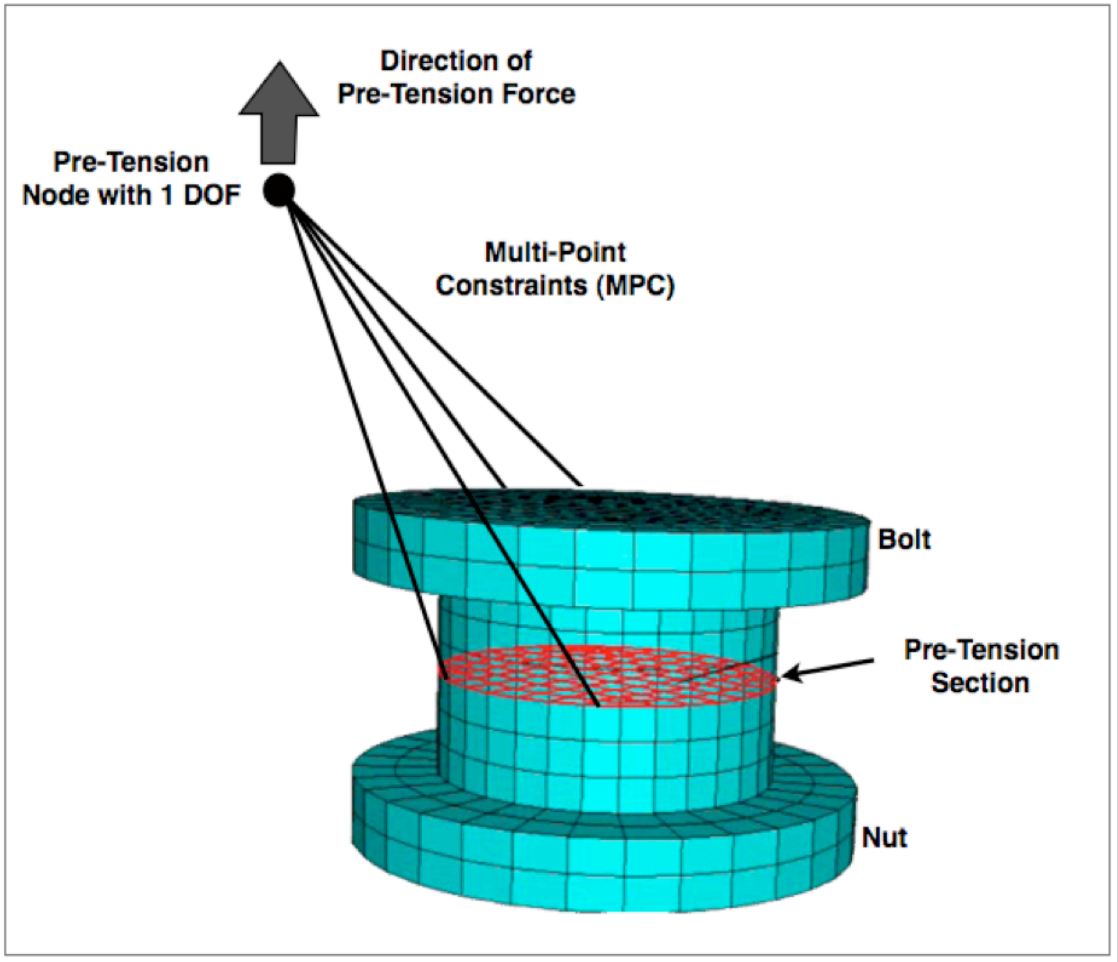

Figure 4-22: Application of Preload Using Pre-Tension Section Method

The Abaqus code command for the application of load in this method is *PRE-TENSION SECTION. This is used in conjunction with pre-tension node and a rigid element. The primary function of the rigid multi-point constraint (MPC) element is to link the pre-tension node to the pre-tension surface and transmit the single degree of freedom constraint to the pre-tension section. This keyword defines the tension or torque in the bolt. As it states, the tension is applied on an earlier defined cross-section at approximately the centre of the bolt shank. As shown in Figure 4-22 above, a pre-tension node is then created and connected to the identified section. The pre-tension node, which has only one degree of freedom, is mainly used to apply preload across the pre-tension section and maintain the tightening adjustment so that the load across the fastener may increase or decrease upon loading of the structure. A point load

applied in a direction normal to pre-tension section mimics the torque applied to connection, and the total force transmitted across the pre-tension section is the combination of the reaction force at the pre-tension node and any other concentrated force at the node [4.23].

The pulling force that creates the pre-tension is applied on the pre-tension node which has a single degree of freedom in the direction perpendicular to the pre-tension section. The pulling force on the node is transmitted to the pre-tension section by use of the rigid element described above using a multi-point constraint keyword, *MCP [4.29]. The basic process flow is shown in Figure 4-23 below.

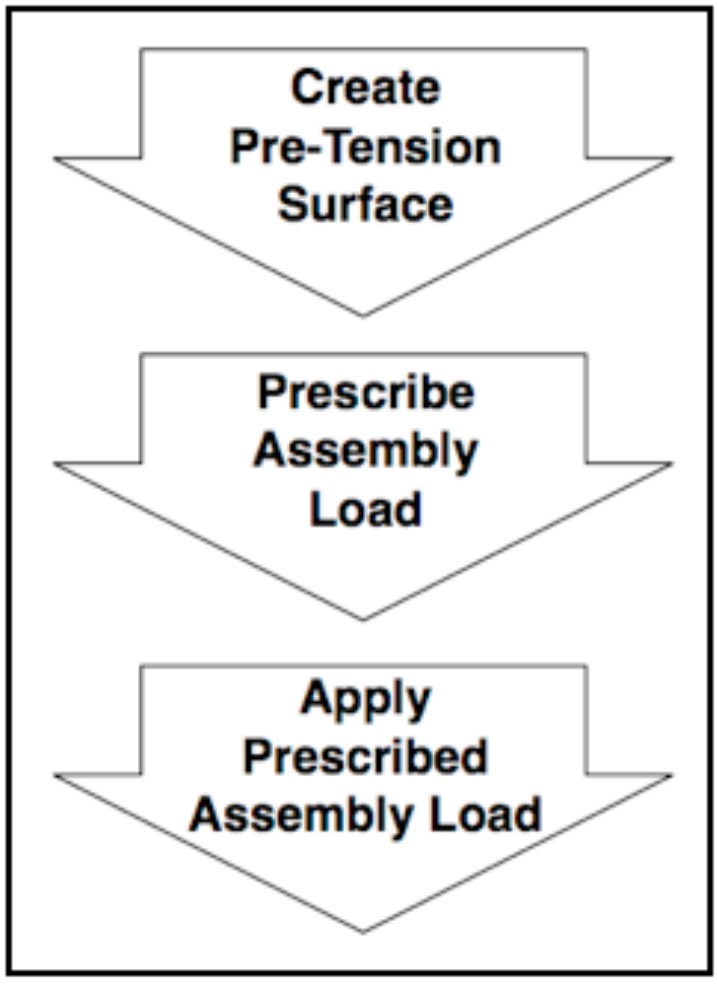

Figure 4-23: Process Algorithm for the Pre-tension Section Method

A set is created in the Abaqus code that consists of the four areas of the model

in contact, namely, the two shoulder surfaces and the two teeth area surfaces of the pin and box.

This method for the application of preload was used to validate the functionality of the 3-D model used in this work. An independent node was introduced into the model and used to apply both axial pull for tensile load and, later, another independent node was used to add rotational load to apply a bend on the model to simulate a dogleg.

4.5.2.2.4 Interference Fit Method of Applying Preload

Because of effects related not only the to the tooth and connection stiffness of the connector but also to its peculiar geometry, numerical and FEA modelling of a threaded connection is complex and values for simulation input are not easily quantifiable. Factors that may affect the construction of the model or the application of modelling input parameters need to be handled carefully. Geometry effects such as the presence of a helix, thread run-out, complex (and often times, different) thread root geometry, the control of load transfer across an abutment and the possible variation of coefficient of friction due to the presence of a lubricant film, or thread dope, between the contacting surfaces all contribute to the accuracy or not of simulation results obtained. Most importantly, unlike in the physical model, the connection cannot be tightened in the FEA model to a make-up torque value to obtain desired preload. The interference fit method achieves this through the resolution of overclosure (overlap) in the contacting parts of the model [4.30].

As such there is a need to formulate and use a preload method that take into consideration most if not all of the factors that may affect the accuracy of the simulation. The Interference Fit method takes into account the absence of both the helix and thread run-out in the model geometry.

Preload application in the 2-D analyses undertaken in this work was executed using the Interference Fit method. This preload method most closely replicates

actual preloading that occurs in practice when the pin is screwed tight into the box. Translating the threads of one of the connecting members (pin or box) in the axial direction in the presence of a force (axial or preload) while disallowing any movement in the abutment faces will result in the application of a preload force in the connector. This is demonstrated in Figure 4-24 below.

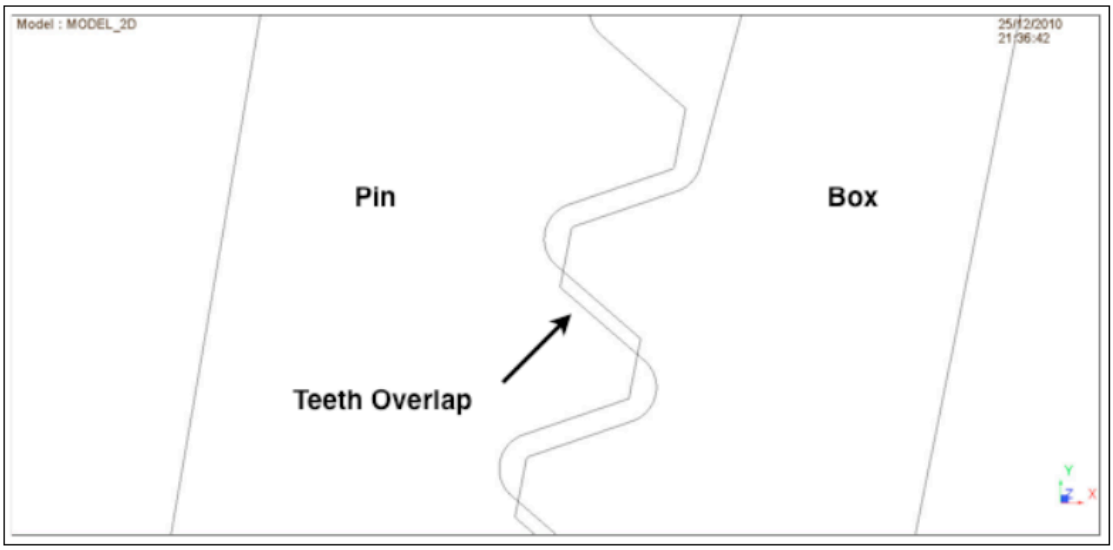

Figure 4-24: Interference Fit Overlap Between Pin and Box Teeth

Translating a set in the model that consists of one set of the teeth (pin or box) is akin to translating the teeth in the axial (Y) direction as one "walks" round the physical connector and therefore loading up the connector through tooth contact on the flanks. So moving the teeth in the model does not violate the sketch but rather shows the effect of the axial movement of one flank against an opposing flank in the presence of an axial force.

This conversion of displacement into a preload force is only possible when a second instruction is inserted in the FEA code to resolve any interference between the contacting surfaces thereby resolving the applied displacement into a contact force. This instruction, the *SHRINK command in Abaqus, will automatically resolve the over-closure in the first step of the analysis and convert the overlap into a pressure force on between the translated and stationary set.

The final model will take into account the contact areas, supports/restraints and expected maximum allowable loads (normally between 50% to 75% of the material's yield strength). Values for the amount of overlap are varied for successive iterations of the simulation until an acceptable amount of preload force is obtained at the shoulder. After the first run is completed, the induced preload in the connector is assessed, and with the knowledge of the materials yield and tensile strength, the maximum allowable preload is determined and the overlap of the FEA model adjusted to approach this preload value.

A step-by-step process to achieve the above is shown in shown in Figure 4-25 below.

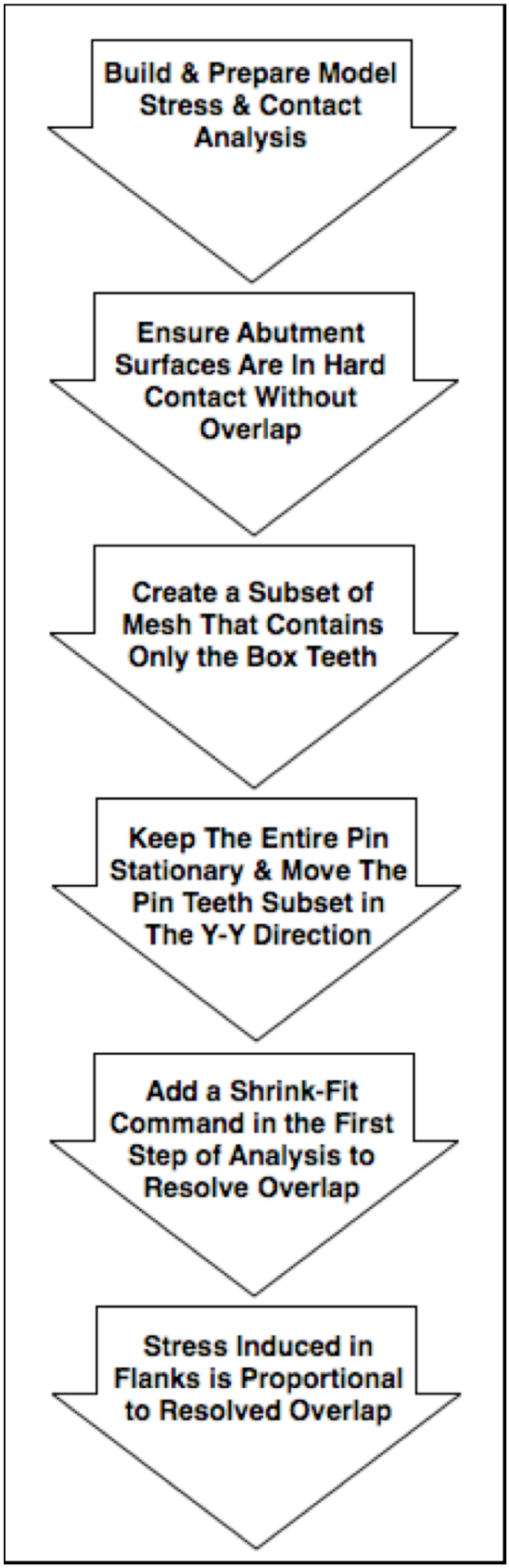

Figure 4-25: Steps for an Interference Fit Preload Simulation

4.5.3 Application of Boundary Conditions to the Model

As mentioned in Section 4.2.2.2. above, the FEA codes understand that each quadrilateral axisymmetric element face (CAX4) represent a complete ring that extends 360^{o} about a given axis. The model is only free to move in the axial (z) direction. Attempt to move an element in the radial (r) direction will only and induce hoop stresses in the model from that movement. The axial direction is therefore the only direction of rigid body motion, which means the model is free to move in the axial (z) direction but it is constrained in at the base by the applied boundary conditions not to move.

Figure 4-26 below shows the stress and strain formulation of an axisymmetric model and the applied boundary conditions of threaded connection.

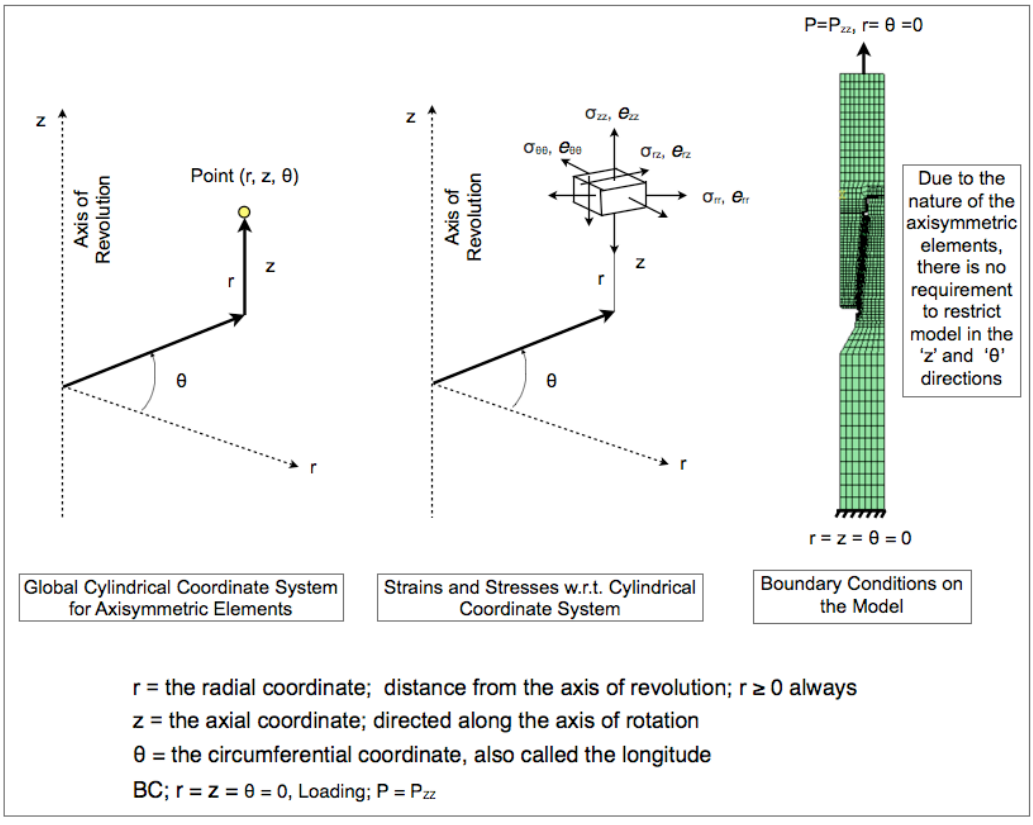

Figure 4-26: Stress/Strain Formulation of Axisymmetric Elements

4.5.4 Determination of Preload Stresses Induced in the Connector

To determine the amount of preload induced in the connector by a certain overlap amount, a geometric line is positioned close to the loaded shoulder of both the pin and box components to read preload stresses induced due to the overlap on the pin and box teeth. The geometric line is a sensor that can be used to read the stresses induced in the connection. This is achieved by reading the nodal stresses in the YY direction along the line, which are then used to calculate the forces on the element face between the two nodes on an element lying along the line. The geometric line and the elements and nodes lying along it are shown in Figure 4-27 below.

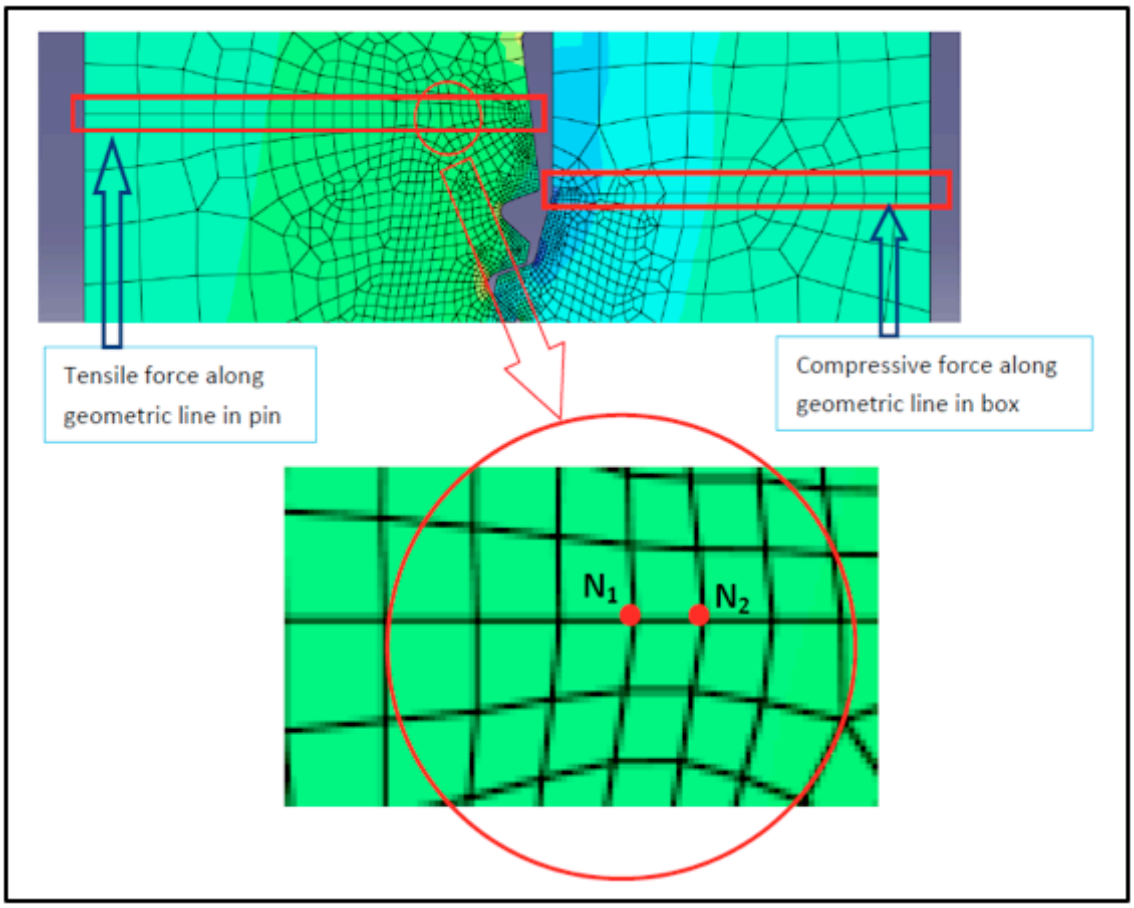

Figure 4-27: Line of Geometry for Calculating Preload Force in the Model

To arrive at the correct amount of overlap that will give the required preload, the

nodal forces along the line of geometry are calculated as;

$$F_{Circumference} = \left[\frac{S_{yy1} + S_{yy2}}{2}\right] \times \left[\frac{\pi}{4}\left(N_1^2 - N_2^2\right)\right] \text{.....4.11}$$

Where $F_{Circumference}$ is the force along the line, S_{yy1} and S_{yy2} are the nodal S_{yy} stress components at nodes 1 and 2, and N_1 and N_2 are the x-coordinate positions of the nodes1 and 2 along the geometric line.

Therefore, for the connection to be in equilibrium, the force along the line of geometry on the pin must be equal and opposite to the force along the line of geometry on the box, or,

$$\sum F_{(Pin-Tensile)} = \sum F_{(Box-Compressive)} \text{.....(4.12)}$$

The amount of stress along the line of geometry will, therefore, be

$$\sigma_{Line} = \left[\frac{\sum F_{(Line)}}{A_{(Line)}}\right] \text{.....(4.13)}$$

From stress data generated by an Abaqus solution values for the NC46 connector, values for S_{yy} and N_i were used to compute the value for σ_{Line}

Full results of the computed force values on elements in the line of geometry are shown all cases of preload force only and the preload + axial load scenarios in Appendix E: Simulation Results.

4.5.4.1 Confirming Preload Forces are Equal and Opposite

Theoretically, in an equilibrium condition, from eq. (4.12) above, the preload force in the pin are expected to be equal and opposite to the preload force in the box. A series of simulations were undertaken on the NC46 connector for various amount of overlap (from 0.05mm to 0.35mm) in order to calculate the preload force in the pin and box using eq. (4.11) above. The result obtained from the simulation is shown in Table 4-2 and Figure 4-28 below.

PRELOAD FORCE DUE TO OVERLAP

OVERLAP AMOUNT (MM)	+VE FORCE IN PIN (MN)	-VE FORCE IN BOX (MN)	% DIFF.
0.05	0.7	-0.7	-0.99
0.10	1.3	-1.3	-0.99
0.15	1.9	-2.0	-0.99
0.20	2.6	-2.6	-0.99
0.25	3.2	-3.2	-0.99
0.30	3.8	-3.8	-0.99
0.35	4.5	-4.6	-0.99

Table 4-2 Equality in Preload Force Values in Pin (+ve) and Box (-ve)

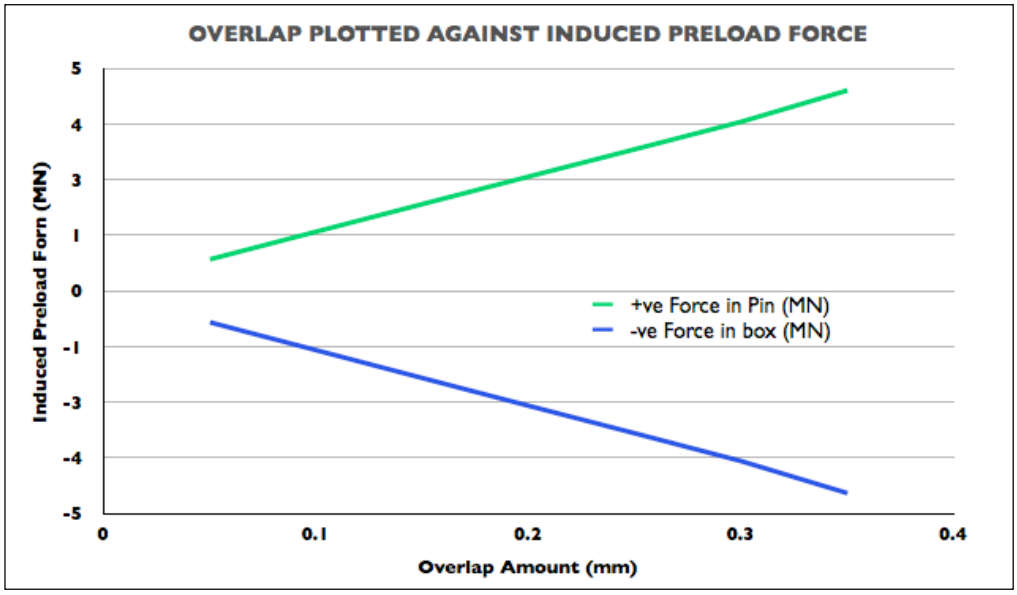

Figure 4-28: Equality in Preload Force Values in Pin (+ve) and Box (-ve)

4.5.4.2 Model Validation with Previous Work Done

Extensive work has been done in the study of the effect and location of peak stress in threaded connections in general and oilwell drillstring threaded connections in particular. In all these studies, the Stress Concentration Factor (SCF), and especially the location of the peak value of this dimensionless

parameter, is used to predict the location for the onset of fatigue failure. The SCF, K_T, is a dimensionless parameter that is the ratio between maximum local stress and the nominal global stress in the body, or mathematically,

$$K_T = \frac{\sigma_{\max}}{\sigma_{\min}} \text{.....(4.14)}$$

However, in Chapter Two, for the root stresses of a drillstring threaded connection, SCF, K_{Ti} was defined as the local peak stress in component near tooth $,i$. σ_i, divided by the local nominal stress in the component's body at tooth i, S_i, or,

$$K_{ti} = \frac{\sigma_i}{S_i} \text{.....(4.15)}$$

Earlier work by Tafreshi & Dover [4.7], Macdonald & Deans [4.31], Baha'I [4.32] and Baragetti & Baryshnikov [4.33], while approaching the problem from different investigative angles, all looked at the relationship of fatigue and drillstring failure from the point of view of stress concentrations at locations of geometric discontinuities such as the thread roots.

In Figure 4-28 below Tafreshi and Dover's results from investigations carried out on an NC46 connector were compared to the results obtained from the two-dimensional FEA model of the NC46 connector developed and used in this work. It should be noted here that just as was done in the earlier investigation by Tafreshi-Dover, the model was tested with axial load only without a preload force and then a preload force was added and tested again with the same axial load.

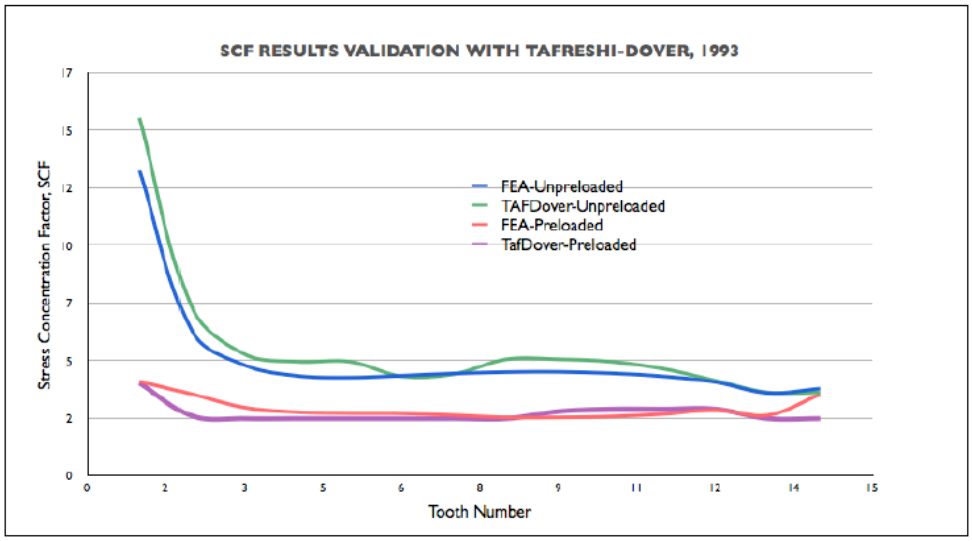

Figure 4-29: Validating the NC46 SCF Results with Tafreshi-Dover Results

The load values in the actual FEA model and in the actual drillstring are obtained by loading up the connector with an external axial load. A reduction of load carried by the first threads engaged limits both failures due to fatigue caused by combined loading and failures induced by galling especially for aluminum drillstring connections. Connections are subjected to stresses induced by make-up torque and the superposition of alternate or pulsating axial and bending stresses, the latter are present if the drill-string has to deviate and follow non-rectilinear routes during actual drilling operations. Lower loads on the first threads engaged mean lower contact pressures which, in turn, reduce galling problems.

4.6 Connection Working Limits and Failure Criteria

4.6.1 Connection Working Limits

API specifications limit only the minimum yield strength of *RSCs* thus allowing the production of rotary-shouldered connections (RSCs) with a broad range of mechanical characteristics [4.34]. For conventional drillpipes, the minimum yield strength can vary from a range of 515 MPa (E75 grade) to 930 MPa (S135 grade) and 830 MPa for tool joints. Any analysis must consider the aforesaid figures in determining the working limits of the drillstring connection.

For different drilling situations, it is important to know the maximum allowable combination of loads that can be applied to the drill string components. These might include loads for make-up and tension or for torsion and tension at a given make-up torque. The analyses must be carried out at loads not exceeding 50% to 75% of the component's minimum yield strength [4.35].

The three points of concern as far as working limits are concerned in the connection are;
1.) Yielding in the pin and box, when the combination of loads in the connection exceeds the component's minimum yield strength,
2.) Application of torsional load that will cause a permanent dimensional change in the component, or torsional yield and, finally,
3.) Separation of the connection at the shoulder that will cancel out the shoulder compressive load induced by the make-up torque.

All simulations undertaken in this work were done with the three concerns mentioned above in mind. Baragetti and Baryshikov [4.33] proposed a method for evaluation of the working limits of rotary shouldered connections under static loading using a numerical procedure confirmed by full scale experimental tests.

4.6.1.1 Yield Validation

The individual teeth and other areas of peak stress in the connection were observed under two limiting conditions of shoulder separation and pin yielding. All validations carried out in this work attempt to look at the stress concentration factor, SCF, at these areas as an indicator of peak stress and possible location of failure initiation. These observations were done under varying cases of two loading criteria – axial tensile load and preload. In the next chapter the author reports on the work that was undertaken comparing (and assessing the suitability) of the various materials that are currently in use or can be used as drillstring materials in deepwater and ERD applications. Failure analysis and validation is undertaken here to investigate yielding of the pin and box materials so as to identify their working limits as defined by the standard industry specifications and the material's properties.

Failure Criteria is defined and calculated for the purpose of determining the load limit in any structure. This load limit relates to an estimate of the yield or failure of the structure or component. The FEA model simulates loading on a structure and reports the response of the structure to such a loading closely, within the limits of the margins of error discussed in earlier chapters, approximates to the expected response of the physical structure.

For Isotropic ductile materials, the most commonly used failure criteria are the Maximum Shear Stress, or Tresca Criterion and the von Mises, (or Maximum Distortion Energy Criterion). Both criteria use principal stresses in their formulation [4.36].

In the Tresca criterion any given point in the body is considered safe as long the maximum shear stress at that point is under the yield shear stress obtained from a uniaxial tensile test. For a two-dimensional stress field the maximum shear stress is related to the difference in the two principal stresses. This means that for the Tresca Criterion, the principal stress difference and the principal stresses themselves must be less than the yield shear stress [4.36].

This can be expressed mathematically as;

$$|\sigma_1| \leq \sigma_y \text{.....} (4.16a)$$

$$|\sigma_2| \leq \sigma_y \text{.....} (4.16b)$$

$$|\sigma_1 - \sigma_2| \leq \sigma_y \text{.....} (4.16c)$$

The von Mises Criterion is based on the determination of the distortion energy in a given material, that is, the energy associated with the change of shape, rather than a change in volume, of the material. According to the von Mises Criterion, a structural material is safe as long the maximum value of the distortion per unit volume in that material remains smaller than the distortion energy per unit volume required to cause yield in a tensile test specified for that material [4.37]. In other words, failure occurs when the energy of distortion reaches the same energy for yield in uniaxial tension. For a three-dimensional stress field, this can be expressed mathematically as;

$$\frac{1}{2}\left[(\sigma_1 - \sigma_2)^2 + (\sigma_2 - \sigma_3)^2 + (\sigma_3 - \sigma_1)^2\right] \leq \sigma_y^2 \text{.....} (4.17a)$$

In case of a plane stress situation (where $\sigma_3 = 0$) eq. (4.27a) reduces to

$$\left(\sigma_1^2 - \sigma_1\sigma_2 + \sigma_2^2\right) \leq \sigma_y^2 \text{.....} (4.17b)$$

Because we are dealing with a principally linear-elastic problem in these FEA analyses and knowing that the materials studied exhibit ductile behaviour, the von Mises failure criterion is ideal in determining the stress level that must not be exceeded for the mechanical behaviour of the material to remain in the linear-elastic region.

A series of analyses were undertaken on the NC46 two-dimensional axisymmetric model in both the preloaded only and the axial plus preloaded cases to determine the maximum amount of load that can be applied without

yielding either of the connection components. Understandably, the first of such analyses undertaken was in the preloaded case. Knowing that the yield strength of the material under analysis (AIS4145H) is 930 MPa, the target will be to determine the amount of preload-inducing overlap that will give a von Mises stress of between 50% and 75% of the yield strength value.

As shown in Table 4-3 below an acceptable value was obtained at an overlap value of 0.2mm. A value below this (<0.2mm) will under-load the connection while at a value above that (>0.2mm) the connection material risks yielding. This is shown graphically in Figure 4-30 below.

The aim of this analysis is develop a benchmark case, using AISI 4145H steel in this case, based on which the model can be fully validated and in the which the benchmark elastic parameters can be substituted for the parameters of other materials to be studied.

YIELD ANALYSIS

OVERLAP AMOUNT (MM)	MATERIAL	YIELD STRENGTH	PEAK VON MISES STRESS	VON MISES STRESS @ 0.2MM	% OF YIELD STRENGTH
0.05	AISI 4145H	940.0	170.50	616.70	18.14
0.10	AISI 4145H	940.0	320.50	616.70	34.10
0.15	AISI 4145H	940.0	469.30	616.70	49.93
0.20	AISI 4145H	940.0	616.70	616.70	65.61
0.25	AISI 4145H	940.0	756.70	616.70	80.50
0.30	AISI 4145H	940.0	902.70	616.70	96.03
0.35	AISI 4145H	940.0	1,048.00	616.70	111.49

Table 4-3 Yield Analysis to Determine Overlap Value for NC46 Connector

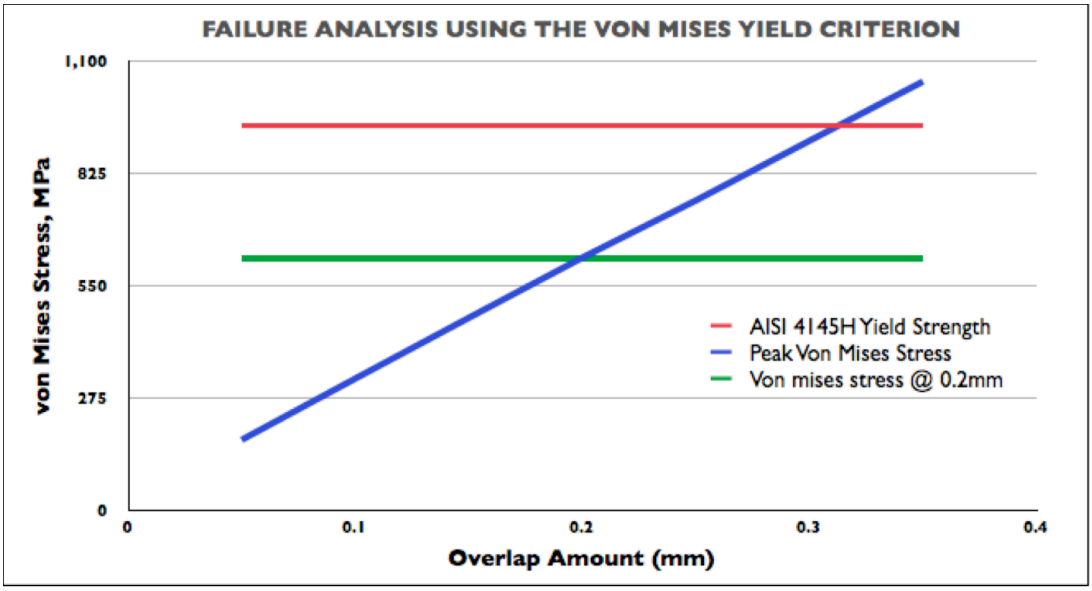

Figure 4-30: von Mises Stress Vs. Overlap Values for Preload

Having determined the amount of overlap required to apply the predetermined preload the next step is to load the connector in tension so as to determine the maximum amount of axial tensile load the connector can withstand before yielding in the presence of preload. To achieve this, the connector was loaded in tension and the von Mises stress was observed in relation to varying amount of applied tensile load. The aim to is to observe what amount of axial load will induce a tensile stress large enough to overcome the compressive stress induced by the preload force and cause yielding in any of the components or a separation at the shoulder.

In accordance with design standards such as the BS 11961:2008 [4.38] the lower value yield strength for a Grade 'S' drillpipe is 930 MPa. This grade of pipe, commonly referred to S135 [4.39], as shown in Table 4-5 below, was chosen for the benchmarking studies because it has the highest yield strength of all conventional grades of steel drillpipes currently in common use in the field.

Conventional Drillpipe Properties	Yield Strength				Minimum Tensile Strength	
	Minimum		Maximum			
Steel Grade	K Psi	MPa	K Psi	MPa	K Psi	MPa
E75	75	515	105		100	690
X95	95	655	125		105	725
G105	105	725	135		115	790
S135	135	930	165		145	1000
Tool Joints	120	830			140	970

Table 4-4 Conventional Drillpipe Grade and Properties

In tensile loading, as depicted by the bolt and nut joint diagram in Section 2.2.3 of Chapter Two, once the connection is optimally preloaded - a positive change in von Mises stresses is only noticeable when the applied axial load is of a magnitude large enough to overcome the preload compressive forces. Figure 4-31 and Figure 4-32 below show a preloaded connection reacting to an increase in external tensile load. In Figure 4-31, the preload force can be seen inducing a maximum von mises stress of 616.7 MPa on the model while in Figure 4-32 the tensile load is seen to have no effect on the von Mises stress value until a certain value (>500KN) is exceeded after which the magnitude of the von Mises stress is seen to vary with the increase in tensile loading.

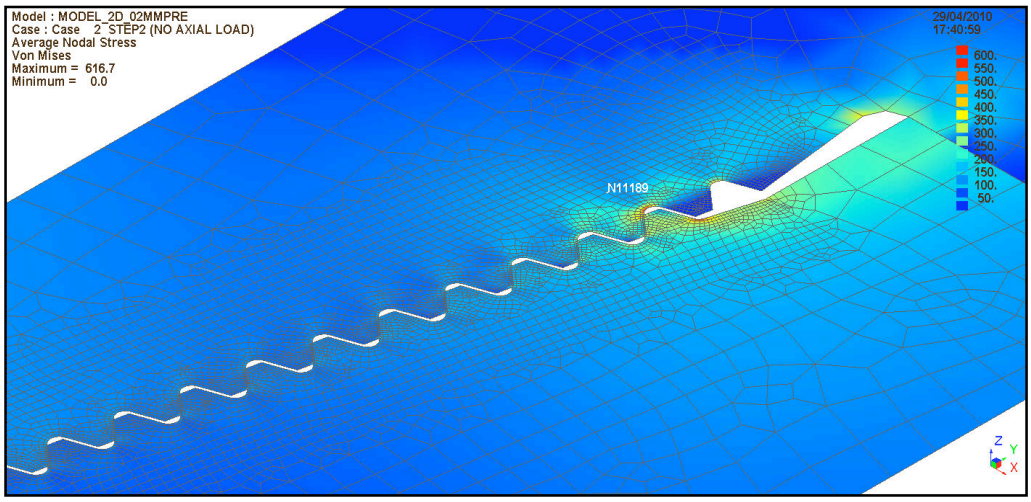

Figure 4-31: Stress Contour of von Mises Stress Value at 0.2mm Overlap

A further observation that additionally validates the model is the increasing inequality in the value of tensile force in the pin and the compressive force in box. As can be seen from Table 4-2 and Figure 4-28 above, during the application of the preload-only force in the connector the forces in the pin and box are equal and opposite. However, upon the introduction of a tensile load on the already preloaded connector, the equality is lost as is shown in Figure 4-33 below.

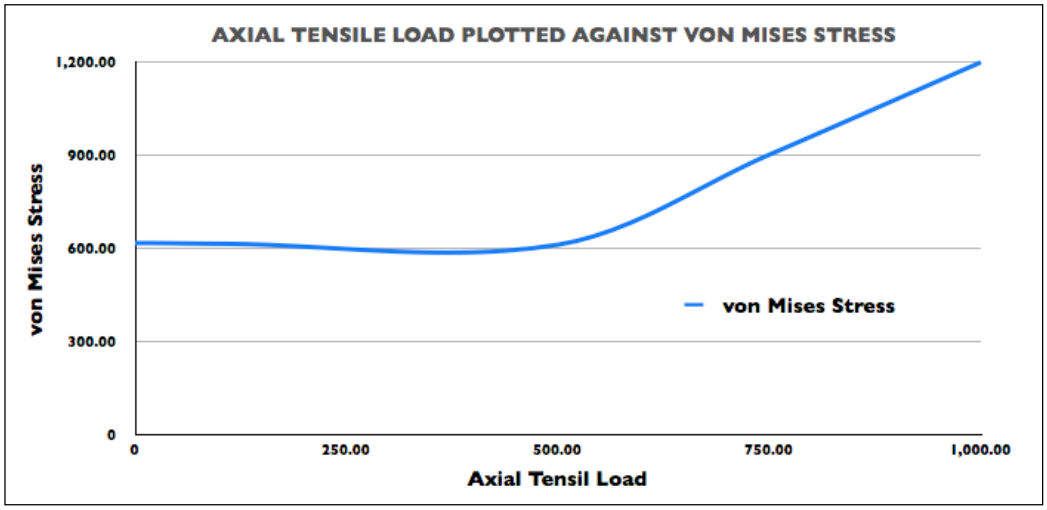

Figure 4-32: Tensile Load Vs von Mises Stress for Preload & Axial Load

Initially, a change is observed from the 20KN to 520KN range where the application external tensile load causes a slight increase in stress in the pin and a non-proportional increase in the compressive force in the box. Between 500KN and 1MN a reverse of the earlier phenomenon is observed whereby the decrease in compressive force in the box levels out but a steep increase in the tensile force in the pin is observed. This observed phenomenon confirms active load 'transfer' between the box and pin and why, in the presence of preload and external axial load, the most critical stress concentration factor is located in the pin. This is shown clearly in Sections 1 and 2 of Appendix E under Benchmark Analyses- AISI4145H Steel.

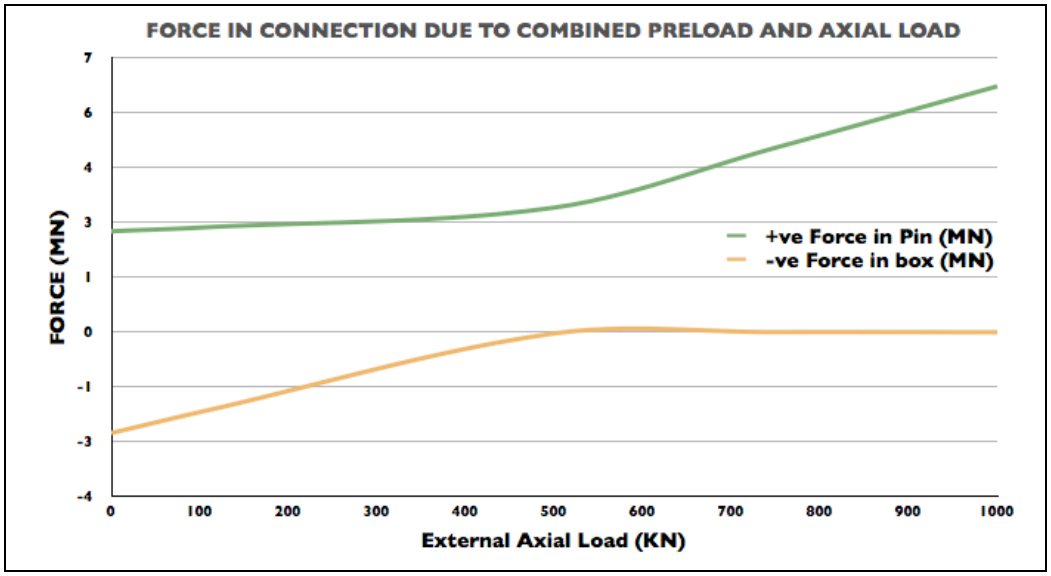

Figure 4-33: Force in Pin and Box After Application of Tensile Load

4.7 Reference

[4.1] **NDE Centre, University College London**, "*Fatigue Analysis of Drillstrings – FADS"*, Final Report, Joint Industry Project, 1990.

[4.2] **NDE Centre, University College London**, *"Prevention of Downhole Failure – PDF"*, Final Report, Joint Industry Project, NDE Centre, Univ. College London

[4.3] **NDE Centre, University College London**, *"Reliable Operations of Drillstrings - RODS"*, Joint Industry Project, Final Report, 2002

[4.4] **Hibbit, Karlson and Sorenson, Inc**, *"ABAQUS User Guide Manual"* , v. 5.8, 1999.

[4.5] **Shir, R.**, *"An introduction to Finite Element Analysis Using Creo Simulation 1.0"* SDC Publications, 2011; Pp. 9-18

[4.6] **Simulia Publications** *"ABAQUS 6.7 User Manual"*, Simulia Publications, 2006

[4.7] **Tafreshi, A., and Dover, W. D.**, *"Stress Analysis of Drillstring Threaded Connections Using the Finite Element Method"*, Int. Journal of Fatigue 15, No 5 (1993) pp 429-438

[4.8] **Yi-Cheng, C., Chung-Biau, T.**, *"Stress Analysis of a Helical Gear Set with Localized Bearing Contact"*; Finite |Elements in Analysis Design, No. 38, pp707-723, 2002

[4.9] **Institut Francais du Petrole**, *"Drilling Data Handbook"*, Institut Francais du Petrol, Sixth Edition, Editions Technip, 1991

[4.10] **Pick, R.J. and Burns, D.J.**, *"Finite Element Analysis of Threaded End Closures of Thick-Walled Vessels"*, Proceedings of the Institute of Mechanical Engineers, Pp. 15-25, January 1971

[4.11] **Jien-Jong Chen, Yan-Shin Shih**, *"A study of the helical effect on the thread connection by three dimensional finite element analysis"*, 2nd

International Workshop on the Integrity of Nuclear Components, Japan 1998, pp13-29.

[4.12] **Simulia Publications** *"ABAQUS 6.7 Theory Manual"*, Simulia Publications, 2006 Section 3.2.8.

[4.13] http://nafems.org/resources/analysis_terms/terms/STRESS-CONCENTRATION/ accessed on 17/12/2011.

[4.14] **Kelley, B. W., Pedersen, R.**, *"The Beam Strength of Modern Gears"*, Trans. of the SAE, 1958; vol 66, pp 137-157

[4.15] **Heywwod, R. B.**, *"Design Against Fatigue"* Chapman and Hall Ltd., London 1962. Pp 261-265.

[4.16] **Pilkey, W. D.**, *"Paterson's Stress Concentration Factors"* John Wiley and Sons, 1997. Pp. 180.

[4.17] **Den Hartog, J.P.**, *"The Mechanics of Plate Rotorsfor Turbo-Generators"* 1929, Trans A.S.M.E., vol. 51, part 1, Applied Mechanics Section, p. 1, Paper No. APM 51-1

[4.18] **Goodier, J.N.**, *"The Distribution of Load on the Threads of Screws"* 1940 Trans. A.S.M.E. vol. 62 p A-10

[4.19] **Weigle, R. E., Laselle, R. R. and Purtell, J. P.**, *"Experimental Investigation of the Fatigue Behaviour of Thread-type Projections"*; Experimental Mechanics, Vol 3, No. 5, May 1963.

[4.20] **Farr,A. P.**, *"Torque Requirements for Rotary Shouldered Connections and Selection of Connections for Drill Collars"*, Paper ASME 5-PET-19 presented at the 1957 ASME Petroleum Mechanical Engineering Conference, September.

[4.21] **Brennan, F.P., Kare, R.F.**, *"An Experimental Analysis of Preload in Threaded Connections"*, Proceedings of the International Conference on Offshore Mechanics and Arctic Engineering – OMAE, Vol. III, pp 235-241, 1994

[4.22] **Bailey, E. I. and Smith, J. E**: *"Testing Thread Compounds for Rotary-Shouldered Connections"* IADC/SPE Paper 23844 presented at the 1992 IADC/SPE Drilling Conference in New Orleans, L.A.

[4.23] **Hibbitt, H. D., Nagtegaal, J. C.**; *"Computer process for prescribing an assembly load to provide pre-tensioning simulation in the design analysis of load-bearing structures"*, July 1999; Source: www.FreePatentsOnline.com (Accessed in January 2011); Patent no.; 5920491

[4.24] **Simulia Publications** *"ABAQUS 6.7 Theory Manual"*, Simulia Publications, 2006 Section 31.2.1.

[4.25] **Simulia Publications**, *"Abaqus Analysis User's Manual; Volume V: Prescribed Conditions, Constraints and Interactions; Version 6.7"*, Simulia Publications; Section 29.2.2.

[4.26] **Simulia Publications**, *"ABAQUS 6.7 User Manual"*, Simulia Publications, 2006

[4.27] **Lyons, W.C. and Plisga, G. J.**, *"Standard Handbook of Petroleum and Natural Gas Engineering"* Gulf Professional Publishing, 2005. Pp. 4-186;

[4.28] **Baragetti, S.**; *"Effects of Taper Variation on Conical Thread Connections Load Distribution"*; Transactions of the ASME; Vol. 124 June 2004; Pg 320-329

[4.29] **Simulia Publications** *"Abaqus Analysis User's Manual, Volume V: Prescribe Conditions, Constraints and Interactions; Version 6.7"*, Simulia Publications; Section 27.5.1.

[4.30] **Simulia Publications**, *"Abaqus Analysis User's Manual; Volume V: Prescribed Conditions, Constraints and Interactions; Version 6.7"*, Simulia Publications; Section 29.2.4.

[4.31] **Macdonald, K. A. and Deans, W. F.**, *"Stress Analysis Of Drillstring Threaded Connections Using The Finite Element Method"*, Engineering Failure Analysis, Vol 2, No. 1 pp. 1-30, 1995

[4.32] **Baha'i, H**, *"A Parametric Model for Axial and Bending Stress Concentration Factors in API Drillstring Threaded Connectors"*; Int. Journal of Pressure Vessels and Piping 78; 2001; pp 495-505

[4.33] **Baragetti, S. and Baryshnikov, A.;** *"Rotary Shouldered Thread Connections: Working Limits Under Combined Static Loading";* Journal of Mechanical Design, Transactions of the ASME; Vol 123, September 2001; pp 456-463

[4.34] **American Petroleum Institute** *"API Specification 7: Specification for Rotary Drillstem Elements"*; Fortieth Edition – 2002, American Petroleum Institute. Pp. 19.

[4.35] **American Petroleum Institute**, *"API RP 7A1 Recommended Practice for Testing of Thread Compound for Rotary Shouldered Connections"* American Petroleum Institute 1st Edition, November 1992

[4.36] **Hibbeler, R. C.**, *"Mechanics of Materials"* Pearson Education, Inc., 2003; Pp. 524-527

[4.37] **Vable, M.**, *"Mechanics of Materials"* Oxford University Press, 2002; Pp 673-4

[4.38] **British Standards**, *"BS EN ISO 11961:2008; Petroleum and natural gas industries. Steel Drill Pipe"* British Standards

[4.39] **Institut Francais du Petrole**, *"Drilling Data Handbook"*, Institut Francais du Petrol, Sixth Edition, Editions Technip, 1991

5 Simulations and Results

Non-Conventional Drillstring Materials: Simulations and Results

5.1 Introduction

The economic demands form a substantial part of the operational demands since drillstring materials are now expected to perform under very tough and exacting standards as far as their physical properties are concerned. In ultra-deep drilling (UDD), failure of the drillstring in a scenario where the material's safe operating envelop is exceeded will translate into substantial operating cost for the operator not only because this has the potential for an undesirable eventuality which may warrant the suspension drilling operations but also because in this particular case, the drillstring failure occurs very deep. This is bound to present a problem that will cost much more remedy than in the case of normal or shallow depth drilling.

The depth at which current exploration campaigns are targeting using UDD and ERD requires an increased number of tubulars to reach the zones of interest. Other factors such as the high tensile hook loads expected to be experienced by strings placed shallower up the wellbore, fatigue due to cyclic stresses in rotating strings (especially if rotating in a dogleg) and increase in torque and drag due to elevated loads require that physical factors such as reduced drillstring weight, material strength and the durability of the drillstring material be studied for various material types and compared with AISI 4145H steel, the material currently in conventional drillstring use. Non-conventional materials currently in use as drillstring materials include aluminium alloy (Al-Zn-Mg-II, 70,000 psi or 480 MPa yield strength) and titanium alloy (Ti-6Al-4AV, 114,000 psi or 827 MPa yield strength). While both of these materials are lighter than the steel type used in the manufacture of drillstring components, the latter comes with a near-prohibitive cost disadvantage while the former is too light and has much weaker elastic properties than steel and titanium alloy. Table 5.1 below

shows the elastic and physical properties of the drillstring materials under study. The applicability of all these materials as DP materials will be discussed in the later part of this chapter.

Non-Conventional Drillpipe Properties					
DP Grade	**Yield Strength (MPa)**	**Young's Modulus, E(MPa)**	**Poisson Ratio**	**S/W Ratio**	**% S/W Ratio Improvement over S135**
Steel (S135)	930	200000	0.3	737.3	0%
Steel (Z-140)	965	200000	0.3	764.6	4%
Steel (V-150)	1034	200000	0.3	819.2	11%
Steel (UD-165)	1137	200000	0.3	901.2	22%
Aluminium Alloy (Al-Zn-Mg II)	480	70000	0.35	823.1	12%
Titanium Alloy (Ti-6Al-4V)	827	114000	0.3	1,012.7	37%

Table 5-1 Elastic Properties of Drillstring Materials [5.1]

As can be seen from Table 5-1 above, other materials considered are the newly-developed steel alloys with higher yield strengths, at least one of which, UD-165, was developed specifically with UDD in mind. These are the Z-140 (140,000 psi or 965 MPa yield strength), the V-150 (150,000 psi or 1,034 MPa yield strength) and the UD-165 (165,000 psi or 1,137 MPa yield strength) steel grades.

The benchmark studies of the model was undertaken in the previous chapter used the elastic properties of the strongest grade of conventional drillstring material, the S-135, made from AISI4145H steel. The study shows the stress response of the material under conditions of varying magnitudes of applied preload and external axial loads.

It should be noted here that, as shown in Figure 5-1 below, aluminium alloy and titanium alloy drillpipes are sometimes manufactured with standard API steel tooljoints which can be handled by already available tubular handling equipment on the drill floor and allows for the deployment of hybrid steel/aluminium alloy

drillstrings. The tool joints are connected to the aluminum alloy or titanium alloy drill pipe using a thermal shrink fit technology, which is recognized for its long-term dependability.

In a certain proprietary case [5.2,], the Aluminum Alloy Drill Pipe (ADP) is machined with six modified Acme threads per inch on 3/8" taper per foot. The end of the pipe is provided with a smooth concentric shoulder. Beyond this point, the pipe is tapered through the transition zone. The inside of the pipe end of the tool joint displays the threads, the end shoulder and the counterbore.

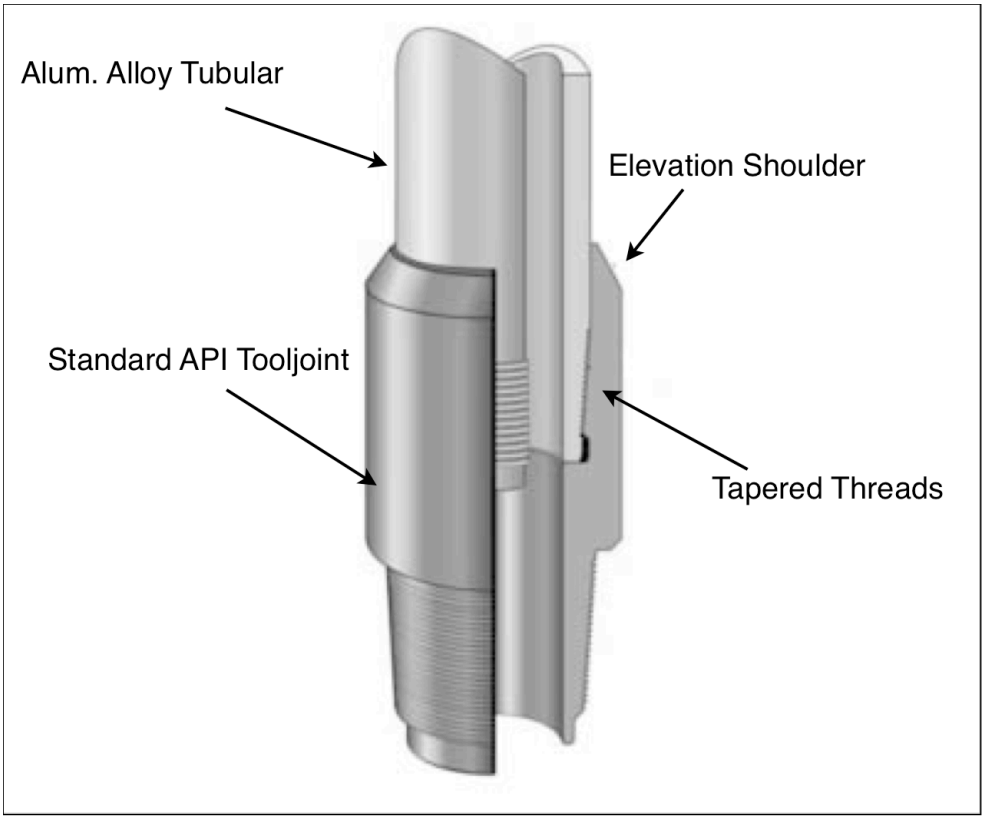

Figure 5-1: Aluminium Drillpipe with Steel Tooljoint [5.2]

Using the FEA model developed, an investigation was undertaken to study the response of the model to other steel and non-steel drillstring materials. The study involved determination of the working limits of the string in terms of the applicable preload and external tensile load using the von Mises failure criterion. The results obtained from the simulation are shown in the two tables below and discussed in more detail in the subsequent sections. Table 5-2 below

shows the amount of overlap that will generate the upper limit value of allowable preload stress using the chosen failure criterion. Table 5-3 below, on the other hand, shows the same value for an axial load limit. The data from which these results are generated is attached as Appendix E: Simulation Results.

PRELOAD YIELD ANALYSIS

PEAK VON MISES STRESS (MPA)														
OVERLAP (MM)		STEEL	STEEL Y.S.	STEEL@ 0.2MM	Z-140 STEEL Y.S.	V-150 STEEL Y.S.	UD165 STEEL Y.S.	STEEL@ 0.25MM	ALUMINIUM ALLOY	ALUMINIUM ALLOY Y.S.	ALUM. ALLOY @0.30MM	TITANIUM ALLOY	TITANIUM ALLOY Y.S.	TITAN. ALLOY @0.35MM
0.05	0.05	170.50	940.00	616.70	965.00	1,034.00	1,137.00	756.00	58.40	480.10	309.10	97.90	880.00	597.30
0.10	0.10	320.50	940.00	616.70	965.00	1,034.00	1,137.00	756.00	109.80	480.10	309.10	182.70	880.00	597.30
0.15	0.15	469.30	940.00	616.70	965.00	1,034.00	1,137.00	756.00	160.60	480.10	309.10	267.50	880.00	597.30
0.20	0.20	616.70	940.00	616.70	965.00	1,034.00	1,137.00	756.00	210.80	480.10	309.10	351.50	880.00	597.30
0.25	0.25	756.70	940.00	616.70	965.00	1,034.00	1,137.00	756.00	259.10	480.10	309.10	431.30	880.00	597.30
0.30	0.30	902.70	940.00	616.70	965.00	1,034.00	1,137.00	756.00	309.10	480.10	309.10	514.50	880.00	597.30
0.35	0.35	1,048.00	940.00	616.70	965.00	1,034.00	1,137.00	756.00	358.90	480.10	309.10	597.30	880.00	597.30
0.40	0.40		940.00	616.70	965.00	1,034.00	1,137.00	756.00	412.10	480.10	309.10	688.10	880.00	597.30
0.45	0.45		940.00	616.70	965.00	1,034.00	1,137.00	756.00		480.10	309.10	775.80	880.00	597.30
0.50	0.50		940.00	616.70	965.00	1,034.00	1,137.00	756.00		480.10	309.10	862.90	880.00	597.30

Table 5-2 Preload Limit of Drillstring Materials under Investigation

AXIAL YIELD ANALYSIS

		STRESS DUE TO AXIAL LOAD				MAXIMUM ALLOWABLE STRESS			
AXIAL LOAD (N)		STEEL S, Z & V	ALUMINIUM ALLOY	TITANIUM ALLOY	STEEL UD165	STEEL	ALUMINIUM ALLOY	TITANIUM ALLOY	STEEL UD165
0	0	616.70	309.90	597.30	756.00	616.70	309.90	597.30	756.00
20	20	616.90	309.90	599.80	756.00	616.70	309.90	597.30	756.00
50	50	616.70	309.90	599.70	756.00	616.70	309.90	597.30	756.00
2000	2000	616.70	309.90	599.10	756.00	616.70	309.90	597.30	756.00
20000	20000	616.70	309.80	598.80	756.00	616.70	309.90	597.30	756.00
100000	100000	614.70	309.30	598.10	756.00	616.70	309.90	597.30	756.00
150000	150000	616.70	308.30	597.70	756.00	616.70	309.90	597.30	756.00
250000	250000	616.70	309.20	595.00	756.00	616.70	309.90	597.30	756.00
300000	300000	616.70	355.00	598.10	756.00	616.70	309.90	597.30	756.00
400000	400000	616.70	473.40	597.70	756.00	616.70	309.90	597.30	756.00
450000	450000	616.70	523.00	595.70	756.00	616.70	309.90	597.30	756.00
500000	500000	611.60	588.10	600.00	753.00	616.70	309.90	597.30	756.00
550000	550000	680.00	659.00	659.70	754.90	616.70	309.90	597.30	756.00
600000	600000	760.00	730.00	718.70	806.80	616.70	309.90	597.30	756.00
750000	750000	901.60	870.00	860.00	901.60	616.70	309.90	597.30	756.00
1000000	1000000	1,199.00	1,258.00	1,180.00	1,198.00	616.70	309.90	597.30	756.00

Table 5-3 Axial Load Limit of Drillstring Materials under Investigation

5.2 Non-Conventional Drillpipe Materials

5.2.1 High-Strength Steels

High-strength steels drillpipes are developed with extended-reach drilling (ERD) in mind [5.3]. They represent a mid- to long-term solution to the problem of strength requirement of drillstrings in such an application. Current high-strength grades available on the market today are Z-140 and V-150. These grades provide 4% and 11% improvement in strength-to-weight ratio respectively when compared to S-135 drill pipe and carry only a relatively small cost premium over S-135 drill pipe, moreover, they exhibit the same elastic and physical properties as conventional steel drillpipes as such no special tables, charts and data is required to arrive at their operational parameters such as string weight, buoyancy and pipe wear over time [5.3]. Another advantage the high-strength steel drillpipes have, especially, over aluminium drillpipes, is that there is no requirement for the modification of the drill floor pipe handling equipment to prevent crushing or plastically damaging the pipe due low stiffness values.

The substantial improvement in obtaining high toughness in high-strength steels has led drill pipe manufacturers towards the development of ultra high-strength steels such as UD-165. The development of the UD-165 grade with 165,000 pounds per square inch yield strength tubes would provide a 22% improvement in strength-to-weight ratio when compared to S-135 drill pipe. This would be second only to Titanium drillpipes in strength-to-weight ratio (SWR). The cost of the UD-165 drillpipe is also substantially less than that of titanium alloy drillpipes.

5.2.2 Steel Drillpipes: Preload Yield Stress Analysis Results (S, V & Z Grades)

As stated in Table 5-2 and Table 5.3 above and shown Figure 5-2 below, at an external tensile load range of >500KN and <600KN for a steel drillstring with 0.2mm overlap and using the von Mises failure criterion, the highest nodal stress was seen to be 611.6 MPa for the conventional drillstring steel material

and 754.9 MPa for the same amount of overlap and an external load limit of 550KN for the UD-165 drillstring.

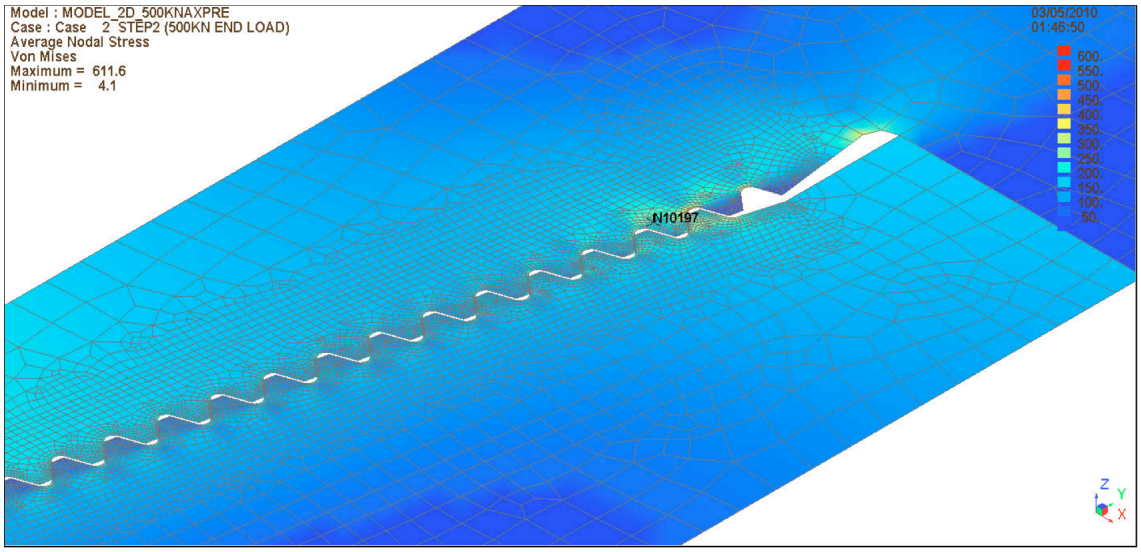

Figure 5-2: von Mises Failure Determination (Steel)

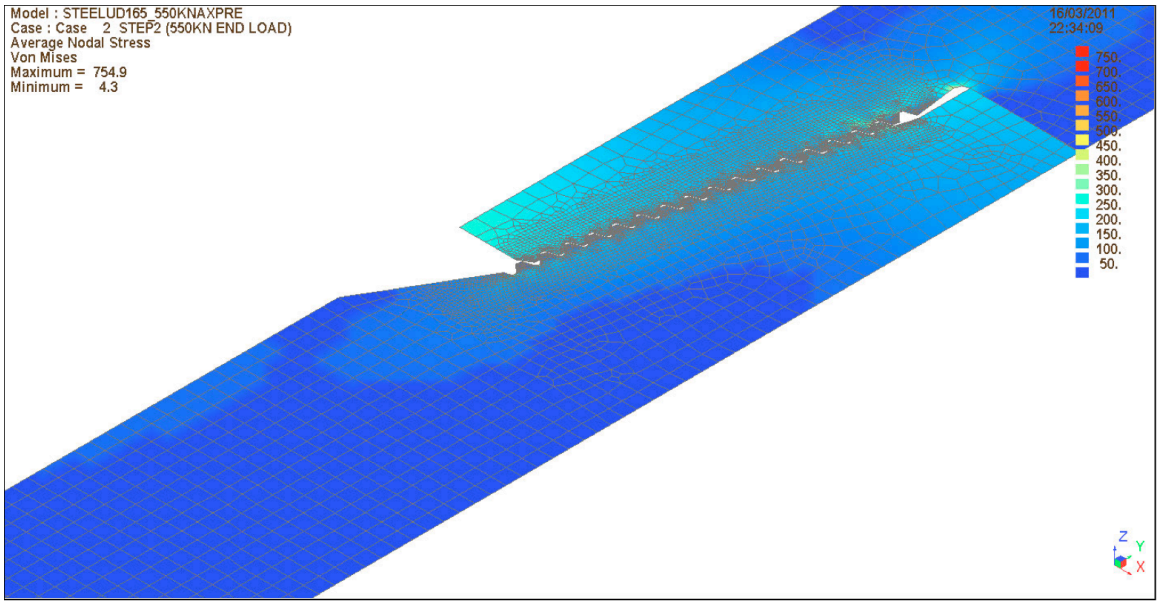

Figure 5-3: von Mises Failure Determination (UD165 Steel)

Figure 5-4 below shows a graphical representation of the results obtained in the preload simulation where the red lines represent the variation of induced

preload force with the amount of overlap at the teeth, the yield strength of steel (upper horizontal red line) and the stress induced in the string at an overlap value that will produce a preload force that is between 50-75 percent of the yield strength value (the lower horizontal line). The other three lines are for the yield strength values of Z-140 (green), V-150 (purple) and UD-165 (green) steels. All the steel grades were simulated using the same elastic properties.

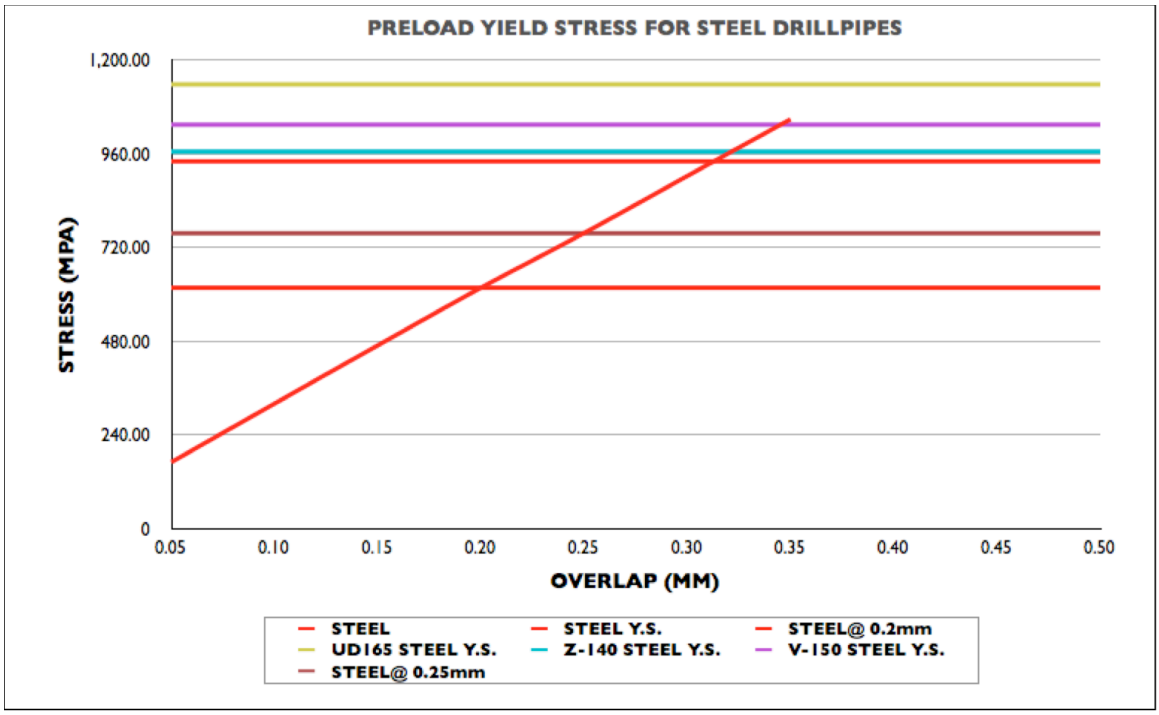

Figure 5-4: Induced Preload Stress Vs Overlap Amount (Steel DPs)

It can be seen from Fig. 5.4 above that the induced preload value for 0.2mm overlap falls within the 50-75% of the yield stress value for all the steel grades. While it is possible to go beyond the 0.2mm overlap in the of UD-165 steel, the simulation will be focusing instead on extending applied external tensile loading in the case of this grade of steel. This is because the grade was developed primarily for ultra-deep drilling applications, hence the name. From Table 5.3 above it can be seen that while the other steel grades (S, Z and V) are limited to tensile load range of 500KN to 550KN, the UD-165 grade will still be within its working limit at a tensile load range of 550KN to 600KN.

5.2.3 Aluminium Alloy Drillpipes

Aluminium Drill Pipes (ADP) technology is one way of applying an existing material to an existing technology to tap into the unique benefits of such a material. The key characteristics of an ADP are specified in the ISO-15546: "Aluminium Alloy Drillpipe for the Oil and Gas Industry" standard. Because the standard calls for the ADP to be handled in a similar manner as steel drillpipes, the ADPs are fitted with steel tooljoints [5.4] to avoid expensive retrofitting of the drillpipe handling tools on the drill floor.

Use of aluminium alloy (Al-Zn-Mg II) drillpipes is not a new concept in oil well drilling as it has been in existence for over half a century in the oilfields of the USSR, and later, Russia. By the beginning of the 1990s, aluminium alloy drillpipes were involved in drilling 70% to 80% of the all oil and gas wells in the Soviet Union. Over a million metres of aluminium alloy drillpipes is currently in operation in Russia [5.5].

The demands of ERD well construction calls for various qualities in a drillstring which may or may not be present in a conventional drillstring built for a directional or horizontal well. In light of this aluminium alloy drillpipes comes with some inherent characteristics that make them ideally suited for ERD applications. These include:

1. Light weight;
2. Impact resistance;
3. Good corrosion resistance;
4. Lower Modulus of Elasticity
5. Non-magnetic (no interference with downhole electronics);
6. Increased rig capacity
7. Reduction in off-bottom torque;
8. Improved over-pull margin;

One of the few disadvantages of aluminium alloy drill pipes is that they

generally require greater wall thickness than steel drill pipes. The other disadvantage is tendency of the yield strength of aluminium alloy drillstrings to fall dramatically at elevated temperatures.

5.2.3.1 Aluminium Alloy: Preload and Tensile Yield Stress Analysis Results

Aluminium alloy drillpipes are made from the Al-Mg-Zn-II alloy. As shown in Table 5-2 and Table 4-3 above and Figure 5-5 below, at an external tensile load range of >300KN and <350KN in an aluminium alloy drillstring with 0.3mm overlap and using the von Mises failure criterion, the highest nodal stress was seen to be 355 MPa. This constitutes about 74% of the yield strength of 480 MPa for this particular alloy.

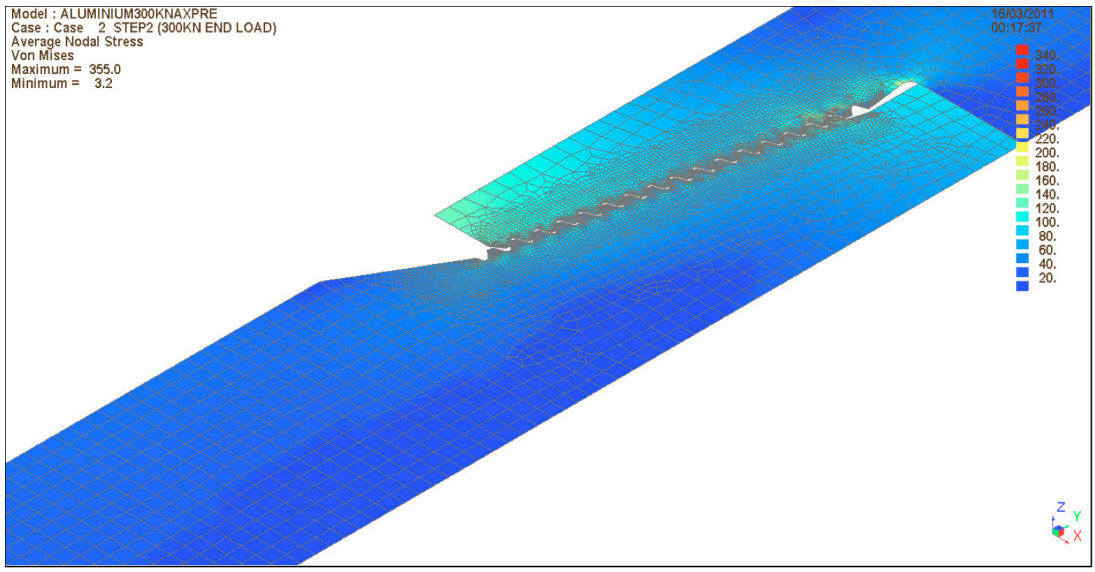

Figure 5-5: von Mises Failure Determination (Aluminium Alloy)

Figure 5-6 below shows a graphical representation of the results obtained in the preload simulation where the green lines represent the variation of induced preload force with the amount of overlap at the teeth, the yield strength of aluminium alloy (upper horizontal line) and the stress induced in the string at an overlap value that will produce a preload force that is between 50-75 percent of the yield strength value (the lower horizontal line). The low stiffness

(compliance) of aluminium alloy accounts for the high overlap value as compared to steel.

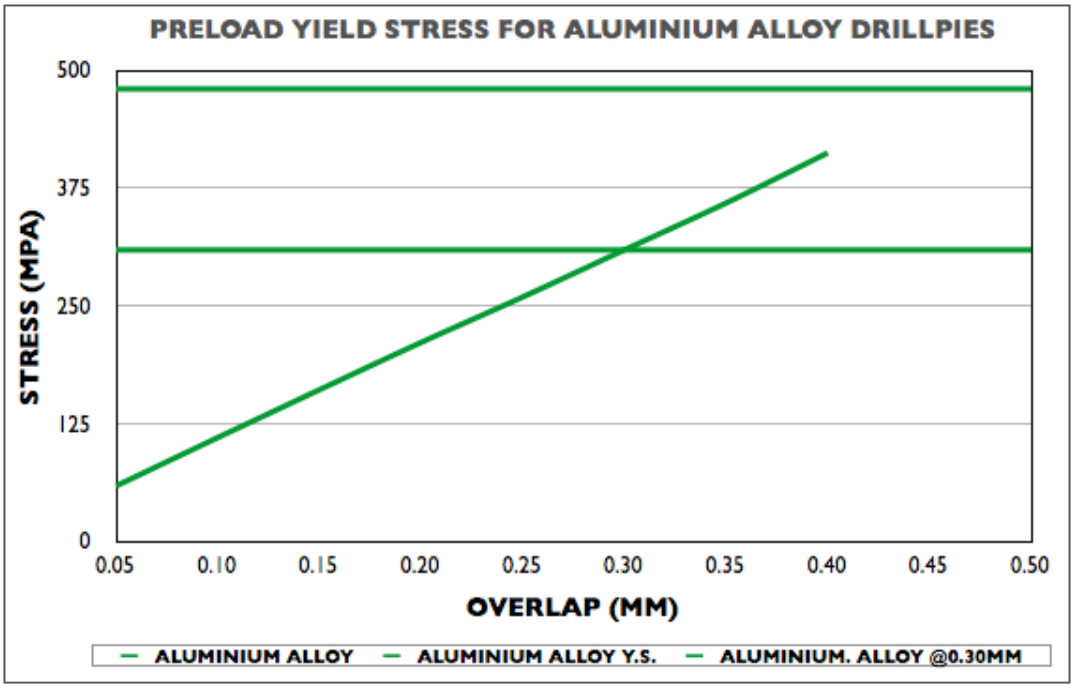

Figure 5-6: Induced Preload Stress Vs Overlap Amount (ADPs)

5.2.4 Titanium Alloy Drillpipes

Titanium alloy (Ti-6Al-4V) drillpipes are made from the Ti-Al-Zn alloy. Titanium alloy drillpipes combine the durability of steel and the flexibility of composite materials. Because of these features, they have found wide applicability in short radius extended reach drilling where high cyclic stresses are encountered, In a typical short radius re-entry programme drillpipes can be expected to have a radius of curvature of less than 60 feet [5.6]. As such titanium alloy drillpipes are mostly employed to take advantage of what is possible when flexible pipes are used in small diameter holes in slimhole drilling such as re-entries of existing wells. Because, globally, there are thousands of straight vertical wells on many existing producing fields that are candidates for re-entry and conversion into horizontal and multilateral wells, titanium drillpipes will continue to be deployed in more and more projects.

However, apart from the aforementioned advantages, the use of Titanium alloy drillpipes in ERD offers significant advantages over conventional steel drillpipe where high cyclic stresses are encountered.

One of the few setbacks for the use Titanium alloy as drillpipe material is its significant wear rates. Thus, mid-body wear of Titanium alloy drillpipe joints is a significant risk that may require development of advanced wear “knots” or other techniques to maximize the usable life of such drillstrings [5.7]. Other disadvantages of Titanium alloy as a drillstring material include the material’s near prohibitive cost. The cost to manufacture Titanium alloy drillpipes is approximately seven to ten times more expensive than that of a conventional steel drill pipe [5.7].

The physical properties worth noting in Titanium when compared to steel include:

1. Lower Elastic Modulus: Titanium’s Modulus of Elasticity of 114,000 MPa is 57% of that of steel at 200,000 MPa. This means titanium is 57% as stiff as steel.
2. High Yield Strength: Titanium alloy’s yield strength of 827 MPa is almost equal to that of the strongest of the steel used for the manufacture of the S135 grade of drillpipes. This translates into a Strength-to-Weight (SWR) of 37% over the S135 steel grade.
3. Low Weight: This means for the same hoisting capacity a rig can handle a titanium drillpipe that is almost double the length the same size steel drillpipe.
4. Good fatigue resistance; Lab tests have shown that for cyclic stresses between 200 MPa and 275 MPa, titanium has a fatigue life almost ten times that of steel.
5. Lower susceptibility to corrosion fatigue; It has also been shown that the fatigue performance in air of titanium alloy drillstrings is sustained in the drilling environment. Titanium is generally unaffected by corrosive elements

such as brine, carbon dioxide and hydrogen sulfide that are encountered while drilling.

5.2.4.1 Titanium Drillpipes: Preload and Tensile Yield Stress Analysis

As stated in Table 5-2 and Table 5-3 above and shown Figure 5-7 below, at an external tensile load range of >500KN and <550KN in a titanium alloy drillstring with 0.35mm overlap and using the von Mises failure criterion, the highest nodal stress was seen to be 659 MPa. This constitutes about 75% of the yield strength of 880 MPa for this particular alloy.

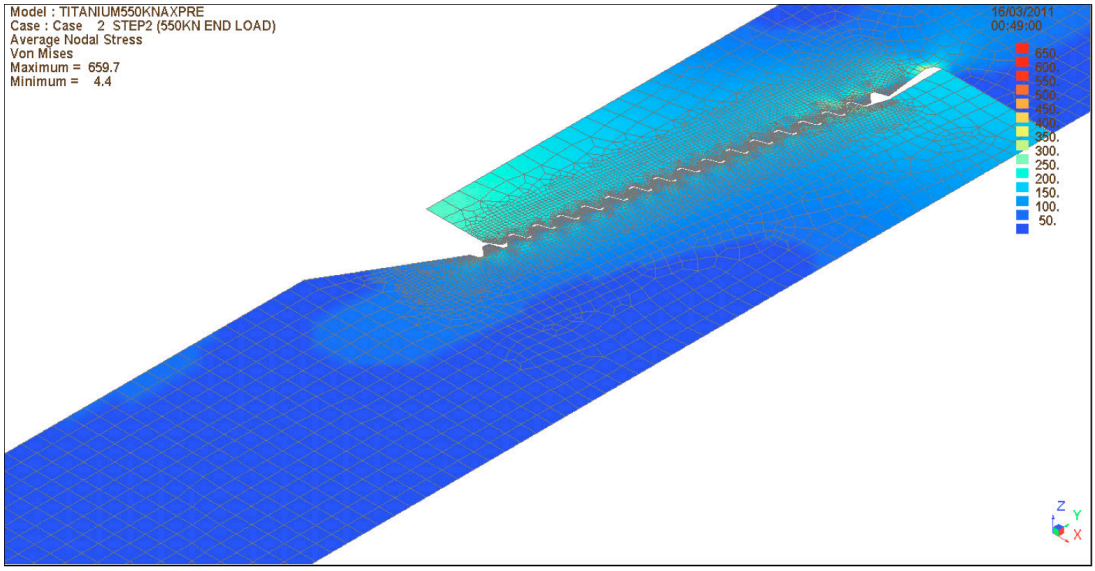

Figure 5-7: von Mises Failure Determination (Titanium Alloy)

Figure 5-8 below shows a graphical representation of the results obtained in the preload simulation where the blue lines represent the variation of induced preload force with the amount of overlap at the teeth, the yield strength of titanium alloy (upper horizontal line) and the stress induced in the string at an overlap value that will produce a preload force that is between 50-75 percent of the yield strength value (the lower horizontal line).

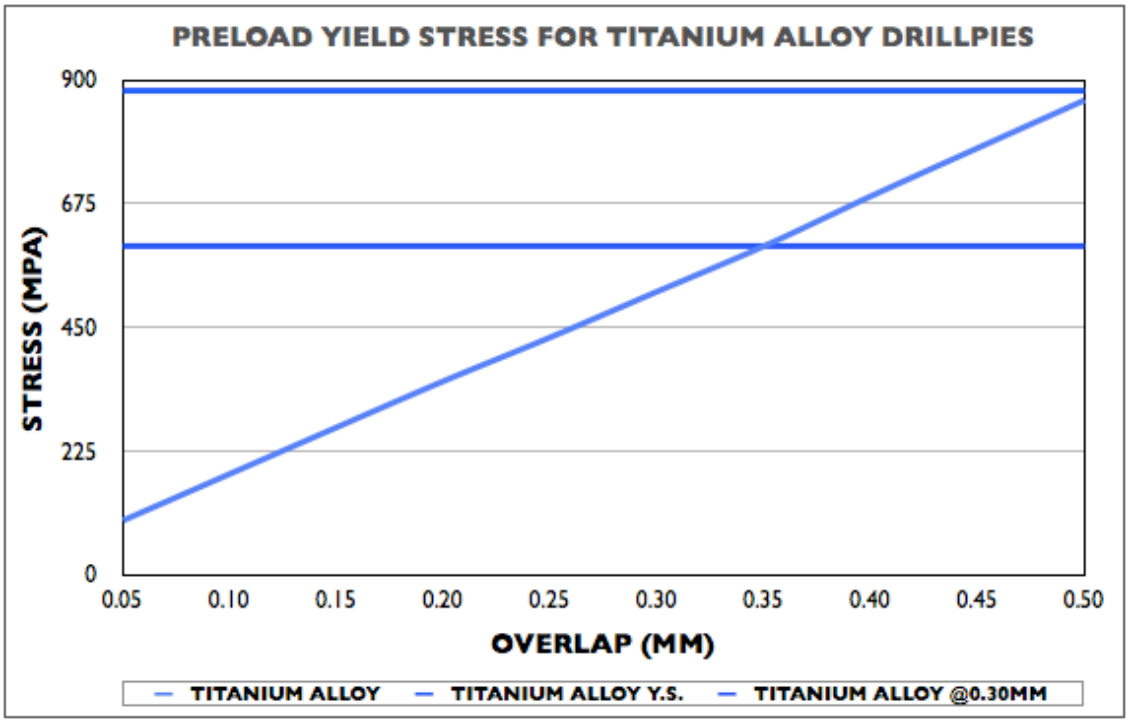

Figure 5-8: Preload Stress Vs Overlap Amount (Titanium Alloy DPs)

5.3 Stress Performance Analyses for the Various Drillstring Materials

From all the three analyses results shown above, the preload stress performance of the materials is plotted below. Because of a combination of high tensile strength and low stiffness, the maximum amount of overlap seen so far, 0.35mm, and thus preload force, can be seen in titanium alloy. This is followed by aluminium alloy with 3.0mm. The lowest value is in steel at 0.2mm. These results are shown in Figure 5-9 below.

Preload stress values are important in ERD applications because of the tendency of a rotating string to gall if its maximum make-up torque limit is exceeded. From the results obtained, coupled with its known property of toughness, it can be deduced that the best performance in this regard is titanium alloy. This makes a good case for titanium alloy tooljoints in equimodulus and hybrid drillstring applications.

The influence of induced preload from overlap lies in the introduction of an internal compressive load in the connection that an external tensile force has to overcome before a net positive tensile stress can be observed in the connection. This brings about a net reduction in the induced stresses in the connection.

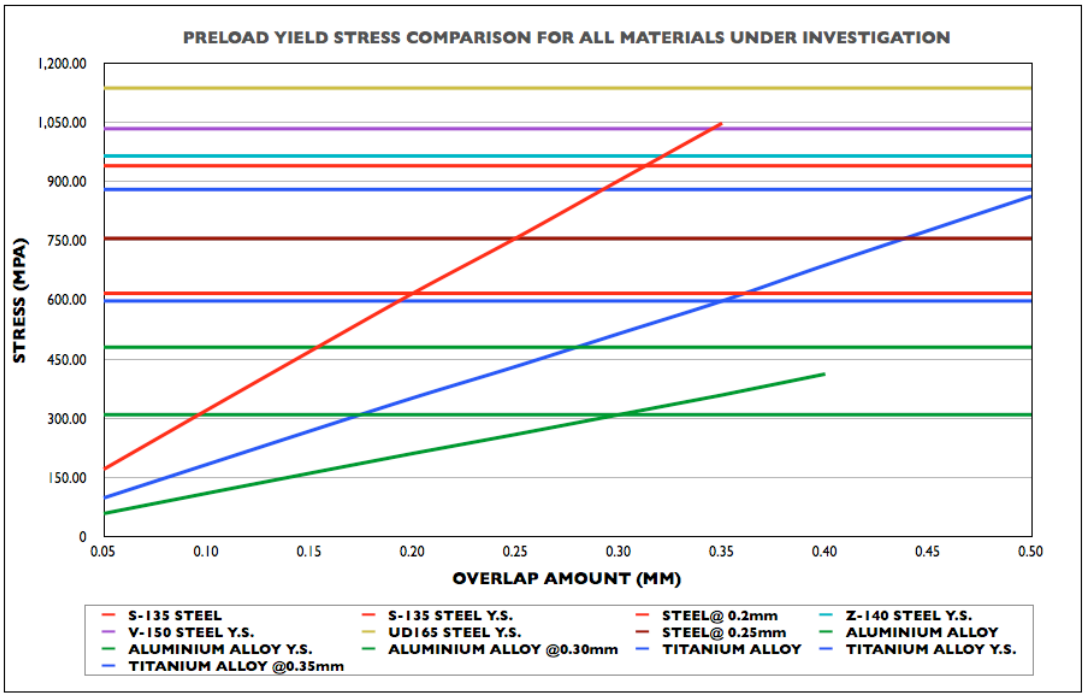

Figure 5-9: Induced Preload Stress Comparison for All Materials

From Figure 5-9 above, which is a superimposition of the observed stress response in preload situation for the materials investigated, the preload performance of the materials under investigation can be seen. The major observation here is that by a combination of lower elastic modulus and toughness, titanium alloy can withstand the highest overlap-induced preload. The practical implication of this is that titanium alloy makes a better material for ERD wells not only because of its inherent toughness but also because of the tendency of contact with the drilled formation to further 'over-tighten' the connections in a rotating string. As it shall be seen later in the discussion on hybrid strings, an ideal combination will be that of a titanium alloy string with aluminium alloy tooljoints that will further reduce the stress concentration factor at the critical root. However, there are currently no aluminium alloy tooljoints manufactured for use with steel or titanium alloy tubulars.

From the results obtained it is observed that in terms of applied axial load, the best performance was observed in the high strength UD-165 steel. While preloaded drillstrings made from other steel grades and titanium alloy are within

their elastic limits for an applied external tensile load of up to 550KN, UD-165 grade of steel is workable up to 600KN. This translates into an ability to support higher hook loads when drilling deeper wells. If this, and cost, are the only criterion then, the UD-165 presents itself as the better alternative in all the strings analysed.

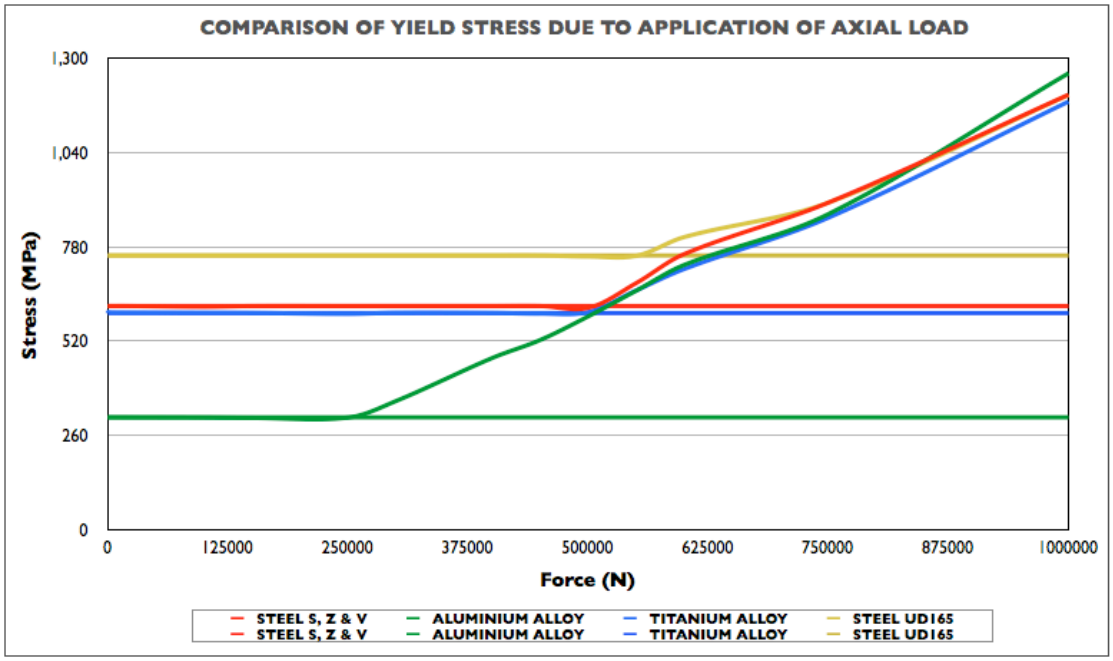

Figure 5-10: Yield Stress Due to Application of Axial Load

Aluminium alloy presents the lowest hook load capacity at 355KN. However, the main reason why aluminium alloy, despite this shortcoming, has remained a good drillstring material is its light weight. A maximum allowable hook load of 355KN for aluminium alloy means strength to weight ratio advantage over steel of 12% (from Table 5-1 above). This, in turn, means rigs can drill to depths with aluminium alloy strings within the same hook load limit that cannot be reached with steel drillstrings.

Aluminium alloy's beneficial buoyancy characteristics, which have not been covered in this work, also point to additional advantages in using aluminium alloy tubulars in actual drilling operation.

When compliance is factored in there is additional advantage of using aluminium alloys as their comparative softness when used in a hybrid string arrangement with either steel or titanium alloy components results in a reduce stress concentration factor (SCF). This is discussed further in the next section.

However, a major disadvantage of aluminium alloys in drillstring application is their low fatigue limit. This means, because fatigue is a major cause of drillstring failure, whatever advantage is exhibited by the material is this application, care must be taken in deploying it in oilwell drilling.

5.4 Reduction in SCF in Hybrid Strings

A lot of research has gone into the various methods of reducing stress concentration at the thread roots, especially the critical root at the last engaged tooth (LET), from which fatigue failure is likely to be initiated. Earlier works have shown that in 65% of the cases failure in threaded connections occur at the LET. To mitigate this type of failure, most investigations propose methods of reducing peak stress values at this location by smoothing out the load distribution across the teeth which will reduce the concentration of the load at the critical location [5.8], [5.9]. Various methods of achieving this effect in loads/stresses have found wide application in fastener technology. Prominent amongst these methods have been discussed earlier in this work.

One of the many proposals suggested by researchers for achieving a reduction in the peak stresses concentration is the use of less stiff materials for the nut in a bolt-nut arrangement, or as in the case of this work, the pin and box of a drillstring threaded connection. Dragoni [5.9] has shown the beneficial effect of varying the bolt and nut material to load and stress distribution in a connection. Starting with the early works on thread load distribution, primarily the work of Sopwith [5.10] and Stoeckly and Macke [5.11] and other investigations that estimated a possible 20% reduction in the thread load concentration factor in an engagement between a steel bolt and titanium alloy nut as compared to an equimodulus connection, he varied the Young's Modulus of the nut to achieve an even further reduction of the peak stresses in the connection.

So far all the finite element analysis investigations carried out in this work were undertaken on equimodulus connections with an overlap-induced preload value and axial tension that is commensurate with the elastic properties of the said materials. In order to extend the work done by Dragoni and present it with the added validation of a finite element study, it was decided to use the already developed NC46 connection model to investigate the effect(s) of varying the material types in a hybrid pin/box arrangement.

A lesser percentage of failures is associated with thread run-out and can be mitigated by decreasing the shank diameter. When the benefits of the a softer box material is combined with a reduction in the shank diameter of the tooljoint, simulated here using the gauge diameters of three different connection geometries, NC40, NC46 and NC50, where the NC50 connection has the smallest shank diameter, then it can be seen that a much greater benefit is derived. The phenomenon of lower SCF in hybrid strings with softer materials is not unconnected with the mechanical compliance of the soft material when in contact with a hard material. In this situation the soft material undergoes greater strain and, if working within its elastic limits, will undergo greater deflections than in an equimodulus situation.

The three different tooljoint geometries (NC40, NC46 and NC50) have the same thread profile (V 0.038R). The loading scenario used in these simulations considers the working limits of the materials of the two connections thus the load input used in the simulation is the lower of the two materials in the hybrid string while the coefficient of friction is maintained at the value used in the previous equimodulus simulations.

For each of the hybrid configurations, six (6) different simulations were undertaken; two each for the three different geometries. The two simulations mimic two scenarios, one a hard box/soft pin and the other a hard pin/soft box. Stress values at the LET thread roots were observed and from these readings a stress concentration factor (SCF) was calculated and compared to the values obtained for an equimodulus string and since the critical LET SCF being observed is in the pin and not the box component of the connection, in both the hard box/soft pin and hard pin/soft box scenarios, it is the critical LET SCF of the pin that is taken as the benchmark. A percentage difference in reduction of SCF was then obtained in each case and presented.

The results obtained from the simulations indicate that a beneficial improvement in SCF is obtained in each case as the string geometry gets smaller. The

significance of this observation is that the benefits of the application of Titanium alloy and Aluminium alloy drillstrings in slimhole drilling can now be viewed from the point of reduced SCF string SCF instead of the only light-weight strings. It was also seen that, as theorised by Dragoni, a more compliant nut, or in our case, a soft box, reduces the peak SCF in the connection when compared to a similar equimodulus connection.

It is important here to mention that the classification of the materials as soft and hard are, in the case of this investigation, a comparison of the stiffness of the materials as depicted by the materials elastic properties and not mechanical hardness as depicted by the material's resistance to plastic deformation as measure in Vicker's and Brinnel hardness tests. All investigations in this work were undertaken within the elastic range. Full finite element analysis simulation results reported here are attached as Appendix E: Simulation Results.

5.4.1 Steel/Titanium Alloy Hybrid String

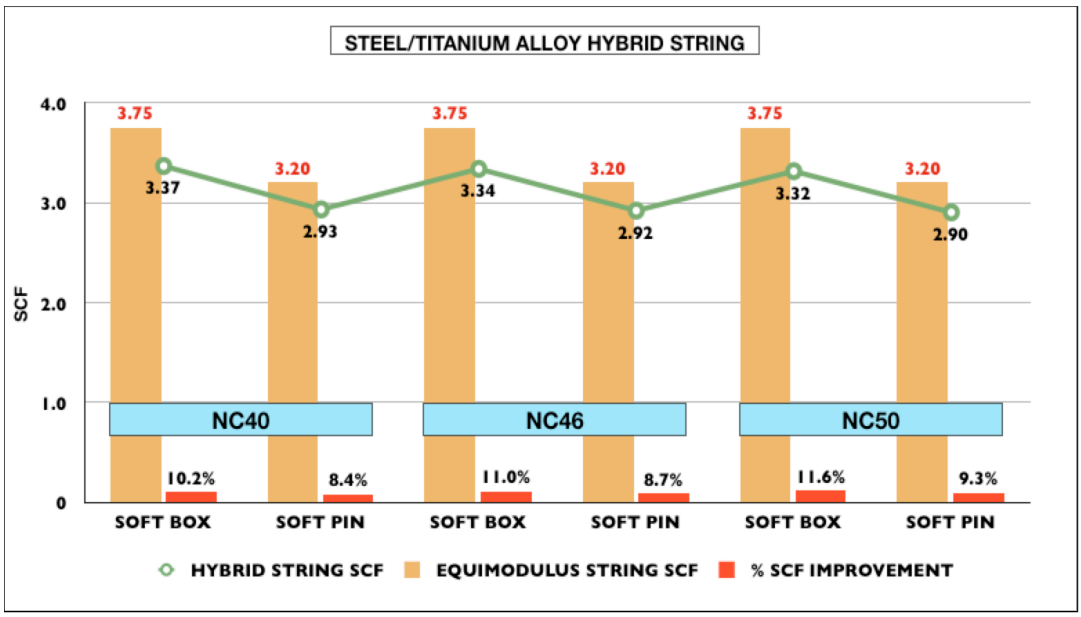

Figure 5-11: SCF Reduction in a Steel/Titanium Alloy Hybrid String

The first hybrid drillstring combination simulated is made up of steel with a Young's Modulus, E, of 200,000 MPa and a Poisson Ratio, η, of 0.3 and titanium alloy with a Young's Modulus, E, of 114,000 MPa and Poisson Ratio, η, of 0.3. In this particular simulation the soft material is titanium alloy while the hard material is steel. To operate within their elastic limits, steel requires an overlap of not greater than 0.2mm while titanium will still be within its safe working limits at an overlap of 0.35mm. Both steel and titanium can support up to 600 KN axial tensile load. In view of this, the simulation was undertaken using an overlap of 0.2mm and an axial load of 600KN.

With a nodal LET stress of 612 MPa was observed in the NC40 connection of steel/titanium hybrid string as against a 791 MPa for an equimodulus steel string. As shown in Figure 5-11 above, the peak SCF value for the equimodulus string is 3.75 while that of the hybrid string with a soft box is 3.37. This difference translates into a beneficial reduction of SCF of about 10% in favour of the hybrid string. For a hybrid string of the same configuration but with a soft pin the reduction in SCF is only 8.4%. There is a further reduction in SCF in both the soft box (11.0%) and soft pin (8.7%) in the case of the NC46 connection and in both the soft box (11.6) and soft pin (9.3%) in the NC50 connection.

In the steel/titanium alloy hybrid string, it can be seen that the largest reduction is SCF (11.6%) is in the NC50 connector where the simulation was undertaken with the box modelled with the elastic properties of the soft material (titanium alloy) and the pin modelled with the elastic properties of the hard material (steel).

5.4.2 Steel/Aluminum Alloy Hybrid String

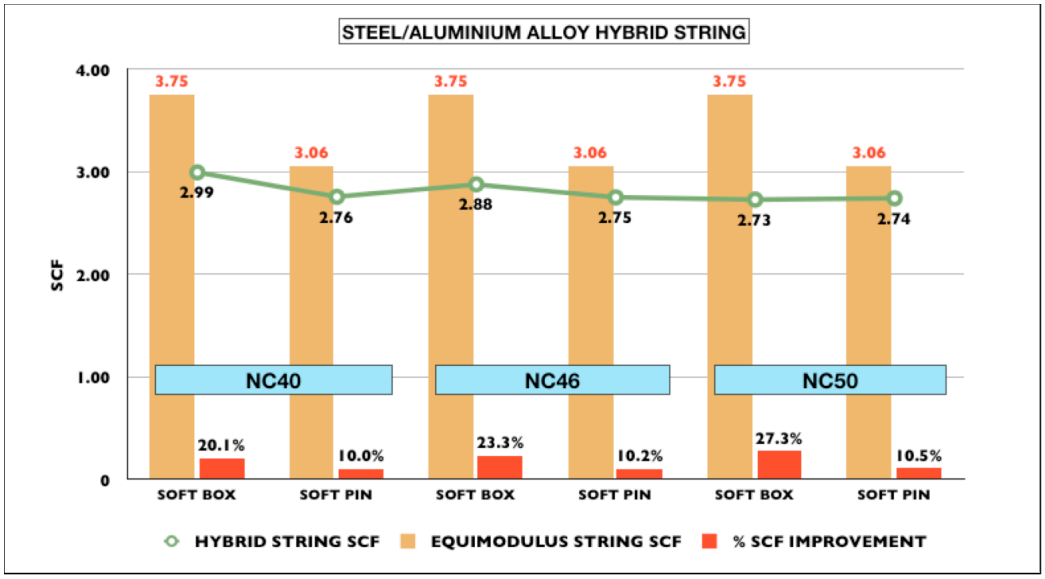

Figure 5-12: SCF Reduction in a Steel/Aluminium Alloy Hybrid String

The model was then used to simulate a preload and axial loading on a hybrid drillstring made up of steel with a Young's Modulus, E, of 200,000 MPa and Poisson Ratio, n, of 0.3 and aluminium alloy with a Young's Modulus, E, of 70,000 MPa and Poisson Ratio, , of 0.35. In this particular simulation the soft material is aluminium alloy while the hard material is steel. To operate within their elastic limits, steel requires an overlap of not greater than 0.2mm while aluminium alloy will still be within its safe working limits at an overlap of 0.3mm. While steel can support up to 600 KN axial tensile load, aluminium alloy will yield at tensile loads in excess of 300KN. In view of this, the simulation was undertaken using an overlap of 0.2mm and an axial load of 300KN in order to stay within the working limits of the softer material.

A peak nodal LET stress of 449.1 MPa was observed in the NC40 connection of steel/titanium hybrid string as against a 392 MPa for an equimodulus steel string. As shown in Fig. 5.12 above, the peak SCF value for the equimodulus string is 3.75 while that of the hybrid string with a soft box is 3.06. This difference translates into a beneficial reduction of SCF of 20.1% in favour of the

hybrid string. For a hybrid string of the same configuration but with a soft pin the reduction in SCF is only 10%. There is a reduction in SCF in both the soft box (23.3%) and soft pin (10.2%) in the case of the NC46 connection and in both the soft box (27.3) and soft pin (10.5%) in the NC50 connection.

In the steel/aluminium alloy hybrid string, it can be seen that the largest reduction is SCF (27.3%) is in the NC50 connector where the simulation was undertaken with the box modelled with the elastic properties of the soft material (aluminium alloy) and the pin modelled with the elastic properties of the hard material (steel). There is a greater amount of compliance between aluminium alloy and steel than between titanium alloy and steel.

5.4.3 Titanium/Aluminium Alloy Hybrid String

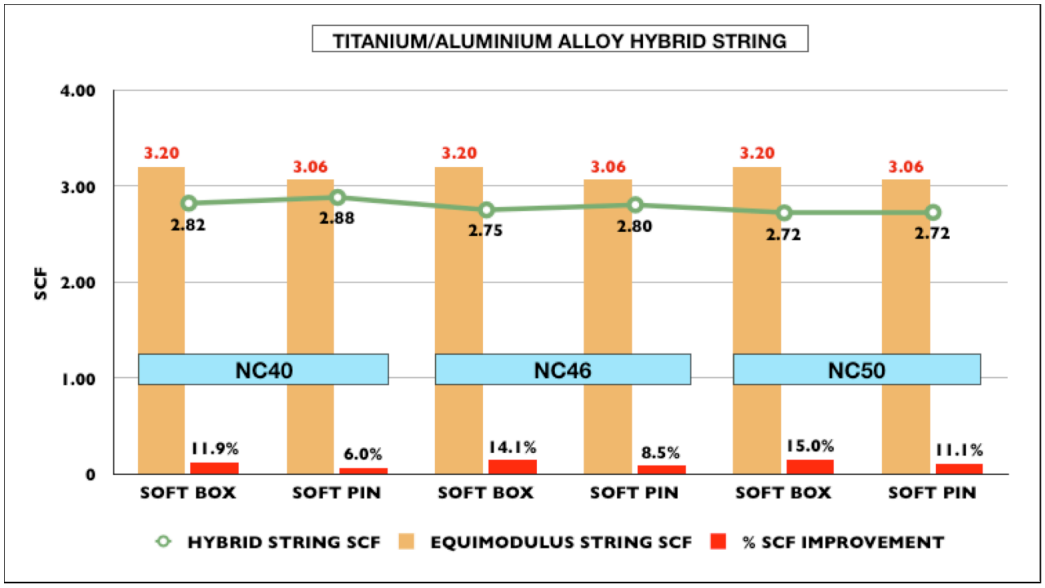

Figure 5-13: SCF Reduction in Titanium/Aluminium Alloy(s) Hybrid String

The last simulation for preload and axial load was undertaken on a hybrid drillstring made up of titanium alloy with a Young's Modulus, E, of 114,000 MPa and Poisson Ratio, η, of 0.3 and aluminium alloy with a Young's Modulus, E, of 70,000 MPa and Poisson Ratio, η, of 0.35. In this simulation the soft material

is aluminium alloy while the hard material is titanium alloy. To operate within their elastic limits, titanium alloy requires an overlap of not greater than 0.3mm while aluminium alloy will still be within its safe working limits at an overlap of 0.35mm. While titanium alloy can support up to 600 KN axial tensile load, aluminium alloy can withstand safely support only 300KN to remain within its working limits. In view of this, the simulation was undertaken using an overlap of 0.3mm and an axial load of 300KN.

A peak nodal LET stress of 449.1 MPa was observed in the NC40 connection of steel/titanium hybrid string as against a 719 MPa for an equimodulus titanium alloy string. As shown in Figure 5-13 above, the peak SCF value for the equimodulus string is 3.20 while that of the hybrid string with a soft box is 2.82. This difference translates into a beneficial reduction of SCF of 11.9% in favour of the hybrid string. For a hybrid string of the same configuration but with a soft pin the reduction in SCF is only 6%. There is a reduction in SCF in both the soft box (14.1%) and soft pin (8.5%) in the case of the NC46 connection and in both the soft box (15.0) and soft pin (11.1%) in the NC50 connection.

In the titanium alloy/aluminium alloy hybrid string, it can be seen that the largest reduction is SCF (15.0%) is in the NC50 connector where the simulation was undertaken with the box modelled with the elastic properties of the soft material (aluminium alloy) and the pin modelled with the elastic properties of the hard material (titanium alloy). This shows compliance that is greater than the one seen between steel and titanium alloy but less than the one between steel and aluminium alloy.

5.5 Conclusion

In total, over eighty (80) simulations runs were undertaken to generate the data used in the analysis. Some of the simulations are for the purpose of studying the robustness of the model and the consistency of the results obtained. Others were undertaken to see if other alloys of the the titanium alloy and aluminium alloy materials will perform any better or any differently from Ti—6AL- 4V and Al-Zn-Mg II respectively. Same was undertaken for different alloys of steel and of varying carbon content. The S, Z, V and UD steels were considered in the case of the hybrid string study as being the same because they share the same elastic properties, which are the primary material inputs in the simulation.

What is with It is noteworthy that in the simulations undertaken care was taken not exceed the operating parametrs of the various materials used in the simulation, especially in terms of the materials' elastic properties and the expected operational parameters in the field. In the case of hybrid strings, particularly, care was taken to use the limiting envelop of the weaker of the two materials in the hybrid in terms of both the tensile axial load and the preload stresses.

The results of the hybrid simulation show the SCF is affected by the compliance of the material, the materials, stiffness (E value) and the geometry of the string. When the geometry of the connection is studied in isolation it is seen that the connections with the smallest diameter give the highest SCF reduction. This makes the case for the application of hybrid strings in slimhole drilling. These observation are further discussed in the next chapter.

5.6 References

[5.1] **Chandler, R.B., Jellison, M.J., Payne, M.L. and Shepard, J.S.**, *"Advanced and Emerging Drillstring Technologies Overcome Operational Challenges"*; World Oil, Vol. 227 No. 10; October, 2006

[5.2] Source:ALCOA; http://www.alcoa.com/oil_gas/en/images/popup/api_diagram.asp; accessed on 12th of December, 2010.

[5.3] **Jellison, M.J., Chandler, B.R., Payne, M.L. and Shepard, J.S.**, *"Ultradeep Drilling Pushes Drillstring Technology Innovation"*, SPE Paper No. 104827 presented at the 15th SPE Middle East Oil & Gas Show and Conference in March 2007

[5.4] **International Standards Organisation**, *"ISO-15546:2011: Aluminium Alloy Drillpipe for the Oil and Gas Industry"*, International Standards Organisation, 2011.

[5.5] **Gelfgat, M. Y., Vakrushev, A. V., Basovich, D. V., Tikhonov, V .S., Odell, A. C. and Brunnert, D. J.**, *"Aluminium Pipes - A Viable Solution To Boost Drilling and Completion Technology"*; International Petroleum Technology Conference (IPTC) Paper 13758, Doha-Qatar December 2009

[5.6] **Smith, J. E., Schutz, R. W. and Bailey, E. I.**, *"Titanium-Drillpipe Development for Short-Radius Drilling"*, SPE Paper 59140 presented at the IADC/SPE Drilling Conference, New Orleans, February 2000

[5.7] **Jellison, M.J., Chandler, R.B., Payne, M.L., and Shepard, J.S.**, *"Drillstring Technology Vanguard for World-Class Extended-Reach Drilling"* OTC Paper 18512 presented at the Offshore Technology Conference, Houston, Texas, May 2007

[5.8] **Patterson, E. A. and Kenny, B.**, *"Stress Analysis of Some Nut-Bolt Connections with Modifications to the External Shape of the Nut"*, The Journal of Strain Analysis for Engineering Design; Vol . 22 No. 4,; Pg. 187-193; 1988

[5.9] **Dragoni, E.**, *"Effect of nut geometries on screw thread stress distribution: Photoelastic results"*, The Journal of Strain Analysis for Engineering Design; Vol . 27 No. 1,; Pg. 1-6; 1992

[5.10] **Sopwith, D.G.**, *"The Distribution of Load in Screw Threads"*, Procedures of the Institution of Mechanical Engineers; 373-383; 391-198; 1948

[5.11] **Stoeckly, E. E. and Macke, H. J.**, *"The Effect of Taper on Screw Thread Load Distribution"*, Transaction of American Society of Mechanical Engineers; Vol. 74, pg. 103-112, 1952

6 Discussion

The need to drill deeper and longer has brought about many new innovations in oil well drilling. New and non-conventional drillstring materials have been introduced and the use of these materials is gaining wide acceptance in the industry [6.1]. There are, however, as presented here, additional optimisations that can be applied to non-conventional strings to reduce the risk of early catastrophic drillstring failure.

The drillstring analysis FE model developed has been used to extend Dragoni's earlier theoretical model about nut compliance. It has now been shown using a validated finite element analysis model that there are great benefits in using softer and more compliant drillstring materials as box connections or tooljoints in the reduction of the load concentration factor which in turn will reduce the stress concentration factor at the critical thread root. This reduction in SCF translates into a much better S-N curve, which means longer service life for the connection under the same stress amplitude.

The current industry convention with hybrid strings is to fit on them steel tooljoints. This, as was explained in previous sections, is to ensure seamless handling of both the titanium and aluminum drill pipes on the drill floor where the pipe handling equipment are those designed for steel drillpipes. In that case, for the industry to fully benefit from the findings in this work it has to come up with ways in which tongs, slips and other drill pipe handling gear can be used on softer materials with damaging the tooljoints. This may require the retro-fitting of the entire pipe handling and hoisting system to accommodate softer drillstring materials. Alternatively, the industry may consider introducing, as was the done in the case tooljoint hard-banding, a way to make the joints stronger and more wear resistant enough to be used on normal drill floors without a need for the replacement of handling equipment. Or alternatively locate strings made from the softer materials in deeper or high-angle sections of the well where they will not be supporting much of the string's hook load.

6.1 Induced Stress in the Connection

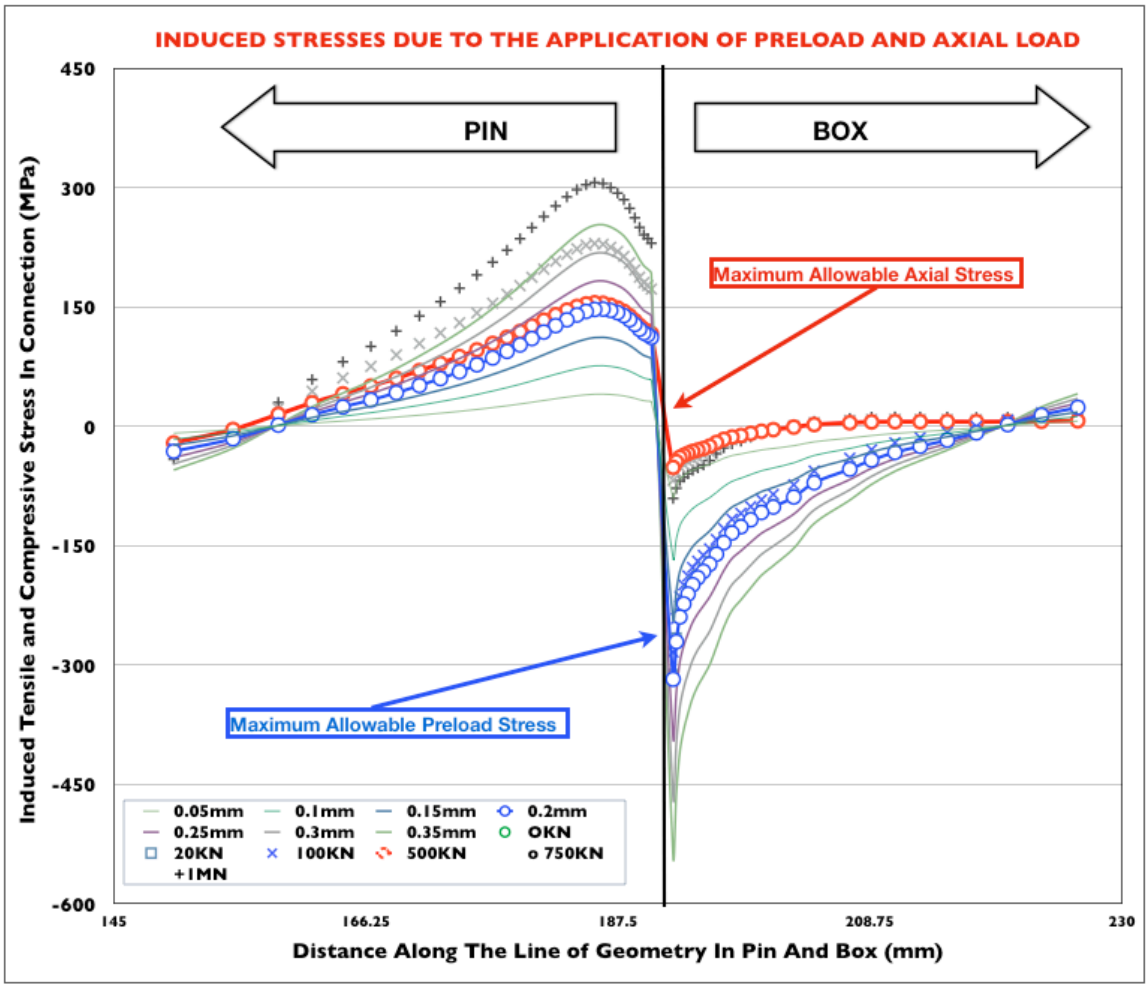

Figure 6-1: Stress Distribution on AISI 4145H Steel Connection

Figure 6-1 above shows the distribution of stresses due to both preload and axial tensile load on nodal points along the geometric lines on the pin and box components of the AISI 4145H material used in the benchmark study. The geometric lines act as sensors located near the loaded of the connection to read the stress in the connection. See Section 4.5.3 in Chapter Four above.

The stresses are plotted from the internal diameter surface of the pin to the outer surface of the box. The blue line shows the stresses due to overlap-induced preload stress at 0.2mm overlap in the pin and box while the red line shows the stresses due to the applied external axial load of 500KN. Stress distribution plots for all the materials simulated and can be seen in Appendix E:

Simulation Results.

In all the simulations undertaken, it was observed that in the presence of preload, applied axial tensile load leads to a reduction in the compressive stress in the box while the limiting factor for applied axial load remains the amount calculated or observed to maintain the integrity of the connection, i.e., an amount that shall not be larger than the axial stress induced in the pin due to only the preload induced compressive stress in the box.

In this particular instance, from the above figure, it is observed that no parting is experienced at the shoulder of the connection because the applied axial tensile load of 500KN does not overcome the axial stress in the pin due to the induced preload compressive stress at 2mm overlap.

It was also observed that the excessive preload-induced compressive stress in the box is greatly reduced from >-300MPa to - 50MPa by the introduction of the external axial load. While failure the connection is more likely to come from tensile rather than compressive stresses, the reduction axial load optimizes the integrity of the connection.

The reason why most failures in the roots of the thread, especially in the LET, occur in the pin - and in the presence of external tensile load, could be explained from the fact that at no point is the box in tension in the teeth region. It can also be noted that in the presence of a more compliant box material in a hybrid connection, the peak tensile stress in the pin will further relieved thereby creating a reduction in the SCF in the pin.

6.2 Fatigue Properties of Drillstring Materials

The observations made in this work were primarily undertaken to study the load/stress response in static loading scenarios of an oilwell drillstring connection. Important as this may be in understanding the expected behaviour of tubular materials under loading, it is essential to keep in mind that most drillstring failures are as a result of fatigue, static loading then becomes the reason why a connection of compromised integrity, due to fatigue crack initiation, fails. Other important causes of failure initiation are impact and torsional loads. Fatigue, or progressive fracture, plays the most important part in the initiation and propagation of drillstring failure mechanism. By some estimation over 73% of the failure of drillstring connections is attributable to phenomenon [6.2]. Since it was recognised as a major structural issue in the 1840s, engineers have been having a running battle with fatigue as most engineering components fail by fatigue than by any other failure phenomenon [6.3].

As a result various methods have been proposed to assess the susceptibility of materials to fatigue failure. Most of these are through the determination of the materials fatigue life or its resistance to failure due to cyclic loading. Some of the engineering models for the prediction of fatigue failure in materials are discussed in Appendix B5: Fatigue Failure in Drillstrings.

6.2.1 Fatigue Life Models

Several empirical models exist for the determination of fatigue life and fatigue crack growth. Rankine's observations [6.4] established the influence of dynamic loads in the sudden failure of components. Then a few years later Wohler's work on failure of components when subjected to cyclic stress repetitions documented the existence of an endurance limit in materials and led to the introduction of the S-N curve concept as the first scientific method of investigating the fatigue life of materials [6.5]. Several other models were proffered but the most widely accepted are those by Gerber in 1874

[6.6], Goodman in 1899 [6.7] Soderberg in 1930 [6.8] and Morrow in 1960 [6.9].

Three main fatigue-failure models are in common use. These are the Stress-Life (S-N), the Strain-Life (e-N) and the Linear Elastic Fracture Mechanics (LEFM) models.

6.2.2 Fatigue Life Comparison of the Connections Studied

Since one of the primary factors that influence fatigue life or failure is a sufficient tensile stress, then it follows that the stronger and tougher materials will resist fatigue more robustly than weaker and softer materials. Conversely, materials with greater modulus of elasticity such as steel are expected to be stiffer and will, going by the discussion in Appendix B5: Fatigue Failure in Drillstrings, have larger lower permissible DLS (C) values, as proffered by Lubinski [6.10]. It is worth noting here that while the C values are dependent a material's modulus of elasticity, the fatigue-life behaviour of materials is not dependent on modulus of elasticity values.

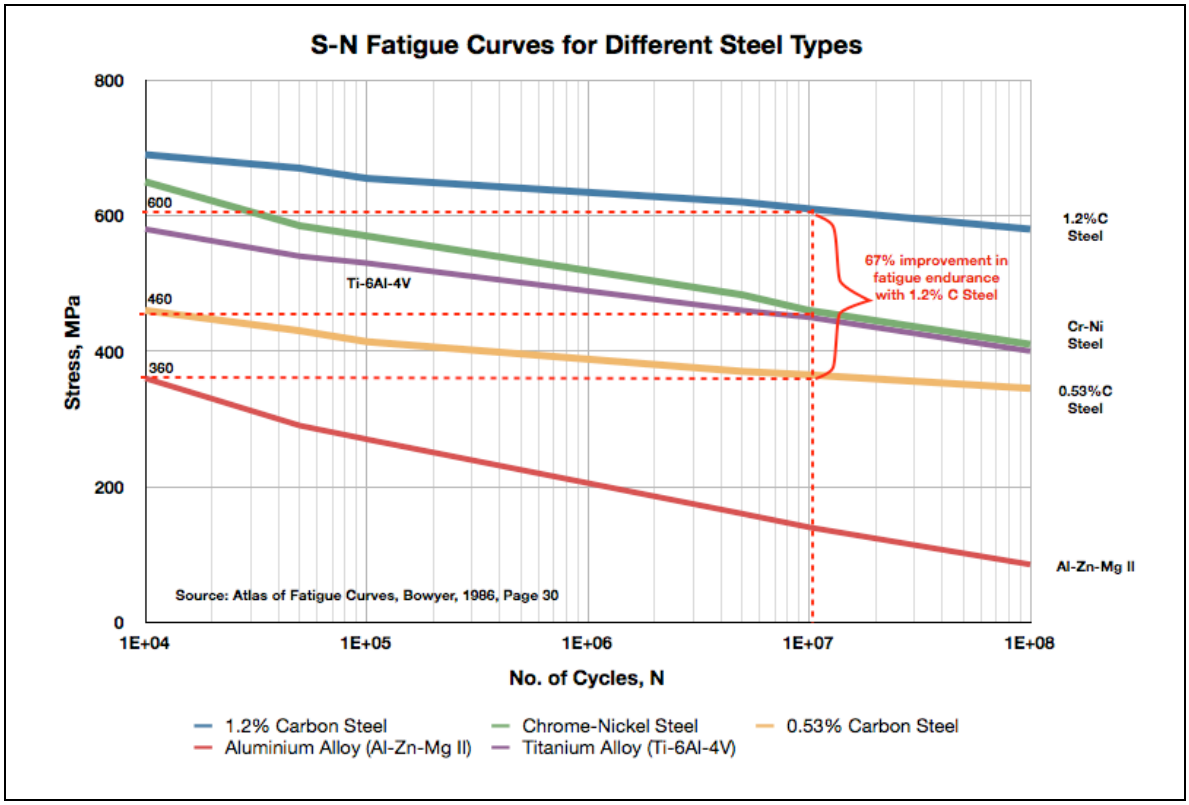

Figure 6-2: S-N Comparison for Steel and Ti and Al Alloys [6.11]

While from an engineering perspective, of the three materials analysed in this work, the best fatigue properties from the S-N curve point of view is obtained from titanium alloy, the prohibitive cost of this material is a major disadvantage. The next best choice in this regard is steel but, as will be seen later in the chapter, hybrid string of steel and aluminium alloy gives a very good reduction in SCF at the LET which will have a positive effect as far as resistance to crack initiation is concerned.

From the foregoing, it can be seen that the fatigue argument makes aluminium alloy less desirable because even though it provides the lowest reduction in SCF when combined with any of the other two materials in a hybrid string scenario, it will fail much sooner due to its low fatigue resistance. But if a 'softer' steel is used in place of Aluminium alloy as the soft component of a steel-on-steel hybrid string, there will, in effect, be an steel-based equimodulus string with the beneficial fatigue resistance of steel - because the modulus of elasticity remains unchanged - and the added benefit of low SCF which is good for

resisting fatigue crack initiation and propagation – a phenomenon observed in all hard/soft material combinations. But, since most carbon steels have near-identical modulus of elasticity of about +/-200 GPa, and the E value is what has been defined as the governing factor as to which material is soft or hard, then other properties, such as fatigue resistance and yield strength shall be the basis upon which the various steels are compared.

In Figure 6-2 above, a comparison is shown of the fatigue resistance of three different steel types; 1.2% carbon steel, Chromium-Nickel steel and 0.5% carbon steel. All three exhibit different levels of fatigue resistance. We can see from the table that the SCF benefits of using 'soft' aluminium alloy can be approached without the prohibitive cost of titanium alloy. This means that these steel types can be used in place of the more common AISI 4145H steel for the manufacture of drillstring components or, at the very least, be used in the manufacture of tooljoints to used on AISI 4145H steel or on aluminium alloy drillpipes as both exhibit lower fatigue resistance than both the 1.2% carbon steel and the Chromium-Molybdenum steel.

The steel grade most commonly used for the manufacture of drillstring materials, the AISI4145H, is a chromium-molybdenum (Chromoly) high carbon steel with 0.42% - 0.49% by weight of carbon. The 'H' at the end signifies the added property of 'hardenability' to the material - which means that the steel can be hardened by heat treatment.

Amount of carbon by weight in a steel composition is used to manipulate and obtain some desired properties in steel. Carbon steels which can successfully undergo heat-treatment have a carbon content in the range of 0.30–1.70% by weight. Trace impurities of various other elements can have a significant effect on the quality of the resulting steel. Medium carbon steel can have approximately 0.30–0.59% carbon content. It balances ductility and strength and has good wear resistance. It is used for large parts, forging and automotive components. AISI4145H steel used in the manufacture of drillstring components

fall within this classification. High carbon steels on the other hand can have approximately 0.6–0.99% carbon content.

Ultra-high carbon steel has approximately 1.0–2.0% carbon content. This class of steels can be tempered to great hardness. They are used in special applications where strength is required such as knives, axles or punches. As is shown in Figure 6-2, steels with higher carbon content of over 1% have been shown to have higher fatigue resistance properties [6.11].

6.3 Analysis of Hybrid String Configurations

Appendix E reports the simulation results undertaken on the equimodulus connections of AISI 4145H steel, aluminium alloy and titanium alloy. Hybrid strings were simulated in a similar way but the elastic modulus of one of the two components (pin or box) that make up the connection was switched to that of a different material.

To effectively study and compare the performance of hybrid strings, three loading scenarios were considered, namely, P1, P2 and P3. P1 considers what has been defined as the minimum depth of an ultra-deep well, which is 25,000 ft or 7600 m. P2 is the depth of the record deepest well, the Knotty Head well drilled in the Grand Canyon in the Gulf of Mexico, which was drilled up to a depth of 34,000ft or 10,420 m. P3 is the margin of overpull that can be exerted on the string in case of stuck pipe or other similar hole problems. This value is the difference between the tensile strength of the string and the hook load.

The hybrid string configurations subjected to these loading scenarios are;

a. Steel/Titanium Alloy
b. Steel/Aluminium Alloy
c. Titanium Alloy/Aluminium Alloy
d. UD-165 Steel/AISI 4145H Steel

Data was collected for both a soft box, where the box material has a lower modulus of elasticity, and a soft pin, where the pin material has a lower modulus of elasticity, scenarios. Using the calculated load limits corresponding to the tensile strength on the material under study, a corresponding maximum allowable stress on the connector was calculated and the peak stress on the LET observed. This was in turn looked at in relation to the materials fatigue strength and the stress concentration factor in the root of the LET.

The results obtained for both the soft pin and the soft box scenarios are shown in Figure 6-2 and Figure 6-3 below. From the results obtained it can be seen that in the P1 and P2 loading scenarios aluminium alloy exhibits the lowest peak stress. This is expected in line with its elastic properties and low yield strength. It can also be seen that all hybrid configurations, apart from the UD-165/Steel hybrid, are too weak to withstand the stress exerted in the overpull (P3) loading scenario. Even in the case of the UD-165/Steel hybrid configuration, the induced stress of 878.8 MPa is 94.4% of the yield strength of the S-135 steel, which at 930 MPa has the lower yield strength of the two materials in the configuration.

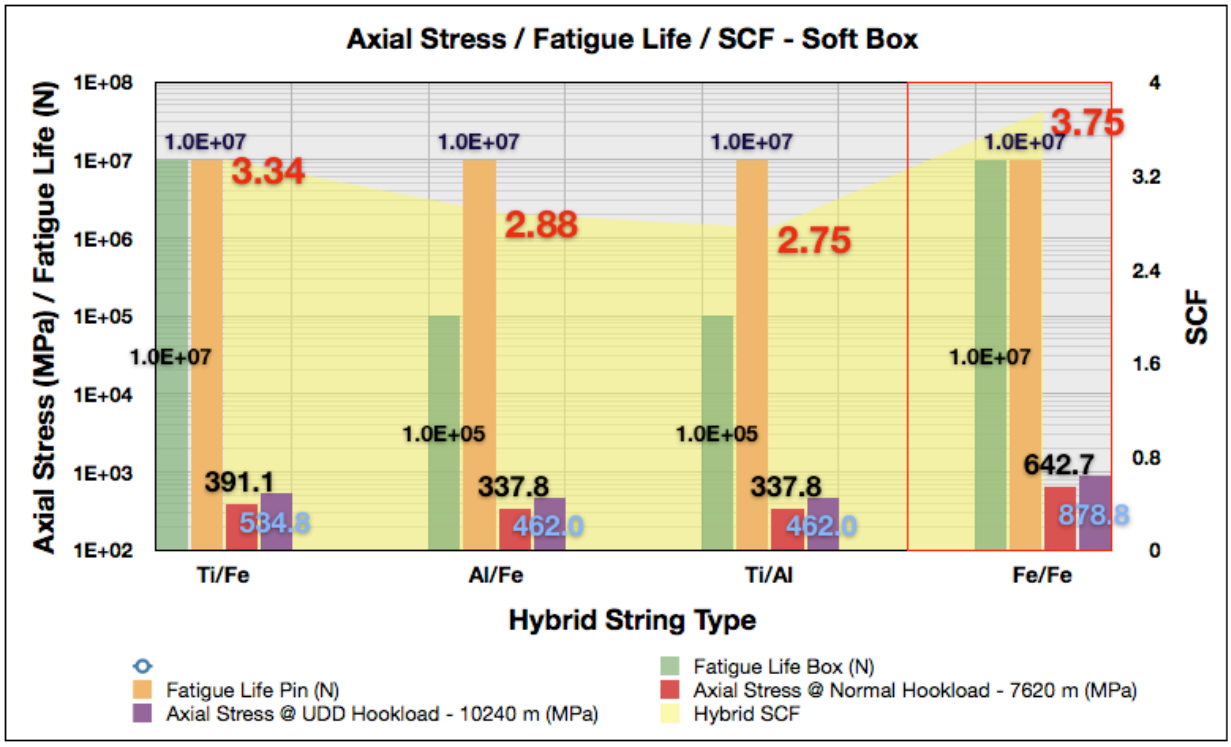

Figure 6-3: Stress and Fatigue Life of Hybrid Strings (Soft Box)

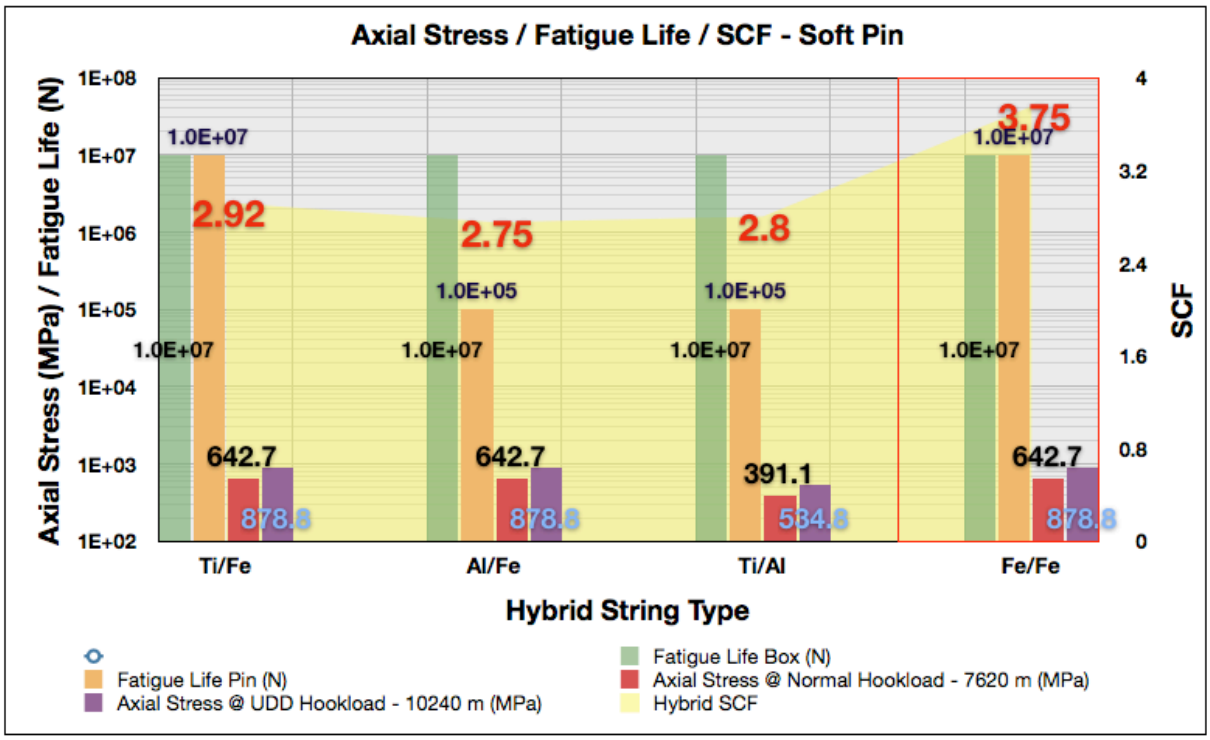

Figure 6-4: Stress and Fatigue Life of Hybrid Strings (Soft Pin)

6.3.1 Elastic Response of Hybrid Strings to Loading Scenarios

It has been shown earlier in Section 5.4 of Chapter Five how Dargoni's investigations in the reduction of SCF in hybrid nut and bolt situations due to material compliance was validated in this work. However, that is but a benchmark study that highlights the beneficial reduction in SCF obtainable vis-à-vis the physical size of the tooljoint (NC40, NC46 and NC50) and the materials that form the hybrid (Steel/Titanium Alloy, Steel/Aluminium Alloy and Titanium Alloy/Aluminium Alloy). Unlike what is being discussed in this section, the benchmark study in Chapter Five does not relate the loading or the elastic response of the connection to actual drilling situations.

Therefore the results presented in Figure 6-2 and Figure 6-3 above tend to be both more practical and realistic as they are obtained with the UDD loading scenarios factored into the simulation. Furthermore, it relates the elastic performance of each hybrid configuration to the fatigue performance of the materials that make up the string.

6.3.1.1 Fatigue and Cost Penalties of Hybrid String Configurations

Looking at the simulation results in isolation as was presented in Chapter Five, a larger reduction in SCF is observed in hybrid configurations that include aluminium alloy. However, when fatigue is factored into the expected performance of the connection, as is shown here, it can be clearly seen that such a large reduction in SCF does not compensate for the low fatigue life obtainable from aluminium. Aluminium alloy exhibits a fatigue life of only 105 cycles at a maximum allowable stress of about 400 MPa.

Advisably, hybrid strings that include aluminium alloy drillpipes should only be run deeper in the well where they support a small fraction of the entire string hookload. They should also be run in drilling situations where the rotation of the bit is provided by a positive displacement mud motor and not the rotary or top drive. When the string is rotated using a positive displacement mud motor the part of the sting upstream from the motor does not rotate, in which case the string is not required to rotate in doglegs that are shallow up the borehole.

The next best SCF reduction scenario is where titanium alloy is used in the hybrid configuration. But even with this and the advantages of titanium discussed earlier in this work the prohibitive cost of titanium makes it economically unfeasible for consideration as drillstring material in deep and ultra-deep drilling. With a lower yield strength than both conventional and UD-165 steels, it is also advisable that, like aluminium alloy, it should be run deeper in the well but unlike aluminium alloy it can be used in both rotary and sliding (mud motor) drilling modes as it has much higher fatigue strength and can thus be employed more readily in areas of high cyclic stress such as doglegs.

6.3.1.2 Overpull Margin in the UD-165 steel connection

Analysing the results shown in Figure 6-2 and Figure 6-3 above, it can be seen that, as expected, the peak SCF in the connection does not change in the UD-165/Steel hybrid string irrespective of which of the two steel types is the box (or

pin). This is expected as they have the same elastic properties. However, as shown in Table 5-1 in Chapter Five, UD-165 has superior yield strength of 1137 MPa thus making the material ideal for ultra-deep drilling. This also means that the material has a more generous margin of overpull in case it is ever required, for example in the event of a stuckpipe situation. Also, as was shown in Figure 4-11 in Chapter Four the SCF value of 3.75 obtained from this hybrid configuration in both the soft box and soft pin scenarios agrees with the FEA results obtained when a simulation was undertaken to validate the model against Tafreshi-Dover's results.

6.3.1.3 More Compliant Steel in a UD-165/Steel Hybrid Configuration

As it has been shown by Dragoni [6.12] and validated in this work, a hybrid connection consisting of more pliant material(s) tends to have a reduced SCF than a similar equimodulus steel connection. It has also been seen that because the elastic properties of UD-165 and conventional steel (E and υ) are the same, no reduction in SCF will be observed.

For most materials, especially steel alloys, it is common knowledge that the method of manufacture, rather than the thread form dominates a connection's fatigue strength.

However, the fact that a reduction in SCF has been shown to be possible in the case of a hybrid string of two different moduli of elasticity whereby the box is made from softer material means that the compliance of the material used in the manufacture of the connection is a function of its elastic properties. As has been shown in the hybrid string analyses undertaken above, the 'soft' and 'hard' terminologies were attached to materials not to denote their hardness (resistance to indentation or scratching) but to their stiffness as exhibited in accordance to their elastic properties.

To see a marked variation in fatigue resistance (as can be registered on an s-n diagram) in a given connection, the variation in elastic moduli across different

steel alloys becomes more important as gains can be shown to be obtained at both ends; namely due to the combination of a ‘hard’ and ‘soft’ materials and the selective transfer of peak SCF in the pin.

Because of the cantilever action that takes place on each thread flank, the axial, bending and torsional loads are likely to induce stresses in the connection that are beyond surface and which may, at higher intensities be through thickness. Nonetheless, to further enhance the fatigue resistance of the connection; a manufacturing method that introduces compressive residual stresses, such as thread cold rolling and shot/laser peening can be used that further increases the fatigue performance of the connection [6.13].

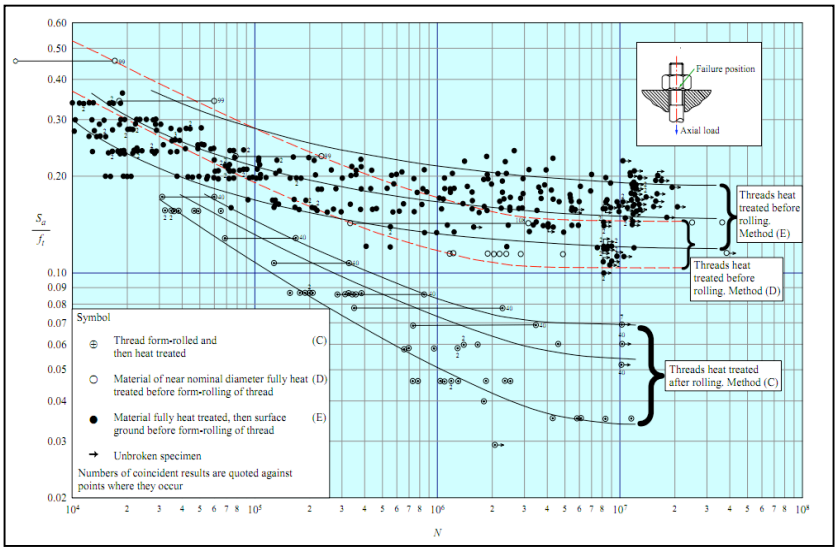

Figure 6-5: Heat and Surface Treatment of Thread Materials [6.13]

It has been shown experimentally that heat-treating threads before rolling increases the fatigue strength of the threads [6.14]. Of the methods shown, method ‘E’ where the material is fully heat-treated and surface ground before rolling the threads results in better fatigue resistance than if the material simply heat-treated before rolling the thread (method ‘D’) or the threads are rolled before the material is heat-treated (method ‘C’). It can be observed here that both the AISI4145H and the 1.2%C steel shown in the S-N diagram above have the ability of being heat treated and surface treated to obtain desired performance properties.

6.3.1.4 Titanium alloy as a Tooljoint Material

A tooljoint made form a different material can be used at the hybrid interface for various reasons. Where aluminium alloy drillpipes are used in place of, or in a hybrid arrangement with, conventional steel drillpipess, most operators are reluctant in retrofitting the drill floor with pipe handling equipment suited for the softer aluminium alloy drillpipe. As such, the aluminium alloy pipes come with friction-welded steel tooljoints.

However, since it is desirable to have a material of reduced stiffness at the hybrid interface as a box material to reduce the SCF in the connection, a steel drillpipe can be made with a box made from either titanium alloy or aluminium alloy. But, again, since aluminium alloy has low fatigue resitance and low tensile strength, titanium alloy would be more ideal for this application.

Due to its prohibitive cost, titanium alloy is not readily used as drillstring material. However, from the results seen in this work, titanium alloy, which is lighter but almost as strong as steel, is ideal as a tooljoint material because its stiffness is higher than that of aluminium alloy but lower than that of steel and much lighter than steel. A light and ultra-slim drillstring made from steel but with titanium alloy tooljoints will have a 15% lower SCF values at the critical thread root than the same string with steel tooljoints. This is in addition to the reduced string weight occasioned by using titanium alloy tooljoints instead of the heavier steel tooljoints. Additionally, when titanium alloy is anodized and coated with dry film lubricants, its metal-to-metal wear resistance properties can be greatly improved [6.15].

6.3.1.5 Lighter Drillstring to Increase Rig Rating

Drilling rigs are rated in accordance to their loading and hoisting capacity. For reasons of safety and stability, the capacity rating of a rig is directly dependent on how much load it can hold on deck and how much weight it can hoist. The latter is directly related to the depth that can be drilled by the rig while the

former is related to logistic costs, depth rating and the stability of the drilling unit as an offshore floating vessel.

Without looking at factors such as the reduction of the hook load due to buoyancy and increase of string weight due to the weight of the bottom hole assembly (BHA), a 5", 19.5 pounds per inch S-135 drill pipe with NC50 connection required to drill 25,000 ft will have a weight in air of (19.5 x 25000=487,500 lbs) or 221,130 kg. The investigations undertaken on titanium alloy drillstrings with the FEA model considered only preload and axial loading. While these contribute to the greater amount of stress the string will experience, bending loads and impact loads will also contribute to such stress.

With a SWR ratio advantage of 37% percent for titanium alloy over steel this means an identical drillstring made from only titanium alloy material will drill up to 34,250 feet before it exerts the same hook load as 25,000 ft of a S-135 steel drillstring. Moreover, in the Steel/Titanium alloy hybrid FEA simulation, by limiting the loading on the string to the capacity of the weaker member in a hybrid configuration, the working safety limit in respect of the stronger (stiffer) member is improved. This in itself is good but when viewed in relation to the expected location of peak stress, which is the LET on the pin, then the benefits become even more pronounced.

The advantage of a lighter string, titanium alloy in this case, is even further improved when it is considered that within the working limits of an aluminium alloy string, the same titanium alloy string run with the softer aluminium alloy tooljoint at the hybrid interface will further reduce the SCF at that point.

Titanium's prohibitive cost must be considered before suggesting its use in a drillstring of whichever style or configuration.

6.4 Conclusion

Three different types of drillstring materials were analysed to establish their working limits and to establish their performance in hybrid string configuration. The analyses were limited to stress response due to applied internal (preload) and external (tensile) loads. While the investigations have confirmed the expected physical and mechanical response of these materials, it has also shown areas of possible modification to current drillstring applications to increase the depths that can be reached by the strings and to reduce fatigue failure through the reduction of peak stress concentration at the critical thread root, the pin LET.

The use of a hybrid string has been found to reduce the peak SCF in the LET in the tooljoints especially in the case of softer box material. This is in addition to the reduced string weight when titanium or aluminium alloys are used as string material in place of steel. This investigation has proven the benefits of a ‘soft’ material tooljoint on the entire string to reduce the SCF and decrease the string weight.

The findings were applied to simulate the expected behaviour of a hybrid string in a ‘real-life’ oilfield drilling situation where the expected hookload of three different wells, a well of a normal deep well, an ultra-deep well and a drilling overpull margin, was used used to see the advantage of the hybrid string over a similar equimodulus string.

Advantages were shown to be not only in the reduced string weight in terms of the use of lighter materials in the hybrid make-up but also in the reduced stress concentration factor (SCF) when a more compliant (softer) material is used as part of a hybrid string.

6.5 REFERENCE

[6.1] **Jellison, M.J., Chandler, R.B., Payne, M.L, Shepard, J.S.**, "*Ultradeep Drilling Pushes Drillstring Technology Innovations"* SPE paper 104827; SPE Drilling & Completion, June 2008

[6.2] **Pitts, J.P.**, *"Trip Inspection, Testing Gain Favor as Insurance"*; *Drill Bit*, 303, 885.

[6.3] **Schutz, W.**, *"A History of Fatigue", Engineering Fracture Mechanics"*, Vol 54, No. 2, 1996, pp. 263-300

[6.4] **Rankine, W.J.M.**, *"On the causes of the unexpected breakage of the journals of railway axles, and on the means of preventing such accidents by observing the law of continuity in their construction". Institution of Civil Engineers,* 1842, *Minutes of Proceedings*, 105-108

[6.5] **Wohler, A.**, "Versuche zur Ermittlung der auf die Eisenbahnwagenachsen ein wirkeden Krafte und die Widerstandsfahigkeit der Wagen-Achsen", Zeitschrit fur Bauwesen, X, 1860, pp 583-616.

[6.6] **Gerber, W.Z.**, *"Calculation of the allowable stresses in iron structures"*; Bayer Archif Engineering;6(6):101-110.

[6.7] **Goodman, J.**, *"Mechanics Applied to Engineering"*, Longman, Green & Company, London, 1899

[6.8] **Soderberg, C. R.**, *"WorkingStress"*, Trans. ASME 52, APM-52-2, 13, 1930

[6.9] **Morrow, J.**, *"Fatigue Properties of Metals"*; Proceedings of Division 4 of the SAE Iron and Steel Technical Committee, Nov. 4, 1964.

[6.10] **Lubinski, A.**, *"Maximum Permissible Doglegs in Rotary Boreholes"*; Journal of Petroleum Technology, February, 1991

[6.11] **Bowyer, H. E.**, *"Atlas of Fatigue Curves"*, Published by ASM International; 1986; Pp. 30.

[6.12] **Dragoni, E.**, *"Effect of nut geometries on screw thread stress distribution: Photoelastic results"*, The Journal of Strain Analysis for Engineering Design; Vol . 27 No. 1,; Pg. 1-6; 1992

[6.13] ESDU 84037

[6.14] **Kristoffersen, S.**, *"Improved Fatigue Performance of Threaded Drillstring Connections by Cold Rolling"*, Dr. Ing Thesis, Norwegian University of Science and Technology, 2002

[6.15] **Budinski, K. G.**, *"Tribological Properties of Titanium Alloys"*, Wear Vol 151, Pp 203-217. 1991

7 Conclusions and Future Work

7.1 Conclusions

This work has succeeded in presenting an analysis of the state of knowledge of stresses induced in threaded connections and applying such knowledge to the novel scenario of an oilwell drillstring. This was achieved through a detailed literature review of the theories and of thread stress and the tools of computational mechanics employed in the analysis carried out in the work.

This work hereby presents a novel way of applying internal stress, also known as preload, in a threaded connection. The method is validated using results of similar theoretical, practical and simulated works carried out in the past by earlier researchers in the field. The method involves using the thread geometry profile which is broken down into sets and also an Abaqus keyword command and keyword to simulate the mechanical response of a threaded connection in the presence of a preload force, Abaqus is the finite element analysis software package used the work. This is termed Interference Fit Method.

Using this method an axisymmetric model of the drillstring threaded connection using the linear elastic properties of the benchmark AISI 4145H steel grade is then developed for the eventual simulations carried out in the work. A total of over sixty simulations were undertaken from which the model was validated with earlier work. The simulations also help to build a pattern of stress response to both axial loading and preload in response to applied load. It is against this pattern of behaviour that the model's response was compared when other type of materials were simulated either in a standalone equimodulus connection or in a hybrid connection.

Three different types of drillstring materials were analysed to establish their working limits and to establish their performance in hybrid string configuration.

The analyses were limited to stress response due to applied internal (preload) and external (tensile) loads. While the investigations have confirmed the expected physical and mechanical response of these materials, it has also shown areas of possible modification to current drillstring applications to increase the depths that can be reached by the strings and to reduce fatigue failure through the reduction of peak stress concentration at the critical thread root, the pin LET.

The use of a hybrid string was found to reduce the peak SCF in the LET in the tooljoints especially in the case of softer box material. This is in addition to the reduced string weight when titanium or aluminium alloys are used as drillstring material in place of the heavier steel. This investigation has proven the benefits of a ‘soft’ material tooljoint on the entire string to reduce the SCF and decrease the string weight.

Because of the positive results to be expected in the deployment lighter equimodulus strings and reduced SCF at the connections in hybrid strings as highlighted in the findings and validations in this research work, every branch of industry in which threaded connections are employed as fastening mechanisms in general but the results of the research will be found especially useful to the global oil and gas industry in which the viability of projects can be directly linked to the assessment of the possibility of getting that bit at the end of thousands of threaded connections to strike that reservoir buried tens of thousands of kilometres in the subsurface.

In this work, a new method of undertaking FEA analysis of drillstring has been developed and is hereby proposed. The old method works on simulating an applied external tensile load to simulate string weight and overpull, a preload force is then introduced at the teeth and abutment to see by how much the tensile stress in the string are reduced due to the compressive preload stress. In practical applications, threaded connections must have an internal load (preload) that locks in the connection’s integrity before an axial force is applied.

Doing it any other way will cause the connection to rattle and be devoid of structural integrity. Furthermore, with the proposed model, a trend prediction system can be developed that will compliment drillstring design calculations by going beyond hook load, overpull, tubular collapse/burst ratings to predict likely failure scenarios based on the expected increase or decrease in stress concentration factors at the critical thread roots occasioned by the use of hybrid strings.

7.2 Suggested Future Work

From the results observed in this work, the following areas of further investigation and future work are hereby proposed:

7.2.1 Three-dimensional FEA to Investigate Bending Stresses

A 3-D FEA model was created by revolving the current model into a 180^{o} geometry thereby converting the CAX4 axisymmetric elements in the 2-D model into C3D8 brick elements. The 3D model was then employed in the study of the stress response of the model to axial and bending loads.

The generated 3-D model has a mesh of 257616 elements made from 286679 nodes. The size of the input file, which has 582192 lines, is 33.8 MB. The 2-D model it was revolved from, on the other hand has a mesh of 4092 elements made from 5848 nodes. The size of the input file, which has 9433 lines, is 1.3MB. It was found to computationally very expensive to run comparative analyses on the 3-D model die to its sheer size. As such only two simulations were run with it; one to test its response to axial loading and the other to test its response to bending.

While the 2-D model was designed to be preloaded using a given amount overlap using the interference-fit method, the 3-D was preloaded using the pre-tension surface method by adding load to a single independent node and the load is then transmitted to a pre-tension surface on the model using multi-point constraint (*MPC) command. The same method was used to add rotation to the model to simulate a dogleg in the bending case.

As part of the validation process in this work, 3-D model was developed and run successfully. Two investigations were undertaken to test the response of the model to axial load and bending force. In the preload and axial load cases, the following codes were used to generate the results shown in Figure 7-1 and Figure 7-2 below.

**NODE*

****NODE 999000 FOR MAIN PRE-LOAD SECTION.*

999000, 0.0000, 0.0000, 0.0000

****NODE 999101 for constraint on top of pin SENA –yes.*

****NODE 999102 for constraint at bottom of box SEX0 – yes*

**** NODES 999101 AND 999102 ARE USED TO CONSTRAIN THE PIN AND BOX IN THE Y-Y DIRECTION WITH PRESCRIBED LOADS.*

999101, 0.0, 750.0, 0.0

999102, 0.0, -550.0, 0.0

**PRE-TENSION SECTION, NODE=999000, SURFACE=SCPT*

**NSET, NSET=PPSET*

999000

****DECLARATION OF THE MULTI-POINT CONSTRAINT COMMAND TO TRANSFER LOADING ON NODES 999001 AND TO 999102 TO MODEL*

**MPC*

BEAM,SENA, 999101

**MPC*

BEAM, SEX0, 999102

**STEP, NLGEOM=YES, INC=300, UNSYMM=NO*

*********** STEP 1 ***************

****STEP FOR THE APPLICATION OF PRE-LOAD*

**STATIC*

0.01,1.0, 1E-06, 1.0

**CLOAD, OP=NEW*

****APPLICATION OF AXIAL PULL ON THE MODEL ON NODE 999000 IN THE Y-Y DIRECTION TO APPLY PRE-LOAD*

999000, 1, 1000000.0

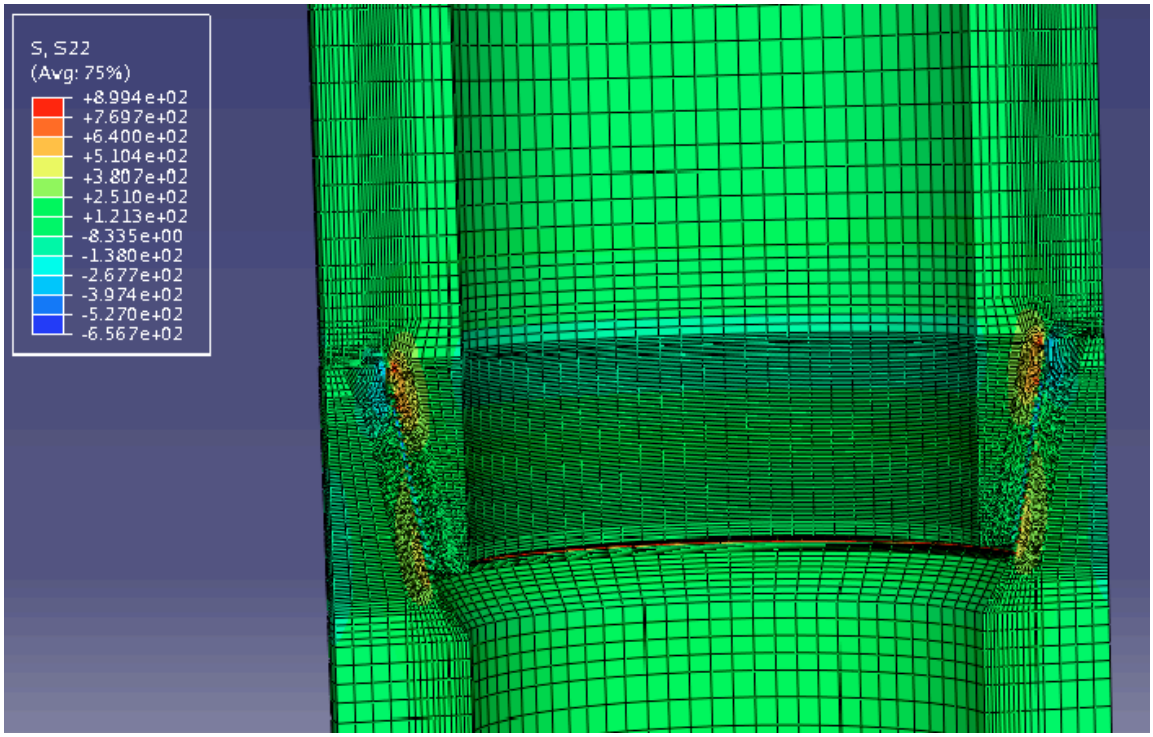

Figure 7-1: Apply Preload in a 3-D Model using Pre-tension Surface

```
 TO APPLY BENDING IN A SEPARATE SIMULATION
 ********** STEP 2 **************
 *STEP, NLGEOM=YES, INC=300, UNSYMM=NO
TENSION
**********************************
*STATIC
0.01, 1.0,1E-06, 1.0

*BOUNDARY,FIXED,OP=NEW
**** FIX THE APPLIED PRE-LOAD FROM PREVIOUS STEP******
999000, 1, 1
**==========**
*BOUNDARY, OP=NEW
**==========**
 SEZ0, 3
**** NODE 999101:-
 999101, 1,6
************
***ADD ROTATIONAL LOAD ON NODE 999102 TO INDUCE BENDING LOAD
AT BOTTOM OF BOX
*****NODE 999102:-
**** DEGREES OF FREEDOM 1 AND 2 ON NODE 999102 ARE FREE
 999102, 3,5
***APPLY ROTATION OF 1° ABOUT THE Z- AXIS (6,6) ON NODE 999102 TO
BEND HE MODEL
 999102, 6,6, 0.017453
```

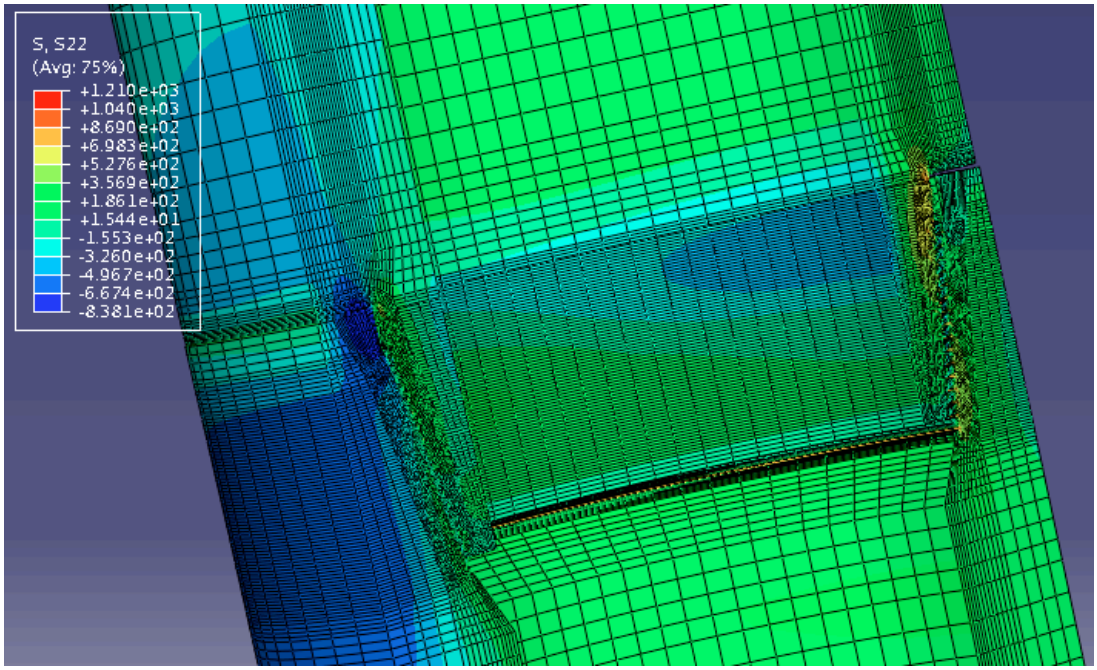

Figure 7-2: Apply Preload in a 3-D Model using Pre-tension Surface

The writer suggests that future researchers should consider using the methods of applying preload used in this work to build models that can be used in different well configurations with varying amount of dogleg severity to test the response of the various materials to bending stresses.

7.2.2 Comaprison of the Materials' Response to Impact Loading

Investigating and comparing response to impact loading of the conventional drillstring (steel), an aluminium alloy string, a titanium alloy string and hybrid strings of all the three materials. Some downhole failures are caused by impact loads especially when drilling through hard or vugular formations. A comparative study of the response of various materials can be undertaken to study areas of string optimisation to mitigate failure due to impact loads. The response of a drillstring components to impact loads can be used to optimise strings designed to work in hard and highly compacted lithologies and also in the design of jarring operations.

7.2.3 Modeling and Analysis of Composite Drillpipe

Many of today's engineering components are manufacture from composites to take advantage of the light weight and strength of composite fibres. Composite drillpipes are employed in short radius horizontal drilling. In one reported case [7.1], the pipe shaft of the composite drillpipe is filament wound 12K carbon fibre combined with glass fibres in eposy resin over an elastomeric liner. Standard API rotary shouldered tool joints overwrapped with the composite materials form the end of the connections.

Chandler, et al. [7.2] reported that while composite drillpipe could cost up triple the cost of conventional drillpipe, its advantages over conventional steel drillpipes include:

a. Lower weight
b. Higher strength-to-weight ratio
c. Superior corrosion resistance
d. Enhanced fatigue resistance, and,
e. They are non-magnetic.

In a study prepared by Dr. James C. Leslie of Advanced Composite Products and Technology, Inc. on behalf of the United States Department of Energy [7.3] he reported of a composite drillpipe developed by his company that has the structural and strength properties comparable to, while weighing only 50% of, its steel counterpart. Among other advantages, he reported that such a superior flexibility and strength to weight (SWR) ratio the composite drillpipe will find wide applications in low curvature ERD and UDD.

Figure 7-3: Demonstrating the Flexibility of a Composite Drillpipe [7.3]

Figure 7-4: Demonstrating the Lightness of Composite Drillpipe [7.3]

Numerical, FEA and full scale analyses of composite drill pipes will go along way further investigate the operational limit of composite drillpipes and to suggest how best they could be used in a hybrid string scenario because of their high cost.

7.2.4 Validation with Full Scale Three-Dimensional Model

Validation of the model with a full scale model tests using a tensile loading rig and a rotating bend rig will achieve increased confidence in the data generated. To the best of the author's knowledge there has not been a full scale experiment undertaken to validate the stress response of hybrid strings to applied internal preloads and and external axial or compressive loads. Tafreshi & Dover [7.4], Macdonald & Deans [7.5], Baragetti & Baryshnikov [7.6], Knight & Brennan, Kristoffersen [7.7] [clxxv] and a host of other investigators all undertook their analysis with comparison and validation with full-scale models.

Using a rotating bend rig and fatigue test rig it is possible to replicate the FEA investigations undertaken in this work with full scale model tests.

7.3 Reference

[7.1] **Composites World**, *"Composite Drillpipe and Available Option"* viewed at www.compositesworld.com/articles/composite-drillpipe-an-available-option accessed on August 23rd, 2011.

[7.2] **Chandler, R.B., Jellison, M.J., Payne, M.L. and Shepard, J.S**, *"Advanced and Emerging Drillstring Technologies Overcome Operational Challenges"*; World Oil, Vol. 227 No. 10; October, 2006

[7.3] **Leslie, J. C.**, "Development and Manufacture of Cost-Effective Composite Drillpipe", December 2008.

[7.4] **Tafreshi, A. and Dover, W.D.**, "Stress Analysis of Drillstring Threaded Connections Using the Finite Element Method", Int. Journal of Fatigue 15, No 5 (1993) pp 429-438

[7.5] **Macdonald, K. A. and Deans, W. F**., *"Stress Analysis Of Drillstring Threaded Connections Using The Finite Element Method"*, Engineering Failure Analysis, Vol 2, No. 1 pp. 1-30, 1995

[7.6] **Baragetti, S. and Baryshnikov, A.**, *"Rotary Shouldered Thread Connections: Working Limits Under Combined Static Loads"*, Transactions of the ASME. Vol. 123, September 2011.

[7.7] **Kristoffersen, S.**, *"Improved Fatigue Performance of Threaded Drillstring Connections by Cold Rolling"*, Dr. Ing Thesis, Norwegian University of Science and Technology, 2002

8 Appendices

8.1 Appendix A: Simulation Workflow

Codes used in the generation of input files and visualising results are Abaqus version 6.7.1 and Roshaz

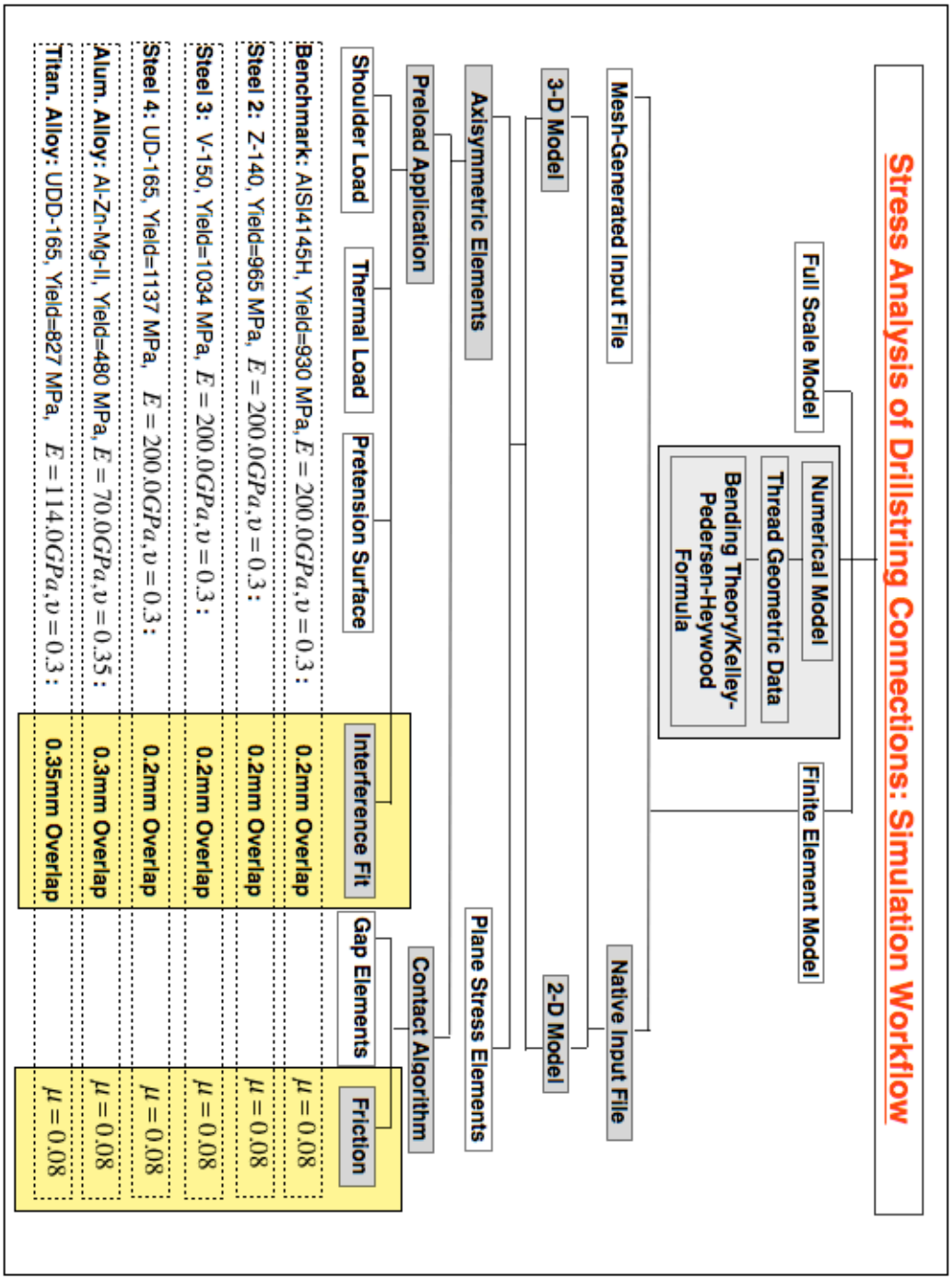

8.1.1 Appendix B3 – Theory of Torque and Preload

Let us consider what takes place when preload is applied to a bolted connection before and after the application of an external axial force.

8.2 Appendix B: Theoretical Background

8.2.1 Appendix B1 – Theory of Torque and Preload

Let us consider what takes place when preload is applied to a bolted connection before and after the application of an external axial force.

Consider a power screw on which a torque is applied to overcome a force F as shown in Figure 2-12, above. The threads on the screw have a pitch, p, a lead angle, γ and a mean diameter, dm. To find the torque required to apply a force, P, equal to the load, F, lets imagine one turn of the thread unrolled on a flat surface such that it forms a right-angled triangle whose hypotenuse is the edge of the thread, the base is the mean diameter, dm, of the thread and the height is the lead as shown in Figure 0-1 below.

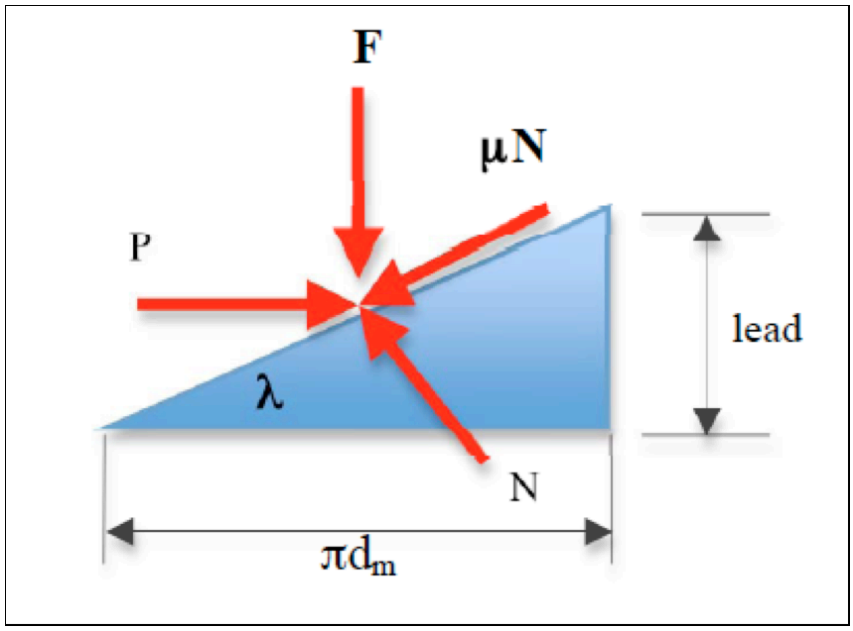

Figure 8-1: Forces Acting on One Turn of Thread

To achieve equilibrium in the system when supporting the load and the force exerted by the screw the vertical and horizontal components of the force are:

$$\sum F_H = P - NSin\lambda - \mu NCos\lambda = 0 \text{.....} B1.1a$$

$$\sum F_V = P - \mu Sin\lambda - NCos\lambda = 0 \text{.....} B1.1b$$

Since the normal force, N, is not important in this case, we can eliminate it and solve for P, this gives;

$$P = \frac{F(\mu Sin\lambda - NCos\lambda)}{Cos\lambda + Sin\lambda} \text{.....} B1.2$$

Since $\lambda = {}^{1}\!/_{d_m}$ and $Tan\lambda = {}^{Sin\lambda}\!/_{Cos\lambda}$ then by dividing the numerator and denominator of eq. (B1.2) by $Cos\lambda$, we obtain

$$P = \frac{F\left[\left({}^{1}\!/_{d_m}\right) + \mu\right]}{1 - \left({}^{1}\!/_{d_m}\right)} \text{.....} B1.3$$

Also, knowing that torque, T, is a product of force, P, and mean radius, ${}^{d_m}\!/_{2}$ eq. (B1.3) can be rewritten to express the torque required to exert force, P.

$$T = \frac{Fd_m}{2}\left(\frac{l + \pi\mu d_m}{\mu d_m - \mu l}\right) \text{.....} B1.4$$

Eq. (B1.4) expresses the torque required to overcome the friction of the thread and to exert the force, P. The above eqs. (B1.1-B1.8) are developed based on the power screw, which has square threads. But unlike power screw, most threads in use today have a thread angle, 2α, which means the load is not parallel to the axis of the screw but inclined to the axis because of the lead angle, γ, and the thread angle 2α. The thread angle's main effect on the thread system is to increase the frictional force by the wedging action on the thread flanks.

To take into account of this effect, the frictional terms in eq. (B3.4) will be divided by the cosine of half the thread angle. This yields;

$$T = \frac{Fd_m}{2}\left(\frac{l + \pi\mu d_m Sec\alpha}{\mu d_m - \mu l Sec\alpha}\right) \ldots\ldots\ldots\ldots B1.5$$

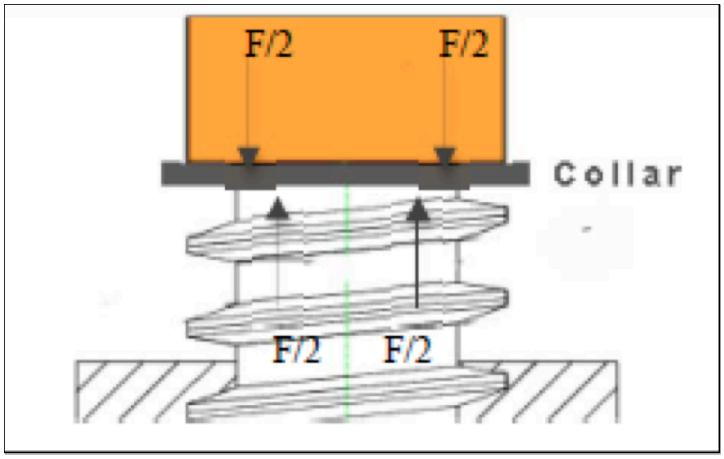

Figure 8-2: Loaded Collar on Power Screw

When a collar or abutment is introduced into the thread system as shown in Figure 0-2 above, an additional component of torque must be added to take into account the force exerted at collar.

If the mean diameter of the collar is d_c and the coefficient of friction at the collar interface is μ_c , then torque, T, required to produce the force, P becomes

$$T = \frac{Fd_m}{2}\left(\frac{l + \pi\mu d_m Sec\alpha}{\mu d_m - \mu l Sec\alpha}\right) + \frac{F\mu_c d_c}{2} \ldots\ldots\ldots\ldots B1.6$$

Because eq. (B1.6) does not take into account the lead angle, it remains an approximation of the torque required to produce a force, P across the threads and the shoulder.

8.2.2 Appendix B2: Governing Equation for Stress Modelling:

As an example, it can be considered that the governing equations for the analysis of stress in a system be taken from the theory of elasticity. In a two-dimensional problem

of a bar in tension, the equations are rendered as;

$$-f_{(x)} = \frac{\partial \sigma_x}{\partial \sigma} + \frac{\partial \tau_{xy}}{\partial y} \text{.....} B2.1a$$

$$-f_{(y)} = \frac{\partial \tau_{xy}}{\partial x} + \frac{\partial \sigma_y}{\partial y} + \text{.....} B2.1b$$

Where σ_x, σ_y, τ_{xy}, are components of the induced stress and f_x and f_y are loads acting on every point in the bar. And to describe the elastic response of the material to applied stress;

$$\sigma_x = \frac{E}{1-\upsilon^2}\varepsilon_x + \frac{E\upsilon}{1-\upsilon^2}\varepsilon_y \text{.....} B2.2a$$

$$\sigma_y = \frac{E\upsilon}{1-\upsilon^2}\varepsilon_x + \frac{E\upsilon}{1-\upsilon^2}\varepsilon_y \text{.....} B2.2b$$

$$\tau_{xy} = \frac{E}{2(1-\upsilon)}\gamma_{xy} \text{.....} B2.2c$$

Where ε_x, ε_y and γ_{xy} are components of strain and the Modulus of Elasticity, E and Poisson Ratio, υ are experimentally measured physical properties of the material.

As the bar deforms, strain-displacement relations can be made to describe the purely geometric aspects of the deformation.

$$\varepsilon_x = \frac{\partial u}{\partial x} \text{.....} B2.3a$$

$$\varepsilon_y = \frac{\partial v}{\partial y} \text{.....} B2.3b$$

$$\gamma_{xy} = \frac{\partial u}{\partial y} + \frac{\partial v}{\partial x} \text{.....} B2.3c$$

Where u and v are displacements of a material point in the bar in the x and y directions respectively.

Substituting eqs. (B2.3a), (B2.3b) and (B2.3c) into eqs. (B2.1a) and (B2.1b) will give,

$$-f_x = \frac{E}{1-\upsilon^2}\frac{\partial^2 u}{\partial x^2} + \frac{E}{2(1-\upsilon)}\frac{\partial^2 \upsilon}{\partial x \partial y} + \frac{E}{2(1-\upsilon)}\frac{\partial^2 u}{\partial y^2} \text{.....} B2.4a$$

$$-f_x = \frac{E}{1-\upsilon^2}\frac{\partial^2 \upsilon}{\partial y^2} + \frac{E}{2(1-\upsilon)}\frac{\partial^2 \upsilon}{\partial x \partial y} + \frac{E}{2(1-\upsilon)}\frac{\partial^2 \upsilon}{\partial x^2} \text{.....} B2.4b$$

Eqs. (B2.4a) and (B2.4b) above are the governing equation that describes the response of the bar to the external applied load. These are a partial differential equations containing two unknown functions u(x,y) and v(x,y). The applied load at the end of the bar can be seen as boundaries of the domain and can be represented as boundary conditions

$$\sigma_x = \frac{P}{A} \text{.....} B2.5$$

applied to both ends of the bar where A is the surface area at ends of the bar and P is the applied load.

Therefore the numerical equations we seek are for the unknown functions $u(x,y,z)$ and $v(x,y,z)$ (the functions u and v are in three dimensions; x y and z) which satisfy both the governing equations (B2.4) and the boundary conditions in eq. (B2.5). The solutions found can then be substituted into the strain-displacement eq. (B2.3) to determine the strains in the bar and then the strains substituted into equations (B2.2) to determine the stress.

Having determined the governing equations and the boundary conditions of the system, the FEA analysis now discretizes the system into elements and attempts to numerically evaluate, for each element in the bar, the element equations, which are algebraic equations, derived from (and approximate to) the governing eq. (B2.4) above. To develop the element equations that approximate to the governing (exact) solution to the problem, we need to construct a trial solution that renders the differential equation in equation (B2.4) to an algebraic equation that can be solved more easily through computation.

Consider the governing equation of a one-dimensional boundary value problem for strain-stress 3-d bar . The equation will be

$$\frac{d}{d_x}\left(x\frac{dU(x)}{dx}\right)=\frac{2}{x^2} \quad .....B2.6$$

Expanding eq. (B2.6) using chain rule of differentiation we have,

$$x\frac{dU(x)}{dx^2}+\frac{dU(x)}{dx}=\frac{2}{x^2} \quad .....B2.7$$

This is a special case for a general second-order differential equation,

$$C_2(x)\frac{d^2U(x)}{dx^2}+C_1(x)\frac{dU(x)}{dx}+C_0(x)U(x)=f(x) \quad .....B2.8$$

Where $c_2(x)=x$, $c_1(x)=1$, $c_0(x)=0$ and $f(x)=2/x^2$. When the coefficients $c_2(x)$ and $c_1(x)$ satisfy the condition,

$$C_1(x)+\frac{dC_2(x)}{dx} \quad .....B2.9$$

Then eq. (B2.8) can be written as,

$$\frac{d}{dx}\left(C_2(x)\frac{d\,U(x)}{dx^2}\right)+C_0(x)U(x)=f(x)\text{.....}B2.10$$

In equations (B2.6 to B2.10)) above, x is the independent variable and the domain of the problem is $1<x<2$ on the x-axis, therefore the boundary of the domain is the two points $x=1$ and $x=2$ In which case the boundary conditions (BCs) are

$$U(1)=2\text{.....}B2.11a$$

and,

$$\left(-x\frac{dU}{dx}\right)_{x=2}=\frac{1}{2}\text{.....}B2.11b$$

If $-x\frac{du}{dx}=\rho$, then

$$U(1)=2\text{.....}B2.12a$$

and

$$\rho(2)=\frac{1}{2}\text{.....}B2.12a$$

FEA will then aim to find an expression for $U_{(x)}$ in terms of known functions that approximately satisfies eq. (B2.10) in the domain of the problem and eqs. ((B2.12a and B2.12b) in the boundary of the problem. Because it is an approximate solution of the problem it is denoted with $\tilde{U}$. As has been mentioned in eq. (B2.12) above, the Error, $E_{(x)}$, of the solution is the difference between the exact solution, $U_{(x)}$, and the approximate solution, $\tilde{U}_{(x)}$.

8.2.3 Appendix B3 – Fatigue Failure in Drillstrings.

8.2.3.1 Crack Initiation Models

In the S-N model, in which the load amplitudes are consistent and predictable over the life of the component, stresses are applied to determine the fatigue life of the component. The cycle stress used in the investigation is kept below the endurance limit of the material. In the e-N model, which is a bit more complicated to use, a reasonably accurate picture of the crack-initiation stage can be obtained. This method can be used to account for cumulative damage due to variations in cyclic load. Low cycle fatigue (LCF) and finite-life scenarios where the stresses are high enough to cause local yielding are better modeled with this method. A combination of fatigue loading and high temperature is also better handled through the e-N approach. The LEFM approach is the best model for the crack propagation stage and can be used to predict the remaining service life of a component that already has an identified crack. This approach, which can be applied to both finite life and LCF situations, relies on the accuracy of the accuracy of the estimate of the initial crack size and and the stress intensity (geometry) factor.

Fatigue failure in drillstrings, like in other engineering components, is influenced by three factors. These are; a tensile stress of a sufficiently high value, a large enough fluctuation in applied stress and sufficiently large number of cycles of the applied stress. Since in a typical fatigue failure a microscopic defect forms at a point of high stress, such as areas of stress concentration, and gradually enlarges as the cyclic loads are applied repeatedly, our examination of the stress at play at the LET will help us and future designers and analysts to relate this study made in static conditions to the expected behaviour of a connection's high stress location when subjected to cyclic dynamic loads as experienced in the drilling situation. Figure 6-1 below show the alternating, mean and range values of three types of cyclic stress encountered.

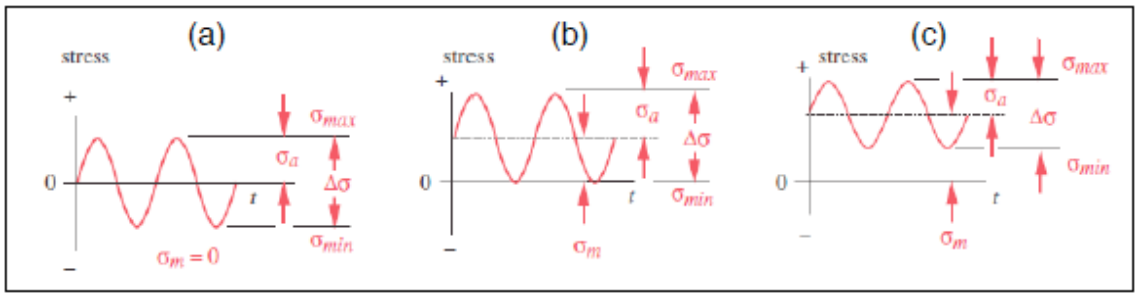

Figure 8-3: Reversed (a), Repeated (b) and Fluctuating (c) Stresses

In order to determine a component's fatigue strength at any point the maximum and minimum stress values at that point are calculated then used to obtain the average stress and the stress amplitude.

Where average stress is;

$$\sigma_{Ave} = \frac{\sigma_{Max} + \sigma_{Min}}{2} \quad \text{.....B3.1}$$

and the stress amplitude

$$\sigma_{Amp} = \frac{\sigma_{Max} + \sigma_{Min}}{2} \quad \text{.....B3.2}$$

Since drillstring components are more likely to fail under high cycle fatigue (HCF) situations where the service life is likely to be dominated by fatigue crack initiation then progressive enlargement of the crack until failure, it is common to use stress-life (S-N) model and empirical fits to the data for the determination of the joint's fatigue strength. The most common methods of plotting the S-N curve is by using Basquin's "Law" which states:

$$\sigma_a N^b = C \quad \text{.....B3.3}$$

Where σ_a = stress amplitude, N = number of cycles to failure, b, C are empirically determined constants of which C is a function of the mean stress and b is between 0.05 and 0.15. Basquin's law can be used for tests undertaken in HCF regime with any fixed value of mean stress.

Goodman's rule, which uses linear interpolation and is expressed as:

$$\sigma_a N^b = C_0 \left(1 - \frac{\sigma_m}{\sigma_m} \right) \quad \text{.....B3.4}$$

Where C_0 is the constant in Basquin's law above but determined by testing at zero (0) mean stress.

Goodman's diagram is a plot of σ_{Ave} vs σ_{Amp}. This plot of values picked at a particular location on the component determines whether that component will have infinite life or fail at that location.

8.2.3.2 Crack Growth Model

In cases where crack growth occupies a significant fraction of the lifetime we can use models for crack growth. It is usually observed that crack growth rate $\frac{da}{dN}$ depends on the stress intensity factor;

$$\Delta K = \Delta\sigma\sqrt{\pi a} \quad \text{.....} B3.5$$

Paris law, which states,

$$\frac{da}{dN} = C\Delta K^m \quad \text{.....} B3.6$$

is then used to determine the remaining life of the component.

where C and m are material constants and ΔK is the stress intensity factor range.

It is noteworthy here that applying the LEFM model is best done in experimental situations as operators will very likely not run a drillstring components that is known to have defect.

In earlier discussions on dog-leg severity (DLS) and its effect on the fatigue life of materials, it was discussed how Lubinski's use of a modified Goodman diagram to propose, depending on the tensile load and pipe's characteristics, means of determining a permissible DLS below which the connection will not fail due to fatigue. For the three materials investigated here, undertaking fatigue tests or using already available fatigue test data will help in the determination of the endurance limit of each of the three materials will help us in assessing the benefits derivable from using one over the other vis-à-vis their fatigue endurance properties.

As stated above the most common type of fatigue test conducted focuses on the nominal stress required to cause a fatigue failure in some number of cycles. The data is obtained by cycling smooth or notched specimens until failure. The usual procedure is to test the first specimen at a

high peak stress where failure is expected in a fairly short number of cycles. The test stress is decreased for each succeeding specimen until one or two specimens do not fail in the specified numbers of cycles, which is usually at least 10^7 cycles. The highest stress at which a "run-out" (non-failure) occurs is taken as the fatigue threshold. Not all materials have a fatigue threshold (most nonferrous metallic alloys do not) and for these materials the test is usually terminated after about 10^8 cycles.

It should be noted that there are several shortcomings of S-N fatigue data. First, the conditions of the test specimens do not always represent actual service conditions. For example, components with surface conditions, such as pitting from corrosion, which differs from the condition of the test specimens will have significantly different fatigue performance. Furthermore, there is often a considerable amount of scatter in fatigue data even when carefully machined standard specimens out of the same lot of material are used. Since there is considerable scatter in the data, a reduction factor is often applied to S-N curves to provide conservative values for the design of components.

The most common type of drill pipe failure is fatigue wear. It generally occurs in dog legs where the pipe goes through cyclic bending stresses. These stresses occur because the outer wall of the pipe in a dog leg is stretched and creates a greater tension load. As the pipe rotates a half cycle, the stresses change to the other side of the pipe, For example, the stress may change from 350 MPa to - 150 MPa and again to 350 MPa in the course of one cycle or rotation of the pipe.

8.2.3.3 Fatigue and Drillstring Stress

Fatigue damage from rotation in doglegs is a significant problem if the angle is greater than some critical value. Lubinski has published several works that describe this value. Rotation in angles below this value does not cause appreciable fatigue. The maximum permissible dogleg severity for fatigue damage consideration can be calculate with the following equations:

$$C = \frac{430{,}000\sigma_b Tanh KL}{\mu EKDL} \quad \text{.....B3.7}$$

$$K = \sqrt{\frac{T}{EI}} \quad \text{.....B3.8}$$

Where

C= maximum permisible dogleg severity,

E = Young' s modulus in psi (30 X 10^6 psi for steel, 10.5 X 10^6 psi for aluminium alloy and 16.5 X 10^6 psi for titanium alloy)

D = drill pipe outer diameter, in.

L = half the distance between tool joints, 180 in. for Range 2 pipe, in.

T= tension below the dog leg, lb

σ_b = maximum permissible bending stress, psi

I = drill pipe moment of inertia = $\frac{\pi}{64}\left(D^4 - d^4\right)$

The maximum permissible bending stress, σ_b, is calculated from the buoyant tensile stress, σ_t (psi), inthe dogleg with the following equations:

$$\sigma_t = \frac{T}{A}$$

Where A is the cross-sectional area of the pipe body in in^2.

For the Grade S-135 we have looked at earlier in the chapter:

$$\sigma_b = 20000\left(1 - \frac{\sigma_t}{145000}\right) \quad \text{.....B3.9}$$

This equation holds true for values of σ_t up to 133,400 psi or 920MPa which is about the yield strength value of the steel material.

Severe pipe damage occurs when dogleg severity is greater than the value computed for *C* above. The damage depends on the type of material the drillpipe is made from (steel, aluminium or titanium), corrosion level in the drilling environment, stress, and the dogleg angle. S-N diagrams that can be used, in this situation, to determine the approximate number of cycles, or rotations, before pipe failure occurs have been established.

The fraction (f) of drill pipe life expended in an interval of a dogleg can thus be calculated as follows:

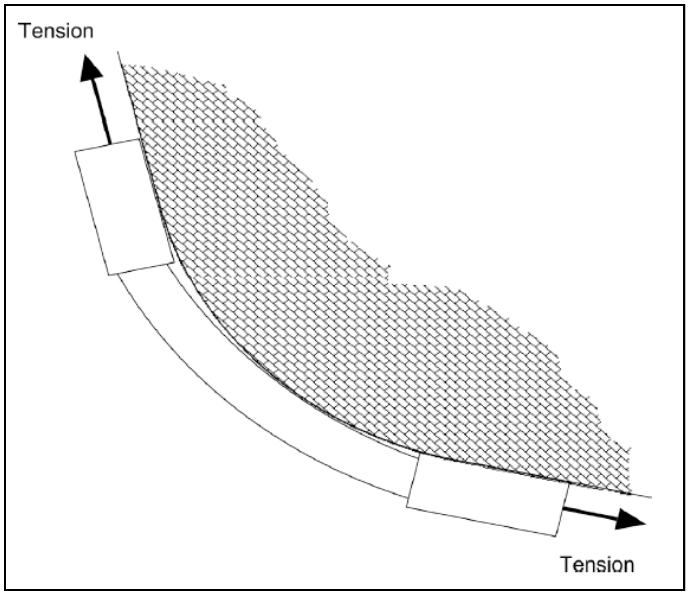

Figure 8-4: Drillpipe in a Dogleg Interval

$$f = \frac{B}{N} \quad \text{.....} B3.10$$

where

f = fraction of life expended

B = number of drill pipe revolution to drill interval

N = number of revolutions to failure of joint of drill pipe

It can be shown that:

$$B = \frac{60RD}{V} \quad \text{.....} B3.11$$

where

R = rotary speed, rpm

d = length of dogleg interval, ft

V = drilling rate ft / hr.

In order to determine (N) the number of revolution to failure of the joint of drill pipe we need to know the actual bending stress (σ_b). This value can be computed as follows:

$$\sigma_b = \frac{EDC_0}{2} \quad \text{.....} B3.12$$

where

D = outside diameter of the pipe, in.

E = Young' s modulus, lb / in

c_o = maximum pipe curvature, radians / in.

The relationship between the hole curvature (c) and the Maximum pipe curvature (c_0) is:

$$C_0 = cKL \quad \text{.....} B3.13$$

where

c = hole curvature, radians / in.

L = one half the length of a drill pipe joint, in.

The effect of bending stress on fatigue cycles before failure for a steel drillpipe is well documented, in the presence for tension, however, the fatigue effect of bending becomes more severe. To make the proper allowances for this, the actual bending stress, (σ_b), must be multiplied by a correction factor, τ , as follows:

$$\tau = \frac{T}{T - \sigma_t} \quad \text{.....} B3.14$$

The vertical axis of the S-N curve should be entered with the product of τ and σ_b or just σ_b . Determine the number of cycles, N, to failure then enter N into the first equation to determine the fraction of the pipe life expended in drilling the section.

It is noteworthy here that, since drillstring components operate in corrosive environments, the standard S-N curve obtained in controlled laboratory tests can only act as a guide to the actual behaviour of these materials in service. However, of the three materials under investigation, Titanium has been seen to have superior corrosion resistance properties.

8.2.4 Appendix B – Bibliography

1. Lubinski, A., *"Maximum Permissible Doglegs in Rotary Boreholes"*; Journal of Petroleum Technology, February, 1991.

2. Grondin, G.Y. and Kulak, G. L.; 'Fatigue Testing of Drillpipe' *Journal of the Society of Petroleum Engineers,* 9, (2), pp. 95-102, June 01, 1994, SPE Paper 24224

3. Schutz, W*., "A History of Fatigue"*, Engineering Fracture Mechanics, Vol. 54, No. 2, 1996, Pp. 263

4. Goodman, J., *"MechanicsApplied to Engineering"*, Longman, Green and Company, London, 1899.

5. Morrow, J., "Fatigue Property of Metals", Proceedings of Division 4 of the SAE Iron and Steel Technical Committee, Nov. 4, 1964

8.3 Appendix C: Summary of Drillstring Investigations Undertaken at the UCL-NDE Centre

8.3.1 Fatigue Analysis of Drillsstrings - FADS (1990)

Sponsored by AGIP, BP and Norsk Hydro, Fatigue Analysis of Drillstrings (FADS) was initiated in 1988 and completed in 1990. The principal aim of the project was the study of the causes of drillstring failure during drilling operations and the prevention of such failure through the development of operational and mathematical parametric models. The main deliverable of FADS was the development of a computer program to be used in the prediction of fatigue life of drillstring components. This was done through the development and analysis of loading models to be used in the prediction of the root or notch stress at the thread roots (SCF determination), crack propagation (SIF determination), material behaviour and environmental variables in a variety of connections. This was done to facilitate fatigue life study and the prediction of fatigue crack growth rates and thus the expected remaining service life of drillstem components.

FADS provided an analysis of two thread geometries, NC50 and API 6-5/8" REG both made from the AISI 4145H steel. Tests were conducted for axial loading of the connection with investigations for bending, torsion and effect of preload. At the end of the study a computer program for calculating the remaining fatigue life based on parametric stress equations, fatigue and fracture mechanics analysis and material data was presented. The computer analysis package presented is a user-friendly software written in Fortran77.

The FADS study, as a means of developing input parameters of the software, undertook a survey of information on failure modes held by the industrial sponsors of the project, thereby generating a materials database. The study also looked at fatigue analysis (both the crack initiation and propagation stages) and a full stress analysis of the loaded connection.

In looking at the drillstring failure records from the industry, the investigators assessed that;

1) The box and pin are both vulnerable to failure, with the box being slightly more vulnerable than the pin,

2) That the failure, which induces both washouts and fractures, has fatigue as its main mechanism with some evidence of brittle fracture in substandard materials,

3) Most incidences of failure occur within 0-300ft of the bit, i.e., the bottom hole assembly (BHA) area, and,

4) That at the tooljoint, the critical location for failure is the last engaged thread of the box or the first engaged thread of the pin.

The foregoing failure survey was used to establish the likely failure mechanisms for drillstrings in service and to confirm the specific areas to be addressed by the FADS project.

A hybrid FEA and Analogue model was used in the study. The FEA part of this hybrid model was done using three axisymmetric thread teeth. The analogue model was shown to be a mechanical system composed of rigid levers joined by springs. Using the analogue model together with an input from the FEA model, a relationship was developed that calculates the SCF values for each tooth.

The results of the hybrid model were compared with those of full scale FEA of the entire connection in a test that models for axial loading and bending. The axial case looked at axial load only, axial load with preload and preload only. The average error of the hybrid model was an overestimation of the local stress by 8%. The range of errors in all cases was -1 to +18%. Bend stress data was also generated using the full FE meshes. The results were similar to those in the axial loading case. Also, photoelastic analysis was further used to provide additional confidence in the hybrid model.

As part of the study the stress concentration factor (SCF) or K_{ti} was defined as the local peak stress in component near tooth i, σ_i, divided by the local nominal stress in the component's body at tooth i, S_i.

$$K_{ti} = \frac{\sigma_i}{S_i} \quad \text{.....} C1.1$$

Where,

$$S_i = \frac{\sum P_i}{A_i} \quad \text{.....} C1.2$$

It can be seen from studying different connection types with varying bore and outside diameters that the local nominal stress is influenced by the local net section of the pipe and local force carried by that section, so to compare the peak local stresses of a connection there is a need to redefine the SCF and obtain a nominal stress remote from the location of peak stress and thus uninfluenced by the local load and geometry.

So results using the definition of SCF from eq. (C1.1) above were re-analysed with nominal stresses remote from the location of loading. The nominal stresses in this reanalysis are taken for a range of bore diameters and outside diameters using the equation

$$\sigma_{nom} = \frac{4P}{\pi(OD^2 - ID^2)} \quad \text{.....C1.3}$$

As a result of this reanalysis, parametric equations such as eq. (C1.5) below were developed to determine the percentage of the load carried by the critical tooth in the connection. This was then used as the basis to allow calculation of local and nominal stresses in the connection using eq. (C1.4) below.

$$\sigma = \frac{P}{LC} \quad \text{.....C1.4}$$

Where P is the externally applied load and LC is the Load Capacity or % of the applied load on the tooth.

$$LC = a(OD^2 - dc^2)^{\alpha}(dc^2 - ID^2)^{\beta} \quad \text{.....C1.5}$$

Where, a, α and β are the parameters to be fitted.

To complete the study, knowledge of the monotonic, cyclic and fatigue properties of the materials used in the making of the drillstem component were required. Pertinent characteristics of materials such as the cyclic stress-strain curve, fatigue strain-life curve, fatigue crack growth equation and the materials S-N curves were included in the software program. Further tests were carried out on the material in different environmental conditions that aim to simulate in-service conditions of the string. These included tests in air, water-based mud, oil-based mud, oil-based mud with copper

containing dope and with zinc containing dope. The tests were carried out under various cyclic frequencies and mud temperatures.

Crack initiation and propagation analysis models were then developed and included as part of FADS. In the case of crack initiation, studies undertaken as part of the FADS project such as local notch tip stress-strain behaviour, response to variable amplitude loading, response to cyclic loading and the material's fatigue properties were used to develop the analysis.

In the case of the crack propagation analysis, fracture mechanics estimates of fatigue life and stress intensity factor (SIF) estimates for drillstring components were used.

The final result of the project was the production of FADS, an interactive computer application for the fatigue analysis of threaded connections. The program allows estimates of initiation life, crack growth curves, S/N curves and stresses to be obtained for a range of drillstring connections studied within the project.

8.3.2 Prevention of Downhole Failure - PDF (1992)

Prevention of Downhole Failure (PDF) was a continuation of the FADS study. PDF extended the original work done in FADS to include all the main connector types beyond the two analysed under FADS, namely NC50 and API 6-5/8" REG. The connectors analysed in PDF are NC46, NC50, 6-5/8"REG and 7-5/8"REG, all in both standard form and with bore back and stress relief groove. The studies were undertaken under axial, bending and torsional loading.

The PDF investigation of axial loading showed clear advantages for the use of bore back and stress relief groove, showing a 9% reduction in the SCF of the last engaged thread of the pin (14% in the case of a shorter stress relief length) and 13% in the first engaged thread of the box due to the bore back.

FE analysis confirmed earlier studies undertaken in FADS and gives further confidence to the extended parametric equations developed. 3D FEA under bending and torsion also confirmed the photoelastic and 2D FEA studies which reported lower SCFs in these cases.

Fatigue life and remaining life predictions in FADS were further validated in PDF by

conducting full scale tests under axial and bending loads on AISI 4145H and non-magnetic steels. Other new features incorporated in the FADS software are the consideration of partial preload mean stress and residual stress on fatigue crack growth and fatigue analysis. Others are crack aspect ratio and failure criteria.

8.3.3 Reliable Operation of Downhole Systems - RODS (2002) [1]

Like the FADS and PDF projects before it, RODS was also an industry-sponsored undertaking of the NDE Centre of the University College London (UCL). It was funded by Shell, Statoil and Saga to build on the gains of FADS and PDF. And like FADS, the main project deliverable is a suite of computer programs that will aid in the prevention of downhole failure.

By combining advanced testing and inspection regimes with materials technology, progressive stress, fatigue/fracture mechanics and failure analysis, RODS proposed a new design philosophy for oilfield downhole components.

The RODS project undertook the study of thread and connection/tooljoint geometry as an addition to earlier work done in FADS and PDF. An analysis of bore eccentricity and its effect on the fatigue life of the connection was also undertaken.

8.3.4 Appendix C – Bibliography

6. “Fatigue Analysis of Drillstrings – FADS”, Final Report, Joint Industry Project, NDE Centre, Univ. Col. London, 1990.

7. “Prevention of Downhole Failure – PDF”, Final Report, Joint Industry Project, NDE Centre, Univ. College London

8. Reliable Operation of Downhole System - RODS, Final Report, Joint Industry Project, NDE Centre - UCL, OCTG Ltd, TSC Ltd, NTNU. 1998

8.4 Appendix C: Overlap and Yield Simulation Results

8.4.1 Benchmark Analyses – AISI4145H Steel

8.4.1.1 Simulation Results Summary

CUMULATIVE PRELOAD FORCE DUE TO OVERLAP

OVERLAP AMOUNT (MM)		+VE FORCE IN PIN (MN)	-VE FORCE IN BOX (MN)	% DIFF.
0.05		0.7	-0.7	-0.99
0.10		1.3	-1.3	-0.99
0.15		1.9	-2.0	-0.99
0.20		2.6	-2.6	-0.99
0.25		3.2	-3.2	-0.99
0.30		3.8	-3.8	-0.99
0.35		4.5	-4.6	-0.99

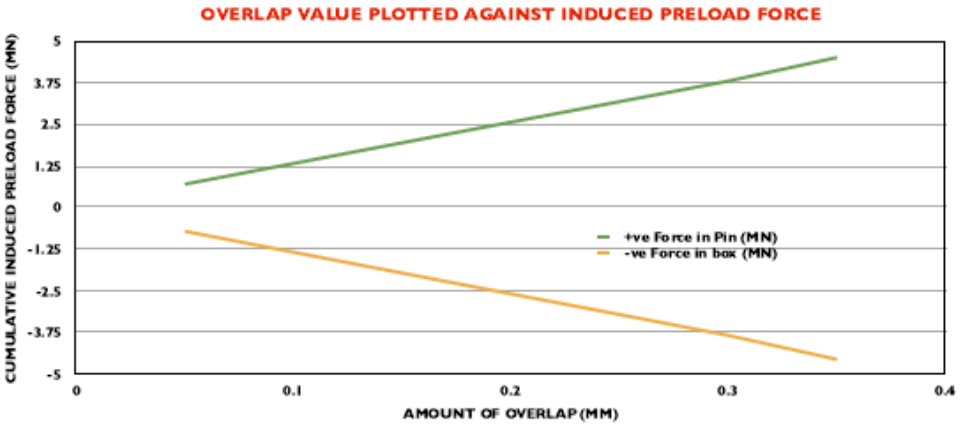

FORCE DUE TO AXIAL LOAD

AXIAL FORCE IN CONNECTOR		+VE FORCE IN PIN (MN)	-VE FORCE IN BOX (MN)	% DIFF.
0	0	2.56342	-2.58629	-0.99
20	20	2.58311	-2.48067	-1.04
100	100	2.65800	-2.05321	-1.29
500	500	3.16828	-0.04378	-72.37
750	750	4.69906	-0.01078	-435.72
1000	1000	6.26613	-0.01384	-452.74

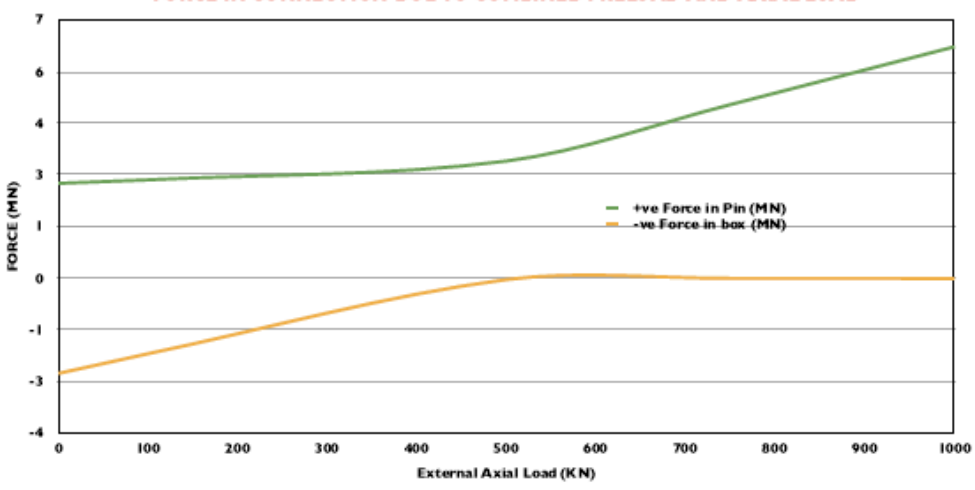

YIELD ANALYSIS - STEEL

OVERLAP AMOUNT (MM)	MATERIAL		YIELD STRENGTH	PEAK VON MISES STRESS	VON MISES STRESS @ 0.2MM	% OF YIELD STRENGTH	AXIAL LOAD (KN)	VON MISES STRESS (MPA)
0.05	AISI 4145H	0.05	940.0	170.50	616.70	18.14	0.00	616.70
0.10	AISI 4145H	0.10	940.0	320.50	616.70	34.10	20.00	616.90
0.15	AISI 4145H	0.15	940.0	469.30	616.70	49.93	100.00	614.70
0.20	AISI 4145H	0.20	940.0	616.70	616.70	65.61	500.00	611.60
0.25	AISI 4145H	0.25	940.0	756.70	616.70	80.50	750.00	901.60
0.30	AISI 4145H	0.30	940.0	902.70	616.70	96.03	1,000.00	1,199.00
0.35	AISI 4145H	0.35	940.0	1,048.00	616.70	111.49		

FAILURE ANALYSIS USING THE VON MISES YIELD CRITERION

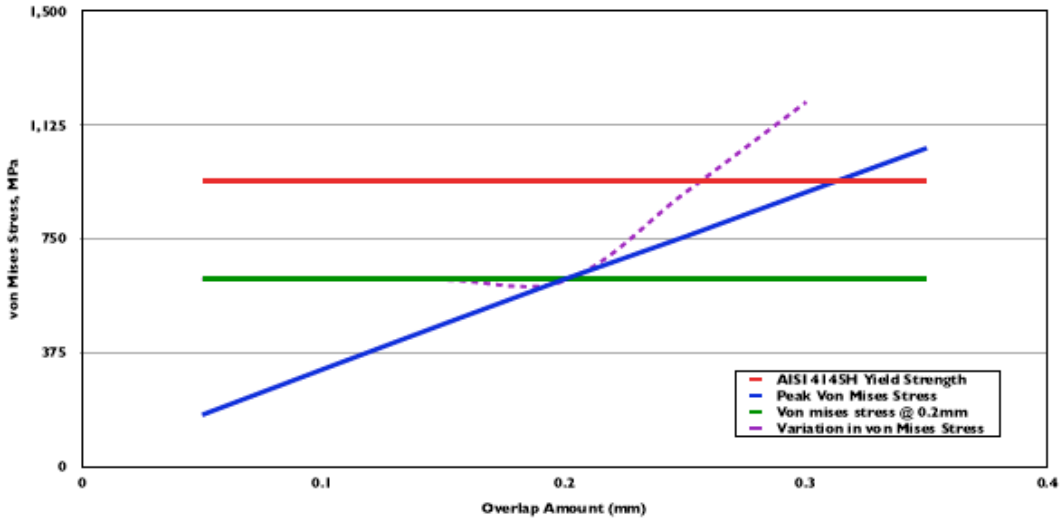

AXIAL TENSILE LOAD PLOTTED AGAINST VON MISES STRESS

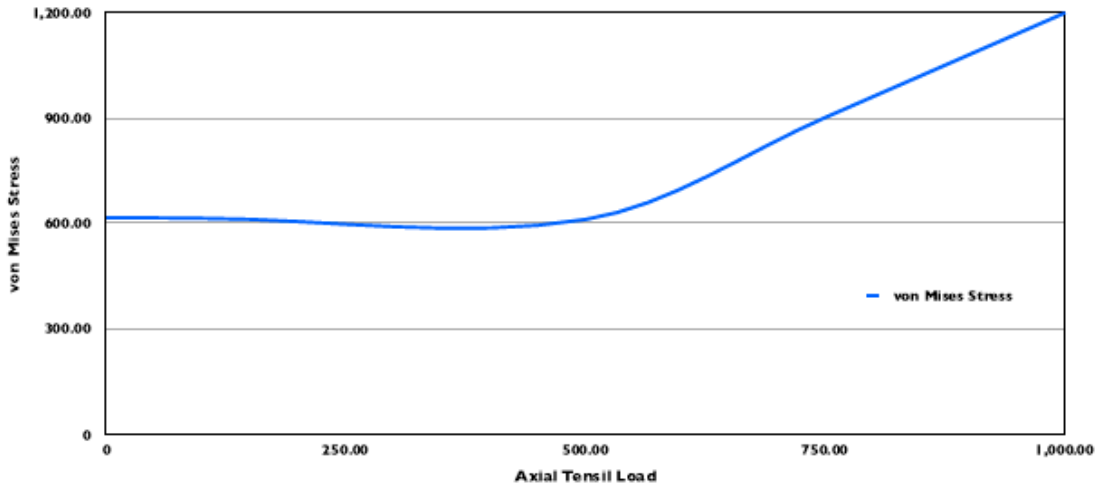

8.4.1.2 Induced Stress in Pin and Box Due to Preload and Axial Load

		Preload Induced Stress (MPa)							Axial Load Induced Stress (MPa)					
		0.05mm	0.1mm	0.15mm	0.2mm	0.25mm	0.3mm	0.35mm	OKN	20KN	100KN	500KN	750KN	1MN
BOX	226.226	6.5517	12.2262	17.9339	23.6704	29.345	35.1295	40.9549	23.6714	24.2401	25.084	6.932	9.4642	12.689
BOX	223.169	3.9104	7.2578	10.6392	14.0514	17.4259	20.8879	24.3883	14.0521	14.9134	17.1538	6.3478	8.7961	11.7826
BOX	220.326	0.6283	1.0745	1.5544	2.0666	2.5511	3.112	3.7075	2.0667	3.3779	7.6401	5.9308	8.4066	11.2473
BOX	217.683	-2.1829	-4.2245	-6.2329	-8.2085	-10.2184	-12.1479	-14.0463	-8.2089	-6.4812	-0.3645	5.7471	8.3176	11.1179
BOX	215.226	-4.7136	-8.9826	-13.2179	-17.4188	-21.659	-25.8137	-29.9396	-17.4196	-15.3876	-7.7828	5.8745	8.6791	11.5928
BOX	212.942	-6.8391	-12.9743	-19.0746	-25.1386	-31.25	-37.2662	-43.2553	-25.1398	-22.8853	-14.1144	5.828	8.7452	11.6794
BOX	210.818	-8.9679	-16.9649	-24.9255	-32.8476	-40.821	-48.6915	-56.5373	-32.8491	-30.4288	-20.7169	5.7898	8.8396	11.8062
BOX	208.844	-11.6361	-21.9576	-32.2383	-42.4758	-52.7551	-62.9304	-73.0826	-42.4777	-39.9305	-29.4262	5.46	8.5879	11.4716
BOX	207.009	-14.7912	-27.8697	-40.9091	-53.906	-66.9313	-79.8638	-92.7821	-53.9084	-51.2435	-40.0484	4.4227	7.3923	9.8779
BOX	204.009	-19.4718	-36.6519	-53.8054	-70.9279	-88.052	-105.13	-122.212	-70.9307	-68.1381	-56.1962	2.1616	4.6136	6.1712
BOX	202.285	-24.3942	-45.8972	-67.3937	-88.8772	-110.325	-131.823	-153.325	-88.88	-85.9792	-73.4624	-0.9699	0.6358	0.8604
BOX	200.56	-27.8539	-52.3956	-76.9417	-101.479	-125.926	-150.602	-175.196	-101.481	-98.4955	-85.5544	-4.2238	-3.7843	-5.0448
BOX	199.56	-29.7313	-55.928	-82.1447	-108.358	-134.462	-161.02	-187.355	-108.36	-105.341	-92.2406	-6.2746	-6.581	-8.7788
BOX	198.654	-32.2437	-60.6415	-89.0663	-117.48	-145.737	-174.631	-203.193	-117.484	-114.404	-101.009	-8.844	-10.0904	-13.4689
BOX	197.827	-34.6792	-65.209	-95.7672	-126.304	-156.617	-187.62	-218.247	-126.311	-123.172	-109.494	-11.6261	-13.9478	-18.6309
BOX	197.073	-36.8264	-69.2399	-101.682	-134.1	-166.252	-199.045	-231.513	-134.11	-130.902	-116.905	-13.5376	-16.5005	-22.0371
BOX	196.386	-40.2338	-75.6338	-111.042	-146.43	-181.456	-217.133	-252.533	-146.438	-143.118	-128.636	-16.3516	-20.2283	-27.0143
BOX	195.76	-44.2539	-83.1571	-122.029	-160.858	-199.2	-238.857	-277.641	-160.869	-157.397	-142.241	-20.3561	-25.7343	-34.3762
BOX	195.19	-47.7572	-89.6964	-131.594	-173.375	-214.61	-257.899	-299.85	-173.415	-169.797	-153.968	-24.9215	-32.2165	-43.0482
BOX	194.669	-50.2758	-94.4228	-138.452	-182.408	-225.667	-270.208	-314.142	-182.379	-178.648	-162.292	-27.8573	-36.3562	-48.5798
BOX	194.195	-52.5181	-98.5996	-144.526	-190.347	-235.429	-280.888	-326.44	-190.316	-186.47	-169.583	-29.8292	-39.0672	-52.193
BOX	193.763	-55.0303	-103.272	-151.319	-199.227	-246.297	-293.675	-341.134	-199.189	-195.199	-177.663	-31.5411	-41.3493	-55.2261
BOX	193.369	-58.3295	-109.409	-160.239	-210.871	-260.548	-310.596	-360.621	-210.822	-206.63	-188.176	-33.9869	-44.6699	-59.64
BOX	193.01	-61.8523	-115.958	-169.744	-223.255	-275.749	-328.608	-381.338	-223.209	-218.791	-199.31	-36.4268	-47.9605	-64.0091
BOX	192.682	-66.5324	-124.698	-182.406	-239.668	-296.047	-352.535	-408.881	-239.628	-234.892	-213.976	-39.0081	-51.3289	-68.4708
BOX	192.384	-75.4489	-141.288	-206.526	-270.856	-334.401	-398.29	-461.461	-270.823	-265.473	-241.812	-44.3618	-58.4272	-77.9016
BOX	192.112	-89.011	-166.31	-242.661	-317.96	-391.709	-467.406	-540.673	-317.927	-311.637	-283.798	-51.6953	-67.9991	-90.6299
	190.27	30.6755	57.7747	84.8036	111.753	138.519	165.394	192.195	111.753	111.801	111.841	116.567	172.492	230.179
PIN	189.97	31.5324	59.3868	87.1671	114.863	142.379	169.997	197.535	114.863	114.898	114.884	119.573	176.922	236.066
PIN	189.64	32.2179	60.6761	89.0565	117.349	145.463	173.672	201.797	117.349	117.374	117.319	122.043	180.56	240.897
PIN	189.28	33.4968	63.0834	92.5872	121.998	151.231	180.553	209.785	121.998	122.012	121.908	126.713	187.454	250.072
PIN	188.88	35.1646	66.2228	97.1924	128.063	158.756	189.53	220.207	128.063	128.061	127.891	132.816	196.466	262.071
PIN	188.44	36.782	69.2675	101.658	133.943	166.052	198.234	230.311	133.943	133.93	133.713	138.875	205.414	273.98
PIN	187.96	38.2161	71.9677	105.619	139.16	172.529	205.961	239.283	139.16	139.142	138.899	144.406	213.592	284.868
PIN	187.43	39.2337	73.8843	108.432	142.865	177.133	211.455	245.662	142.865	142.849	142.615	148.62	219.831	293.174
PIN	186.84	40.0042	75.3366	110.564	145.674	180.632	215.631	250.512	145.674	145.669	145.473	152.134	225.043	300.113
PIN	186	40.4614	76.1998	111.833	147.348	182.728	218.135	253.422	147.348	147.359	147.232	154.688	228.846	305.178
PIN	185.49	40.3432	75.9802	111.513	146.931	182.236	217.551	252.747	146.931	146.968	146.944	155.288	229.769	306.409
PIN	184.78	39.6327	74.6457	109.559	144.361	179.076	213.785	248.377	144.361	144.433	144.553	153.87	227.715	303.675
PIN	184	38.4017	72.3314	106.167	139.898	173.573	207.222	240.76	139.898	140.015	140.32	150.707	223.087	297.513
PIN	183.16	36.7258	69.1796	101.547	133.818	166.069	198.271	230.369	133.818	133.988	134.514	146.054	216.263	288.426
PIN	182.21	34.7158	65.3987	96.004	126.522	157.057	187.522	217.889	126.522	126.748	127.506	140.175	207.625	276.923
PIN	181.21	32.4959	61.2221	89.8798	118.46	147.09	175.631	204.083	118.46	118.74	119.724	133.396	197.655	263.644
PIN	180.21	30.2493	56.9944	83.6793	110.296	136.987	163.577	190.085	110.296	110.625	111.817	126.312	187.224	249.749
PIN	179.21	28.0518	52.8581	77.6118	102.306	127.091	151.767	176.369	102.306	102.679	104.062	119.217	176.77	235.819
PIN	178.11	25.8256	48.6668	71.4626	94.2069	117.052	139.786	162.454	94.207	94.6228	96.1866	111.884	165.956	221.408
PIN	176.90	23.5487	44.3794	65.1712	85.919	106.771	127.515	148.199	85.919	86.3749	88.1107	104.217	154.644	206.329
PIN	175.56	21.1784	39.915	58.6186	77.2852	96.051	114.717	133.331	77.2851	77.7787	79.6766	96.039	142.567	190.226
PIN	174	18.7991	35.4323	52.0377	68.612	85.2713	101.847	118.377	68.6118	69.1389	71.1815	87.6121	130.112	173.614
PIN	172.5	16.4396	30.9856	45.5078	60.0037	74.5623	89.0586	103.516	60.0035	60.5594	62.7258	79.0189	117.399	156.651
PIN	170.72	14.0272	26.4379	38.8278	51.1952	63.5951	75.9598	88.2912	51.1949	51.7754	54.0471	69.9747	104.007	138.775
PIN	168.77	11.5458	21.7583	31.9525	42.1269	52.2969	62.4637	72.6026	42.1265	42.7275	45.0852	60.3887	89.7999	119.805
PIN	166.63	9.0769	17.1013	25.1086	33.098	41.0413	49.0166	56.9688	33.0975	33.7142	36.1351	50.5766	75.2456	100.366
PIN	164.27	6.6834	12.5851	18.4702	24.3384	30.1165	35.963	41.7905	24.3379	24.965	27.4253	40.8192	60.7621	81.0153
PIN	161.67	3.9688	7.462	10.9387	14.3992	17.7174	21.1468	24.5615	14.3986	15.0357	17.5306	29.5995	44.1013	58.7521
PIN	158.82	0.4472	0.8159	1.1681	1.5046	1.8295	2.1225	2.2062	1.5039	2.1562	4.7037	15.0715	22.528	29.9235
PIN	155	-4.2572	-8.0612	-11.8813	-15.7155	-19.853	-23.7464	-27.6414	-15.7165	-15.0357	-12.3828	-3.9576	-5.7152	-7.814
PIN	150	-8.5759	-16.2088	-23.8564	-31.5158	-39.5583	-47.2897	-55.0149	-31.5169	-30.7993	-28.0016	-20.9117	-30.8595	-41.405

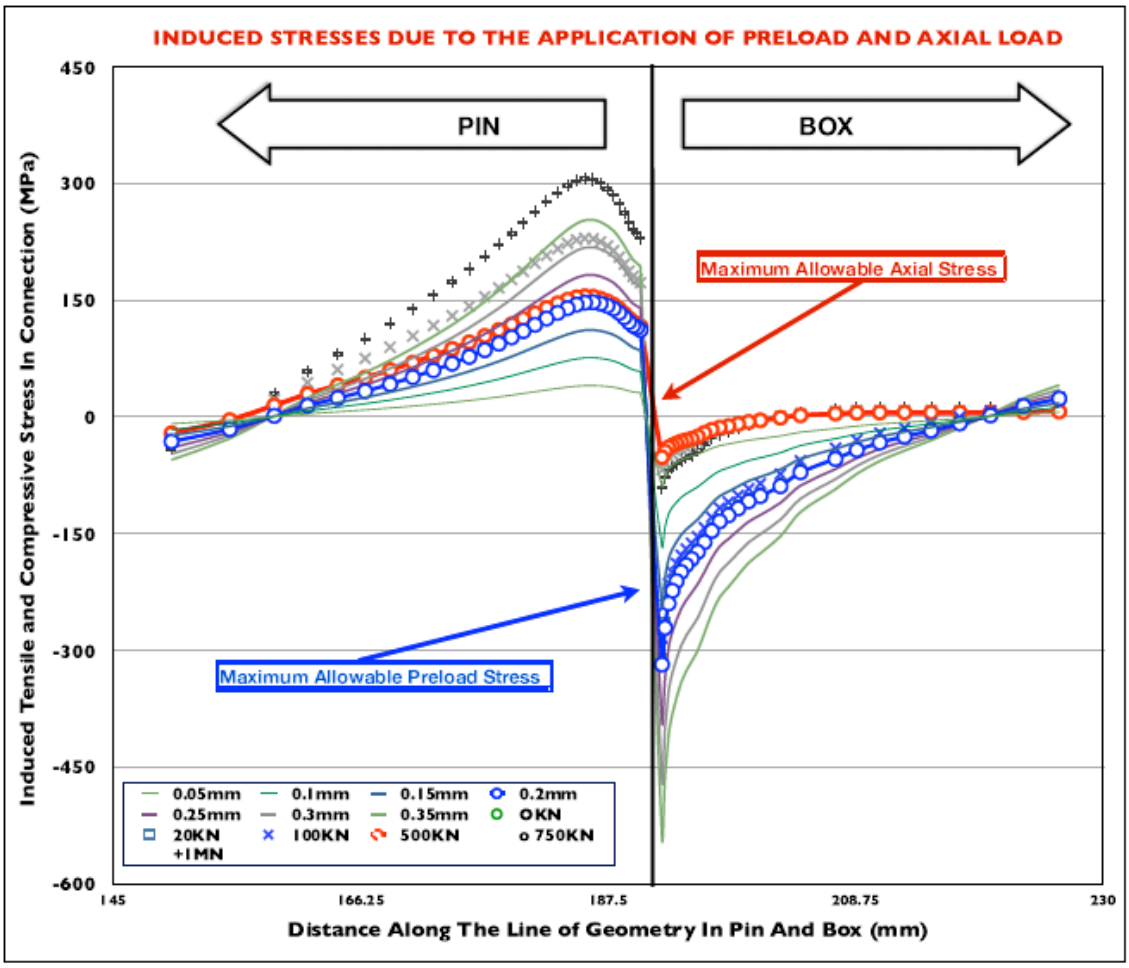
INDUCED STRESSES DUE TO THE APPLICATION OF PRELOAD AND AXIAL LOAD
PIN
BOX
Maximum Allowable Axial Stress
Maximum Allowable Preload Stress
0.05mm
0.1mm
0.15mm
0.2mm
0.25mm
0.3mm
0.35mm
OKN
20KN
100KN
500KN
o 750KN
+1MN
450
300
150
0
-150
-300
-450
-600
145
166.25
187.5
208.75
230
Induced Tensile and Compressive Stress In Connection (MPa)
Distance Along The Line of Geometry In Pin And Box (mm)

8.4.1.3 Simulation Data Pages

RESULTS SNAPSHOT 0.05MM

COMPONENT	LENGTH (MM)	PEAK S22 STRESS (MPA)	PRELOAD FORCE IN COMPONENT (MN)
PIN	40.3	40.5	0.70
BOX	34.1	-89.0	-0.71
		%Difference	-0.99

YIELD ANALYSIS 0.05MM

COMPONENT	MATERIAL	YIELD STRENGTH	PEAK VON MISES STRESS
PIN	AISI 4145H	940.0	170.50
BOX	AISI 4145H	940.0	
		% of Yield	18.14

PIN PRELOAD STRESS VALUES

NODE	X	S22	TRUE ELEMENT FORCE	AVE. NODAL STRESS	FORCE ON ELEMENT FACE	VON MISES STRESS
158	190.27	30.6755	3.58E+02	3.11E+01	1.11E+04	29.5386
1828	189.97	31.5324	3.94E+02	3.19E+01	1.25E+04	29.9934
1829	189.64	32.2179	4.32E+02	3.29E+01	1.42E+04	30.2411
1830	189.28	33.4968	4.75E+02	3.43E+01	1.63E+04	31.661
1831	188.88	35.1646	5.20E+02	3.60E+01	1.87E+04	33.6968
1832	188.44	36.782	5.71E+02	3.75E+01	2.14E+04	35.9131
1833	187.96	38.2161	6.26E+02	3.87E+01	2.43E+04	37.9227
1834	187.43	39.2337	6.88E+02	3.96E+01	2.73E+04	39.4618
1835	186.84	40.0042	7.54E+02	4.02E+01	3.03E+04	40.7355
1836	186	40.4614	8.26E+02	4.04E+01	3.34E+04	41.5603
1837	185.49	40.3432	8.32E+02	4.00E+01	3.33E+04	41.6169
1838	184.78	39.6327	9.01E+02	3.90E+01	3.52E+04	40.8431
1839	184	38.4017	9.75E+02	3.76E+01	3.66E+04	39.3127
1840	183.16	36.7258	1.09E+03	3.57E+01	3.90E+04	37.1632
1841	182.21	34.7158	1.14E+03	3.36E+01	3.84E+04	34.6158
1842	181.21	32.4959	1.14E+03	3.14E+01	3.56E+04	31.8017
160	180.21	30.2493	1.13E+03	2.92E+01	3.29E+04	29.1085
1843	179.21	28.0518	1.23E+03	2.69E+01	3.33E+04	26.6356
1844	178.11	25.8256	1.35E+03	2.47E+01	3.33E+04	24.229
1845	176.90	23.5487	1.47E+03	2.24E+01	3.30E+04	21.9023
1846	175.56	21.1784	1.61E+03	2.00E+01	3.21E+04	19.6288
1847	174	18.7991	1.75E+03	1.76E+01	3.09E+04	17.5199
1848	172.5	16.4396	1.91E+03	1.52E+01	2.91E+04	15.6219
1849	170.72	14.0272	2.08E+03	1.28E+01	2.66E+04	13.8436
1850	168.77	11.5458	2.26E+03	1.03E+01	2.33E+04	12.1194
1851	166.63	9.0769	2.45E+03	7.88E+00	1.93E+04	10.5356
1852	164.27	6.6834	2.66E+03	5.33E+00	1.41E+04	9.1836
1853	161.67	3.9688	2.87E+03	2.21E+00	6.34E+03	7.8184
1854	158.82	0.4472	3.77E+03	-1.91E+00	-7.18E+03	6.5061
1855	155	-4.2572	4.79E+03	-6.42E+00	-3.07E+04	6.4418
159	150	-8.5759	7.07E+04	-4.29E+00		9.6628
				Tensile Preload Force in Pin	7.04E+05	

BOX PRELOAD STRESS VALUES

NODE	X	S22	TRUE ELEMENT FORCE	AVE. NODAL STRESS	FORCE ON ELEMENT FACE	VON MISES STRESS
77	226.2	6.5517	4.32E+03	5.23E+00	2.26E+04	26.4257
761	223.2	3.9104	3.96E+03	2.27E+00	8.99E+03	26.6112
762	220.3	0.6283	3.64E+03	-7.77E-01	-2.83E+03	27.7524
763	217.7	-2.183	3.34E+03	-3.45E+00	-1.15E+04	28.9436
764	215.2	-4.714	3.07E+03	-5.78E+00	-1.77E+04	30.1158
765	212.9	-6.839	2.83E+03	-7.90E+00	-2.23E+04	31.2031
766	210.8	-8.968	2.60E+03	-1.03E+01	-2.68E+04	32.2995
767	208.8	-11.64	2.40E+03	-1.32E+01	-3.17E+04	33.5405
78	207	-14.79	3.87E+03	-1.71E+01	-6.64E+04	35.1005
896	204	-19.47	2.20E+03	-2.19E+01	-4.83E+04	37.5527
895	202.3	-24.39	2.18E+03	-2.61E+01	-5.70E+04	40.3262
894	200.6	-27.85	1.26E+03	-2.88E+01	-3.62E+04	42.6574
82	199.6	-29.73	1.13E+03	-3.10E+01	-3.51E+04	44.0083
893	198.7	-32.24	1.03E+03	-3.35E+01	-3.45E+04	45.6801
892	197.8	-34.68	9.35E+02	-3.58E+01	-3.34E+04	47.3762
891	197.1	-36.83	8.49E+02	-3.85E+01	-3.27E+04	49.0075
890	196.4	-40.23	7.71E+02	-4.22E+01	-3.26E+04	51.5977
889	195.8	-44.25	7.00E+02	-4.60E+01	-3.22E+04	54.5293
888	195.2	-47.76	6.38E+02	-4.90E+01	-3.13E+04	57.2599
887	194.7	-50.28	5.79E+02	-5.14E+01	-2.98E+04	59.2611
886	194.2	-52.52	5.27E+02	-5.38E+01	-2.83E+04	61.0422
885	193.8	-55.03	4.79E+02	-5.67E+01	-2.72E+04	62.7636
884	193.4	-58.33	4.36E+02	-6.01E+01	-2.62E+04	65.2876
883	193	-61.85	3.97E+02	-6.42E+01	-2.55E+04	68.0175
882	192.7	-66.53	3.60E+02	-7.10E+01	-2.56E+04	71.3638
881	192.4	-75.45	3.29E+02	-8.22E+01	-2.70E+04	78.5943
69	192.1	-89.01	1.16E+05	-4.45E+01		94.4089
				Compressive Preload Force in Box	-7.11E+05	

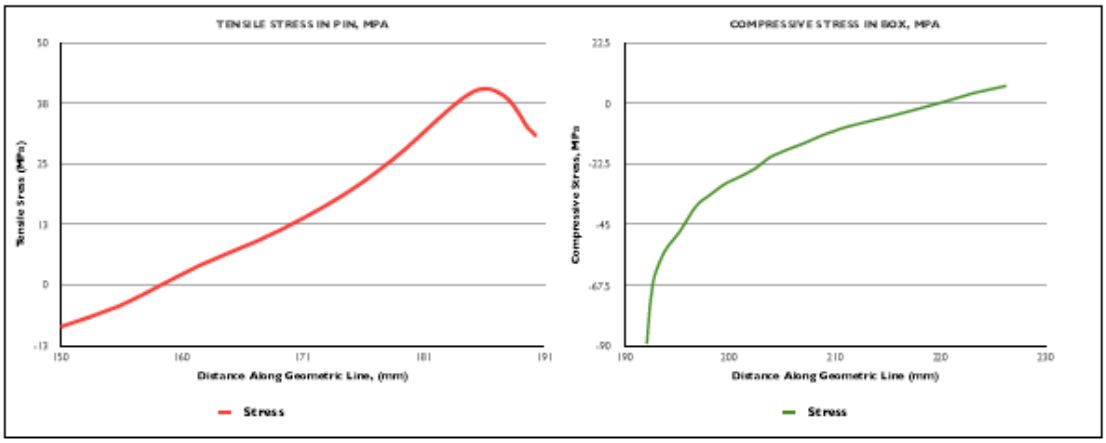

RESULTS SNAPSHOT-0.1MM

COMPONENT	LENGTH (MM)	PEAK S22 STRESS (MPA)	PRELOAD FORCE IN COMPONENT (MN)
PIN	40.3	76.2	1.33
BOX	34.1	-166.3	-1.34
		% Difference	-0.99

YIELD ANALYSIS-0.1MM

COMPONENT	MATERIAL	YIELD STRENGTH	PEAK VON MISES STRESS
PIN	AISI 4145H	940.0	320.50
BOX	AISI 4145H	940.0	
		% of Yield	34.10

PIN PRELOAD STRESS VALUES

NODE	X	S22	TRUE ELEMENT FORCE	AVE. NODAL STRESS	FORCE ON ELEMENT FACE	VON MISES STRESS
158	190.27	57.7747	3.58E+02	5.86E+01	2.10E+04	81.6368
1828	189.97	59.3868	3.94E+02	6.00E+01	2.36E+04	82.8932
1829	189.64	60.6761	4.32E+02	6.19E+01	2.67E+04	83.5764
1830	189.28	63.0834	4.75E+02	6.47E+01	3.07E+04	87.4987
1831	188.88	66.2228	5.20E+02	6.77E+01	3.53E+04	93.1234
1832	188.44	69.2675	5.71E+02	7.06E+01	4.03E+04	99.2469
1833	187.96	71.9677	6.26E+02	7.29E+01	4.57E+04	104.801
1834	187.43	73.8843	6.88E+02	7.46E+01	5.13E+04	109.058
1835	186.84	75.3366	7.54E+02	7.58E+01	5.71E+04	112.583
1836	186	76.1998	8.26E+02	7.61E+01	6.28E+04	114.872
1837	185.49	75.9802	8.32E+02	7.53E+01	6.26E+04	115.04
1838	184.78	74.6457	9.01E+02	7.35E+01	6.62E+04	112.915
1839	184	72.3314	9.75E+02	7.08E+01	6.90E+04	108.7
1840	183.16	69.1796	1.09E+03	6.73E+01	7.34E+04	102.773
1841	182.21	65.3987	1.14E+03	6.33E+01	7.23E+04	95.7463
1842	181.21	61.2221	1.14E+03	5.91E+01	6.71E+04	87.9793
160	180.21	56.9944	1.13E+03	5.49E+01	6.20E+04	80.5415
1843	179.21	52.8581	1.23E+03	5.08E+01	6.27E+04	73.7084
1844	178.11	48.6668	1.35E+03	4.65E+01	6.28E+04	67.0547
1845	176.90	44.3794	1.47E+03	4.21E+01	6.21E+04	60.6184
1846	175.56	39.915	1.61E+03	3.77E+01	6.06E+04	54.3247
1847	174	35.4323	1.75E+03	3.32E+01	5.82E+04	48.482
1848	172.5	30.9856	1.91E+03	2.87E+01	5.49E+04	43.2193
1849	170.72	26.4379	2.08E+03	2.41E+01	5.01E+04	38.2847
1850	168.77	21.7583	2.26E+03	1.94E+01	4.39E+04	33.4969
1851	166.63	17.1013	2.45E+03	1.48E+01	3.64E+04	29.0968
1852	164.27	12.5851	2.66E+03	1.00E+01	2.66E+04	25.3405
1853	161.67	7.462	2.87E+03	4.14E+00	1.19E+04	21.5503
1854	158.82	0.8159	3.77E+03	-3.62E+00	-1.36E+04	17.922
1855	155	-8.0612	4.79E+03	-1.21E+01	-5.81E+04	17.8037
159	150	-16.2088	7.07E+04	-8.10E+00		26.7968
				Tensile Preload Force in Pin	1.33E+06	

BOX PRELOAD STRESS VALUES

NODE	X	S22	TRUE ELEMENT FORCE	AVE. NODAL STRESS	FORCE ON ELEMENT FACE	VON MISES STRESS
77	226.2	12.226	4.32E+03	9.74E+00	4.21E+04	73.2072
761	223.2	7.2578	3.96E+03	4.17E+00	1.65E+04	73.7398
762	220.3	1.0745	3.64E+03	-1.58E+00	-5.73E+03	76.9062
763	217.7	-4.225	3.34E+03	-6.60E+00	-2.21E+04	80.2123
764	215.2	-8.983	3.07E+03	-1.10E+01	-3.37E+04	83.4628
765	212.9	-12.97	2.83E+03	-1.50E+01	-4.23E+04	86.4701
766	210.8	-16.96	2.60E+03	-1.95E+01	-5.06E+04	89.4974
767	208.8	-21.96	2.40E+03	-2.49E+01	-5.97E+04	92.9244
78	207	-27.87	3.87E+03	-3.23E+01	-1.25E+05	97.2321
896	204	-36.65	2.20E+03	-4.13E+01	-9.08E+04	104.003
895	202.3	-45.9	2.18E+03	-4.91E+01	-1.07E+05	111.665
894	200.6	-52.4	1.26E+03	-5.42E+01	-6.81E+04	118.097
82	199.6	-55.93	1.13E+03	-5.83E+01	-6.61E+04	121.834
893	198.7	-60.64	1.03E+03	-6.29E+01	-6.48E+04	126.441
892	197.8	-65.21	9.35E+02	-6.72E+01	-6.29E+04	131.098
891	197.1	-69.24	8.49E+02	-7.24E+01	-6.15E+04	135.582
890	196.4	-75.63	7.71E+02	-7.94E+01	-6.12E+04	142.701
889	195.8	-83.16	7.00E+02	-8.64E+01	-6.05E+04	150.726
888	195.2	-89.7	6.38E+02	-9.21E+01	-5.87E+04	158.184
887	194.7	-94.42	5.79E+02	-9.65E+01	-5.59E+04	163.622
886	194.2	-98.6	5.27E+02	-1.01E+02	-5.31E+04	168.438
885	193.8	-103.3	4.79E+02	-1.06E+02	-5.10E+04	173.095
884	193.4	-109.4	4.36E+02	-1.13E+02	-4.91E+04	179.919
883	193	-116	3.97E+02	-1.20E+02	-4.78E+04	187.28
882	192.7	-124.7	3.60E+02	-1.33E+02	-4.79E+04	196.344
881	192.4	-141.3	3.29E+02	-1.54E+02	-5.05E+04	215.962
69	192.1	-166.3	1.16E+05	-8.32E+01		257.985
				Compressive Preload Force in Box	-1.34E+06	

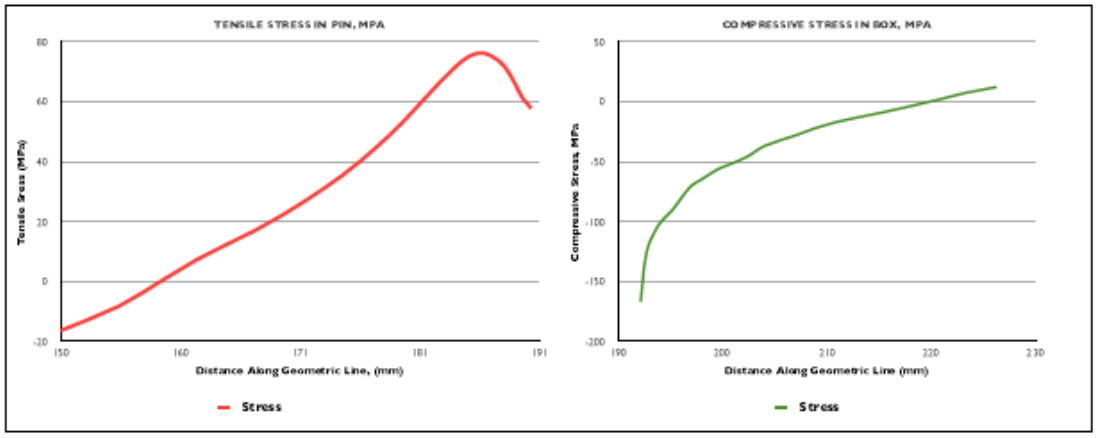

RESULTS SNAPSHOT-0.15MM

COMPONENT	LENGTH (MM)	PEAK S22 STRESS (MPA)	PRELOAD FORCE IN COMPONENT (MN)
PIN	40.3	111.8	1.95
BOX	34.1	-242.7	-1.96
		% Difference	-0.99

YIELD ANALYSIS-0.15MM

COMPONENT	MATERIAL	YIELD STRENGTH	PEAK VON MISES STRESS
PIN	AISI 4145H	940.0	469.30
BOX	AISI 4145H	940.0	
		% of Yield	49.93

PIN PRELOAD STRESS VALUES

NODE	X	S22	TRUE ELEMENT FORCE	AVE. NODAL STRESS	FORCE ON ELEMENT FACE	VON MISES STRESS
158	190.27	84.8036	3.58E+02	8.60E+01	3.08E+04	81.6368
1828	189.97	87.1671	3.94E+02	8.81E+01	3.47E+04	82.8932
1829	189.64	89.0565	4.32E+02	9.08E+01	3.92E+04	83.5764
1830	189.28	92.5872	4.75E+02	9.49E+01	4.51E+04	87.4987
1831	188.88	97.1924	5.20E+02	9.94E+01	5.17E+04	93.1234
1832	188.44	101.658	5.71E+02	1.04E+02	5.92E+04	99.2469
1833	187.96	105.619	6.26E+02	1.07E+02	6.70E+04	104.801
1834	187.43	108.432	6.88E+02	1.09E+02	7.53E+04	109.058
1835	186.84	110.564	7.54E+02	1.11E+02	8.38E+04	112.583
1836	186	111.833	8.26E+02	1.12E+02	9.22E+04	114.872
1837	185.49	111.513	8.32E+02	1.11E+02	9.19E+04	115.04
1838	184.78	109.559	9.01E+02	1.08E+02	9.72E+04	112.915
1839	184	106.167	9.75E+02	1.04E+02	1.01E+05	108.7
1840	183.16	101.547	1.09E+03	9.88E+01	1.08E+05	102.773
1841	182.21	96.004	1.14E+03	9.29E+01	1.06E+05	95.7463
1842	181.21	89.8798	1.14E+03	8.68E+01	9.85E+04	87.9793
160	180.21	83.6793	1.13E+03	8.06E+01	9.11E+04	80.5415
1843	179.21	77.6118	1.23E+03	7.45E+01	9.20E+04	73.7084
1844	178.11	71.4626	1.35E+03	6.83E+01	9.22E+04	67.0547
1845	176.90	65.1712	1.47E+03	6.19E+01	9.12E+04	60.6184
1846	175.56	58.6186	1.61E+03	5.53E+01	8.90E+04	54.3247
1847	174	52.0377	1.75E+03	4.88E+01	8.55E+04	48.482
1848	172.5	45.5078	1.91E+03	4.22E+01	8.06E+04	43.2193
1849	170.72	38.8278	2.08E+03	3.54E+01	7.36E+04	38.2847
1850	168.77	31.9525	2.26E+03	2.85E+01	6.44E+04	33.4969
1851	166.63	25.1086	2.45E+03	2.18E+01	5.34E+04	29.0968
1852	164.27	18.4702	2.66E+03	1.47E+01	3.91E+04	25.3405
1853	161.67	10.9387	2.87E+03	6.05E+00	1.74E+04	21.5503
1854	158.82	1.1681	3.77E+03	-5.36E+00	-2.02E+04	17.922
1855	155	-11.8813	4.79E+03	-1.79E+01	-8.56E+04	17.8037
159	150	-23.8564	7.07E+04	-1.19E+01		26.7968
				Tensile Preload Force in Pin	1.95E+06	

BOX PRELOAD STRESS VALUES

NODE	X	S22	TRUE ELEMENT FORCE	AVE. NODAL STRESS	FORCE ON ELEMENT FACE	VON MISES STRESS
77	226.2	17.934	4.32E+03	1.43E+01	6.17E+04	73.2072
761	223.2	10.639	3.96E+03	6.10E+00	2.42E+04	73.7398
762	220.3	1.5544	3.64E+03	-2.34E+00	-8.51E+03	76.9062
763	217.7	-6.233	3.34E+03	-9.73E+00	-3.25E+04	80.2123
764	215.2	-13.22	3.07E+03	-1.61E+01	-4.96E+04	83.4628
765	212.9	-19.07	2.83E+03	-2.20E+01	-6.22E+04	86.4701
766	210.8	-24.93	2.60E+03	-2.86E+01	-7.44E+04	89.4974
767	208.8	-32.24	2.40E+03	-3.66E+01	-8.77E+04	92.9244
78	207	-40.91	3.87E+03	-4.74E+01	-1.83E+05	97.2321
896	204	-53.81	2.20E+03	-6.06E+01	-1.33E+05	104.003
895	202.3	-67.39	2.18E+03	-7.22E+01	-1.58E+05	111.665
894	200.6	-76.94	1.26E+03	-7.95E+01	-1.00E+05	118.097
82	199.6	-82.14	1.13E+03	-8.56E+01	-9.70E+04	121.834
893	198.7	-89.07	1.03E+03	-9.24E+01	-9.52E+04	126.441
892	197.8	-95.77	9.35E+02	-9.87E+01	-9.23E+04	131.098
891	197.1	-101.7	8.49E+02	-1.06E+02	-9.03E+04	135.582
890	196.4	-111	7.71E+02	-1.17E+02	-8.99E+04	142.701
889	195.8	-122	7.00E+02	-1.27E+02	-8.88E+04	150.726
888	195.2	-131.6	6.38E+02	-1.35E+02	-8.62E+04	158.184
887	194.7	-138.5	5.79E+02	-1.41E+02	-8.19E+04	163.622
886	194.2	-144.5	5.27E+02	-1.48E+02	-7.79E+04	168.438
885	193.8	-151.3	4.79E+02	-1.56E+02	-7.46E+04	173.095
884	193.4	-160.2	4.36E+02	-1.65E+02	-7.19E+04	179.919
883	193	-169.7	3.97E+02	-1.76E+02	-7.00E+04	187.28
882	192.7	-182.4	3.60E+02	-1.94E+02	-7.01E+04	196.344
881	192.4	-206.5	3.29E+02	-2.25E+02	-7.38E+04	215.962
69	192.1	-242.7	1.16E+05	-1.21E+02		257.985
				Compressive Preload Force in Box	-1.96E+06	

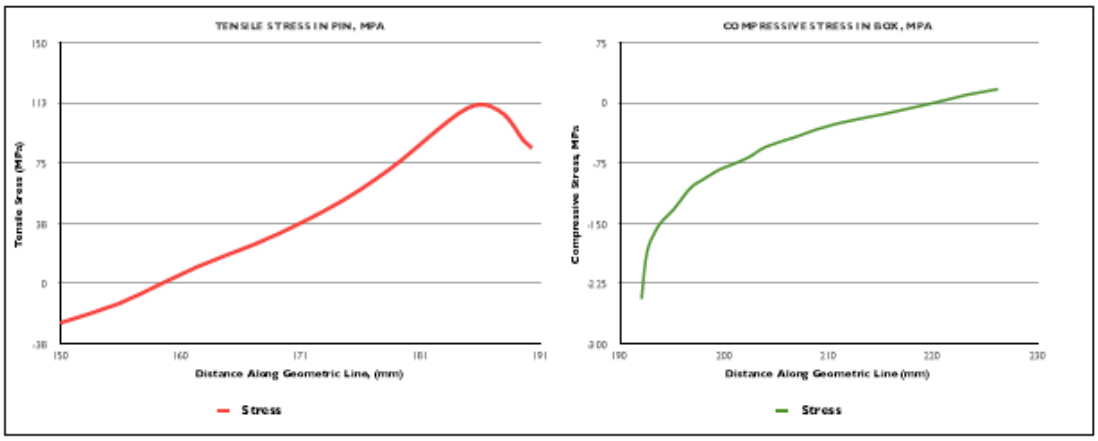

RESULTS SNAPSHOT-0.2MM

COMPONENT	LENGTH (MM)	PEAK S22 STRESS (MPA)	PRELOAD FORCE IN COMPONENT (MN)
PIN	40.3	147.3	2.56
BOX	34.1	-318.0	-2.59
		%Difference	-0.99

YIELD ANALYSIS-0.2MM

COMPONENT	MATERIAL	YIELD STRENGTH	PEAK VON MISES STRESS
PIN	AISI 4145H	940.0	616.70
BOX	AISI 4145H	940.0	
		% of Yield	65.61

PIN PRELOAD STRESS VALUES

NODE	X	S22	TRUE ELEMENT FORCE	AVE. NODAL STRESS	FORCE ON ELEMENT FACE	VON MISES STRESS
158	190.27	111.753	3.58E+02	1.13E+02	4.06E+04	107.571
1828	189.97	114.863	3.94E+02	1.16E+02	4.57E+04	109.226
1829	189.64	117.349	4.32E+02	1.20E+02	5.17E+04	110.125
1830	189.28	121.998	4.75E+02	1.25E+02	5.94E+04	115.291
1831	188.88	128.063	5.20E+02	1.31E+02	6.82E+04	122.7
1832	188.44	133.943	5.71E+02	1.37E+02	7.80E+04	130.767
1833	187.96	139.16	6.26E+02	1.41E+02	8.83E+04	138.085
1834	187.43	142.865	6.88E+02	1.44E+02	9.92E+04	143.694
1835	186.84	145.674	7.54E+02	1.47E+02	1.10E+05	148.342
1836	186	147.348	8.26E+02	1.47E+02	1.21E+05	151.362
1837	185.49	146.931	8.32E+02	1.46E+02	1.21E+05	151.591
1838	184.78	144.361	9.01E+02	1.42E+02	1.28E+05	148.8
1839	184	139.898	9.75E+02	1.37E+02	1.33E+05	143.254
1840	183.16	133.818	1.09E+03	1.30E+02	1.42E+05	135.455
1841	182.21	126.522	1.14E+03	1.22E+02	1.40E+05	126.205
1842	181.21	118.46	1.14E+03	1.14E+02	1.30E+05	115.979
160	180.21	110.296	1.13E+03	1.06E+02	1.20E+05	106.183
1843	179.21	102.306	1.23E+03	9.83E+01	1.21E+05	97.181
1844	178.11	94.2069	1.35E+03	9.01E+01	1.22E+05	88.4134
1845	176.90	85.919	1.47E+03	8.16E+01	1.20E+05	79.9299
1846	175.56	77.2852	1.61E+03	7.29E+01	1.17E+05	71.6318
1847	174	68.612	1.75E+03	6.43E+01	1.13E+05	63.9256
1848	172.5	60.0037	1.91E+03	5.56E+01	1.06E+05	56.9818
1849	170.72	51.1952	2.08E+03	4.67E+01	9.70E+04	50.4686
1850	168.77	42.1269	2.26E+03	3.76E+01	8.49E+04	44.1478
1851	166.63	33.098	2.45E+03	2.87E+01	7.04E+04	38.3379
1852	164.27	24.3384	2.66E+03	1.94E+01	5.14E+04	33.3782
1853	161.67	14.3992	2.87E+03	7.95E+00	2.28E+04	28.3757
1854	158.82	1.5046	3.77E+03	-7.11E+00	-2.68E+04	23.5952
1855	155	-15.7155	4.79E+03	-2.36E+01	-1.13E+05	23.4704
159	150	-31.5158	7.07E+04	-1.58E+01		35.3647
				Tensile Preload Force in Pin	2.56E+06	

BOX PRELOAD STRESS VALUES

NODE	X	S22	TRUE ELEMENT FORCE	AVE. NODAL STRESS	FORCE ON ELEMENT FACE	VON MISES STRESS
77	226.2	23.67	4.32E+03	1.89E+01	8.15E+04	96.5385
761	223.2	14.051	3.96E+03	8.06E+00	3.19E+04	97.2392
762	220.3	2.0666	3.64E+03	-3.07E+00	-1.12E+04	101.414
763	217.7	-8.209	3.34E+03	-1.28E+01	-4.28E+04	105.775
764	215.2	-17.42	3.07E+03	-2.13E+01	-6.54E+04	110.063
765	212.9	-25.14	2.83E+03	-2.90E+01	-8.20E+04	114.027
766	210.8	-32.85	2.60E+03	-3.77E+01	-9.80E+04	118.017
767	208.8	-42.48	2.40E+03	-4.82E+01	-1.16E+05	122.534
78	207	-53.91	3.87E+03	-6.24E+01	-2.42E+05	128.214
896	204	-70.93	2.20E+03	-7.99E+01	-1.76E+05	137.146
895	202.3	-88.88	2.18E+03	-9.52E+01	-2.08E+05	147.265
894	200.6	-101.5	1.26E+03	-1.05E+02	-1.32E+05	155.747
82	199.6	-108.4	1.13E+03	-1.13E+02	-1.28E+05	160.679
893	198.7	-117.5	1.03E+03	-1.22E+02	-1.26E+05	166.752
892	197.8	-126.3	9.35E+02	-1.30E+02	-1.22E+05	172.88
891	197.1	-134.1	8.49E+02	-1.40E+02	-1.19E+05	178.785
890	196.4	-146.4	7.71E+02	-1.54E+02	-1.18E+05	188.171
889	195.8	-160.9	7.00E+02	-1.67E+02	-1.17E+05	198.729
888	195.2	-173.4	6.38E+02	-1.78E+02	-1.14E+05	208.495
887	194.7	-182.4	5.79E+02	-1.86E+02	-1.08E+05	215.665
886	194.2	-190.3	5.27E+02	-1.95E+02	-1.03E+05	221.953
885	193.8	-199.2	4.79E+02	-2.05E+02	-9.83E+04	228.053
884	193.4	-210.9	4.36E+02	-2.17E+02	-9.46E+04	236.963
883	193	-223.3	3.97E+02	-2.31E+02	-9.20E+04	246.556
882	192.7	-239.7	3.60E+02	-2.55E+02	-9.20E+04	258.309
881	192.4	-270.9	3.29E+02	-2.94E+02	-9.67E+04	283.601
69	192.1	-318	1.16E+05	-1.59E+02		338.334
				Compressive Preload Force in Box	-2.59E+06	

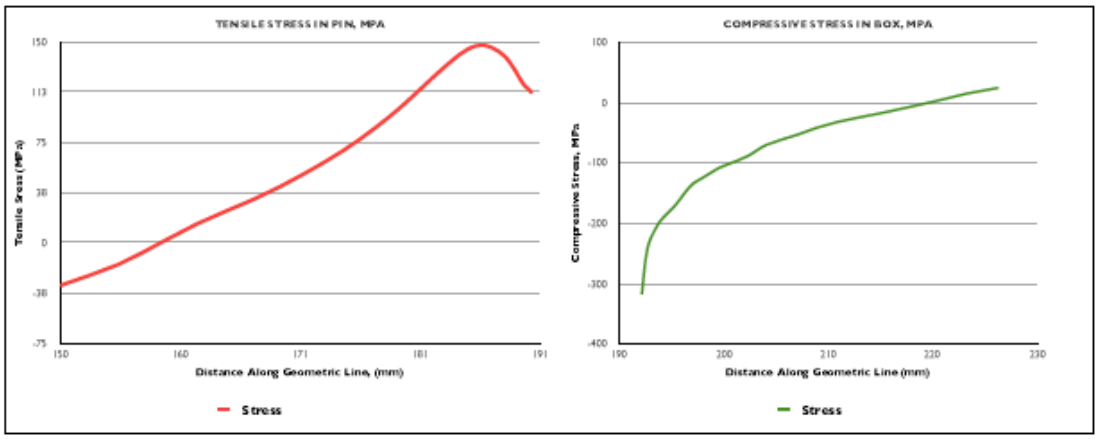

RESULTS SNAPSHOT-0.25MM

COMPONENT	LENGTH (MM)	PEAK S22 STRESS (MPA)	PRELOAD FORCE IN COMPONENT (MN)
PIN	40.3	182.7	3.18
BOX	34.1	-391.7	-3.21
		% Difference	-0.99

YIELD ANALYSIS-0.25MM

COMPONENT	MATERIAL	YIELD STRENGTH	PEAK VON MISES STRESS
PIN	AISI 4145H	940.0	756.70
BOX	AISI 4145H	940.0	
		% of Yield	80.50

PIN PRELOAD STRESS VALUES

NODE	X	S22	TRUE ELEMENT FORCE	AVE. NODAL STRESS	FORCE ON ELEMENT FACE	VON MISES STRESS
158	190.27	138.519	3.58E+02	1.40E+02	5.03E+04	133.29
1828	189.97	142.379	3.94E+02	1.44E+02	5.66E+04	135.347
1829	189.64	145.463	4.32E+02	1.48E+02	6.41E+04	136.465
1830	189.28	151.231	4.75E+02	1.55E+02	7.37E+04	142.878
1831	188.88	158.756	5.20E+02	1.62E+02	8.45E+04	152.074
1832	188.44	166.052	5.71E+02	1.69E+02	9.67E+04	162.086
1833	187.96	172.529	6.26E+02	1.75E+02	1.09E+05	171.173
1834	187.43	177.133	6.88E+02	1.79E+02	1.23E+05	178.144
1835	186.84	180.632	7.54E+02	1.82E+02	1.37E+05	183.928
1836	186	182.726	8.26E+02	1.82E+02	1.51E+05	187.699
1837	185.49	182.236	8.32E+02	1.81E+02	1.50E+05	188.012
1838	184.78	179.076	9.01E+02	1.76E+02	1.59E+05	184.577
1839	184	173.573	9.75E+02	1.70E+02	1.66E+05	177.729
1840	183.16	166.069	1.09E+03	1.62E+02	1.76E+05	168.085
1841	182.21	157.057	1.14E+03	1.52E+02	1.74E+05	156.635
1842	181.21	147.09	1.14E+03	1.42E+02	1.61E+05	143.965
160	180.21	136.987	1.13E+03	1.32E+02	1.49E+05	131.813
1843	179.21	127.091	1.23E+03	1.22E+02	1.51E+05	120.634
1844	178.11	117.052	1.35E+03	1.12E+02	1.51E+05	109.735
1845	176.90	106.771	1.47E+03	1.01E+02	1.49E+05	99.1803
1846	175.56	96.051	1.61E+03	9.07E+01	1.46E+05	88.8457
1847	174	85.2713	1.75E+03	7.99E+01	1.40E+05	79.2386
1848	172.5	74.5623	1.91E+03	6.91E+01	1.32E+05	70.5742
1849	170.72	63.5951	2.08E+03	5.79E+01	1.20E+05	62.4423
1850	168.77	52.2969	2.26E+03	4.67E+01	1.05E+05	54.5514
1851	166.63	41.0413	2.45E+03	3.56E+01	8.72E+04	47.3017
1852	164.27	30.1165	2.66E+03	2.39E+01	6.35E+04	41.121
1853	161.67	17.7174	2.87E+03	9.67E+00	2.78E+04	34.9015
1854	158.82	1.6295	3.77E+03	-9.11E+00	-3.43E+04	29.0162
1855	155	-19.853	4.79E+03	-2.97E+01	-1.42E+05	29.0958
159	150	-39.5583	7.07E+04	-1.98E+01		44.1362
				Tensile Preload Force in Pin	3.18E+06	

BOX PRELOAD STRESS VALUES

NODE	X	S22	TRUE ELEMENT FORCE	AVE. NODAL STRESS	FORCE ON ELEMENT FACE	VON MISES STRESS
77	226.2	29.345	4.32E+03	2.34E+01	1.01E+05	119.544
761	223.2	17.426	3.96E+03	9.99E+00	3.96E+04	120.408
762	220.3	2.5511	3.64E+03	-3.83E+00	-1.39E+04	125.577
763	217.7	-10.22	3.34E+03	-1.59E+01	-5.33E+04	130.984
764	215.2	-21.66	3.07E+03	-2.65E+01	-8.13E+04	136.305
765	212.9	-31.25	2.83E+03	-3.60E+01	-1.02E+05	141.219
766	210.8	-40.82	2.60E+03	-4.68E+01	-1.22E+05	146.164
767	208.8	-52.76	2.40E+03	-5.98E+01	-1.43E+05	151.773
78	207	-66.93	3.87E+03	-7.75E+01	-3.00E+05	158.828
896	204	-88.05	2.20E+03	-9.92E+01	-2.18E+05	169.934
895	202.3	-110.3	2.18E+03	-1.18E+02	-2.58E+05	182.517
894	200.6	-125.9	1.26E+03	-1.30E+02	-1.64E+05	193.017
82	199.6	-134.5	1.13E+03	-1.40E+02	-1.59E+05	199.119
893	198.7	-145.7	1.03E+03	-1.51E+02	-1.56E+05	206.636
892	197.8	-156.6	9.35E+02	-1.61E+02	-1.51E+05	214.188
891	197.1	-166.3	8.49E+02	-1.74E+02	-1.48E+05	221.468
890	196.4	-181.5	7.71E+02	-1.90E+02	-1.47E+05	233.059
889	195.8	-199.2	7.00E+02	-2.07E+02	-1.45E+05	246.063
888	195.2	-214.6	6.38E+02	-2.20E+02	-1.40E+05	258.092
887	194.7	-225.7	5.79E+02	-2.31E+02	-1.34E+05	266.851
886	194.2	-235.4	5.27E+02	-2.41E+02	-1.27E+05	274.583
885	193.8	-246.3	4.79E+02	-2.53E+02	-1.21E+05	282.045
884	193.4	-260.5	4.36E+02	-2.68E+02	-1.17E+05	292.956
883	193	-275.7	3.97E+02	-2.86E+02	-1.14E+05	304.735
882	192.7	-296	3.60E+02	-3.15E+02	-1.14E+05	319.319
881	192.4	-334.4	3.29E+02	-3.63E+02	-1.19E+05	350.518
69	192.1	-391.7	1.16E+05	-1.96E+02		417.066
				Compressive Preload Force in Box	-3.21E+06	

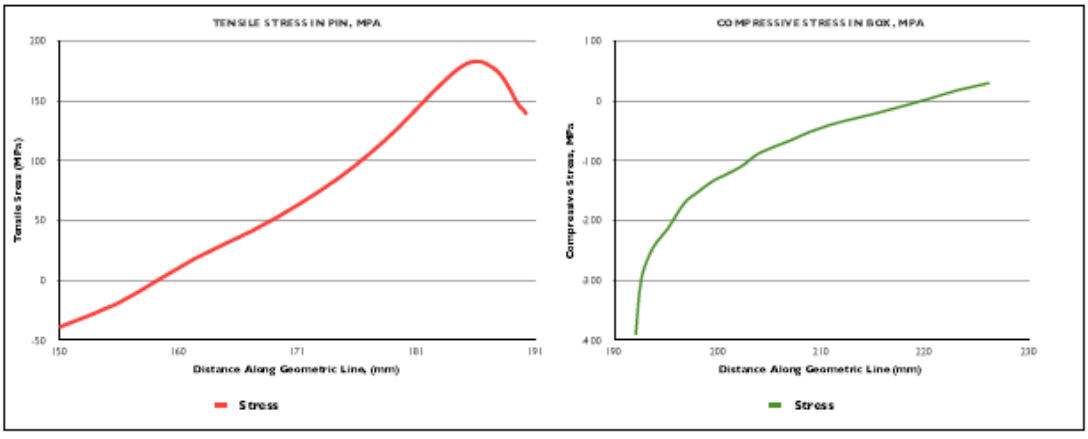

RESULTS SNAPSHOT-0.3MM

COMPONENT	LENGTH (MM)	PEAK S22 STRESS (MPA)	PRELOAD FORCE IN COMPONENT (MN)
PIN	40.3	218.1	3.79
BOX	34.1	-467.4	-3.83
		% Difference	-0.99

YIELD ANALYSIS-0.3MM

COMPONENT	MATERIAL	YIELD STRENGTH	PEAK VON MISES STRESS
PIN	AISI 4145H	940.0	902.70
BOX	AISI 4145H	940.0	
		% of Yield	96.03

PIN PRELOAD STRESS VALUES

NODE	X	S22	TRUE ELEMENT FORCE	AVE. NODAL STRESS	FORCE ON ELEMENT FACE	VON MISES STRESS
158	190.27	165.394	3.58E+02	1.68E+02	6.01E+04	159.133
1828	189.97	169.997	3.94E+02	1.72E+02	6.76E+04	161.586
1829	189.64	173.672	4.32E+02	1.77E+02	7.65E+04	162.919
1830	189.28	180.553	4.75E+02	1.85E+02	8.79E+04	170.571
1831	188.88	189.53	5.20E+02	1.94E+02	1.01E+05	181.545
1832	188.44	198.234	5.71E+02	2.02E+02	1.15E+05	193.494
1833	187.96	205.961	6.26E+02	2.09E+02	1.31E+05	204.339
1834	187.43	211.455	6.88E+02	2.14E+02	1.47E+05	212.661
1835	186.84	215.631	7.54E+02	2.17E+02	1.63E+05	219.567
1836	186	218.135	8.26E+02	2.18E+02	1.80E+05	224.073
1837	185.49	217.551	8.32E+02	2.16E+02	1.79E+05	224.452
1838	184.78	213.785	9.01E+02	2.11E+02	1.90E+05	220.36
1839	184	207.222	9.75E+02	2.03E+02	1.98E+05	212.193
1840	183.16	198.271	1.09E+03	1.93E+02	2.10E+05	200.69
1841	182.21	187.522	1.14E+03	1.82E+02	2.07E+05	187.031
1842	181.21	175.631	1.14E+03	1.70E+02	1.93E+05	171.912
160	180.21	163.577	1.13E+03	1.58E+02	1.78E+05	157.409
1843	179.21	151.767	1.23E+03	1.46E+02	1.80E+05	144.064
1844	178.11	139.786	1.35E+03	1.34E+02	1.80E+05	131.053
1845	176.90	127.515	1.47E+03	1.21E+02	1.78E+05	118.449
1846	175.56	114.717	1.61E+03	1.08E+02	1.74E+05	106.106
1847	174	101.847	1.75E+03	9.55E+01	1.67E+05	94.6286
1848	172.5	89.0586	1.91E+03	8.25E+01	1.58E+05	84.2752
1849	170.72	75.9598	2.08E+03	6.92E+01	1.44E+05	74.5557
1850	168.77	62.4637	2.26E+03	5.57E+01	1.26E+05	65.1227
1851	166.63	49.0166	2.45E+03	4.25E+01	1.04E+05	56.4549
1852	164.27	35.963	2.66E+03	2.86E+01	7.58E+04	49.0652
1853	161.67	21.1468	2.87E+03	1.15E+01	3.31E+04	41.6305
1854	158.82	1.9225	3.77E+03	-1.09E+01	-4.11E+04	34.6019
1855	155	-23.7464	4.79E+03	-3.55E+01	-1.70E+05	34.7251
159	150	-47.2897	7.07E+04	-2.36E+01		52.7248
			Tensile Preload Force in Pin		3.79E+06	

BOX PRELOAD STRESS VALUES

NODE	X	S22	TRUE ELEMENT FORCE	AVE. NODAL STRESS	FORCE ON ELEMENT FACE	VON MISES STRESS
77	226.2	35.13	4.32E+03	2.80E+01	1.21E+05	142.775
761	223.2	20.888	3.96E+03	1.20E+01	4.75E+04	143.801
762	220.3	3.112	3.64E+03	-4.52E+00	-1.64E+04	149.973
763	217.7	-12.15	3.34E+03	-1.90E+01	-6.34E+04	156.432
764	215.2	-25.81	3.07E+03	-3.15E+01	-9.69E+04	162.788
765	212.9	-37.27	2.83E+03	-4.30E+01	-1.22E+05	168.656
766	210.8	-46.69	2.60E+03	-5.58E+01	-1.45E+05	174.559
767	208.8	-62.93	2.40E+03	-7.14E+01	-1.71E+05	181.255
78	207	-79.86	3.87E+03	-9.25E+01	-3.58E+05	189.681
896	204	-105.1	2.20E+03	-1.18E+02	-2.61E+05	202.956
895	202.3	-131.8	2.18E+03	-1.41E+02	-3.08E+05	218.033
894	200.6	-150.6	1.26E+03	-1.56E+02	-1.96E+05	230.67
82	199.6	-161	1.13E+03	-1.68E+02	-1.90E+05	238.092
893	198.7	-174.6	1.03E+03	-1.81E+02	-1.87E+05	247.177
892	197.8	-187.6	9.35E+02	-1.93E+02	-1.81E+05	256.186
891	197.1	-199	8.49E+02	-2.08E+02	-1.77E+05	264.876
890	196.4	-217.1	7.71E+02	-2.28E+02	-1.76E+05	278.718
889	195.8	-238.9	7.00E+02	-2.48E+02	-1.74E+05	294.935
888	195.2	-257.9	6.38E+02	-2.64E+02	-1.68E+05	309.81
887	194.7	-270.2	5.79E+02	-2.76E+02	-1.60E+05	319.137
886	194.2	-280.9	5.27E+02	-2.87E+02	-1.51E+05	327.475
885	193.8	-293.7	4.79E+02	-3.02E+02	-1.45E+05	336.382
884	193.4	-310.6	4.36E+02	-3.20E+02	-1.39E+05	349.422
883	193	-328.6	3.97E+02	-3.41E+02	-1.35E+05	363.4
882	192.7	-352.5	3.60E+02	-3.75E+02	-1.35E+05	380.614
881	192.4	-398.3	3.29E+02	-4.33E+02	-1.42E+05	417.59
69	192.1	-467.4	1.16E+05	-2.34E+02		497.58
			Compressive Preload Force in Box		-3.83E+06	

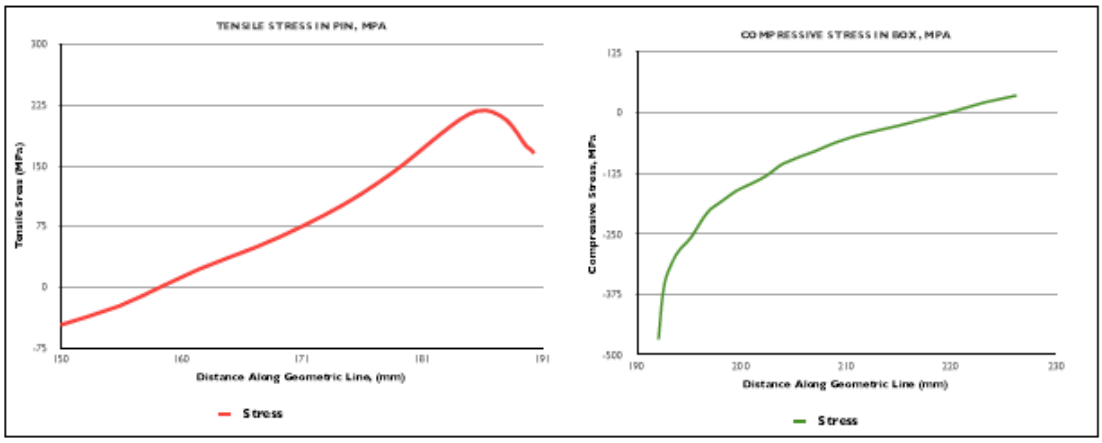

RESULTS SNAPSHOT - 0.35 MM

COMPONENT	LENGTH (MM)	PEAK S22 STRESS (MPA)	PRELOAD FORCE IN COMPONENT (MN)
PIN	40.3	253.4	4.41
BOX	34.1	-540.7	-4.45
		%Difference	-0.99

YIELD ANALYSIS - 0.35 MM

COMPONENT	MATERIAL	YIELD STRENGTH	PEAK VON MISES STRESS
PIN	AISI 4145H	940.0	1,048.00
BOX	AISI 4145H	940.0	
		% of Yield	111.49

PIN PRELOAD STRESS VALUES

NODE	X	S22	TRUE ELEMENT FORCE	AVE. NODAL STRESS	FORCE ON ELEMENT FACE	VON MISES STRESS
158	190.27	192.195	3.58E+02	1.95E+02	6.98E+04	107.571
1828	189.97	197.535	3.94E+02	2.00E+02	7.86E+04	109.226
1829	189.64	201.797	4.32E+02	2.06E+02	8.89E+04	110.125
1830	189.28	209.785	4.75E+02	2.15E+02	1.02E+05	115.291
1831	188.88	220.207	5.20E+02	2.25E+02	1.17E+05	122.7
1832	188.44	230.311	5.71E+02	2.35E+02	1.34E+05	130.767
1833	187.96	239.283	6.26E+02	2.42E+02	1.52E+05	138.085
1834	187.43	245.662	6.88E+02	2.48E+02	1.71E+05	143.694
1835	186.84	250.512	7.54E+02	2.52E+02	1.90E+05	148.342
1836	186	253.422	8.26E+02	2.53E+02	2.09E+05	151.362
1837	185.49	252.747	8.32E+02	2.51E+02	2.08E+05	151.591
1838	184.78	248.377	9.01E+02	2.45E+02	2.20E+05	148.8
1839	184	240.76	9.75E+02	2.36E+02	2.30E+05	143.254
1840	183.16	230.369	1.09E+03	2.24E+02	2.44E+05	135.455
1841	182.21	217.889	1.14E+03	2.11E+02	2.41E+05	126.205
1842	181.21	204.083	1.14E+03	1.97E+02	2.24E+05	115.979
160	180.21	190.085	1.13E+03	1.83E+02	2.07E+05	106.183
1843	179.21	176.369	1.23E+03	1.69E+02	2.09E+05	97.181
1844	178.11	162.454	1.35E+03	1.55E+02	2.10E+05	88.4134
1845	176.90	148.199	1.47E+03	1.41E+02	2.07E+05	79.9299
1846	175.56	133.331	1.61E+03	1.26E+02	2.02E+05	71.6318
1847	174	118.377	1.75E+03	1.11E+02	1.94E+05	63.9256
1848	172.5	103.516	1.91E+03	9.59E+01	1.83E+05	56.9818
1849	170.72	88.2912	2.08E+03	8.04E+01	1.67E+05	50.4686
1850	168.77	72.6026	2.26E+03	6.48E+01	1.46E+05	44.1478
1851	166.63	56.9688	2.45E+03	4.94E+01	1.21E+05	38.3379
1852	164.27	41.7905	2.66E+03	3.32E+01	8.81E+04	33.3782
1853	161.67	24.5615	2.87E+03	1.34E+01	3.84E+04	28.3757
1854	158.82	2.2062	3.77E+03	-1.27E+01	-4.79E+04	23.5952
1855	155	-27.6414	4.79E+03	-4.13E+01	-1.98E+05	23.4704
159	150	-55.0149	7.07E+04	-2.75E+01		35.3647
				Tensile Preload Force in Pin	4.41E+06	

BOX PRELOAD STRESS VALUES

NODE	X	S22	TRUE ELEMENT FORCE	AVE. NODAL STRESS	FORCE ON ELEMENT FACE	VON MISES STRESS
77	226.2	40.955	4.32E+03	3.27E+01	1.41E+05	184.904
761	223.2	24.388	3.96E+03	1.40E+01	5.56E+04	187.752
762	220.3	3.7075	3.64E+03	-5.17E+00	-1.88E+04	189.297
763	217.7	-14.05	3.34E+03	-2.20E+01	-7.35E+04	198.183
764	215.2	-29.94	3.07E+03	-3.66E+01	-1.12E+05	210.927
765	212.9	-43.26	2.83E+03	-4.99E+01	-1.41E+05	224.804
766	210.8	-56.54	2.60E+03	-6.48E+01	-1.69E+05	237.401
767	208.8	-73.08	2.40E+03	-8.29E+01	-1.99E+05	247.069
78	207	-92.78	3.87E+03	-1.07E+02	-4.16E+05	255.093
896	204	-122.2	2.20E+03	-1.38E+02	-3.03E+05	260.332
895	202.3	-153.3	2.18E+03	-1.64E+02	-3.59E+05	260.779
894	200.6	-175.2	1.26E+03	-1.81E+02	-2.28E+05	256.035
82	199.6	-187.4	1.13E+03	-1.95E+02	-2.21E+05	246.557
893	198.7	-203.2	1.03E+03	-2.11E+02	-2.17E+05	233.203
892	197.8	-218.2	9.35E+02	-2.25E+02	-2.10E+05	217.345
891	197.1	-231.5	8.49E+02	-2.42E+02	-2.06E+05	199.789
890	196.4	-252.5	7.71E+02	-2.65E+02	-2.04E+05	182.945
889	195.8	-277.6	7.00E+02	-2.89E+02	-2.02E+05	167.443
888	195.2	-299.9	6.38E+02	-3.07E+02	-1.96E+05	152.328
887	194.7	-314.1	5.79E+02	-3.20E+02	-1.85E+05	137.682
886	194.2	-326.4	5.27E+02	-3.34E+02	-1.76E+05	123.337
885	193.8	-341.1	4.79E+02	-3.51E+02	-1.68E+05	109.995
884	193.4	-360.6	4.36E+02	-3.71E+02	-1.62E+05	97.9572
883	193	-381.3	3.97E+02	-3.95E+02	-1.57E+05	86.6536
882	192.7	-408.9	3.60E+02	-4.35E+02	-1.57E+05	75.681
881	192.4	-461.5	3.29E+02	-5.01E+02	-1.65E+05	65.5973
69	192.1	-540.7	1.16E+05	-2.70E+02		57.0001
				Compressive Preload Force in Box	-4.45E+06	

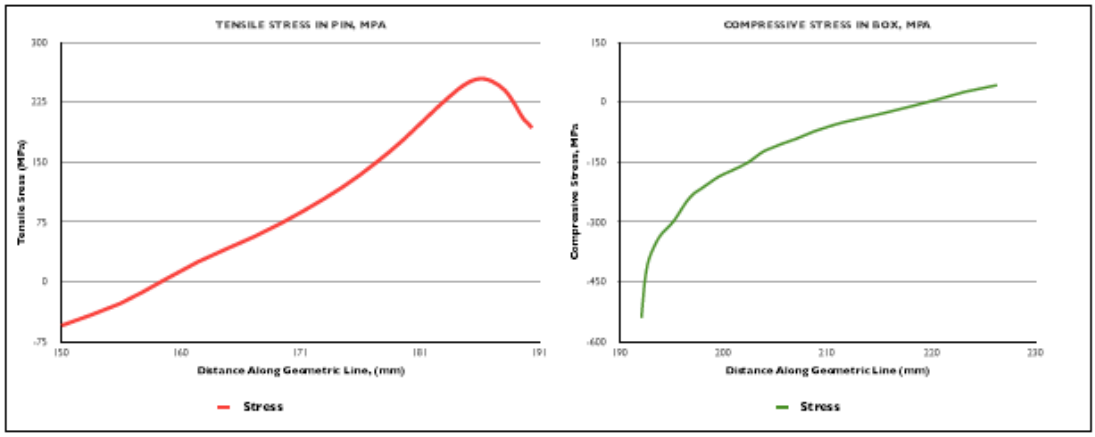

RESULTS SNAPSHOT-0 KN

COMPONENT	LENGTH (MM)	PEAK S22 STRESS (MPA)	PRELOAD FORCE IN COMPONENT (MN)
PIN	40.3	147.3	2.56
BOX	34.1	-317.9	-2.59
		%Difference	-0.99

YIELD ANALYSIS-0 KN

COMPONENT	MATERIAL	YIELD STRENGTH	PEAK VON MISES STRESS
PIN	AISI 4145H	940.0	616.70
BOX	AISI 4145H	940.0	
		% of Yield	65.61

PIN PRELOAD STRESS VALUES

NODE	X	S22	TRUE ELEMENT FORCE	AVE. NODAL STRESS	FORCE ON ELEMENT FACE	VON MISES STRESS
158	190.27	111.753	3.58E+02	1.13E+02	4.06E+04	107.571
1828	189.97	114.863	3.94E+02	1.16E+02	4.57E+04	109.226
1829	189.64	117.349	4.32E+02	1.20E+02	5.17E+04	110.125
1830	189.28	121.998	4.75E+02	1.25E+02	5.94E+04	115.291
1831	188.88	128.063	5.20E+02	1.31E+02	6.82E+04	122.7
1832	188.44	133.943	5.71E+02	1.37E+02	7.80E+04	130.767
1833	187.96	139.16	6.26E+02	1.41E+02	8.83E+04	138.085
1834	187.43	142.865	6.88E+02	1.44E+02	9.92E+04	143.694
1835	186.84	145.674	7.54E+02	1.47E+02	1.10E+05	148.342
1836	186	147.348	8.26E+02	1.47E+02	1.21E+05	151.362
1837	185.49	146.931	8.32E+02	1.46E+02	1.21E+05	151.591
1838	184.78	144.361	9.01E+02	1.42E+02	1.28E+05	148.8
1839	184	139.898	9.75E+02	1.37E+02	1.33E+05	143.254
1840	183.16	133.818	1.09E+03	1.30E+02	1.42E+05	135.455
1841	182.21	126.522	1.14E+03	1.22E+02	1.40E+05	126.205
1842	181.21	118.46	1.14E+03	1.14E+02	1.30E+05	115.978
160	180.21	110.296	1.13E+03	1.06E+02	1.20E+05	106.183
1843	179.21	102.306	1.23E+03	9.83E+01	1.21E+05	97.1805
1844	178.11	94.207	1.35E+03	9.01E+01	1.22E+05	88.4129
1845	176.90	85.919	1.47E+03	8.16E+01	1.20E+05	79.9293
1846	175.56	77.2851	1.61E+03	7.29E+01	1.17E+05	71.6312
1847	174	68.6118	1.75E+03	6.43E+01	1.13E+05	63.9249
1848	172.5	60.0035	1.91E+03	5.56E+01	1.06E+05	56.9811
1849	170.72	51.1949	2.08E+03	4.67E+01	9.70E+04	50.4679
1850	168.77	42.1265	2.26E+03	3.76E+01	8.49E+04	44.1471
1851	166.63	33.0975	2.45E+03	2.87E+01	7.04E+04	38.3372
1852	164.27	24.3379	2.66E+03	1.94E+01	5.14E+04	33.3775
1853	161.67	14.3986	2.87E+03	7.95E+00	2.28E+04	28.3751
1854	158.82	1.5039	3.77E+03	-7.11E+00	-2.68E+04	23.5947
1855	155	-15.7165	4.79E+03	-2.36E+01	-1.13E+05	20.4705
159	150	-31.5169	7.07E+04	-1.58E+01		35.3653
				Tensile Force in Pin	2.56E+06	

BOX PRELOAD STRESS VALUES

NODE	X	S22	TRUE ELEMENT FORCE	AVE. NODAL STRESS	FORCE ON ELEMENT FACE	VON MISES STRESS
77	226.2	23.671	4.32E+03	1.89E+01	8.15E+04	96.5375
761	223.2	14.052	3.96E+03	8.06E+00	3.19E+04	97.238
762	220.3	2.0667	3.64E+03	-3.07E+00	-1.12E+04	101.413
763	217.7	-8.209	3.34E+03	-1.28E+01	-4.28E+04	105.774
764	215.2	-17.42	3.07E+03	-2.13E+01	-6.54E+04	110.062
765	212.9	-25.14	2.83E+03	-2.90E+01	-8.20E+04	114.026
766	210.8	-32.85	2.60E+03	-3.77E+01	-9.80E+04	118.016
767	208.8	-42.48	2.40E+03	-4.82E+01	-1.16E+05	122.533
78	207	-53.91	3.87E+03	-6.24E+01	-2.42E+05	128.214
896	204	-70.93	2.20E+03	-7.99E+01	-1.76E+05	137.147
895	202.3	-88.88	2.18E+03	-9.52E+01	-2.08E+05	147.266
894	200.6	-101.5	1.26E+03	-1.05E+02	-1.32E+05	155.748
82	199.6	-108.4	1.13E+03	-1.13E+02	-1.28E+05	160.681
893	198.7	-117.5	1.03E+03	-1.22E+02	-1.26E+05	166.755
892	197.8	-126.3	9.35E+02	-1.30E+02	-1.22E+05	172.887
891	197.1	-134.1	8.49E+02	-1.40E+02	-1.19E+05	178.793
890	196.4	-146.4	7.71E+02	-1.54E+02	-1.18E+05	188.18
889	195.8	-160.9	7.00E+02	-1.67E+02	-1.17E+05	198.736
888	195.2	-173.4	6.38E+02	-1.78E+02	-1.14E+05	208.524
887	194.7	-182.4	5.79E+02	-1.86E+02	-1.08E+05	215.625
886	194.2	-190.3	5.27E+02	-1.95E+02	-1.03E+05	221.919
885	193.8	-199.2	4.79E+02	-2.05E+02	-9.82E+04	228.011
884	193.4	-210.8	4.36E+02	-2.17E+02	-9.46E+04	236.915
883	193	-223.2	3.97E+02	-2.31E+02	-9.20E+04	246.515
882	192.7	-239.6	3.60E+02	-2.55E+02	-9.20E+04	258.276
881	192.4	-270.8	3.29E+02	-2.94E+02	-9.67E+04	283.575
69	192.1	-317.9	1.16E+05	-1.59E+02		338.307
				Compressive Force in Box	-2.59E+06	

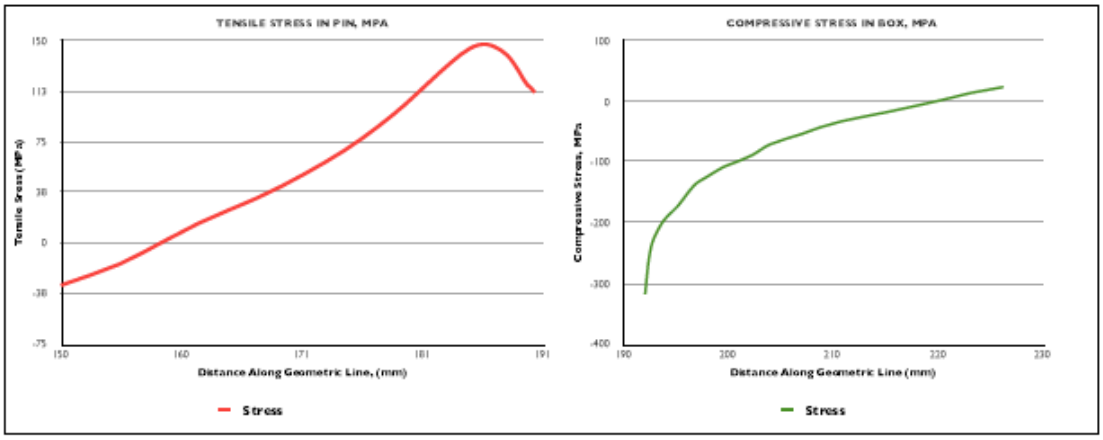

RESULTS SNAPSHOT-20 KN

COMPONENT	LENGTH (MM)	PEAK S22 STRESS (MPA)	PRELOAD FORCE IN COMPONENT (MN)
PIN	40.3	147.4	2.58
BOX	34.1	-311.6	-2.48
		%Difference	-1.04

YIELD ANALYSIS-20 KN

COMPONENT	MATERIAL	YIELD STRENGTH	PEAK VON MISES STRESS
PIN	AISI 4145H	940.0	616.90
BOX	AISI 4145H	940.0	
		% of Yield	65.63

PIN PRELOAD STRESS VALUES

NODE	X	S22	TRUE ELEMENT FORCE	AVE. NODAL STRESS	FORCE ON ELEMENT FACE	VON MISES STRESS
158	190.27	111.801	3.58E+02	1.13E+02	4.06E+04	107.884
1828	189.97	114.898	3.94E+02	1.16E+02	4.57E+04	109.526
1829	189.64	117.374	4.32E+02	1.20E+02	5.17E+04	110.421
1830	189.28	122.012	4.75E+02	1.25E+02	5.94E+04	115.569
1831	188.88	128.061	5.20E+02	1.31E+02	6.82E+04	122.95
1832	188.44	133.93	5.71E+02	1.37E+02	7.80E+04	130.989
1833	187.96	139.142	6.26E+02	1.41E+02	8.83E+04	138.285
1834	187.43	142.849	6.88E+02	1.44E+02	9.92E+04	143.882
1835	186.84	145.669	7.54E+02	1.47E+02	1.10E+05	148.522
1836	186	147.359	8.26E+02	1.47E+02	1.21E+05	151.543
1837	185.49	146.968	8.32E+02	1.46E+02	1.21E+05	151.779
1838	184.78	144.433	9.01E+02	1.42E+02	1.28E+05	149.007
1839	184	140.015	9.75E+02	1.37E+02	1.34E+05	143.5
1840	183.16	133.988	1.09E+03	1.30E+02	1.42E+05	135.755
1841	182.21	126.748	1.14E+03	1.23E+02	1.40E+05	126.564
1842	181.21	118.74	1.14E+03	1.15E+02	1.30E+05	116.401
160	180.21	110.625	1.13E+03	1.07E+02	1.20E+05	106.663
1843	179.21	102.679	1.23E+03	9.87E+01	1.22E+05	97.713
1844	178.11	94.6228	1.35E+03	9.05E+01	1.22E+05	88.9977
1845	176.90	86.3749	1.47E+03	8.21E+01	1.21E+05	80.5643
1846	175.56	77.7787	1.61E+03	7.35E+01	1.18E+05	72.313
1847	174	69.1389	1.75E+03	6.48E+01	1.14E+05	64.6469
1848	172.5	60.5594	1.91E+03	5.62E+01	1.07E+05	57.7341
1849	170.72	51.7754	2.08E+03	4.73E+01	9.82E+04	51.2431
1850	168.77	42.7275	2.26E+03	3.82E+01	8.63E+04	44.9408
1851	166.63	33.7142	2.45E+03	2.93E+01	7.19E+04	39.1436
1852	164.27	24.965	2.66E+03	2.00E+01	5.31E+04	34.1919
1853	161.67	15.0357	2.87E+03	8.60E+00	2.47E+04	29.1844
1854	158.82	2.1562	3.77E+03	-6.44E+00	-2.43E+04	24.311
1855	155	-15.0357	4.79E+03	-2.29E+01	-1.10E+05	23.8261
159	150	-30.7993	7.07E+04	-1.54E+01		35.2508
				Tensile Force in Pin	2.58E+06	

BOX PRELOAD STRESS VALUES

NODE	X	S22	TRUE ELEMENT FORCE	AVE. NODAL STRESS	FORCE ON ELEMENT FACE	VON MISES STRESS
77	226.2	24.24	4.32E+03	1.96E+01	8.45E+04	96.4164
761	223.2	14.913	3.96E+03	9.15E+00	3.62E+04	97.086
762	220.3	3.3779	3.64E+03	-1.55E+00	-5.64E+03	101.166
763	217.7	-6.481	3.34E+03	-1.09E+01	-3.65E+04	105.402
764	215.2	-15.39	3.07E+03	-1.91E+01	-5.88E+04	109.559
765	212.9	-22.89	2.83E+03	-2.67E+01	-7.54E+04	113.421
766	210.8	-30.43	2.60E+03	-3.52E+01	-9.16E+04	117.32
767	208.8	-39.93	2.40E+03	-4.56E+01	-1.09E+05	121.707
78	207	-51.24	3.87E+03	-5.97E+01	-2.31E+05	127.24
896	204	-68.14	2.20E+03	-7.71E+01	-1.70E+05	135.92
895	202.3	-85.98	2.18E+03	-9.22E+01	-2.01E+05	145.808
894	200.6	-98.5	1.26E+03	-1.02E+02	-1.28E+05	154.133
82	199.6	-105.3	1.13E+03	-1.10E+02	-1.25E+05	159.011
893	198.7	-114.4	1.03E+03	-1.19E+02	-1.22E+05	164.974
892	197.8	-123.2	9.35E+02	-1.27E+02	-1.19E+05	171.009
891	197.1	-130.9	8.49E+02	-1.37E+02	-1.16E+05	176.825
890	196.4	-143.1	7.71E+02	-1.50E+02	-1.16E+05	186.046
889	195.8	-157.4	7.00E+02	-1.64E+02	-1.15E+05	196.415
888	195.2	-169.8	6.38E+02	-1.74E+02	-1.11E+05	206.046
887	194.7	-178.6	5.79E+02	-1.83E+02	-1.06E+05	213.037
886	194.2	-186.5	5.27E+02	-1.91E+02	-1.00E+05	219.215
885	193.8	-195.2	4.79E+02	-2.01E+02	-9.63E+04	225.184
884	193.4	-206.6	4.36E+02	-2.13E+02	-9.27E+04	233.895
883	193	-218.8	3.97E+02	-2.27E+02	-9.02E+04	243.282
882	192.7	-234.9	3.60E+02	-2.50E+02	-9.02E+04	254.768
881	192.4	-265.5	3.29E+02	-2.89E+02	-9.48E+04	279.478
69	192.1	-311.6	1.16E+05	-1.56E+02		332.9
				Compressive Force in Box	-2.48E+06	

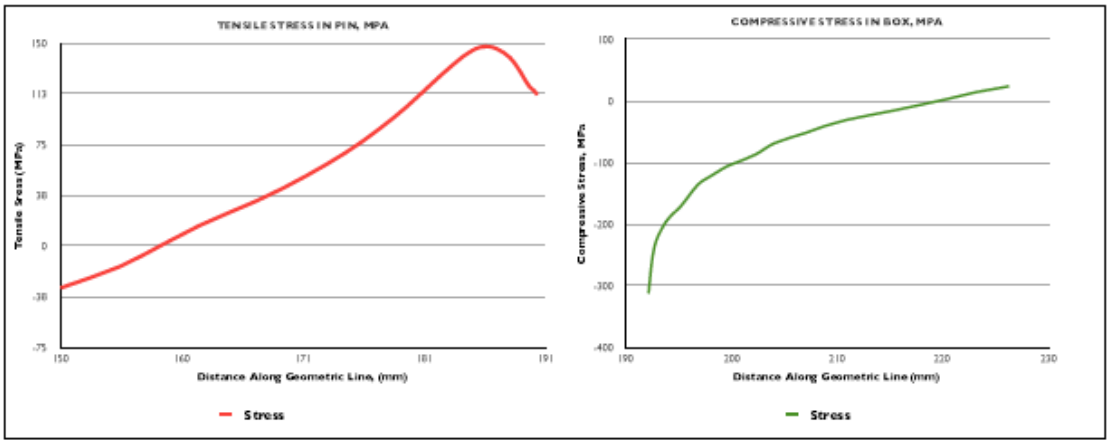

RESULTS SNAPSHOT- 100 KN

COMPONENT	LENGTH (MM)	PEAK S22 STRESS (MPA)	PRELOAD FORCE IN COMPONENT (MN)
PIN	40.3	147.2	2.66
BOX	34.1	-283.8	-2.05
		% Difference	-1.29

YIELD ANALYSIS- 100 KN

COMPONENT	MATERIAL	YIELD STRENGTH	PEAK VON MISES STRESS
PIN	AISI 4145H	940.0	614.70
BOX	AISI 4145H	940.0	
		% of Yield	65.39

PIN PRELOAD STRESS VALUES

NODE	X	S22	TRUE ELEMENT FORCE	AVE. NODAL STRESS	FORCE ON ELEMENT FACE	VON MISES STRESS
158	190.27	111.841	3.58E+02	1.13E+02	4.06E+04	109.022
1828	189.97	114.884	3.94E+02	1.16E+02	4.57E+04	110.614
1829	189.64	117.319	4.32E+02	1.20E+02	5.17E+04	111.496
1830	189.28	121.908	4.75E+02	1.25E+02	5.94E+04	116.565
1831	188.88	127.891	5.20E+02	1.31E+02	6.81E+04	123.826
1832	188.44	133.713	5.71E+02	1.36E+02	7.79E+04	131.745
1833	187.96	138.899	6.26E+02	1.41E+02	8.81E+04	138.948
1834	187.43	142.615	6.88E+02	1.44E+02	9.91E+04	144.492
1835	186.84	145.473	7.54E+02	1.46E+02	1.10E+05	149.103
1836	186	147.232	8.26E+02	1.47E+02	1.21E+05	152.127
1837	185.49	146.944	8.32E+02	1.46E+02	1.21E+05	152.4
1838	184.78	144.553	9.01E+02	1.42E+02	1.28E+05	149.723
1839	184	140.32	9.75E+02	1.37E+02	1.34E+05	144.388
1840	183.16	134.514	1.09E+03	1.31E+02	1.43E+05	136.878
1841	182.21	127.506	1.14E+03	1.24E+02	1.41E+05	127.949
1842	181.21	119.724	1.14E+03	1.16E+02	1.31E+05	118.065
160	180.21	111.817	1.13E+03	1.08E+02	1.22E+05	108.583
1843	179.21	104.062	1.23E+03	1.00E+02	1.24E+05	99.8648
1844	178.11	96.1866	1.35E+03	9.21E+01	1.24E+05	91.3798
1845	176.90	88.1107	1.47E+03	8.39E+01	1.24E+05	83.1674
1846	175.56	79.6766	1.61E+03	7.54E+01	1.21E+05	75.1216
1847	174	71.1815	1.75E+03	6.70E+01	1.17E+05	67.6324
1848	172.5	62.7258	1.91E+03	5.84E+01	1.12E+05	60.8572
1849	170.72	54.0471	2.08E+03	4.96E+01	1.03E+05	54.4674
1850	168.77	45.0852	2.26E+03	4.06E+01	9.17E+04	48.2489
1851	166.63	36.1351	2.45E+03	3.18E+01	7.79E+04	42.5111
1852	164.27	27.4253	2.66E+03	2.25E+01	5.97E+04	37.599
1853	161.67	17.5306	2.87E+03	1.11E+01	3.19E+04	32.5902
1854	158.82	4.7037	3.77E+03	-3.84E+00	-1.45E+04	27.436
1855	155	-12.3828	4.79E+03	-2.02E+01	-9.67E+04	25.7169
159	150	-28.0016	7.07E+04	-1.40E+01		35.2176
				Tensile Force in Pin	2.66E+06	

BOX PRELOAD STRESS VALUES

NODE	X	S22	TRUE ELEMENT FORCE	AVE. NODAL STRESS	FORCE ON ELEMENT FACE	VON MISES STRESS
77	226.2	25.084	4.32E+03	2.11E+01	9.12E+04	96.1613
761	223.2	17.154	3.96E+03	1.24E+01	4.91E+04	96.8856
762	220.3	7.6401	3.64E+03	3.64E+00	1.32E+04	100.708
763	217.7	-0.365	3.34E+03	-4.07E+00	-1.36E+04	104.557
764	215.2	-7.783	3.07E+03	-1.09E+01	-3.36E+04	108.26
765	212.9	-14.11	2.83E+03	-1.74E+01	-4.92E+04	111.719
766	210.8	-20.72	2.60E+03	-2.51E+01	-6.52E+04	115.232
767	208.8	-29.43	2.40E+03	-3.47E+01	-8.33E+04	119.049
78	207	-40.05	3.87E+03	-4.81E+01	-1.86E+05	123.911
898	204	-56.2	2.20E+03	-6.48E+01	-1.43E+05	131.404
895	202.3	-73.46	2.18E+03	-7.95E+01	-1.74E+05	140.166
894	200.6	-85.55	1.26E+03	-8.89E+01	-1.12E+05	147.723
82	199.6	-92.24	1.13E+03	-9.66E+01	-1.10E+05	152.306
893	198.7	-101	1.03E+03	-1.05E+02	-1.08E+05	157.73
892	197.8	-109.5	9.35E+02	-1.13E+02	-1.06E+05	163.286
891	197.1	-116.9	8.49E+02	-1.23E+02	-1.04E+05	168.67
890	196.4	-128.6	7.71E+02	-1.35E+02	-1.04E+05	177.138
889	195.8	-142.2	7.00E+02	-1.48E+02	-1.04E+05	186.668
888	195.2	-154	6.38E+02	-1.58E+02	-1.01E+05	195.573
887	194.7	-162.3	5.79E+02	-1.66E+02	-9.61E+04	202.056
886	194.2	-169.6	5.27E+02	-1.74E+02	-9.14E+04	207.709
885	193.8	-177.7	4.79E+02	-1.83E+02	-8.77E+04	213.135
884	193.4	-188.2	4.36E+02	-1.94E+02	-8.44E+04	220.974
883	193	-199.3	3.97E+02	-2.07E+02	-8.21E+04	229.404
882	192.7	-214	3.60E+02	-2.28E+02	-8.22E+04	239.659
881	192.4	-241.8	3.29E+02	-2.63E+02	-8.63E+04	261.735
69	192.1	-283.8	1.16E+05	-1.42E+02		309.322
				Compressive Force in Box	-2.05E+06	

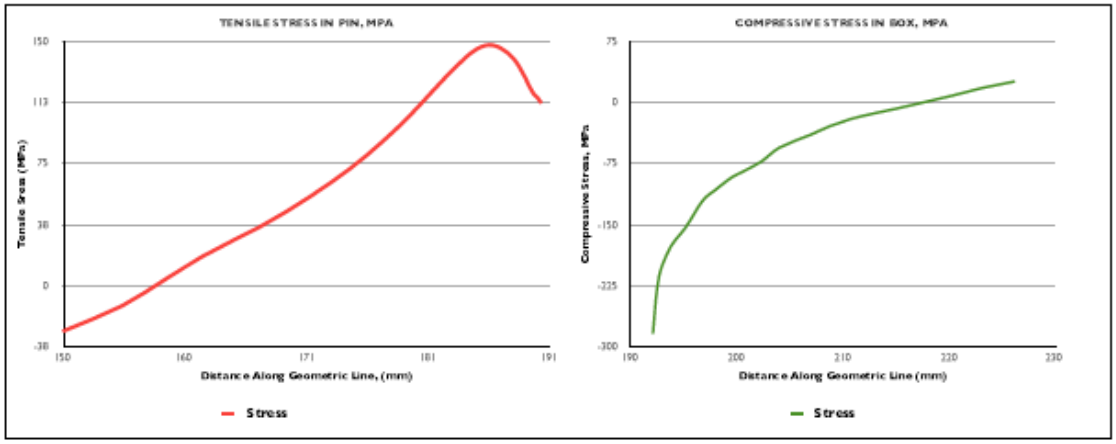

RESULTS SNAPSHOT-500 KN

COMPONENT	LENGTH (MM)	PEAK S22 STRESS (MPA)	PRELOAD FORCE IN COMPONENT (MN)
PIN	40.3	155.3	3.17
BOX	34.1	-51.7	-0.04
		% Difference	-72.37

YIELD ANALYSIS-500 KN

COMPONENT	MATERIAL	YIELD STRENGTH	PEAK VON MISES STRESS
PIN	AISI 4145H	940.0	611.60
BOX	AISI 4145H	940.0	
		% of Yield	65.06

PIN PRELOAD STRESS VALUES

NODE	X	S22	TRUE ELEMENT FORCE	AVE. NODAL STRESS	FORCE ON ELEMENT FACE	VON MISES STRESS
158	190.27	116.567	3.58E+02	1.18E+02	4.23E+04	118.057
1828	189.97	119.573	3.94E+02	1.21E+02	4.75E+04	119.587
1829	189.64	122.043	4.32E+02	1.24E+02	5.37E+04	120.539
1830	189.28	126.713	4.75E+02	1.30E+02	6.17E+04	125.573
1831	188.88	132.816	5.20E+02	1.36E+02	7.07E+04	132.766
1832	188.44	138.875	5.71E+02	1.42E+02	8.09E+04	140.674
1833	187.96	144.406	6.26E+02	1.47E+02	9.17E+04	147.973
1834	187.43	148.62	6.88E+02	1.50E+02	1.03E+05	153.784
1835	186.84	152.134	7.54E+02	1.53E+02	1.16E+05	158.795
1836	186	154.688	8.26E+02	1.55E+02	1.28E+05	162.377
1837	185.49	155.268	8.32E+02	1.55E+02	1.29E+05	163.265
1838	184.78	153.87	9.01E+02	1.52E+02	1.37E+05	161.336
1839	184	150.707	9.75E+02	1.48E+02	1.45E+05	156.993
1840	183.16	146.054	1.09E+03	1.43E+02	1.56E+05	150.659
1841	182.21	140.175	1.14E+03	1.37E+02	1.56E+05	142.926
1842	181.21	133.396	1.14E+03	1.30E+02	1.47E+05	134.188
160	180.21	126.312	1.13E+03	1.23E+02	1.39E+05	125.636
1843	179.21	119.217	1.23E+03	1.16E+02	1.43E+05	117.661
1844	178.11	111.884	1.35E+03	1.08E+02	1.46E+05	109.822
1845	176.90	104.217	1.47E+03	1.00E+02	1.48E+05	102.118
1846	175.56	96.039	1.61E+03	9.18E+01	1.48E+05	94.3997
1847	174	87.6121	1.75E+03	8.33E+01	1.46E+05	87.0218
1848	172.5	79.0189	1.91E+03	7.45E+01	1.42E+05	80.1212
1849	170.72	69.9747	2.08E+03	6.52E+01	1.35E+05	73.3629
1850	168.77	60.3887	2.26E+03	5.55E+01	1.25E+05	66.5793
1851	166.63	50.5766	2.45E+03	4.57E+01	1.12E+05	60.1122
1852	164.27	40.8192	2.66E+03	3.52E+01	9.35E+04	54.433
1853	161.67	29.5995	2.87E+03	2.23E+01	6.42E+04	48.4965
1854	158.82	15.0715	3.77E+03	5.56E+00	2.09E+04	41.7913
1855	155	-3.9576	4.79E+03	-1.24E+01	-5.96E+04	37.0245
159	150	-20.9117	7.07E+04	-1.05E+01		41.5602
				Tensile Force in Pin	3.17E+06	

BOX PRELOAD STRESS VALUES

NODE	X	S22	TRUE ELEMENT FORCE	AVE. NODAL STRESS	FORCE ON ELEMENT FACE	VON MISES STRESS
77	226.2	6.932	4.32E+03	6.64E+00	2.87E+04	106.964
761	223.2	6.3478	3.96E+03	6.14E+00	2.43E+04	108.293
762	220.3	5.9308	3.64E+03	5.84E+00	2.12E+04	110.948
763	217.7	5.7471	3.34E+03	5.81E+00	1.94E+04	113.516
764	215.2	5.8745	3.07E+03	5.85E+00	1.80E+04	116.038
765	212.9	5.828	2.83E+03	5.81E+00	1.64E+04	118.474
766	210.8	5.7898	2.60E+03	5.62E+00	1.46E+04	120.95
767	208.8	5.46	2.40E+03	4.94E+00	1.18E+04	123.424
78	207	4.4227	3.87E+03	3.29E+00	1.28E+04	126.318
896	204	2.1616	2.20E+03	5.96E-01	1.31E+03	129.933
895	202.3	-0.97	2.18E+03	-2.60E+00	-5.67E+03	133.151
894	200.6	-4.224	1.26E+03	-5.25E+00	-6.60E+03	135.831
82	199.6	-6.275	1.13E+03	-7.56E+00	-8.57E+03	137.62
893	198.7	-8.844	1.03E+03	-1.02E+01	-1.05E+04	138.838
892	197.8	-11.63	9.35E+02	-1.26E+01	-1.18E+04	139.925
891	197.1	-13.54	8.49E+02	-1.49E+01	-1.27E+04	141.165
890	196.4	-16.35	7.71E+02	-1.84E+01	-1.42E+04	142.378
889	195.8	-20.36	7.00E+02	-2.26E+01	-1.58E+04	143.124
888	195.2	-24.92	6.38E+02	-2.64E+01	-1.68E+04	144.165
887	194.7	-27.86	5.79E+02	-2.88E+01	-1.67E+04	145.074
886	194.2	-29.83	5.27E+02	-3.07E+01	-1.62E+04	145.4
885	193.8	-31.54	4.79E+02	-3.28E+01	-1.57E+04	145.435
884	193.4	-33.99	4.36E+02	-3.52E+01	-1.53E+04	145.774
883	193	-36.43	3.97E+02	-3.77E+01	-1.50E+04	146.337
882	192.7	-39.01	3.60E+02	-4.17E+01	-1.50E+04	146.799
881	192.4	-44.36	3.29E+02	-4.80E+01	-1.58E+04	148.61
69	192.1	-51.7	1.16E+05	-2.58E+01		151.87
				Compressive Force in Box	-4.38E+04	

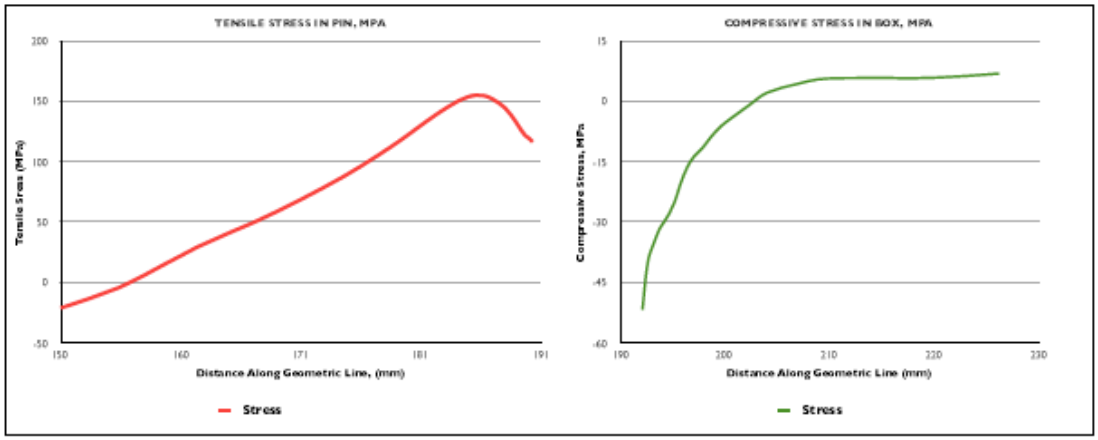

RESULTS SNAPSHOT-750 KN

COMPONENT	LENGTH (MM)	PEAK S22 STRESS (MPA)	PRELOAD FORCE IN COMPONENT (MN)
PIN	40.3	229.8	4.70
BOX	34.1	-68.0	-0.01
		%Difference	-435.72

YIELD ANALYSIS-750 KN

COMPONENT	MATERIAL	YIELD STRENGTH	PEAK VON MISES STRESS
PIN	AISI 4145H	940.0	901.60
BOX	AISI 4145H	940.0	
		% of Yield	95.91

PIN PRELOAD STRESS VALUES

NODE	X	S22	TRUE ELEMENT FORCE	AVE. NODAL STRESS	FORCE ON ELEMENT FACE	VON MISES STRESS
158	190.27	172.492	3.58E+02	1.75E+02	6.26E+04	174.778
1828	189.97	176.922	3.94E+02	1.79E+02	7.03E+04	177.034
1829	189.64	180.56	4.32E+02	1.84E+02	7.95E+04	178.439
1830	189.28	187.454	4.75E+02	1.92E+02	9.12E+04	185.873
1831	188.88	196.466	5.20E+02	2.01E+02	1.05E+05	196.495
1832	188.44	205.414	5.71E+02	2.10E+02	1.20E+05	208.176
1833	187.96	213.592	6.26E+02	2.17E+02	1.36E+05	218.964
1834	187.43	219.831	6.88E+02	2.22E+02	1.53E+05	227.562
1835	186.84	225.043	7.54E+02	2.27E+02	1.71E+05	234.984
1836	186	228.846	8.26E+02	2.29E+02	1.89E+05	240.306
1837	185.49	229.769	8.32E+02	2.29E+02	1.90E+05	241.654
1838	184.78	227.715	9.01E+02	2.25E+02	2.03E+05	238.846
1839	184	223.087	9.75E+02	2.20E+02	2.14E+05	232.48
1840	183.16	216.263	1.09E+03	2.12E+02	2.31E+05	223.177
1841	182.21	207.625	1.14E+03	2.03E+02	2.31E+05	211.806
1842	181.21	197.655	1.14E+03	1.92E+02	2.18E+05	198.945
160	180.21	187.224	1.13E+03	1.82E+02	2.05E+05	186.346
1843	179.21	176.77	1.23E+03	1.71E+02	2.12E+05	174.589
1844	178.11	165.956	1.35E+03	1.60E+02	2.16E+05	163.024
1845	176.90	154.644	1.47E+03	1.49E+02	2.19E+05	151.651
1846	175.56	142.567	1.61E+03	1.36E+02	2.19E+05	140.244
1847	174	130.112	1.75E+03	1.24E+02	2.17E+05	129.33
1848	172.5	117.399	1.91E+03	1.11E+02	2.12E+05	119.108
1849	170.72	104.007	2.08E+03	9.69E+01	2.01E+05	109.084
1850	168.77	89.7999	2.26E+03	8.25E+01	1.86E+05	99.011
1851	166.63	75.2456	2.45E+03	6.80E+01	1.67E+05	89.3976
1852	164.27	60.7621	2.66E+03	5.24E+01	1.39E+05	80.9473
1853	161.67	44.1013	2.87E+03	3.33E+01	9.57E+04	72.1102
1854	158.82	22.528	3.77E+03	8.41E+00	3.17E+04	62.1253
1855	155	-5.7152	4.79E+03	-1.83E+01	-8.76E+04	55.0125
159	150	-30.8595	7.07E+04	-1.54E+01		61.6689
				Tensile Force in Pin	4.70E+06	

BOX PRELOAD STRESS VALUES

NODE	X	S22	TRUE ELEMENT FORCE	AVE. NODAL STRESS	FORCE ON ELEMENT FACE	VON MISES STRESS
77	226.2	9.4642	4.32E+03	9.13E+00	3.94E+04	9.4642
761	223.2	8.7961	3.96E+03	8.60E+00	3.41E+04	8.7961
762	220.3	8.4066	3.64E+03	8.36E+00	3.04E+04	8.4066
763	217.7	8.3176	3.34E+03	8.50E+00	2.84E+04	8.3176
764	215.2	8.6791	3.07E+03	8.71E+00	2.68E+04	8.6791
765	212.9	8.7452	2.83E+03	8.79E+00	2.49E+04	8.7452
766	210.8	8.8396	2.60E+03	8.71E+00	2.27E+04	8.8396
767	208.8	8.5879	2.40E+03	7.99E+00	1.92E+04	8.5879
78	207	7.3923	3.87E+03	6.00E+00	2.33E+04	7.3923
896	204	4.6136	2.20E+03	2.62E+00	5.78E+03	4.6136
895	202.3	0.6358	2.18E+03	-1.57E+00	-3.44E+03	0.6358
894	200.6	-3.784	1.26E+03	-5.18E+00	-6.51E+03	-3.7843
82	199.6	-6.581	1.13E+03	-8.34E+00	-9.45E+03	-6.581
893	198.7	-10.09	1.03E+03	-1.20E+01	-1.24E+04	-10.0904
892	197.8	-13.95	9.35E+02	-1.52E+01	-1.42E+04	-13.9478
891	197.1	-16.5	8.49E+02	-1.84E+01	-1.56E+04	-16.5005
890	196.4	-20.23	7.71E+02	-2.30E+01	-1.77E+04	-20.2283
889	195.8	-25.73	7.00E+02	-2.90E+01	-2.03E+04	-25.7343
888	195.2	-32.22	6.38E+02	-3.43E+01	-2.19E+04	-32.2165
887	194.7	-36.36	5.79E+02	-3.77E+01	-2.18E+04	-36.3562
886	194.2	-39.07	5.27E+02	-4.02E+01	-2.12E+04	-39.0672
885	193.8	-41.35	4.79E+02	-4.30E+01	-2.06E+04	-41.3493
884	193.4	-44.67	4.36E+02	-4.63E+01	-2.02E+04	-44.6699
883	193	-47.96	3.97E+02	-4.96E+01	-1.97E+04	-47.9605
882	192.7	-51.33	3.60E+02	-5.49E+01	-1.98E+04	-51.3289
881	192.4	-58.43	3.29E+02	-6.32E+01	-2.08E+04	-58.4272
69	192.1	-68	1.16E+05	-3.40E+01		-67.9991
				Compressive Force in Box	-1.08E+04	

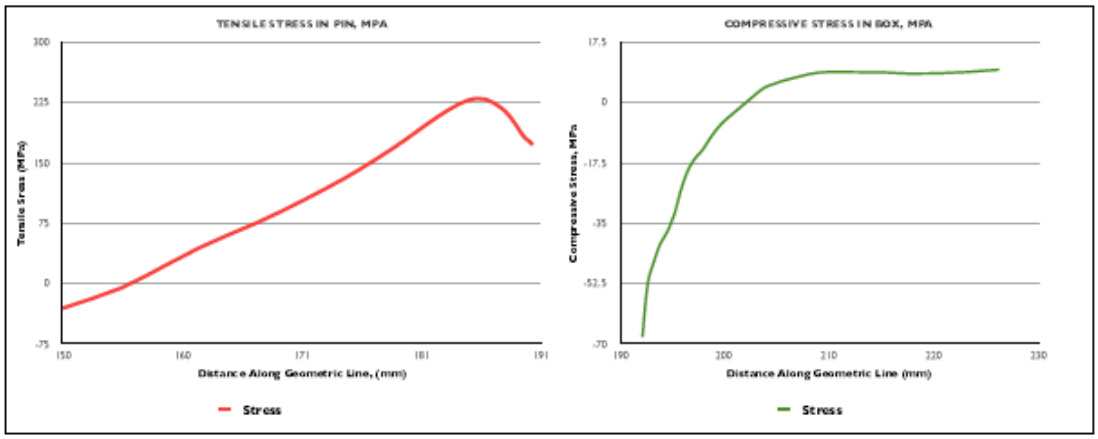

RESULTS SNAPSHOT- 1 MN

COMPONENT	LENGTH (MM)	PEAK S22 STRESS (MPA)	PRELOAD FORCE IN COMPONENT (MN)
PIN	40.3	306.4	6.27
BOX	34.1	-90.6	-0.01
		% Difference	-452.74

YIELD ANALYSIS- 1 MN

COMPONENT	MATERIAL	YIELD STRENGTH	PEAK VON MISES STRESS
PIN	AISI 4145H	940.0	1,199.00
BOX	AISI 4145H	940.0	
		% of Yield	127.55

PIN PRELOAD STRESS VALUES

NODE	X	S22	TRUE ELEMENT FORCE	AVE. NODAL STRESS	FORCE ON ELEMENT FACE	VON MISES STRESS
158	190.27	230.179	3.58E+02	2.33E+02	8.35E+04	233.244
1828	189.97	236.066	3.94E+02	2.38E+02	9.39E+04	236.245
1829	189.64	240.897	4.32E+02	2.45E+02	1.06E+05	238.11
1830	189.28	250.072	4.75E+02	2.56E+02	1.22E+05	246.012
1831	188.88	262.071	5.20E+02	2.68E+02	1.39E+05	262.161
1832	188.44	273.98	5.71E+02	2.79E+02	1.60E+05	277.723
1833	187.96	284.868	6.26E+02	2.89E+02	1.81E+05	292.1
1834	187.43	293.174	6.88E+02	2.97E+02	2.04E+05	303.559
1835	186.84	300.113	7.54E+02	3.03E+02	2.28E+05	313.456
1836	186	305.178	8.26E+02	3.06E+02	2.52E+05	320.557
1837	185.49	306.409	8.32E+02	3.05E+02	2.54E+05	322.368
1838	184.78	303.675	9.01E+02	3.01E+02	2.71E+05	318.64
1839	184	297.513	9.75E+02	2.93E+02	2.86E+05	310.171
1840	183.16	288.426	1.09E+03	2.83E+02	3.08E+05	297.788
1841	182.21	276.923	1.14E+03	2.70E+02	3.09E+05	282.648
1842	181.21	263.644	1.14E+03	2.57E+02	2.91E+05	265.517
160	180.21	249.749	1.13E+03	2.43E+02	2.74E+05	248.731
1843	179.21	235.819	1.23E+03	2.29E+02	2.82E+05	233.062
1844	178.11	221.408	1.35E+03	2.14E+02	2.89E+05	217.644
1845	176.90	206.329	1.47E+03	1.98E+02	2.92E+05	202.478
1846	175.56	190.226	1.61E+03	1.82E+02	2.93E+05	187.262
1847	174	173.614	1.75E+03	1.65E+02	2.89E+05	172.696
1848	172.5	156.651	1.91E+03	1.48E+02	2.82E+05	159.05
1849	170.72	138.775	2.08E+03	1.29E+02	2.69E+05	145.661
1850	168.77	119.805	2.26E+03	1.10E+02	2.49E+05	132.203
1851	166.63	100.366	2.45E+03	9.07E+01	2.22E+05	119.357
1852	164.27	81.0153	2.66E+03	6.99E+01	1.86E+05	108.065
1853	161.67	58.7521	2.87E+03	4.43E+01	1.27E+05	96.2583
1854	158.82	29.9235	3.77E+03	1.11E+01	4.16E+04	82.9359
1855	155	-7.814	4.79E+03	-2.46E+01	-1.18E+05	73.4901
159	150	-41.405	7.07E+04	-2.07E+01		82.4573
				Tensile Force in Pin	6.27E+06	

BOX PRELOAD STRESS VALUES

NODE	X	S22	TRUE ELEMENT FORCE	AVE. NODAL STRESS	FORCE ON ELEMENT FACE	VON MISES STRESS
77	226.2	12.689	4.32E+03	1.22E+01	5.28E+04	212.803
761	223.2	11.783	3.96E+03	1.15E+01	4.56E+04	215.413
762	220.3	11.247	3.64E+03	1.12E+01	4.07E+04	220.605
763	217.7	11.118	3.34E+03	1.14E+01	3.79E+04	225.627
764	215.2	11.593	3.07E+03	1.16E+01	3.57E+04	230.564
765	212.9	11.679	2.83E+03	1.17E+01	3.32E+04	235.34
766	210.8	11.806	2.60E+03	1.16E+01	3.03E+04	240.211
767	208.8	11.472	2.40E+03	1.07E+01	2.56E+04	245.085
78	207	9.8779	3.87E+03	8.02E+00	3.11E+04	250.805
896	204	6.1712	2.20E+03	3.52E+00	7.74E+03	257.991
895	202.3	0.8604	2.18E+03	-2.09E+00	-4.57E+03	264.393
894	200.6	-5.045	1.26E+03	-6.91E+00	-8.69E+03	269.644
82	199.6	-8.779	1.13E+03	-1.11E+01	-1.26E+04	273.141
893	198.7	-13.47	1.03E+03	-1.60E+01	-1.65E+04	275.491
892	197.8	-18.63	9.35E+02	-2.03E+01	-1.90E+04	277.525
891	197.1	-22.04	8.49E+02	-2.45E+01	-2.08E+04	279.854
890	196.4	-27.01	7.71E+02	-3.07E+01	-2.37E+04	282.078
889	195.8	-34.38	7.00E+02	-3.87E+01	-2.71E+04	283.269
888	195.2	-43.05	6.38E+02	-4.58E+01	-2.92E+04	284.96
887	194.7	-48.58	5.79E+02	-5.04E+01	-2.92E+04	286.493
886	194.2	-52.19	5.27E+02	-5.37E+01	-2.83E+04	286.902
885	193.8	-55.23	4.79E+02	-5.74E+01	-2.75E+04	286.74
884	193.4	-59.64	4.36E+02	-6.18E+01	-2.69E+04	287.115
883	193	-64.01	3.97E+02	-6.62E+01	-2.63E+04	287.926
882	192.7	-68.47	3.60E+02	-7.32E+01	-2.64E+04	288.497
881	192.4	-77.9	3.29E+02	-8.43E+01	-2.77E+04	291.391
69	192.1	-90.63	1.16E+05	-4.53E+01		296.55
				Compressive Force in Box	-1.38E+04	

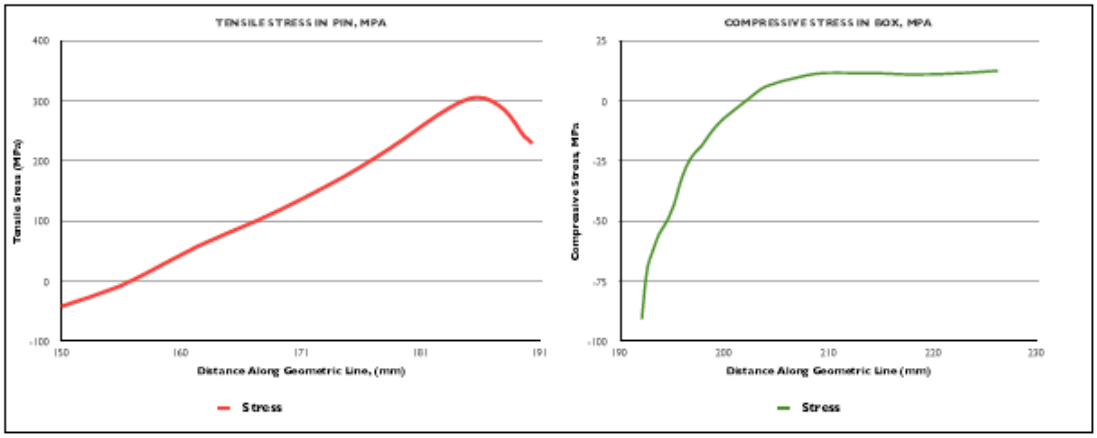

8.4.2 Aluminium Alloy – AL-ZN-MG-II Simulation Results

8.4.2.1 Simulation Results Summary

PRELOAD FORCE DUE TO OVERLAP

OVERLAP AMOUNT (MM)	+VE FORCE IN PIN (MN)	-VE FORCE IN BOX (MN)	% DIFF.
0.05	0.2	-0.2	-0.99
0.10	0.5	-0.5	-0.99
0.15	0.7	-0.7	-0.99
0.20	0.9	-0.9	-0.99
0.25	1.1	-1.1	-0.99
0.30	1.3	-1.3	-0.99
0.35	1.5	-1.5	-0.99

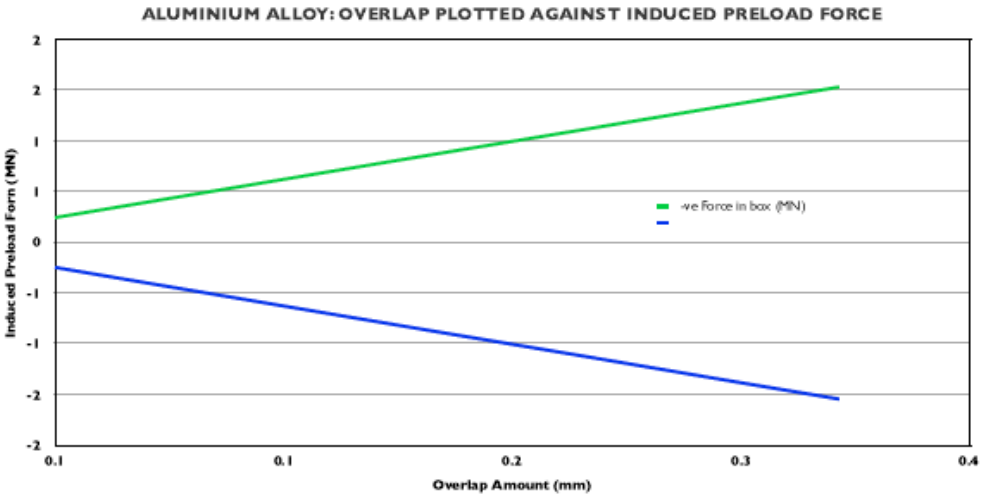

FORCE DUE TO AXIAL LOAD

AXIAL FORCE IN CONNECTOR		+VE FORCE IN PIN (MN)	-VE FORCE IN BOX (MN)	% DIFF.
0	0	1.31536	-1.32698	-0.99
20	20	1.31741	-1.31658	-1.00
100	100	1.41910	-0.80195	-1.77
150	150	1.47461	-0.54313	-2.72
300	300	1.88041	-0.00745	-252.51
400	400	2.50744	-0.00964	-260.07
500	500	3.13436	-0.01169	-268.19

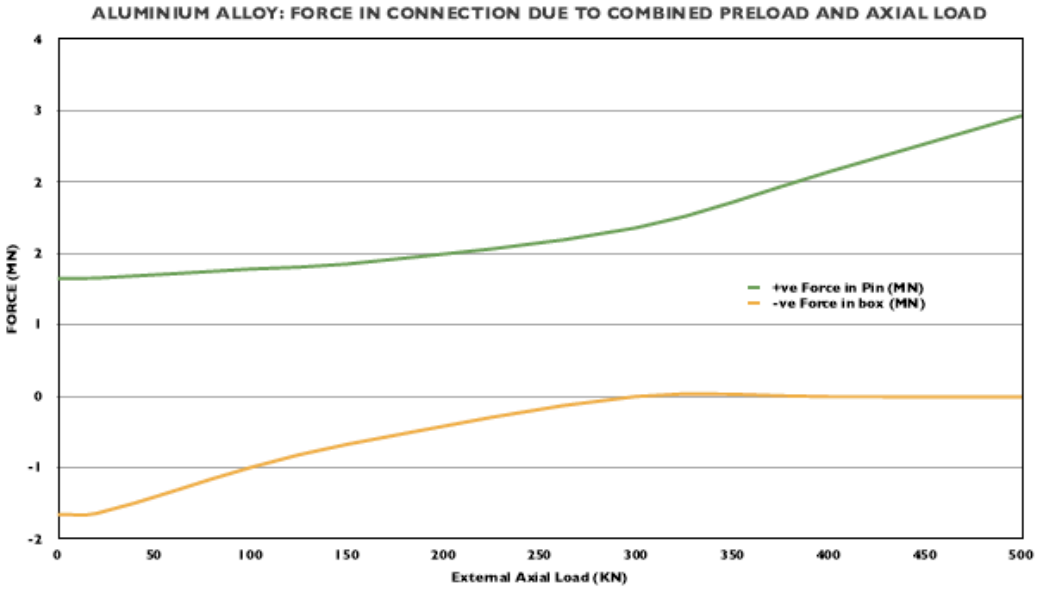

PRELOAD AND AXIAL LOAD YIELD ANALYSIS

OVERLAP AMOUNT (MM)	MATERIAL		YIELD STRENGTH	PEAK VON MISES STRESS	% OF YIELD STRENGTH	VON MISES STRESS @ 0.3MM	AXIAL LOAD (KN)	PEAK VON MISES STRESS (MPA)	% OF YIELD STRENGTH
0.05	Al Zn Mg II	0.05	480.1	58.40	12.16	309.10	0.00	309.90	0.00
0.10	Al Zn Mg II	0.10	480.1	109.80	22.87	309.10	2.00	309.80	0.42
0.15	Al Zn Mg II	0.15	480.1	160.60	33.45	309.10	100.00	309.30	20.83
0.20	Al Zn Mg II	0.20	480.1	210.80	43.91	309.10	250.00	309.20	52.07
0.25	Al Zn Mg II	0.25	480.1	259.10	53.97	309.10	300.00	355.00	62.49
0.30	Al Zn Mg II	0.30	480.1	309.10	64.38	309.10	400.00	473.40	83.32
0.35	Al Zn Mg II	0.35	480.1	358.90	74.76	309.10	500.00	588.10	104.14
0.40	Al Zn Mg II	0.40	480.1	412.10	85.84	309.10			

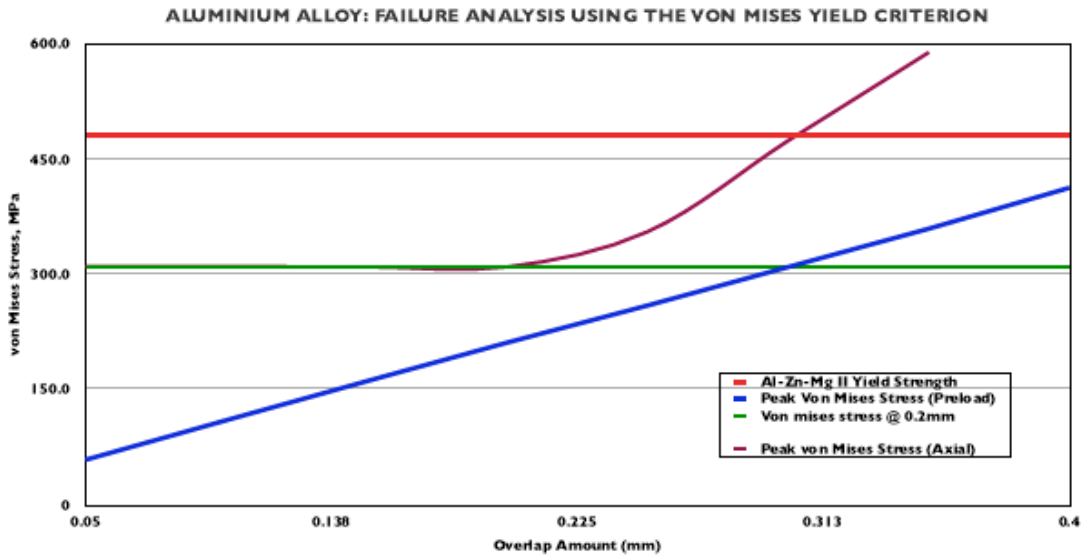

8.4.2.2 Induced Stress in Pin and Box Due to Preload and Axial Load

		Preload Induced Stress (MPa)								Axial Load Induced Stress						
		0.05mm	0.1mm	0.15mm	0.2mm	0.25mm	0.3mm	0.35mm	0.4mm	0N	2KN	100KN	150KN	300KN	400KN	500KN
BOX	226.23	2.34	4.3645	6.4009	8.4486	10.471	12.535	14.61	18.74	14.02	13.991	12.234	10.292	3.6907	4.9912	6.21
BOX	223.17	1.44	2.6702	3.9135	5.1703	6.411	7.6792	8.96	12.21	9.15	9.1523	9.2054	8.1535	3.4472	4.6646	5.80
BOX	220.33	0.30	0.5311	0.771	1.0268	1.2718	1.5311	1.81	4.02	3.06	3.1158	5.6743	5.7634	3.3289	4.4987	5.59
BOX	217.68	-0.67	-1.3015	-1.922	-2.525	-3.1389	-3.746	-4.33	-3.00	-2.29	-2.186	2.7071	3.837	3.3166	4.4688	5.55
BOX	215.23	-1.55	-2.9566	-4.3515	-5.727	-7.1131	-8.498	-9.85	-9.56	-7.13	-6.984	8.07E-0	2.2383	3.4598	4.6461	5.78
BOX	212.94	-2.30	-4.359	-6.4089	-8.437	-10.478	-12.52	-14.53	-15.25	-11.31	-11.12	-2.191	0.8816	3.5354	4.7332	5.89
BOX	210.82	-3.06	-5.7897	-8.5062	-11.2	-13.905	-16.61	-19.29	-21.13	-15.86	-15.64	-4.904	-0.797	3.5704	4.7657	5.94
BOX	208.84	-4.01	-7.5671	-11.1091	-14.62	-18.148	-21.68	-25.17	-28.54	-21.49	-21.23	-8.678	-3.345	3.4439	4.5841	5.73
BOX	207.01	-5.12	-9.6504	-14.1644	-18.65	-23.141	-27.65	-32.12	-36.99	-28.00	-27.71	-13.6	-7.058	2.9878	3.9634	4.96
BOX	204.01	-6.77	-12.737	-18.6973	-24.63	-30.561	-36.53	-42.46	-50.02	-37.85	-37.53	-21.6	-13.39	1.7664	2.3211	2.92
BOX	202.29	-8.50	-15.982	-23.4672	-30.93	-38.377	-45.91	-53.39	-60.94	-46.18	-45.83	-28.81	-19.5	0.4027	0.4938	0.65
BOX	200.56	-9.72	-18.279	-26.8417	-35.38	-43.892	-52.55	-61.13	-68.97	-52.46	-52.11	-34.48	-24.42	-1.02	-1.406	-1.71
BOX	199.56	-10.38	-19.531	-28.6868	-37.82	-46.918	-56.24	-65.44	-76.65	-58.08	-57.71	-39.39	-28.62	-2.422	-3.274	-4.04
BOX	198.65	-11.28	-21.214	-31.1573	-41.08	-50.94	-61.1	-71.09	-83.69	-64.09	-63.71	-44.73	-33.31	-4.217	-5.666	-7.03
BOX	197.83	-12.16	-22.86	-33.5719	-44.25	-54.859	-65.77	-76.51	-90.69	-68.76	-68.37	-48.9	-37.01	-5.806	-7.781	-9.67
BOX	197.07	-12.92	-24.288	-35.6683	-47.01	-58.273	-69.82	-81.21	-97.74	-72.97	-72.57	-52.62	-40.28	-7.124	-9.535	-11.86
BOX	196.39	-14.10	-26.502	-38.91	-51.28	-63.539	-76.1	-88.50	-104.65	-78.01	-77.6	-56.99	-44.09	-8.728	-11.67	-14.53
BOX	195.76	-15.51	-29.15	-42.7779	-56.36	-69.784	-83.73	-97.33	-111.75	-83.63	-83.2	-61.78	-48.21	-10.53	-14.07	-17.53
BOX	195.19	-16.75	-31.46	-46.1561	-60.78	-75.225	-90.48	-105.20	-118.85	-90.22	-89.77	-67.32	-52.95	-12.6	-16.83	-20.97
BOX	194.67	-17.65	-33.144	-48.6004	-63.99	-79.164	-94.89	-110.32	-126.65	-95.77	-95.31	-71.94	-56.88	-14.48	-19.33	-24.09
BOX	194.2	-18.44	-34.622	-50.7496	-66.8	-82.616	-98.65	-114.66	-133.84	-100.72	-100.2	-75.96	-60.26	-16.03	-21.39	-26.66
BOX	193.76	-19.33	-36.277	-53.1547	-69.94	-86.462	-103.2	-119.85	-141.05	-105.64	-105.1	-79.84	-63.42	-17.09	-22.81	-28.43
BOX	193.37	-20.49	-38.438	-56.2968	-74.04	-91.48	-109.1	-126.72	-148.83	-111.71	-111.2	-84.53	-67.19	-18.4	-24.56	-30.59
BOX	193.01	-21.73	-40.736	-59.6308	-78.38	-96.808	-115.5	-133.98	-157.95	-118.84	-118.3	-89.97	-71.55	-19.96	-26.65	-33.18
BOX	192.68	-23.38	-43.816	-64.0936	-84.16	-103.96	-123.9	-143.69	-170.11	-128.19	-127.6	-97.02	-77.13	-21.77	-29.08	-36.18
BOX	192.38	-26.56	-49.741	-72.7068	-95.3	-117.65	-140.2	-162.46	-192.59	-146.36	-145.7	-110.7	-87.98	-25.23	-33.7	-41.92
BOX	192.11	-31.28	-58.441	-85.2726	-111.7	-137.56	-164.2	-190.00	-226.74	-172.64	-171.8	57.836	-103.6	-29.71	-39.69	-49.34
PIN	190.27	10.65	20.0616	29.4475	38.779	48.0937	57.438	66.74	75.88	57.35	57.36	59.382	58.188	69.085	92.53	6.21
PIN	189.97	10.95	20.6218	30.2688	39.859	49.4344	59.038	68.60	77.98	58.94	58.952	60.627	59.719	70.859	94.897	115.29
PIN	189.64	11.19	21.072	30.9286	40.727	50.5108	60.322	70.09	79.67	60.22	60.229	62.978	60.957	72.32	96.842	118.23
PIN	189.28	11.63	21.9087	32.1559	42.341	52.5151	62.714	72.87	82.81	62.60	62.612	66.084	63.302	75.08	100.53	120.65
PIN	188.88	12.22	23.0148	33.7786	44.477	55.1654	65.878	76.54	86.98	65.76	65.763	69.104	66.401	78.735	105.42	125.24
PIN	188.44	12.79	24.083	35.3454	46.538	57.7243	68.932	80.09	90.99	68.80	68.805	71.805	69.426	82.348	110.24	131.31
PIN	187.96	13.29	25.0294	36.7339	48.365	59.9936	71.642	83.23	94.56	71.50	71.502	73.766	72.146	85.649	114.65	137.31
PIN	187.43	13.65	25.7019	37.7208	49.664	61.6085	73.57	85.47	97.09	73.41	73.421	75.298	74.146	88.168	118.02	142.80
PIN	186.84	13.92	26.2106	38.4677	50.647	62.8334	75.034	87.17	99.01	74.87	74.875	76.276	75.734	90.268	120.83	147.00
PIN	186	14.08	26.5124	38.9114	51.231	63.5655	75.909	88.19	100.15	75.73	75.742	76.216	76.787	91.796	122.87	150.49
PIN	185.49	14.04	26.4361	38.8004	51.086	63.3937	75.706	87.96	99.87	75.52	75.534	75.1	76.817	92.169	123.37	153.05
PIN	184.78	13.79	25.975	38.1252	50.198	62.3018	74.405	86.45	98.15	74.21	74.231	73.046	75.808	91.359	122.29	153.68
PIN	184	13.36	25.1696	36.9448	48.645	60.3863	72.121	83.79	95.13	71.93	71.949	70.194	73.879	89.505	119.81	152.35
PIN	183.16	12.78	24.0705	35.3337	46.525	57.7688	69	80.17	91.01	68.81	68.833	66.732	71.167	86.764	116.14	149.29
PIN	182.21	12.08	22.755	33.405	43.988	54.6325	65.259	75.83	86.07	65.07	65.098	62.867	67.847	83.3	111.51	144.75
PIN	181.21	11.31	21.3038	31.277	41.188	51.1685	61.127	71.03	80.61	60.94	60.974	58.902	64.113	79.309	106.17	139.01
PIN	180.21	10.52	19.829	29.114	38.342	47.6436	56.921	66.15	75.06	56.73	56.778	54.994	60.263	75.117	100.55	132.39
PIN	179.21	9.76	18.3853	26.9962	35.555	44.1887	52.798	61.36	69.62	52.62	52.665	51.015	56.454	70.911	94.916	125.43
PIN	178.11	8.98	16.9232	24.8511	32.732	40.686	48.619	56.50	64.11	48.45	48.497	46.919	52.563	66.562	89.084	118.44
PIN	176.90	8.19	15.4277	22.6565	29.843	37.0986	44.337	51.53	58.46	44.17	44.228	42.626	48.542	62.011	82.976	111.20
PIN	175.56	7.36	13.8723	20.3735	26.838	33.3624	39.878	46.35	52.58	39.73	39.785	38.282	44.311	57.158	76.457	103.62
PIN	174	6.53	12.3105	18.0805	23.819	29.6051	35.393	41.14	46.67	35.26	35.317	33.93	40.009	52.151	69.727	95.52
PIN	172.5	5.71	10.7595	15.8029	20.819	25.8682	30.932	35.95	40.79	30.82	30.877	29.437	35.678	47.034	62.842	87.15
PIN	170.72	4.87	9.1719	13.4709	17.748	22.0377	26.358	30.64	34.77	26.27	26.328	24.771	31.182	41.637	55.575	78.60
PIN	168.77	4.00	7.5373	11.069	14.583	18.0887	21.643	25.16	28.56	21.58	21.642	20.103	26.487	35.907	47.854	69.56
PIN	166.63	3.14	5.9155	8.6855	11.442	14.1663	16.959	19.71	22.40	16.93	16.992	15.541	21.764	30.051	39.962	59.95
PIN	164.27	2.31	4.343	6.374	8.3953	10.3598	12.413	14.42	16.43	12.42	12.482	10.329	17.125	24.223	32.102	50.13
PIN	161.67	1.36	2.5532	3.7426	4.9264	6.0246	7.2355	8.40	9.63	7.29	7.349	3.5858	11.812	17.495	23.028	40.34
PIN	158.82	0.13	0.2348	0.334	0.4327	0.4083	0.5275	0.60	0.83	0.64	0.7004	-5.373	4.9402	8.7951	11.291	29.04
PIN	155	-1.51	-2.8644	-4.2221	-5.573	-7.097	-8.436	-9.82	-10.95	-8.25	-8.189	-13.34	-4.154	-2.601	-4.086	14.43
PIN	150	-2.99	-5.6467	-8.31	-10.96	-13.831	-16.48	-19.17	-21.52	-16.23	-16.17	57.836	-12.2	-12.53	-17.48	-4.71

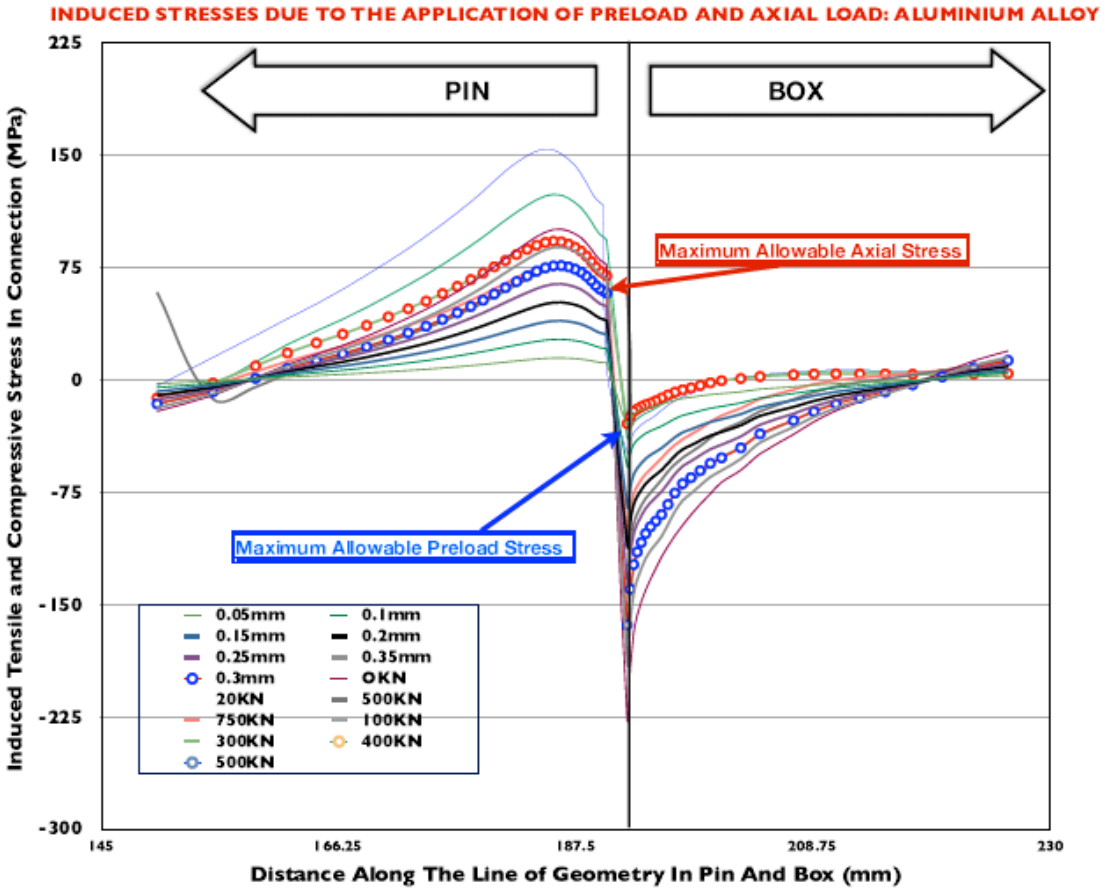
INDUCED STRESSES DUE TO THE APPLICATION OF PRELOAD AND AXIAL LOAD: ALUMINIUM ALLOY
PIN
BOX
Maximum Allowable Axial Stress
Maximum Allowable Preload Stress
0.05mm
0.1mm
0.15mm
0.2mm
0.25mm
0.35mm
0.3mm
0KN
20KN
500KN
750KN
100KN
300KN
400KN
500KN
225
150
75
0
-75
-150
-225
-300
145
166.25
187.5
208.75
230
Induced Tensile and Compressive Stress In Connection (MPa)
Distance Along The Line of Geometry In Pin And Box (mm)

8.4.2.3 Simulation Data Pages

RESULTS SNAPSHOT-0.05MM

COMPONENT	LENGTH (MM)	PEAK S22 STRESS (MPA)	PRELOAD FORCE IN COMPONENT (MN)
PIN	40.3	14.1	0.24
BOX	34.1	2.3	-0.25
		%Difference	-0.99

YIELD ANALYSIS-0.05MM

COMPONENT	MATERIAL	YIELD STRENGTH	PEAK VON MISES STRESS
PIN	AL-MG-ZN-II	480.0	58.40
BOX	AL-MG-ZN-II	480.0	
		% of Yield	12.17

PIN PRELOAD STRESS VALUES

NODE	X	S22	TRUE ELEMENT FORCE	AVE. NODAL STRESS	FORCE ON ELEMENT FACE	VON MISES STRESS
158	190.27	10.65	3.58E+02	1.06E+01	3.87E+03	31.7051
1828	189.97	10.95	3.94E+02	1.11E+01	4.36E+03	32.1932
1829	189.64	11.19	4.32E+02	1.14E+01	4.93E+03	32.4589
1830	189.28	11.63	4.75E+02	1.19E+01	5.67E+03	33.9827
1831	188.88	12.22	5.20E+02	1.25E+01	6.51E+03	36.1678
1832	188.44	12.79	5.71E+02	1.30E+01	7.45E+03	38.5466
1833	187.96	13.29	6.26E+02	1.35E+01	8.43E+03	40.7039
1834	187.43	13.65	6.88E+02	1.38E+01	9.48E+03	42.3567
1835	186.84	13.92	7.54E+02	1.40E+01	1.05E+04	43.7251
1836	186	14.08	8.26E+02	1.41E+01	1.16E+04	44.6124
1837	185.49	14.04	8.32E+02	1.39E+01	1.16E+04	44.6757
1838	184.78	13.79	9.01E+02	1.36E+01	1.22E+04	43.8479
1839	184	13.36	9.75E+02	1.31E+01	1.27E+04	42.208
1840	183.16	12.78	1.09E+03	1.24E+01	1.36E+04	39.9036
1841	182.21	12.08	1.14E+03	1.17E+01	1.33E+04	37.1719
1842	181.21	11.31	1.14E+03	1.09E+01	1.24E+04	34.1533
160	180.21	10.52	1.13E+03	1.01E+01	1.14E+04	31.2634
1843	179.21	9.76	1.23E+03	9.37E+00	1.16E+04	28.6092
1844	178.11	8.98	1.35E+03	8.58E+00	1.16E+04	26.0254
1845	176.90	8.19	1.47E+03	7.77E+00	1.15E+04	23.5266
1846	175.56	7.36	1.61E+03	6.95E+00	1.12E+04	21.084
1847	174	6.53	1.75E+03	6.12E+00	1.07E+04	18.8172
1848	172.5	5.71	1.91E+03	5.29E+00	1.01E+04	16.7762
1849	170.72	4.87	2.08E+03	4.43E+00	9.21E+03	14.8631
1850	168.77	4.00	2.26E+03	3.57E+00	8.06E+03	13.0075
1851	166.63	3.14	2.45E+03	2.72E+00	6.68E+03	11.3024
1852	164.27	2.31	2.66E+03	1.83E+00	4.87E+03	9.8467
1853	161.67	1.36	2.87E+03	7.44E-01	2.14E+03	8.3774
1854	158.82	0.13	3.77E+03	-6.91E-01	-2.60E+03	6.9682
1855	155	-1.51	4.79E+03	-2.25E+00	-1.08E+04	6.9123
159	150	-2.99	7.07E+04	-1.49E+00		10.3903
			Tensile Preload Force in Pin		2.44E+05	

BOX PRELOAD STRESS VALUES

NODE	X	S22	TRUE ELEMENT FORCE	AVE. NODAL STRESS	FORCE ON ELEMENT FACE	VON MISES STRESS
77	226.23	2.34	4.32E+03	1.89E+00	8.16E+03	28.4058
761	223.17	1.44	3.96E+03	8.71E-01	3.45E+03	26.6115
762	220.33	0.30	3.64E+03	-1.83E-01	-6.66E+02	29.84
763	217.68	-0.67	3.34E+03	-1.11E+00	-3.71E+03	31.1222
764	215.23	-1.55	3.07E+03	-1.92E+00	-5.91E+03	32.3829
765	212.94	-2.30	2.83E+03	-2.68E+00	-7.57E+03	33.5504
766	210.82	-3.06	2.60E+03	-3.54E+00	-9.20E+03	34.7262
767	208.84	-4.01	2.40E+03	-4.57E+00	-1.09E+04	36.057
78	207.01	-5.12	3.87E+03	-5.94E+00	-2.30E+04	37.7295
896	204.01	-6.77	2.20E+03	-7.63E+00	-1.68E+04	40.3574
895	202.29	-8.50	2.18E+03	-9.11E+00	-1.99E+04	43.3289
894	200.56	-9.72	1.26E+03	-1.01E+01	-1.26E+04	45.8252
82	199.56	-10.38	1.13E+03	-1.08E+01	-1.23E+04	47.2732
893	198.65	-11.28	1.03E+03	-1.17E+01	-1.21E+04	49.0608
892	197.83	-12.16	9.35E+02	-1.25E+01	-1.17E+04	50.872
891	197.07	-12.92	8.49E+02	-1.35E+01	-1.15E+04	52.6164
890	196.39	-14.10	7.71E+02	-1.48E+01	-1.14E+04	55.3869
889	195.76	-15.51	7.00E+02	-1.61E+01	-1.13E+04	58.5166
888	195.19	-16.75	6.38E+02	-1.72E+01	-1.10E+04	61.4211
887	194.67	-17.65	5.79E+02	-1.80E+01	-1.04E+04	63.5616
886	194.2	-18.44	5.27E+02	-1.89E+01	-9.94E+03	65.4486
885	193.76	-19.33	4.79E+02	-1.99E+01	-9.54E+03	67.2722
884	193.37	-20.49	4.36E+02	-2.11E+01	-9.20E+03	69.9446
883	193.01	-21.73	3.97E+02	-2.26E+01	-8.96E+03	72.8336
882	192.68	-23.38	3.60E+02	-2.50E+01	-9.00E+03	76.3982
881	192.38	-26.56	3.29E+02	-2.89E+01	-9.50E+03	84.0778
69	192.11	-31.28	1.16E+05	-1.56E+01		100.685
			Compressive Preload Force in Box		-2.47E+05	

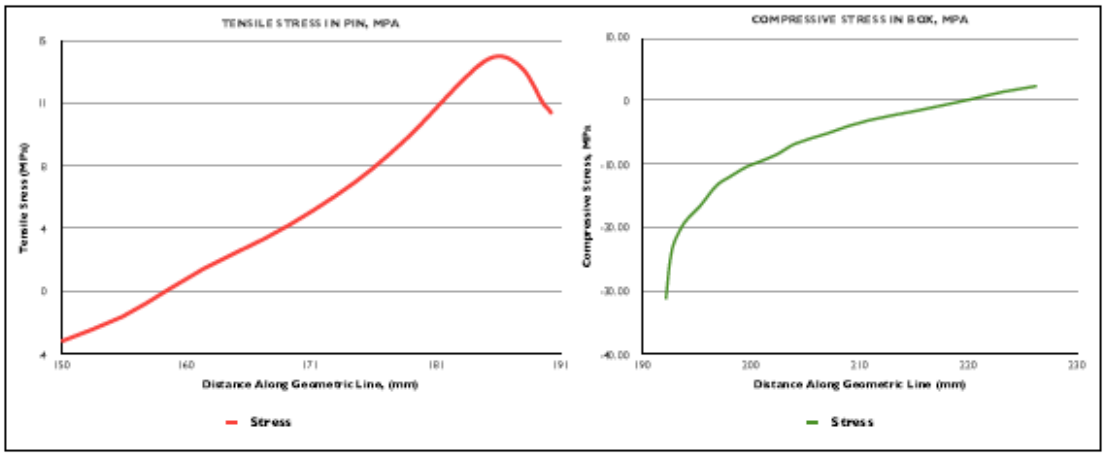

RESULTS SNAPSHOT-0.1 MM

COMPONENT	LENGTH (MM)	PEAK S22 STRESS (MPA)	PRELOAD FORCE IN COMPONENT (MN)
PIN	40.3	26.5	0.46
BOX	34.1	4.4	-0.46
		%Difference	-0.99

YIELD ANALYSIS-0.1 MM

COMPONENT	MATERIAL	YIELD STRENGTH	PEAK VON MISES STRESS
PIN	AL-MG-ZN-II	480.0	58.40
BOX	AL-MG-ZN-II	480.0	
		% of Yield	12.17

PIN PRELOAD STRESS VALUES

NODE	X	S22	TRUE ELEMENT FORCE	AVE. NODAL STRESS	FORCE ON ELEMENT FACE	VON MISES STRESS
158	190.27	20.062	3.58E+02	2.03E+01	7.29E+03	31.7051
1828	189.97	20.622	3.94E+02	2.08E+01	8.20E+03	32.1932
1829	189.64	21.072	4.32E+02	2.15E+01	9.29E+03	32.4589
1830	189.26	21.909	4.75E+02	2.25E+01	1.07E+04	33.9827
1831	188.88	23.015	5.20E+02	2.35E+01	1.23E+04	36.1678
1832	188.44	24.083	5.71E+02	2.46E+01	1.40E+04	38.5466
1833	187.96	25.029	6.26E+02	2.54E+01	1.59E+04	40.7039
1834	187.43	25.702	6.88E+02	2.60E+01	1.79E+04	42.3567
1835	186.84	26.211	7.54E+02	2.64E+01	1.99E+04	43.7251
1836	186	26.512	8.26E+02	2.65E+01	2.19E+04	44.6124
1837	185.49	26.436	8.32E+02	2.62E+01	2.18E+04	44.6757
1838	184.78	25.975	9.01E+02	2.56E+01	2.30E+04	43.8479
1839	184	25.17	9.75E+02	2.46E+01	2.40E+04	42.208
1840	183.16	24.071	1.09E+03	2.34E+01	2.55E+04	39.9036
1841	182.21	22.755	1.14E+03	2.20E+01	2.52E+04	37.1719
1842	181.21	21.304	1.14E+03	2.06E+01	2.34E+04	34.1533
160	180.21	19.829	1.13E+03	1.91E+01	2.16E+04	31.2634
1843	179.21	18.385	1.23E+03	1.77E+01	2.18E+04	28.6092
1844	178.11	16.923	1.35E+03	1.62E+01	2.18E+04	26.0254
1845	176.90	15.428	1.47E+03	1.47E+01	2.16E+04	23.5266
1846	175.56	13.872	1.61E+03	1.31E+01	2.11E+04	21.084
1847	174	12.311	1.75E+03	1.15E+01	2.02E+04	18.8172
1848	172.5	10.76	1.91E+03	9.97E+00	1.90E+04	16.7762
1849	170.72	9.1719	2.08E+03	8.35E+00	1.74E+04	14.8631
1850	168.77	7.5373	2.26E+03	6.73E+00	1.52E+04	13.0075
1851	166.63	5.9155	2.45E+03	5.13E+00	1.26E+04	11.3024
1852	164.27	4.343	2.66E+03	3.45E+00	9.16E+03	9.8467
1853	161.67	2.5532	2.87E+03	1.39E+00	4.00E+03	8.3774
1854	158.82	0.2348	3.77E+03	-1.31E+00	-4.95E+03	6.9682
1855	155	-2.864	4.79E+03	-4.26E+00	-2.04E+04	6.9123
159	150	-5.647	7.07E+04	-2.82E+00		10.3903
			Tensile Preload Force in Pin		4.60E+05	

BOX PRELOAD STRESS VALUES

NODE	X	S22	TRUE ELEMENT FORCE	AVE. NODAL STRESS	FORCE ON ELEMENT FACE	VON MISES STRESS
77	226.23	4.365	4.32E+03	3.52E+00	1.52E+04	28.4058
761	223.17	2.67	3.96E+03	1.60E+00	6.34E+03	28.6115
762	220.33	0.531	3.64E+03	-3.85E-01	-1.40E+03	29.84
763	217.66	-1.302	3.34E+03	-2.13E+00	-7.11E+03	31.1222
764	215.23	-2.957	3.07E+03	-3.66E+00	-1.12E+04	32.3829
765	212.94	-4.359	2.83E+03	-5.07E+00	-1.43E+04	33.5504
766	210.82	-5.79	2.60E+03	-6.68E+00	-1.74E+04	34.7262
767	208.84	-7.567	2.40E+03	-8.61E+00	-2.06E+04	36.057
78	207.01	-9.65	3.87E+03	-1.12E+01	-4.34E+04	37.7295
896	204.01	-12.74	2.20E+03	-1.44E+01	-3.16E+04	40.3574
895	202.29	-15.98	2.18E+03	-1.71E+01	-3.74E+04	43.3289
894	200.56	-18.28	1.26E+03	-1.89E+01	-2.38E+04	45.8252
82	199.56	-19.53	1.13E+03	-2.04E+01	-2.31E+04	47.2732
893	198.65	-21.21	1.03E+03	-2.20E+01	-2.27E+04	49.0608
892	197.83	-22.86	9.35E+02	-2.36E+01	-2.21E+04	50.872
891	197.07	-24.29	8.49E+02	-2.54E+01	-2.16E+04	52.6164
890	196.39	-26.5	7.71E+02	-2.78E+01	-2.15E+04	55.3869
889	195.76	-29.15	7.00E+02	-3.03E+01	-2.12E+04	58.5166
888	195.19	-31.46	6.38E+02	-3.23E+01	-2.06E+04	61.4211
887	194.67	-33.14	5.79E+02	-3.39E+01	-1.96E+04	63.5616
886	194.2	-34.62	5.27E+02	-3.54E+01	-1.87E+04	65.4486
885	193.76	-36.28	4.79E+02	-3.74E+01	-1.79E+04	67.2722
884	193.37	-38.44	4.36E+02	-3.96E+01	-1.73E+04	69.9446
883	193.01	-40.74	3.97E+02	-4.23E+01	-1.68E+04	72.8336
882	192.68	-43.82	3.60E+02	-4.68E+01	-1.69E+04	76.3982
881	192.38	-49.74	3.29E+02	-5.41E+01	-1.78E+04	84.0778
69	192.11	-58.44	1.16E+05	-2.92E+01		100.685
in Box					-4.64E+05	

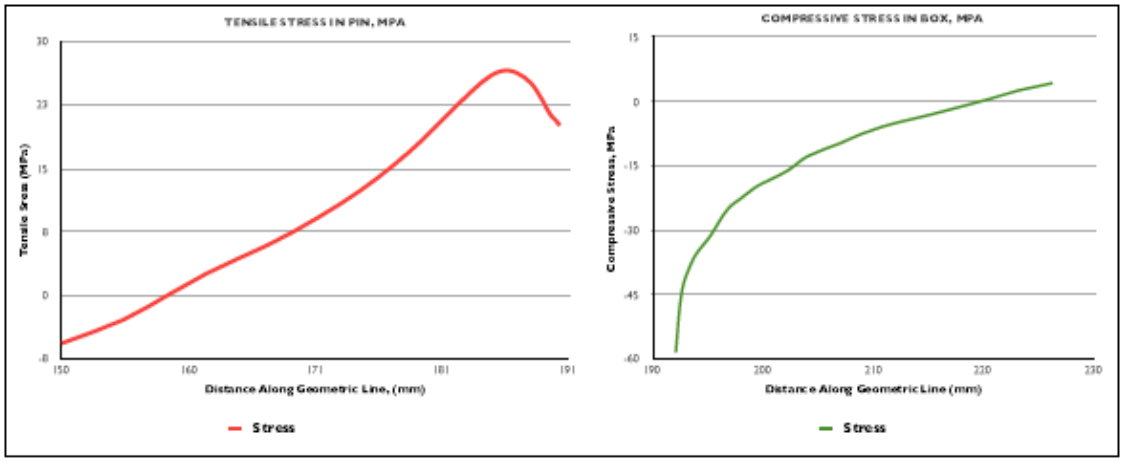

RESULTS SNAPSHOT-0.15MM

COMPONENT	LENGTH (MM)	PEAK S22 STRESS (MPA)	PRELOAD FORCE IN COMPONENT (MN)
PIN	40.3	38.9	0.68
BOX	34.1	6.4	-0.68
		% Difference	-0.99

YIELD ANALYSIS-0.15MM

COMPONENT	MATERIAL	YIELD STRENGTH	PEAK VON MISES STRESS
PIN	AL-MG-ZN-II	480.0	58.40
BOX	AL-MG-ZN-II	480.0	
		% of Yield	12.17

PIN PRELOAD STRESS VALUES

NODE	X	S22	TRUE ELEMENT FORCE	AVE. NODAL STRESS	FORCE ON ELEMENT FACE	VON MISES STRESS
158	190.27	29.448	3.58E+02	2.99E+01	1.07E+04	31.7051
1828	189.97	30.269	3.94E+02	3.06E+01	1.20E+04	32.1932
1829	189.64	30.929	4.32E+02	3.15E+01	1.36E+04	32.4589
1830	189.28	32.156	4.75E+02	3.30E+01	1.57E+04	33.9827
1831	188.88	33.779	5.20E+02	3.46E+01	1.80E+04	36.1678
1832	188.44	35.345	5.71E+02	3.60E+01	2.06E+04	38.5466
1833	187.96	36.734	6.26E+02	3.72E+01	2.33E+04	40.7039
1834	187.43	37.721	6.88E+02	3.81E+01	2.62E+04	42.3567
1835	186.84	38.468	7.54E+02	3.87E+01	2.92E+04	43.7251
1836	186	38.911	8.26E+02	3.89E+01	3.21E+04	44.6124
1837	185.49	38.8	8.32E+02	3.85E+01	3.20E+04	44.6757
1838	184.78	38.125	9.01E+02	3.75E+01	3.38E+04	43.8479
1839	184	36.945	9.75E+02	3.61E+01	3.52E+04	42.208
1840	183.16	35.334	1.09E+03	3.44E+01	3.75E+04	39.9036
1841	182.21	33.405	1.14E+03	3.23E+01	3.69E+04	37.1719
1842	181.21	31.277	1.14E+03	3.02E+01	3.43E+04	34.1533
160	180.21	29.114	1.13E+03	2.81E+01	3.17E+04	31.2634
1843	179.21	26.996	1.23E+03	2.59E+01	3.20E+04	28.6092
1844	178.11	24.851	1.35E+03	2.38E+01	3.21E+04	26.0254
1845	176.90	22.657	1.47E+03	2.15E+01	3.17E+04	23.5266
1846	175.56	20.374	1.61E+03	1.92E+01	3.09E+04	21.084
1847	174	18.081	1.75E+03	1.69E+01	2.97E+04	18.8172
1848	172.5	15.803	1.91E+03	1.46E+01	2.80E+04	16.7762
1849	170.72	13.471	2.08E+03	1.23E+01	2.55E+04	14.8631
1850	168.77	11.069	2.26E+03	9.88E+00	2.23E+04	13.0075
1851	166.63	8.6855	2.45E+03	7.53E+00	1.85E+04	11.3024
1852	164.27	6.374	2.66E+03	5.06E+00	1.34E+04	9.8467
1853	161.67	3.7426	2.87E+03	2.04E+00	5.86E+03	8.3774
1854	158.82	0.334	3.77E+03	-1.94E+00	-7.32E+03	6.9682
1855	155	-4.222	4.79E+03	-6.27E+00	-3.00E+04	6.9123
159	150	-8.31	7.07E+04	-4.16E+00		10.3903
			Tensile Preload Force in Pin		6.75E+05	

BOX PRELOAD STRESS VALUES

NODE	X	S22	TRUE ELEMENT FORCE	AVE. NODAL STRESS	FORCE ON ELEMENT FACE	VON MISES STRESS
77	226.23	6.401	4.32E+03	5.16E+00	2.23E+04	28.4058
761	223.17	3.914	3.96E+03	2.34E+00	9.28E+03	28.6115
762	220.33	0.771	3.64E+03	-5.76E-01	-2.09E+03	29.84
763	217.68	-1.922	3.34E+03	-3.14E+00	-1.05E+04	31.1222
764	215.23	-4.352	3.07E+03	-5.38E+00	-1.65E+04	32.3829
765	212.94	-6.409	2.83E+03	-7.46E+00	-2.11E+04	33.5504
766	210.82	-8.506	2.60E+03	-9.81E+00	-2.55E+04	34.7262
767	208.84	-11.11	2.40E+03	-1.26E+01	-3.03E+04	36.057
78	207.01	-14.16	3.87E+03	-1.64E+01	-6.36E+04	37.7295
896	204.01	-18.7	2.20E+03	-2.11E+01	-4.64E+04	40.3574
895	202.29	-23.47	2.18E+03	-2.52E+01	-5.49E+04	43.3289
894	200.56	-28.84	1.26E+03	-2.78E+01	-3.49E+04	45.8252
82	199.56	-28.69	1.13E+03	-2.99E+01	-3.39E+04	47.2732
893	196.65	-31.16	1.03E+03	-3.24E+01	-3.33E+04	49.0608
892	197.83	-33.57	9.35E+02	-3.46E+01	-3.24E+04	50.872
891	197.07	-35.67	8.49E+02	-3.73E+01	-3.17E+04	52.6164
890	196.39	-38.91	7.71E+02	-4.08E+01	-3.15E+04	55.3869
889	195.76	-42.78	7.00E+02	-4.45E+01	-3.11E+04	58.5166
888	195.19	-46.16	6.38E+02	-4.74E+01	-3.02E+04	61.4211
887	194.67	-48.6	5.79E+02	-4.97E+01	-2.88E+04	63.5616
886	194.2	-50.75	5.27E+02	-5.20E+01	-2.74E+04	65.4486
885	193.76	-53.15	4.79E+02	-5.47E+01	-2.62E+04	67.2722
884	193.37	-56.3	4.36E+02	-5.80E+01	-2.53E+04	69.9446
883	193.01	-59.63	3.97E+02	-6.19E+01	-2.46E+04	72.8336
882	192.68	-64.09	3.60E+02	-6.84E+01	-2.47E+04	76.3982
881	192.38	-72.71	3.29E+02	-7.90E+01	-2.60E+04	84.0778
69	192.11	-85.27	1.16E+05	-4.26E+01		100.685
			Compressive Preload Force in Box		-6.81E+05	

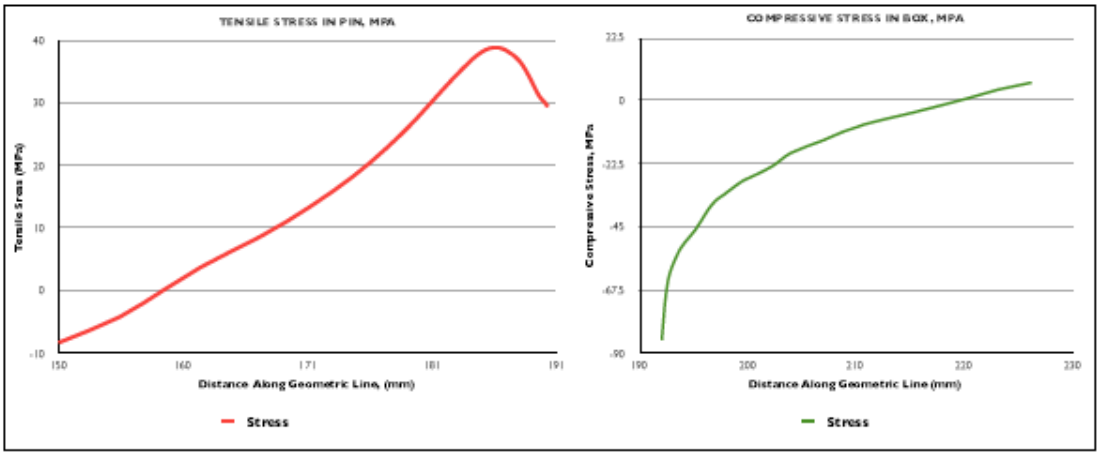

RESULTS SNAPSHOT-0.2MM

COMPONENT	LENGTH (MM)	PEAK S22 STRESS (MPA)	PRELOAD FORCE IN COMPONENT (MN)
PIN	40.3	51.2	0.89
BOX	34.1	8.4	-0.90
		% Difference	-0.99

YIELD ANALYSIS-0.2MM

COMPONENT	MATERIAL	YIELD STRENGTH	PEAK VON MISES STRESS
PIN	AL-MG-ZN-II	480.0	58.40
BOX	AL-MG-ZN-II	480.0	
		% of Yield	12.17

PIN PRELOAD STRESS VALUES

NODE	X	S22	TRUE ELEMENT FORCE	AVE. NODAL STRESS	FORCE ON ELEMENT FACE	VON MISES STRESS
158	190.27	38.779	3.58E+02	3.93E+01	1.41E+04	31.7051
1828	189.97	39.859	3.94E+02	4.03E+01	1.59E+04	32.1932
1829	189.64	40.727	4.32E+02	4.15E+01	1.79E+04	32.4589
1830	189.28	42.341	4.75E+02	4.34E+01	2.06E+04	33.9827
1831	188.88	44.477	5.20E+02	4.55E+01	2.37E+04	36.1678
1832	188.44	46.538	5.71E+02	4.75E+01	2.71E+04	38.5466
1833	187.96	48.365	6.26E+02	4.90E+01	3.07E+04	40.7039
1834	187.43	49.664	6.88E+02	5.02E+01	3.45E+04	42.3567
1835	186.84	50.647	7.54E+02	5.09E+01	3.84E+04	43.7251
1836	186	51.231	8.26E+02	5.12E+01	4.22E+04	44.6124
1837	185.49	51.086	8.32E+02	5.06E+01	4.21E+04	44.6757
1838	184.78	50.198	9.01E+02	4.94E+01	4.45E+04	43.8479
1839	184	48.645	9.75E+02	4.76E+01	4.64E+04	42.208
1840	183.16	46.525	1.09E+03	4.53E+01	4.93E+04	39.9036
1841	182.21	43.988	1.14E+03	4.26E+01	4.86E+04	37.1719
1842	181.21	41.188	1.14E+03	3.98E+01	4.51E+04	34.1533
160	180.21	38.342	1.13E+03	3.69E+01	4.17E+04	31.2634
1843	179.21	35.555	1.23E+03	3.41E+01	4.22E+04	28.6092
1844	178.11	32.732	1.35E+03	3.13E+01	4.22E+04	26.0254
1845	176.90	29.843	1.47E+03	2.83E+01	4.18E+04	23.5266
1846	175.56	26.838	1.61E+03	2.53E+01	4.07E+04	21.084
1847	174	23.819	1.75E+03	2.23E+01	3.91E+04	18.8172
1848	172.5	20.819	1.91E+03	1.93E+01	3.68E+04	16.7762
1849	170.72	17.748	2.08E+03	1.62E+01	3.36E+04	14.8631
1850	168.77	14.583	2.26E+03	1.30E+01	2.94E+04	13.0075
1851	166.63	11.442	2.45E+03	9.92E+00	2.43E+04	11.3024
1852	164.27	8.3953	2.66E+03	6.66E+00	1.77E+04	9.8467
1853	161.67	4.9264	2.87E+03	2.68E+00	7.70E+03	8.3774
1854	158.82	0.4327	3.77E+03	-2.57E+00	-9.68E+03	6.9682
1855	155	-5.573	4.79E+03	-8.27E+00	-3.96E+04	6.9123
159	150	-10.96	7.07E+04	-5.48E+00		10.3903
			Tensile Preload Force in Pin		8.89E+05	

BOX PRELOAD STRESS VALUES

NODE	X	S22	TRUE ELEMENT FORCE	AVE. NODAL STRESS	FORCE ON ELEMENT FACE	VON MISES STRESS
77	226.23	8.449	4.32E+03	6.81E+00	2.94E+04	28.4058
761	223.17	5.17	3.96E+03	3.10E+00	1.23E+04	28.6115
762	220.33	1.027	3.64E+03	-7.49E-01	-2.72E+03	29.84
763	217.68	-2.525	3.34E+03	-4.13E+00	-1.38E+04	31.1222
764	215.23	-5.727	3.07E+03	-7.08E+00	-2.18E+04	32.3829
765	212.94	-8.437	2.83E+03	-9.82E+00	-2.78E+04	33.5504
766	210.82	-11.2	2.60E+03	-1.29E+01	-3.36E+04	34.7262
767	208.84	-14.62	2.40E+03	-1.66E+01	-3.99E+04	36.057
78	207.01	-18.65	3.87E+03	-2.16E+01	-8.36E+04	37.7295
896	204.01	-24.63	2.20E+03	-2.78E+01	-6.11E+04	40.3574
895	202.29	-30.93	2.18E+03	-3.32E+01	-7.24E+04	43.3289
894	200.56	-35.38	1.26E+03	-3.66E+01	-4.60E+04	45.8252
82	199.56	-37.82	1.13E+03	-3.94E+01	-4.47E+04	47.2732
893	198.65	-41.08	1.03E+03	-4.27E+01	-4.39E+04	49.0608
892	197.83	-44.25	9.35E+02	-4.56E+01	-4.27E+04	50.872
891	197.07	-47.01	8.49E+02	-4.91E+01	-4.17E+04	52.6164
890	196.39	-51.28	7.71E+02	-5.38E+01	-4.15E+04	55.3869
889	195.76	-56.36	7.00E+02	-5.86E+01	-4.10E+04	58.5166
888	195.19	-60.78	6.38E+02	-6.24E+01	-3.98E+04	61.4211
887	194.67	-63.99	5.79E+02	-6.54E+01	-3.79E+04	63.5616
886	194.2	-66.8	5.27E+02	-6.84E+01	-3.60E+04	65.4486
885	193.76	-69.94	4.79E+02	-7.20E+01	-3.45E+04	67.2722
884	193.37	-74.04	4.36E+02	-7.62E+01	-3.32E+04	69.9446
883	193.01	-78.38	3.97E+02	-8.13E+01	-3.23E+04	72.6336
882	192.68	-84.16	3.60E+02	-8.97E+01	-3.23E+04	76.3982
881	192.38	-95.3	3.29E+02	-1.03E+02	-3.40E+04	84.0778
69	192.11	-111.7	1.16E+05	-5.58E+01		100.685
			Compressive Preload Force in Box		-8.97E+05	

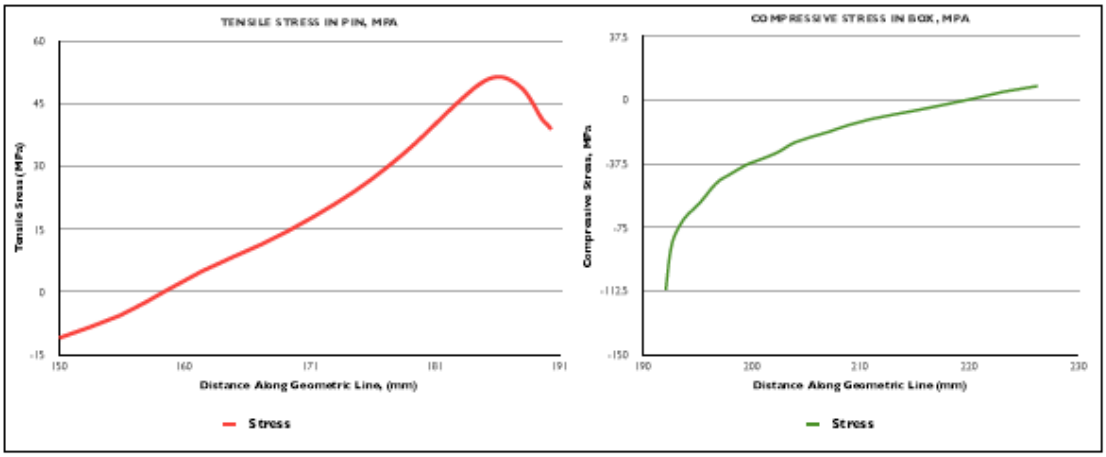

RESULTS SNAPSHOT-0.25MM

COMPONENT	LENGTH (MM)	PEAK S22 STRESS (MPA)	PRELOAD FORCE IN COMPONENT (MN)
PIN	40.3	63.6	1.10
BOX	34.1	10.5	-1.11
		% Difference	-0.99

YIELD ANALYSIS-0.25MM

COMPONENT	MATERIAL	YIELD STRENGTH	PEAK VON MISES STRESS
PIN	AL-MG-ZN-II	480.0	58.40
BOX	AL-MG-ZN-II	480.0	
		% of Yield	12.17

PIN PRELOAD STRESS VALUES

NODE	X	S22	TRUE ELEMENT FORCE	AVE. NODAL STRESS	FORCE ON ELEMENT FACE	VON MISES STRESS
158	190.27	48.094	3.58E+02	4.88E+01	1.75E+04	31.7051
1828	189.97	49.434	3.94E+02	5.00E+01	1.97E+04	32.1932
1829	189.64	50.511	4.32E+02	5.15E+01	2.23E+04	32.4589
1830	189.28	52.515	4.75E+02	5.38E+01	2.56E+04	33.9827
1831	188.88	55.165	5.20E+02	5.64E+01	2.94E+04	36.1678
1832	188.44	57.724	5.71E+02	5.89E+01	3.36E+04	38.5466
1833	187.96	59.994	6.26E+02	6.08E+01	3.81E+04	40.7039
1834	187.43	61.609	6.88E+02	6.22E+01	4.28E+04	42.3567
1835	186.84	62.833	7.54E+02	6.32E+01	4.76E+04	43.7251
1836	186	63.566	8.26E+02	6.35E+01	5.24E+04	44.6124
1837	185.49	63.394	8.32E+02	6.28E+01	5.23E+04	44.6757
1838	184.78	62.302	9.01E+02	6.13E+01	5.53E+04	43.8479
1839	184	60.386	9.75E+02	5.91E+01	5.76E+04	42.208
1840	183.16	57.769	1.09E+03	5.62E+01	6.13E+04	39.9036
1841	182.21	54.633	1.14E+03	5.29E+01	6.04E+04	37.1719
1842	181.21	51.169	1.14E+03	4.94E+01	5.61E+04	34.1533
160	180.21	47.644	1.13E+03	4.59E+01	5.18E+04	31.2634
1843	179.21	44.189	1.23E+03	4.24E+01	5.24E+04	28.6092
1844	178.11	40.686	1.35E+03	3.89E+01	5.25E+04	26.0254
1845	176.90	37.099	1.47E+03	3.52E+01	5.19E+04	23.5266
1846	175.56	33.362	1.61E+03	3.15E+01	5.06E+04	21.084
1847	174	29.605	1.75E+03	2.77E+01	4.86E+04	18.8172
1848	172.5	25.868	1.91E+03	2.40E+01	4.58E+04	16.7762
1849	170.72	22.038	2.08E+03	2.01E+01	4.17E+04	14.8631
1850	168.77	18.089	2.26E+03	1.61E+01	3.64E+04	13.0075
1851	166.63	14.166	2.45E+03	1.23E+01	3.01E+04	11.3024
1852	164.27	10.36	2.66E+03	8.19E+00	2.18E+04	9.8467
1853	161.67	6.0246	2.87E+03	3.22E+00	9.24E+03	8.3774
1854	158.82	0.4083	3.77E+03	-3.34E+00	-1.26E+04	6.9682
1855	155	-7.097	4.79E+03	-1.05E+01	-5.01E+04	6.9123
159	150	-13.83	7.07E+04	-6.92E+00		10.3903
			Tensile Preload Force in Pin		1.10E+06	

BOX PRELOAD STRESS VALUES

NODE	X	S22	TRUE ELEMENT FORCE	AVE. NODAL STRESS	FORCE ON ELEMENT FACE	VON MISES STRESS
77	226.23	10.47	4.32E+03	8.44E+00	3.65E+04	28.4058
761	223.17	6.411	3.96E+03	3.84E+00	1.52E+04	28.6115
762	220.33	1.272	3.64E+03	-9.34E-01	-3.40E+03	29.84
763	217.68	-3.139	3.34E+03	-5.13E+00	-1.71E+04	31.1222
764	215.23	-7.113	3.07E+03	-8.80E+00	-2.70E+04	32.3629
765	212.94	-10.48	2.83E+03	-1.22E+01	-3.45E+04	33.5504
766	210.82	-13.91	2.60E+03	-1.60E+01	-4.17E+04	34.7262
767	208.84	-18.15	2.40E+03	-2.06E+01	-4.95E+04	36.057
78	207.01	-23.14	3.67E+03	-2.69E+01	-1.04E+05	37.7295
896	204.01	-30.56	2.20E+03	-3.45E+01	-7.59E+04	40.3574
895	202.29	-36.38	2.18E+03	-4.11E+01	-8.98E+04	43.3289
894	200.56	-43.89	1.26E+03	-4.54E+01	-5.71E+04	45.8252
82	199.56	-46.92	1.13E+03	-4.89E+01	-5.55E+04	47.2732
893	198.65	-50.94	1.03E+03	-5.29E+01	-5.45E+04	49.0608
892	197.83	-54.86	9.35E+02	-5.66E+01	-5.29E+04	50.872
891	197.07	-58.27	8.49E+02	-6.09E+01	-5.17E+04	52.6164
890	196.39	-63.54	7.71E+02	-6.67E+01	-5.14E+04	55.3869
889	195.76	-69.78	7.00E+02	-7.25E+01	-5.08E+04	58.5166
888	195.19	-75.22	6.38E+02	-7.72E+01	-4.93E+04	61.4211
887	194.67	-79.16	5.79E+02	-8.09E+01	-4.68E+04	63.5616
886	194.2	-82.62	5.27E+02	-8.45E+01	-4.45E+04	65.4486
885	193.76	-86.46	4.79E+02	-8.90E+01	-4.26E+04	67.2722
884	193.37	-91.48	4.36E+02	-9.41E+01	-4.10E+04	69.9446
883	193.01	-96.81	3.97E+02	-1.00E+02	-3.99E+04	72.6336
882	192.68	-104	3.60E+02	-1.11E+02	-3.99E+04	76.3962
881	192.38	-117.6	3.29E+02	-1.28E+02	-4.19E+04	84.0778
69	192.11	-137.6	1.16E+05	-6.88E+01		100.685
			Compressive Preload Force in Box		-1.11E+06	

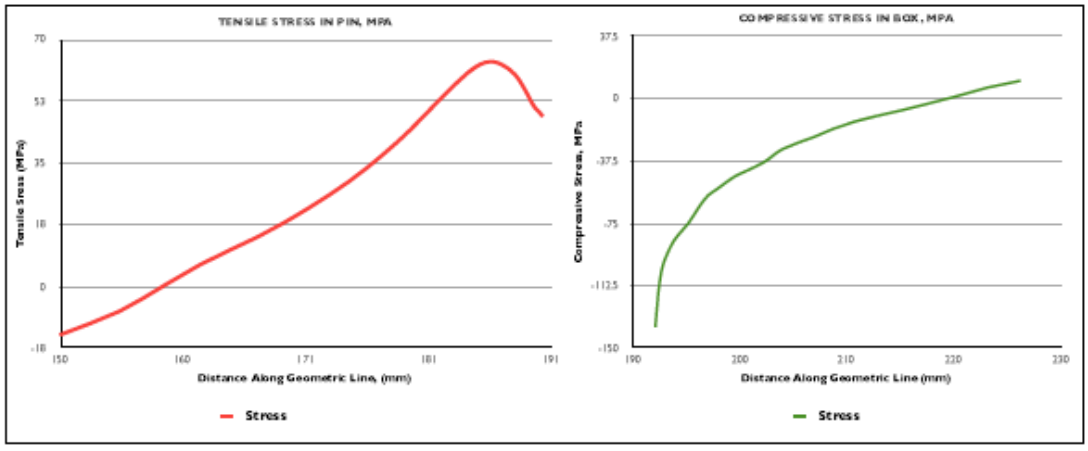

RESULTS SNAPSHOT-0.3MM

COMPONENT	LENGTH (MM)	PEAK S22 STRESS (MPA)	PRELOAD FORCE IN COMPONENT (MN)
PIN	40.3	75.9	1.32
BOX	34.1	12.5	-1.33
		% Difference	-0.99

YIELD ANALYSIS-0.3MM

COMPONENT	MATERIAL	YIELD STRENGTH	PEAK VON MISES STRESS
PIN	AL-MG-ZN-II	480.0	58.40
BOX	AL-MG-ZN-II	480.0	
		% of Yield	12.17

PIN PRELOAD STRESS VALUES

NODE	X	S22	TRUE ELEMENT FORCE	AVE. NODAL STRESS	FORCE ON ELEMENT FACE	VON MISES STRESS
158	190.27	57.438	3.58E+02	5.82E+01	2.09E+04	31.7051
1828	189.97	59.038	3.94E+02	5.97E+01	2.35E+04	32.1932
1829	189.64	60.322	4.32E+02	6.15E+01	2.66E+04	32.4589
1830	189.28	62.714	4.75E+02	6.43E+01	3.06E+04	33.9827
1831	188.88	65.878	5.20E+02	6.74E+01	3.51E+04	36.1678
1832	188.44	68.932	5.71E+02	7.03E+01	4.01E+04	38.5466
1833	187.96	71.642	6.26E+02	7.26E+01	4.55E+04	40.7039
1834	187.43	73.57	6.88E+02	7.43E+01	5.11E+04	42.3567
1835	186.84	75.034	7.54E+02	7.55E+01	5.69E+04	43.7251
1836	186	75.909	8.26E+02	7.58E+01	6.26E+04	44.6124
1837	185.49	75.706	8.32E+02	7.51E+01	6.24E+04	44.6757
1838	184.78	74.405	9.01E+02	7.33E+01	6.60E+04	43.8479
1839	184	72.121	9.75E+02	7.06E+01	6.88E+04	42.208
1840	183.16	69	1.09E+03	6.71E+01	7.32E+04	39.9036
1841	182.21	65.259	1.14E+03	6.32E+01	7.21E+04	37.1719
1842	181.21	61.127	1.14E+03	5.90E+01	6.70E+04	34.1533
160	180.21	56.921	1.13E+03	5.49E+01	6.19E+04	31.2634
1843	179.21	52.798	1.23E+03	5.07E+01	6.26E+04	28.6092
1844	178.11	48.619	1.35E+03	4.65E+01	6.27E+04	26.0254
1845	176.90	44.337	1.47E+03	4.21E+01	6.21E+04	23.5266
1846	175.56	39.878	1.61E+03	3.76E+01	6.05E+04	21.084
1847	174	35.393	1.75E+03	3.32E+01	5.81E+04	18.8172
1848	172.5	30.932	1.91E+03	2.86E+01	5.47E+04	16.7762
1849	170.72	26.358	2.08E+03	2.40E+01	4.99E+04	14.8631
1850	168.77	21.643	2.26E+03	1.93E+01	4.36E+04	13.0075
1851	166.63	16.959	2.45E+03	1.47E+01	3.60E+04	11.3024
1852	164.27	12.413	2.66E+03	9.82E+00	2.61E+04	9.8467
1853	161.67	7.2355	2.87E+03	3.88E+00	1.11E+04	8.3774
1854	158.82	0.5275	3.77E+03	-3.95E+00	-1.49E+04	6.9682
1855	155	-8.436	4.79E+03	-1.25E+01	-5.97E+04	6.9123
159	150	-16.48	7.07E+04	-8.24E+00		10.3903
				Tensile Preload Force in Pin	1.32E+06	

BOX PRELOAD STRESS VALUES

NODE	X	S22	TRUE ELEMENT FORCE	AVE. NODAL STRESS	FORCE ON ELEMENT FACE	VON MISES STRESS
77	226.23	12.53	4.32E+03	1.01E+01	4.36E+04	28.4058
761	223.17	7.679	3.96E+03	4.61E+00	1.82E+04	28.6115
762	220.33	1.531	3.64E+03	-1.11E+00	-4.03E+03	29.84
763	217.68	-3.746	3.34E+03	-6.12E+00	-2.05E+04	31.1222
764	215.23	-8.498	3.07E+03	-1.05E+01	-3.23E+04	32.3829
765	212.94	-12.52	2.83E+03	-1.46E+01	-4.12E+04	33.5504
766	210.82	-16.61	2.60E+03	-1.91E+01	-4.98E+04	34.7262
767	208.84	-21.68	2.40E+03	-2.47E+01	-5.91E+04	36.057
78	207.01	-27.65	3.87E+03	-3.21E+01	-1.24E+05	37.7295
896	204.01	-36.53	2.20E+03	-4.12E+01	-9.07E+04	40.3574
895	202.29	-45.91	2.18E+03	-4.92E+01	-1.07E+05	43.3289
894	200.56	-52.55	1.26E+03	-5.44E+01	-6.84E+04	45.8252
82	199.56	-56.24	1.13E+03	-5.87E+01	-6.65E+04	47.2732
893	198.65	-61.1	1.03E+03	-6.34E+01	-6.53E+04	49.0608
892	197.83	-65.77	9.35E+02	-6.78E+01	-6.34E+04	50.872
891	197.07	-69.82	8.49E+02	-7.30E+01	-6.20E+04	52.6164
890	196.39	-76.1	7.71E+02	-7.99E+01	-6.16E+04	55.3869
889	195.76	-83.73	7.00E+02	-8.71E+01	-6.10E+04	58.5166
888	195.19	-90.48	6.38E+02	-9.27E+01	-5.91E+04	61.4211
887	194.67	-94.89	5.79E+02	-9.68E+01	-5.60E+04	63.5616
886	194.2	-98.65	5.27E+02	-1.01E+02	-5.31E+04	65.4486
885	193.76	-103.2	4.79E+02	-1.06E+02	-5.09E+04	67.2722
884	193.37	-109.1	4.36E+02	-1.12E+02	-4.89E+04	69.9446
883	193.01	-115.5	3.97E+02	-1.20E+02	-4.76E+04	72.6336
882	192.68	-123.9	3.60E+02	-1.32E+02	-4.76E+04	76.3982
881	192.38	-140.2	3.29E+02	-1.52E+02	-5.00E+04	84.0778
69	192.11	-164.2	1.16E+05	-8.21E+01		100.685
				Compressive Preload Force in Box	-1.33E+06	

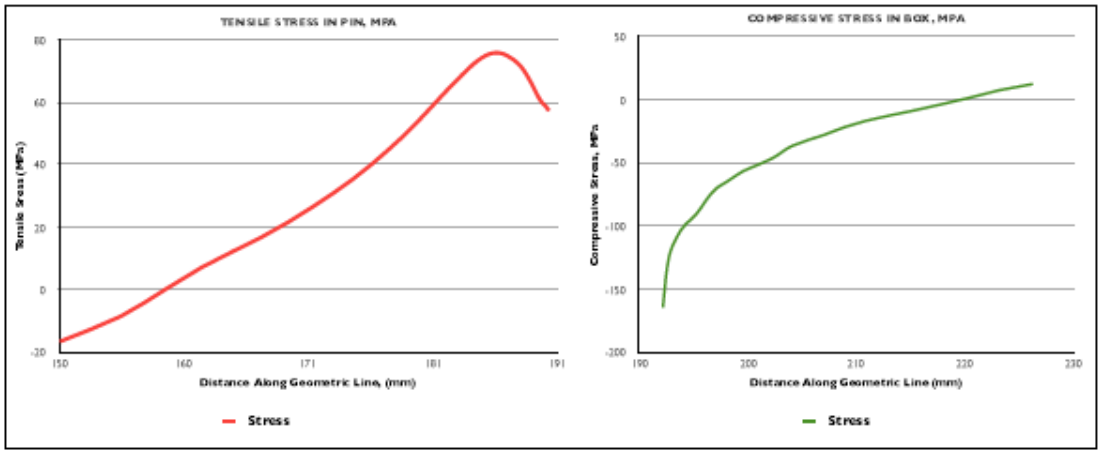

RESULTS SNAPSHOT-0.35MM

COMPONENT	LENGTH (MM)	PEAK S22 STRESS (MPA)	PRELOAD FORCE IN COMPONENT (MN)
PIN	40.3	88.2	1.53
BOX	34.1	14.6	-1.54
		% Difference	-0.99

YIELD ANALYSIS-0.35MM

COMPONENT	MATERIAL	YIELD STRENGTH	PEAK VON MISES STRESS
PIN	AL-MG-ZN-II	480.0	58.40
BOX	AL-MG-ZN-II	480.0	
		% of Yield	12.17

PIN PRELOAD STRESS VALUES

NODE	X	S22	TRUE ELEMENT FORCE	AVE. NODAL STRESS	FORCE ON ELEMENT FACE	VON MISES STRESS
158	190.27	66.74	3.58E+02	6.77E+01	2.43E+04	31.7051
1828	189.97	68.60	3.94E+02	6.93E+01	2.73E+04	32.1932
1829	189.64	70.09	4.32E+02	7.15E+01	3.09E+04	32.4589
1830	189.28	72.87	4.75E+02	7.47E+01	3.55E+04	33.9827
1831	188.88	76.54	5.20E+02	7.83E+01	4.08E+04	36.1678
1832	188.44	80.09	5.71E+02	8.17E+01	4.66E+04	38.5466
1833	187.96	83.23	6.26E+02	8.44E+01	5.28E+04	40.7039
1834	187.43	85.47	6.88E+02	8.63E+01	5.94E+04	42.3567
1835	186.84	87.17	7.54E+02	8.77E+01	6.61E+04	43.7251
1836	186	88.19	8.26E+02	8.81E+01	7.27E+04	44.6124
1837	185.49	87.96	8.32E+02	8.72E+01	7.25E+04	44.6757
1838	184.78	86.45	9.01E+02	8.51E+01	7.67E+04	43.8479
1839	184	83.79	9.75E+02	8.20E+01	7.99E+04	42.208
1840	183.16	80.17	1.09E+03	7.80E+01	8.51E+04	39.9036
1841	182.21	75.83	1.14E+03	7.34E+01	8.38E+04	37.1719
1842	181.21	71.03	1.14E+03	6.86E+01	7.79E+04	34.1533
160	180.21	66.15	1.13E+03	6.38E+01	7.20E+04	31.2634
1843	179.21	61.36	1.23E+03	5.89E+01	7.26E+04	28.6092
1844	178.11	56.50	1.35E+03	5.40E+01	7.29E+04	26.0254
1845	176.90	51.53	1.47E+03	4.89E+01	7.21E+04	23.5266
1846	175.56	46.35	1.61E+03	4.37E+01	7.03E+04	21.084
1847	174	41.14	1.75E+03	3.85E+01	6.76E+04	18.8172
1848	172.5	35.95	1.91E+03	3.33E+01	6.36E+04	16.7762
1849	170.72	30.64	2.08E+03	2.79E+01	5.80E+04	14.8631
1850	168.77	25.16	2.26E+03	2.24E+01	5.07E+04	13.0075
1851	166.63	19.71	2.45E+03	1.71E+01	4.18E+04	11.3024
1852	164.27	14.42	2.66E+03	1.14E+01	3.03E+04	9.8467
1853	161.67	8.40	2.87E+03	4.50E+00	1.29E+04	8.3774
1854	158.82	0.60	3.77E+03	-4.61E+00	-1.74E+04	6.9682
1855	155	-9.82	4.79E+03	-1.45E+01	-6.94E+04	6.9123
159	150	-19.17	7.07E+04	-9.59E+00		10.3903
			Tensile Preload Force in Pin		1.53E+06	

BOX PRELOAD STRESS VALUES

NODE	X	S22	TRUE ELEMENT FORCE	AVE. NODAL STRESS	FORCE ON ELEMENT FACE	VON MISES STRESS
77	226.23	14.61	4.32E+03	1.18E+01	5.09E+04	28.4056
761	223.17	8.96	3.96E+03	5.39E+00	2.13E+04	26.6115
762	220.33	1.81	3.64E+03	-1.26E+00	-4.58E+03	29.84
763	217.68	-4.33	3.34E+03	-7.09E+00	-2.37E+04	31.1222
764	215.23	-9.85	3.07E+03	-1.22E+01	-3.75E+04	32.3829
765	212.94	-14.53	2.83E+03	-1.69E+01	-4.78E+04	33.5504
766	210.82	-19.29	2.60E+03	-2.22E+01	-5.79E+04	34.7262
767	208.84	-25.17	2.40E+03	-2.86E+01	-6.87E+04	36.057
78	207.01	-32.12	3.87E+03	-3.73E+01	-1.44E+05	37.7295
896	204.01	-42.46	2.20E+03	-4.79E+01	-1.05E+05	40.3574
895	202.29	-53.39	2.18E+03	-5.73E+01	-1.25E+05	43.3289
894	200.56	-61.13	1.26E+03	-6.33E+01	-7.96E+04	45.8252
82	199.56	-65.44	1.13E+03	-6.83E+01	-7.74E+04	47.2732
893	198.65	-71.09	1.03E+03	-7.38E+01	-7.60E+04	49.0608
892	197.83	-76.51	9.35E+02	-7.89E+01	-7.38E+04	50.872
891	197.07	-81.21	8.49E+02	-8.49E+01	-7.21E+04	52.6164
890	196.39	-88.50	7.71E+02	-9.29E+01	-7.17E+04	55.3869
889	195.76	-97.33	7.00E+02	-1.01E+02	-7.09E+04	58.5166
888	195.19	-105.20	6.38E+02	-1.08E+02	-6.88E+04	61.4211
887	194.67	-110.32	5.79E+02	-1.12E+02	-6.51E+04	63.5616
886	194.2	-114.66	5.27E+02	-1.17E+02	-6.17E+04	65.4486
885	193.76	-119.85	4.79E+02	-1.23E+02	-5.91E+04	67.2722
884	193.37	-126.72	4.36E+02	-1.30E+02	-5.68E+04	69.9446
883	193.01	-133.98	3.97E+02	-1.39E+02	-5.52E+04	72.8336
882	192.68	-143.69	3.60E+02	-1.53E+02	-5.52E+04	76.3982
881	192.38	-162.46	3.29E+02	-1.76E+02	-5.79E+04	84.0778
69	192.11	-190.00	1.16E+05	-9.50E+01		100.685
			Compressive Preload Force in Box		-1.54E+06	

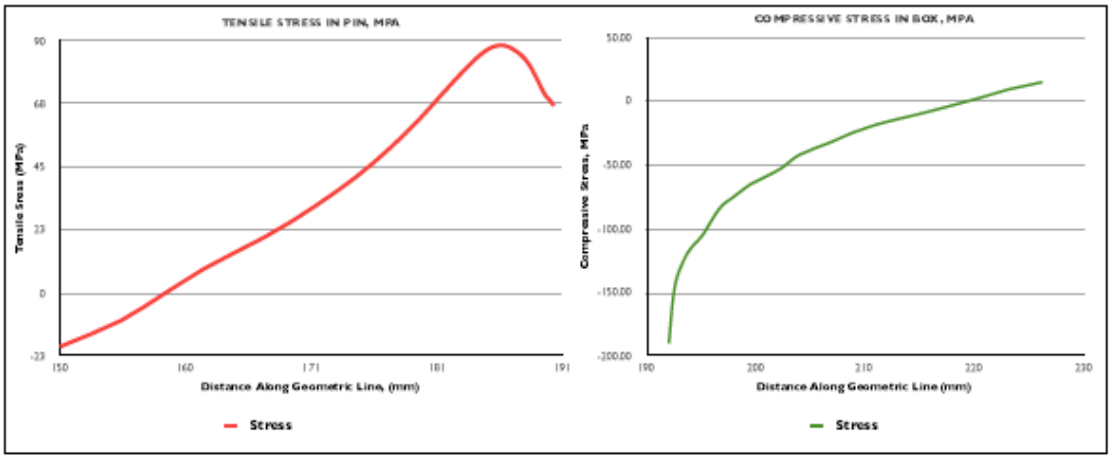

RESULTS SNAPSHOT-0.4MM

COMPONENT	LENGTH (MM)	PEAK S22 STRESS (MPA)	PRELOAD FORCE IN COMPONENT (MN)
PIN	40.3	100.2	1.74
BOX	34.1	18.7	-1.76
		%Difference	-0.99

YIELD ANALYSIS-0.4MM

COMPONENT	MATERIAL	YIELD STRENGTH	PEAK VON MISES STRESS
PIN	AL-MG-ZN-II	480.0	58.40
BOX	AL-MG-ZN-II	480.0	
		% of Yield	12.17

PIN PRELOAD STRESS VALUES

NODE	X	S22	TRUE ELEMENT FORCE	AVE. NODAL STRESS	FORCE ON ELEMENT FACE	VON MISES STRESS
158	190.27	75.88	3.58E+02	7.69E+01	2.76E+04	31.7051
1828	189.97	77.98	3.94E+02	7.88E+01	3.10E+04	32.1932
1829	189.64	79.67	4.32E+02	8.12E+01	3.51E+04	32.4589
1830	189.28	82.81	4.75E+02	8.49E+01	4.03E+04	33.9827
1831	188.88	86.98	5.20E+02	8.90E+01	4.63E+04	36.1678
1832	188.44	90.99	5.71E+02	9.28E+01	5.30E+04	38.5466
1833	187.96	94.56	6.26E+02	9.58E+01	6.00E+04	40.7039
1834	187.43	97.09	6.88E+02	9.80E+01	6.74E+04	42.3567
1835	186.84	99.01	7.54E+02	9.96E+01	7.50E+04	43.7251
1836	186	100.15	8.26E+02	1.00E+02	8.26E+04	44.6124
1837	185.49	99.87	8.32E+02	9.90E+01	8.24E+04	44.6757
1838	184.78	98.15	9.01E+02	9.66E+01	8.71E+04	43.8479
1839	184	95.13	9.75E+02	9.31E+01	9.07E+04	42.208
1840	183.16	91.01	1.09E+03	8.85E+01	9.65E+04	39.9036
1841	182.21	86.07	1.14E+03	8.33E+01	9.51E+04	37.1719
1842	181.21	80.61	1.14E+03	7.78E+01	8.84E+04	34.1533
160	180.21	75.06	1.13E+03	7.23E+01	8.17E+04	31.2634
1843	179.21	69.62	1.23E+03	6.69E+01	8.26E+04	28.6092
1844	178.11	64.11	1.35E+03	6.13E+01	8.27E+04	26.0254
1845	176.90	58.46	1.47E+03	5.55E+01	8.18E+04	23.5266
1846	175.56	52.58	1.61E+03	4.96E+01	7.98E+04	21.084
1847	174	46.67	1.75E+03	4.37E+01	7.67E+04	18.8172
1848	172.5	40.79	1.91E+03	3.78E+01	7.22E+04	16.7762
1849	170.72	34.77	2.08E+03	3.17E+01	6.58E+04	14.8631
1850	168.77	28.56	2.26E+03	2.55E+01	5.75E+04	13.0075
1851	166.63	22.40	2.45E+03	1.94E+01	4.76E+04	11.3024
1852	164.27	16.43	2.66E+03	1.30E+01	3.46E+04	9.8467
1853	161.67	9.63	2.87E+03	5.23E+00	1.50E+04	8.3774
1854	158.82	0.83	3.77E+03	-5.06E+00	-1.91E+04	6.9682
1855	155	-10.95	4.79E+03	-1.62E+01	-7.78E+04	6.9123
159	150	-21.52	7.07E+04	-1.08E+01		10.3903
			Tensile Preload Force in Pin		1.74E+06	

BOX PRELOAD STRESS VALUES

NODE	X	S22	TRUE ELEMENT FORCE	AVE. NODAL STRESS	FORCE ON ELEMENT FACE	VON MISES STRESS
77	226.23	18.74	4.32E+03	1.55E+01	6.68E+04	28.4058
761	223.17	12.21	3.96E+03	8.12E+00	3.22E+04	26.6115
762	220.33	4.02	3.64E+03	5.12E-01	1.86E+03	29.84
763	217.68	-3.00	3.34E+03	-6.28E+00	-2.10E+04	31.1222
764	215.23	-9.56	3.07E+03	-1.24E+01	-3.81E+04	32.3829
765	212.94	-15.25	2.83E+03	-1.82E+01	-5.14E+04	33.5504
766	210.82	-21.13	2.60E+03	-2.48E+01	-6.46E+04	34.7262
767	208.84	-28.54	2.40E+03	-3.28E+01	-7.86E+04	36.057
78	207.01	-36.99	3.87E+03	-4.35E+01	-1.69E+05	37.7295
896	204.01	-50.02	2.20E+03	-5.55E+01	-1.22E+05	40.3574
895	202.29	-60.94	2.18E+03	-6.50E+01	-1.42E+05	43.3289
894	200.56	-68.97	1.26E+03	-7.28E+01	-9.15E+04	45.8252
82	199.56	-76.65	1.13E+03	-8.02E+01	-9.09E+04	47.2732
893	198.65	-83.69	1.03E+03	-8.72E+01	-8.98E+04	49.0606
892	197.83	-90.69	9.35E+02	-9.42E+01	-8.81E+04	50.872
891	197.07	-97.74	8.49E+02	-1.01E+02	-8.59E+04	52.6164
890	196.39	-104.65	7.71E+02	-1.08E+02	-8.34E+04	55.3869
889	195.76	-111.75	7.00E+02	-1.15E+02	-8.07E+04	58.5166
888	195.19	-118.85	6.38E+02	-1.23E+02	-7.83E+04	61.4211
887	194.67	-126.65	5.79E+02	-1.30E+02	-7.54E+04	63.5616
886	194.2	-133.84	5.27E+02	-1.37E+02	-7.24E+04	65.4486
885	193.76	-141.05	4.79E+02	-1.45E+02	-6.95E+04	67.2722
884	193.37	-148.83	4.36E+02	-1.53E+02	-6.68E+04	69.9446
883	193.01	-157.95	3.97E+02	-1.64E+02	-6.52E+04	72.8336
882	192.68	-170.11	3.60E+02	-1.81E+02	-6.54E+04	76.3982
881	192.38	-192.59	3.29E+02	-2.10E+02	-6.89E+04	84.0778
69	192.11	-226.74	1.16E+05	-1.13E+02		100.685
			Compressive Preload Force in Box		-1.76E+06	

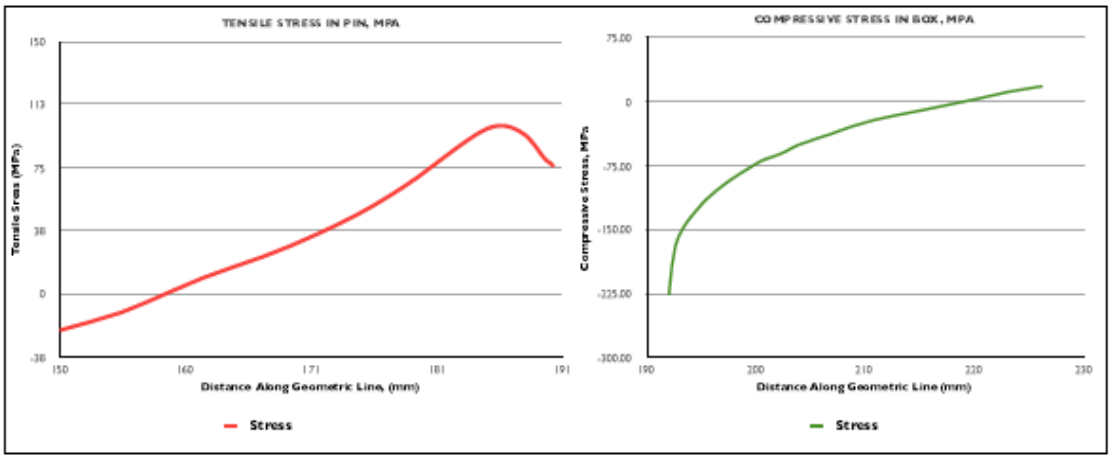

RESULTS SNAPSHOT-0KN

COMPONENT	LENGTH (MM)	PEAK S22 STRESS (MPA)	AXIAL FORCE IN COMPONENT (MN)
PIN	40.3	75.7	1.32
BOX	34.1	14.0	-1.33
		%Difference	-0.99

YIELD ANALYSIS-0KN

COMPONENT	MATERIAL	YIELD STRENGTH	PEAK VON MISES STRESS
PIN	AL-MG-ZN-II	480.0	58.40
BOX	AL-MG-ZN-II	480.0	
		% of Yield	12.17

PIN PRELOAD STRESS VALUES

NODE	X	S22	TRUE ELEMENT FORCE	AVE. NODAL STRESS	FORCE ON ELEMENT FACE	VON MISES STRESS
158	190.27	57.35	3.58E+02	5.81E+01	2.06E+04	31.7051
1828	189.97	58.94	3.94E+02	5.96E+01	2.34E+04	32.1932
1829	189.64	60.22	4.32E+02	6.14E+01	2.65E+04	32.4589
1830	189.28	62.60	4.75E+02	6.42E+01	3.05E+04	33.9827
1831	188.88	65.76	5.20E+02	6.73E+01	3.50E+04	36.1678
1832	188.44	68.80	5.71E+02	7.01E+01	4.01E+04	38.5466
1833	187.96	71.50	6.26E+02	7.25E+01	4.54E+04	40.7039
1834	187.43	73.41	6.88E+02	7.41E+01	5.10E+04	42.3567
1835	186.84	74.87	7.54E+02	7.53E+01	5.67E+04	43.7251
1836	186	75.73	8.26E+02	7.56E+01	6.24E+04	44.6124
1837	185.49	75.52	8.32E+02	7.49E+01	6.23E+04	44.6757
1838	184.78	74.21	9.01E+02	7.31E+01	6.59E+04	43.8479
1839	184	71.93	9.75E+02	7.04E+01	6.86E+04	42.208
1840	183.16	68.81	1.09E+03	6.69E+01	7.30E+04	39.9036
1841	182.21	65.07	1.14E+03	6.30E+01	7.19E+04	37.1719
1842	181.21	60.94	1.14E+03	5.88E+01	6.68E+04	34.1533
160	180.21	56.73	1.13E+03	5.47E+01	6.17E+04	31.2634
1843	179.21	52.62	1.23E+03	5.05E+01	6.24E+04	28.6092
1844	178.11	48.45	1.35E+03	4.63E+01	6.25E+04	26.0254
1845	176.90	44.17	1.47E+03	4.20E+01	6.18E+04	23.5266
1846	175.56	39.73	1.61E+03	3.75E+01	6.03E+04	21.064
1847	174	35.26	1.75E+03	3.30E+01	5.79E+04	18.8172
1848	172.5	30.82	1.91E+03	2.85E+01	5.45E+04	16.7762
1849	170.72	26.27	2.08E+03	2.39E+01	4.97E+04	14.8631
1850	168.77	21.58	2.26E+03	1.93E+01	4.35E+04	13.0075
1851	166.63	16.93	2.45E+03	1.47E+01	3.60E+04	11.3024
1852	164.27	12.42	2.66E+03	9.85E+00	2.62E+04	9.8467
1853	161.67	7.29	2.87E+03	3.97E+00	1.14E+04	8.3774
1854	158.82	0.64	3.77E+03	-3.80E+00	-1.43E+04	6.9662
1855	155	-8.25	4.79E+03	-1.22E+01	-5.86E+04	6.9123
159	150	-16.23	7.07E+04	-8.11E+00		10.3903
				Tensile Force in Pin	1.32E+06	

BOX PRELOAD STRESS VALUES

NODE	X	S22	TRUE ELEMENT FORCE	AVE. NODAL STRESS	FORCE ON ELEMENT FACE	VON MISES STRESS
77	226.23	14.02	4.32E+03	1.16E+01	5.00E+04	28.4058
761	223.17	9.15	3.96E+03	6.11E+00	2.42E+04	28.6115
762	220.33	3.06	3.64E+03	3.88E-01	1.41E+03	29.84
763	217.68	-2.29	3.34E+03	-4.71E+00	-1.57E+04	31.1222
764	215.23	-7.13	3.07E+03	-9.22E+00	-2.83E+04	32.3829
765	212.94	-11.31	2.83E+03	-1.36E+01	-3.84E+04	33.5504
766	210.82	-15.86	2.60E+03	-1.87E+01	-4.86E+04	34.7262
767	208.84	-21.49	2.40E+03	-2.47E+01	-5.93E+04	36.057
78	207.01	-28.00	3.87E+03	-3.29E+01	-1.28E+05	37.7295
896	204.01	-37.85	2.20E+03	-4.20E+01	-9.24E+04	40.3574
895	202.29	-46.18	2.18E+03	-4.93E+01	-1.08E+05	43.3289
894	200.56	-52.46	1.26E+03	-5.53E+01	-6.95E+04	45.8252
82	199.56	-58.06	1.13E+03	-6.11E+01	-6.92E+04	47.2732
893	198.65	-64.09	1.03E+03	-6.64E+01	-6.84E+04	49.0608
892	197.83	-68.76	9.35E+02	-7.09E+01	-6.63E+04	50.872
891	197.07	-72.97	8.49E+02	-7.55E+01	-6.41E+04	52.6164
890	196.39	-78.01	7.71E+02	-8.08E+01	-6.23E+04	55.3869
889	195.76	-83.63	7.00E+02	-8.69E+01	-6.09E+04	58.5166
888	195.19	-90.22	6.38E+02	-9.30E+01	-5.93E+04	61.4211
887	194.67	-95.77	5.79E+02	-9.82E+01	-5.69E+04	63.5616
886	194.2	-100.72	5.27E+02	-1.03E+02	-5.43E+04	65.4486
885	193.76	-105.64	4.79E+02	-1.09E+02	-5.21E+04	67.2722
884	193.37	-111.71	4.36E+02	-1.15E+02	-5.02E+04	69.9446
883	193.01	-118.84	3.97E+02	-1.24E+02	-4.91E+04	72.8336
882	192.68	-128.19	3.60E+02	-1.37E+02	-4.95E+04	76.3962
881	192.38	-146.36	3.29E+02	-1.59E+02	-5.24E+04	84.0778
69	192.11	-172.64	1.16E+05	-8.63E+01		100.685
				Compressive Force in Box	-1.33E+06	

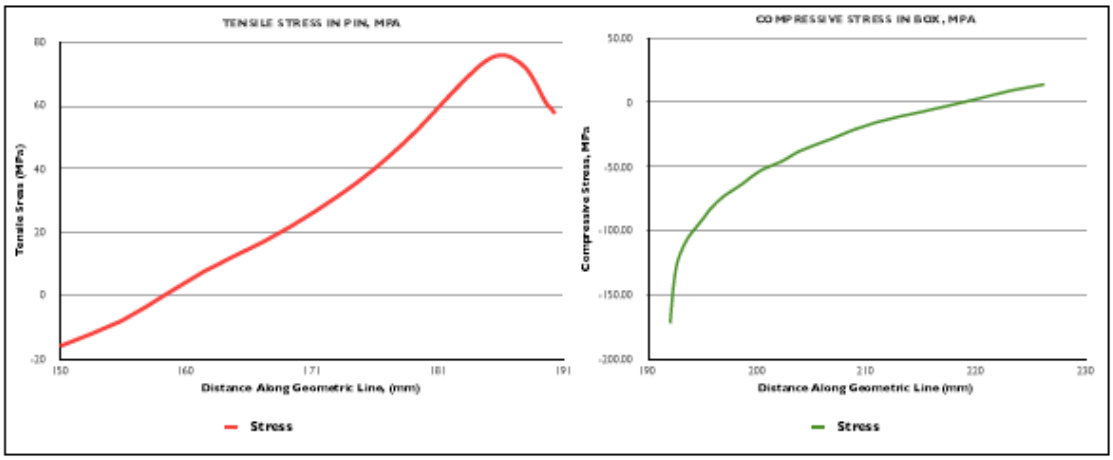

RESULTS SNAPSHOT-2KN

COMPONENT	LENGTH (MM)	PEAK S22 STRESS (MPA)	PRELOAD FORCE IN COMPONENT (MN)
PIN	40.3	75.7	1.32
BOX	34.1	14.0	-1.32
		% Difference	-1.00

YIELD ANALYSIS-2KN

COMPONENT	MATERIAL	YIELD STRENGTH	PEAK VON MISES STRESS
PIN	AL-MG-ZN-II	480.0	58.40
BOX	AL-MG-ZN-II	480.0	
		% of Yield	12.17

PIN PRELOAD STRESS VALUES

NODE	X	S22	TRUE ELEMENT FORCE	AVE. NODAL STRESS	FORCE ON ELEMENT FACE	VON MISES STRESS
158	190.27	57.36	3.58E+02	5.82E+01	2.08E+04	31.7051
1828	189.97	58.952	3.94E+02	5.96E+01	2.35E+04	32.1932
1829	189.64	60.229	4.32E+02	6.14E+01	2.65E+04	32.4589
1830	189.28	62.612	4.75E+02	6.42E+01	3.05E+04	33.9827
1831	188.88	65.763	5.20E+02	6.73E+01	3.50E+04	36.1678
1832	188.44	68.805	5.71E+02	7.02E+01	4.01E+04	38.5466
1833	187.96	71.502	6.26E+02	7.25E+01	4.54E+04	40.7039
1834	187.43	73.421	6.88E+02	7.41E+01	5.10E+04	42.3567
1835	186.84	74.875	7.54E+02	7.53E+01	5.67E+04	43.7251
1836	186	75.742	8.26E+02	7.56E+01	6.24E+04	44.6124
1837	185.49	75.534	8.32E+02	7.49E+01	6.23E+04	44.6757
1838	184.78	74.231	9.01E+02	7.31E+01	6.59E+04	43.8479
1839	184	71.949	9.75E+02	7.04E+01	6.86E+04	42.208
1840	183.16	68.833	1.09E+03	6.70E+01	7.30E+04	39.9036
1841	182.21	65.098	1.14E+03	6.30E+01	7.20E+04	37.1719
1842	181.21	60.974	1.14E+03	5.89E+01	6.68E+04	34.1533
160	180.21	56.778	1.13E+03	5.47E+01	6.18E+04	31.2634
1843	179.21	52.665	1.23E+03	5.06E+01	6.25E+04	28.6092
1844	178.11	48.497	1.35E+03	4.64E+01	6.26E+04	26.0254
1845	176.90	44.228	1.47E+03	4.20E+01	6.19E+04	23.5266
1846	175.56	39.785	1.61E+03	3.76E+01	6.04E+04	21.084
1847	174	35.317	1.75E+03	3.31E+01	5.80E+04	18.8172
1848	172.5	30.877	1.91E+03	2.86E+01	5.46E+04	16.7762
1849	170.72	26.328	2.08E+03	2.40E+01	4.99E+04	14.8631
1850	168.77	21.642	2.26E+03	1.93E+01	4.36E+04	13.0075
1851	166.63	16.992	2.45E+03	1.47E+01	3.61E+04	11.3024
1852	164.27	12.482	2.66E+03	9.92E+00	2.63E+04	9.8467
1853	161.67	7.349	2.87E+03	4.02E+00	1.16E+04	8.3774
1854	158.82	0.7004	3.77E+03	-3.74E+00	-1.41E+04	6.9682
1855	155	-8.189	4.79E+03	-1.22E+01	-5.84E+04	6.9123
159	150	-16.17	7.07E+04	-8.09E+00		10.3903
			Tensile Preload Force in Pin		1.32E+06	

BOX PRELOAD STRESS VALUES

NODE	X	S22	TRUE ELEMENT FORCE	AVE. NODAL STRESS	FORCE ON ELEMENT FACE	VON MISES STRESS
77	226.23	13.99	4.32E+03	1.16E+01	5.00E+04	28.4058
761	223.17	9.152	3.96E+03	6.13E+00	2.43E+04	28.6115
762	220.33	3.116	3.64E+03	4.65E-01	1.69E+03	29.84
763	217.68	-2.186	3.34E+03	-4.59E+00	-1.53E+04	31.1222
764	215.23	-6.984	3.07E+03	-9.05E+00	-2.78E+04	32.3829
765	212.94	-11.12	2.83E+03	-1.34E+01	-3.78E+04	33.5504
766	210.82	-15.64	2.60E+03	-1.84E+01	-4.80E+04	34.7262
767	208.84	-21.23	2.40E+03	-2.45E+01	-5.87E+04	36.057
78	207.01	-27.71	3.87E+03	-3.26E+01	-1.26E+05	37.7295
896	204.01	-37.53	2.20E+03	-4.17E+01	-9.17E+04	40.3574
895	202.29	-45.83	2.18E+03	-4.90E+01	-1.07E+05	43.3289
894	200.56	-52.11	1.26E+03	-5.49E+01	-6.90E+04	45.8252
82	199.56	-57.71	1.13E+03	-6.07E+01	-6.88E+04	47.2732
893	198.65	-63.71	1.03E+03	-6.60E+01	-6.80E+04	49.0608
892	197.83	-68.37	9.35E+02	-7.05E+01	-6.59E+04	50.872
891	197.07	-72.57	8.49E+02	-7.51E+01	-6.38E+04	52.6164
890	196.39	-77.6	7.71E+02	-8.04E+01	-6.20E+04	55.3869
889	195.76	-83.2	7.00E+02	-8.65E+01	-6.05E+04	58.5166
888	195.19	-89.77	6.38E+02	-9.25E+01	-5.90E+04	61.4211
887	194.67	-95.31	5.79E+02	-9.78E+01	-5.66E+04	63.5616
886	194.2	-100.2	5.27E+02	-1.03E+02	-5.41E+04	65.4486
885	193.76	-105.1	4.79E+02	-1.08E+02	-5.18E+04	67.2722
884	193.37	-111.2	4.36E+02	-1.15E+02	-5.00E+04	69.9446
883	193.01	-118.3	3.97E+02	-1.23E+02	-4.89E+04	72.8336
882	192.68	-127.6	3.60E+02	-1.37E+02	-4.93E+04	76.3962
881	192.36	-145.7	3.29E+02	-1.59E+02	-5.22E+04	84.0778
69	192.11	-171.8	1.16E+05	-8.59E+01		100.685
			Compressive Force in Box		-1.32E+06	

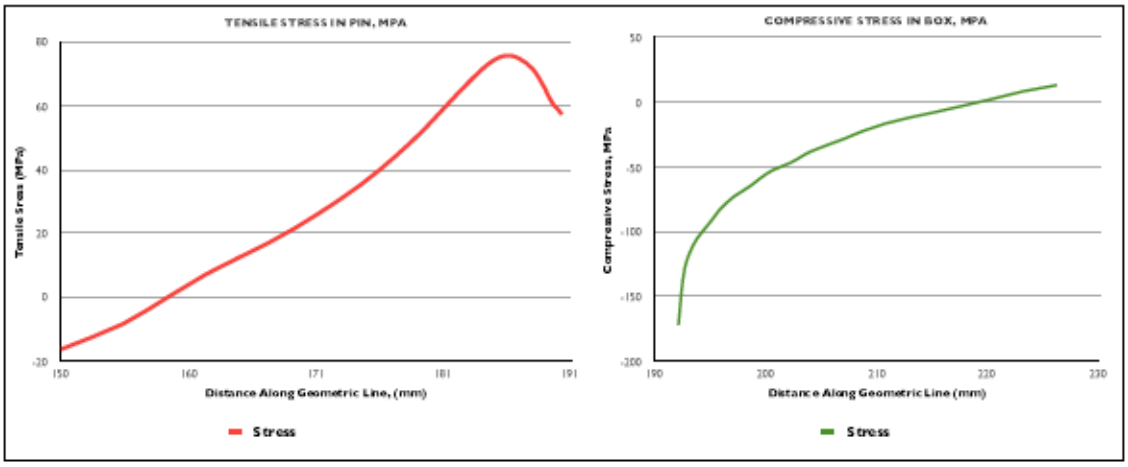

RESULTS SNAPSHOT-100KN

COMPONENT	LENGTH (MM)	PEAK S22 STRESS (MPA)	PRELOAD FORCE IN COMPONENT (MN)
PIN	40.3	76.3	1.42
BOX	34.1	12.2	-0.80
		% Difference	-1.77

YIELD ANALYSIS-100KN

COMPONENT	MATERIAL	YIELD STRENGTH	PEAK VON MISES STRESS
PIN	AL-MG-ZN-II	480.0	56.40
BOX	AL-MG-ZN-II	480.0	
		% of Yield	12.17

PIN PRELOAD STRESS VALUES

NODE	X	S22	TRUE ELEMENT FORCE	AVE. NODAL STRESS	FORCE ON ELEMENT FACE	VON MISES STRESS
158	190.27	57.836	3.58E+02	5.86E+01	2.10E+04	31.7051
1828	189.97	59.382	3.94E+02	6.00E+01	2.36E+04	32.1932
1829	189.64	60.627	4.32E+02	6.18E+01	2.67E+04	32.4589
1830	189.28	62.978	4.75E+02	6.45E+01	3.07E+04	33.9827
1831	188.88	66.084	5.20E+02	6.76E+01	3.52E+04	36.1678
1832	188.44	69.104	5.71E+02	7.05E+01	4.02E+04	38.5466
1833	187.96	71.805	6.26E+02	7.28E+01	4.56E+04	40.7039
1834	187.43	73.766	6.88E+02	7.45E+01	5.13E+04	42.3567
1835	186.84	75.298	7.54E+02	7.58E+01	5.71E+04	43.7251
1836	186	76.276	8.26E+02	7.62E+01	6.29E+04	44.6124
1837	185.49	76.216	8.32E+02	7.57E+01	6.29E+04	44.6757
1838	184.78	75.1	9.01E+02	7.41E+01	6.68E+04	43.8479
1839	184	73.046	9.75E+02	7.16E+01	6.98E+04	42.208
1840	183.16	70.194	1.09E+03	6.85E+01	7.47E+04	39.9036
1841	182.21	66.732	1.14E+03	6.48E+01	7.40E+04	37.1719
1842	181.21	62.867	1.14E+03	6.09E+01	6.91E+04	34.1533
160	180.21	58.902	1.13E+03	5.69E+01	6.43E+04	31.2634
1843	179.21	54.994	1.23E+03	5.30E+01	6.54E+04	28.6092
1844	178.11	51.015	1.35E+03	4.90E+01	6.61E+04	26.0254
1845	176.90	46.919	1.47E+03	4.48E+01	6.60E+04	23.5266
1846	175.56	42.626	1.61E+03	4.05E+01	6.51E+04	21.084
1847	174	38.282	1.75E+03	3.61E+01	6.33E+04	18.8172
1848	172.5	33.93	1.91E+03	3.17E+01	6.05E+04	16.7762
1849	170.72	29.437	2.08E+03	2.71E+01	5.63E+04	14.8631
1850	168.77	24.771	2.26E+03	2.24E+01	5.07E+04	13.0075
1851	166.63	20.103	2.45E+03	1.78E+01	4.37E+04	11.3024
1852	164.27	15.541	2.66E+03	1.29E+01	3.44E+04	9.8467
1853	161.67	10.329	2.87E+03	6.96E+00	2.00E+04	8.3774
1854	158.82	3.5858	3.77E+03	-8.94E-01	-3.37E+03	6.9662
1855	155	-5.373	4.79E+03	-9.36E+00	-4.48E+04	6.9123
159	150	-13.34	7.07E+04	-6.67E+00		10.3903
				Tensile Force in Pin	1.42E+06	

BOX PRELOAD STRESS VALUES

NODE	X	S22	TRUE ELEMENT FORCE	AVE. NODAL STRESS	FORCE ON ELEMENT FACE	VON MISES STRESS
77	226.23	12.23	4.32E+03	1.07E+01	4.63E+04	28.4058
761	223.17	9.205	3.96E+03	7.44E+00	2.95E+04	26.6115
762	220.33	5.674	3.64E+03	4.19E+00	1.52E+04	29.84
763	217.68	2.707	3.34E+03	1.39E+00	4.66E+03	31.1222
764	215.23	8.07E-	3.07E+03	-1.06E+00	-3.24E+03	32.3629
765	212.94	-2.191	2.83E+03	-3.55E+00	-1.00E+04	33.5504
766	210.82	-4.904	2.60E+03	-6.79E+00	-1.77E+04	34.7262
767	208.84	-8.678	2.40E+03	-1.11E+01	-2.67E+04	36.057
78	207.01	-13.6	3.87E+03	-1.76E+01	-6.82E+04	37.7295
896	204.01	-21.6	2.20E+03	-2.52E+01	-5.55E+04	40.3574
895	202.29	-28.81	2.18E+03	-3.16E+01	-6.91E+04	43.3289
894	200.56	-34.48	1.26E+03	-3.69E+01	-4.64E+04	45.8252
82	199.56	-39.39	1.13E+03	-4.21E+01	-4.77E+04	47.2732
893	198.65	-44.73	1.03E+03	-4.68E+01	-4.82E+04	49.0608
892	197.83	-48.9	9.35E+02	-5.08E+01	-4.75E+04	50.872
891	197.07	-52.62	8.49E+02	-5.48E+01	-4.65E+04	52.6164
890	196.39	-56.99	7.71E+02	-5.94E+01	-4.58E+04	55.3869
889	195.76	-61.78	7.00E+02	-6.45E+01	-4.52E+04	58.5166
888	195.19	-67.32	6.38E+02	-6.96E+01	-4.44E+04	61.4211
887	194.67	-71.94	5.79E+02	-7.39E+01	-4.28E+04	63.5616
886	194.2	-75.96	5.27E+02	-7.79E+01	-4.10E+04	65.4486
885	193.76	-79.84	4.79E+02	-8.22E+01	-3.94E+04	67.2722
884	193.37	-84.53	4.36E+02	-8.73E+01	-3.80E+04	69.9446
883	193.01	-89.97	3.97E+02	-9.35E+01	-3.72E+04	72.8336
882	192.68	-97.02	3.60E+02	-1.04E+02	-3.74E+04	76.3982
881	192.38	-110.7	3.29E+02	-1.21E+02	-3.96E+04	84.0778
69	192.11	-130.4	1.16E+05	-6.52E+01		100.685
				Compressive Force in Box	-8.02E+05	

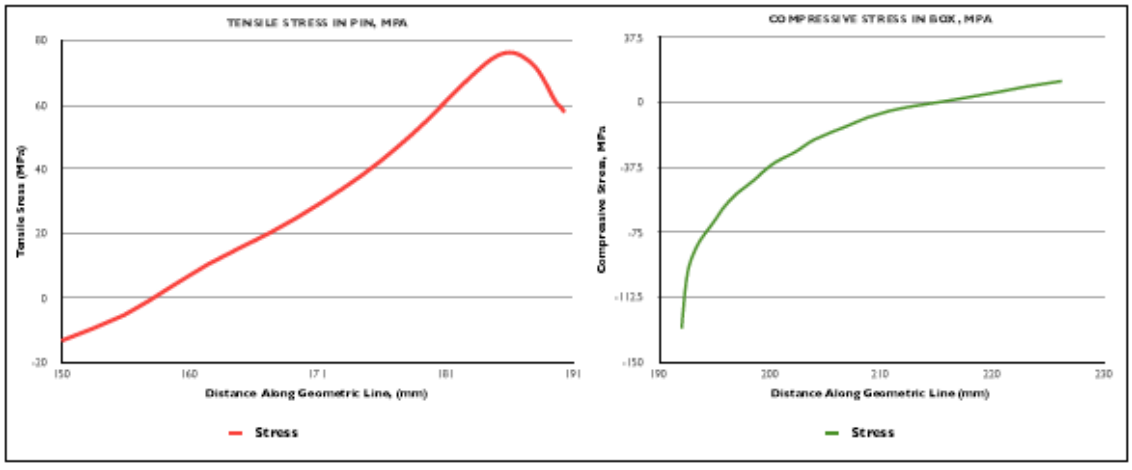

RESULTS SNAPSHOT - 150KN

COMPONENT	LENGTH (MM)	PEAK S22 STRESS (MPA)	PRELOAD FORCE IN COMPONENT (MN)
PIN	40.3	76.8	1.47
BOX	34.1	10.3	-0.54
		% Difference	-2.72

YIELD ANALYSIS - 150KN

COMPONENT	MATERIAL	YIELD STRENGTH	PEAK VON MISES STRESS
PIN	AL-MG-ZN-II	480.0	58.40
BOX	AL-MG-ZN-II	480.0	
		% of Yield	12.17

PIN PRELOAD STRESS VALUES

NODE	X	S22	TRUE ELEMENT FORCE	AVE. NODAL STRESS	FORCE ON ELEMENT FACE	VON MISES STRESS
158	190.27	58.188	3.58E+02	5.90E+01	2.11E+04	31.7051
1828	189.97	59.719	3.94E+02	6.03E+01	2.37E+04	32.1932
1829	189.64	60.957	4.32E+02	6.21E+01	2.68E+04	32.4589
1830	189.28	63.302	4.75E+02	6.49E+01	3.08E+04	33.9827
1831	188.88	66.401	5.20E+02	6.79E+01	3.53E+04	36.1678
1832	188.44	69.426	5.71E+02	7.08E+01	4.04E+04	38.5466
1833	187.96	72.146	6.26E+02	7.31E+01	4.58E+04	40.7039
1834	187.43	74.146	6.88E+02	7.49E+01	5.15E+04	42.3567
1835	186.84	75.734	7.54E+02	7.63E+01	5.75E+04	43.7251
1836	186	76.787	8.26E+02	7.68E+01	6.34E+04	44.6124
1837	185.49	76.817	8.32E+02	7.63E+01	6.35E+04	44.6757
1838	184.78	75.808	9.01E+02	7.48E+01	6.75E+04	43.8479
1839	184	73.879	9.75E+02	7.25E+01	7.07E+04	42.208
1840	183.16	71.167	1.09E+03	6.95E+01	7.58E+04	39.9036
1841	182.21	67.847	1.14E+03	6.60E+01	7.53E+04	37.1719
1842	181.21	64.113	1.14E+03	6.22E+01	7.06E+04	34.1533
160	180.21	60.263	1.13E+03	5.84E+01	6.59E+04	31.2634
1843	179.21	56.454	1.23E+03	5.45E+01	6.73E+04	28.6092
1844	178.11	52.563	1.35E+03	5.06E+01	6.82E+04	26.0254
1845	176.90	48.542	1.47E+03	4.64E+01	6.84E+04	23.5266
1846	175.56	44.311	1.61E+03	4.22E+01	6.78E+04	21.084
1847	174	40.009	1.75E+03	3.78E+01	6.63E+04	18.8172
1848	172.5	35.678	1.91E+03	3.34E+01	6.39E+04	16.7762
1849	170.72	31.182	2.08E+03	2.88E+01	5.99E+04	14.8631
1850	168.77	26.487	2.26E+03	2.41E+01	5.45E+04	13.0075
1851	166.63	21.764	2.45E+03	1.94E+01	4.77E+04	11.3024
1852	164.27	17.125	2.66E+03	1.45E+01	3.84E+04	9.8467
1853	161.67	11.812	2.87E+03	8.38E+00	2.41E+04	8.3774
1854	158.82	4.9402	3.77E+03	3.93E-01	1.48E+03	6.9682
1855	155	-4.154	4.79E+03	-8.18E+00	-3.92E+04	6.9123
159	150	-12.2	7.07E+04	-6.10E+00		10.3903
				Tensile Force in Pin	1.47E+06	

BOX PRELOAD STRESS VALUES

NODE	X	S22	TRUE ELEMENT FORCE	AVE. NODAL STRESS	FORCE ON ELEMENT FACE	VON MISES STRESS
77	226.23	10.29	4.32E+03	9.22E+00	3.98E+04	28.4058
761	223.17	8.154	3.96E+03	6.96E+00	2.76E+04	26.6115
762	220.33	5.763	3.64E+03	4.80E+00	1.75E+04	29.84
763	217.68	3.837	3.34E+03	3.04E+00	1.02E+04	31.1222
764	215.23	2.238	3.07E+03	1.56E+00	4.79E+03	32.3629
765	212.94	0.882	2.83E+03	4.22E-02	1.19E+02	33.5504
766	210.82	-0.797	2.60E+03	-2.07E+00	-5.39E+03	34.7262
767	208.84	-3.345	2.40E+03	-5.20E+00	-1.25E+04	36.057
78	207.01	-7.058	3.87E+03	-1.02E+01	-3.96E+04	37.7295
896	204.01	-13.39	2.20E+03	-1.64E+01	-3.62E+04	40.3574
895	202.29	-19.5	2.18E+03	-2.20E+01	-4.79E+04	43.3289
894	200.56	-24.42	1.26E+03	-2.65E+01	-3.33E+04	45.8252
82	199.56	-28.62	1.13E+03	-3.10E+01	-3.51E+04	47.2732
893	198.65	-33.31	1.03E+03	-3.52E+01	-3.62E+04	49.0608
892	197.83	-37.01	9.35E+02	-3.86E+01	-3.61E+04	50.872
891	197.07	-40.28	8.49E+02	-4.22E+01	-3.58E+04	52.6164
890	196.39	-44.09	7.71E+02	-4.62E+01	-3.56E+04	55.3869
889	195.76	-48.21	7.00E+02	-5.06E+01	-3.54E+04	58.5166
888	195.19	-52.95	6.38E+02	-5.49E+01	-3.50E+04	61.4211
887	194.67	-56.88	5.79E+02	-5.86E+01	-3.39E+04	63.5616
886	194.2	-60.26	5.27E+02	-6.18E+01	-3.26E+04	65.4486
885	193.76	-63.42	4.79E+02	-6.53E+01	-3.13E+04	67.2722
884	193.37	-67.19	4.36E+02	-6.94E+01	-3.02E+04	69.9446
883	193.01	-71.55	3.97E+02	-7.43E+01	-2.95E+04	72.8336
882	192.68	-77.13	3.60E+02	-8.26E+01	-2.98E+04	76.3982
881	192.38	-87.98	3.29E+02	-9.58E+01	-3.15E+04	84.0778
69	192.11	-103.6	1.16E+05	-5.18E+01		100.685
				Compressive Force in Box	-5.43E+05	

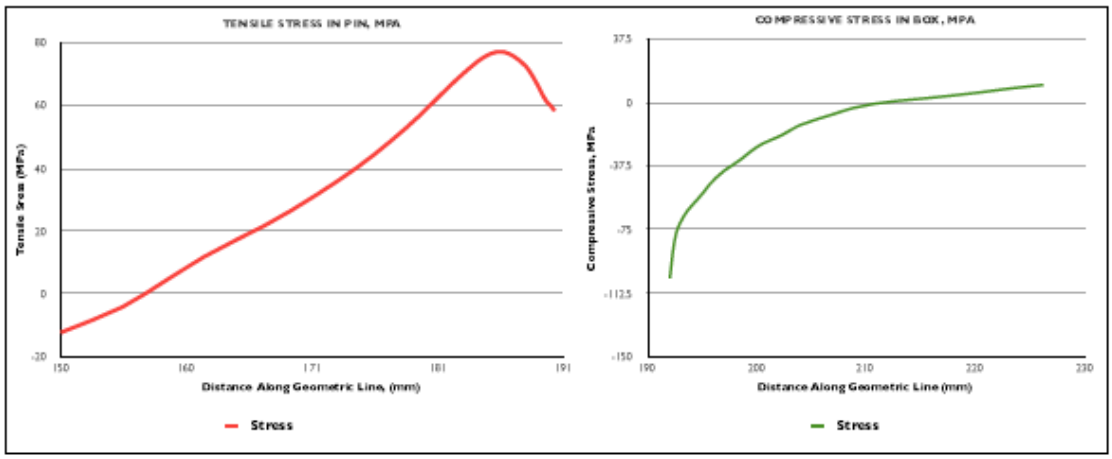

RESULTS SNAPSHOT-200KN

COMPONENT	LENGTH (MM)	PEAK S22 STRESS (MPA)	PRELOAD FORCE IN COMPONENT (MN)
PIN	40.3	92.2	1.88
BOX	34.1	3.7	-0.01
		% Difference	-252.51

YIELD ANALYSIS-200KN

COMPONENT	MATERIAL	YIELD STRENGTH	PEAK VON MISES STRESS
PIN	AL-MG-ZN-II	480.0	58.40
BOX	AL-MG-ZN-II	480.0	
		% of Yield	12.17

PIN PRELOAD STRESS VALUES

NODE	X	S22	TRUE ELEMENT FORCE	AVE. NODAL STRESS	FORCE ON ELEMENT FACE	VON MISES STRESS
158	190.27	69.085	3.58E+02	7.00E+01	2.51E+04	31.7051
1828	189.97	70.859	3.94E+02	7.16E+01	2.82E+04	32.1932
1829	189.64	72.32	4.32E+02	7.37E+01	3.18E+04	32.4589
1830	189.28	75.08	4.75E+02	7.69E+01	3.65E+04	33.9827
1831	188.88	78.735	5.20E+02	8.05E+01	4.19E+04	36.1678
1832	188.44	82.348	5.71E+02	8.40E+01	4.80E+04	38.5466
1833	187.96	85.649	6.26E+02	8.69E+01	5.44E+04	40.7039
1834	187.43	88.168	6.88E+02	8.92E+01	6.14E+04	42.3567
1835	186.84	90.268	7.54E+02	9.10E+01	6.86E+04	43.7251
1836	186	91.796	8.26E+02	9.20E+01	7.59E+04	44.6124
1837	185.49	92.169	8.32E+02	9.18E+01	7.63E+04	44.6757
1838	184.78	91.359	9.01E+02	9.04E+01	8.15E+04	43.8479
1839	184	89.505	9.75E+02	8.81E+01	8.59E+04	42.208
1840	183.16	86.764	1.09E+03	8.50E+01	9.27E+04	39.9036
1841	182.21	83.3	1.14E+03	8.13E+01	9.28E+04	37.1719
1842	181.21	79.309	1.14E+03	7.72E+01	8.77E+04	34.1533
160	180.21	75.117	1.13E+03	7.30E+01	8.24E+04	31.2634
1843	179.21	70.911	1.23E+03	6.87E+01	8.49E+04	28.6092
1844	178.11	66.562	1.35E+03	6.43E+01	8.68E+04	26.0254
1845	176.90	62.011	1.47E+03	5.96E+01	8.78E+04	23.5266
1846	175.56	57.158	1.61E+03	5.47E+01	8.79E+04	21.084
1847	174	52.151	1.75E+03	4.96E+01	8.69E+04	18.8172
1848	172.5	47.034	1.91E+03	4.43E+01	8.47E+04	16.7762
1849	170.72	41.637	2.08E+03	3.88E+01	8.06E+04	14.8631
1850	168.77	35.907	2.26E+03	3.30E+01	7.45E+04	13.0075
1851	166.63	30.051	2.45E+03	2.71E+01	6.65E+04	11.3024
1852	164.27	24.223	2.66E+03	2.09E+01	5.54E+04	9.8467
1853	161.67	17.495	2.87E+03	1.31E+01	3.78E+04	8.3774
1854	158.82	8.7951	3.77E+03	3.10E+00	1.17E+04	6.9682
1855	155	-2.601	4.79E+03	-7.57E+00	-3.62E+04	6.9123
159	150	-12.53	7.07E+04	-6.26E+00		10.3903
				Tensile Force in Pin	1.88E+06	

BOX PRELOAD STRESS VALUES

NODE	X	S22	TRUE ELEMENT FORCE	AVE. NODAL STRESS	FORCE ON ELEMENT FACE	VON MISES STRESS
77	226.23	3.691	4.32E+03	3.57E+00	1.54E+04	28.4058
761	223.17	3.447	3.96E+03	3.39E+00	1.34E+04	28.6115
762	220.33	3.329	3.64E+03	3.32E+00	1.21E+04	29.84
763	217.68	3.317	3.34E+03	3.39E+00	1.13E+04	31.1222
764	215.23	3.46	3.07E+03	3.50E+00	1.07E+04	32.3629
765	212.94	3.535	2.83E+03	3.55E+00	1.00E+04	33.5504
766	210.82	3.57	2.60E+03	3.51E+00	9.13E+03	34.7262
767	208.84	3.444	2.40E+03	3.22E+00	7.71E+03	36.057
78	207.01	2.988	3.87E+03	2.38E+00	9.21E+03	37.7295
896	204.01	1.766	2.20E+03	1.08E+00	2.39E+03	40.3574
895	202.29	0.403	2.18E+03	-3.06E-01	-6.73E+02	43.3289
894	200.56	-1.02	1.26E+03	-1.72E+00	-2.16E+03	45.8252
82	199.56	-2.422	1.13E+03	-3.32E+00	-3.76E+03	47.2732
893	198.65	-4.217	1.03E+03	-5.01E+00	-5.16E+03	49.0608
892	197.83	-5.806	9.35E+02	-6.47E+00	-6.05E+03	50.872
891	197.07	-7.124	8.49E+02	-7.93E+00	-6.73E+03	52.6164
890	196.39	-8.726	7.71E+02	-9.63E+00	-7.43E+03	55.3869
889	195.76	-10.53	7.00E+02	-1.16E+01	-8.10E+03	58.5166
888	195.19	-12.6	6.38E+02	-1.35E+01	-8.64E+03	61.4211
887	194.67	-14.48	5.79E+02	-1.53E+01	-8.83E+03	63.5616
886	194.2	-16.03	5.27E+02	-1.66E+01	-8.72E+03	65.4486
885	193.76	-17.09	4.79E+02	-1.77E+01	-8.50E+03	67.2722
884	193.37	-18.4	4.36E+02	-1.92E+01	-8.36E+03	69.9446
883	193.01	-19.96	3.97E+02	-2.09E+01	-8.29E+03	72.8336
882	192.68	-21.77	3.60E+02	-2.35E+01	-8.47E+03	76.3982
881	192.38	-25.23	3.29E+02	-2.75E+01	-9.03E+03	84.0778
69	192.11	-29.71	1.16E+05	-1.49E+01		100.685
				Compressive Force in Box	-7.45E+03	

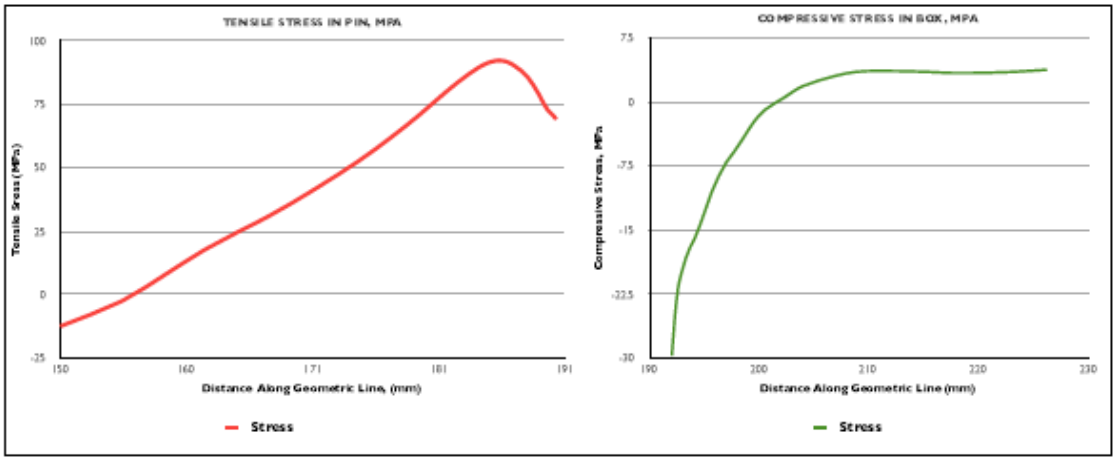

RESULTS SNAPSHOT-400KN

COMPONENT	LENGTH (MM)	PEAK S22 STRESS (MPA)	PRELOAD FORCE IN COMPONENT (MN)
PIN	40.3	123.4	2.51
BOX	34.1	5.0	-0.01
		%Difference	-260.07

YIELD ANALYSIS-400KN

COMPONENT	MATERIAL	YIELD STRENGTH	PEAK VON MISES STRESS
PIN	AL-MG-ZN-II	480.0	58.40
BOX	AL-MG-ZN-II	480.0	
		% of Yield	12.17

PIN PRELOAD STRESS VALUES

NODE	X	S22	TRUE ELEMENT FORCE	AVE. NODAL STRESS	FORCE ON ELEMENT FACE	VON MISES STRESS
158	190.27	92.53	3.58E+02	9.37E+01	3.36E+04	31.7051
1828	189.97	94.897	3.94E+02	9.59E+01	3.77E+04	32.1932
1829	189.64	96.842	4.32E+02	9.87E+01	4.26E+04	32.4589
1830	189.28	100.53	4.75E+02	1.03E+02	4.89E+04	33.9627
1831	188.88	105.42	5.20E+02	1.08E+02	5.61E+04	36.1678
1832	188.44	110.24	5.71E+02	1.12E+02	6.42E+04	38.5466
1833	187.96	114.65	6.26E+02	1.16E+02	7.29E+04	40.7039
1834	187.43	118.02	6.88E+02	1.19E+02	8.21E+04	42.3567
1835	186.84	120.83	7.54E+02	1.22E+02	9.18E+04	43.7251
1836	186	122.87	8.26E+02	1.23E+02	1.02E+05	44.6124
1837	185.49	123.37	8.32E+02	1.23E+02	1.02E+05	44.6757
1838	184.78	122.29	9.01E+02	1.21E+02	1.09E+05	43.8479
1839	184	119.81	9.75E+02	1.18E+02	1.15E+05	42.208
1840	183.16	116.14	1.09E+03	1.14E+02	1.24E+05	39.9036
1841	182.21	111.51	1.14E+03	1.09E+02	1.24E+05	37.1719
1842	181.21	106.17	1.14E+03	1.03E+02	1.17E+05	34.1533
160	180.21	100.55	1.13E+03	9.77E+01	1.10E+05	31.2634
1843	179.21	94.916	1.23E+03	9.20E+01	1.14E+05	28.6092
1844	178.11	89.084	1.35E+03	8.60E+01	1.16E+05	26.0254
1845	176.90	82.976	1.47E+03	7.97E+01	1.17E+05	23.5266
1846	175.56	76.457	1.61E+03	7.31E+01	1.18E+05	21.064
1847	174	69.727	1.75E+03	6.63E+01	1.16E+05	18.8172
1848	172.5	62.842	1.91E+03	5.92E+01	1.13E+05	16.7762
1849	170.72	55.575	2.08E+03	5.17E+01	1.07E+05	14.8631
1850	168.77	47.854	2.26E+03	4.39E+01	9.91E+04	13.0075
1851	166.63	39.962	2.45E+03	3.60E+01	8.63E+04	11.3024
1852	164.27	32.102	2.66E+03	2.76E+01	7.32E+04	9.8467
1853	161.67	23.028	2.87E+03	1.72E+01	4.93E+04	8.3774
1854	158.82	11.291	3.77E+03	3.60E+00	1.36E+04	6.9682
1855	155	-4.086	4.79E+03	-1.08E+01	-5.17E+04	6.9123
159	150	-17.48	7.07E+04	-8.74E+00		10.3903
				Tensile Force in Pin	2.51E+06	

BOX PRELOAD STRESS VALUES

NODE	X	S22	TRUE ELEMENT FORCE	AVE. NODAL STRESS	FORCE ON ELEMENT FACE	VON MISES STRESS
77	226.23	4.991	4.32E+03	4.83E+00	2.09E+04	28.4058
761	223.17	4.665	3.96E+03	4.58E+00	1.81E+04	26.6115
762	220.33	4.499	3.64E+03	4.48E+00	1.63E+04	29.84
763	217.68	4.469	3.34E+03	4.56E+00	1.52E+04	31.1222
764	215.23	4.646	3.07E+03	4.69E+00	1.44E+04	32.3829
765	212.94	4.733	2.83E+03	4.75E+00	1.34E+04	33.5504
766	210.82	4.766	2.60E+03	4.67E+00	1.22E+04	34.7262
767	208.84	4.584	2.40E+03	4.27E+00	1.02E+04	36.057
78	207.01	3.963	3.87E+03	3.14E+00	1.22E+04	37.7295
896	204.01	2.321	2.20E+03	1.41E+00	3.10E+03	40.3574
895	202.29	0.494	2.18E+03	-4.56E-01	-9.96E+02	43.3289
894	200.56	-1.406	1.26E+03	-2.34E+00	-2.94E+03	45.6252
82	199.56	-3.274	1.13E+03	-4.47E+00	-5.07E+03	47.2732
893	198.65	-5.666	1.03E+03	-6.72E+00	-6.93E+03	49.0608
892	197.83	-7.781	9.35E+02	-8.66E+00	-8.10E+03	50.872
891	197.07	-9.535	8.49E+02	-1.06E+01	-9.00E+03	52.6164
890	196.39	-11.67	7.71E+02	-1.29E+01	-9.93E+03	55.3869
889	195.76	-14.07	7.00E+02	-1.55E+01	-1.08E+04	58.5166
888	195.19	-16.83	6.38E+02	-1.81E+01	-1.15E+04	61.4211
887	194.67	-19.33	5.79E+02	-2.04E+01	-1.18E+04	63.5616
886	194.2	-21.39	5.27E+02	-2.21E+01	-1.16E+04	65.4486
885	193.76	-22.81	4.79E+02	-2.37E+01	-1.14E+04	67.2722
884	193.37	-24.56	4.36E+02	-2.56E+01	-1.12E+04	69.9446
883	193.01	-26.65	3.97E+02	-2.79E+01	-1.11E+04	72.6336
882	192.68	-29.08	3.60E+02	-3.14E+01	-1.13E+04	76.3982
881	192.38	-33.7	3.29E+02	-3.67E+01	-1.21E+04	84.0778
69	192.11	-39.69	1.16E+05	-1.98E+01		100.685
				Compressive P Force in Box	-9.64E+03	

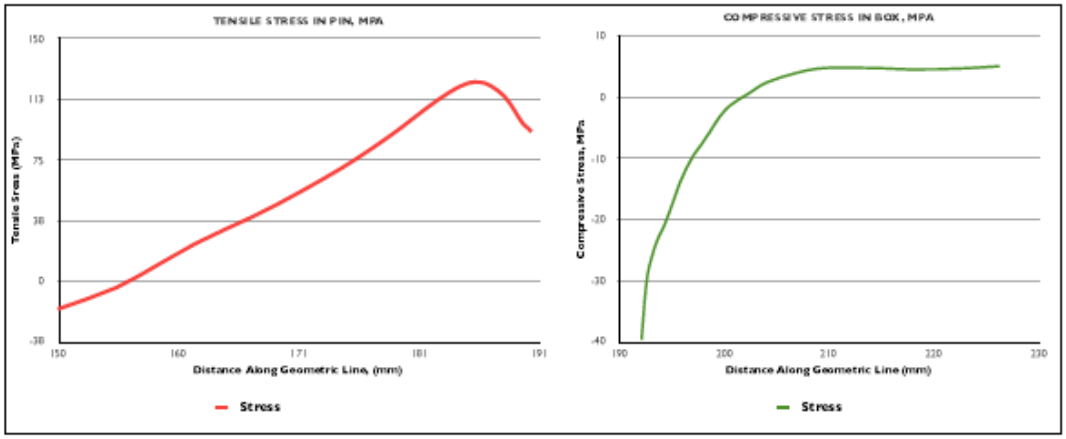

RESULTS SNAPSHOT-500KN

COMPONENT	LENGTH (MM)	PEAK S22 STRESS (MPA)	PRELOAD FORCE IN COMPONENT (MN)
PIN	40.3	153.7	3.13
BOX	34.1	6.2	-0.01
		%Difference	-268.19

YIELD ANALYSIS-500KN

COMPONENT	MATERIAL	YIELD STRENGTH	PEAK VON MISES STRESS
PIN	AL-MG-ZN-II	480.0	58.40
BOX	AL-MG-ZN-II	480.0	
		% of Yield	12.17

PIN PRELOAD STRESS VALUES

NODE	X	S22	TRUE ELEMENT FORCE	AVE. NODAL STRESS	FORCE ON ELEMENT FACE	VON MISES STRESS
158	190.27	115.29	3.58E+02	1.17E+02	4.18E+04	31.7051
1828	189.97	118.23	3.94E+02	1.19E+02	4.70E+04	32.1932
1829	189.64	120.65	4.32E+02	1.23E+02	5.31E+04	32.4589
1830	189.28	125.24	4.75E+02	1.28E+02	6.10E+04	33.9627
1831	188.88	131.31	5.20E+02	1.34E+02	6.99E+04	36.1678
1832	188.44	137.31	5.71E+02	1.40E+02	8.00E+04	38.5466
1833	187.96	142.80	6.26E+02	1.45E+02	9.07E+04	40.7039
1834	187.43	147.00	6.88E+02	1.49E+02	1.02E+05	42.3567
1835	186.84	150.49	7.54E+02	1.52E+02	1.14E+05	43.7251
1836	186	153.05	8.26E+02	1.53E+02	1.27E+05	44.6124
1837	185.49	153.68	8.32E+02	1.53E+02	1.27E+05	44.6757
1838	184.78	152.35	9.01E+02	1.51E+02	1.36E+05	43.8479
1839	184	149.29	9.75E+02	1.47E+02	1.43E+05	42.208
1840	183.16	144.75	1.09E+03	1.42E+02	1.55E+05	39.9036
1841	182.21	139.01	1.14E+03	1.36E+02	1.55E+05	37.1719
1842	181.21	132.39	1.14E+03	1.29E+02	1.46E+05	34.1533
160	180.21	125.43	1.13E+03	1.22E+02	1.38E+05	31.2634
1843	179.21	118.44	1.23E+03	1.15E+02	1.42E+05	28.6092
1844	178.11	111.20	1.35E+03	1.07E+02	1.45E+05	26.0254
1845	176.90	103.62	1.47E+03	9.96E+01	1.47E+05	23.5266
1846	175.56	95.52	1.61E+03	9.13E+01	1.47E+05	21.084
1847	174	87.15	1.75E+03	8.29E+01	1.45E+05	18.8172
1848	172.5	78.60	1.91E+03	7.41E+01	1.42E+05	16.7762
1849	170.72	69.56	2.08E+03	6.48E+01	1.35E+05	14.8631
1850	168.77	59.95	2.26E+03	5.50E+01	1.24E+05	13.0075
1851	166.63	50.13	2.45E+03	4.52E+01	1.11E+05	11.3024
1852	164.27	40.34	2.66E+03	3.47E+01	9.21E+04	9.8467
1853	161.67	29.04	2.87E+03	2.17E+01	6.24E+04	8.3774
1854	158.82	14.43	3.77E+03	4.86E+00	1.83E+04	6.9682
1855	155	-4.71	4.79E+03	-1.30E+01	-6.25E+04	6.9123
159	150	-21.37	7.07E+04	-1.07E+01		10.3903
				Tensile Force in Pin	3.13E+06	

BOX PRELOAD STRESS VALUES

NODE	X	S22	TRUE ELEMENT FORCE	AVE. NODAL STRESS	FORCE ON ELEMENT FACE	VON MISES STRESS
77	226.23	6.21	4.32E+03	6.01E+00	2.59E+04	28.4058
761	223.17	5.80	3.96E+03	5.69E+00	2.25E+04	28.6115
762	220.33	5.59	3.64E+03	5.57E+00	2.03E+04	29.84
763	217.68	5.55	3.34E+03	5.66E+00	1.89E+04	31.1222
764	215.23	5.78	3.07E+03	5.84E+00	1.79E+04	32.3829
765	212.94	5.89	2.83E+03	5.92E+00	1.67E+04	33.5504
766	210.82	5.94	2.60E+03	5.84E+00	1.52E+04	34.7262
767	208.84	5.73	2.40E+03	5.34E+00	1.28E+04	36.057
78	207.01	4.96	3.87E+03	3.94E+00	1.53E+04	37.7295
896	204.01	2.92	2.20E+03	1.79E+00	3.93E+03	40.3574
895	202.29	0.65	2.18E+03	-5.30E-01	-1.16E+03	43.3289
894	200.56	-1.71	1.26E+03	-2.88E+00	-3.62E+03	45.8252
82	199.56	-4.04	1.13E+03	-5.53E+00	-6.27E+03	47.2732
893	198.65	-7.03	1.03E+03	-8.35E+00	-8.60E+03	49.0608
892	197.83	-9.67	9.35E+02	-1.08E+01	-1.01E+04	50.872
891	197.07	-11.86	8.49E+02	-1.32E+01	-1.12E+04	52.6164
890	196.39	-14.53	7.71E+02	-1.60E+01	-1.24E+04	55.3869
889	195.76	-17.53	7.00E+02	-1.92E+01	-1.35E+04	58.5166
888	195.19	-20.97	6.38E+02	-2.25E+01	-1.44E+04	61.4211
887	194.67	-24.09	5.79E+02	-2.54E+01	-1.47E+04	63.5616
886	194.2	-26.66	5.27E+02	-2.75E+01	-1.45E+04	65.4486
885	193.76	-28.43	4.79E+02	-2.95E+01	-1.41E+04	67.2722
884	193.37	-30.59	4.36E+02	-3.19E+01	-1.39E+04	69.9446
883	193.01	-33.18	3.97E+02	-3.47E+01	-1.38E+04	72.8336
882	192.68	-36.18	3.60E+02	-3.90E+01	-1.41E+04	76.3982
881	192.38	-41.92	3.29E+02	-4.56E+01	-1.50E+04	84.0778
69	192.11	-49.34	1.16E+05	-2.47E+01		100.685
				Compressive Force in Box	-1.17E+04	

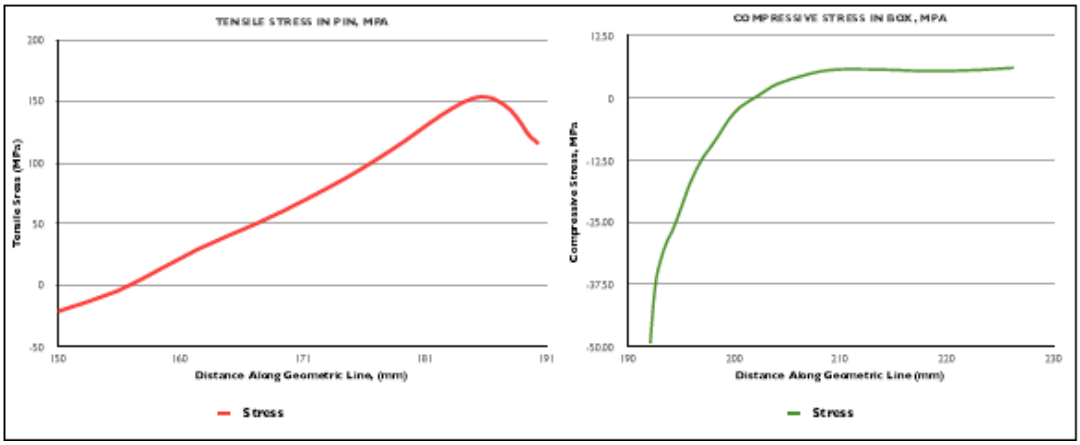

8.4.3 Titanium Alloy – TI-6AL-4V Simulation Results

8.4.3.1 Simulation Results Summary

CUMULATIVE PRELOAD FORCE DUE TO OVERLAP

OVERLAP AMOUNT (MM)		+VE FORCE IN PIN (MN)	-VE FORCE IN BOX (MN)	% DIFF.
0.05		0.4	-0.4	-0.99
0.10		0.8	-0.8	-0.99
0.15		1.1	-1.1	-0.99
0.20		1.5	-1.5	-0.99
0.25		1.8	-1.8	-0.99
0.30		2.2	-2.2	-0.99
0.35		2.5	-2.5	-0.99
0.40		4.6	-4.6	-0.99

TITANIUM ALLOY: OVERLAP VALUE PLOTTED AGAINST INDUCED PRELOAD FORCE

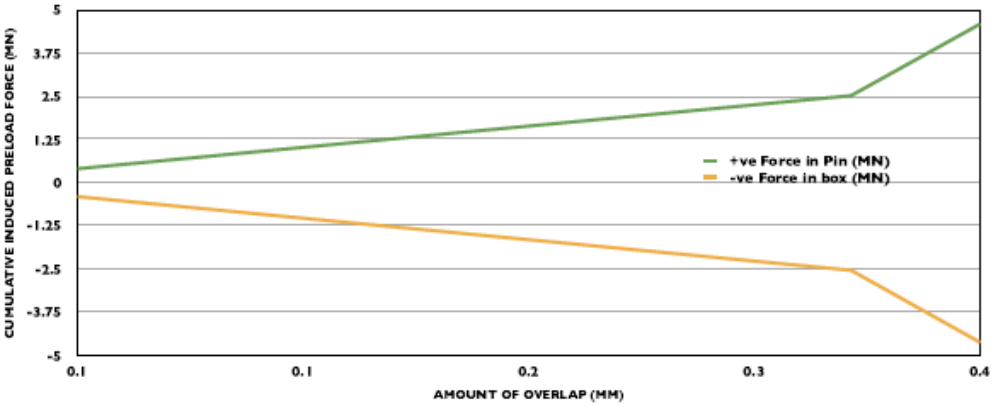

FORCE DUE TO AXIAL LOAD

AXIAL FORCE IN CONNECTOR		+VE FORCE IN PIN (MN)	-VE FORCE IN BOX (MN)	% DIFF.
0	0	2.50800	-2.53600	-0.99
2	2	2.51000	-2.52600	-0.99
100	100	2.61000	-2.00900	-1.30
150	150	2.66100	-1.74500	-1.52
250	250	2.76600	-1.22000	-2.27
450	450	3.70500	-0.10000	-37.05
550	550	3.44600	-0.02000	-172.30
600	600	3.75900	-0.02000	-187.95
1000	1000	6.26800	-0.03000	-208.93

TITANIUM ALLOY: FORCE IN CONNECTION DUE TO COMBINED PRELOAD AND AXIAL LOAD

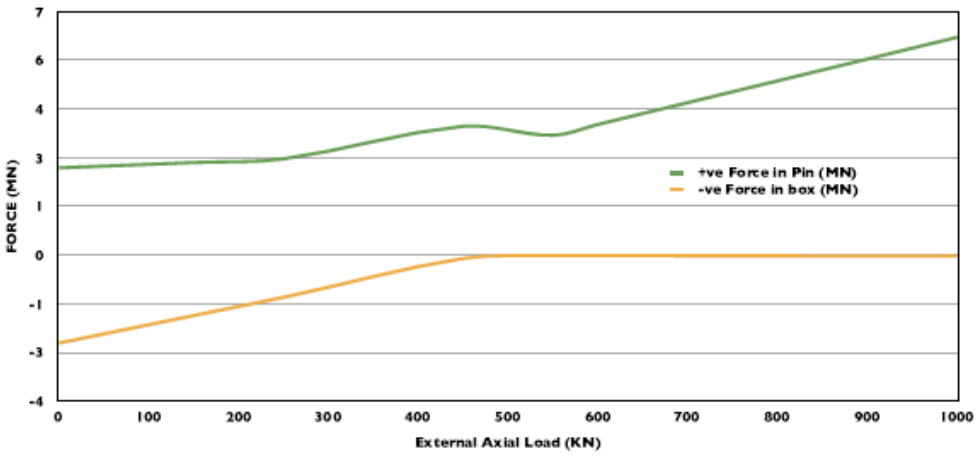

TITANIUM ALLOY YIELD ANALYSIS

OVERLAP AMOUNT (MM)	MATERIAL		YIELD STRENGTH	PEAK VON MISES STRESS	VON MISES STRESS @ 0.35MM	% OF YIELD STRENGTH	AXIAL LOAD (KN)	VON MISES STRESS (MPA)
0.05	Ti 6Al-4V	0.05	880.0	97.19	597.30	11.04	0.00	599.80
0.10	Ti 6Al-4V	0.10	880.0	182.7	597.30	20.76	20.00	599.10
0.15	Ti 6Al-4V	0.15	880.0	267.5	597.30	30.40	100.00	599.10
0.20	Ti 6Al-4V	0.20	880.0	351.5	597.30	39.94	150.00	597.70
0.25	Ti 6Al-4V	0.25	880.0	413.3	597.30	46.97	250.00	595.90
0.30	Ti 6Al-4V	0.30	880.0	514.4	597.30	58.45	450.00	597.70
0.35	Ti 6Al-4V	0.35	880.0	597.3	597.30	67.88	550.00	659.70
0.40	Ti 6Al-4V	0.40	880.0	688.1	597.30	78.19	600.00	718.70
							1,000.00	1180

TITANIUM ALLOY: FAILURE ANALYSIS USING THE VON MISES YIELD CRITERION

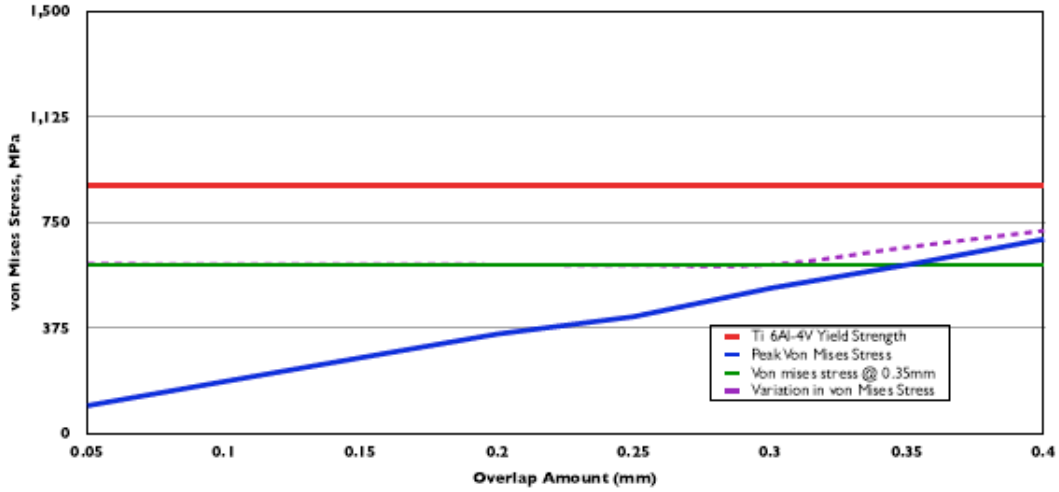

TITANIUM ALLOY: AXIAL TENSILE LOAD PLOTTED AGAINST VON MISES STRESS

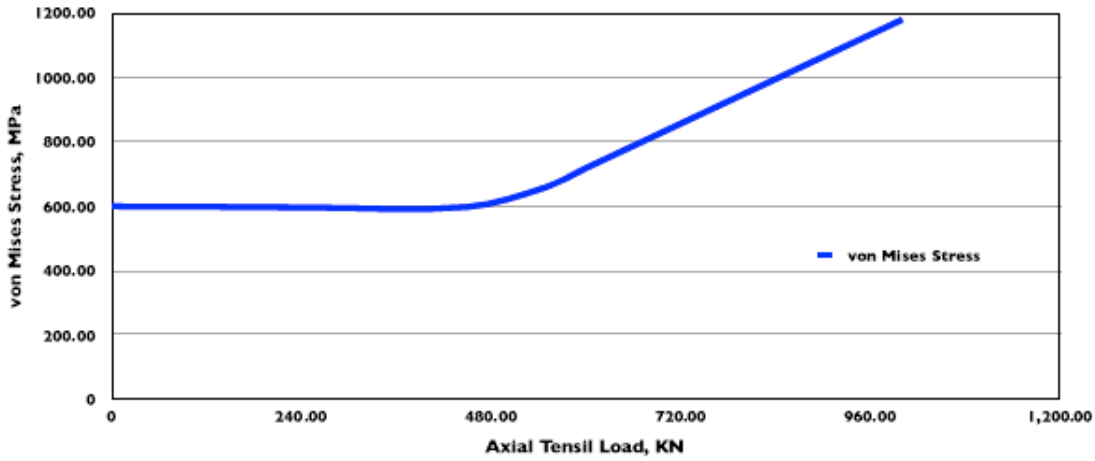

8.4.3.2 Induced Stress in Pin and Box Due to Preload and Axial Load

		Preload Induced Stress (MPa)								Axial Load Induced Stress (MPa)								
		0.05mm	0.1mm	0.15mm	0.2mm	0.25mm	0.3mm	0.35mm	0.4mm	20 N	2KN	100KN	150KN	250KN	450KN	550KN	600KN	1MN
BOX	226.23	2.23	4.14	6.06	8.01	9.93	11.91	13.90	26.07	17.16	17.17	17.32	17.39	16.49	9.63	6.95	7.60	13.27
BOX	223.17	0.36	0.61	0.89	1.18	1.45	1.77	2.11	4.37	5.45	5.51	8.17	9.53	11.07	8.36	6.48	7.08	12.32
BOX	220.33	-1.24	-2.41	-3.55	-4.68	-5.82	-6.92	-8.01	-14.28	-4.56	-4.46	0.53	3.08	6.85	7.15	6.20	6.77	11.68
BOX	217.68	-2.69	-5.12	-7.53	-9.93	-12.35	-14.71	-17.07	-30.96	-14.40	-14.25	-6.96	-3.25	2.83	6.37	6.15	6.72	11.47
BOX	215.23	-3.90	-7.40	-10.87	-14.33	-17.81	-21.24	-24.66	-44.96	-22.99	-22.80	-13.58	-8.88	-0.81	5.79	6.30	6.88	11.62
BOX	212.94	-5.11	-9.67	-14.21	-18.72	-23.27	-27.75	-32.23	-58.89	-31.00	-30.78	-19.89	-14.35	-4.41	5.24	6.34	6.92	11.61
BOX	210.82	-6.63	-12.52	-18.38	-24.21	-30.07	-35.87	-41.66	-76.17	-41.49	-41.23	-28.58	-22.13	-10.07	4.80	6.48	7.07	11.78
BOX	208.84	-8.43	-15.89	-23.32	-30.73	-38.15	-45.52	-52.89	-96.75	-53.78	-53.49	-39.32	-32.08	-18.05	3.60	6.18	6.74	11.15
BOX	207.01	-11.10	-20.89	-30.67	-40.43	-50.19	-59.92	-69.66	-127.83	-72.30	-71.98	-56.04	-47.91	-31.38	1.40	5.32	5.80	9.51
BOX	204.01	-13.90	-26.16	-38.41	-50.66	-62.89	-75.14	-87.40	-160.71	-88.21	-87.86	-70.86	-62.18	-44.09	-3.00	3.09	3.37	5.34
BOX	202.29	-15.88	-29.87	-43.86	-57.84	-71.78	-85.84	-99.86	-183.42	-99.96	-99.61	-82.01	-73.00	-53.97	-7.73	0.54	0.59	0.62
BOX	200.56	-16.95	-31.88	-46.82	-61.76	-76.64	-91.78	-106.79	-196.21	-110.36	-109.99	-91.72	-82.44	-62.44	-11.89	-2.08	-2.27	-4.19
BOX	199.56	-18.38	-34.57	-50.77	-66.96	-83.07	-99.54	-115.82	-212.74	-121.60	-121.22	-102.31	-92.88	-71.96	-15.58	-4.59	-5.00	-8.74
BOX	198.65	-19.77	-37.17	-54.59	-71.99	-89.27	-106.94	-124.40	-228.24	-130.38	-129.99	-110.60	-100.97	-79.38	-20.04	-7.83	-8.55	-14.65
BOX	197.83	-20.99	-39.47	-57.96	-76.44	-94.76	-113.46	-131.96	-242.26	-138.36	-137.96	-118.09	-108.26	-86.01	-23.81	-10.76	-11.74	-19.96
BOX	197.07	-22.93	-43.11	-63.29	-83.47	-103.43	-123.77	-143.94	-264.49	-148.01	-147.59	-127.06	-116.75	-93.66	-27.05	-13.19	-14.40	-24.38
BOX	196.39	-25.22	-47.40	-69.56	-91.69	-113.54	-136.15	-158.26	-289.40	-159.43	-159.00	-137.59	-126.19	-102.07	-30.90	-16.16	-17.64	-29.74
BOX	195.76	-27.22	-51.13	-75.01	-98.82	-122.33	-147.00	-170.91	-309.89	-170.77	-170.32	-148.02	-137.20	-111.78	-35.41	-19.74	-21.55	-36.21
BOX	195.19	-28.66	-53.82	-78.92	-103.97	-128.63	-154.02	-179.06	-324.49	-180.65	-180.18	-157.01	-146.13	-119.62	-39.96	-23.42	-25.57	-42.86
BOX	194.67	-29.94	-56.20	-82.38	-108.50	-134.20	-160.11	-186.07	-337.89	-191.48	-190.99	-166.73	-153.86	-126.30	-43.60	-26.27	-28.67	-47.97
BOX	194.2	-31.37	-58.87	-86.25	-113.56	-140.39	-167.39	-194.45	-353.03	-201.26	-200.75	-175.45	-161.54	-132.79	-47.28	-29.11	-31.77	-53.06
BOX	193.76	-33.25	-62.36	-91.34	-120.20	-148.51	-177.04	-205.55	-372.85	-213.64	-213.10	-186.34	-170.95	-140.62	-50.39	-31.43	-34.30	-57.21
BOX	193.37	-35.26	-66.10	-96.75	-127.26	-157.18	-187.31	-217.36	-393.59	-225.61	-225.04	-196.82	-181.99	-149.75	-54.16	-34.29	-37.41	-62.31
BOX	193.01	-37.92	-71.08	-103.97	-136.61	-168.75	-200.95	-233.06	-419.98	-242.11	-241.50	-211.17	-196.23	-161.43	-57.69	-36.92	-40.29	-67.02
BOX	192.68	-43.01	-80.53	-117.72	-154.39	-190.61	-227.03	-263.03	-470.84	-275.55	-274.85	-240.27	-223.45	-183.72	-62.03	-39.90	-43.52	-72.33
BOX	192.38	-50.74	-94.80	-138.32	-181.24	-223.27	-266.42	-308.18	-547.18	-325.65	-324.82	-283.81	-263.91	-216.82	9.63	-46.14	-50.32	-83.53
BOX	192.11	17.49	32.93	48.34	63.70	78.96	94.27	109.55	200.17	109.35	109.36	109.76	109.96	110.46	8.36	-54.39	-59.32	-98.38
PIN	190.27	17.97	33.85	49.69	65.47	81.16	96.90	112.60	205.70	112.38	112.39	112.74	112.92	113.37	113.38	126.57	138.12	231.41
PIN	189.97	18.36	34.59	50.76	66.89	82.91	98.99	115.02	210.10	114.79	114.80	115.12	115.28	115.71	116.30	129.81	141.65	237.26
PIN	189.64	19.09	35.96	52.77	69.54	86.20	102.92	119.58	218.39	119.33	119.33	119.62	119.76	120.16	118.68	132.47	144.55	242.03
PIN	189.28	20.04	37.75	55.40	73.00	90.49	108.03	125.52	229.20	125.24	125.25	125.48	125.60	125.97	123.21	137.52	150.05	251.18
PIN	188.88	20.97	39.48	57.95	76.35	94.65	112.99	131.28	239.69	130.97	130.98	131.19	131.30	131.65	129.13	144.12	157.25	263.15
PIN	188.44	21.78	41.02	60.20	79.32	98.34	117.40	136.39	249.01	136.06	136.06	136.28	136.39	136.76	134.98	150.67	164.39	275.02
PIN	187.96	22.36	42.11	61.81	81.43	100.97	120.53	140.03	255.64	139.67	139.68	139.93	140.06	140.49	140.32	156.66	170.92	285.88
PIN	187.43	22.80	42.94	63.02	83.03	102.96	122.91	142.79	260.71	142.41	142.42	142.75	142.92	143.43	144.35	161.23	175.90	294.15
PIN	186.84	23.06	43.43	63.74	83.99	104.16	124.34	144.45	263.77	144.04	144.05	144.50	144.72	145.37	147.68	165.05	180.07	301.05
PIN	186	23.00	43.31	63.56	83.75	103.87	124.00	144.07	263.12	143.64	143.65	144.25	144.54	145.35	150.06	167.84	183.10	306.09
PIN	185.49	22.59	42.55	62.45	82.29	102.07	121.86	141.58	258.65	141.14	141.15	141.93	142.33	143.34	150.53	168.51	183.84	307.30
PIN	184.78	21.89	41.23	60.52	79.74	98.94	118.12	137.23	250.80	136.79	136.81	137.82	138.33	139.58	149.03	167.01	182.20	304.54
PIN	184	20.93	39.43	57.88	76.28	94.66	113.02	131.31	240.06	130.87	130.89	132.17	132.82	134.35	145.83	163.62	178.51	298.35
PIN	183.16	19.79	37.28	54.72	72.12	89.52	106.89	124.20	227.19	123.76	123.79	125.34	126.13	127.95	141.17	158.62	173.06	289.24
PIN	182.21	18.52	34.90	51.23	67.52	83.84	100.11	116.33	212.91	115.89	115.93	117.75	118.67	120.75	135.32	152.29	166.16	277.71
PIN	181.21	17.24	32.49	47.70	62.87	78.08	93.24	108.35	198.41	107.92	107.97	110.02	111.06	113.38	128.61	144.99	158.19	264.41
PIN	180.21	15.99	30.13	44.24	58.31	72.44	86.51	100.53	184.17	100.12	100.17	102.43	103.58	106.11	121.62	137.35	148.86	250.49
PIN	179.21	14.72	27.74	40.73	53.70	66.72	79.68	92.60	169.72	92.21	92.25	94.71	95.96	98.68	114.65	129.68	141.50	236.53
PIN	178.11	13.42	25.30	37.15	48.97	60.86	72.68	84.47	154.88	84.10	84.15	86.79	88.13	91.02	107.45	121.76	132.85	222.08
PIN	176.90	12.07	22.75	33.41	44.05	54.75	65.39	76.00	139.39	75.66	75.71	78.50	79.92	82.96	99.94	113.46	123.81	206.95
PIN	175.56	10.72	20.20	29.66	39.11	48.60	58.05	67.47	123.78	67.17	67.22	70.14	71.63	74.78	91.96	104.61	114.15	190.79
PIN	174	9.37	17.66	25.94	34.20	42.50	50.76	59.00	108.23	58.74	58.80	61.81	63.34	66.57	83.75	95.47	104.18	174.10
PIN	172.5	8.00	15.07	22.13	29.18	36.25	43.30	50.33	92.28	50.11	50.17	53.25	54.81	58.08	75.40	86.14	94.00	157.03
PIN	170.72	6.58	12.40	18.21	24.01	29.81	35.60	41.38	75.81	41.23	41.30	44.40	45.97	49.23	66.63	76.31	83.27	139.03
PIN	168.77	5.17	9.75	14.31	18.87	23.39	27.94	32.47	59.38	32.40	32.46	35.55	37.12	40.33	57.36	65.88	71.89	119.90
PIN	166.63	3.81	7.17	10.53	13.87	17.17	20.50	23.82	43.41	23.83	23.89	26.93	28.48	31.60	47.90	55.20	60.22	100.29
PIN	164.27	2.26	4.25	6.24	8.21	10.10	12.05	14.00	25.26	14.12	14.18	17.14	18.66	21.65	38.52	44.56	48.61	80.74
PIN	161.67	0.25	0.47	0.67	0.86	0.93	1.10	1.26	1.72	1.51	1.57	4.45	5.92	8.76	27.74	32.32	35.25	58.23
PIN	158.82	-2.43	-4.59	-6.77	-8.96	-11.32	-13.54	-15.76	-29.71	-15.33	-15.27	-12.45	-11.00	-8.31	13.78	16.48	17.95	29.06
PIN	155	-4.89	-9.24	-13.60	-17.96	-22.55	-26.96	-31.36	-58.50	-30.80	-30.74	-27.89	-26.43	-23.79	113.38	-4.26	-4.70	-9.07
PIN	150	3.73	6.97	10.22	13.49	16.73	20.02	23.34	43.38	26.80	26.77	25.05	24.16	21.39	116.30	-22.73	-24.86	-43.02

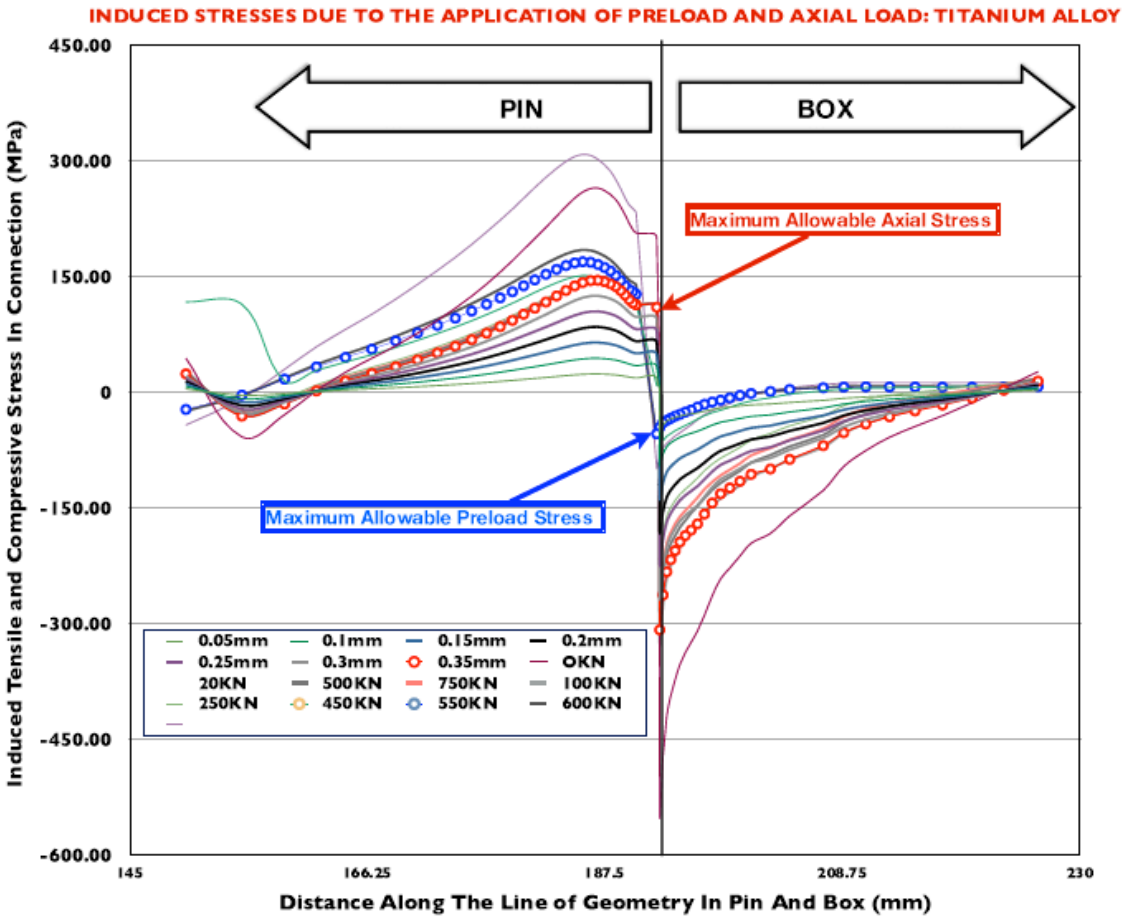
INDUCED STRESSES DUE TO THE APPLICATION OF PRELOAD AND AXIAL LOAD: TITANIUM ALLOY
PIN
BOX
Maximum Allowable Axial Stress
Maximum Allowable Preload Stress
0.05mm
0.1mm
0.15mm
0.2mm
0.25mm
0.3mm
0.35mm
0KN
20KN
500KN
750KN
100KN
250KN
450KN
550KN
600KN
450.00
300.00
150.00
0
-150.00
-300.00
-450.00
-600.00
145
166.25
187.5
208.75
230
Induced Tensile and Compressive Stress In Connection (MPa)
Distance Along The Line of Geometry In Pin And Box (mm)

8.4.3.3 Simulation Data Pages

RESULTS SNAPSHOT-0.05 MM

COMPONENT	LENGTH (MM)	PEAK S22 STRESS (MPA)	PRELOAD FORCE IN COMPONENT (MN)
PIN	40.3	23.1	0.40
BOX	34.1	-50.7	-0.41
		% Difference	-0.99

YIELD ANALYSIS-0.05MM

COMPONENT	MATERIAL	YIELD STRENGTH	PEAK VON MISES STRESS
PIN	Ti 6Al-4V	880.0	97.19
BOX	Ti 6Al-4V	880.0	
	Ti 6Al-4V	% of Yield	11.04

PIN PRELOAD STRESS VALUES

NODE	X	S22	TRUE ELEMENT FORCE	AVE. NODAL STRESS	FORCE ON ELEMENT FACE	VON MISES STRESS
158	190.27	17.4851	3.58E+02	1.77E+01	6.35E+03	16.837
1828	189.97	17.9735	3.94E+02	1.82E+01	7.15E+03	17.0962
1829	189.64	18.3642	4.32E+02	1.87E+01	8.09E+03	17.2375
1830	189.28	19.0932	4.75E+02	1.96E+01	9.30E+03	18.0468
1831	188.88	20.0438	5.20E+02	2.05E+01	1.07E+04	19.2072
1832	188.44	20.9658	5.71E+02	2.14E+01	1.22E+04	20.4705
1833	187.96	21.7832	6.26E+02	2.21E+01	1.38E+04	21.6159
1834	187.43	22.3632	6.88E+02	2.26E+01	1.55E+04	22.4933
1835	186.84	22.8024	7.54E+02	2.29E+01	1.73E+04	23.2192
1836	186	23.063	8.26E+02	2.30E+01	1.90E+04	23.6894
1837	185.49	22.9956	8.32E+02	2.28E+01	1.90E+04	23.7216
1838	184.78	22.5906	9.01E+02	2.22E+01	2.00E+04	23.2806
1839	184	21.889	9.75E+02	2.14E+01	2.09E+04	22.4082
1840	183.16	20.9337	1.09E+03	2.04E+01	2.22E+04	21.183
1841	182.21	19.788	1.14E+03	1.92E+01	2.19E+04	19.731
1842	181.21	18.5227	1.14E+03	1.79E+01	2.03E+04	18.127
160	180.21	17.2421	1.13E+03	1.66E+01	1.88E+04	16.5918
1843	179.21	15.9895	1.23E+03	1.54E+01	1.90E+04	15.1823
1844	178.11	14.7206	1.35E+03	1.41E+01	1.90E+04	13.8105
1845	176.90	13.4228	1.47E+03	1.27E+01	1.88E+04	12.4843
1846	175.56	12.0717	1.61E+03	1.14E+01	1.83E+04	11.1884
1847	174	10.7155	1.75E+03	1.00E+01	1.76E+04	9.9863
1848	172.5	9.3706	1.91E+03	8.68E+00	1.66E+04	8.9045
1849	170.72	7.9955	2.08E+03	7.29E+00	1.51E+04	7.8909
1850	168.77	6.5811	2.26E+03	5.88E+00	1.33E+04	6.9081
1851	166.63	5.1739	2.45E+03	4.49E+00	1.10E+04	6.0053
1852	164.27	3.8096	2.66E+03	3.04E+00	8.06E+03	5.2347
1853	161.67	2.2622	2.87E+03	1.26E+00	3.62E+03	4.4565
1854	158.82	0.2549	3.77E+03	-1.09E+00	-4.09E+03	3.7085
1855	155	-2.4266	4.79E+03	-3.66E+00	-1.75E+04	3.6718
159	150	-4.8883	7.07E+04	-2.44E+00		5.5078
				Tensile Preload Force in Pin	4.01E+05	

BOX PRELOAD STRESS VALUES

NODE	X	S22	TRUE ELEMENT FORCE	AVE. NODAL STRESS	FORCE ON ELEMENT FACE	VON MISES STRESS
77	226.2	3.7345	4.32E+03	2.98E+00	1.29E+04	15.0626
761	223.2	2.2289	3.96E+03	1.29E+00	5.12E+03	15.1684
762	220.3	0.3581	3.64E+03	-4.43E-01	-1.61E+03	15.8189
763	217.7	-1.244	3.34E+03	-1.97E+00	-6.57E+03	16.498
764	215.2	-2.687	3.07E+03	-3.29E+00	-1.01E+04	17.166
765	212.9	-3.898	2.83E+03	-4.51E+00	-1.27E+04	17.7858
766	210.8	-5.112	2.60E+03	-5.87E+00	-1.53E+04	18.4107
767	208.8	-6.633	2.40E+03	-7.53E+00	-1.81E+04	19.1181
78	207	-8.431	3.87E+03	-9.76E+00	-3.78E+04	20.0073
896	204	-11.1	2.20E+03	-1.25E+00	-2.75E+04	21.405
895	202.3	-13.9	2.18E+03	-1.49E+00	-3.25E+04	22.986
894	200.6	-15.88	1.26E+03	-1.64E+00	-2.06E+04	24.3147
82	199.6	-16.95	1.13E+03	-1.77E+00	-2.00E+04	25.0847
893	198.7	-18.38	1.03E+03	-1.91E+00	-1.96E+04	26.0377
892	197.8	-19.77	9.35E+02	-2.04E+00	-1.91E+04	27.0044
891	197.1	-20.99	8.49E+02	-2.20E+00	-1.87E+04	27.9343
890	196.4	-22.93	7.71E+02	-2.41E+00	-1.86E+04	29.4107
889	195.8	-25.22	7.00E+02	-2.62E+00	-1.84E+04	31.0817
888	195.2	-27.22	6.38E+02	-2.79E+00	-1.78E+04	32.6382
887	194.7	-28.66	5.79E+02	-2.93E+00	-1.70E+04	33.7789
886	194.2	-29.94	5.27E+02	-3.07E+00	-1.61E+04	34.794
885	193.8	-31.37	4.79E+02	-3.23E+00	-1.55E+04	35.7753
884	193.4	-33.25	4.36E+02	-3.43E+00	-1.49E+04	37.2139
883	193	-35.26	3.97E+02	-3.66E+00	-1.45E+04	38.77
882	192.7	-37.92	3.60E+02	-4.05E+00	-1.46E+04	40.6773
881	192.4	-43.01	3.29E+02	-4.69E+00	-1.54E+04	44.7987
69	192.1	-50.74	1.16E+05	-2.54E+00		53.8131
				Compressive Preload Force in Box	-4.05E+05	

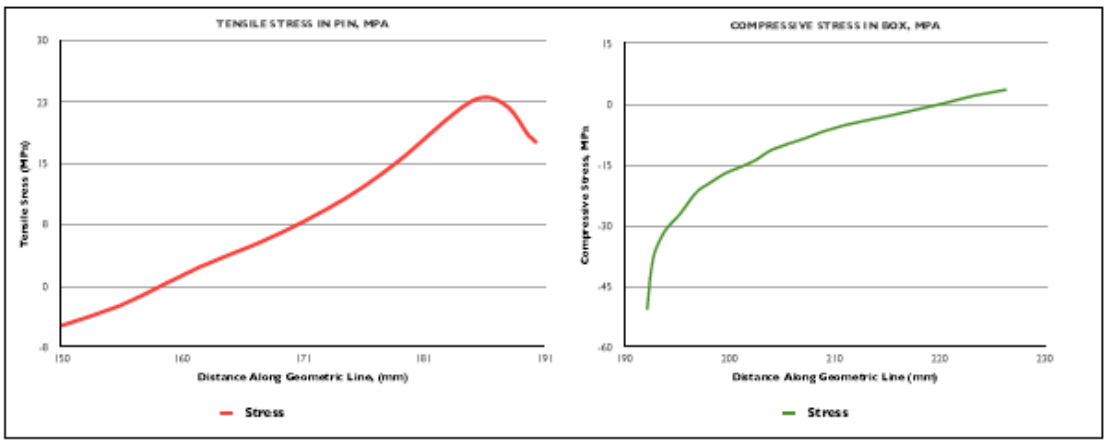

RESULTS SNAPSHOT-0.1MM

COMPONENT	LENGTH (MM)	PEAK S11 STRESS (MPA)	PRELOAD FORCE IN COMPONENT (MN)
PIN	40.3	43.4	0.76
BOX	34.1	-94.8	-0.76
		%Difference	-0.99

YIELD ANALYSIS-0.1MM

COMPONENT	MATERIAL	YIELD STRENGTH	PEAK VON MISES STRESS
PIN	Ti 6Al-4V	880.0	182.70
BOX	Ti 6Al-4V	880.0	
		% of Yield	20.76

PIN PRELOAD STRESS VALUES

NODE	X	S22	TRUE ELEMENT FORCE	AVE. NODAL STRESS	FORCE ON ELEMENT FACE	VON MISES STRESS
158	190.27	32.9316	3.58E+02	3.34E+01	1.20E+04	31.7051
1828	189.97	33.8505	3.94E+02	3.42E+01	1.35E+04	32.1932
1829	189.64	34.5854	4.32E+02	3.53E+01	1.52E+04	32.4589
1830	189.28	35.9575	4.75E+02	3.69E+01	1.75E+04	33.9827
1831	188.88	37.747	5.20E+02	3.86E+01	2.01E+04	36.1678
1832	188.44	39.4825	5.71E+02	4.03E+01	2.30E+04	38.5466
1833	187.96	41.0216	6.26E+02	4.16E+01	2.60E+04	40.7039
1834	187.43	42.114	6.88E+02	4.25E+01	2.93E+04	42.3567
1835	186.84	42.9419	7.54E+02	4.32E+01	3.25E+04	43.7251
1836	186	43.4339	8.26E+02	4.34E+01	3.58E+04	44.6124
1837	185.49	43.3087	8.32E+02	4.29E+01	3.57E+04	44.6757
1838	184.78	42.5481	9.01E+02	4.19E+01	3.78E+04	43.8479
1839	184	41.2289	9.75E+02	4.03E+01	3.93E+04	42.208
1840	183.16	39.4323	1.09E+03	3.84E+01	4.18E+04	39.9036
1841	182.21	37.2773	1.14E+03	3.61E+01	4.12E+04	37.1719
1842	181.21	34.8966	1.14E+03	3.37E+01	3.83E+04	34.1533
160	180.21	32.4868	1.13E+03	3.13E+01	3.54E+04	31.2634
1843	179.21	30.1291	1.23E+03	2.89E+01	3.57E+04	28.6092
1844	178.11	27.7401	1.35E+03	2.65E+01	3.58E+04	26.0254
1845	176.90	25.2963	1.47E+03	2.40E+01	3.54E+04	23.5266
1846	175.56	22.7515	1.61E+03	2.15E+01	3.45E+04	21.084
1847	174	20.1964	1.75E+03	1.89E+01	3.32E+04	18.8172
1848	172.5	17.6618	1.91E+03	1.64E+01	3.13E+04	16.7762
1849	170.72	15.0696	2.08E+03	1.37E+01	2.86E+04	14.8631
1850	168.77	12.4023	2.26E+03	1.11E+01	2.50E+04	13.0075
1851	166.63	9.7477	2.45E+03	8.46E+00	2.07E+04	11.3024
1852	164.27	7.1735	2.66E+03	5.71E+00	1.52E+04	9.8467
1853	161.67	4.2533	2.87E+03	2.36E+00	6.78E+03	8.3774
1854	158.82	0.4651	3.77E+03	-2.06E+00	-7.78E+03	6.9682
1855	155	-4.5949	4.79E+03	-6.92E+00	-3.31E+04	6.9123
159	150	-9.239	7.07E+04	-4.62E+00		10.3903
			Tensile Preload Force in Pin		7.56E+05	

BOX PRELOAD STRESS VALUES

NODE	X	S22	TRUE ELEMENT FORCE	AVE. NODAL STRESS	FORCE ON ELEMENT FACE	VON MISES STRESS
77	226.2	6.969	4.32E+03	5.55E+00	2.40E+04	28.4058
761	223.2	4.137	3.96E+03	2.37E+00	9.41E+03	28.6115
762	220.3	0.6124	3.64E+03	-8.98E-01	-3.27E+03	29.84
763	217.7	-2.408	3.34E+03	-3.76E+00	-1.26E+04	31.1222
764	215.2	-5.12	3.07E+03	-6.26E+00	-1.92E+04	32.3829
765	212.9	-7.395	2.83E+03	-8.53E+00	-2.41E+04	33.5504
766	210.8	-9.67	2.60E+03	-1.11E+01	-2.89E+04	34.7262
767	208.8	-12.52	2.40E+03	-1.42E+01	-3.40E+04	36.057
78	207	-15.89	3.87E+03	-1.84E+01	-7.12E+04	37.7295
896	204	-20.89	2.20E+03	-2.35E+01	-5.18E+04	40.3574
895	202.3	-26.16	2.18E+03	-2.80E+01	-6.12E+04	43.3289
894	200.6	-29.87	1.26E+03	-3.09E+01	-3.88E+04	45.8252
82	199.6	-31.88	1.13E+03	-3.32E+01	-3.77E+04	47.2732
893	198.7	-34.57	1.03E+03	-3.59E+01	-3.69E+04	49.0608
892	197.8	-37.17	9.35E+02	-3.83E+01	-3.58E+04	50.872
891	197.1	-39.47	8.49E+02	-4.13E+01	-3.51E+04	52.6164
890	196.4	-43.11	7.71E+02	-4.53E+01	-3.49E+04	55.3869
889	195.8	-47.4	7.00E+02	-4.93E+01	-3.45E+04	58.5166
888	195.2	-51.13	6.38E+02	-5.25E+01	-3.35E+04	61.4211
887	194.7	-53.82	5.79E+02	-5.50E+01	-3.19E+04	63.5616
886	194.2	-56.2	5.27E+02	-5.75E+01	-3.03E+04	65.4486
885	193.8	-58.87	4.79E+02	-6.06E+01	-2.90E+04	67.2722
884	193.4	-62.36	4.36E+02	-6.42E+01	-2.80E+04	69.9446
883	193	-66.1	3.97E+02	-6.86E+01	-2.73E+04	72.8336
882	192.7	-71.08	3.60E+02	-7.58E+01	-2.73E+04	76.3982
881	192.4	-80.53	3.29E+02	-8.77E+01	-2.88E+04	84.0778
69	192.1	-94.8	1.16E+05	-4.74E+01		100.685
			Compressive Preload Force in Box		-7.63E+05	

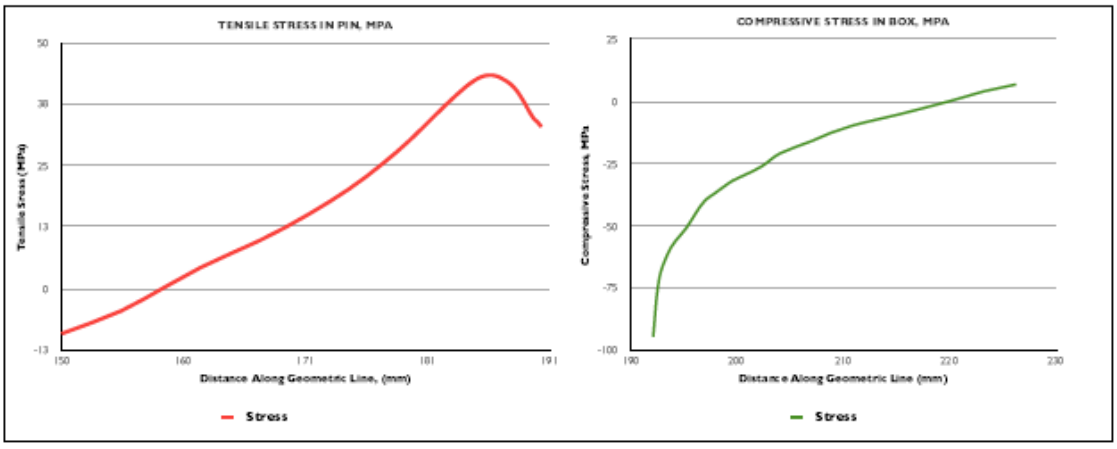

RESULTS SNAPSHOT-0.15MM

COMPONENT	LENGTH (MM)	PEAK S22 STRESS (MPA)	PRELOAD FORCE IN COMPONENT (MN)
PIN	40.3	63.7	1.11
BOX	34.1	-138.3	-1.12
		%Difference	-0.99

YIELD ANALYSIS-0.15MM

COMPONENT	MATERIAL	YIELD STRENGTH	PEAK VON MISES STRESS
PIN	Ti 6Al-4V	880.0	267.50
BOX	Ti 6Al-4V	880.0	
		% of Yield	30.40

PIN PRELOAD STRESS VALUES

NODE	X	S22	TRUE ELEMENT FORCE	AVE. NODAL STRESS	FORCE ON ELEMENT FACE	VON MISES STRESS
158	190.27	48.338	3.58E+02	4.90E+01	1.76E+04	48.338
1828	189.97	49.6852	3.94E+02	5.02E+01	1.98E+04	49.6852
1829	189.64	50.7622	4.32E+02	5.18E+01	2.24E+04	50.7622
1830	189.28	52.7747	4.75E+02	5.41E+01	2.57E+04	52.7747
1831	188.88	55.3996	5.20E+02	5.67E+01	2.95E+04	55.3996
1832	188.44	57.9451	5.71E+02	5.91E+01	3.37E+04	57.9451
1833	187.96	60.2031	6.26E+02	6.10E+01	3.82E+04	60.2031
1834	187.43	61.8061	6.88E+02	6.24E+01	4.29E+04	61.8061
1835	186.84	63.0214	7.54E+02	6.34E+01	4.78E+04	63.0214
1836	186	63.7446	8.26E+02	6.37E+01	5.26E+04	63.7446
1837	185.49	63.5627	8.32E+02	6.30E+01	5.24E+04	63.5627
1838	184.78	62.4486	9.01E+02	6.15E+01	5.54E+04	62.4486
1839	184	60.5153	9.75E+02	5.92E+01	5.77E+04	60.5153
1840	183.16	57.8818	1.09E+03	5.63E+01	6.14E+04	57.8818
1841	182.21	54.7223	1.14E+03	5.30E+01	6.05E+04	54.7223
1842	181.21	51.2315	1.14E+03	4.95E+01	5.62E+04	51.2315
160	180.21	47.6972	1.13E+03	4.60E+01	5.19E+04	47.6972
1843	179.21	44.2387	1.23E+03	4.25E+01	5.25E+04	44.2387
1844	178.11	40.7337	1.35E+03	3.89E+01	5.25E+04	40.7337
1845	176.90	37.1476	1.47E+03	3.53E+01	5.20E+04	37.1476
1846	175.56	33.4126	1.61E+03	3.15E+01	5.07E+04	33.4126
1847	174	29.6615	1.75E+03	2.78E+01	4.87E+04	29.6615
1848	172.5	25.9395	1.91E+03	2.40E+01	4.59E+04	25.9395
1849	170.72	22.1319	2.08E+03	2.02E+01	4.19E+04	22.1319
1850	168.77	18.2129	2.26E+03	1.63E+01	3.67E+04	18.2129
1851	166.63	14.3119	2.45E+03	1.24E+01	3.04E+04	14.3119
1852	164.27	10.528	2.66E+03	8.38E+00	2.23E+04	10.528
1853	161.67	6.2351	2.87E+03	3.45E+00	9.91E+03	6.2351
1854	158.82	0.6658	3.77E+03	-3.05E+00	-1.15E+04	0.6658
1855	155	-6.7723	4.79E+03	-1.02E+01	-4.88E+04	-6.7723
159	150	-13.5981	7.07E+04	-6.80E+00		-13.5981
				Tensile Preload Force in Pin	1.11E+06	

BOX PRELOAD STRESS VALUES

NODE	X	S22	TRUE ELEMENT FORCE	AVE. NODAL STRESS	FORCE ON ELEMENT FACE	VON MISES STRESS
77	226.2	10.222	4.32E+03	8.14E+00	3.52E+04	41.7281
761	223.2	6.0643	3.96E+03	3.48E+00	1.38E+04	42.0317
762	220.3	0.886	3.64E+03	-1.33E+0	-4.85E+03	43.8365
763	217.7	-3.553	3.34E+03	-5.54E+0	-1.85E+04	45.721
764	215.2	-7.534	3.07E+03	-9.20E+0	-2.83E+04	47.5738
765	212.9	-10.87	2.83E+03	-1.25E+0	-3.55E+04	49.288
766	210.8	-14.21	2.60E+03	-1.63E+0	-4.24E+04	51.0135
767	208.8	-18.38	2.40E+03	-2.08E+0	-5.00E+04	52.9669
78	207	-23.32	3.87E+03	-2.70E+0	-1.05E+05	55.4223
896	204	-30.67	2.20E+03	-3.45E+0	-7.60E+04	59.2817
895	202.3	-38.41	2.18E+03	-4.11E+0	-8.98E+04	63.6491
894	200.6	-43.86	1.26E+03	-4.53E+0	-5.70E+04	67.3151
82	199.6	-46.82	1.13E+03	-4.88E+0	-5.53E+04	69.4453
893	198.7	-50.77	1.03E+03	-5.27E+0	-5.43E+04	72.0712
892	197.8	-54.59	9.35E+02	-5.63E+0	-5.26E+04	74.7261
891	197.1	-57.96	8.49E+02	-6.06E+0	-5.15E+04	77.2816
890	196.4	-63.29	7.71E+02	-6.64E+0	-5.12E+04	81.3397
889	195.8	-69.56	7.00E+02	-7.23E+0	-5.06E+04	85.9137
888	195.2	-75.01	6.38E+02	-7.70E+0	-4.91E+04	90.1651
887	194.7	-78.92	5.79E+02	-8.06E+0	-4.67E+04	93.2647
886	194.2	-82.38	5.27E+02	-8.43E+0	-4.44E+04	96.0097
885	193.8	-86.25	4.79E+02	-8.88E+0	-4.25E+04	98.664
884	193.4	-91.34	4.36E+02	-9.40E+0	-4.10E+04	102.554
883	193	-96.75	3.97E+02	-1.00E+0	-3.99E+04	106.75
882	192.7	-104	3.60E+02	-1.11E+0	-4.00E+04	111.916
881	192.4	-117.7	3.29E+02	-1.28E+0	-4.21E+04	123.098
69	192.1	-138.3	1.16E+05	-6.92E+0		147.052
				Compressive Preload Force in Box	-1.12E+06	

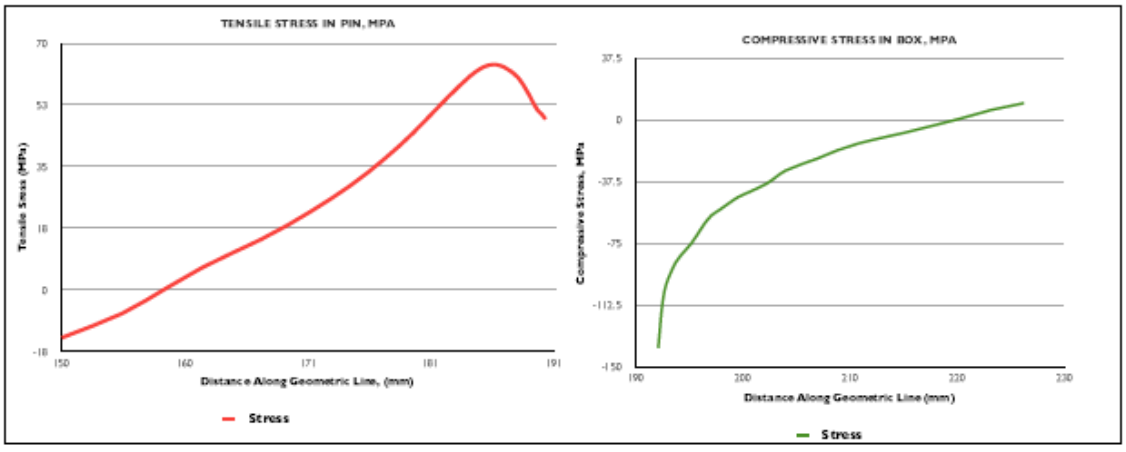

RESULTS SNAPSHOT-0.2MM

COMPONENT	LENGTH (MM)	PEAK S22 STRESS (MPA)	PRELOAD FORCE IN COMPONENT (MN)
PIN	40.3	84.0	1.46
BOX	34.1	-181.2	-1.47
		%Difference	-0.99

YIELD ANALYSIS-0.2MM

COMPONENT	MATERIAL	YIELD STRENGTH	PEAK VON MISES STRESS
PIN	Ti6Al-4V	880.0	351.50
BOX	Ti6Al-4V	880.0	
	Ti6Al-4V	% of Yield	39.94

PIN PRELOAD STRESS VALUES

NODE	X	S22	TRUE ELEMENT FORCE	AVE. NODAL STRESS	FORCE ON ELEMENT FACE	VON MISES STRESS
158	190.27	63.699	3.58E+02	6.46E+01	2.31E+04	61.3156
1828	189.97	65.4722	3.94E+02	6.62E+01	2.60E+04	62.2588
1829	189.64	66.889	4.32E+02	6.82E+01	2.95E+04	62.7711
1830	189.28	69.539	4.75E+02	7.13E+01	3.39E+04	65.7159
1831	188.88	72.9957	5.20E+02	7.47E+01	3.89E+04	69.9391
1832	188.44	76.3474	5.71E+02	7.78E+01	4.45E+04	74.537
1833	187.96	79.3212	6.26E+02	8.04E+01	5.03E+04	78.7083
1834	187.43	81.4328	6.88E+02	8.22E+01	5.66E+04	81.9058
1835	186.84	83.0341	7.54E+02	8.35E+01	6.29E+04	84.555
1836	186	83.9882	8.26E+02	8.39E+01	6.92E+04	86.2766
1837	185.49	83.7507	8.32E+02	8.30E+01	6.90E+04	86.4071
1838	184.78	82.2858	9.01E+02	8.10E+01	7.30E+04	84.8158
1839	184	79.7419	9.75E+02	7.80E+01	7.60E+04	81.6548
1840	183.16	76.2762	1.09E+03	7.42E+01	8.09E+04	77.2095
1841	182.21	72.1175	1.14E+03	6.98E+01	7.97E+04	71.9369
1842	181.21	67.5223	1.14E+03	6.52E+01	7.40E+04	66.1078
160	180.21	62.8689	1.13E+03	6.06E+01	6.84E+04	60.5242
1843	179.21	58.3144	1.23E+03	5.60E+01	6.92E+04	55.3932
1844	178.11	53.6979	1.35E+03	5.13E+01	6.93E+04	50.3957
1845	176.90	48.9738	1.47E+03	4.65E+01	6.86E+04	45.56
1846	175.56	44.0526	1.61E+03	4.16E+01	6.69E+04	40.8301
1847	174	39.1088	1.75E+03	3.67E+01	6.43E+04	36.4376
1848	172.5	34.2021	1.91E+03	3.17E+01	6.06E+04	32.4796
1849	170.72	29.1813	2.08E+03	2.66E+01	5.53E+04	28.7671
1850	168.77	24.0123	2.26E+03	2.14E+01	4.84E+04	25.1642
1851	166.63	18.8659	2.45E+03	1.64E+01	4.01E+04	21.8526
1852	164.27	13.8729	2.66E+03	1.10E+01	2.93E+04	19.0256
1853	161.67	8.2075	2.87E+03	4.53E+00	1.30E+04	16.1742
1854	158.82	0.8576	3.77E+03	-4.05E+00	-1.53E+04	13.4493
1855	155	-8.9579	4.79E+03	-1.35E+01	-6.45E+04	13.3781
159	150	-17.964	7.07E+04	-8.98E+00		20.1579
				Tensile Preload Force in Pin	1.46E+06	

BOX PRELOAD STRESS VALUES

NODE	X	S22	TRUE ELEMENT FORCE	AVE. NODAL STRESS	FORCE ON ELEMENT FACE	VON MISES STRESS
77	226.2	13.492	4.32E+03	1.08E+01	4.64E+04	55.027
761	223.2	8.0093	3.96E+03	4.59E+00	1.82E+04	55.4263
762	220.3	1.178	3.64E+03	-1.75E+0	-6.37E+03	57.8059
763	217.7	-4.679	3.34E+03	-7.30E+0	-2.44E+04	60.2916
764	215.2	-9.929	3.07E+03	-1.21E+0	-3.73E+04	62.7358
765	212.9	-14.33	2.83E+03	-1.65E+0	-4.67E+04	64.9954
766	210.8	-18.72	2.60E+03	-2.15E+0	-5.59E+04	67.2694
767	208.8	-24.21	2.40E+03	-2.75E+0	-6.59E+04	69.8442
78	207	-30.73	3.87E+03	-3.56E+0	-1.38E+05	73.0819
896	204	-40.43	2.20E+03	-4.55E+0	-1.00E+05	78.1735
895	202.3	-50.66	2.18E+03	-5.43E+0	-1.18E+05	83.9411
894	200.6	-57.84	1.26E+03	-5.98E+0	-7.52E+04	88.7758
82	199.6	-61.76	1.13E+03	-6.44E+0	-7.30E+04	91.5872
893	198.7	-66.96	1.03E+03	-6.95E+0	-7.16E+04	95.0484
892	197.8	-71.99	9.35E+02	-7.42E+0	-6.94E+04	98.5417
891	197.1	-76.44	8.49E+02	-8.00E+0	-6.79E+04	101.907
890	196.4	-83.47	7.71E+02	-8.76E+0	-6.75E+04	107.258
889	195.8	-91.69	7.00E+02	-9.53E+0	-6.67E+04	113.276
888	195.2	-98.82	6.38E+02	-1.01E+0	-6.47E+04	118.842
887	194.7	-104	5.79E+02	-1.06E+0	-6.15E+04	122.929
886	194.2	-108.5	5.27E+02	-1.11E+0	-5.85E+04	126.513
885	193.8	-113.6	4.79E+02	-1.17E+0	-5.60E+04	129.99
884	193.4	-120.2	4.36E+02	-1.24E+0	-5.39E+04	135.069
883	193	-127.3	3.97E+02	-1.32E+0	-5.24E+04	140.537
882	192.7	-136.6	3.60E+02	-1.45E+0	-5.25E+04	147.236
881	192.4	-154.4	3.29E+02	-1.68E+0	-5.51E+04	161.652
69	192.1	-181.2	1.16E+05	-9.06E+0		192.851
				Compressive Preload Force in Box	-1.47E+06	

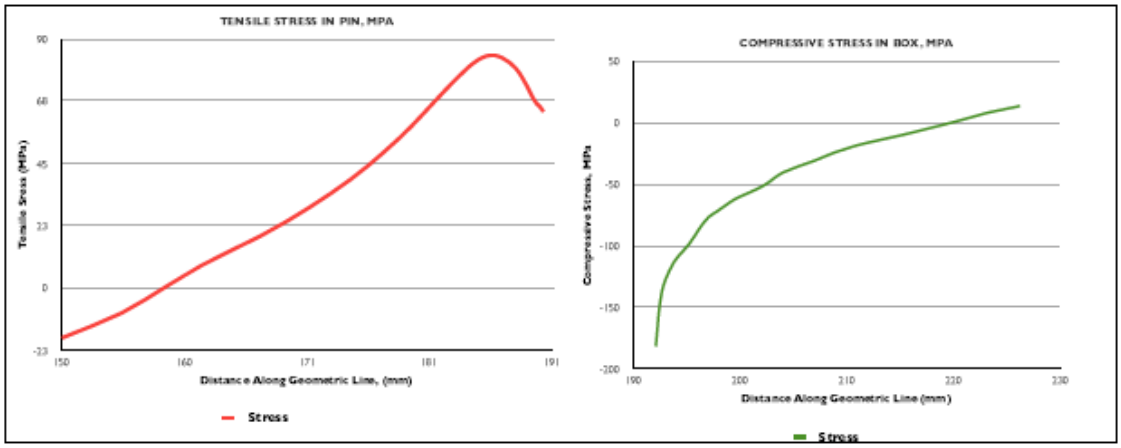

RESULTS SNAPSHOT-0.25MM

COMPONENT	LENGTH (MM)	PEAK S22 STRESS (MPA)	PRELOAD FORCE IN COMPONENT (MN)
PIN	40.3	104.2	1.81
BOX	34.1	-223.3	-1.83
		%Difference	-0.99

YIELD ANALYSIS-0.25MM

COMPONENT	MATERIAL	YIELD STRENGTH	PEAK VON MISES STRESS
PIN	Ti 6Al-4V	880.0	431.30
BOX	Ti 6Al-4V	880.0	
		% of Yield	49.01

PIN PRELOAD STRESS VALUES

NODE	X	S22	TRUE ELEMENT FORCE	AVE. NODAL STRESS	FORCE ON ELEMENT FACE	VON MISES STRESS
158	190.27	78.9559	3.58E+02	8.01E+01	2.87E+04	75.9754
1828	189.97	81.1562	3.94E+02	8.20E+01	3.23E+04	77.1479
1829	189.64	82.914	4.32E+02	8.46E+01	3.65E+04	77.7851
1830	189.28	86.2019	4.75E+02	8.83E+01	4.20E+04	81.4402
1831	188.88	90.4909	5.20E+02	9.26E+01	4.82E+04	86.682
1832	188.44	94.6497	5.71E+02	9.65E+01	5.51E+04	92.3892
1833	187.96	98.3413	6.26E+02	9.97E+01	6.24E+04	97.5686
1834	187.43	100.966	6.88E+02	1.02E+02	7.01E+04	101.542
1835	186.84	102.96	7.54E+02	1.04E+02	7.80E+04	104.839
1836	186	104.155	8.26E+02	1.04E+02	8.59E+04	106.988
1837	185.49	103.874	8.32E+02	1.03E+02	8.56E+04	107.167
1838	184.78	102.073	9.01E+02	1.01E+02	9.06E+04	105.209
1839	184	98.9367	9.75E+02	9.68E+01	9.43E+04	101.305
1840	183.16	94.6591	1.09E+03	9.21E+01	1.00E+05	95.8083
1841	182.21	89.5223	1.14E+03	8.67E+01	9.90E+04	89.2821
1842	181.21	83.8413	1.14E+03	8.10E+01	9.19E+04	82.0601
160	180.21	78.0827	1.13E+03	7.53E+01	8.50E+04	75.1335
1843	179.21	72.4417	1.23E+03	6.96E+01	8.59E+04	68.7611
1844	178.11	66.7198	1.35E+03	6.38E+01	8.61E+04	62.5492
1845	176.90	60.8596	1.47E+03	5.78E+01	8.52E+04	56.5328
1846	175.56	54.7491	1.61E+03	5.17E+01	8.31E+04	50.642
1847	174	48.6046	1.75E+03	4.56E+01	7.99E+04	45.166
1848	172.5	42.5005	1.91E+03	3.94E+01	7.52E+04	40.2273
1849	170.72	36.2492	2.08E+03	3.30E+01	6.87E+04	35.5921
1850	168.77	29.8092	2.26E+03	2.66E+01	6.01E+04	31.0943
1851	166.63	23.3935	2.45E+03	2.03E+01	4.97E+04	26.962
1852	164.27	17.1664	2.66E+03	1.36E+01	3.62E+04	23.4389
1853	161.67	10.0989	2.87E+03	5.51E+00	1.58E+04	19.8938
1854	158.82	0.9288	3.77E+03	-5.19E+00	-1.96E+04	16.5393
1855	155	-11.3162	4.79E+03	-1.69E+01	-8.11E+04	16.5846
159	150	-22.5482	7.07E+04	-1.13E+01		25.1576
				Tensile Preload Force in Pin	1.81E+06	

BOX PRELOAD STRESS VALUES

NODE	X	S22	TRUE ELEMENT FORCE	AVE. NODAL STRESS	FORCE ON ELEMENT FACE	VON MISES STRESS
77	226.2	16.727	4.32E+03	1.33E+01	5.76E+04	68.14
761	223.2	9.9328	3.96E+03	5.69E+00	2.26E+04	68.6324
762	220.3	1.4541	3.64E+03	-2.19E+0	-7.95E+03	71.5789
763	217.7	-5.825	3.34E+03	-9.09E+0	-3.04E+04	74.661
764	215.2	-12.35	3.07E+03	-1.51E+0	-4.63E+04	77.6938
765	212.9	-17.81	2.83E+03	-2.05E+0	-5.81E+04	80.495
766	210.8	-23.27	2.60E+03	-2.67E+0	-6.94E+04	83.3134
767	208.8	-30.07	2.40E+03	-3.41E+0	-8.18E+04	86.5104
78	207	-38.15	3.87E+03	-4.42E+0	-1.71E+05	90.5321
896	204	-50.19	2.20E+03	-5.65E+0	-1.24E+05	96.8626
895	202.3	-62.89	2.18E+03	-6.73E+0	-1.47E+05	104.034
894	200.6	-71.78	1.26E+03	-7.42E+0	-9.33E+04	110.019
82	199.6	-76.64	1.13E+03	-7.99E+0	-9.05E+04	113.498
893	198.7	-83.07	1.03E+03	-8.62E+0	-8.88E+04	117.782
892	197.8	-89.27	9.35E+02	-9.20E+0	-8.61E+04	122.087
891	197.1	-94.76	8.49E+02	-9.91E+0	-8.42E+04	126.237
890	196.4	-103.4	7.71E+02	-1.08E+0	-8.37E+04	132.844
889	195.8	-113.5	7.00E+02	-1.18E+0	-8.26E+04	140.256
888	195.2	-122.3	6.38E+02	-1.25E+0	-8.01E+04	147.112
887	194.7	-128.6	5.79E+02	-1.31E+0	-7.61E+04	152.105
886	194.2	-134.2	5.27E+02	-1.37E+0	-7.23E+04	156.512
885	193.8	-140.4	4.79E+02	-1.44E+0	-6.92E+04	160.766
884	193.4	-148.5	4.36E+02	-1.53E+0	-6.66E+04	166.985
883	193	-157.2	3.97E+02	-1.63E+0	-6.48E+04	173.699
882	192.7	-168.7	3.60E+02	-1.80E+0	-6.48E+04	182.012
881	192.4	-190.6	3.29E+02	-2.07E+0	-6.80E+04	199.795
69	192.1	-223.3	1.16E+05	-1.12E+0		237.727
				Compressive Preload Force in Box	-1.83E+06	

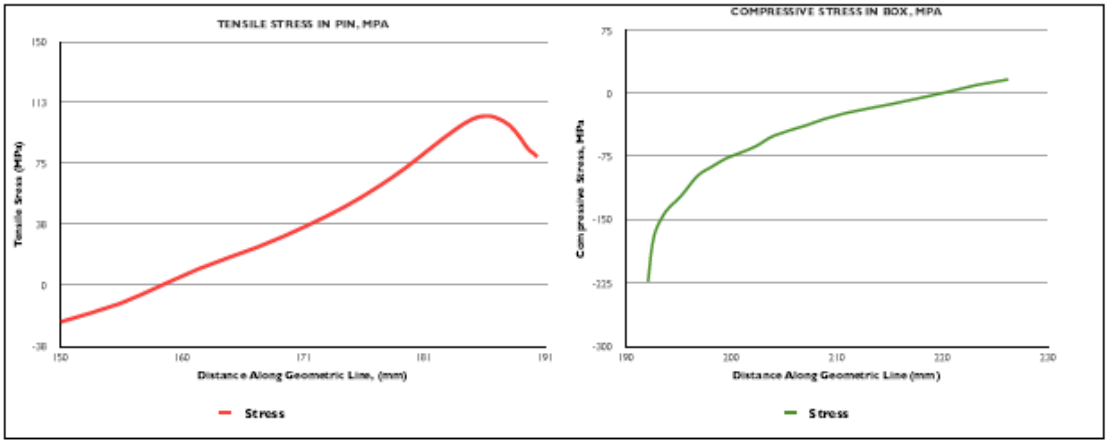

RESULTS SNAPSHOT-0.30MM

COMPONENT	LENGTH (MM)	PEAK S22 STRESS (MPA)	PRELOAD FORCE IN COMPONENT (MN)
PIN	40.3	124.3	2.16
BOX	34.1	-266.4	-2.18
		%Difference	-0.99

YIELD ANALYSIS-0.30MM

COMPONENT	MATERIAL	YIELD STRENGTH	PEAK VON MISES STRESS
PIN	Ti 6Al-4V	880.0	514.50
BOX	Ti 6Al-4V	880.0	
		% of Yield	58.47

PIN PRELOAD STRESS VALUES

NODE	X	S22	TRUE ELEMENT FORCE	AVE. NODAL STRESS	FORCE ON ELEMENT FACE	VON MISES STRESS
158	190.27	94.2749	3.58E+02	9.56E+01	3.43E+04	90.7055
1828	189.97	96.8983	3.94E+02	9.79E+01	3.85E+04	92.1042
1829	189.64	98.9931	4.32E+02	1.01E+02	4.36E+04	92.8636
1830	189.28	102.915	4.75E+02	1.05E+02	5.01E+04	97.2253
1831	188.88	108.032	5.20E+02	1.11E+02	5.75E+04	103.481
1832	188.44	112.993	5.71E+02	1.15E+02	6.58E+04	110.291
1833	187.96	117.398	6.26E+02	1.19E+02	7.45E+04	116.473
1834	187.43	120.529	6.88E+02	1.22E+02	8.37E+04	121.217
1835	186.84	122.91	7.54E+02	1.24E+02	9.32E+04	125.153
1836	186	124.337	8.26E+02	1.24E+02	1.03E+05	127.721
1837	185.49	124.004	8.32E+02	1.23E+02	1.02E+05	127.938
1838	184.78	121.857	9.01E+02	1.20E+02	1.08E+05	125.605
1839	184	118.117	9.75E+02	1.16E+02	1.13E+05	120.95
1840	183.16	113.015	1.09E+03	1.10E+02	1.20E+05	114.393
1841	182.21	106.887	1.14E+03	1.03E+02	1.18E+05	106.607
1842	181.21	100.11	1.14E+03	9.67E+01	1.10E+05	97.9899
160	180.21	93.2388	1.13E+03	8.99E+01	1.01E+05	89.7231
1843	179.21	86.5072	1.23E+03	8.31E+01	1.03E+05	82.1165
1844	178.11	79.6782	1.35E+03	7.62E+01	1.03E+05	74.7002
1845	176.90	72.6835	1.47E+03	6.90E+01	1.02E+05	67.5159
1846	175.56	65.3888	1.61E+03	6.17E+01	9.93E+04	60.4802
1847	174	58.0527	1.75E+03	5.44E+01	9.54E+04	53.9383
1848	172.5	50.7634	1.91E+03	4.70E+01	8.99E+04	48.0368
1849	170.72	43.2971	2.08E+03	3.95E+01	8.20E+04	42.4968
1850	168.77	35.6043	2.26E+03	3.18E+01	7.17E+04	37.1199
1851	166.63	27.9394	2.45E+03	2.42E+01	5.94E+04	32.1793
1852	164.27	20.4989	2.66E+03	1.63E+01	4.32E+04	27.9672
1853	161.67	12.0537	2.87E+03	6.57E+00	1.89E+04	23.7294
1854	158.82	1.0958	3.77E+03	-6.22E+00	-2.34E+04	19.7231
1855	155	-13.5354	4.79E+03	-2.02E+01	-9.70E+04	19.7933
159	150	-26.9551	7.07E+04	-1.35E+01		30.0531
			Tensile Preload Force in Pin		2.16E+06	

BOX PRELOAD STRESS VALUES

NODE	X	S22	TRUE ELEMENT FORCE	AVE. NODAL STRESS	FORCE ON ELEMENT FACE	VON MISES STRESS
77	226.2	20.024	4.32E+03	1.60E+01	6.89E+04	81.382
761	223.2	11.906	3.96E+03	6.84E+00	2.71E+04	81.9664
762	220.3	1.7738	3.64E+03	-2.58E+0	-9.37E+03	85.4845
763	217.7	-6.924	3.34E+03	-1.08E+0	-3.62E+04	89.1662
764	215.2	-14.71	3.07E+03	-1.80E+0	-5.52E+04	92.7893
765	212.9	-21.24	2.83E+03	-2.45E+0	-6.93E+04	96.1342
766	210.8	-27.75	2.60E+03	-3.18E+0	-8.28E+04	99.4988
767	208.8	-35.87	2.40E+03	-4.07E+0	-9.76E+04	103.315
78	207	-45.52	3.87E+03	-5.27E+0	-2.04E+05	108.118
896	204	-59.92	2.20E+03	-6.75E+0	-1.49E+05	115.685
895	202.3	-75.14	2.18E+03	-8.05E+0	-1.76E+05	124.279
894	200.6	-85.84	1.26E+03	-8.88E+0	-1.12E+05	131.482
82	199.6	-91.78	1.13E+03	-9.57E+0	-1.08E+05	135.713
893	198.7	-99.54	1.03E+03	-1.03E+0	-1.06E+05	140.891
892	197.8	-106.9	9.35E+02	-1.10E+0	-1.03E+05	146.026
891	197.1	-113.5	8.49E+02	-1.19E+0	-1.01E+05	150.979
890	196.4	-123.8	7.71E+02	-1.30E+0	-1.00E+05	158.869
889	195.8	-136.1	7.00E+02	-1.42E+0	-9.91E+04	168.113
888	195.2	-147	6.38E+02	-1.51E+0	-9.60E+04	176.592
887	194.7	-154	5.79E+02	-1.57E+0	-9.09E+04	181.908
886	194.2	-160.1	5.27E+02	-1.64E+0	-8.62E+04	186.661
885	193.8	-167.4	4.79E+02	-1.72E+0	-8.25E+04	191.738
884	193.4	-177	4.36E+02	-1.82E+0	-7.94E+04	199.171
883	193	-187.3	3.97E+02	-1.94E+0	-7.72E+04	207.138
882	192.7	-200.9	3.60E+02	-2.14E+0	-7.71E+04	216.95
881	192.4	-227	3.29E+02	-2.47E+0	-8.11E+04	238.027
69	192.1	-266.4	1.16E+05	-1.33E+0		283.62
			Compressive Preload Force in Box		-2.18E+06	

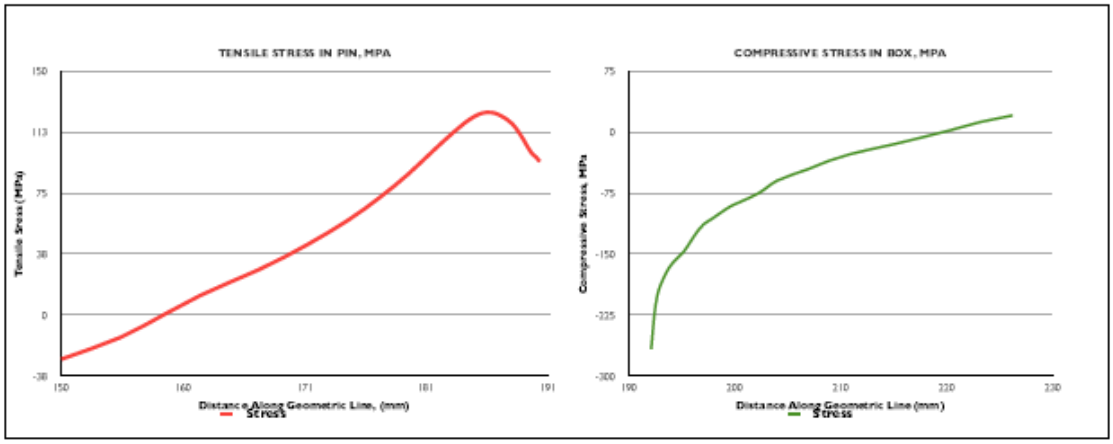

RESULTS SNAPSHOT-0.35MM

COMPONENT	LENGTH (MM)	PEAK S22 STRESS (MPA)	PRELOAD FORCE IN COMPONENT (MN)
PIN	40.3	144.5	2.51
BOX	34.1	-308.2	-2.54
		% Difference	-0.99

YIELD ANALYSIS-0.35MM

COMPONENT	MATERIAL	YIELD STRENGTH	PEAK VON MISES STRESS
PIN	Ti6Al-4V	880.0	597.30
BOX	Ti6Al-4V	880.0	
	Ti6Al-4V	880.0	97.19

PIN PRELOAD STRESS VALUES

NODE	X	S22	TRUE ELEMENT FORCE	AVE. NODAL STRESS	FORCE ON ELEMENT FACE	VON MISES STRESS
158	190.27	109.551	3.58E+02	1.11E+02	3.98E+04	105.395
1828	189.97	112.595	3.94E+02	1.14E+02	4.48E+04	107.019
1829	189.64	115.024	4.32E+02	1.17E+02	5.07E+04	107.899
1830	189.28	119.577	4.75E+02	1.23E+02	5.82E+04	112.964
1831	188.88	125.518	5.20E+02	1.28E+02	6.68E+04	120.229
1832	188.44	131.277	5.71E+02	1.34E+02	7.64E+04	128.138
1833	187.96	136.391	6.26E+02	1.38E+02	8.65E+04	135.319
1834	187.43	140.027	6.88E+02	1.41E+02	9.73E+04	140.829
1835	186.84	142.792	7.54E+02	1.44E+02	1.08E+05	145.403
1836	186	144.451	8.26E+02	1.44E+02	1.19E+05	148.389
1837	185.49	144.066	8.32E+02	1.43E+02	1.19E+05	148.644
1838	184.78	141.575	9.01E+02	1.39E+02	1.26E+05	145.94
1839	184	137.233	9.75E+02	1.34E+02	1.31E+05	140.537
1840	183.16	131.31	1.09E+03	1.28E+02	1.39E+05	132.926
1841	182.21	124.196	1.14E+03	1.20E+02	1.37E+05	123.886
1842	181.21	116.327	1.14E+03	1.12E+02	1.28E+05	113.88
160	180.21	108.348	1.13E+03	1.04E+02	1.18E+05	104.279
1843	179.21	100.53	1.23E+03	9.66E+01	1.19E+05	95.4427
1844	178.11	92.5987	1.35E+03	8.85E+01	1.19E+05	86.8267
1845	176.90	84.4735	1.47E+03	8.02E+01	1.18E+05	78.4788
1846	175.56	75.9989	1.61E+03	7.17E+01	1.15E+05	70.302
1847	174	67.4748	1.75E+03	6.32E+01	1.11E+05	62.6974
1848	172.5	59.004	1.91E+03	5.47E+01	1.04E+05	55.8356
1849	170.72	50.326	2.08E+03	4.59E+01	9.53E+04	49.3925
1850	168.77	41.3835	2.26E+03	3.69E+01	8.34E+04	43.1382
1851	166.63	32.4722	2.45E+03	2.81E+01	6.90E+04	37.3905
1852	164.27	23.8206	2.66E+03	1.89E+01	5.02E+04	32.4901
1853	161.67	14	2.87E+03	7.63E+00	2.19E+04	27.5607
1854	158.82	1.2576	3.77E+03	-7.25E+00	-2.73E+04	22.9044
1855	155	-15.7556	4.79E+03	-2.36E+01	-1.13E+05	23.001
159	150	-31.3585	7.07E+04	-1.57E+01		34.9446
				Tensile Preload Force in Pin	2.51E+06	

BOX PRELOAD STRESS VALUES

NODE	X	S22	TRUE ELEMENT FORCE	AVE. NODAL STRESS	FORCE ON ELEMENT FACE	VON MISES STRESS
77	226.2	23.344	4.32E+03	1.86E+01	8.04E+04	94.6137
761	223.2	13.901	3.96E+03	8.01E+00	3.17E+04	95.2877
762	220.3	2.1133	3.64E+03	-2.95E+0	-1.07E+04	99.3765
763	217.7	-8.006	3.34E+03	-1.25E+0	-4.19E+04	103.658
764	215.2	-17.07	3.07E+03	-2.09E+0	-6.41E+04	107.871
765	212.9	-24.66	2.83E+03	-2.84E+0	-8.04E+04	111.759
766	210.8	-32.23	2.60E+03	-3.69E+0	-9.61E+04	115.67
767	208.8	-41.66	2.40E+03	-4.73E+0	-1.13E+05	120.106
78	207	-52.89	3.87E+03	-6.13E+0	-2.37E+05	125.691
896	204	-69.66	2.20E+03	-7.85E+0	-1.73E+05	134.495
895	202.3	-87.4	2.18E+03	-9.36E+0	-2.04E+05	144.507
894	200.6	-99.86	1.26E+03	-1.03E+0	-1.30E+05	152.888
82	199.6	-106.8	1.13E+03	-1.11E+0	-1.26E+05	157.817
893	198.7	-115.8	1.03E+03	-1.20E+0	-1.24E+05	163.844
892	197.8	-124.4	9.35E+02	-1.28E+0	-1.20E+05	169.792
891	197.1	-132	8.49E+02	-1.38E+0	-1.17E+05	175.539
890	196.4	-143.9	7.71E+02	-1.51E+0	-1.17E+05	184.718
889	195.8	-158.3	7.00E+02	-1.65E+0	-1.15E+05	195.421
888	195.2	-170.9	6.38E+02	-1.75E+0	-1.12E+05	205.332
887	194.7	-179.1	5.79E+02	-1.83E+0	-1.06E+05	211.497
886	194.2	-186.1	5.27E+02	-1.90E+0	-1.00E+05	216.959
885	193.8	-194.4	4.79E+02	-2.00E+0	-9.58E+04	222.797
884	193.4	-205.6	4.36E+02	-2.11E+0	-9.21E+04	231.369
883	193	-217.4	3.97E+02	-2.25E+0	-8.95E+04	240.542
882	192.7	-233.1	3.60E+02	-2.48E+0	-8.94E+04	251.851
881	192.4	-263	3.29E+02	-2.86E+0	-9.38E+04	276.082
69	192.1	-308.2	1.16E+05	-1.54E+0		328.297
				Compressive Preload Force in Box	-2.54E+06	

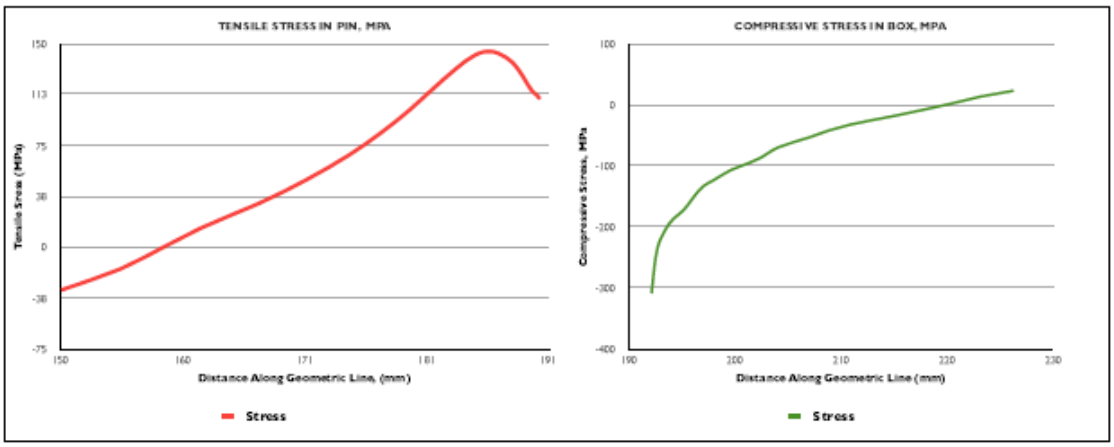

RESULTS SNAPSHOT-0.4MM

COMPONENT	LENGTH (MM)	PEAK S22 STRESS (MPA)	PRELOAD FORCE IN COMPONENT (MN)
PIN	40.3	263.8	4.59
BOX	34.1	-547.2	-4.62
		%Difference	-0.99

YIELD ANALYSIS-0.4MM

COMPONENT	MATERIAL	YIELD STRENGTH	PEAK VON MISES STRESS
PIN	Ti 6Al-4V	880.0	688.10
BOX	Ti 6Al-4V	880.0	
		% of Yield	78.19

PIN PRELOAD STRESS VALUES

NODE	X	S22	TRUE ELEMENT FORCE	AVE. NODAL STRESS	FORCE ON ELEMENT FACE	VON MISES STRESS
158	190.27	200.174	3.58E+02	2.03E+02	7.27E+04	192.442
1828	189.97	205.701	3.94E+02	2.08E+02	8.18E+04	195.402
1829	189.64	210.1	4.32E+02	2.14E+02	9.26E+04	196.999
1830	189.28	218.387	4.75E+02	2.24E+02	1.06E+05	206.236
1831	188.88	229.203	5.20E+02	2.34E+02	1.22E+05	219.487
1832	188.44	239.686	5.71E+02	2.44E+02	1.40E+05	233.918
1833	187.96	249.006	6.26E+02	2.52E+02	1.58E+05	247.032
1834	187.43	255.644	6.88E+02	2.58E+02	1.78E+05	257.112
1835	186.84	260.708	7.54E+02	2.62E+02	1.98E+05	265.499
1836	186	263.772	8.26E+02	2.63E+02	2.17E+05	271.011
1837	185.49	263.124	8.32E+02	2.61E+02	2.17E+05	271.555
1838	184.78	258.646	9.01E+02	2.55E+02	2.30E+05	266.704
1839	184	250.801	9.75E+02	2.45E+02	2.39E+05	256.935
1840	183.16	240.082	1.09E+03	2.34E+02	2.55E+05	243.134
1841	182.21	227.19	1.14E+03	2.20E+02	2.51E+05	226.714
1842	181.21	212.909	1.14E+03	2.06E+02	2.34E+05	208.503
160	180.21	198.406	1.13E+03	1.91E+02	2.16E+05	190.992
1843	179.21	184.173	1.23E+03	1.77E+02	2.18E+05	174.845
1844	178.11	169.715	1.35E+03	1.62E+02	2.19E+05	159.073
1845	176.90	154.884	1.47E+03	1.47E+02	2.17E+05	143.763
1846	175.56	139.388	1.61E+03	1.32E+02	2.12E+05	128.736
1847	174	123.775	1.75E+03	1.16E+02	2.03E+05	114.73
1848	172.5	108.23	1.91E+03	1.00E+02	1.92E+05	102.063
1849	170.72	92.2764	2.08E+03	8.40E+01	1.75E+05	90.1451
1850	168.77	75.8112	2.26E+03	6.76E+01	1.53E+05	78.5663
1851	166.63	59.3801	2.45E+03	5.14E+01	1.26E+05	67.9227
1852	164.27	43.4078	2.66E+03	3.43E+01	9.12E+04	58.8599
1853	161.67	25.2644	2.87E+03	1.35E+01	3.88E+04	49.7783
1854	158.82	1.718	3.77E+03	-1.40E+01	-5.27E+04	41.3479
1855	155	-29.7052	4.79E+03	-4.41E+01	-2.11E+05	42.0925
159	150	-58.4988	7.07E+04	-2.92E+01		64.6124
			Tensile Preload Force in Pin		4.59E+06	

BOX PRELOAD STRESS VALUES

NODE	X	S22	TRUE ELEMENT FORCE	AVE. NODAL STRESS	FORCE ON ELEMENT FACE	VON MISES STRESS
77	226.2	43.375	4.32E+03	3.47E+01	1.50E+05	173.039
761	223.2	26.067	3.96E+03	1.52E+01	6.03E+04	174.218
762	220.3	4.3713	3.64E+03	-4.96E+0	-1.80E+04	181.68
763	217.7	-14.28	3.34E+03	-2.26E+0	-7.56E+04	189.531
764	215.2	-30.98	3.07E+03	-3.80E+0	-1.17E+05	197.272
765	212.9	-44.96	2.83E+03	-5.19E+0	-1.47E+05	204.397
766	210.8	-58.89	2.60E+03	-6.75E+0	-1.76E+05	211.557
767	208.8	-76.17	2.40E+03	-8.65E+0	-2.07E+05	219.697
78	207	-96.75	3.87E+03	-1.12E+0	-4.35E+05	229.943
896	204	-127.8	2.20E+03	-1.44E+0	-3.17E+05	246.206
895	202.3	-160.7	2.18E+03	-1.72E+0	-3.76E+05	264.783
894	200.6	-183.4	1.26E+03	-1.90E+0	-2.39E+05	280.012
82	199.6	-196.2	1.13E+03	-2.04E+0	-2.32E+05	289.046
893	198.7	-212.7	1.03E+03	-2.20E+0	-2.27E+05	300.133
892	197.8	-228.2	9.35E+02	-2.35E+0	-2.20E+05	310.829
891	197.1	-242.3	8.49E+02	-2.53E+0	-2.15E+05	321.249
890	196.4	-264.5	7.71E+02	-2.77E+0	-2.14E+05	338.544
889	195.8	-289.4	7.00E+02	-3.00E+0	-2.10E+05	357.186
888	195.2	-309.9	6.38E+02	-3.17E+0	-2.02E+05	372.908
887	194.7	-324.5	5.79E+02	-3.31E+0	-1.92E+05	384.342
886	194.2	-337.9	5.27E+02	-3.45E+0	-1.82E+05	395.082
885	193.8	-353	4.79E+02	-3.63E+0	-1.74E+05	405.935
884	193.4	-372.8	4.36E+02	-3.83E+0	-1.67E+05	421.258
883	193	-393.6	3.97E+02	-4.07E+0	-1.62E+05	437.248
882	192.7	-420	3.60E+02	-4.45E+0	-1.61E+05	456.144
881	192.4	-470.8	3.29E+02	-5.09E+0	-1.67E+05	497.35
69	192.1	-547.2	1.16E+05	-2.74E+0		585.293
			Compressive Preload Force in Box		-4.62E+06	

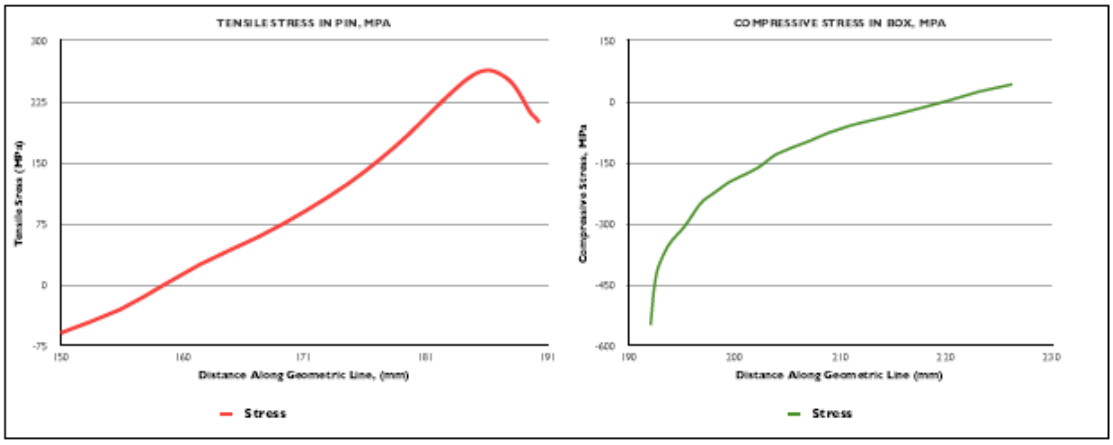

RESULTS SNAPSHOT-20N

COMPONENT	LENGTH (MM)	PEAK S22 STRESS (MPA)	PRELOAD FORCE IN COMPONENT (MN)
PIN	40.3	144.0	2.51
BOX	34.1	-325.6	-2.54
		%Difference	-0.99

YIELD ANALYSIS-20N

COMPONENT	MATERIAL	YIELD STRENGTH	PEAK VON MISES STRESS
PIN	Ti 6Al-4V	880.0	599.80
BOX	Ti 6Al-4V	880.0	
		% of Yield	68.16

PIN PRELOAD STRESS VALUES

NODE	X	S22	TRUE ELEMENT FORCE	AVE. NODAL STRESS	FORCE ON ELEMENT FACE	VON MISES STRESS
158	190.27	109.35	3.58E+02	1.11E+02	3.97E+04	48.338
1828	189.97	112.379	3.94E+02	1.14E+02	4.47E+04	49.6852
1829	189.64	114.793	4.32E+02	1.17E+02	5.06E+04	50.7622
1830	189.28	119.327	4.75E+02	1.22E+02	5.81E+04	52.7747
1831	188.88	125.24	5.20E+02	1.28E+02	6.67E+04	55.3996
1832	188.44	130.971	5.71E+02	1.34E+02	7.63E+04	57.9451
1833	187.96	136.058	6.26E+02	1.38E+02	8.63E+04	60.2031
1834	187.43	139.67	6.88E+02	1.41E+02	9.70E+04	61.8061
1835	186.84	142.409	7.54E+02	1.43E+02	1.08E+05	63.0214
1836	186	144.044	8.26E+02	1.44E+02	1.19E+05	63.7446
1837	185.49	143.64	8.32E+02	1.42E+02	1.18E+05	63.5627
1838	184.78	141.137	9.01E+02	1.39E+02	1.25E+05	62.4486
1839	184	136.79	9.75E+02	1.34E+02	1.30E+05	60.5153
1840	183.16	130.867	1.09E+03	1.27E+02	1.39E+05	57.8818
1841	182.21	123.756	1.14E+03	1.20E+02	1.37E+05	54.7223
1842	181.21	115.893	1.14E+03	1.12E+02	1.27E+05	51.2315
160	180.21	107.924	1.13E+03	1.04E+02	1.17E+05	47.6972
1843	179.21	100.119	1.23E+03	9.62E+01	1.19E+05	44.2387
1844	178.11	92.205	1.35E+03	8.82E+01	1.19E+05	40.7337
1845	176.90	84.1017	1.47E+03	7.99E+01	1.18E+05	37.1476
1846	175.56	75.655	1.61E+03	7.14E+01	1.15E+05	33.4126
1847	174	67.1656	1.75E+03	6.30E+01	1.10E+05	29.6615
1848	172.5	58.7369	1.91E+03	5.44E+01	1.04E+05	25.9395
1849	170.72	50.1116	2.08E+03	4.57E+01	9.49E+04	22.1319
1850	168.77	41.2348	2.26E+03	3.68E+01	8.31E+04	18.2129
1851	166.63	32.4004	2.45E+03	2.81E+01	6.89E+04	14.3119
1852	164.27	23.8327	2.66E+03	1.90E+01	5.04E+04	10.528
1853	161.67	14.1158	2.87E+03	7.81E+00	2.24E+04	6.2351
1854	158.82	1.5109	3.77E+03	-6.91E+00	-2.60E+04	0.6656
1855	155	-15.3317	4.79E+03	-2.31E+01	-1.10E+05	-6.7723
159	150	-30.7963	7.07E+04	-1.54E+01		-13.5981
				Tensile Force in Pin	2.51E+06	

BOX PRELOAD STRESS VALUES

NODE	X	S22	TRUE ELEMENT FORCE	AVE. NODAL STRESS	FORCE ON ELEMENT FACE	VON MISES STRESS
77	226.2	26.802	4.32E+03	2.20E+01	9.49E+04	41.7281
761	223.2	17.162	3.96E+03	1.13E+01	4.48E+04	42.0317
762	220.3	5.4514	3.64E+03	4.45E-01	1.62E+03	43.8365
763	217.7	-4.561	3.34E+03	-9.48E+0	-3.17E+04	45.721
764	215.2	-14.4	3.07E+03	-1.87E+0	-5.74E+04	47.5738
765	212.9	-22.99	2.83E+03	-2.70E+0	-7.63E+04	49.288
766	210.8	-31	2.60E+03	-3.62E+0	-9.43E+04	51.0135
767	208.8	-41.49	2.40E+03	-4.76E+0	-1.14E+05	52.9669
78	207	-53.78	3.87E+03	-6.30E+0	-2.44E+05	55.4223
896	204	-72.3	2.20E+03	-8.03E+0	-1.77E+05	59.2817
895	202.3	-88.21	2.18E+03	-9.41E+0	-2.05E+05	63.6491
894	200.6	-99.96	1.26E+03	-1.05E+0	-1.32E+05	67.3151
82	199.6	-110.4	1.13E+03	-1.16E+0	-1.31E+05	69.4453
893	198.7	-121.6	1.03E+03	-1.26E+0	-1.30E+05	72.0712
892	197.8	-130.4	9.35E+02	-1.34E+0	-1.26E+05	74.7261
891	197.1	-138.4	8.49E+02	-1.43E+0	-1.22E+05	77.2816
890	196.4	-148	7.71E+02	-1.54E+0	-1.19E+05	81.3397
889	195.8	-159.4	7.00E+02	-1.65E+0	-1.16E+05	85.9137
888	195.2	-170.8	6.38E+02	-1.76E+0	-1.12E+05	90.1651
887	194.7	-180.6	5.79E+02	-1.86E+0	-1.08E+05	93.2647
886	194.2	-191.5	5.27E+02	-1.96E+0	-1.03E+05	96.0097
885	193.8	-201.3	4.79E+02	-2.07E+0	-9.94E+04	98.664
884	193.4	-213.6	4.36E+02	-2.20E+0	-9.57E+04	102.554
883	193	-225.6	3.97E+02	-2.34E+0	-9.29E+04	106.75
882	192.7	-242.1	3.60E+02	-2.59E+0	-9.33E+04	111.916
881	192.4	-275.6	3.29E+02	-3.01E+0	-9.88E+04	123.098
69	192.1	-325.6	1.16E+05	-1.63E+0		147.052
				Compressive Force in Box	-2.54E+06	

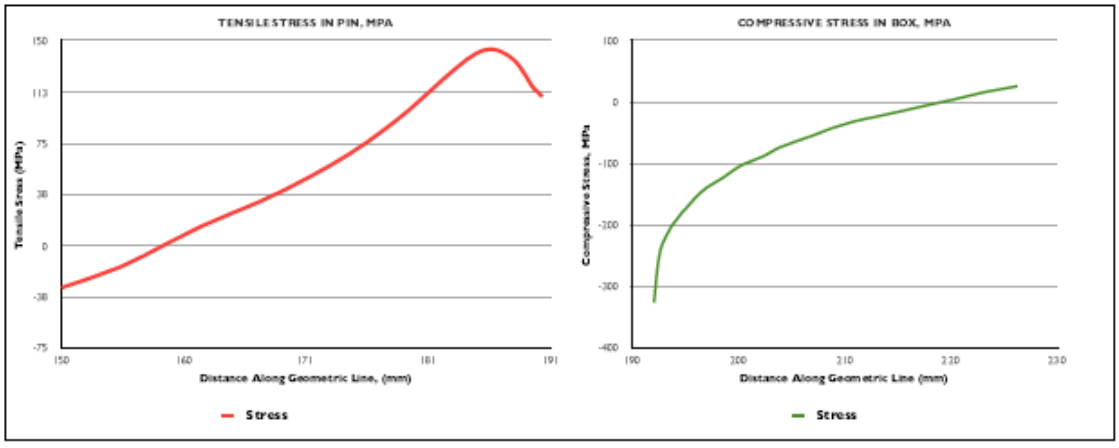

RESULTS SNAPSHOT-2KN

COMPONENT	LENGTH (MM)	PEAK S22 STRESS (MPA)	PRELOAD FORCE IN COMPONENT (MN)
PIN	40.3	144.1	2.51
BOX	34.1	-324.8	-2.53
		% Difference	-0.99

YIELD ANALYSIS-2KN

COMPONENT	MATERIAL	YIELD STRENGTH	PEAK VON MISES STRESS
PIN	Ti 6Al-4V	880.0	599.10
BOX	Ti 6Al-4V	880.0	
	Ti 6Al-4V	880.0	97.19

PIN PRELOAD STRESS VALUES

NODE	X	S22	TRUE ELEMENT FORCE	AVE. NODAL STRESS	FORCE ON ELEMENT FACE	VON MISES STRESS
158	190.27	109.359	3.58E+02	1.11E+02	3.97E+04	16.837
1828	189.97	112.386	3.94E+02	1.14E+02	4.47E+04	17.0962
1829	189.64	114.8	4.32E+02	1.17E+02	5.06E+04	17.2375
1830	189.28	119.333	4.75E+02	1.22E+02	5.81E+04	18.0468
1831	188.88	125.245	5.20E+02	1.28E+02	6.67E+04	19.2072
1832	188.44	130.976	5.71E+02	1.34E+02	7.63E+04	20.4705
1833	187.96	136.063	6.26E+02	1.38E+02	8.63E+04	21.6159
1834	187.43	139.675	6.88E+02	1.41E+02	9.70E+04	22.4933
1835	186.84	142.416	7.54E+02	1.43E+02	1.08E+05	23.2192
1836	186	144.053	8.26E+02	1.44E+02	1.19E+05	23.6894
1837	185.49	143.652	8.32E+02	1.42E+02	1.18E+05	23.7216
1838	184.78	141.153	9.01E+02	1.39E+02	1.25E+05	23.2806
1839	184	136.811	9.75E+02	1.34E+02	1.30E+05	22.4082
1840	183.16	130.893	1.09E+03	1.27E+02	1.39E+05	21.183
1841	182.21	123.788	1.14E+03	1.20E+02	1.37E+05	19.731
1842	181.21	115.93	1.14E+03	1.12E+02	1.27E+05	18.127
160	180.21	107.965	1.13E+03	1.04E+02	1.18E+05	16.5918
1843	179.21	100.165	1.23E+03	9.62E+01	1.19E+05	15.1823
1844	178.11	92.2546	1.35E+03	8.82E+01	1.19E+05	13.8105
1845	176.90	84.1549	1.47E+03	7.99E+01	1.18E+05	12.4843
1846	175.56	75.7114	1.61E+03	7.15E+01	1.15E+05	11.1884
1847	174	67.2245	1.75E+03	6.30E+01	1.10E+05	9.9863
1848	172.5	58.7977	1.91E+03	5.45E+01	1.04E+05	8.9045
1849	170.72	50.1737	2.08E+03	4.57E+01	9.51E+04	7.8909
1850	168.77	41.2974	2.26E+03	3.69E+01	8.33E+04	6.9081
1851	166.63	32.4627	2.45E+03	2.82E+01	6.91E+04	6.0053
1852	164.27	23.8941	2.66E+03	1.90E+01	5.06E+04	5.2347
1853	161.67	14.1758	2.87E+03	7.87E+00	2.26E+04	4.4565
1854	158.82	1.5691	3.77E+03	-6.85E+00	-2.58E+04	3.7085
1855	155	-15.2747	4.79E+03	-2.30E+01	-1.10E+05	3.6718
159	150	-30.7388	7.07E+04	-1.54E+01		5.5078
				Tensile Force in Pin	2.51E+06	

BOX PRELOAD STRESS VALUES

NODE	X	S22	TRUE ELEMENT FORCE	AVE. NODAL STRESS	FORCE ON ELEMENT FACE	VON MISES STRESS
77	226.2	26.767	4.32E+03	2.20E+01	9.49E+04	15.0626
761	223.2	17.165	3.96E+03	1.13E+01	4.49E+04	15.1684
762	220.3	5.5054	3.64E+03	5.23E-01	1.90E+03	15.8189
763	217.7	-4.46	3.34E+03	-9.35E+00	-3.13E+04	16.498
764	215.2	-14.25	3.07E+03	-1.85E+01	-5.69E+04	17.166
765	212.9	-22.8	2.83E+03	-2.68E+01	-7.57E+04	17.7858
766	210.8	-30.78	2.60E+03	-3.60E+01	-9.37E+04	18.4107
767	208.8	-41.23	2.40E+03	-4.74E+01	-1.14E+05	19.1181
78	207	-53.49	3.87E+03	-6.27E+01	-2.43E+05	20.0073
896	204	-71.98	2.20E+03	-7.99E+01	-1.76E+05	21.405
895	202.3	-87.86	2.18E+03	-9.37E+01	-2.05E+05	22.986
894	200.6	-99.61	1.26E+03	-1.05E+02	-1.32E+05	24.3147
82	199.6	-110	1.13E+03	-1.16E+02	-1.31E+05	25.0847
893	198.7	-121.2	1.03E+03	-1.26E+02	-1.29E+05	26.0377
892	197.8	-130	9.35E+02	-1.34E+02	-1.25E+05	27.0044
891	197.1	-138	8.49E+02	-1.43E+02	-1.21E+05	27.9343
890	196.4	-147.6	7.71E+02	-1.53E+02	-1.18E+05	29.4107
889	195.8	-159	7.00E+02	-1.65E+02	-1.15E+05	31.0817
888	195.2	-170.3	6.38E+02	-1.75E+02	-1.12E+05	32.6382
887	194.7	-180.2	5.79E+02	-1.86E+02	-1.07E+05	33.7789
886	194.2	-191	5.27E+02	-1.96E+02	-1.03E+05	34.794
885	193.8	-200.7	4.79E+02	-2.07E+02	-9.92E+04	35.7753
884	193.4	-213.1	4.36E+02	-2.19E+02	-9.55E+04	37.2139
883	193	-225	3.97E+02	-2.33E+02	-9.27E+04	38.77
882	192.7	-241.5	3.60E+02	-2.58E+02	-9.31E+04	40.6773
881	192.4	-274.9	3.29E+02	-3.00E+02	-9.85E+04	44.7987
69	192.1	-324.8	1.16E+05	-1.62E+02		53.8131
				Compressive Force in Box	-2.53E+06	

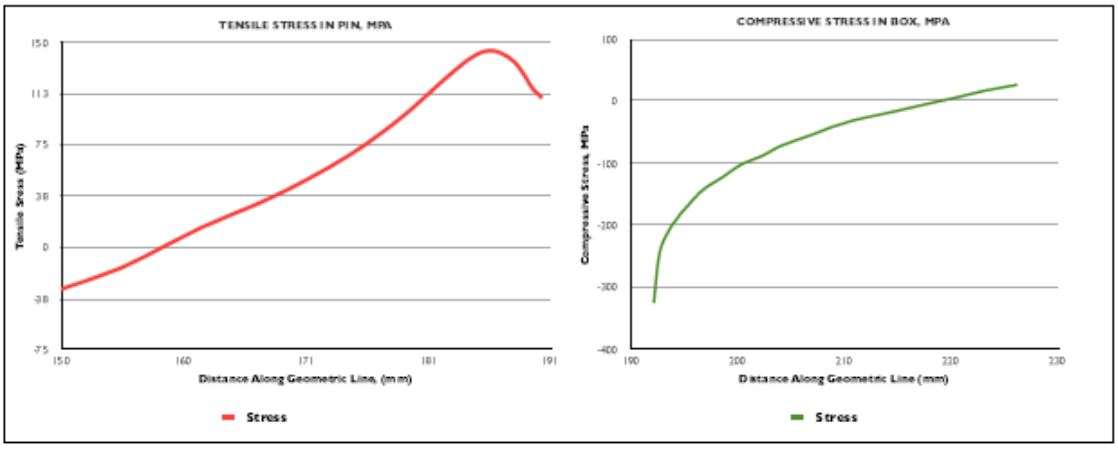

RESULTS SNAPSHOT- 100KN

COMPONENT	LENGTH (MM)	PEAK S22 STRESS (MPA)	PRELOAD FORCE IN COMPONENT (MN)
PIN	40.3	144.5	2.61
BOX	34.1	-283.8	-2.01
		% Difference	-1.30

YIELD ANALYSIS- 100KN

COMPONENT	MATERIAL	YIELD STRENGTH	PEAK VON MISES STRESS
PIN	Ti 6Al-4V	880.0	599.10
BOX	Ti 6Al-4V	880.0	
		% of Yield	68.08

PIN PRELOAD STRESS VALUES

NODE	X	S22	TRUE ELEMENT FORCE	AVE. NODAL STRESS	FORCE ON ELEMENT FACE	VON MISES STRESS
158	190.27	109.761	3.58E+02	1.11E+02	3.99E+04	31.7051
1828	189.97	112.739	3.94E+02	1.14E+02	4.48E+04	32.1932
1829	189.64	115.12	4.32E+02	1.17E+02	5.07E+04	32.4589
1830	189.28	119.618	4.75E+02	1.23E+02	5.82E+04	33.9827
1831	188.88	125.483	5.20E+02	1.28E+02	6.68E+04	36.1678
1832	188.44	131.19	5.71E+02	1.34E+02	7.64E+04	38.5466
1833	187.96	136.279	6.26E+02	1.38E+02	8.65E+04	40.7039
1834	187.43	139.932	6.88E+02	1.41E+02	9.72E+04	42.3567
1835	186.84	142.75	7.54E+02	1.44E+02	1.08E+05	43.7251
1836	186	144.498	8.26E+02	1.44E+02	1.19E+05	44.6124
1837	185.49	144.245	8.32E+02	1.43E+02	1.19E+05	44.6757
1838	184.78	141.933	9.01E+02	1.40E+02	1.26E+05	43.8479
1839	184	137.821	9.75E+02	1.35E+02	1.32E+05	42.208
1840	183.16	132.171	1.09E+03	1.29E+02	1.40E+05	39.9036
1841	182.21	125.342	1.14E+03	1.22E+02	1.39E+05	37.1719
1842	181.21	117.747	1.14E+03	1.14E+02	1.29E+05	34.1533
160	180.21	110.018	1.13E+03	1.06E+02	1.20E+05	31.2634
1843	179.21	102.426	1.23E+03	9.86E+01	1.22E+05	28.6092
1844	178.11	94.7097	1.35E+03	9.07E+01	1.22E+05	26.0254
1845	176.90	86.7863	1.47E+03	8.26E+01	1.22E+05	23.5266
1846	175.56	78.4995	1.61E+03	7.43E+01	1.20E+05	21.084
1847	174	70.1405	1.75E+03	6.60E+01	1.16E+05	18.8172
1848	172.5	61.8083	1.91E+03	5.75E+01	1.10E+05	16.7762
1849	170.72	53.2458	2.08E+03	4.88E+01	1.01E+05	14.8631
1850	168.77	44.3953	2.26E+03	4.00E+01	9.03E+04	13.0075
1851	166.63	35.5489	2.45E+03	3.12E+01	7.66E+04	11.3024
1852	164.27	26.9341	2.66E+03	2.20E+01	5.85E+04	9.8467
1853	161.67	17.1444	2.87E+03	1.08E+01	3.10E+04	8.3774
1854	158.82	4.4531	3.77E+03	-4.00E+00	-1.51E+04	6.9682
1855	155	-12.4476	4.79E+03	-2.02E+01	-9.66E+04	6.9123
159	150	-27.8882	7.07E+04	-1.39E+01		10.3903
				Tensile Force in Pin	2.61E+06	

BOX PRELOAD STRESS VALUES

NODE	X	S22	TRUE ELEMENT FORCE	AVE. NODAL STRESS	FORCE ON ELEMENT FACE	VON MISES STRESS
77	226.2	25.045	4.32E+03	2.12E+01	9.15E+04	28.4058
761	223.2	17.317	3.96E+03	1.27E+01	5.05E+04	28.6115
762	220.3	8.1719	3.64E+03	4.35E+00	1.58E+04	29.84
763	217.7	0.5317	3.34E+03	-3.21E+00	-1.07E+04	31.1222
764	215.2	-6.961	3.07E+03	-1.03E+01	-3.16E+04	32.3829
765	212.9	-13.58	2.83E+03	-1.67E+01	-4.73E+04	33.5504
766	210.8	-19.89	2.60E+03	-2.42E+01	-6.31E+04	34.7262
767	208.8	-28.58	2.40E+03	-3.39E+01	-8.14E+04	36.057
78	207	-39.32	3.87E+03	-4.77E+01	-1.85E+05	37.7295
896	204	-56.04	2.20E+03	-6.34E+01	-1.40E+05	40.3574
895	202.3	-70.86	2.18E+03	-7.64E+01	-1.67E+05	43.3289
894	200.6	-82.01	1.26E+03	-8.69E+01	-1.09E+05	45.8252
82	199.6	-91.72	1.13E+03	-9.70E+01	-1.10E+05	47.2732
893	198.7	-102.3	1.03E+03	-1.06E+02	-1.10E+05	49.0608
892	197.8	-110.6	9.35E+02	-1.14E+02	-1.07E+05	50.872
891	197.1	-118.1	8.49E+02	-1.23E+02	-1.04E+05	52.6164
890	196.4	-127.1	7.71E+02	-1.32E+02	-1.02E+05	55.3869
889	195.8	-137.6	7.00E+02	-1.43E+02	-1.00E+05	58.5166
888	195.2	-148	6.38E+02	-1.53E+02	-9.73E+04	61.4211
887	194.7	-157	5.79E+02	-1.62E+02	-9.37E+04	63.5616
886	194.2	-166.7	5.27E+02	-1.71E+02	-9.01E+04	65.4486
885	193.8	-175.4	4.79E+02	-1.81E+02	-8.67E+04	67.2722
884	193.4	-186.3	4.36E+02	-1.92E+02	-8.35E+04	69.9446
883	193	-196.8	3.97E+02	-2.04E+02	-8.11E+04	72.8336
882	192.7	-211.2	3.60E+02	-2.26E+02	-8.14E+04	76.3982
881	192.4	-240.3	3.29E+02	-2.62E+02	-8.61E+04	84.0778
69	192.1	-283.8	1.16E+05	-1.42E+02		100.685
				Compressive Force in Box	-2.01E+06	

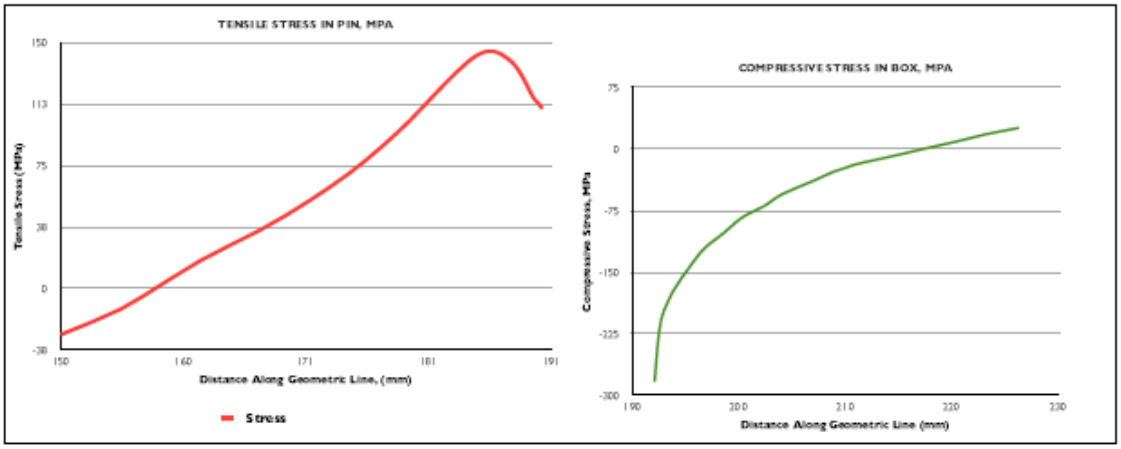

RESULTS SNAPSHOT- 150KN

COMPONENT	LENGTH (MM)	PEAK S22 STRESS (MPA)	PRELOAD FORCE IN COMPONENT (MN)
PIN	40.3	144.7	2.66
BOX	34.1	-263.9	-1.75
		% Difference	-1.52

YIELD ANALYSIS- 150KN

COMPONENT	MATERIAL	YIELD STRENGTH	PEAK VON MISES STRESS
PIN	Ti 6Al-4V	880.0	597.70
BOX	Ti 6Al-4V	880.0	
		% of Yield	67.92

PIN PRELOAD STRESS VALUES

NODE	X	S22	TRUE ELEMENT FORCE	AVE. NODAL STRESS	FORCE ON ELEMENT FACE	VON MISES STRESS
158	190.27	109.963	3.58E+02	1.11E+02	3.99E+04	48.338
1828	189.97	112.916	3.94E+02	1.14E+02	4.49E+04	49.6852
1829	189.64	115.281	4.32E+02	1.18E+02	5.08E+04	50.7622
1830	189.28	119.761	4.75E+02	1.23E+02	5.83E+04	52.7747
1831	188.88	125.602	5.20E+02	1.28E+02	6.68E+04	55.3996
1832	188.44	131.296	5.71E+02	1.34E+02	7.64E+04	57.9451
1833	187.96	136.385	6.26E+02	1.38E+02	8.66E+04	60.2031
1834	187.43	140.06	6.88E+02	1.41E+02	9.73E+04	61.8061
1835	186.84	142.917	7.54E+02	1.44E+02	1.08E+05	63.0214
1836	186	144.721	8.26E+02	1.45E+02	1.19E+05	63.7446
1837	185.49	144.543	8.32E+02	1.43E+02	1.19E+05	63.5627
1838	184.78	142.327	9.01E+02	1.40E+02	1.26E+05	62.4486
1839	184	138.333	9.75E+02	1.36E+02	1.32E+05	60.5153
1840	183.16	132.819	1.09E+03	1.29E+02	1.41E+05	57.8818
1841	182.21	126.132	1.14E+03	1.22E+02	1.40E+05	54.7223
1842	181.21	118.671	1.14E+03	1.15E+02	1.30E+05	51.2315
160	180.21	111.062	1.13E+03	1.07E+02	1.21E+05	47.6972
1843	179.21	103.577	1.23E+03	9.98E+01	1.23E+05	44.2387
1844	178.11	95.9593	1.35E+03	9.20E+01	1.24E+05	40.7337
1845	176.90	88.1261	1.47E+03	8.40E+01	1.24E+05	37.1476
1846	175.56	79.9194	1.61E+03	7.58E+01	1.22E+05	33.4126
1847	174	71.6258	1.75E+03	6.75E+01	1.18E+05	29.6615
1848	172.5	63.3422	1.91E+03	5.91E+01	1.13E+05	25.9395
1849	170.72	54.8114	2.08E+03	5.04E+01	1.05E+05	22.1319
1850	168.77	45.9744	2.26E+03	4.15E+01	9.38E+04	18.2129
1851	166.63	37.1223	2.45E+03	3.28E+01	8.04E+04	14.3119
1852	164.27	28.4844	2.66E+03	2.36E+01	6.26E+04	10.528
1853	161.67	18.6587	2.87E+03	1.23E+01	3.53E+04	6.2351
1854	158.82	5.9248	3.77E+03	-2.54E+00	-9.57E+03	0.6658
1855	155	-11.0042	4.79E+03	-1.87E+01	-8.97E+04	-6.7723
159	150	-26.4322	7.07E+04	-1.32E+01		-13.5981
				Tensile Force in Pin	2.66E+06	

BOX PRELOAD STRESS VALUES

NODE	X	S22	TRUE ELEMENT FORCE	AVE. NODAL STRESS	FORCE ON ELEMENT FACE	VON MISES STRESS
77	226.2	24.164	4.32E+03	2.08E+01	8.97E+04	41.7281
761	223.2	17.392	3.96E+03	1.35E+01	5.33E+04	42.0317
762	220.3	9.53	3.64E+03	6.30E+00	2.29E+04	43.8365
763	217.7	3.0755	3.34E+03	-8.55E-0	-2.86E+02	45.721
764	215.2	-3.247	3.07E+03	-6.06E+0	-1.86E+04	47.5738
765	212.9	-8.883	2.83E+03	-1.16E+0	-3.28E+04	49.288
766	210.8	-14.35	2.60E+03	-1.82E+0	-4.75E+04	51.0135
767	208.8	-22.13	2.40E+03	-2.71E+0	-6.50E+04	52.9669
78	207	-32.08	3.87E+03	-4.00E+0	-1.55E+05	55.4223
896	204	-47.91	2.20E+03	-5.50E+0	-1.21E+05	59.2817
895	202.3	-62.18	2.18E+03	-6.76E+0	-1.48E+05	63.6491
894	200.6	-73	1.26E+03	-7.77E+0	-9.77E+04	67.3151
82	199.6	-82.44	1.13E+03	-8.77E+0	-9.94E+04	69.4453
893	198.7	-92.88	1.03E+03	-9.69E+0	-9.98E+04	72.0712
892	197.8	-101	9.35E+02	-1.05E+0	-9.79E+04	74.7261
891	197.1	-108.3	8.49E+02	-1.13E+0	-9.55E+04	77.2816
890	196.4	-116.7	7.71E+02	-1.21E+0	-9.37E+04	81.3397
889	195.8	-126.2	7.00E+02	-1.32E+0	-9.22E+04	85.9137
888	195.2	-137.2	6.38E+02	-1.42E+0	-9.04E+04	90.1651
887	194.7	-146.1	5.79E+02	-1.50E+0	-8.69E+04	93.2647
886	194.2	-153.9	5.27E+02	-1.58E+0	-8.30E+04	96.0097
885	193.8	-161.5	4.79E+02	-1.66E+0	-7.97E+04	98.664
884	193.4	-171	4.36E+02	-1.76E+0	-7.69E+04	102.554
883	193	-182	3.97E+02	-1.89E+0	-7.52E+04	106.75
882	192.7	-196.2	3.60E+02	-2.10E+0	-7.56E+04	111.916
881	192.4	-223.4	3.29E+02	-2.44E+0	-8.01E+04	123.098
69	192.1	-263.9	1.16E+05	-1.32E+0		147.052
				Compressive Force in Box	-1.75E+06	

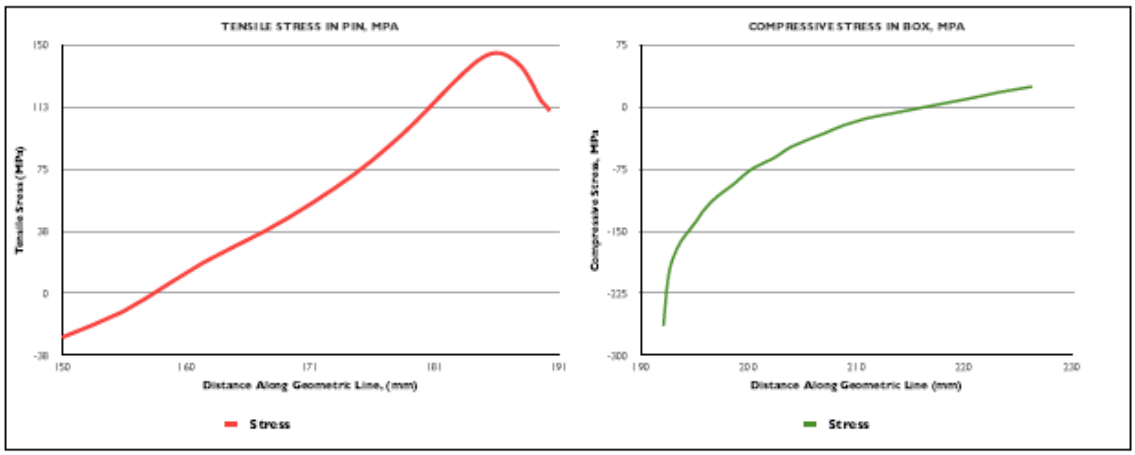

RESULTS SNAPSHOT-250KN

COMPONENT	LENGTH (MM)	PEAK S22 STRESS (MPA)	PRELOAD FORCE IN COMPONENT (MN)
PIN	40.3	145.4	2.77
BOX	34.1	-216.8	-1.22
		%Difference	-2.27

YIELD ANALYSIS-250KN

COMPONENT	MATERIAL	YIELD STRENGTH	PEAK VON MISES STRESS
PIN	Ti6Al-4V	880.0	595.90
BOX	Ti6Al-4V	880.0	
		% of Yield	67.72

PIN PRELOAD STRESS VALUES

NODE	X	S22	TRUE ELEMENT FORCE	AVE. NODAL STRESS	FORCE ON ELEMENT FACE	VON MISES STRESS
158	190.27	110.458	3.58E+02	1.12E+02	4.01E+04	48.338
1828	189.97	113.369	3.94E+02	1.15E+02	4.51E+04	49.6852
1829	189.64	115.708	4.32E+02	1.18E+02	5.10E+04	50.7622
1830	189.28	120.161	4.75E+02	1.23E+02	5.85E+04	52.7747
1831	188.88	125.967	5.20E+02	1.29E+02	6.70E+04	55.3996
1832	188.44	131.65	5.71E+02	1.34E+02	7.66E+04	57.9451
1833	187.96	136.755	6.26E+02	1.39E+02	8.68E+04	60.2031
1834	187.43	140.485	6.88E+02	1.42E+02	9.76E+04	61.8061
1835	186.84	143.434	7.54E+02	1.44E+02	1.09E+05	63.0214
1836	186	145.365	8.26E+02	1.45E+02	1.20E+05	63.7446
1837	185.49	145.35	8.32E+02	1.44E+02	1.20E+05	63.5627
1838	184.78	143.336	9.01E+02	1.41E+02	1.28E+05	62.4486
1839	184	139.584	9.75E+02	1.37E+02	1.33E+05	60.5153
1840	183.16	134.348	1.09E+03	1.31E+02	1.43E+05	57.8818
1841	182.21	127.945	1.14E+03	1.24E+02	1.42E+05	54.7223
1842	181.21	120.753	1.14E+03	1.17E+02	1.33E+05	51.2315
160	180.21	113.382	1.13E+03	1.10E+02	1.24E+05	47.6972
1843	179.21	106.106	1.23E+03	1.02E+02	1.26E+05	44.2387
1844	178.11	98.6794	1.35E+03	9.48E+01	1.28E+05	40.7337
1845	176.90	91.0167	1.47E+03	8.70E+01	1.28E+05	37.1476
1846	175.56	82.9572	1.61E+03	7.89E+01	1.27E+05	33.4126
1847	174	74.7776	1.75E+03	7.07E+01	1.24E+05	29.6615
1848	172.5	66.5699	1.91E+03	6.23E+01	1.19E+05	25.9395
1849	170.72	58.0756	2.08E+03	5.37E+01	1.12E+05	22.1319
1850	168.77	49.2318	2.26E+03	4.48E+01	1.01E+05	18.2129
1851	166.63	40.329	2.45E+03	3.60E+01	8.82E+04	14.3119
1852	164.27	31.6015	2.66E+03	2.66E+01	7.07E+04	10.528
1853	161.67	21.6504	2.87E+03	1.52E+01	4.37E+04	6.2351
1854	158.82	8.7606	3.77E+03	2.24E-01	8.45E+02	0.6658
1855	155	-8.312	4.79E+03	-1.60E+01	-7.69E+04	-6.7723
159	150	-23.7852	7.07E+04	-1.19E+01		-13.5981
				Tensile Force in Pin	2.77E+06	

BOX PRELOAD STRESS VALUES

NODE	X	S22	TRUE ELEMENT FORCE	AVE. NODAL STRESS	FORCE ON ELEMENT FACE	VON MISES STRESS
77	226.2	21.385	4.32E+03	1.89E+01	8.18E+04	41.7281
761	223.2	16.494	3.96E+03	1.38E+01	5.46E+04	42.0317
762	220.3	11.069	3.64E+03	8.96E+00	3.26E+04	43.8365
763	217.7	6.8475	3.34E+03	4.84E+00	1.62E+04	45.721
764	215.2	2.8297	3.07E+03	1.01E+00	3.11E+03	47.5738
765	212.9	-0.808	2.83E+03	-2.61E+00	-7.38E+03	49.288
766	210.8	-4.411	2.60E+03	-7.24E+00	-1.89E+04	51.0135
767	208.8	-10.07	2.40E+03	-1.41E+01	-3.37E+04	52.9669
78	207	-18.05	3.87E+03	-2.47E+01	-9.57E+04	55.4223
896	204	-31.38	2.20E+03	-3.77E+01	-8.30E+04	59.2817
895	202.3	-44.09	2.18E+03	-4.90E+01	-1.07E+05	63.6491
894	200.6	-53.97	1.26E+03	-5.82E+01	-7.32E+04	67.3151
82	199.6	-62.44	1.13E+03	-6.72E+01	-7.62E+04	69.4453
893	198.7	-71.96	1.03E+03	-7.57E+01	-7.79E+04	72.0712
892	197.8	-79.38	9.35E+02	-8.27E+01	-7.74E+04	74.7261
891	197.1	-86.01	8.49E+02	-8.98E+01	-7.63E+04	77.2816
890	196.4	-93.66	7.71E+02	-9.79E+01	-7.55E+04	81.3397
889	195.8	-102.1	7.00E+02	-1.07E+02	-7.49E+04	85.9137
888	195.2	-111.8	6.38E+02	-1.16E+02	-7.38E+04	90.1651
887	194.7	-119.6	5.79E+02	-1.23E+02	-7.12E+04	93.2647
886	194.2	-126.3	5.27E+02	-1.30E+02	-6.82E+04	96.0097
885	193.8	-132.8	4.79E+02	-1.37E+02	-6.55E+04	98.664
884	193.4	-140.6	4.36E+02	-1.45E+02	-6.33E+04	102.554
883	193	-149.7	3.97E+02	-1.56E+02	-6.18E+04	106.75
882	192.7	-161.4	3.60E+02	-1.73E+02	-6.22E+04	111.916
881	192.4	-183.7	3.29E+02	-2.00E+02	-6.58E+04	123.098
69	192.1	-216.8	1.16E+05	-1.08E+02		147.052
				Compressive Force in Box	-1.22E+06	

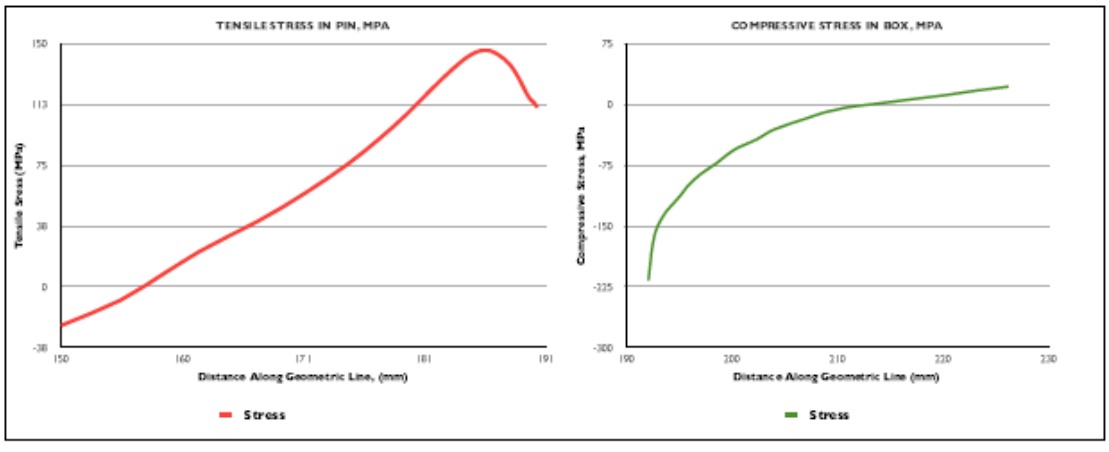

RESULTS SNAPSHOT-450KN

COMPONENT	LENGTH (MM)	PEAK S22 STRESS (MPA)	PRELOAD FORCE IN COMPONENT (MN)
PIN	40.3	150.5	3.70
BOX	34.1	-62.0	-0.10
		%Difference	-38.41

YIELD ANALYSIS-450KN

COMPONENT	MATERIAL	YIELD STRENGTH	PEAK VON MISES STRESS
PIN	Ti 6Al-4V	880.0	597.70
BOX	Ti 6Al-4V	880.0	
	Ti 6Al-4V	880.0	97.19

PIN PRELOAD STRESS VALUES

NODE	X	S22	TRUE ELEMENT FORCE	AVE. NODAL STRESS	FORCE ON ELEMENT FACE	VON MISES STRESS
158	190.27	100.485	3.58E+02	9.92E+01	3.56E+04	16.837
1828	189.97	97.9735	3.94E+02	1.06E+02	4.16E+04	17.0962
1829	189.64	113.382	4.32E+02	1.15E+02	4.96E+04	17.2375
1830	189.28	116.299	4.75E+02	1.17E+02	5.58E+04	18.0468
1831	188.88	118.682	5.20E+02	1.21E+02	6.29E+04	19.2072
1832	188.44	123.21	5.71E+02	1.26E+02	7.21E+04	20.4705
1833	187.96	129.127	6.26E+02	1.32E+02	8.27E+04	21.6159
1834	187.43	134.984	6.88E+02	1.38E+02	9.47E+04	22.4933
1835	186.84	140.316	7.54E+02	1.42E+02	1.07E+05	23.2192
1836	186	144.348	8.26E+02	1.46E+02	1.21E+05	23.6894
1837	185.49	147.68	8.32E+02	1.49E+02	1.24E+05	23.7216
1838	184.78	150.062	9.01E+02	1.50E+02	1.35E+05	23.2806
1839	184	150.534	9.75E+02	1.50E+02	1.46E+05	22.4082
1840	183.16	149.034	1.09E+03	1.47E+02	1.61E+05	21.183
1841	182.21	145.829	1.14E+03	1.43E+02	1.64E+05	19.731
1842	181.21	141.169	1.14E+03	1.38E+02	1.57E+05	18.127
160	180.21	135.319	1.13E+03	1.32E+02	1.49E+05	16.5918
1843	179.21	128.61	1.23E+03	1.25E+02	1.54E+05	15.1823
1844	178.11	121.623	1.35E+03	1.18E+02	1.59E+05	13.8105
1845	176.90	114.645	1.47E+03	1.11E+02	1.64E+05	12.4843
1846	175.56	107.45	1.61E+03	1.04E+02	1.67E+05	11.1884
1847	174	99.9442	1.75E+03	9.60E+01	1.68E+05	9.9863
1848	172.5	91.9569	1.91E+03	8.79E+01	1.68E+05	8.9045
1849	170.72	83.7466	2.08E+03	7.96E+01	1.65E+05	7.8909
1850	168.77	75.3955	2.26E+03	7.10E+01	1.60E+05	6.9081
1851	166.63	66.6288	2.45E+03	6.20E+01	1.52E+05	6.0053
1852	164.27	57.3633	2.66E+03	5.26E+01	1.40E+05	5.2347
1853	161.67	47.9037	2.87E+03	4.32E+01	1.24E+05	4.4565
1854	158.82	38.5166	3.77E+03	3.31E+01	1.25E+05	3.7085
1855	155	27.7367	4.79E+03	2.08E+01	9.94E+04	3.6718
159	150	13.7778	7.07E+04	6.89E+00		5.5078
				Tensile Force in Pin	3.70E+06	

BOX PRELOAD STRESS VALUES

NODE	X	S22	TRUE ELEMENT FORCE	AVE. NODAL STRESS	FORCE ON ELEMENT FACE	VON MISES STRESS
77	226.2	3.7345	4.32E+03	2.98E+00	1.29E+04	15.0626
761	223.2	2.2289	3.96E+03	5.93E+00	2.35E+04	15.1684
762	220.3	9.6308	3.64E+03	8.99E+00	3.27E+04	15.8189
763	217.7	8.3556	3.34E+03	7.75E+00	2.59E+04	16.498
764	215.2	7.15	3.07E+03	6.76E+00	2.08E+04	17.166
765	212.9	6.37	2.83E+03	6.08E+00	1.72E+04	17.7858
766	210.8	5.7904	2.60E+03	5.51E+00	1.44E+04	18.4107
767	208.8	5.2391	2.40E+03	5.02E+00	1.20E+04	19.1181
78	207	4.7954	3.87E+03	4.20E+00	1.63E+04	20.0073
896	204	3.6039	2.20E+03	2.50E+00	5.51E+03	21.405
895	202.3	1.3996	2.18E+03	-8.00E-01	-1.75E+03	22.986
894	200.6	-2.999	1.26E+03	-5.36E+00	-6.74E+03	24.3147
82	199.6	-7.727	1.13E+03	-9.81E+00	-1.11E+04	25.0847
893	198.7	-11.89	1.03E+03	-1.37E+01	-1.41E+04	26.0377
892	197.8	-15.58	9.35E+02	-1.78E+01	-1.67E+04	27.0044
891	197.1	-20.04	8.49E+02	-2.19E+01	-1.86E+04	27.9343
890	196.4	-23.81	7.71E+02	-2.54E+01	-1.96E+04	29.4107
889	195.8	-27.05	7.00E+02	-2.90E+01	-2.03E+04	31.0817
888	195.2	-30.9	6.38E+02	-3.32E+01	-2.12E+04	32.6382
887	194.7	-35.41	5.79E+02	-3.77E+01	-2.18E+04	33.7789
886	194.2	-39.96	5.27E+02	-4.18E+01	-2.20E+04	34.794
885	193.8	-43.6	4.79E+02	-4.54E+01	-2.18E+04	35.7753
884	193.4	-47.28	4.36E+02	-4.88E+01	-2.13E+04	37.2139
883	193	-50.39	3.97E+02	-5.23E+01	-2.08E+04	38.77
882	192.7	-54.16	3.60E+02	-5.59E+01	-2.02E+04	40.6773
881	192.4	-57.69	3.29E+02	-5.99E+01	-1.97E+04	44.7987
69	192.1	-62.03	1.16E+05	-3.10E+00		53.8131
				Compressive Force in Box	-9.65E+04	

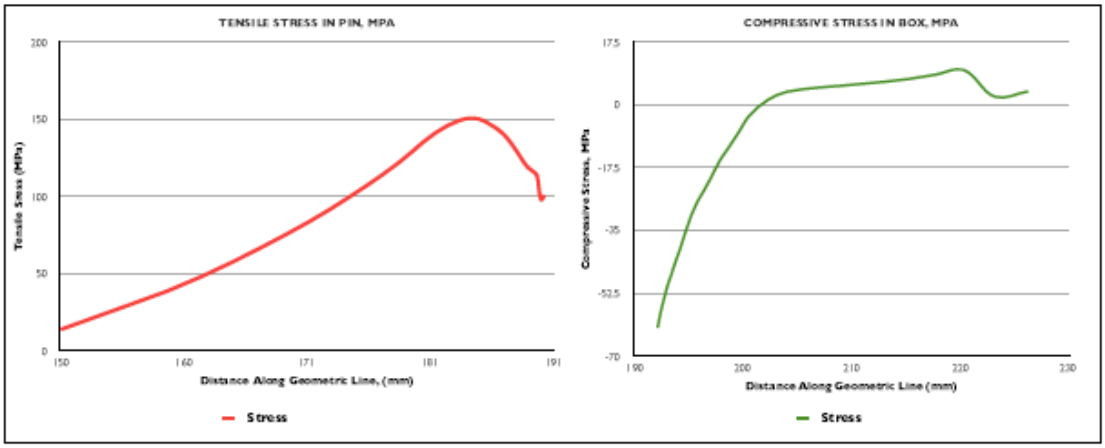

RESULTS SNAPSHOT-550KN

COMPONENT	LENGTH (MM)	PEAK S22 STRESS (MPA)	PRELOAD FORCE IN COMPONENT (MN)
PIN	40.3	168.5	3.45
BOX	34.1	-54.4	-0.02
		% Difference	-214.75

YIELD ANALYSIS-550KN

COMPONENT	MATERIAL	YIELD STRENGTH	PEAK VON MISES STRESS
PIN	Ti 6Al-4V	880.0	659.70
BOX	Ti 6Al-4V	880.0	
		% of Yield	74.97

PIN PRELOAD STRESS VALUES

NODE	X	S22	TRUE ELEMENT FORCE	AVE. NODAL STRESS	FORCE ON ELEMENT FACE	VON MISES STRESS
158	190.27	126.574	3.58E+02	1.28E+02	4.59E+04	31.7051
1828	189.97	129.814	3.94E+02	1.31E+02	5.16E+04	32.1932
1829	189.64	132.472	4.32E+02	1.35E+02	5.83E+04	32.4589
1830	189.28	137.52	4.75E+02	1.41E+02	6.69E+04	33.9827
1831	188.88	144.12	5.20E+02	1.47E+02	7.67E+04	36.1678
1832	188.44	150.672	5.71E+02	1.54E+02	8.78E+04	38.5466
1833	187.96	156.661	6.26E+02	1.59E+02	9.95E+04	40.7039
1834	187.43	161.231	6.88E+02	1.63E+02	1.12E+05	42.3567
1835	186.84	165.048	7.54E+02	1.66E+02	1.25E+05	43.7251
1836	186	167.835	8.26E+02	1.68E+02	1.39E+05	44.6124
1837	185.49	168.512	8.32E+02	1.68E+02	1.40E+05	44.6757
1838	184.78	167.008	9.01E+02	1.65E+02	1.49E+05	43.8479
1839	184	163.619	9.75E+02	1.61E+02	1.57E+05	42.208
1840	183.16	158.62	1.09E+03	1.55E+02	1.70E+05	39.9036
1841	182.21	152.293	1.14E+03	1.49E+02	1.70E+05	37.1719
1842	181.21	144.988	1.14E+03	1.41E+02	1.60E+05	34.1533
160	180.21	137.345	1.13E+03	1.34E+02	1.51E+05	31.2634
1843	179.21	129.683	1.23E+03	1.26E+02	1.55E+05	28.6092
1844	178.11	121.756	1.35E+03	1.18E+02	1.59E+05	26.0254
1845	176.90	113.462	1.47E+03	1.09E+02	1.61E+05	23.5266
1846	175.56	104.606	1.61E+03	1.00E+02	1.61E+05	21.084
1847	174	95.4701	1.75E+03	9.08E+01	1.59E+05	18.8172
1848	172.5	86.1427	1.91E+03	8.12E+01	1.55E+05	16.7762
1849	170.72	76.3138	2.08E+03	7.11E+01	1.48E+05	14.8631
1850	168.77	65.8844	2.26E+03	6.05E+01	1.37E+05	13.0075
1851	166.63	55.1982	2.45E+03	4.99E+01	1.22E+05	11.3024
1852	164.27	44.5616	2.66E+03	3.84E+01	1.02E+05	9.8467
1853	161.67	32.3248	2.87E+03	2.44E+01	7.01E+04	8.3774
1854	158.82	16.4795	3.77E+03	6.11E+00	2.30E+04	6.9682
1855	155	-4.2636	4.79E+03	-1.35E+01	-6.47E+04	6.9123
159	150	-22.7291	7.07E+04	-1.14E+01		10.3903
				Tensile Force in Pin	3.45E+06	

BOX PRELOAD STRESS VALUES

NODE	X	S22	TRUE ELEMENT FORCE	AVE. NODAL STRESS	FORCE ON ELEMENT FACE	VON MISES STRESS
77	226.2	6.9512	4.32E+03	6.71E+0	2.90E+04	28.4058
761	223.2	6.4758	3.96E+03	6.34E+0	2.51E+04	28.6115
762	220.3	6.1972	3.64E+03	6.17E+0	2.25E+04	29.84
763	217.7	6.1514	3.34E+03	6.22E+0	2.08E+04	31.1222
764	215.2	6.2983	3.07E+03	6.32E+0	1.94E+04	32.3829
765	212.9	6.3411	2.83E+03	6.41E+0	1.81E+04	33.5504
766	210.8	6.4771	2.60E+03	6.33E+0	1.65E+04	34.7262
767	208.8	6.1805	2.40E+03	5.75E+0	1.38E+04	36.057
78	207	5.3175	3.87E+03	4.20E+0	1.63E+04	37.7295
896	204	3.0907	2.20E+03	1.82E+0	4.00E+03	40.3574
895	202.3	0.5411	2.18E+03	-7.68E-0	-1.68E+03	43.3289
894	200.6	-2.077	1.26E+03	-3.33E+0	-4.19E+03	45.8252
82	199.6	-4.585	1.13E+03	-6.21E+0	-7.04E+03	47.2732
893	198.7	-7.832	1.03E+03	-9.29E+0	-9.57E+03	49.0608
892	197.8	-10.76	9.35E+02	-1.20E+0	-1.12E+04	50.872
891	197.1	-13.19	8.49E+02	-1.47E+0	-1.25E+04	52.6164
890	196.4	-16.16	7.71E+02	-1.80E+0	-1.38E+04	55.3869
889	195.8	-19.74	7.00E+02	-2.16E+0	-1.51E+04	58.5166
888	195.2	-23.42	6.38E+02	-2.48E+0	-1.59E+04	61.4211
887	194.7	-26.27	5.79E+02	-2.77E+0	-1.60E+04	63.5616
886	194.2	-29.11	5.27E+02	-3.03E+0	-1.59E+04	65.4486
885	193.8	-31.43	4.79E+02	-3.29E+0	-1.57E+04	67.2722
884	193.4	-34.29	4.36E+02	-3.56E+0	-1.55E+04	69.9446
883	193	-36.92	3.97E+02	-3.84E+0	-1.53E+04	72.8336
882	192.7	-39.9	3.60E+02	-4.30E+0	-1.55E+04	76.3982
881	192.4	-46.14	3.29E+02	-5.03E+0	-1.65E+04	84.0778
69	192.1	-54.39	1.16E+05	-2.72E+0		100.685
				Compressive Force in Box	-1.60E+04	

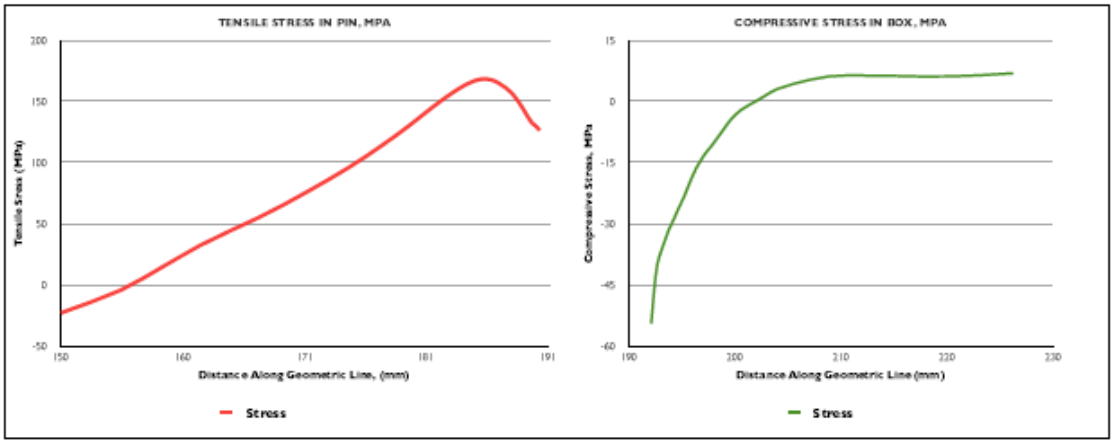

RESULTS SNAPSHOT-600KN

COMPONENT	LENGTH (MM)	PEAK S22 STRESS (MPA)	PRELOAD FORCE IN COMPONENT (MN)
PIN	40.3	183.8	3.76
BOX	34.1	-59.3	-0.02
		%Difference	-216.15

YIELD ANALYSIS-600KN

COMPONENT	MATERIAL	YIELD STRENGTH	PEAK VON MISES STRESS
PIN	Ti 6Al-4V	880.0	718.70
BOX	Ti 6Al-4V	880.0	
		% of Yield	81.67

PIN PRELOAD STRESS VALUES

NODE	X	S22	TRUE ELEMENT FORCE	AVE. NODAL STRESS	FORCE ON ELEMENT FACE	VON MISES STRESS
158	190.27	138.12	3.58E+02	1.40E+02	5.01E+04	48.338
1828	189.97	141.65	3.94E+02	1.43E+02	5.63E+04	49.6852
1829	189.64	144.546	4.32E+02	1.47E+02	6.37E+04	50.7622
1830	189.28	150.05	4.75E+02	1.54E+02	7.30E+04	52.7747
1831	188.88	157.246	5.20E+02	1.61E+02	8.37E+04	55.3996
1832	188.44	164.39	5.71E+02	1.68E+02	9.58E+04	57.9451
1833	187.96	170.92	6.26E+02	1.73E+02	1.09E+05	60.2031
1834	187.43	175.902	6.88E+02	1.78E+02	1.22E+05	61.8061
1835	186.84	180.065	7.54E+02	1.82E+02	1.37E+05	63.0214
1836	186	183.104	8.26E+02	1.83E+02	1.51E+05	63.7446
1837	185.49	183.842	8.32E+02	1.83E+02	1.52E+05	63.5627
1838	184.78	182.203	9.01E+02	1.80E+02	1.63E+05	62.4486
1839	184	178.507	9.75E+02	1.76E+02	1.71E+05	60.5153
1840	183.16	173.057	1.09E+03	1.70E+02	1.85E+05	57.8818
1841	182.21	166.158	1.14E+03	1.62E+02	1.85E+05	54.7223
1842	181.21	158.192	1.14E+03	1.54E+02	1.75E+05	51.2315
160	180.21	149.857	1.13E+03	1.46E+02	1.64E+05	47.6972
1843	179.21	141.5	1.23E+03	1.37E+02	1.69E+05	44.2387
1844	178.11	132.854	1.35E+03	1.28E+02	1.73E+05	40.7337
1845	176.90	123.807	1.47E+03	1.19E+02	1.75E+05	37.1476
1846	175.56	114.146	1.61E+03	1.09E+02	1.76E+05	33.4126
1847	174	104.178	1.75E+03	9.91E+01	1.74E+05	29.6615
1848	172.5	93.9995	1.91E+03	8.86E+01	1.69E+05	25.9395
1849	170.72	83.2723	2.08E+03	7.76E+01	1.61E+05	22.1319
1850	168.77	71.8883	2.26E+03	6.61E+01	1.49E+05	18.2129
1851	166.63	60.2226	2.45E+03	5.44E+01	1.33E+05	14.3119
1852	164.27	48.6098	2.66E+03	4.19E+01	1.11E+05	10.528
1853	161.67	35.249	2.87E+03	2.66E+01	7.64E+04	6.2351
1854	158.82	17.9481	3.77E+03	6.62E+00	2.50E+04	0.6658
1855	155	-4.6995	4.79E+03	-1.48E+01	-7.08E+04	-6.7723
159	150	-24.8588	7.07E+04	-1.24E+01		-13.5981
				Tensile Force in Pin	3.76E+06	

BOX PRELOAD STRESS VALUES

NODE	X	S22	TRUE ELEMENT FORCE	AVE. NODAL STRESS	FORCE ON ELEMENT FACE	VON MISES STRESS
77	226.2	7.6003	4.32E+03	7.34E+00	3.17E+04	41.7281
761	223.2	7.0782	3.96E+03	6.92E+00	2.74E+04	42.0317
762	220.3	6.7703	3.64E+03	6.74E+00	2.45E+04	43.8365
763	217.7	6.7174	3.34E+03	6.80E+00	2.27E+04	45.721
764	215.2	6.8752	3.07E+03	6.90E+00	2.12E+04	47.5738
765	212.9	6.9206	2.83E+03	6.99E+00	1.98E+04	49.288
766	210.8	7.0683	2.60E+03	6.91E+00	1.80E+04	51.0135
767	208.8	6.744	2.40E+03	6.27E+00	1.50E+04	52.9669
78	207	5.8019	3.87E+03	4.59E+00	1.78E+04	55.4223
896	204	3.3712	2.20E+03	1.98E+00	4.36E+03	59.2817
895	202.3	0.5884	2.18E+03	-8.40E-01	-1.83E+03	63.6491
894	200.6	-2.268	1.26E+03	-3.64E+00	-4.57E+03	67.3151
82	199.6	-5.004	1.13E+03	-6.78E+00	-7.68E+03	69.4453
893	198.7	-8.548	1.03E+03	-1.01E+01	-1.05E+04	72.0712
892	197.8	-11.74	9.35E+02	-1.31E+01	-1.22E+04	74.7261
891	197.1	-14.4	8.49E+02	-1.60E+01	-1.36E+04	77.2816
890	196.4	-17.64	7.71E+02	-1.96E+01	-1.51E+04	81.3397
889	195.8	-21.55	7.00E+02	-2.36E+01	-1.65E+04	85.9137
888	195.2	-25.57	6.38E+02	-2.71E+01	-1.73E+04	90.1651
887	194.7	-28.67	5.79E+02	-3.02E+01	-1.75E+04	93.2647
886	194.2	-31.77	5.27E+02	-3.30E+01	-1.74E+04	96.0097
885	193.8	-34.3	4.79E+02	-3.59E+01	-1.72E+04	98.664
884	193.4	-37.41	4.36E+02	-3.89E+01	-1.69E+04	102.554
883	193	-40.29	3.97E+02	-4.19E+01	-1.67E+04	106.75
882	192.7	-43.52	3.60E+02	-4.69E+01	-1.69E+04	111.916
881	192.4	-50.32	3.29E+02	-5.48E+01	-1.80E+04	123.098
69	192.1	-59.32	1.16E+05	-2.97E+01		147.052
				Compressive Force in Box	-1.74E+04	

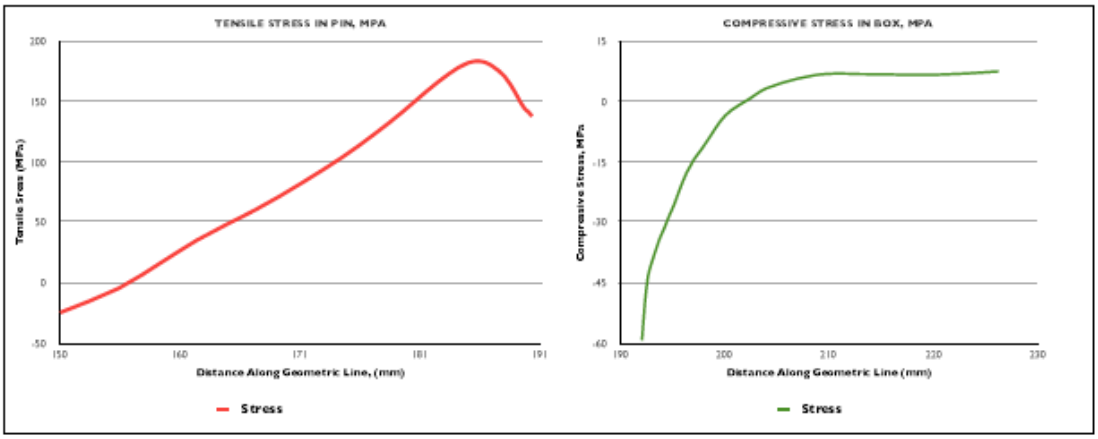

RESULTS SNAPSHOT- IMN

COMPONENT	LENGTH (MM)	PEAK S22 STRESS (MPA)	PRELOAD FORCE IN COMPONENT (MN)
PIN	40.3	307.3	6.27
BOX	34.1	-98.4	-0.03
		%Difference	-227.54

YIELD ANALYSIS- IMN

COMPONENT	MATERIAL	YIELD STRENGTH	PEAK VON MISES STRESS
PIN	Ti 6Al-4V	880.0	1,180.00
BOX	Ti 6Al-4V	880.0	
		% of Yield	134.09

PIN PRELOAD STRESS VALUES

NODE	X	S22	TRUE ELEMENT FORCE	AVE. NODAL STRESS	FORCE ON ELEMENT FACE	VON MISES STRESS
158	190.27	231.408	3.58E+02	2.34E+02	8.40E+04	31.7051
1828	189.97	237.257	3.94E+02	2.40E+02	9.43E+04	32.1932
1829	189.64	242.03	4.32E+02	2.47E+02	1.07E+05	32.4589
1830	189.28	251.18	4.75E+02	2.57E+02	1.22E+05	33.9827
1831	188.88	263.151	5.20E+02	2.69E+02	1.40E+05	36.1678
1832	188.44	275.022	5.71E+02	2.80E+02	1.60E+05	38.5466
1833	187.96	285.878	6.26E+02	2.90E+02	1.82E+05	40.7039
1834	187.43	294.149	6.88E+02	2.98E+02	2.05E+05	42.3567
1835	186.84	301.053	7.54E+02	3.04E+02	2.29E+05	43.7251
1836	186	306.09	8.26E+02	3.07E+02	2.53E+05	44.6124
1837	185.49	307.296	8.32E+02	3.06E+02	2.54E+05	44.6757
1838	184.78	304.538	9.01E+02	3.01E+02	2.72E+05	43.8479
1839	184	298.349	9.75E+02	2.94E+02	2.86E+05	42.208
1840	183.16	289.236	1.09E+03	2.83E+02	3.09E+05	39.9036
1841	182.21	277.708	1.14E+03	2.71E+02	3.09E+05	37.1719
1842	181.21	264.406	1.14E+03	2.57E+02	2.92E+05	34.1533
160	180.21	250.488	1.13E+03	2.44E+02	2.75E+05	31.2634
1843	179.21	236.528	1.23E+03	2.29E+02	2.83E+05	28.6092
1844	178.11	222.079	1.35E+03	2.15E+02	2.89E+05	26.0254
1845	176.90	206.952	1.47E+03	1.99E+02	2.93E+05	23.5266
1846	175.56	190.787	1.61E+03	1.82E+02	2.93E+05	21.084
1847	174	174.095	1.75E+03	1.66E+02	2.90E+05	18.8172
1848	172.5	157.032	1.91E+03	1.48E+02	2.83E+05	16.7762
1849	170.72	139.029	2.08E+03	1.29E+02	2.69E+05	14.8631
1850	168.77	119.904	2.26E+03	1.10E+02	2.49E+05	13.0075
1851	166.63	100.287	2.45E+03	9.05E+01	2.22E+05	11.3024
1852	164.27	80.7389	2.66E+03	6.95E+01	1.85E+05	9.8467
1853	161.67	58.2338	2.87E+03	4.37E+01	1.25E+05	8.3774
1854	158.82	29.0843	3.77E+03	1.00E+01	3.77E+04	6.9682
1855	155	-9.0718	4.79E+03	-2.60E+01	-1.25E+05	6.9123
159	150	-43.0229	7.07E+04	-2.15E+01		10.3903
				Tensile Force in Pin	6.27E+06	

BOX PRELOAD STRESS VALUES

NODE	X	S22	TRUE ELEMENT FORCE	AVE. NODAL STRESS	FORCE ON ELEMENT FACE	VON MISES STRESS
77	226.2	13.271	4.32E+03	1.28E+01	5.53E+04	28.4058
761	223.2	12.316	3.96E+03	1.20E+01	4.75E+04	28.6115
762	220.3	11.682	3.64E+03	1.16E+01	4.21E+04	29.84
763	217.7	11.475	3.34E+03	1.15E+01	3.86E+04	31.1222
764	215.2	11.624	3.07E+03	1.16E+01	3.57E+04	32.3829
765	212.9	11.609	2.83E+03	1.17E+01	3.31E+04	33.5504
766	210.8	11.777	2.60E+03	1.15E+01	2.98E+04	34.7262
767	208.8	11.155	2.40E+03	1.03E+01	2.48E+04	36.057
78	207	9.5055	3.87E+03	7.42E+00	2.88E+04	37.7295
896	204	5.3443	2.20E+03	2.98E+00	6.56E+03	40.3574
895	202.3	0.615	2.18E+03	-1.79E+0	-3.90E+03	43.3289
894	200.6	-4.189	1.26E+03	-6.46E+0	-8.13E+03	45.8252
82	199.6	-8.741	1.13E+03	-1.17E+0	-1.33E+04	47.2732
893	198.7	-14.65	1.03E+03	-1.73E+0	-1.78E+04	49.0608
892	197.8	-19.98	9.35E+02	-2.22E+0	-2.07E+04	50.872
891	197.1	-24.38	8.49E+02	-2.71E+0	-2.30E+04	52.6164
890	196.4	-29.74	7.71E+02	-3.30E+0	-2.54E+04	55.3869
889	195.8	-36.21	7.00E+02	-3.95E+0	-2.77E+04	58.5166
888	195.2	-42.86	6.38E+02	-4.54E+0	-2.90E+04	61.4211
887	194.7	-47.97	5.79E+02	-5.05E+0	-2.93E+04	63.5616
886	194.2	-53.06	5.27E+02	-5.51E+0	-2.90E+04	65.4486
885	193.8	-57.21	4.79E+02	-5.98E+0	-2.86E+04	67.2722
884	193.4	-62.31	4.36E+02	-6.47E+0	-2.82E+04	69.9446
883	193	-67.02	3.97E+02	-6.97E+0	-2.77E+04	72.8336
882	192.7	-72.33	3.60E+02	-7.79E+0	-2.81E+04	76.3982
881	192.4	-83.53	3.29E+02	-9.10E+0	-2.99E+04	84.0778
69	192.1	-98.38	1.16E+05	-4.92E+0		100.685
				Compressive Force in Box	-2.75E+04	

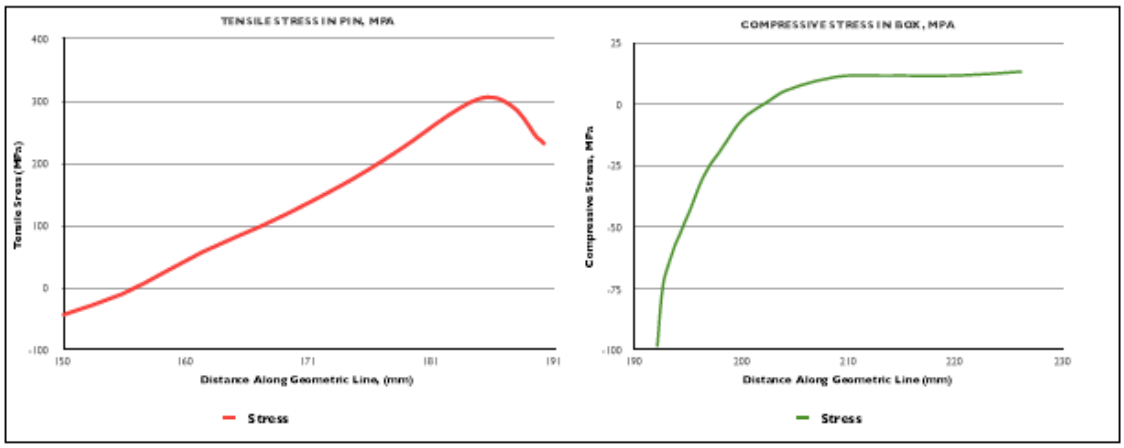

8.5 Appendix D: FORTRAN77 Mesh Generator and Input Files

8.5.1 FORTRAN77 Mesh Generator

----- FORTRAN77 MESH GENERATOR ELECTRONICALLY ATTACHED -------

8.5.2 FORTRAN77 Mesh-Generated Input File (Abridged)

----- FULL NPUT FILE ELECTRONICALLY ATTACHED -------

```
*HEADING
Default
****----------------------------------------------------------------------
**   Outer diameter  =    165.000 mm
**    Inner diameter  =     75.000  mm
**    Bevel dia. of shoulder =    165.000 mm
**    Length of the assembly =    412.500 mm
**
**     Axial Loading Only
**     Total Axial Load  =   169714.282NEWTONS
**
*PREPRINT,  ECHO =  NO, MODEL = NO, HISTORY=NO
*RESTART,WRITE,FREQUENCY =   20
*NODE,  NSET = BOX
1 ,  0.63081592E+02, -0.22225000E+02
2 ,  0.63425536E+02, -0.23888879E+02
3 ,  0.63769479E+02, -0.25552757E+02
131 ,  0.57304119E+02, -0.22225000E+02
    .
    .
    .
4953 ,  0.82500000E+02, -0.12475620E+02
4954 ,  0.61086456E+02, -0.13665780E+02
4955 ,  0.65503769E+02, -0.13665780E+02

*NODE,  NSET = PIN
134 ,  0.56468714E+02, -0.22474812E+02
135 ,  0.56565138E+02, -0.22707600E+02
256 ,  0.54505426E+02, -0.22225000E+02
    .
    .
    .
5749 ,  0.69642857E+02,  0.25477047E+02
5750 ,  0.76071429E+02,  0.25477047E+02
5751 ,  0.82500000E+02,  0.25477047E+02

*NSET ,  NSET = BOXEND
4306 ,
4307 ,
4308 ,
4309 ,
4310 ,
4311 ,
4312 ,
4313 ,
4314 ,
4315 ,
4316 ,
4317 ,
```

```
4318 ,
4319 ,    4320
*NSET ,  NSET = PINEND
5499 ,
5500 ,
5501 ,
5502 ,
5503 ,
5504 ,
5505 ,
5506 ,
5507 ,
5508 ,
5509 ,
5510 ,
5511 ,
5512 ,    5513

***Alternating BOXT and PINT  elements
*ELEMENT , TYPE = CAX8, ELSET e= BOXT1 ***
1,   133,   21,   60,   131,   20,   47,   85,   132
2,   21,   23,   62,   60,   22,   48,   61,   47
3,   23,   25,   64,   62,   24,   49,   63,   48
4,   25,   27,   66,   64,   26,   50,   65,   49
     .
     .
     .
1784,  5735,  5490,  5492,  5737,  5747,  5491,  5748,  5736
1785,  5737,  5492,  5494,  5739,  5748,  5493,  5749,  5738
1786,  5739,  5494,  5496,  5741,  5749,  5495,  5750,  5740
1787,  5741,  5496,  5498,  5743,  5750,  5497,  5751,  5742

*ELSET ,  ELSET =  BOXEND
1457 ,
1456 ,
1455 ,
1454 ,
1453 ,
1452 ,    1451
*ELSET ,  ELSET =  PINEND
1787 ,
1786 ,
1785 ,
1784 ,
1783 ,
1781 ,    1780
*ELSET, ELSET  =  TRBOX
BOXT1 ,
BOXT2 ,
BOXT3 ,
BOXT4 ,
BOXT5 ,
BOXT6 ,
BOXT7 ,
BOXT8 ,
BOXT9 ,
BOXT10 ,
BOXT11 ,
BOXT12 ,  BOXT13
*ELSET, ELSET  =  TRPIN
PINT1 ,
PINT2 ,
PINT3 ,
PINT4 ,
```

```
PINT5 ,
PINT6 ,
PINT7 ,
PINT8 ,
PINT9 ,
PINT10 ,
PINT11 ,
PINT12 ,  PINT13
*ELSET , ELSET = BOX
UNBOX1, UNBOX2
*ELSET , ELSET =  SCFBX 1
893 ,
894 ,
895 ,
896 ,
897 ,     898
*ELSET , ELSET =  SCFBX 2
819 ,
820 ,
821 ,
822 ,
823 ,     824
*ELSET , ELSET =  SCFBX 3
745 ,
746 ,
747 ,
748 ,
749 ,     750
*ELSET , ELSET =  SCFBX 4
671 ,
672 ,
673 ,
674 ,
675 ,     676
*ELSET , ELSET =  SCFBX 5
597 ,
598 ,
599 ,
600 ,
601 ,     602
*ELSET , ELSET =  SCFBX 6
523 ,
524 ,
525 ,
526 ,
527 ,     528
*ELSET , ELSET =  SCFBX 7
449 ,
450 ,
451 ,
452 ,
453 ,     454
*ELSET , ELSET =  SCFBX 8
375 ,
376 ,
377 ,
378 ,
379 ,     380
*ELSET , ELSET =  SCFBX 9
301 ,
302 ,
303 ,
304 ,
305 ,     306
```

```
*ELSET , ELSET =  SCFBX10
227 ,
228 ,
229 ,
230 ,
231 ,     232
*ELSET , ELSET =  SCFBX11
153 ,
154 ,
155 ,
156 ,
157 ,     158
*ELSET , ELSET =  SCFBX12
79 ,
80 ,
81 ,
82 ,
83 ,      84
*ELSET , ELSET =  SCFBX13
5 ,
6 ,
7 ,
8 ,
9 ,      10
*ELSET  , ELSET = SCUBX0
1502 ,
1503 ,
1504 ,
1505 ,
1506 ,    1507
*ELSET  , ELSET = SCUBX1
1227 ,
1228 ,
1229 ,
1230 ,
1231 ,
1232 ,
1231 ,    1232
*ELSET  , ELSET = SCUBX2
1261 ,
1262 ,
1263 ,
1264 ,
1265 ,    1266
*ELSET ,  ELSET = SCFPN 1
35 ,
36 ,
37 ,
1548 ,   1549,    1550
*ELSET ,  ELSET = SCFPN 2
109 ,
110 ,
111 ,
46 ,    47,     48
*ELSET ,  ELSET = SCFPN 3
183 ,
184 ,
185 ,
120 ,    121,    122
*ELSET ,  ELSET = SCFPN 4
257 ,
258 ,
259 ,
194 ,    195,    196
```

```
*ELSET ,  ELSET = SCFPN 5
331 ,
332 ,
333 ,
268 ,    269,     270
*ELSET ,  ELSET = SCFPN 6
405 ,
406 ,
407 ,
342 ,    343,     344
*ELSET ,  ELSET = SCFPN 7
479 ,
480 ,
481 ,
416 ,    417,     418
*ELSET ,  ELSET = SCFPN 8
553 ,
554 ,
555 ,
490 ,    491,     492
*ELSET ,  ELSET = SCFPN 9
627 ,
628 ,
629 ,
564 ,    565,     566
*ELSET ,  ELSET = SCFPN10
701 ,
702 ,
703 ,
638 ,    639,     640
*ELSET ,  ELSET = SCFPN11
775 ,
776 ,
777 ,
712 ,    713,     714
*ELSET ,  ELSET = SCFPN12
849 ,
850 ,
851 ,
786 ,    787,     788
*ELSET ,  ELSET = SCFPN13
923 ,
924 ,
925 ,
860 ,    861,     862
*ELSET ,  ELSET = SCFPN14
934 ,
935 ,
936 ,
1459 ,   1460,    1461
*ELSET, ELSET = SCUPN1
1559 ,
1560 ,
1561 ,
1562 ,
1563 ,     1564
*ELSET,  ELSET = ROOTP
1650 ,     1651
*ELSET , ELSET = SCFBOX
SCFBX 1,
SCFBX 2,
SCFBX 3,
SCFBX 4,
SCFBX 5,
```

```
SCFBX 6,
SCFBX 7,
SCFBX 8,
SCFBX 9,
SCFBX10,
SCFBX11,
SCFBX12,
SCFBX13,
SCUBX1, SCUBX2,  SCUBX0
*ELSET , ELSET = SCFPIN
SCFPN 1,
SCFPN 2,
SCFPN 3,
SCFPN 4,
SCFPN 5,
SCFPN 6,
SCFPN 7,
SCFPN 8,
SCFPN 9,
SCFPN10,
SCFPN11,
SCFPN12,
SCFPN13,
SCFPN14,
SCUPN1, ROOTP
*SOLID SECTION,   ELSET = BOX , MATERIAL = STEEL
*SOLID SECTION,   ELSET = PIN , MATERIAL = STEEL
*SOLID SECTION,   ELSET = TRBOX ,MATERIAL = STEEL
*SOLID SECTION,   ELSET = TRPIN ,MATERIAL = STEEL
*MATERIAL , NAME  =  STEEL
*ELASTIC
203.E+03,  0.3
***PLOT
***DRAW
*STEP, INC=20
*STATIC
0.2, 1.0,  0.2
*BOUNDARY
BOXEND,    2
4306, 1
*CLOAD
5513 , 2,  0.40408162E+04
5500 , 2,  0.16163265E+05
5502 , 2,  0.16163265E+05
5504 , 2,  0.16163265E+05
5506 , 2,  0.16163265E+05
5508 , 2,  0.16163265E+05
5510 , 2,  0.16163265E+05
5512 , 2,  0.16163265E+05
5500 , 2,  0.80816325E+04
5502 , 2,  0.80816325E+04
5504 , 2,  0.80816325E+04
5506 , 2,  0.80816325E+04
5508 , 2,  0.80816325E+04
5510 , 2,  0.80816325E+04
5499 , 2,  0.40408162E+04
*ELPRINT, ELSET = SCFBOX, FREQUENCY=20,
POSITION= AVERAGED AT NODES , SUMMARY = YES
S , MISES, SP
*PRINT, CONTACT = YES
*ELPRINT, ELSET = SCFPIN, FREQUENCY=20,
POSITION= AVERAGED AT NODES , SUMMARY = YES
S, MISES , SP
*ENDSTEP
```

8.5.3 Developed 2-D Model Input File - Preload (Abridged)

----------Full Input Files of All Developed Models Attached Electronically----------

---Models Developed With King Assistance of Mr. Bob Johnson of DAMT Ltd---

```
*HEADING
Model: Model_2D_Final Date: 29/04/2010  13:04:25
**
** COORDINATES
*NODE, NSET=NALL
      1,   150.00000    ,   59.965270    ,   0.0000000
      2,   168.92883    ,   92.334180    ,   0.0000000
      3,   170.46879    ,   92.862620    ,   0.0000000
         .
         .
         .
  12684,   188.24437    ,  -458.13861    ,  0.16364378E-20
  12685,   188.24437    ,  -463.16153    ,  0.16563944E-20
  12686,   188.24437    ,  -468.18446    ,  0.16763509E-20
**
** ELEMENT TOPOLOGY
*Solid Section, elset=E1   , material=M1
*ELEMENT, TYPE=CAX4  ,ELSET=E1
      1,     72,    732,   2160,    676
      2,      1,    691,   2161,    739
      3,     74,    752,   2162,    712
         .
         .
         .
  10338,   10868,   11321,   11320,   11185
  10339,   11211,   11260,   11315,   11210
  10340,   11315,   11260,   11192,   11212
*
*Solid Section, elset=E1   , material=M1
*ELEMENT, TYPE=CAX4  ,ELSET=E1
  10341,     73,    2054,   11322,    690
  10342,   2054,    2055,   11323,   11322
  10343,   2055,    2056,   11324,   11323
         .
         .
         .
```

```
  11810,  12611,  12612,  12605,  12606
  11811,  12610,  12611,  12606,  12607
  11812,  12609,  12610,  12607,  12608
**
** MATERIAL PROPERTIES
** M1
*MATERIAL, NAME=M1
*ELASTIC, TYPE=ISOTROPIC
   70000.   ,  0.35000
*DENSITY
  0.270600E-08,
*EXPANSION, TYPE=ISO
  2.310000E-05,
**
** M2
*MATERIAL, NAME=M2
*ELASTIC, TYPE=ISOTROPIC
   70000.   ,  0.35000
*DENSITY
  0.270600E-08,
*EXPANSION, TYPE=ISO
  2.310000E-05,
**
** SLIDELINES
** Slideline part = Set   SC11  (MASTER)
*SURFACE, NAME=  surf_SC11 , TYPE=ELEMENT
    852,  S1
    852,  S4
    853,  S1
    853,  S4
          .
          .
          .
   1537,  S1
   1538,  S1
   1539,  S2
**
** Slideline part = Set   SC21   (SLAVE)
*SURFACE, NAME=  surf_SC21 , TYPE=ELEMENT
   7118,  S4
   7120,  S1
   7120,  S4
          .
```

```
          .
          .
    7793,  S4
    7794,  S4
    7795,  S3
**
** Slideline part = Set   SC12  (MASTER)
*SURFACE, NAME=  surf_SC12 , TYPE=ELEMENT
     353,  S1
     354,  S4
     355,  S1
     355,  S4
     359,  S1
     360,  S2
     361,  S1
     362,  S1
     363,  S1
     364,  S1
     365,  S1
     366,  S2
     403,  S1
     404,  S1
     404,  S4
     405,  S4
     412,  S1
     413,  S2
     414,  S1
     415,  S2
**
** Slideline part = Set   SC22   (SLAVE)
*SURFACE, NAME=  surf_SC22 , TYPE=ELEMENT
    6214,  S4
    6215,  S1
    6215,  S4
    6236,  S4
    6237,  S4
    6238,  S4
    6239,  S3
    6240,  S4
    6241,  S4
    6242,  S4
    6243,  S4
    6244,  S4
```

```
   6245,  S4
   6246,  S4
   6247,  S4
   6248,  S4
   6276,  S4
   6277,  S4
**
** contact definition C1
** Master part = Set   SC11
** Slave  part = Set   SC21
**
*CONTACT PAIR, INTERACTION=SMOOTH1
     surf_SC21,      surf_SC11
*SURFACE INTERACTION, NAME=SMOOTH1
*FRICTION
   0.0800,
**
** contact definition C2
** Master part = Set   SC12
** Slave  part = Set   SC22
**
*CONTACT PAIR, INTERACTION=SMOOTH2
     surf_SC22,      surf_SC12
*SURFACE INTERACTION, NAME=SMOOTH2
*FRICTION
   0.0800,
**
** EARTH SPRINGS
**
** FIXED FREEDOMS
**
*BOUNDARY
    162, 2
    163, 2
   2145, 2
   2146, 2
   2147, 2
   2148, 2
   2149, 2
   2150, 2
   2151, 2
   2152, 2
   2153, 2
```

```
   2154, 2
   2155, 2
   2156, 2
   2157, 2
   2158, 2
   2159, 2
*INITIAL CONDITIONS,TYPE=TEMPERATURE
Nall, 0.0
**
** LOADING
**
*Step, INC=100, NLGEOM=YES
Case    1  STEP1 (RESOLVE OVERLAP)
*Static
     0.10000,     1.00000, 1e-05, 1.0
*CONTROLS,PARAMETERS=TIME INCREMENTATION
, , , , , , 25, , ,
**
*contact interference, shrink
surf_SC21, surf_SC11
surf_SC22, surf_SC12
**
** LOADS
**
**
** OUTPUT REQUESTS
**
*Restart, write, frequency=     1
*Output, field, op=NEW, frequency=     1
*Node Output
U, RF, CF
*Element Output
S, E, NFORC
*Output, history, op=NEW, frequency=     1
*El Print, frequency=     1
*NODE PRINT, totals=yes, frequency=     1
   cf,
   rf,
*File format, ascii
*NODE FILE, FREQUENCY=     1
U
*EL FILE, POSITION=NODES, FREQUENCY=     1
S,  E
```

```
NFORC
*End Step
*Step, INC=100, NLGEOM=YES
Case    2  STEP2 (NO AXIAL LOAD)
*Static
    0.10000,     1.00000, 1e-05, 1.0
*CONTROLS,PARAMETERS=TIME INCREMENTATION
, , , , , , 25, , ,
**
** LOADS
**
**  Load  Case
**     1   2 Line  SLOD , traction      0.0 , Pressure      0.0
**
*Cload,OP=NEW
**
*End Step
```

8.5.4 Developed 2-D Model Input File – Axial + Preload (Abridged)

```
*HEADING
Model: MODEL_2D_FINAL Date: 07/03/2011  00:44:56
**
** COORDINATES
**
*NODE, NSET=NALL
      1,   150.00000    ,   59.965270    ,   0.0000000
      2,   168.92883    ,   92.234180    ,   0.0000000
      3,   170.46879    ,   92.762620    ,   0.0000000
          .
          .
          .
  12706,   188.24437    ,  -458.17122    ,   0.0000000
  12707,   188.24437    ,  -463.19088    ,   0.0000000
  12708,   188.24436    ,  -468.21055    ,   0.0000000
**
** ELEMENT TOPOLOGY
**
*Solid Section, elset=E1   , material=M1
*ELEMENT, TYPE=CAX4  ,ELSET=E1
```

```
      1,     72,    732,   2160,    676
      2,      1,    691,   2161,    739
      3,     74,    752,   2162,    712
         .
         .
         .
   4759,    992,    993,   5992,   6316
   4760,   5992,   6207,   6307,   6316
   4761,   6307,   5991,    992,   6316

*Solid Section, elset=E2   , material=M2
*ELEMENT, TYPE=CAX4  ,ELSET=E2
   4762,    157,   1739,   6317,   1759
   4763,   1759,   6317,   6318,   1758
   4764,   1758,   6318,   6319,   1757
         .
         .
         .
  10360,  10890,  11343,  11342,  11207
  10361,  11233,  11282,  11337,  11232
  10362,  11337,  11282,  11214,  11234
*
*Solid Section, elset=E1   , material=M1
*ELEMENT, TYPE=CAX4  ,ELSET=E1
  10363,     73,   2054,  11344,    690
  10364,   2054,   2055,  11345,  11344
  10365,   2055,   2056,  11346,  11345
         .
         .
         .
  11832,  12633,  12634,  12627,  12628
  11833,  12632,  12633,  12628,  12629
  11834,  12631,  12632,  12629,  12630
**
** MATERIAL PROPERTIES
**
** M1
*MATERIAL, NAME=M1
*ELASTIC, TYPE=ISOTROPIC
   70000.   ,  0.35000
*DENSITY
  0.270600E-08,
*EXPANSION, TYPE=ISO
```

```
  2.310000E-05,
**
** M2
*MATERIAL, NAME=M2
*ELASTIC, TYPE=ISOTROPIC
   70000.    ,  0.35000
*DENSITY
  0.270600E-08,
*EXPANSION, TYPE=ISO
  2.310000E-05,
**
**
** SLIDELINES
**
** Slideline part = Set   SC11  (MASTER)
**
*SURFACE, NAME=  surf_SC11 , TYPE=ELEMENT
    847,  S1
    847,  S4
    848,  S1
    848,  S4
          .
          .
          .
   1532,  S1
   1533,  S1
   1534,  S2
**
** Slideline part = Set   SC21   (SLAVE)
**
*SURFACE, NAME=  surf_SC21 , TYPE=ELEMENT
   7140,  S4
   7142,  S1
   7142,  S4
          .
          .
          .
   7814,  S4
   7815,  S4
   7816,  S4
   7817,  S3
**
** Slideline part = Set   SC12  (MASTER)
```

```
**
*SURFACE, NAME=  surf_SC12 , TYPE=ELEMENT
    353,  S1
    354,  S4
    355,  S1
    355,  S4
    359,  S1
    360,  S2
    361,  S1
    362,  S1
    363,  S1
    364,  S1
    365,  S1
    366,  S2
    408,  S1
    409,  S1
    409,  S4
    410,  S4
    417,  S1
    418,  S2
    419,  S1
    420,  S2
**
** Slideline part = Set   SC22   (SLAVE)
**
*SURFACE, NAME=  surf_SC22 , TYPE=ELEMENT
   6236,  S4
   6237,  S1
   6237,  S4
   6258,  S4
   6259,  S4
   6260,  S4
   6261,  S3
   6262,  S4
   6263,  S4
   6264,  S4
   6265,  S4
   6266,  S4
   6267,  S4
   6268,  S4
   6269,  S4
   6270,  S4
   6298,  S4
```

```
   6299,  S4
**
** contact definition C1
** Master part = Set   SC11
** Slave  part = Set   SC21
**
*CONTACT PAIR, INTERACTION=SMOOTH1
     surf_SC21,      surf_SC11
*SURFACE INTERACTION, NAME=SMOOTH1
*FRICTION
   0.0500,
**
** contact definition C2
** Master part = Set   SC12
** Slave  part = Set   SC22
**
*CONTACT PAIR, INTERACTION=SMOOTH2
     surf_SC22,      surf_SC12
*SURFACE INTERACTION, NAME=SMOOTH2
*FRICTION
   0.0500,
**
** EARTH SPRINGS
**
** FIXED FREEDOMS
**
*BOUNDARY
    162, 2
    163, 2
   2145, 2
   2146, 2
   2147, 2
   2148, 2
   2149, 2
   2150, 2
   2151, 2
   2152, 2
   2153, 2
   2154, 2
   2155, 2
   2156, 2
   2157, 2
   2158, 2
```

```
   2159, 2
*INITIAL CONDITIONS,TYPE=TEMPERATURE
Nall, 0.0
**
** LOADING
**
*Step, INC=100, NLGEOM=YES
Case    1  STEP1 (RESOLVE OVERLAP)
*Static
     0.10000,     1.00000, 1e-05, 1.0
*CONTROLS,PARAMETERS=TIME INCREMENTATION
, , , , , , 25, , ,
**
*contact interference, shrink
surf_SC21, surf_SC11
surf_SC22, surf_SC12
**
** LOADS
**
** OUTPUT REQUESTS
**
*Restart, write, frequency=     1
*Output, field, op=NEW, frequency=     1
*Node Output
U, RF, CF
*Element Output
S, E, NFORC
*Output, history, op=NEW, frequency=     1
*El Print, frequency=     1
*NODE PRINT, totals=yes, frequency=     1
  cf,
  rf,
*File format, ascii
*NODE FILE, FREQUENCY=     1
U
*EL FILE, POSITION=NODES, FREQUENCY=     1
S, E
NFORC
*End Step
*Step, INC=100, NLGEOM=YES
Case    2  STEP2 (1MN END LOAD)
*Static
     0.10000,     1.00000, 1e-05, 1.0
```

```
*CONTROLS,PARAMETERS=TIME INCREMENTATION
, , , , , , 25, , ,
**
** LOADS
**
**  Load  Case
**     1   2 Line  SLOD , traction      0.0 , Pressure -69.2178
**
*Cload,OP=NEW
    99,1,  0.31222409E-08
    99,2,   232392.99
   100,1,  0.20970936E-08
   100,2,   156874.50
  1139,1,  0.42948242E-08
  1139,2,   320315.82
  1140,1,  0.44268971E-08
  1140,2,   330166.06
  1141,1,  0.45589700E-08
  1141,2,   340016.30
  1142,1,  0.46910429E-08
  1142,2,   349866.54
  1143,1,  0.48231158E-08
  1143,2,   359716.78
  1144,1,  0.49551887E-08
  1144,2,   369567.02
  1145,1,  0.50872616E-08
  1145,2,   379417.25
  1146,1,  0.52193345E-08
  1146,2,   389267.49
  1147,1,  0.53514075E-08
  1147,2,   399117.73
  1148,1,  0.54834804E-08
  1148,2,   408967.97
  1149,1,  0.56155533E-08
  1149,2,   418818.21
  1150,1,  0.57476262E-08
  1150,2,   428668.45
  1151,1,  0.58796991E-08
  1151,2,   438518.69
  1152,1,  0.60117720E-08
  1152,2,   448368.92
  1153,1,  0.61438449E-08
  1153,2,   458219.16
```

**
*End Step

8.5.5 Developed 3-D Model Input File - Preload (Abridged)

```
*HEADING
**
**
**  IMPOSED DISPLACEMENT ***
**  ************************
**  STEP1: PRE-LOAD THE CONNECTOR
**  STEP2: APPLY EXTENSION
**
*NODE, NSET=SN01, NSET=SN02
   19705, -167.469772,   97.669983,   -0.000060
   19745, -165.858582,   97.669983,   -0.000059
   19781, -164.247406,   97.669983,   -0.000059
   19832, -162.636215,   97.669983,   -0.000058
          .
          .
          .
 257180,  173.126038,  214.255005,  145.270020
 257181,  145.269989,  214.255005,  173.126068
 257226,  159.806122,  214.255005,  159.806152
***
*ELEMENT, TYPE=C3D8, ELSET=SET01
 119521, 223959, 224401, 224692, 224065, 224969, 225384, 225693, 225089,
 119522, 224401, 224755, 225269, 224692, 225384, 225768, 226291, 225693,
 119523, 224755, 225052, 225778, 225269, 225768, 226090, 226786, 226291,
          .
          .
          .

 257614, 225260, 225151, 226594, 226664, 224124, 223996, 225471, 225535,
 257615, 225151, 225025, 226543, 226594, 223996, 223881, 225392, 225471,
 257616, 225025, 224905, 226450, 226543, 223881, 223770, 225318, 225392,
```

```
***
*ELEMENT, TYPE=C3D8, ELSET=SET02
     1, 215972, 214898, 215402, 216201, 217126, 216024, 216505, 217329,
     2, 214898, 213800, 214571, 215402, 216024, 214954, 215697, 216505,
     3, 213800, 212687, 213745, 214571, 214954, 213857, 214890, 215697,
          .
          .
          .
 286652,  286653,  286654,  286655,  286656,  286657,  286658,  286659
 286660,  286661,  286662,  286663,  286664,  286665,  286666,  286667
 286668,  286669,  286670,  286671,  286672,  286673,  286674,  286675
 286676,
**
*SURFACE, TYPE=ELEMENT, NAME=SCAA
*********************************
  119521,  S3
  119522,  S3
  119523,  S3
          .
          .
          .
  257423,  S5
  257424,  S4
  257424,  S5
**
**
*SURFACE, TYPE=ELEMENT, NAME=SCAB
*********************************
  135436,  S4
  135440,  S4
  135444,  S4
          .
          .
          .
  253570,  S3
  253571,  S3
  253572,  S3
**
**
*SURFACE, TYPE=ELEMENT, NAME=SCBA
*********************************
       1,  S6
       5,  S6
```

```
      9,  S6
          .
          .
          .
  117568,  S3
  117569,  S3
  117570,  S3
**
**
*SURFACE, TYPE=ELEMENT, NAME=SCBB
*********************************
   14497,  S6
   14501,  S6
   14505,  S6
          .
          .
          .
  115054,  S5
  115055,  S5
  115056,  S5
**
**
*SURFACE, TYPE=ELEMENT, NAME=SCPT
*********************************
  135337,  S3
  135338,  S3
  135339,  S3
          .
          .
          .
  252808,  S4
  252812,  S4
  252816,  S4
**
**
*SURFACE, TYPE=ELEMENT, NAME=SLOD
*********************************
   14209,  S3
   14210,  S3
   14211,  S3
          .
          .
          .
```

```
  257313,  S6
  257317,  S6
  257321,  S6
  257325,  S6
****
*MATERIAL, NAME=PAR01
*ELASTIC, TYPE=ISO
208000.0, 0.30,
*PLASTIC
 600.0, 0.0
 900.0, 0.2
**********
****
****
*SOLID SECTION, ELSET=SET01, MATERIAL=PAR01
****
****
****
*MATERIAL, NAME=PAR02
*ELASTIC, TYPE=ISO
208000.0, 0.30,
*PLASTIC
 600.0, 0.0
 900.0, 0.2
**********
****
****
*SOLID SECTION, ELSET=SET02, MATERIAL=PAR02
****
****
****
*ORIENTATION, SYS=RECT, NAME=CARTG
1.0, 0.0, 0.0,    0.0, 1.0, 0.0,    0.0, 0.0, 0.0
**SECOND LINE DEFAULT (1,0.0)**
**
**
****
****
****
****
*CONTACT PAIR, INTERACT=FRIC81, SMALL SLIDING, TYPE=NODE TO SURFACE
*****************
***SLAVE, MASTER**
```

```
******************
SCBA, SCAA
SCBB, SCAB
****
****
****
*SURFACE INTERACTION, NAME=FRIC81
*FRICTION
0.08
**
****
*NODE
***NODE 999000 FOR MAIN PRE-LOAD SECTION
 999000,  0.0000,   0.0000,   0.0000
***
***NODE 999101 for  constraint on top of pin SENA -yes
***NODE 999102 for constraint at bottom of box SEX0 - yes
 999101,       0.0,     750.0,   0.0
 999102,       0.0,    -550.0,   0.0
**
****
*PRE-TENSION SECTION, NODE=999000, SURFACE=SCPT
***********************************************
***
*NSET, NSET=PPSET
 999000
*******
*MPC
BEAM,SENA, 999101
*MPC
BEAM, SEX0, 999102
******************
*STEP, NLGEOM=YES, INC=300, UNSYMM=NO
************************************
********** STEP 1 ***************
************************************
**
STEP FOR PRE-LOAD
*****************
*STATIC
0.01,1.0, 1E-06, 1.0
**
**
```

```
*CLOAD, OP=NEW
**============**
999000, 1, 1000000.0
***
*BOUNDARY, OP=NEW
**=============**
  SEZ0, 3
 999101, 1,6
****
****
*CONTACT INTERFERENCE, SHRINK
*****************************
SCBA, SCAA
SCBB, SCAB
****
*EL PRINT, FREQ=0, POSITION=AVERAGED AT NODES
**
*NODE PRINT, FREQ=1, NSET=PPSET
U
RF
**
*NODE FILE, FREQ=1
U
**
*EL FILE, POSITION=AVERAGED AT NODES, FREQ=1
S
PE
*File format, ascii
*END STEP
**
```

8.5.6 Developed 3-D Model Input File – Preload + Bend (Abridged)

```
*HEADING
**
**
**  IMPOSED DISPLACEMENT ***
**  ************************
**  STEP1: PRE-LOAD THE CONNECTOR
**  STEP2: APPLY EXTENSION
**
```

```
**
*NODE, NSET=SN01, NSET=SN02
   19705, -167.469772,   97.669983,   -0.000060
   19745, -165.858582,   97.669983,   -0.000059
   19781, -164.247406,   97.669983,   -0.000059
   19832, -162.636215,   97.669983,   -0.000058
          .
          .
          .
  257180,  173.126038,  214.255005,  145.270020
  257181,  145.269989,  214.255005,  173.126068
  257226,  159.806122,  214.255005,  159.806152
***
*ELEMENT, TYPE=C3D8, ELSET=SET01
 119521, 223959, 224401, 224692, 224065, 224969, 225384, 225693, 225089,
 119522, 224401, 224755, 225269, 224692, 225384, 225768, 226291, 225693,
 119523, 224755, 225052, 225778, 225269, 225768, 226090, 226786, 226291,
          .
          .
          .

 257614, 225260, 225151, 226594, 226664, 224124, 223996, 225471, 225535,
 257615, 225151, 225025, 226543, 226594, 223996, 223881, 225392, 225471,
 257616, 225025, 224905, 226450, 226543, 223881, 223770, 225318, 225392,
***
*ELEMENT, TYPE=C3D8, ELSET=SET02
      1, 215972, 214898, 215402, 216201, 217126, 216024, 216505, 217329,
      2, 214898, 213800, 214571, 215402, 216024, 214954, 215697, 216505,
      3, 213800, 212687, 213745, 214571, 214954, 213857, 214890, 215697,
          .
          .
          .
  286652,  286653,  286654,  286655,  286656,  286657,  286658,  286659
  286660,  286661,  286662,  286663,  286664,  286665,  286666,  286667
  286668,  286669,  286670,  286671,  286672,  286673,  286674,  286675
  286676,
**
**
*SURFACE, TYPE=ELEMENT, NAME=SCAA
*********************************
   119521,  S3
   119522,  S3
   119523,  S3
```

.
.
.
257423, S5
257424, S4
257424, S5
**
**
*SURFACE, TYPE=ELEMENT, NAME=SCAB
****
135436, S4
135440, S4
135444, S4
.
.
.
253570, S3
253571, S3
253572, S3
**
**
*SURFACE, TYPE=ELEMENT, NAME=SCBA
****
1, S6
5, S6
9, S6
.
.
.
117568, S3
117569, S3
117570, S3
**
**
*SURFACE, TYPE=ELEMENT, NAME=SCBB
****
14497, S6
14501, S6
14505, S6
.
.
.
115054, S5

```
  115055,  S5
  115056,  S5
**
**
*SURFACE, TYPE=ELEMENT, NAME=SCPT
**********************************
  135337,  S3
  135338,  S3
  135339,  S3
        .
        .
        .
  252808,  S4
  252812,  S4
  252816,  S4
**
**
*SURFACE, TYPE=ELEMENT, NAME=SLOD
*********************************
   14209,  S3
   14210,  S3
   14211,  S3
        .
        .
        .
  257313,  S6
  257317,  S6
  257321,  S6
  257325,  S6
****
****
*MATERIAL, NAME=PAR01
*ELASTIC, TYPE=ISO
208000.0, 0.30,
*PLASTIC
 600.0, 0.0
 900.0, 0.2
**********
*SOLID SECTION, ELSET=SET01, MATERIAL=PAR01
****
*MATERIAL, NAME=PAR02
*ELASTIC, TYPE=ISO
208000.0, 0.30,
```

```
*PLASTIC
 600.0, 0.0
 900.0, 0.2
**********
****
****
*SOLID SECTION, ELSET=SET02, MATERIAL=PAR02
****
*ORIENTATION, SYS=RECT, NAME=CARTG
1.0, 0.0, 0.0,    0.0, 1.0, 0.0,    0.0, 0.0, 0.0
**SECOND LINE DEFAULT (1,0.0)**
**
**
*CONTACT PAIR, INTERACT=FRIC81, SMALL SLIDING, TYPE=NODE TO SURFACE
*****************
***SLAVE, MASTER**
*****************
SCBA, SCAA
SCBB, SCAB
****
*SURFACE INTERACTION, NAME=FRIC81
*FRICTION
0.08
**
**
*****
*NODE
***NODE 999000 FOR MAIN PRE-LOAD SECTION
 999000,  0.0000,   0.0000,   0.0000
***
***NODE 999101 for  constraint on top of pin SENA -yes
***NODE 999102 for constraint at bottom of box SEX0 - yes
 999101,       0.0,     750.0,   0.0
 999102,       0.0,    -550.0,   0.0
**
****
*PRE-TENSION SECTION, NODE=999000, SURFACE=SCPT
*********************************************
*NSET, NSET=PPSET
 999000
*******
**
**
```

```
****
****
*MPC
BEAM,SENA, 999101
*MPC
BEAM, SEX0, 999102
******************
*STEP, NLGEOM=YES, INC=300, UNSYMM=NO
************************************
********** STEP 1 ***************
************************************
**
STEP FOR PRE-LOAD
*****************
*STATIC
0.01,1.0, 1E-06, 1.0
**
**
*CLOAD, OP=NEW
**=============**
999000, 1, 5000000.0
***
*BOUNDARY, OP=NEW
**==============**
  SEZ0, 3
 999101, 1,6
****
*CONTACT INTERFERENCE, SHRINK
*****************************
SCBA, SCAA
SCBB, SCAB
****
**
*EL PRINT, FREQ=0, POSITION=AVERAGED AT NODES
**
*NODE PRINT, FREQ=1, NSET=PPSET
U
RF
**
*NODE FILE, FREQ=1
U
**
*EL FILE, POSITION=AVERAGED AT NODES, FREQ=1
```

```
S
PE
*END STEP
**
*STEP, NLGEOM=YES, INC=300, UNSYMM=NO
**************************************
********** STEP 2 ******************
**************************************
**
TENSION
****************
*STATIC
0.01,1.0, 1E-06, 1.0
**
*BOUNDARY,FIXED,OP=NEW
**** FIX THE PRE-LOAD ******
999000, 1, 1
**==============**
*BOUNDARY, OP=NEW
**==============**
 SEZ0, 3
**** NODE 999101:-
 999101, 1,6
*************
*****NODE 999102:-
***** FREEDOMS 1 AND 2 ARE FREE
 999102, 3,5
 999102, 6,6, 0.016453
****
**
*EL PRINT, FREQ=0, POSITION=AVERAGED AT NODES
**
*NODE PRINT, FREQ=1, NSET=PPSET
U
RF
**
*NODE FILE, FREQ=1
U
**
*EL FILE, POSITION=AVERAGED AT NODES, FREQ=1
S
PE
*END STEP
```